Juerg Hodler
Rahel A. Kubik-Huch
Gustav K. von Schulthess
Editors

Musculoskeletal Diseases 2021–2024

Diagnostic Imaging

IDKD Diagnostic
Imaging Courses

OPEN ACCESS

Springer

IDKD Springer Series

Series Editors

Juerg Hodler
Department of Radiology
University Hospital of Zurich
Zurich, Switzerland

Rahel A. Kubik-Huch
Department of Radiology
Kantonsspital Baden
Baden, Switzerland

Gustav K. von Schulthess
Professor and Director
Emeritus Nuclear Medicine
University Hospital
Zurich, Switzerland

The world-renowned International Diagnostic Course in Davos (IDKD) represents a unique learning experience for imaging specialists in training as well as for experienced radiologists and clinicians. IDKD reinforces his role of educator offering to the scientific community tools of both basic knowledge and clinical practice. Aim of this Series, based on the faculty of the Davos Course and now launched as open access publication, is to provide a periodically renewed update on the current state of the art and the latest developments in the field of organ-based imaging (chest, neuro, MSK, and abdominal).

More information about this series at http://www.springer.com/series/15856

Juerg Hodler • Rahel A. Kubik-Huch
Gustav K. von Schulthess

Editors

Musculoskeletal Diseases 2021–2024

Diagnostic Imaging

✸ Springer

Editors
Juerg Hodler
Department of Radiology
University Hospital of Zurich
Zurich
Switzerland

Rahel A. Kubik-Huch
Department of Radiology
Kantonsspital Baden
Baden, Aargau
Switzerland

Gustav K. von Schulthess
Professor and Director
Emeritus Nuclear Medicine
University Hospital
Zurich
Switzerland

Contents

Shoulder: Instability

1

Michael J. Tuite and Christian W. A. Pfirrmann

Learning Objectives
- To know the types of glenohumeral instability and anatomic factors for the development of glenohumeral instability.
- To understand the concept of the glenoid track and the engaging Hill-Sachs lesion.
- To understand the MR appearance of SLAP tears, overhead thrower labral tears, and the labral tears associated with spinoglenoid notch cysts.
- To understand how to distinguish labral tears from normal labral variants.

1.1 Glenohumeral Instability

Glenohumeral instability is the inability to keep the humeral head centered in the glenoid fossa. Glenohumeral instability can be classified according to etiology and direction of instability.

Glenohumeral instability can be classified into static instabilities, dynamic instabilities, and voluntary dislocation [1].

Static instability is associated with significant structural alteration of the shoulder, for example, large rotator cuff tears or a glenoid dysplasia with consecutive static decentering of the humeral head.

Dynamic instability is the classic form of instability, commonly caused by trauma, and is usually associated with injuries to the labrum, to the glenohumeral ligaments, and often with fractures of the glenoid rim. Dynamic instability may also be associated with general hyperlaxity.

M. J. Tuite (✉)
Department of Radiology, University of Wisconsin, Madison, WI, USA
e-mail: mjtuite@wisc.edu

C. W. A. Pfirrmann
MRI—Medical Radiological Institute, Zurich, Zurich, Switzerland
e-mail: christian.pfirrmann@pfirrmann.ch

Glenohumeral instability may be *unidirectional* (anterior instability or posterior instability) or *multidirectional*. Multidirectional instability is affecting a minority of patients.

The classification *in traumatic instability and atraumatic instability* is important from an imaging perspective. Both instabilities are characterized by recurrent dislocations of the glenohumeral joint. However, in traumatic instabilities, structural changes such as labral, ligamentous, and bony lesions are highly prevalent. In atraumatic instabilities the glenohumeral joint may not exhibit any injuries [2].

Key Point
- In atraumatic instabilities the glenohumeral joint may be normal at imaging.

The labrum, the ligaments, and the bony structures contribute to the stability of the glenohumeral joint. Usually, the labrum receives the highest attention at imaging. However, the glenoid labrum only contributes about 10% to the stability glenohumeral joint. Therefore, it is important to also include the glenohumeral ligaments and the bony structures into a comprehensive imaging assessment.

1.2 Anterior Instability

1.2.1 Labral Lesions in Anterior Instability

Bankart lesion: The "Bankart lesion" was described by A. S. Blundell Bankart in the *British Medical Journal* in 1923 [3]. The Bankart lesion consists of a tear of the anteroinferior labrum. The labrum and the periosteum are completely detached. Therefore, the labrum seems to float distant to the glenoid rim when viewed at arthroscopy or on transverse MRI sections (Fig. 1.1).
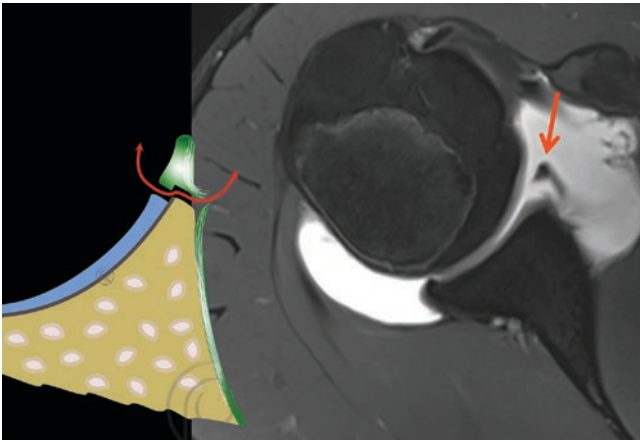
Fig. 1.1 Bankart lesion
Axial fluid sensitive fat-saturated MR arthrography image shows a Bankart lesion (red arrow) consisting of a tear of the antero-inferior labrum. The labrum and the periosteum are completely detached. Therefore, the labrum seems to float distant to the glenoid rim
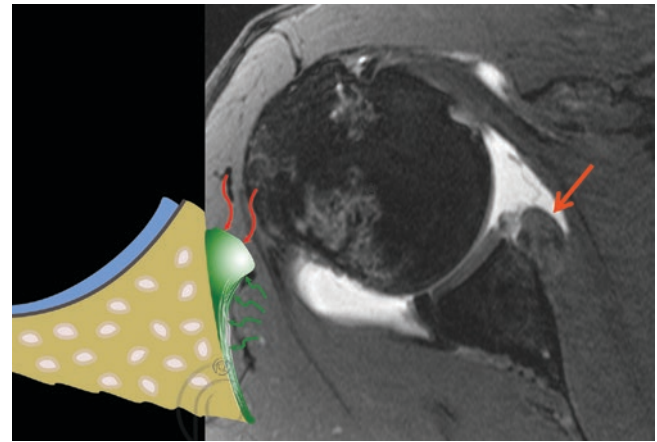
Fig. 1.3 ALPSA lesion
Axial fluid sensitive fat-saturated MR arthrography image shows an ALPSA lesion (red arrow). The detached labrum is medially displaced and scarred to the glenoid neck
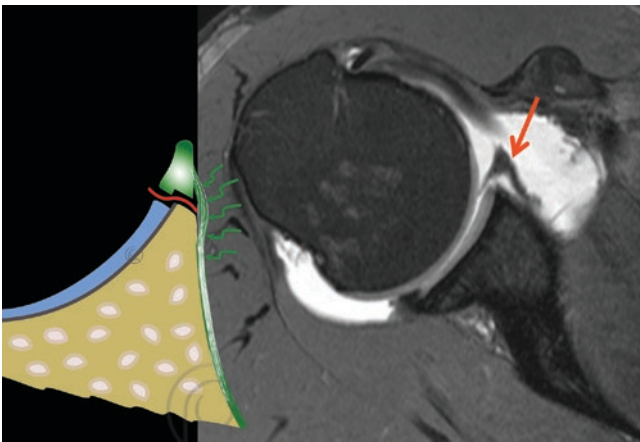
Fig. 1.2 Perthes lesion
Axial fluid sensitive fat-saturated MR arthrography image shows the anteroinferior labrum (red arrow) detached from the edge of the glenoid but still attached to the intact periosteum

Fig. 1.4 GLAD lesion
Axial fluid sensitive fat-saturated MR arthrography image shows a GLAD lesion. A portion of the anterior inferior glenoid articular cartilage is avulsed associated with a partial labral tear. The labrum is not detached or dislocated

Perthes lesion: The Perthes lesion was described some years earlier than the Bankart lesion in 1906 [4]. The antero-inferior labrum is detached from the edge of the glenoid but still attached to the intact periosteum. Often the labrum may be almost normally positioned at imaging. However, functionally the labrum no longer adds to the stability glenohumeral joint (Fig. 1.2).

ALPSA lesion: In 1993 Neviaser [5] described the anterior labro-ligamentous periosteal sleeve avulsion (ALPSA) lesion as a cause for anterior instability of the shoulder. In the ALPSA lesion, the periosteum between the labrum and glenoid remains intact. The detached labrum displaces medially and inferiorly. The labrum and the periosteum heal on the scapular neck (Fig. 1.3).

GLAD lesion: GLAD stands for "glenolabral articular disruption" and was also described by Neviaser in 1993 [6]. The GLAD lesion consists of an anteroinferior glenoid articular cartilage injury associated with a partial labral tear. The labrum is not detached or dislocated. Patients with GLAD lesions usually have a stable glenohumeral joint and present with anterior shoulder pain (Fig. 1.4).

1.2.2 Ligament Lesions in Anterior Instability

One of the most important stabilizers for the glenohumeral joint is the inferior glenohumeral ligament (IGHL). The IGHL connects the glenoid to the humerus and has the shape

of a hammock with a strong anterior and posterior bundle. Two distinct patterns of the attachment of the IGHL to the glenoid are described [7]. In most joints (80%) the IGHL attaches directly to the labrum with some fibers extending onto the glenoid neck. Less commonly (20%) the IGHL attaches only to the glenoid neck. Therefore, a detachment of the glenoid labrum is a detachment of the IGHL in most cases. Most frequently the failure of the IGHL is on the glenoid side. Failure on the humeral side is termed "humeral avulsion of glenohumeral ligament" or HAGL lesion. HAGL lesions may be difficult to be diagnosed at arthroscopy. The J sign (the axillary recess is normally U-shaped—conversion to a J shape is called the J sign) and axillary fluid extravasation at MR arthrography are suggestive of a HAGL lesion. However, a false-positive diagnosis of HAGL lesions is not uncommon at MRI [8]. Fluid extravasation at MR arthrography may occur with an intact IGHL or also in a mid-substance tear of the IGHL.

> **Key Point**
> - The inferior glenohumeral ligament attaches directly to the labrum in most joints. Therefore, a detachment of the glenoid labrum is a detachment of the IGHL in most cases.

1.2.3 Bony Lesions in Anterior Instability

1.2.3.1 Glenoid
A bony defect of the glenoid rim is probably the most important factor for the development of an unstable glenohumeral joint. Bony defects of the glenoid that are more than half of the maximal AP diameter of the glenoid in length lead to a significant loss of dislocation resistance. This may not be compensated for by a Bankart repair or labral reconstruction alone. A bony procedure such as a Latarjet procedure or bone grafting procedure to augment the anterior glenoid rim is often necessary.

A bony defect can be congenital, can be a result of a glenoid rim fracture, or can be the result of the chronic instability. Repetitive anterior subluxations of the humeral head lead to glenoid bone loss without the presence of a fragment at the glenoid rim.

1.2.3.2 Humerus
In 1940 Harold A. Hill and Maurice D. Sachs described the grooved defect of the humeral head in the journal *Radiology*. The presence of a Hill-Sachs lesion confirms the diagnosis of anterior instability of the glenohumeral joint. The prevalence of Hill-Sachs lesion that needs to be treated is about 7% [9].

Therefore, the size, location, and relation to the glenoid need to be addressed.

Some types of Hill-Sachs are at risk for an engaging lesion and need to be treated: risk factors are a large and wide Hill-Sachs lesion, a medially located Hill-Sachs lesion, or a Hill-Sachs lesion with an oblique orientation on neutral position of the humerus. Cases with an engaging Hill-Sachs lesion present with a large bony defect of the glenoid at the same time (bipolar lesion).

1.2.3.3 Glenoid Track Theory, On-Track and Off-Track Lesions
In the abduction and external rotation (ABER) position of the shoulder, patients with glenohumeral instability experience subluxation and apprehension. Apprehension is the fear of imminent dislocation of a patient anterior instability with when placing the arm in an ABER position.

The "glenoid track" is the contact area of the glenoid surface onto the posterosuperior humeral head in the ABER position (Fig. 1.5).

The contact area between the glenoid and the humeral head, e.g., the "glenoid track," measures approximately 84% of the glenoid transverse diameter, whereas reminder of glenoid (16%) contacts with the medial margin of the rotator cuff footprint [10].

- On-track: Hill-Sachs lesion remains within the glenoid track.
- Off-track: Hill-Sachs lesion extends past the glenoid track medially and is therefore at risk for engaging.

> **Key Point**
> - Reasons for the "off-track" lesion are a large Hill-Sachs lesion, a medially located Hill-Sachs lesion, and/or a bony defect of the glenoid rim.

1.3 Posterior Instability

1.3.1 Labral Lesions in Posterior Instability

Posterior instability of the glenohumeral joint is common in young active patients. Posterior instability of the glenohumeral joint is most prevalent in young men, for example, the military population. Posterior instability of the glenohumeral joint is often caused by repetitive microtrauma. Repetitive pushups, pullups, or heavy weightlifting (bench press) may promote posterior instability of the glenohumeral joint. Also, in swimming and golf which puts stress on the posterior capsule, posterior instability of the glenohumeral joint may be seen.
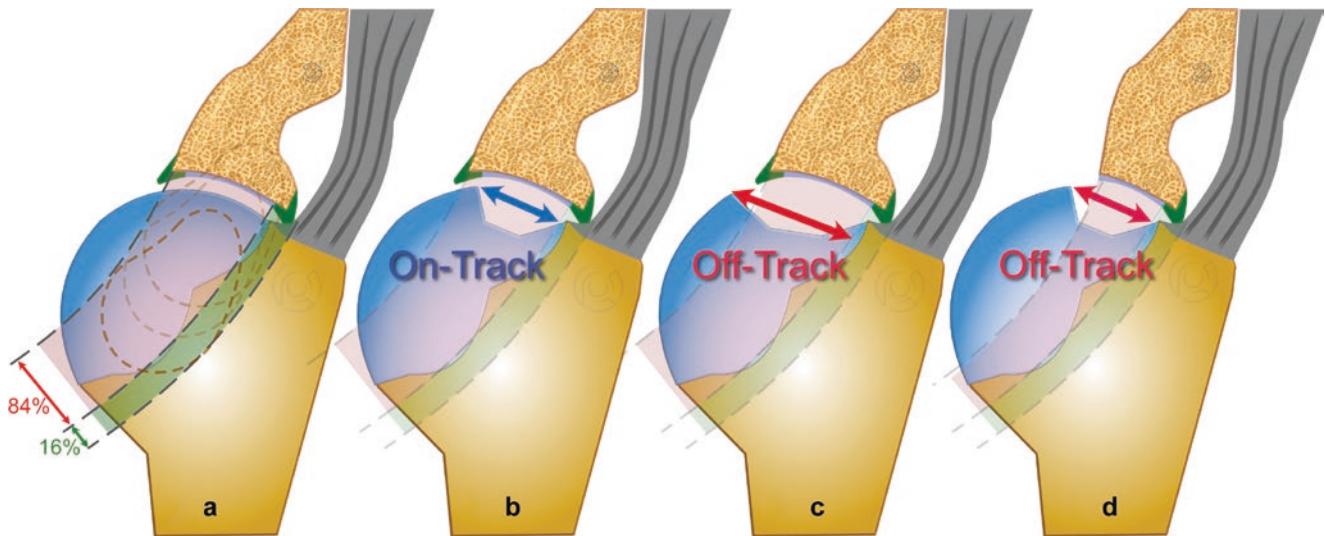
Fig. 1.5 Glenoid track theory, on-track situation, and off-track situation The "glenoid track" is the contact area of the glenoid surface onto the humeral head in the ABER position (**a**). On-track situation: the Hill-Sachs lesion remains within the glenoid track, and the Hill-Sachs lesion is not engaging (**b**). Off-track situation: the Hill-Sachs lesion extends past glenoid track medially, and the Hill-Sachs lesion is engaging (**c**). Off-track situation: the bony defect of the glenoid rim narrows the glenoid track humeral head. Hill-Sachs lesion extends past glenoid track medially, and the Hill-Sachs lesion is engaging (**d**)

Key Points
Anatomic risk factors for posterior instability of the glenohumeral joint include:

- Increased glenoid retroversion.
- Increased humeral head retroversion.
- Posterior glenoid dysplasia (brachial plexus birth palsy).

The Kim lesion, named after the author who first described this lesion, represents a posteroinferior labrum avulsion [11]. Often the labral lesion is concealed. Adjacent a marginal chondrolabral junction, lesion caused by repetitive posterior subluxations of the humeral head is observed (Fig. 1.6).

Kim's triad includes:

- Concealed posteroinferior labral tear.
- Marginal chondral lesion.
- Retroversion of the glenoid.

1.4 Labral Tears Without Overt Instability

1.4.1 Superior Labrum Anterior-Posterior (SLAP) Tears

SLAP tears are superior labral tears that occur in the region of the biceps anchor. SLAP tears are one of the more common tears of the glenoid labrum, with a prevalence at arthros-
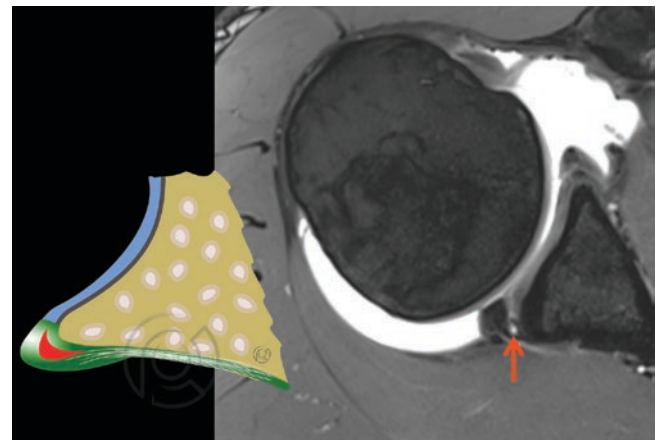
Fig. 1.6 Kim's lesion
Axial fluid sensitive fat-saturated MR arthrography image shows a posteroinferior labrum avulsion lesion (red arrow)

copy of 5–38% [12]. Although SLAP tears are often painful, smaller tears can be asymptomatic and identified incidentally at surgery or on a shoulder MR scan done for other reasons. SLAP tears can occur acutely after a fall on an outstretched hand or from either acute or repetitive biceps traction on the superior labrum. The SLAP tears in overhead throwing athletes will be discussed further in the next section on Overhead Thrower Injuries.

SLAP tears can have a variety of tear orientations, so are often subdivided into several types. A type 1 SLAP tear refers to a frayed free edge of the superior labrum and is a common finding in older individuals. Type 1 SLAP tears are usually degenerative or from overuse and may be minimal or asymptomatic.

The higher-type SLAP tears are longitudinal tears of the superior labrum, and these tears may require surgery to alleviate symptoms. The most common higher-type SLAP tear is a type 2 SLAP tear, which is a partial-thickness longitudinal tear of the superior labrum. These tears can have either a stable or unstable biceps anchor depending on their size and specific site of involvement. Distinguishing a stable from an unstable type 2 SLAP tear can be difficult on MR images, but in general larger tears at the base of the labrum that weaken the biceps anchor are more unstable.

The anterior to posterior length of type 2 SLAP tears varies in different individuals. Some have subcategorized type 2 SLAP tears as 2A (anterosuperior), 2B (posterosuperior), or 2C (involving the entire superior labrum from anterior to posterior). The posterosuperior type 2B SLAP tears are sometimes seen in overhead throwing athletes and in patients with a spinoglenoid notch paralabral cyst, both discussed in a later section.

A type 3 SLAP tear is a full-thickness tear resulting in a bucket handle torn labral segment. Type 3 SLAP tears tend to have a stable biceps anchor. A type 4 SLAP tear extends into the biceps tendon. There are currently some 12 types of SLAP tears described, and the type 5 and above tears mainly involve extension to other parts of the labrum or adjacent structures.

SLAP tears appear on MR images as linear increased signal extending to an articular surface of the labrum between the 11:00 and 1:00 position of the glenoid rim [13] (Fig. 1.7). Because some patients have a superior recess normal variant in this region of the labrum, there are several MR signs that have been proposed to help distinguish a SLAP tear from a normal recess. The findings of a SLAP tear include the linear increased signal being irregular, extending across the entire labrum on an oblique coronal image, curving laterally, there being two increased signal lines (a recess that is more medial, and the tear which is located more laterally, also called the "double oreo" sign), or signal width > 2 mm on MR or 3 mm at MR arthrography. High signal at the labral-chondral junction posterior to the biceps anchor has been proposed as a possible MR sign of a SLAP tear; however several studies have found that at MR arthrography a normal superior recess can extend posterior to the biceps in up to 90% of individuals.

> **Key Point**
> - For SLAP tears the linear increased signal usually curves laterally, in distinction from a normal labral variant superior sublabral recess which curves medially.

1.4.2 Overhead Thrower Labrocapsular Injuries

Overhead throwing athletes can develop an overuse injury of the shoulder that includes a superior labral tear. There are two related etiologies that have been described for why labral tears occur in these athletes, glenohumeral internal rotation deficit (GIRD) and internal impingement. GIRD results from thickening and fibrosis of the posterior band inferior glenohumeral ligament and capsule and results from repetitive traction during the deceleration phase of

Fig. 1.7 Superior labrum anterior–posterior (SLAP) tear
Two consecutive oblique coronal fat-suppressed T2-weighted images show irregular, laterally curving high signal (arrow) in the superior labrum
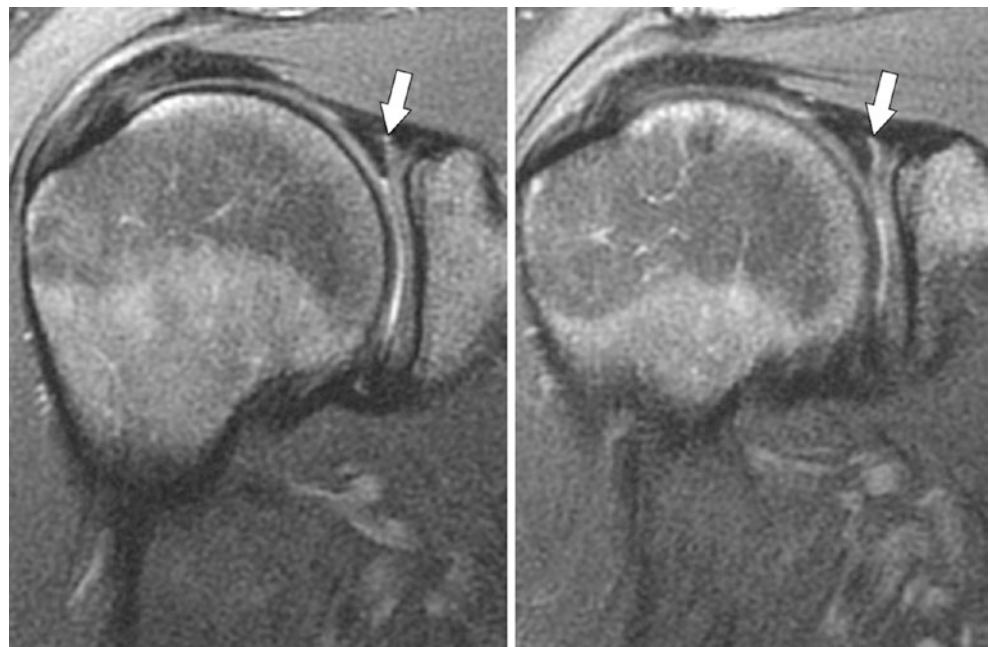
throwing. Internal impingement presents as pain in the late cocking phase of throwing with decreased throwing velocity. Internal impingement is felt to be a shoulder microinstability condition due to a posterosuperior shift of the humeral head contact point with the glenoid due to GIRD, a stretched anterior capsule, and muscle fatigue that allows increased contact of the under surface of the rotator cuff with the posterosuperior labrum [14].

There are two main mechanisms that are believed to lead to labral injury in patients with GIRD and internal impingement. The first is repetitive forceful contact between the greater tuberosity and the posterosuperior glenoid rim during abduction and external rotation, which causes fraying or tears of the posterosuperior labrum. The other is longitudinal twisting of the long head biceps tendon at full external rotation of the humerus, which twists the biceps anchor resulting in a "peel-back" SLAP tear. The biceps muscle also contracts late in the throwing motion during deceleration so as to slow the extension of the elbow, and this applies repetitive traction forces on the superior labrum and may exacerbate tears.

The posterosuperior labral tears with internal impingement appear similar on MR to SLAP tears from other mechanisms. Overhead throwers can develop free edge fraying in the posterosuperior labrum, which other than their distinctive posterosuperior location appear similar to other type 1 SLAP tears on MR with blunting and irregularity of the free edge. The other common SLAP tear in overhead throwers is a type 2B SLAP tear which will appear as irregular laterally curved high signal (Fig. 1.8). Other throwers may have a smaller focal tear of the posterosuperior labrum that does not extend to the 12:00 position of the glenoid. Because these
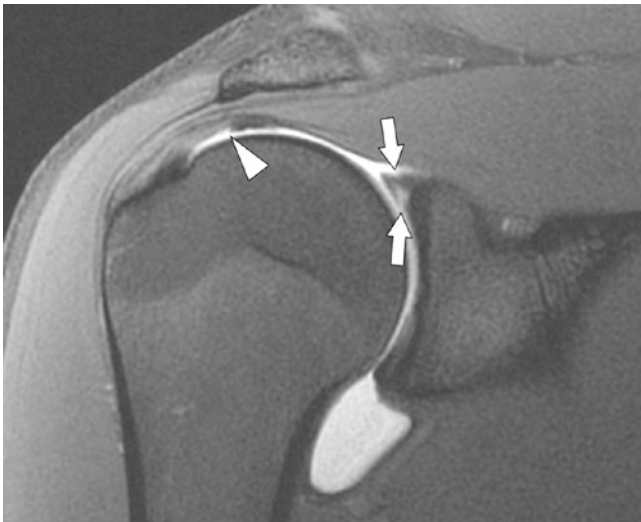
Fig. 1.8 Overhead thrower labral tear
Oblique coronal fat-suppressed T1-weighted MR arthrogram image in a 21-year-old baseball pitcher who has pain with throwing shows a tear of the posterosuperior labrum (arrows). There is also an articular surface partial thickness rotator cuff tear (arrowhead)

tears can be small, they are often better seen on MR arthrography with abduction and external rotation (ABER) images.

There are several other lesions of the labrocapsular complex that can be seen in throwing athletes. Patients with GIRD can have focal thickening of the posterior band inferior glenohumeral ligament near the labral insertion, with loss of the normal labrocapsular recess in this region. These athletes can also have an exostosis in this region, the Bennett lesion, which is felt to result from repetitive traction leading to ossification of the posterior band inferior glenohumeral ligament at the glenoid insertion. Throwers often develop a chronically stretched anterior capsule which allows the increased external rotation in the late cocking phase of the throwing motion that is associated with increased throwing velocity, although this can be difficult to diagnose on MR images. They can also develop tears of the anterior capsule due to tensile overload; these tears are more common in older overhead throwing athletes where the capsule has become less pliable.

There are several additional findings in the shoulder associated with internal impingement. The most important is an articular surface partial thickness cuff tear of the posterior supraspinatus or anterior infraspinatus tendon (Fig. 1.8). Another common finding in throwers is prominent posterior humeral head cysts. These have been sometimes called a "pseudo Hill-Sachs" lesion, but they occur more posterior than a true posterolateral Hill-Sachs lesion. A partial tear of the inferior subscapularis muscle-tendon junction has also been described in throwing athletes.

1.4.3 Spinoglenoid Notch Cyst and Posterosuperior Labral Tear

Shoulder paralabral cysts are pseudocysts that result from a labrocapsular tear that allows joint fluid to extravasate into the paralabral soft tissues. Paralabral cysts can occur at any point around the glenoid rim, but are most common adjacent to the posterosuperior region of the glenoid rim. The posterosuperior location is common because cysts can form here easily in the fat plane between the supraspinatus and infraspinatus muscles lateral to the scapular spine, an area known as the spinoglenoid notch.

The labral tears associated with spinoglenoid notch paralabral cysts can be type 2B SLAP tears (superior labral tears that extend posteriorly) or focal posterosuperior labral tears. Focal tears in the posterosuperior labrum can occur after acute trauma such as a fall on an outstretched hand or from repetitive trauma. Labral tears in this region are not uncommon in overhead throwers, but most are not associated with a paralabral cyst in this group of athletes.

Spinoglenoid notch paralabral cysts are symptomatic because they often compress the suprascapular nerve, which
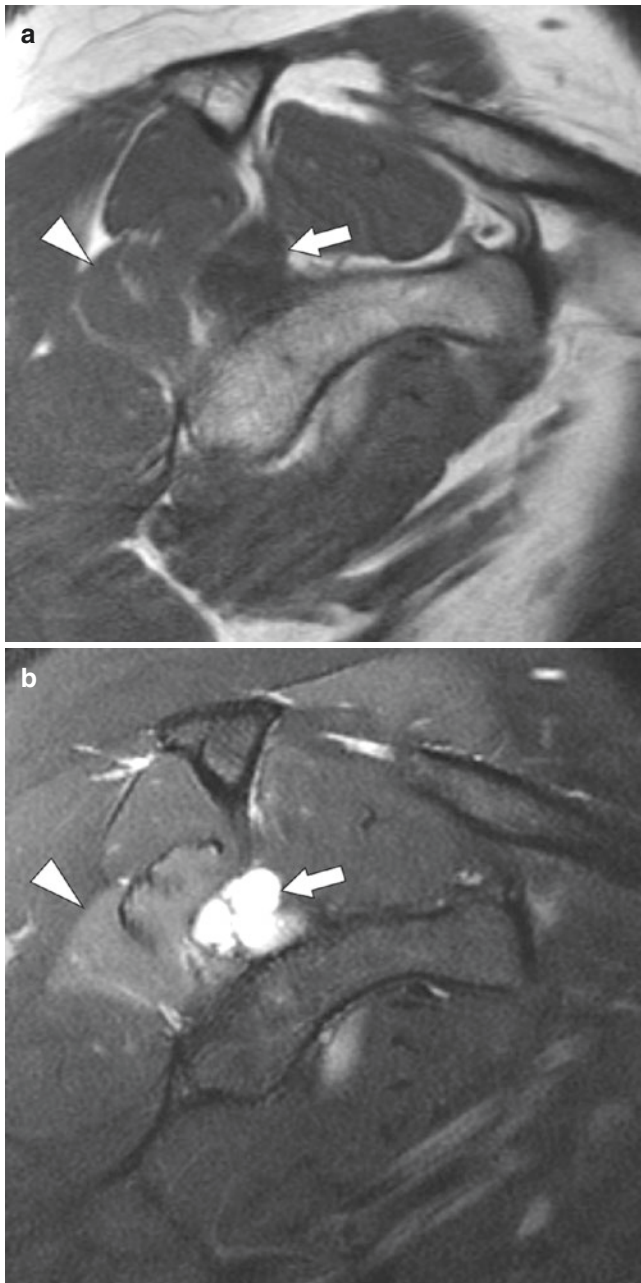
Fig. 1.9 Spinoglenoid notch cyst
(**a**) Oblique sagittal T1-weighted and (**b**) oblique sagittal fat-suppressed T2-weighted images show a paralabral cyst in the spinoglenoid notch (arrows) and denervation edema (arrowheads) within the caudal portion of the infraspinatus muscle

courses through the fat plane between the supraspinatus and infraspinatus muscles. The suprascapular nerve contains sensory fibers that supply the posterior joint capsule and acromioclavicular joint and motor fibers that innervate the infraspinatus and supraspinatus muscles. The most common presentation of a spinoglenoid notch paralabral cyst is pain, and half the patients who are symptomatic will have only pain due to the sensory fibers being primarily affected. Motor

symptoms are usually external rotation weakness from denervation of the infraspinatus muscle; large cysts that extend superiorly into the suprascapular notch can also involve the motor branch to the supraspinatus muscle causing arm abduction weakness.

On MR, paralabral cysts appear as a well-defined T2 high signal mass medial and adjacent to the posterosuperior labrum (Fig. 1.9) [15, 16]. On MR arthrography, there is variable filling of the cyst with intraarticular contrast. Although 85% of cysts are associated with a labral tear, the tear often partially heals so that fluid in the glenohumeral joint and the paralabral cyst may not have a bidirectional communication.

The infraspinatus muscle may appear normal on MR even if the patient is experiencing pain, possibly due to nerve impingement affecting the sensory fibers more than the motor fibers. Other spinoglenoid notch cysts will have associated increased T2 signal in the infraspinatus muscle, termed denervation edema. If the cyst is left untreated, the patient may develop fat replacement and atrophy of the muscle. If a cyst is large and extends up to the suprascapular notch region, there may also be T2 high signal in the supraspinatus muscle. Again, if the cyst is long-standing, there may be fat replacement atrophy of both the infraspinatus and supraspinatus muscles.

1.5 Normal Labral Variants

One of the difficulties with accurately diagnosing labral tears on MR imaging is the normal labral variants, which can sometimes appear similar to tears. The most common location for the labral variants is from 11:00 posterosuperiorly to the 3:00 anteriorly on the glenoid rim. The labral variants are mainly sections of the labrum that are partially or completely unattached to the glenoid rim.

The most common labral variant is a superior sublabral recess, which is a partially unattached superior labrum between 11:00 and 1:00 that is seen in 74% of people [17]. The recess formed by the partially unattached superior labrum occurs at the articular surface of the labral-chondral junction; the peripheral superomedial margin of the superior labrum remains adherent to the glenoid rim. Some have classified the attachment of the superior labrum to the glenoid rim into one of three "biceps-labral complexes": type 1 (entire medial base of the labrum adherent to the glenoid rim), type 2 (superior recess ≤2 mm), or type 3 (superior recess >2 mm) [18]. On MR images, a superior sublabral recess will appear as smooth medially curving linear high signal at the labral-chondral junction which does not extend outward across the entire base of the labrum.

The next most common location for labral variants is in the anterosuperior (1:00–3:00) labrum between the origins

of the middle and inferior glenohumeral ligaments. There are three labral variants that can occur in the anterosuperior labrum. One is a sublabral foramen, where the labrum is focally unattached to the glenoid rim, and is present in 10–15% of individuals [19]. The second is a Buford complex where the anterosuperior portion of the labrum is absent and there is a thick, cord-like middle glenohumeral ligament, and this is seen in 1–2% of individuals. The third is an anterosuperior sublabral recess where the labrum is only attached to the glenoid rim at its outer margin, similar to a superior sublabral recess. There is an increased association of these anterosuperior labral variants with the more common superior sublabral recess.

The sublabral foramen and anterosuperior recess will appear on MR images as high signal between the labrum and glenoid rim. The Buford complex appears on MR images as a segment of the anterosuperior glenoid rim where no labrum is visible, although the patient also has a thick middle glenohumeral ligament which may lie against the glenoid rim and mimic the unattached labrum of a sublabral foramen (Fig. 1.10).

> **Key Point**
> - On MR, increased signal between the labrum and glenoid rim isolated to the anterosuperior labrum is more likely to be a sublabral foramen normal variant than to be a tear.

Although less common than in the 11:00–3:00 region, a shallow recess at the inner labral-chondral junction can also occur at other regions around the glenoid rim [20]. These smooth, less than 2 mm deep recesses should not be confused with a labral tear.

There is controversy whether these labral variants are congenital or developmental such as from prior post-traumatic detachment. For the superior recess, De Palma found these recesses were more prevalent with increasing age and therefore believed they were an acquired lesion possibly from chronic repetitive traction [21]. Tena-Arregui et al. found that a superior recess was not present in still-born fetal specimens and came to the same conclusion but did observe that 10% of fetuses had a sublabral foramen, a similar prevalence to adults [22]. It may be that some variants are congenital and others acquired. In any case, most believe that a superior recess or an anterosuperior labral variant is an incidental finding and if "repaired" at surgery will only worsen symptoms.

Finally, there is a finding on oblique coronal MR images called a "pseudoSLAP," where T2 high signal fluid is present between the long head biceps tendon and the anterior-superior labrum on oblique coronal images. This occurs because the long head biceps tendon can pass over the anter-
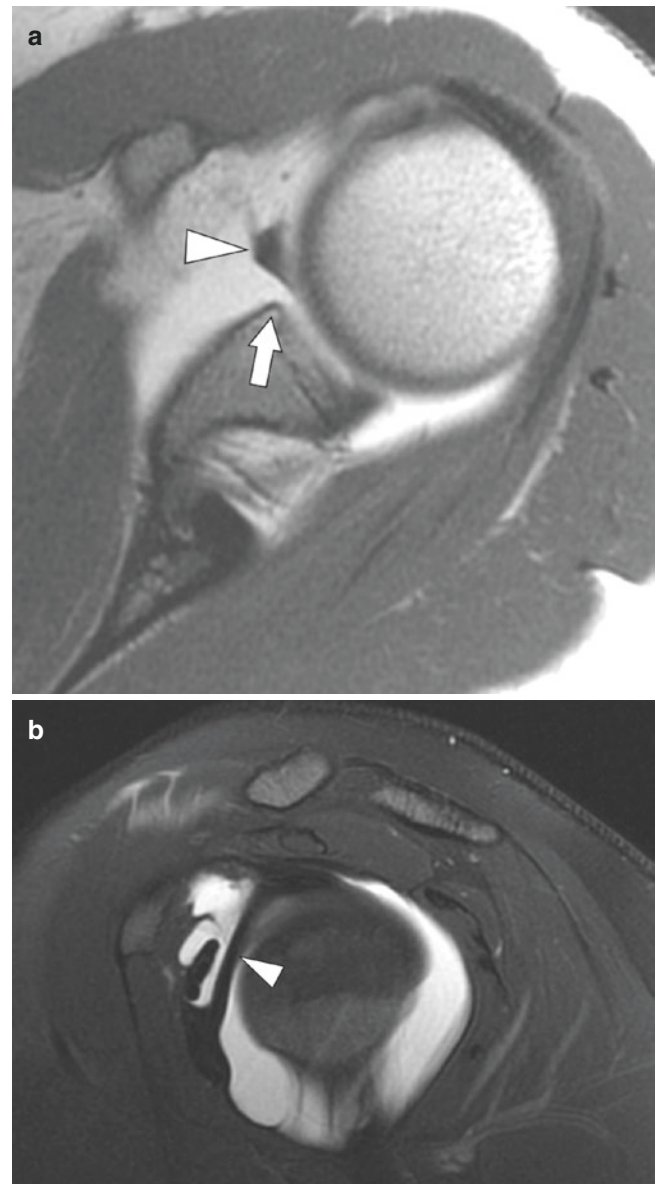
Fig. 1.10 Buford complex normal labral variant (**a**) Axial T1-weighted and (**b**) oblique sagittal fat-suppressed T2-weighted images show an absent anterosuperior labrum (arrow) and a thick, cord-like middle glenohumeral ligament (arrowheads), known as a Buford complex

osuperior labrum to insert directly onto the supraglenoid tubercle in some individuals. This pitfall should not be mistaken for a biceps-labral junction tear.

1.6 Concluding Remarks

MR is the best modality for imaging the glenoid labrum and instability, but even with high-quality images, accurately diagnosing pathology can be challenging. Learning the varied MR appearances of labral tears and injuries to the capsule is important to help confirm the clinical findings and guide

presurgical planning. Recognizing labral tears above the midpoint of the glenoid, and distinguishing them from the normal labral variants, is important in identifying several of the causes of shoulder pain.

> **Take Home Messages**
> - The classification in traumatic instability and atraumatic instability is very important because the examination in a patient with an atraumatic instability of the glenohumeral joint may be normal.
> - All structures (labrum, ligament, bone) contributing to glenohumeral instability must be addressed.
> - The increased signal on MR seen in SLAP tears is often irregular, directed cranially or curves laterally, and extends into the superior labrum.
> - The increased signal on MR of a normal variant superior sublabral recess is smooth, curves medially, and occurs at the labral/glenoid junction.

References

1. Gerber C, Nyffeler RW. Classification of glenohumeral joint instability. Clin Orthop Relat Res. 2002;400:65–76.
2. Matsen FA 3rd, Harryman DT 2nd, Sidles JA. Mechanics of glenohumeral instability. Clin Sports Med. 1991;10(4):783–8.
3. Bankart AS. Recurrent or habitual dislocation of the shoulder joint. Br Med J. 1923;2(3285):1132–3. https://doi.org/10.1136/bmj.2.3285.1132.
4. Perthes G. Über operationen bei habitueller Schulterluxationen. Deutsch Z Chir. 1906;85:199–227.
5. Neviaser TJ. The anterior labroligamentous periosteal sleeve avulsion lesion: a cause of anterior instability of the shoulder. Arthroscopy. 1993;9:17–21.
6. Neviaser TJ. The GLAD lesion: another cause of anterior shoulder pain. Arthroscopy. 1993;9(1):22–3.
7. Eberly VC, McMahon PJ, Lee TQ. Variation in the glenoid origin of the anteroinferior glenohumeral capsulolabrum. Clin Orthop Relat Res. 2002;400:26–31.
8. Melvin JS, Mackenzie JD, Nacke E, Sennett BJ, Wells L. MRI of HAGL lesions: four arthroscopically confirmed cases of false-positive diagnosis. Am J Roentgenol. 2008;191(3):730–4.
9. Kurokawa D, Yamamoto N, Nagamoto H, Omori Y, Tanaka M, Sano H, Itoi E. The prevalence of a large Hill-Sachs lesion that needs to be treated. J Shoulder Elb Surg. 2013;22(9):1285–9.
10. Gyftopoulos S, Yemin A, Beltran L, Babb J, Bencardino J. Engaging Hill-Sachs lesion: is there an association between this lesion and findings on MRI? Am J Roentgenol. 2013;201(4):W633–8.
11. Kim SH, Ha KI, Yoo JC, Noh KC. Kim's lesion: an incomplete and concealed avulsion of the posteroinferior labrum in posterior or multidirectional posteroinferior instability of the shoulder. Arthroscopy. 2004;20(7):712–20.
12. Mohana-Borges A, Chung C, Resnick D. Superior labral anteroposterior tear: classification and diagnosis on MRI and MR arthrography. AJR. 2003;181:1449–62.
13. Symanski JS, Subhas N, Babb J, Nicholson J, Gyftopoulos S. Diagnosis of superior labrum anterior-to-posterior tears by using MR imaging and MR arthrography: a systematic review and meta-analysis. Radiology. 2017;285(1):101–13.
14. Lin DJ, Wong TT, Kazam JK. Shoulder injuries in the overhead-throwing athlete: epidemiology, mechanisms of injury, and imaging findings. Radiology. 2018;286(2):370–87. https://doi.org/10.1148/radiol.2017170481.
15. Tung GA, Entzian D, Stern JB, et al. MR imaging and MR arthrography of paraglenoid labral cysts. Am J Roentgenol. 2000;174:1707–15.
16. Guven F, Ogul H, Kaya S, Kantarci M. MR arthrographic evaluation of posterior paraglenoid labral cysts: a retrospective study. Acta Radiol. 2020;61(6):789–95.
17. Smith DK, Chopp TM, Aufdemorte TB, Witkowski EG, Jones RC. Sublabral recess of the superior glenoid labrum: study of cadavers with conventional nonenhanced MR imaging, MR arthrography, anatomic dissection, and limited histologic examination. Radiology. 1996;201(1):251–6. PMID: 8816553. https://doi.org/10.1148/radiology.201.1.8816553.
18. De Coninck T, Ngai SS, Tafur M, Chung CB. Imaging the glenoid labrum and labral tears. Radiographics. 2016;36(6):1628–47. https://doi.org/10.1148/rg.2016160020.
19. Tuite MJ, Orwin JF. Anterosuperior labral variants of the shoulder: appearance on gradient-recalled-echo and fast spin-echo MR images. Radiology. 1996;199(2):537–40.
20. Tuite MJ, Currie JW, Orwin JF, Baer GS, del Rio AM. Sublabral clefts and recesses in the anterior, inferior, and posterior glenoid labrum at MR arthrography. Skelet Radiol. 2013;42(3):353–62. https://doi.org/10.1007/s00256-012-1496-0.
21. DePalma A. Surgery of the shoulder. 2nd ed. Philadelphia: JB Lippincott; 1973. p. 206–35.
22. Tena-Arregui J, Barrio-Asensio C, Puerta-Fonolla J, Murillo-Gonzalez J. Arthroscopic study of the shoulder joint in fetuses. Arthroscopy. 2005;21(9):1114–9.

Rotator Cuff

2

Eva Llopis, Alexeys Perez, and Luis Cerezal

Learning Objectives
- Review new anatomical concepts of the rotator cuff.
- Review characteristics of the anterior rotator cuff, subscapularis and posterior rotator cuff, and supraspinatus and infraspinatus for partial- and full-thickness and massive tears.
- Describe the more important differential diagnosis when facing a MR request for shoulder pain.
- Learn how to do standardized reports and what information should be included in a report for decision-making.

Key Points
- Knowledge of anatomy and biomechanics of rotator cuff tears is essential for understanding tear patterns.
- Rotator cuff should be divided into anterior and posterior tendon injuries.
- Reports should include location, size, retraction, pattern, and fatty atrophy.

2.1 Anatomy

The shoulder is the most flexible and movable synovial joint allowing a huge ROM.

Its anatomy allows abduction, adduction, flexion, extension, and medial and lateral rotation but sacrifices stability.

E. Llopis (✉)
Hospital de la Ribera, Hospital IMSKE, Valencia, Spain

A. Perez
CST, Consorsi Sanitari de Terrassa, Terrassa, Spain

L. Cerezal
DMC, Diagnostico mÉdico Cantabria, Santander, Spain

Rotator cuff tendons and muscles are the dynamic stabilizers of the shoulder helping the bone discrepancy between the glenoid and the humeral head to avoid shoulder dislocation. The origin of the rotator cuff is the scapula, and they insert into the humeral head forming parallel structures (Fig. 2.1). Although the rotator cuff is separate at the origin, the rotator cuff is organized in a five-layer structure where they approach each other near the insertion. This layered structure explains the appearance of delaminating tears. In the lower level, there are some perpendicular lineal fibers that represent an extension of the coracohumeral ligament and extend from the rotator interval through the supraspinatus and the infraspinatus. It is called the rotator cable and has biomechanical implications in stress shielding, acting like a suspension bridge. It can be depicted on US and MR, especially in

Fig. 2.1 Anatomy of the shoulder, sagittal PD FSE fat sat WI, 1 subscapularis; 2 long head of the biceps tendon; 3 supraspinatus; 4 infraspinatus; 5 teres minus; 6 coracoid process; 7 acromioclavicular joint

Fig. 2.2 Anatomy of the shoulder, sagittal PD FSE fat sat WI, rotator cable is shown as an extension of the coracohumeral ligament crossing the underlying fibers of the supraspinatus and infraspinatus

Fig. 2.3 Coronal PD fat sat WI, demonstrates high signal intensity within the insertion of the supraspinatus without disruption

ABER position where the fibers of the supraspinatus relax [1–7] (Fig. 2.2).

The posterior rotator cuff tendons include the supraspinatus and infraspinatus that have a bursal and an articular site. The teres minus is rarely injured, and its function on the biomechanics of the shoulder is still to be determined. The supraspinatus inserts onto the anterior part of the greater tuberosity. It is important to realize that it has some anterior extensions to the lesser tuberosity reinforcing the rotator interval and merging with the subscapularis. The infraspinatus origins in the infraspinatus fossa at the inferior part of the scapula and inserts into the greater trochanter with a trapezoidal shape appearance. It has a wide insertion covering part of the supraspinatus insertion [8, 9].

The subscapularis has the largest tendon, with many fascicles. Its superior fascicles have a tendinous insertion, many of which insert into the lesser tuberosity, while some cross toward the greater tuberosity, whereas its inferior fascicles have a muscular insertion onto the humerus. Its function is anterior stabilization of the shoulder and of the long head of the biceps tendon [10].

2.2 Posterior Rotator Cuff, Supraspinatus and Infraspinatus

1. Tendinopathy.

Secondary to repetitive contact of the tendons with movements between the acromioclavicular arch and the

humeral head and between the joint capsule and the glenoid rim, the tendons experience structural changes. These changes represent histologically a continuum model of different progressive changes that start in reactive tendinopathy and continue into tendon disrepair and degenerative tendinopathy and end in tendon rupture. Initially those changes are reversible but shift to degeneration and rupture when the capacity of the tissue to repair is not enough. Our role would be to be sensitive enough to depict changes that are reversible. Initially the reaction of the tendon to load, friction, and activity results in small changes with disorganized extracellular matrix and subtle inflammatory reaction around the tendon that can be seen on imaging as peritendinitis and focal thickness of the tendon on high-resolution MR or US. In an attempt to heal matrix breakdown with collagen, separation and proliferation of abnormal tenocytes and increase of vascularization occur, which on imaging can be seen as low echogenicity areas on US and focal areas of high signal intensity on fluid-sensitive MRI. Progressively histological changes evolve to cellular and matrix changes with mucoid degeneration, chondral metaplasia, and amyloid deposition together with reparative changes and inflammation such as an increase of fibroblastic cells and neovascularization. These changes represent degenerative tendinopathy, and they are precursors of tendon tears. On imaging an increase in tendon thickness and changes of intrasubstance echogenicity on US and signal intensity on MR can be depicted [11, 12] (Fig. 2.3).

2. Partial Tears.

The incapacity to heal and restore the native structure of the tendon leads to partial tear with scar formation with disorganized tissue that decreases mechanical properties. On imaging this is seen as focal areas of fluid echogenicity or high signal intensity on fluid-sensitive sequences, particularly PD fat saturation or T2 fat saturation sequences. They can be divided depending on the location, in articular, intrasubstance, or bursal partial tears (Fig. 2.4). Tears that are bigger than 50% have higher probability to progression to a full-thickness tear than those that are smaller than 50% of the thickness. Tears that are smaller than 50% are usually treated conservatively; surgical treatment is only recommended when conservative measures fail [13, 14].

Bursal-side tears are associated with subacromial and coracohumeral arch degenerative changes. The presence of fluid in the subacromial bursa facilitates the radiological diagnosis. These tears are occult to arthroscopy. Because of their adequate blood supply, they have a tendency to heal [13, 14].

Partial articular surface tears are the more frequent; they have been named as PASTA (partial articular supraspinatus tendon avulsion) lesions or rim rent tears. They don't heal properly and have a tendency to progress to full-thickness tears. Insertional tears occur in younger population and are related to traumatic events, whereas more proximal tears in the critical zone are associated with degenerative changes. Partial tears have a vertical component that should be measured in mm and is easy to be seen in conventional projections; its horizontal component is more difficult, and ABER position helps to depict its full extension. Partial articular surface tears occurring within the 2nd and 3rd layer may extend horizontally and might involve the supraspinatus and the infraspinatus in a delaminating type of injury without retraction [15–18] (Fig. 2.5).

Fig. 2.4 Two different cases on coronal PD fat sat FSE WI. (**a**) Articular side partial (arrows) rupture of more than 50% of tendon thickness; (**b**) bursal side partial rupture (arrows) affecting less than 50% of the tendon thickness

Fig. 2.5 Coronal PD fat sat WI, showing delaminating partial rupture with fluid between the different layers without disruption of its articular side insertion

Intrasubstance tears occur within the tendon and usually are associated with intense pain.

3. Full-Thickness Tears.

Full-thickness tears are those tears that extend from the articular side to the bursal side; they don't have to involve the entire tendon in other planes. It is important to describe the size of the tear, the number of tendons affected, the retraction, and the shape of the tear. The size of the tear is categorized as smaller than 2 cm, between 3 and 4 cm, or greater than 5 cm. The retraction is defined as no retraction, small retraction if it doesn't reach the level of the acromioclavicular joint, and large when it passes the AC joint. Arthroscopically the pattern of the tear is described as crescent, U-, or L-shaped [15–18] (Figs. 2.6 and 2.7).

Fat atrophy has implication on the therapeutic approach and patient prognosis. If the atrophy is greater than 50% of the muscle, there is a high rate of recurrence after
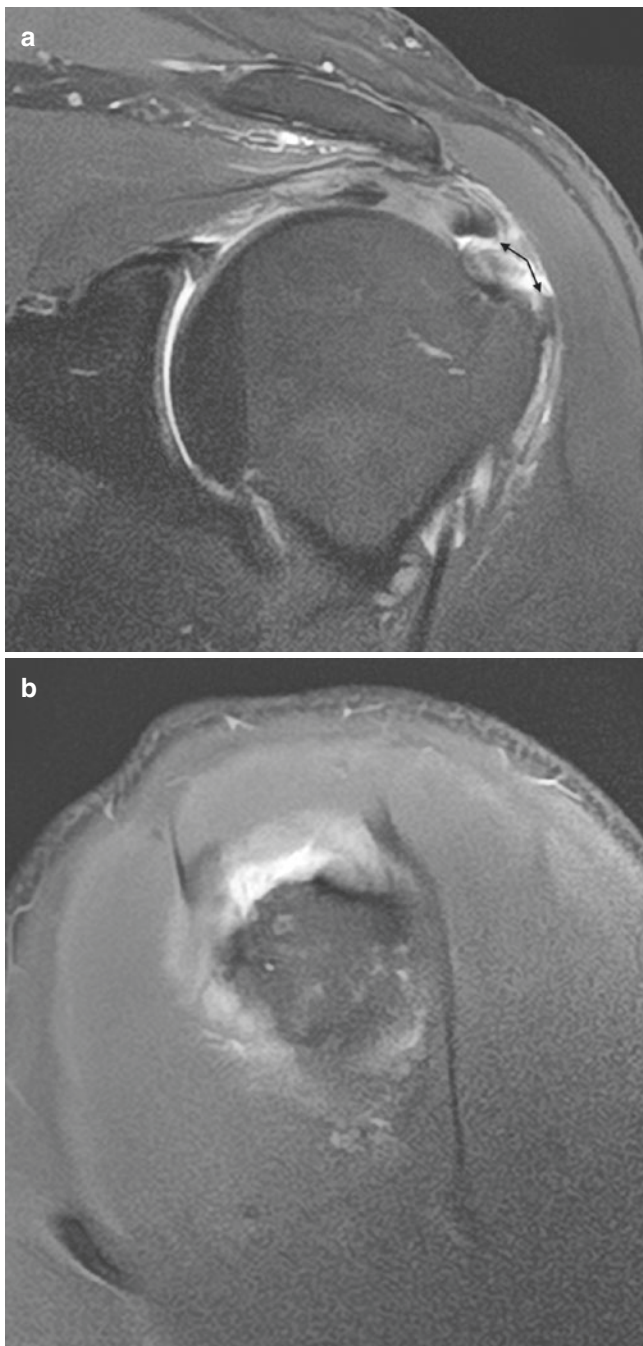
Fig. 2.6 Full-thickness tear of the supraspinatus, coronal (**a**) and sagittal (**b**) PD fat sat WI
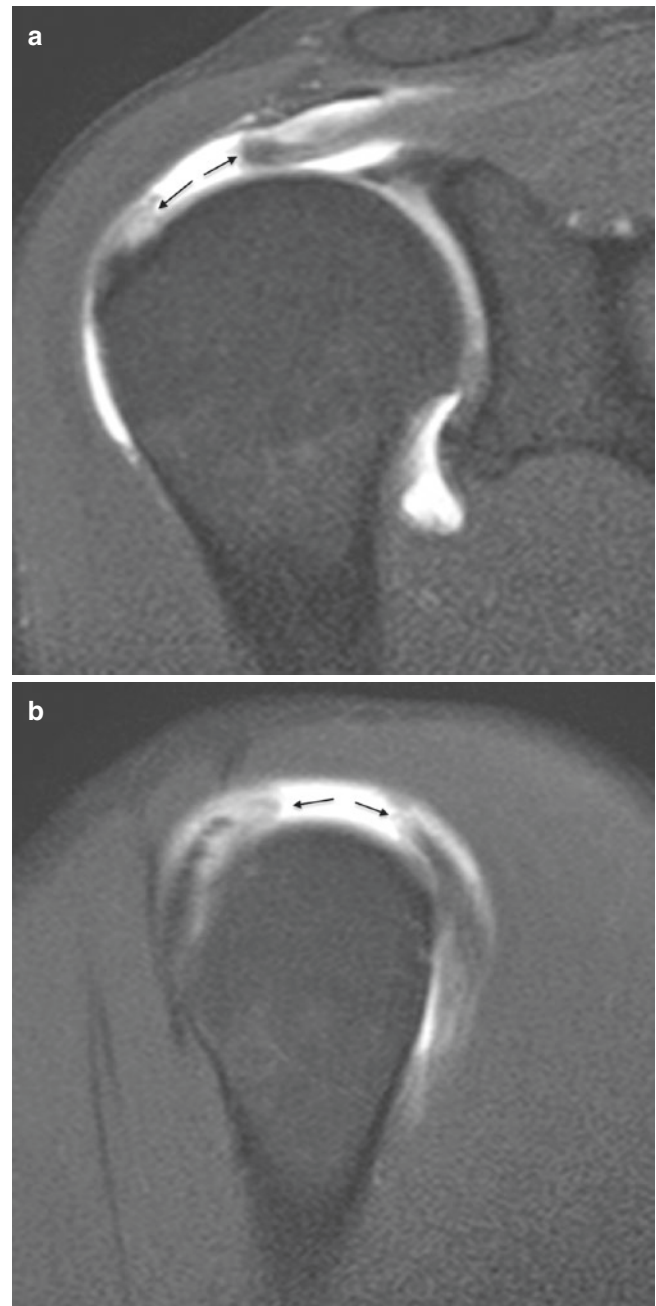
Fig. 2.7 MRI arthrography of the shoulder coronal (**a**) and sagittal (**b**) T1 FSE fat sat WI demonstrating full-thickness complete rupture of the supraspinatus

Table 2.1 Lafosse classification

Grade I	Partial lesion of the superior one third
Grade II	Complete lesion of the superior one third
Grade III	Complete lesion of the superior two thirds
Grade IV	Complete lesion with head centered and fatty degeneration < stage 3
Grade V	Complete lesion with eccentric head and fatty degeneration > stage 3

Fig. 2.9 Coronal PD FSE WI of a massive rupture of the rotator cuff showing superior migration of the humeral head (black arrow), remodelation of the acromioclavicular arch (black arrow head), glehohumeral degenerative changes, and fatty atrophy of the supraspinatus (*)

Glenohumeral arthrosis can be seen as loss of the joint space and presence of inferior humeral osteophytes. In the last stages and on imaging, we can depict subchondral cyst formation, secondary areas of avascular necrosis and bone marrow edema, and ultimately collapse of the humeral head [13, 21–23].

For treatment purposes it is important to describe the morphology and bone stock of the glenoid, the deltoid, and the alignment [21–23] (Fig. 2.9).

Fig. 2.8 Sagittal FSE T1WI showing moderate atrophy of the supraspinatus [1] and severe atrophy of the infraspinatus

repair. There have been different classifications for fat atrophy. The Goutallier system is based on the percentage of fat within the muscle on CT axial planes; Zanetti and Thomazeau analyzed the supraspinatus fossa on T1-weighted sagittal MR images, and recently ISAKOS defined four different grades [13, 19–21] (Table 2.1) (Fig. 2.8).

4. Massive Rotator Cuff Tears, Rotator Cuff Arthropathy.

A massive rotator cuff tear is characterized by the involvement of two or more tendons or a retraction greater than 5 cm. As the rotator cuff centralizes the humeral head into the glenoid and serves as the fulcrum when the deltoid abducts and elevates the arm, its deficiency changes the biomechanics. There is progressive migration of the humeral head superiorly causing adaptive changes on the coracoacromial arch with acetabulization.

2.3 Subscapularis Tendon Tears

Subscapularis tendon tears are more frequent than previously thought. They have been found in cadavers in more than 30%. They are underestimated in all imaging techniques. The sagittal plane is the best for its MR evaluation. On MR arthrography we strongly recommend external forced rotation for better depiction of partial articular side tears. Most missed are partial- and full-thickness tears of the posterior fibers of the subscapularis. They are closely related to the rotator interval and the anterior crossing fibers of the supraspinatus. Lafosse classification is the most accepted one; it is divided into five grades (Table 2.2). Subscapularis tears are associated with anterosuperior impingement. Anterosuperior impingement was described by Gerber arthroscopically revealing impingement of the undersurface of the subscapularis tendon against the anterosuperior glenoid rim in the position of flexion and internal rotation. It is less common than posterosuperior impingement. There are

Table 2.2 Fatty atrophy

Grade 0	Normal muscle
Grade 1	Some fatty streaks
Grade 2	Less than 50% of fatty infiltration
Grade 3	50% equal fat to muscle
Grade 4	More than 50% fatty infiltration

ISAKOS adopted Goutallier and Fuchs classification of the fatty atrophy valid for CT and MRI
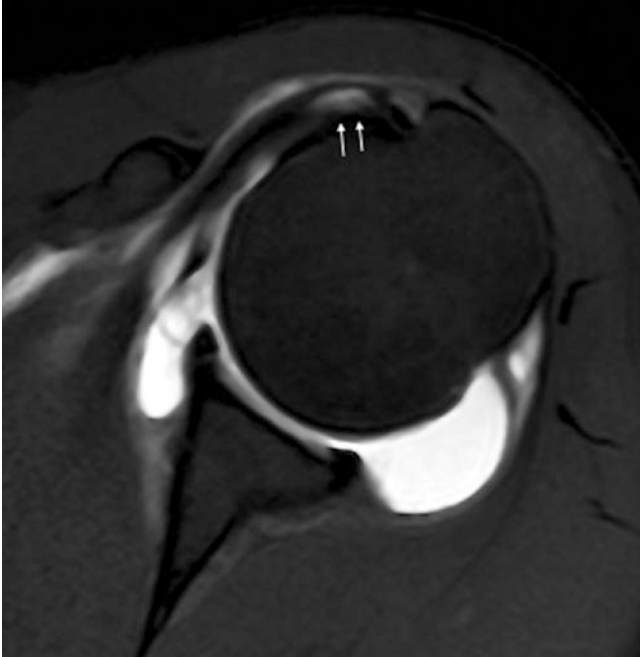
Fig. 2.10 Axial arthro-MRI FSE T1 fat sat WI demonstrates partial articular side tear of the subscapularis

associated rotator interval lesions, long head of the biceps tendon lesions and dislocation, and SLAP lesions [24–26] (Fig. 2.10).

2.4 Differential Diagnosis

It is important to know some entities that clinically can mimic rotator cuff lesions.

1. Calcified Tendinopathy.

   Crystal deposition, especially CPPD deposits on the tendon, causes inflammation and is an important cause of shoulder pain in young adults. Its cause is still unknown although microtrauma, ischemia, and metaplasia have been proposed as causes. It is usually a self-limited disease with spontaneous resolution in a high percentage of cases. Different clinical stages have been described: a precalcification phase which is clinically silent; the calcification phase in which crystal deposition occurs, subsequently the start of a resorptive phase with inflammatory reaction that causes severe pain; and the end a post-calcification phase (Fig. 2.11). The deposits of CPPD might migrate to the subacromial bursa causing bursitis or less frequent into the bone at the lesser or greater tuberosity. It is important to know this potential involvement of the numeral head to avoid confusion with a tumor. MRI shows a sclerotic or lytic lesion surrounded by peripheral bone marrow edema. The key for the diagnosis is the association with calcifications within the proximal tendon [27, 28] (Fig. 2.12).
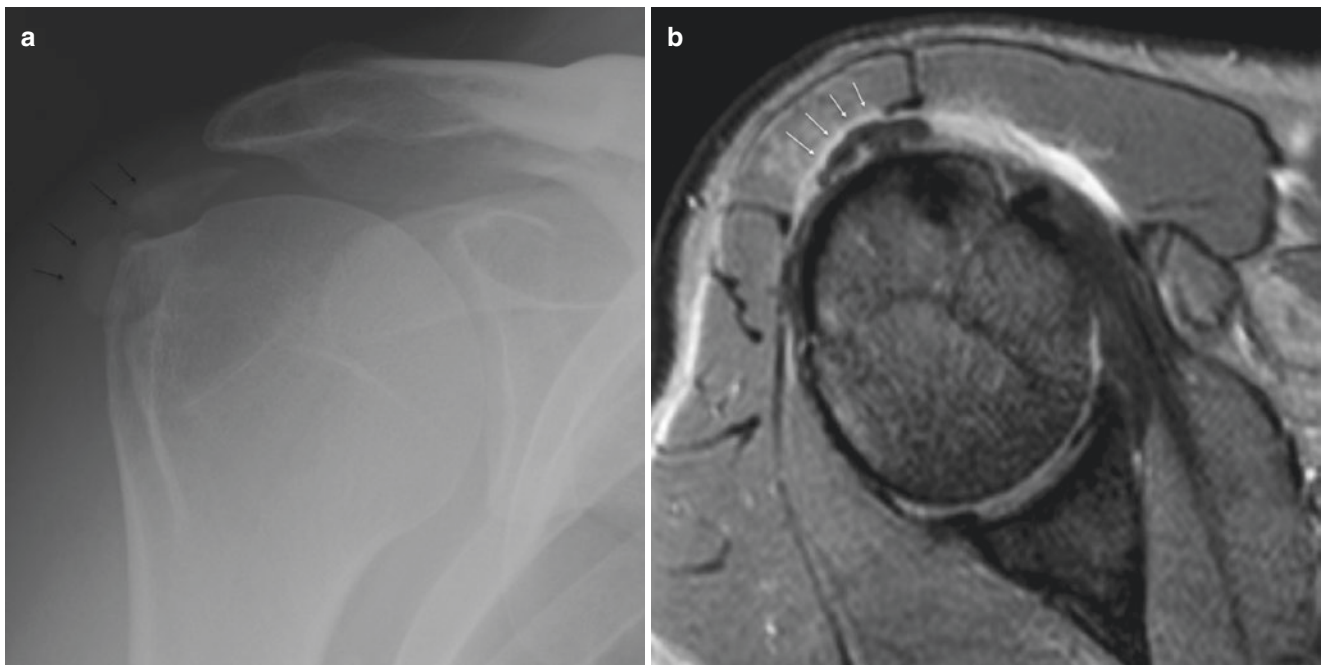
Fig. 2.11 Rotator cuff hydroxyapatite deposition disease. (**a**) AP radiograph shows periarticular calcifications; (**b**) axial GET2; (**c**) coronal PD FSE fat sat WI shows coarse ovoid calcification in the subacromial subdeltoid bursa surrounded by fluid indicating inflammation
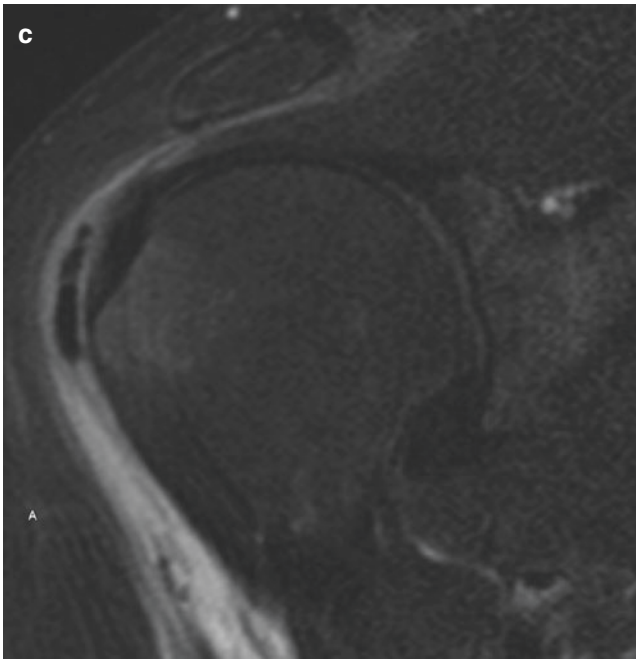
Fig. 2.11 (continued)

2. Adhesive Capsulitis.

Adhesive capsulitis is a clinical diagnosis characterized by pain and marked decrease of the range of motion, especially to external rotation. MRI findings are usually not specific but can correlate with the clinical stages. In the acute inflammatory phase, MRI can show axillary capsular thickening and capsular edema and rotator interval synovitis. Progressively hypervascularization and fibrosis occur, which may be reflected on MRI images by thickening of the coracohumeral ligament, subcoracoid fibrosis, and capsular thickening. On MR arthrography classic findings are low volume injection, often less than 8 ml, and thickening of the structures [29, 30] (Fig. 2.13).

3. Nerve Denervation Syndromes.

There are two main nerve denervation syndromes around the shoulder secondary to the suprascapular nerve and to the axillary nerve. Suprascapular neuropathy can be related to compression of an associated paralabral cyst in a superior labrum injury. When there is no compression, there are two main origins: a viral inflammation and or overuse in athletes with overhead activities. On imaging in the acute phase, supraspinatus and infraspinatus muscle edema is seen, whereas in chronic phases fatty atrophy and volume loss of the muscle are shown [31] (Fig. 2.14).

The causes of axillary nerve denervation can be secondary to injury of the axillary nerve in anterior inferior shoulder dislocation especially in patients older than 40 years of age; can be secondary to compression due to a lesion in the quadrilateral space; or can be idiopathic. The role of MRI is to rule out compression causes and
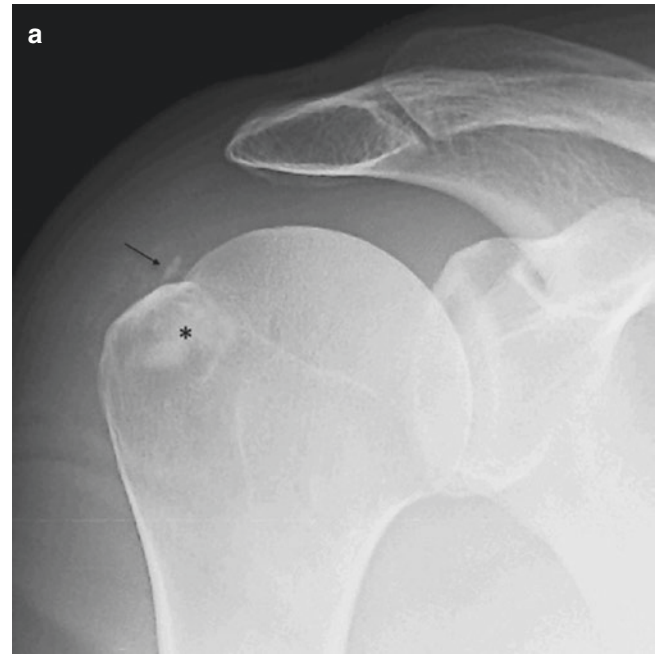
Fig. 2.12 Intrabone migration of hydroxyapatite deposition, (**a**) AP radiographs demonstrate calcifications in the greater tuberosity surrounded by a radiolucency area (*). Calcifications within the rotator cuff space help for the diagnosis of hydroxyapatite deposition disease. (**b**) Coronal FSE PD fat sat WI shows the same features of calcifications within the greater tuberosity (*) surrounded by a hyperintense halo (arrow)

associated injuries in shoulder dislocation. MRI will demonstrate secondary to the lesion of the axillary nerve edema of the teres minus or fatty atrophy on chronic stages [31] (Fig. 2.15).
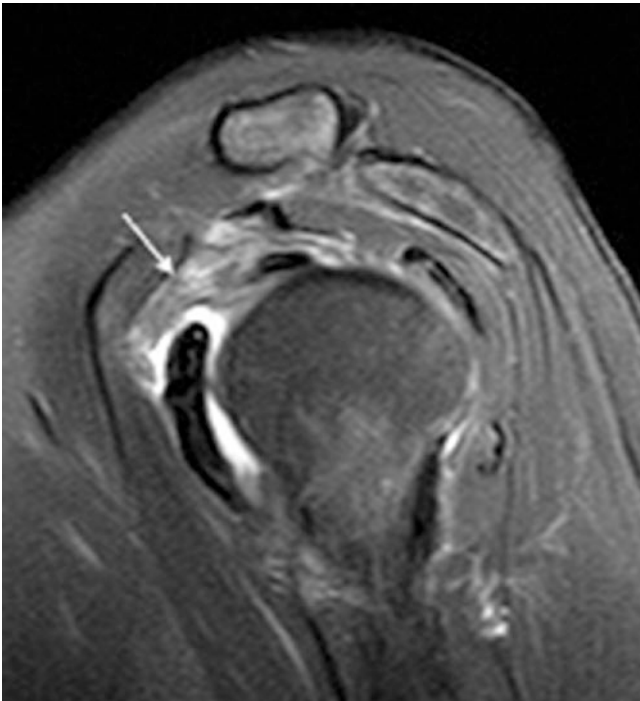
Fig. 2.13 Patient with decreased external rotation, sagittal FSE PD fat sat WI shows thickening of the coracohumeral ligament with soft tissue edema

4. Isolated Greater Tuberosity Fractures.

   Isolated fractures of the greater tuberosity can be secondary to shoulder direct or indirect trauma or in older population to minor trauma in osteoporotic patients. When there is little or no displacement (<5 mm), they might be difficult to see on plain films especially if only one projection is seen. They can be seen on US as a discontinuity of cortical bone line and are easy to be diagnosed on MRI [32] (Fig. 2.16).

2.5 Conclusions

Our radiological report in rotator cuff injuries plays a critical role in the decision-making process for the surgeon and the patient outcome. Spend time recognizing the pattern. The report should be simple and standardized. The radiologist must be aware of the treatment implications of the different types of tear and understand the parameters used to evaluate rotator cuff tears on MRI.

Diagnosis of concomitant lesions and knowing the differential diagnosis are very important.
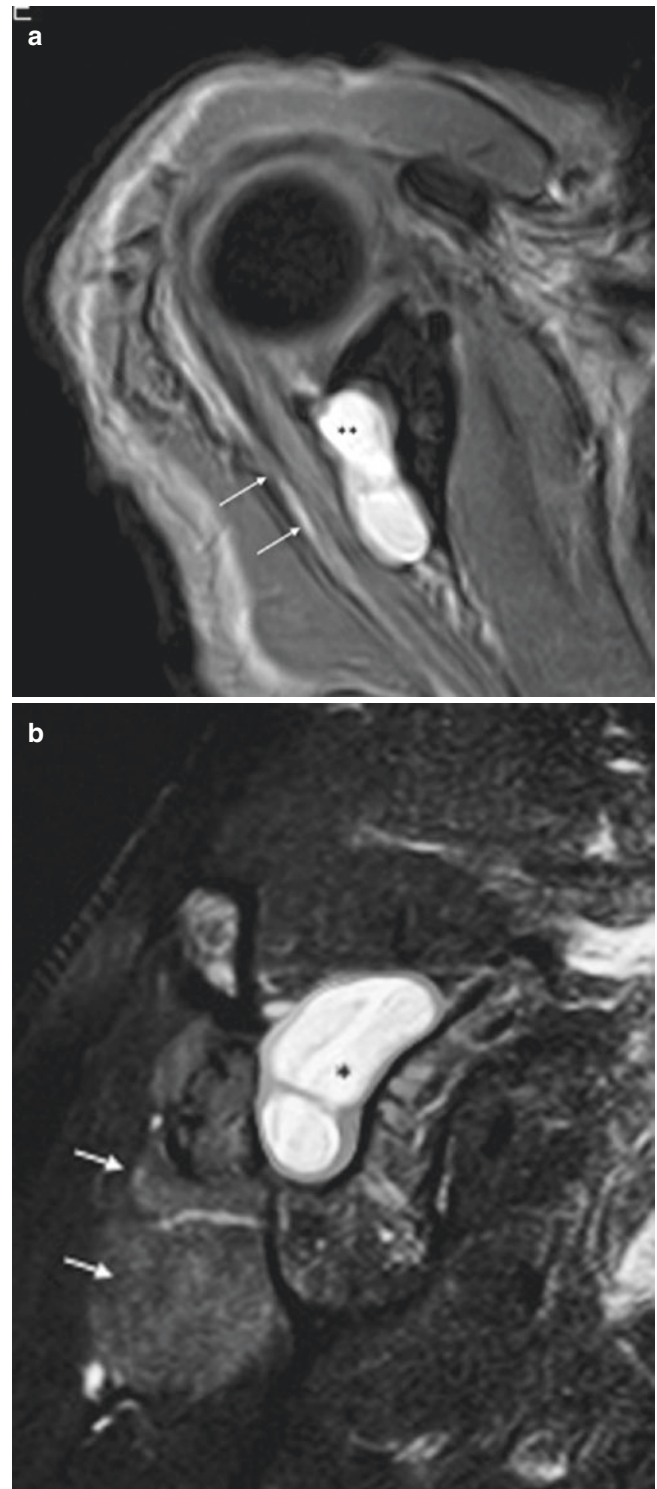
Fig. 2.14 (**a**) axial GE T2 WI and (**b**) sagittal FSE T2 WI of a paralabral cyst (*) in the supraglenoid notch causing entrapment of the suprascapularis nerve and secondary edema in the infraspinatus (arrow)
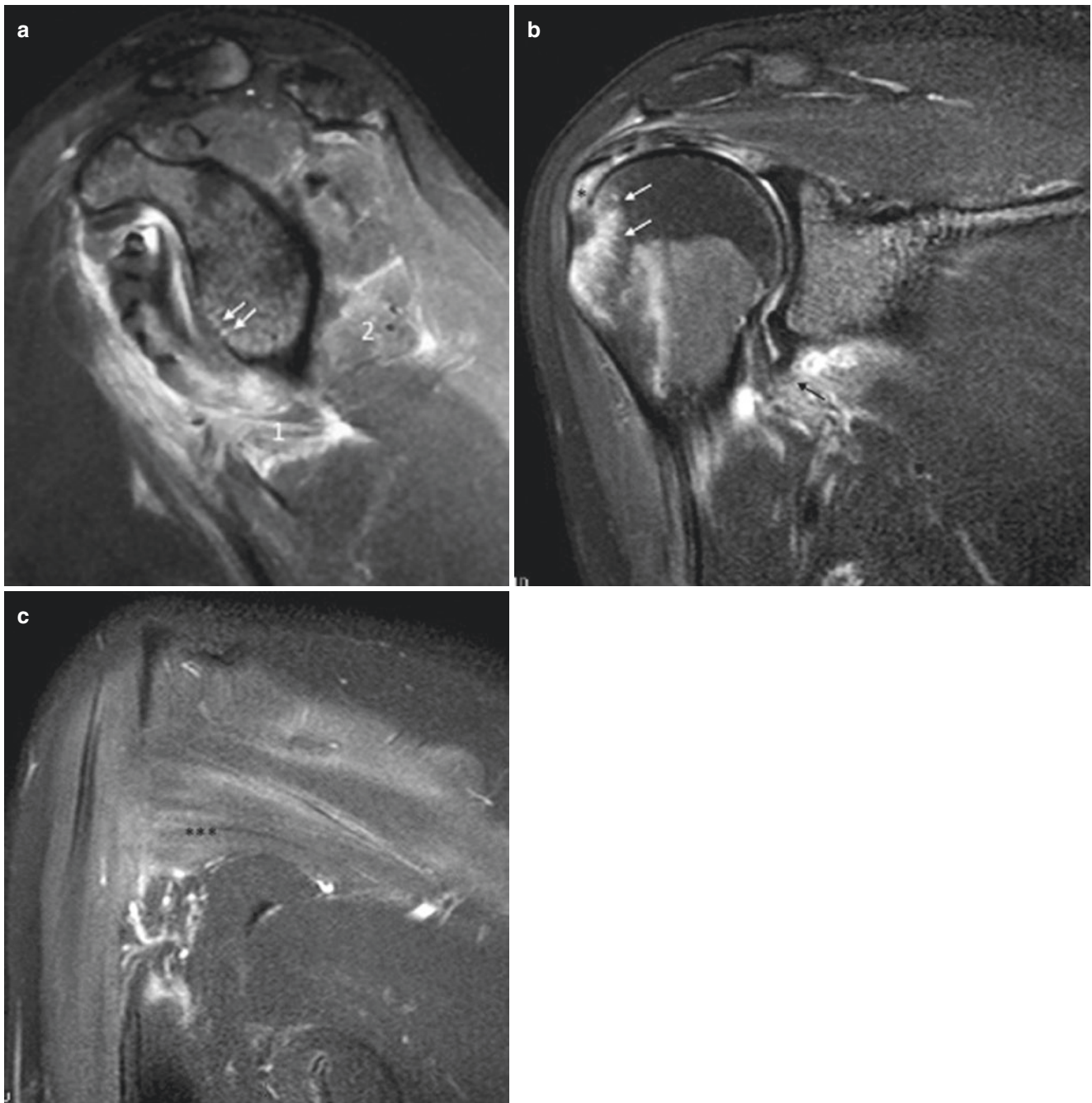
Fig. 2.15 A 48-year-old patient with anterior and inferior dislocation of the shoulder and associated complications like partial tear of the supraspinatus, greater tuberosity fracture, and axillary nerve injury with soft tissue edema of the teres minor. (**a**) Sagittal FSE PD fat sat WI shows anteroinferior glenoid-labral complex lesion (white arrow) soft tissue edema and effusion in the axillary recess [1] and edema in the teres minus [2]; (**b**) coronal FSE PD fat sat WI demonstrates small partial tear of the supraspinatus (*), non-displaced fracture of the greater tuberosity (white arrows), and soft tissue edema of the axillary recess (black arrow); (**c**) posterior plane on coronal FSE PD fat sat WI demonstrates edema of the teres minor secondary to axillary nerve lesion
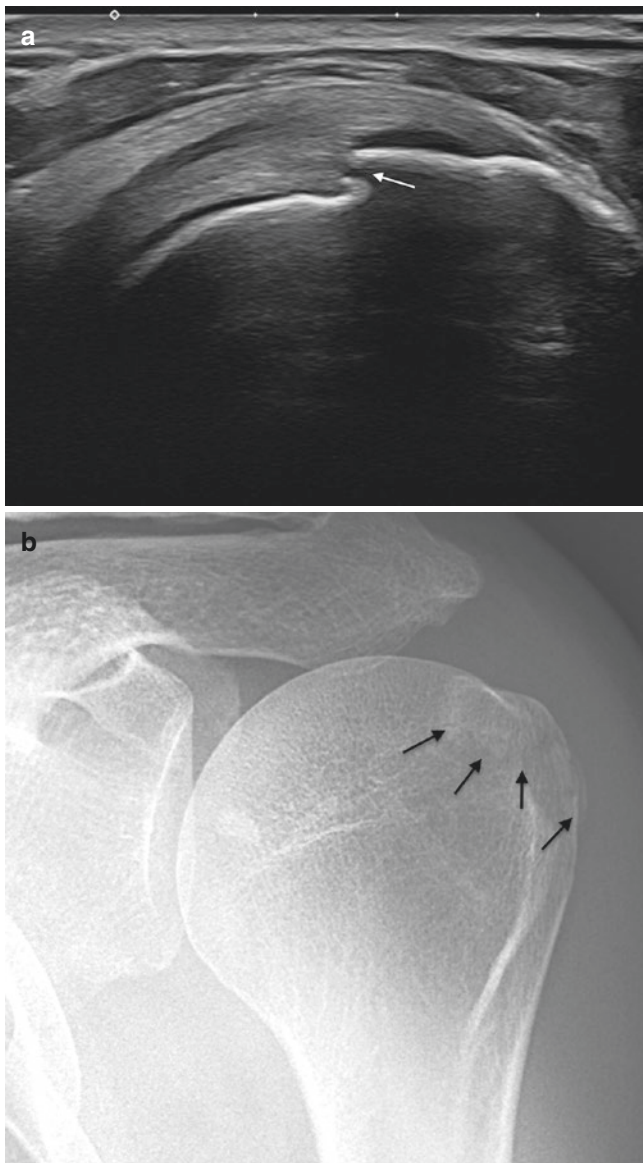
Fig. 2.16 A 45-year-old male with a request of US to rule out rotator cuff lesion after indirect trauma; (**a**) US of the shoulder shows discontinuity of the cortical bone of the greater tuberosity (arrow); (**b**) AP radiograph performed later demonstrates the small non-displaced fracture (arrows)

Key Points
- Anterior rotator cuff, subscapularis and posterior rotator cuff, and supraspinatus and infraspinatus are slightly different.
- Superior fibers of the subscapularis and anterior fibers of the supraspinatus weaved together are closely related to biceps tendon and rotator interval tears.
- New patterns of injuries such as delamination tears can be depicted with high-resolution MRI.
- Reports should include pattern, size, retraction, shape, and fatty atrophy.

Take Home Messages
- Reports of rotator cuff tears should follow a structured form including size of the lesion, retraction, shape, and atrophy.
- It is important to remember that despite the rotator cuff muscles origin are separate when they insert, they weave together being these areas the more difficult to depict on MRI.
- Differential diagnosis should include other causes of shoulder pain that might be clinically mimickers.

References

1. Clark JM, Harryman DT 2nd. Tendons, ligaments, and capsule of the rotator cuff. Gross and microscopic anatomy. J Bone Joint Surg Am. 1992;74(5):713–25.
2. De Franco MJ, Cole BJ. Current perspective on rotator cuff anatomy. J Arthroscop Rel Surg. 2009;25(3):305–20.
3. Llopis E, Montesinos P, Guedez MT, et al. Normal Shoulder MRI and MR arthrography: anatomy and technique. Semin Musculoskelet Radiol. 2015;19(3):212–30.
4. Lee SY, Lee JK. Horizontal component of partial-thickness tears of rotator cuff: imaging characteristics and comparison of ABER view with oblique coronal view at MR arthrography initial results. Radiology. 2002;224(2):470–6.
5. Burkhart SS, Esch JC, Jolson RS. The rotator crescent and rotator cable: an anatomic description of the shoulder's "suspension bridge". Arthroscopy. 1993;9(6):611–6.
6. Morag Y, Jamadar DA, Boon TA. Ultrasound of the rotator cable: prevalence and morphology in asymptomatic shoulders. Am J Roentgenol. 2012;198:W27–30.
7. Gyftopoulos S, Bencardino J, Nevsky G, et al. Rotator cable: MRI study of its appearance in the intact rotator cuff with anatomic and histologic orrelation. Am J Roentgenol. 2013;200(5):1101–005.
8. Moser TP, Cardinal E, Bureau NJ, et al. The aponeurotic expansion of the supraspinatus tendon: anatomy and prevalence in a series of 150 shoulder MRIs. Skelet Radiol. 2015;44:223–31.
9. Curtis AS, Burbank KM, Tierney JJ, et al. The insertional footprint of the rotator cuff: an anatomic study. Arthroscopy. 2006;22(6):609–11.
10. Morag Y, Jamadar DA, Miller B, et al. The subscapularis: anatomy, injury and imaging. Skelet Radiol. 2011;40(3):255–69.
11. Buck F, Grehn H, Hilbe M, et al. Magnetic resonance histologic correlation in rotator cuff tendons. J MRI. 2010;32:165–72.
12. Cook JL, Rio E, Purdam CR, et al. Revisiting the continuum model of tendon pathology: what is its merit in clinical practice and research. Br J Sports Med. 2016;0:1–7.
13. Imhoff AB, Savoie FH. Rotator cuff across the life span ISAKOS consensus book. Berlin, Heidelberg, New York: Springer; 2019.
14. Morag Y, Jacobson JA, Miller B, et al. MR imaging of rotator cuff injury: What the clinician need to know. Radiographics. 2006;26(4):1045–65.
15. Tuite MJ, Turnbull JR, Orwin JF. Anterior versus posterior, and rim-rent rotator cuff tears: prevalence and MR sensitivity. Skelet Radiol. 1998;27:237–43.
16. Fukuda H, Hamada K, Nakajima T, et al. Partial-thickness tears of the rotator cuff. A clinicopathological review based on 66 surgically verified cases. Int Orthop. 1996;20(4):257–65.
17. Cha SW, Lee CK, Sugaya H, et al. Retraction pattern of delaminated rotator cuff tears: dual-layer rotator cuff repair. J Orthop Surg Res. 2016;11:75–85.

18. Choo HJ, sj L, Kim JH, et al. Delaminated tears of the rotator cuff: prevalence, characteristics, and diagnostic accuracy using indirect MR arthrography. Am J Roentgenol. 2015;204:360–6.

19. Davidson J, Burkhart SS. The geometric classification of rotator cuff tears: a system linking tear pattern to treatment and prognosis. Arthroscopy. 2010;26(3):417–24.

20. Goutallier D, Postel JM, Gleyze P, et al. Influence of cuff muscle fatty degeneration on anatomic and functional outcomes after simple suture of full thickness tears. J Shoulder Elb Surg. 2003;12(6):550–4.

21. Zanetti M, Gerber C, Hodler J. Quantitative assessment of the muscles of the rotator cuff with MRI. Investig Radiol. 1998;33(3):163–70.

22. Di Benedetto P, Beltrame A, Cicuto C, et al. Rotator cuff tears reparability index based on preoperative MRI: our experience. Acta Biomed. 2019;90:36–46.

23. Samim M, Walsh P, Gyftopoulos S, et al. Postoperative MRI of massive rotator cuff tears. Am J Roentgenol. 2018;211(1):146–54.

24. Pfirrmann CW, Zanetti M, Weishaupt D, et al. Subscapularis tendon tears: detection and grading at MR arthrography. Radiology. 1999;213(3):709–14.

25. Lafosse L, Jost B, Reiland Y, et al. Structural integrity and clinical outcomes after arthroscopic repair of isolated subscapularis tears. J Bone Jt Surg A. 2007;89(6):1184–93.

26. Habermeyer P, Krieter C, Tang KL, et al. A new arthroscopic classification of articular-sided supraspinatus footprint lesions: a prospective comparison with Snyder's and Ellman's classification. J Shoulder Elb Surg. 2008;17(6):909–13.

27. Siegal D, Wu JS, Newman JS, et al. Calcific tendinitis: a pictorial review. Can Assoc Radiol J. 2009;60(5):263–72.

28. Speed CA, Hazleman BL. Calcific tendinitis of the shoulder. N Engl J Med. 1999;340(20):1582–4.

29. Park S, Lee DH, Yoon SH, et al. Evaluation of adhesive capsulitis of the shoulder with fat-suppressed T2-weighted MRI: association between clinical features and MRI finding. Am J Roentgenol. 2016;207:135–41.

30. Lee SY, Park J, Song SW. Correlation of MR arthrographic findings and range of shoulder motion in patients with frozen shoulder. Am J Roentgenol. 2012;198:173–9.

31. Yanny S, Toms AP. MR patterns of denervation around the shoulder. Am J Roentgenol. 2010;195:W157–63.

32. Kim E, Shin HK, Kim CH. Characteristics of an isolated greater tuberosity fracture of the humerus. J Orthop Sci. 2005;10(5):441–4.

Elbow Imaging with an Emphasis on MRI

3

Mark W. Anderson and Christine B. Chung

Learning Objectives
- To review challenges in MR imaging of the elbow and identify strategies to optimize imaging protocols.
- To review osseous and soft tissue anatomy of the elbow.
- To demonstrate the MR imaging appearance of commonly encountered pathology of the elbow.

3.1 Introduction

The elbow is a complex joint made up of three separate articulations within a common capsule. The proximal ulna articulates with the trochlea and functions as a hinge joint, while the proximal radioulnar joint provides for rotational movement of the forearm. The radiocapitellar joint allows for both hinge and rotational movements. Together, these allow for flexion and extension of the arm and, in conjunction with the distal radioulnar joint at the wrist, pronation and supination as well.

This article will discuss the normal anatomy of the elbow and the most common types of elbow pathology as well as their appearances on various imaging studies, with an emphasis on MR imaging.

M. W. Anderson (✉)
Department of Radiology, University of Virginia, Charlottesville, VA, USA
e-mail: mwa3a@virginia.edu

C. B. Chung
Department of Radiology, University of California, San Diego, La Jolla, CA, USA
e-mail: cbchung@ucsd.edu

3.2 MR Technique

Challenges associated with elbow MRI include the complex anatomy of this relatively small joint, as well as technical considerations related to MR acquisition. If the patient is scanned in a supine position with arms extended along the sides, this may result in some degradation of image quality given the off-center position within the magnet. Images can be acquired with the patient prone and the arm extended over the head (superman position), placing the region of interest closer to the magnet isocenter; however patient discomfort can lead to increased motion artifact.

MR imaging studies of the elbow are commonly performed at field strengths of 1.5 T or higher. Imaging at 3.0 T is increasingly common, with ultra-high field systems (7.0 T) deployed in the research setting [1]. Higher field strength and dedicated coils for elbow MR provide much needed improvements in signal-to-noise ratio (SNR), resulting in improved image resolution. Surface coils are essential for the acquisition of optimal MR images.

Imaging protocols should cover the joint in multiple planes and with multiple different tissue contrasts [2]. The coronal oblique imaging plane is oriented parallel to the humeral epicondylar axis as seen in the axial plane, and sagittal sequences are oriented perpendicular to that axis. Axial images should always extend distal to the radial tuberosity.

Suggested protocol parameters for elbow MR imaging include a field of view (FOV) of 12–15 cm. Slice thickness from 2 to 3 mm is generally accepted with a matrix of 256×256 to 512×512. Conventional MR protocols include some combination of non-fat-suppressed T1- or PD-weighted, fat-suppressed PD- or T2-weighted, or short tau inversion recovery (STIR) sequences.

Direct MR arthrography is an alternative to conventional MR imaging that provides joint distention for better delineation and visualization of structures. Its primary application in clinical practice is for identification and characterization of intraarticular bodies and osteochondral lesions [3]. The optimum

gadolinium concentration for maximal signal-to-noise ratios at 1.5–3.0 T ranges from 0.7 to 3.4 mmol/L [4]. The capacity of the joint for purposes of MR arthrography is 5–10 mL.

Although fat-suppressed T1-, PD-, and T2-weighted sequences are typically used, non-fat-suppressed sequences should be included if visualization of fat is desired.

3.3 Bones and Cartilage

3.3.1 Normal Anatomy

The humerus, ulna, and radius all contribute to the elbow joint [5]. Two epicondyles project from the distal humerus. The larger medial epicondyle is the site of attachment of the common flexor/pronator tendon as well as the ulnar collateral ligament. The lateral epicondyle gives rise to the common extensor/supinator tendon and the extensor carpi ulnaris tendon. The radial collateral and lateral ulnar collateral ligaments also arise from the lateral epicondyle. The distal articular surface of the humerus is divided into the trough-like trochlea that articulates with the proximal ulna and the rounded capitellum that articulates with the radial head. Dorsally, the deep, olecranon fossa of the humerus accepts the tip of the olecranon when the elbow is extended, while the smaller coronoid fossa along the ventral aspect of the humerus receives the coronoid process in flexion. Prominent extrasynovial fat pads are present within both fossae.

The trochlear notch of the ulna forms a hinge joint with the trochlea. The radial notch of the ulna lies along the lateral aspect of the coronoid process and articulates with the radial head to form the proximal radioulnar joint. The slightly concave radial head articulates with the capitellum. The radial tuberosity along the medial aspect of the proximal radius provides the attachment site for the distal biceps tendon.

The articular cartilage of the elbow is so thin that it's often difficult to evaluate with MR imaging. It's also important to recognize that the articular cartilage of the capitellum is found along its anterior convexity only, and not along its irregular, posterior non-articular aspect.

3.3.2 Bones and Cartilage: Potential Pitfalls

With the elbow extended, the border between the articular cartilage of the capitellum and its irregular non-articular posterior surface may mimic an osteochondral lesion on coronal MR images. This pitfall can be easily avoided by cross-referencing the level of the coronal scan with a sagittal image (Fig. 3.1). Another osseous variant is a transverse bony ridge in the mid-trochlear notch that may mimic a loose body or osteophyte on sagittal images (Fig. 3.2).
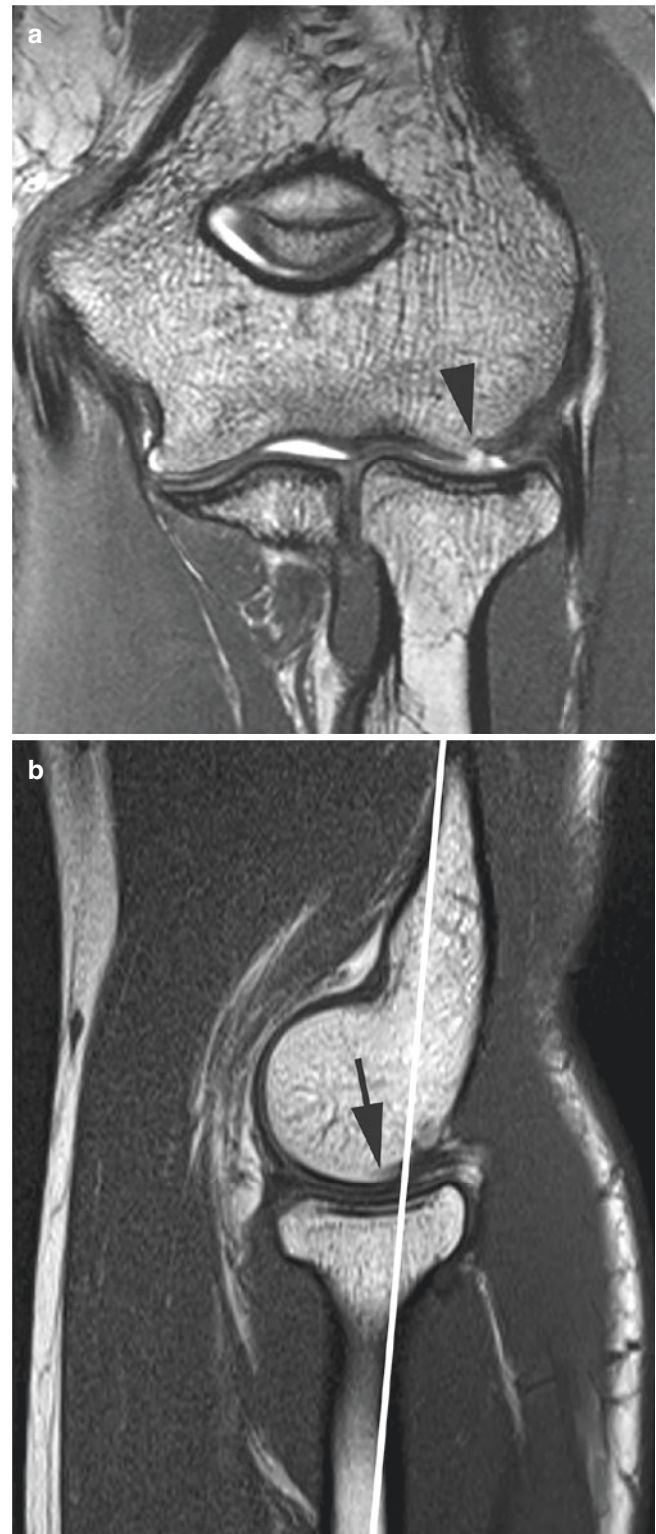
Fig. 3.1 Pseudodefect of the capitellum. (**a**) Coronal gradient echo T2*-weighted image shows an apparent osteochondral lesion along the surface of the capitellum (arrowhead). (**b**) Correlative sagittal T1-weighted image reveals that the coronal slice (white line) lies just posterior margin of the articular surface (arrow)

Fig. 3.2 Transverse trochlear ridge. Sagittal T1-weighted image demonstrates the normal transverse trochlear ridge (arrow) of the ulna, the anatomic landmark between the olecranon and coronoid

3.3.3 Bones: Pathology

3.3.3.1 Acute Trauma

In a patient presenting with elbow pain after an acute injury, often the only radiographic finding is elevation of the posterior and/or anterior fat pads indicating an effusion. Several studies have demonstrated a high incidence of associated osseous contusions or fractures in these patients which are well demonstrated with MR imaging [6]. A bone contusion is most easily identified by its edema-like signal intensity on fat-saturated T2-weighted images. In the case of a fracture, a linear component may be seen within the edema on T2W images or may be better demonstrated as a low signal intensity line on a T1-weighted image (Fig. 3.3). In the setting of a radiographically apparent fracture, MR imaging is able to assess any associated ligament or cartilage abnormalities as well. Contusions or fractures involving the radial head and posterior capitellum are commonly seen after a posterior dislocation and should prompt close inspection of the collateral ligaments which are often concurrently disrupted [7].

3.3.3.2 Stress Fractures

Stress fractures occur much less commonly in the upper than the lower extremities. In the elbow stress fractures involve the olecranon in 98% of cases [8]. The mechanism of injury is thought to be related to chronic traction of the triceps
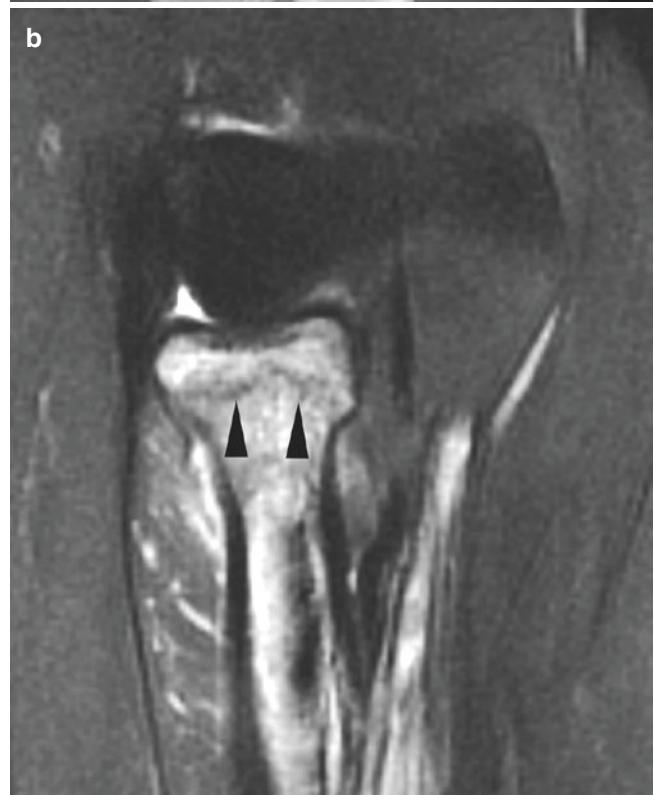
Fig. 3.3 Radiographically occult fracture. (**a**) Oblique radiograph of the elbow shows no evidence of fracture. (**b**) Coronal fat-saturated T2-weighted image reveals a non-displaced fracture of the radial head (arrowheads) with surrounding marrow edema. Used by permission of Springer Nature
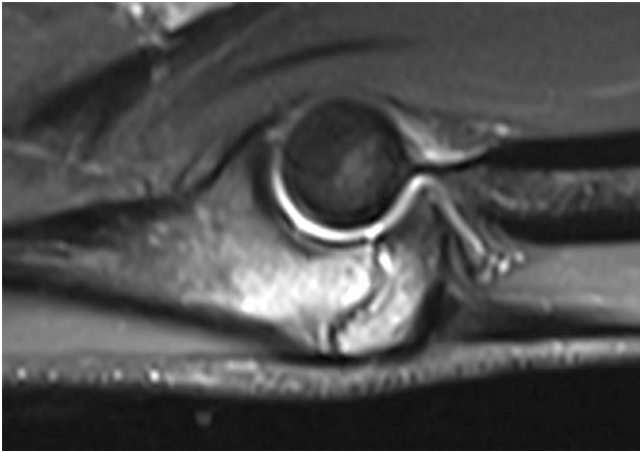
Fig. 3.4 Stress fracture. A 17-year-old male with 6-month history of posterior elbow pain exacerbated by weight lifting. Sagittal STIR image demonstrates a non-displaced fracture and prominent marrow edema in the olecranon. The olecranon physis was found to be fused in the opposite elbow on radiographs

tendon or forces along the posteromedial joint that occur in the valgus overload syndrome (see below). MR imaging findings are those of stress injuries anywhere in the body with edema-like abnormal signal intensity in the marrow indicating a stress reaction with or without a fracture line (Fig. 3.4).

3.3.3.3 Osteochondral Lesions

Osteochondral lesions of the elbow are thought to result from repetitive impaction or shear forces that damage the articular cartilage and underlying subchondral bone. Formerly known as osteochondritis dissecans (OCD), these injuries occur most often in adolescent throwing athletes or gymnasts.

The repetitive valgus forces that occur at the elbow during the throwing motion result in tensile forces across the medial joint that may produce laxity or tearing of the ulnar collateral ligament and/or the common flexor tendon. As these medial stabilizers fail, impaction and shear forces occur across the lateral aspect of the joint resulting in injury to the cartilage and subchondral bone of the capitellum and, less commonly, radial head [9]. These osteochondral lesions most commonly involve the anterolateral capitellum but have also been described in the trochlea in young athletes [10].

On MR images, osteochondral lesions demonstrate abnormal subchondral signal intensity as well as irregularity of the chondral surface, disruption or irregularity of the subchondral bone plate, and/or the presence of a subchondral fragment (Fig. 3.5). The primary role of imaging is to provide information regarding the stability of the osteochondral fragment. MRI, with its excellent soft tissue contrast, allows

Fig. 3.5 Osteochondral lesion. A 14-year-old male baseball player with lateral elbow pain. Axial fat-saturated T2-wieghted image reveals extensive marrow edema and a subchondral fracture line in the anterior capitellum (arrow). The overlying cartilage appears to be intact, and there is no fluid undercutting the lesion to suggest this is an unstable fragment

direct visualization of the articular cartilage, as well as of the character of the interface of the osteochondral lesion with the native bone. The presence of joint fluid completely encircling the fragment generally indicates an unstable lesion [11]. Direct MR arthrography can be helpful in identifying an unstable fragment, and CT arthrography can also be used for this purpose.

3.4 Ligaments

3.4.1 Ligaments: Normal Anatomy

The ulnar collateral ligament (UCL) is made up of three bundles (Fig. 3.6). Its anterior bundle courses from the undersurface of the medial epicondyle to the sublime tubercle along the medial margin of the coronoid process. It is the most important stabilizer of the elbow, especially during throwing and other overhead motions. The posterior bundle of the UCL extends from the medial epicondyle in a fan-like distribution to the medial margin of the trochlear notch of the olecranon and forms the floor of the cubital tunnel. The small transverse bundle of the UCL runs from the olecranon to the coronoid process and does not play a significant role in stabilizing the elbow.

On the lateral side (Fig. 3.7), the radial collateral ligament (RCL) lies just deep to the common extensor tendon and courses from the lateral epicondyle to blend with the annular ligament along the volar aspect of the radiocarpal joint. The lateral ulnar collateral ligament (LUCL) also originates on
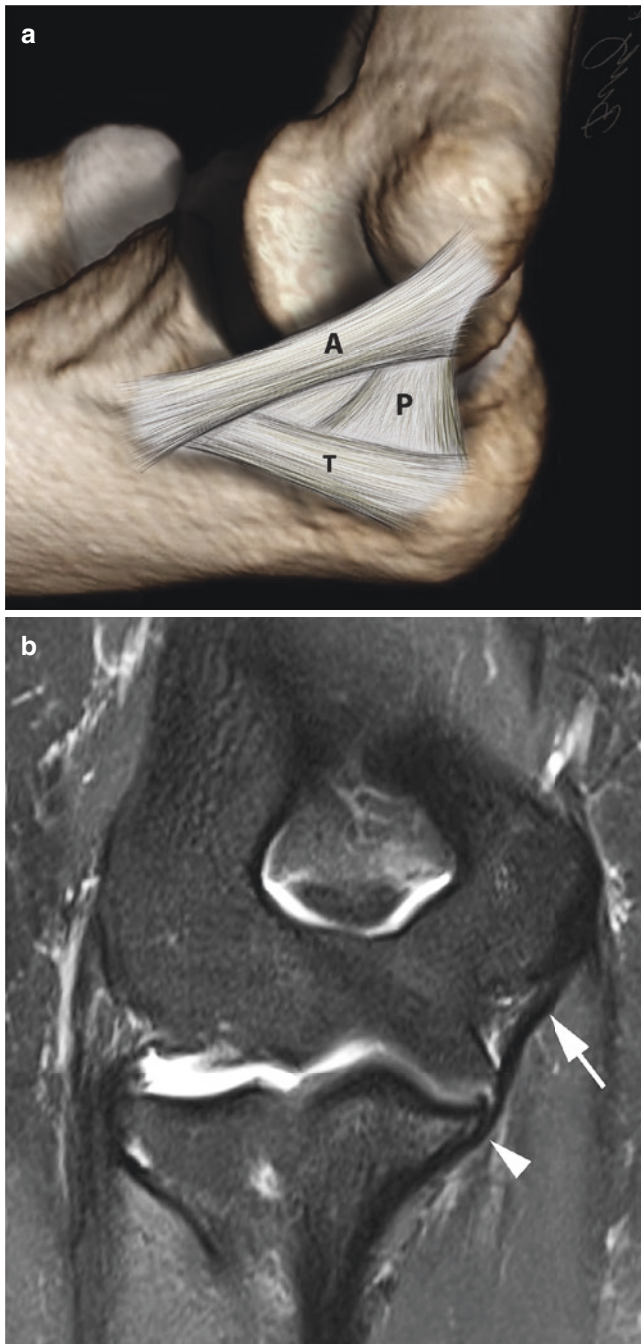
Fig. 3.6 Normal ulnar collateral ligament (UCL). (**a**) Diagram showing the anterior (A), posterior (P), and transverse (T) bundles of the UCL. (**b**) The anterior bundle is well seen on a coronal fat-saturated T2-weighted image (arrow). Note its uninterrupted distal attachment at the sublime tubercle of the ulna (arrowhead). Illustration courtesy of Dr. Brady Huang, San Diego, CA

the lateral epicondyle and extends behind the radial head to attach to the supinator crest along the lateral aspect of the proximal ulna. It provides posterolateral stability for the radiocapitellar joint. The annular ligament runs from the ventral aspect of the radial notch of the ulna around the radial head to attach along with the LUCL along the supinator crest and stabilizes the proximal radioulnar joint [12]. Although these are described as individual structures, studies suggest that they function together as a continuous sheet, rather than as individual entities.

3.4.2 Ligaments: Pathology

3.4.2.1 Valgus Instability

The UCL and, in particular, its anterior band are the most important medial stabilizer of the elbow. The most common mechanisms of ulnar collateral ligament insufficiency are chronic attenuation, as seen in throwing or other overhead athletes, and acute post-traumatic disruption, usually after a fall on an outstretched arm.

During the throwing motion, high valgus stresses are placed on the elbow with resulting tensile forces along its medial aspect with the maximum stress on the ulnar collateral ligament occurring during the late cocking and acceleration phases [13]. Repetitive insults to the ligament produce microscopic tears that progress to significant attenuation or frank tearing within its substance. Complete, full-thickness tears are often well demonstrated on conventional MR imaging studies (Fig. 3.8), but partial tears can be subtle and are best seen with MR arthrography [14]. A partial-thickness undersurface tear will often result in a "T-sign" which is best demonstrated using MR arthrography (see Fig. 3.7).

In the skeletally immature patient, the apophysis is the weakest link in the muscle-tendon-bone complex. Chronic valgus stress may result in a condition known as "Little Leaguer's Elbow" in which repetitive stresses across the medial epicondylar apophysis result in its apparent widening on radiographs (also known as "epiphysiolysis"), displacement or fragmentation [15]. MR imaging demonstrates extension of physeal cartilage into the metaphysis and/or marrow edema within the apophysis and also allows for assessment of the UCL, which is usually normal in these patients (Fig. 3.9).

3.4.2.2 Valgus Overload Syndrome

Throwing athletes and others involved in overhead sports often develop a constellation of injuries known as the valgus overload syndrome [16]. This is related to the strong valgus forces generated at the elbow which may lead to tensile failure of the UCL, an osteochondral lesion in the capitellum and/or subchondral edema, cartilage loss, and osteophyte formation along the posteromedial elbow joint secondary to increased shear forces in that region (Fig. 3.10). A careful inspection of these three areas should be carried out when viewing an MR imaging study in an overhead athlete presenting with elbow pain.
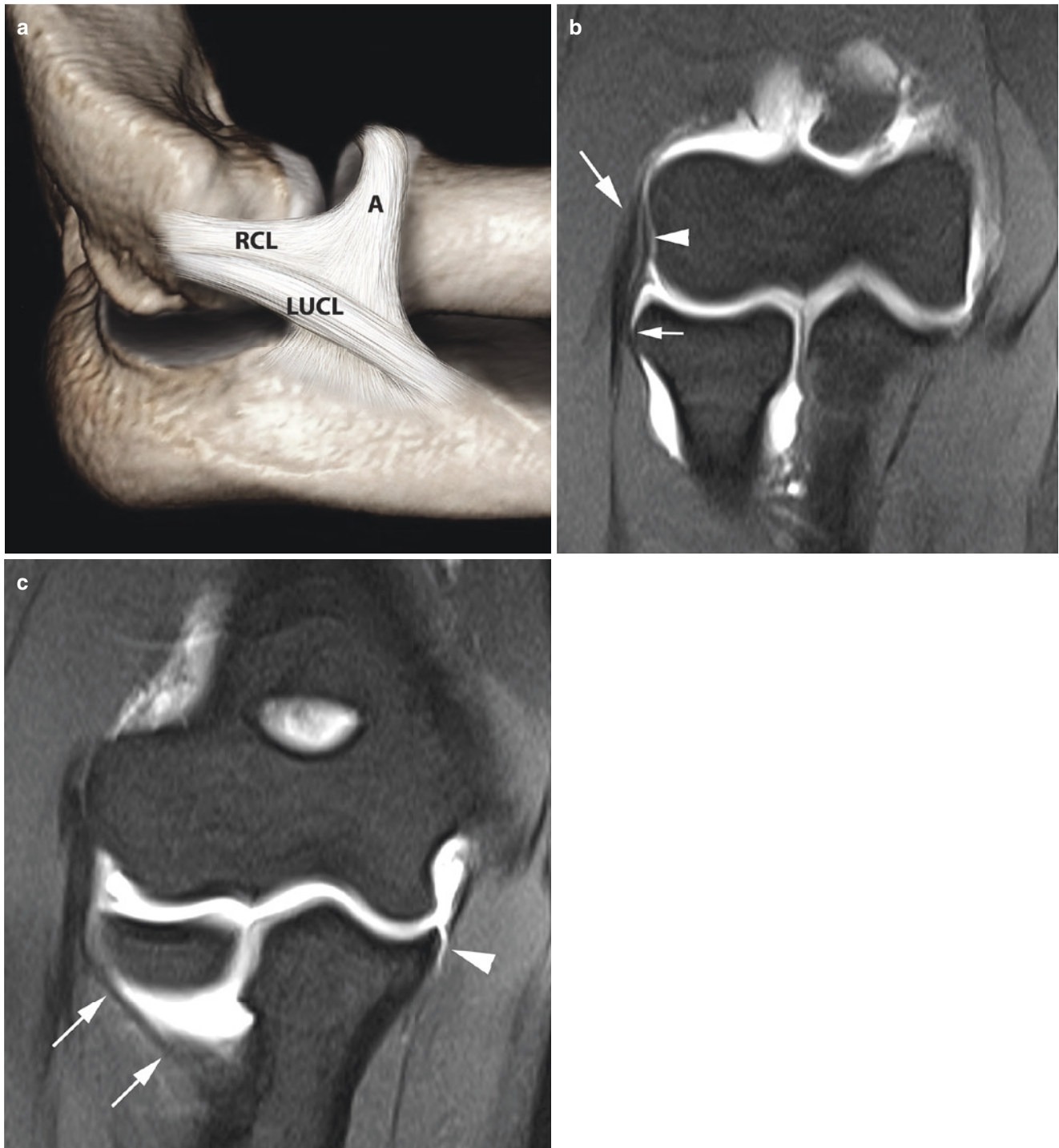
Fig. 3.7 Normal lateral ligaments. (**a**) Diagram showing the lateral collateral ligament complex including the radial collateral ligament (RCL), lateral ulnar collateral ligament (LUCL), and annular ligament (A). (**b**) Coronal fat-saturated T1-weighted image (MR arthrogram) shows the RCL (arrowhead) just deep to the common extensor tendon (arrow) and merging distally with the annular ligament (small arrow). (**c**) A more posterior image demonstrates the LUCL (arrows) as it courses behind the radial head to insert on the supinator crest of the ulna. Note also a partial tear of the distal ulnar collateral ligament forming a "T sign" (arrowhead). Illustration courtesy of Dr. Brady Huang, San Diego, CA
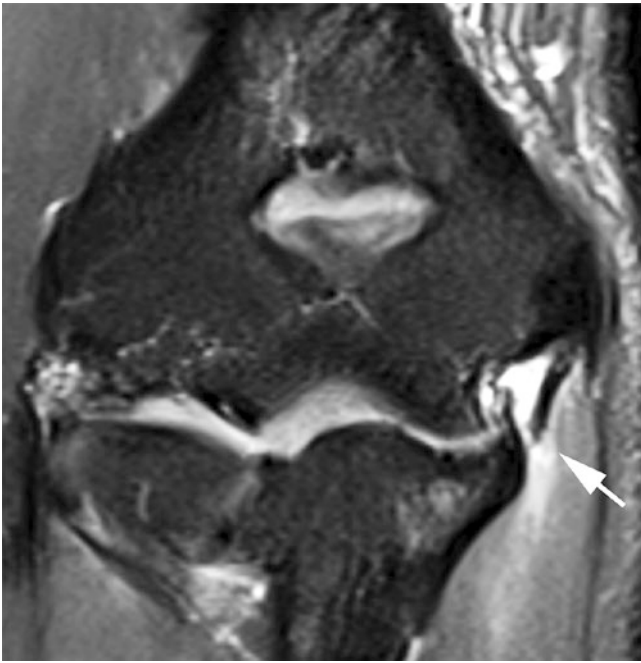
Fig. 3.8 Ulnar collateral ligament tear. An 18-year-old college baseball pitcher who felt a "pop" in his elbow while throwing and presented with medial elbow pain. Coronal fat-saturated T2-weighted image reveals a full-thickness tear of the anterior bundle of the UCL at its ulnar attachment (arrow) and edema in the adjacent flexor musculature

Fig. 3.10 Valgus overload syndrome: posteromedial joint. Axial T1-weighted image (MR arthrogram) demonstrates prominent osteophytes along the posteromedial joint (large arrow) as well as a small focus of cartilage loss along the posterior trochlea (small arrow). Used by permission of Springer Nature

3.4.2.3   Posterolateral Rotatory Instability and Elbow Dislocation (Fig. 3.11)

Posterolateral rotatory instability (PLRI) is the most common pattern of recurrent elbow instability and is often the sequela of a prior elbow dislocation. With an elbow dislocation, soft tissue injuries classically have been thought to proceed from lateral to medial along a spectrum of severity consisting of three stages: stage 1, posterolateral subluxation of the ulna on the humerus resulting in injury to the lateral ulnar collateral ligament; stage 2, incomplete dislocation with perching of the coronoid under the trochlea and tearing of the radial collateral ligament and joint capsule in addition to the lateral ulnar collateral ligament; and stage 3, complete dislocation with the coronoid located behind the humerus. Severe injuries may also result in additional tearing of the ulnar collateral ligament [17].

In addition to the soft tissue injuries, fractures involving the coronoid process and radial head commonly occur with an elbow dislocation, and the constellation of findings is referred to as the "terrible triad" of the elbow [18]. A fracture of the coronoid process is pathognomonic of an episode of elbow subluxation or dislocation, and the larger the coronoid fracture fragment, the more pronounced the degree of posterolateral instability.

Fig. 3.9 Medial apophysitis ("Little Leaguer's Elbow"). Coronal fat-saturated T2-weighted image (MR arthrogram) displays marrow edema within the medial epicondylar apophysis (arrow) in a 14-year-old baseball player. Note also the normal UCL (arrowhead)
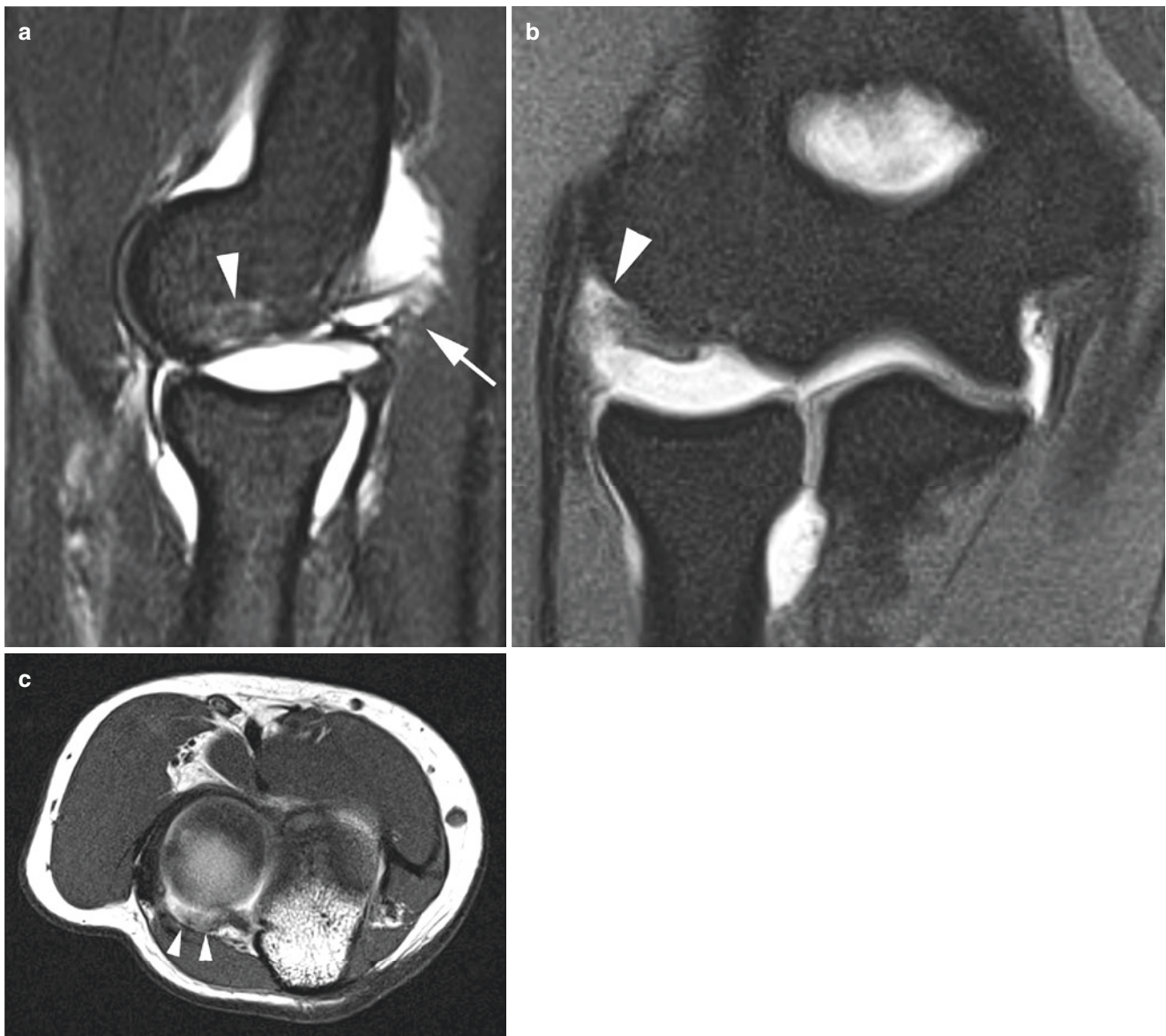
Fig. 3.11 Elbow dislocation. (**a**) Sagittal STIR image (MR arthrogram) shows posterior subluxation of the radial head and posterior ligamentous/capsular tearing (arrow) as well a subtle bone marrow contusion in the posterior capitellum (arrowhead). (**b**) Coronal fat-saturated T1-weighted image displays high-grade tearing of the RCL from its humeral attachment and an axial T1-weighted image (**c**) reveals tearing of the LUCL distally (arrowheads)

Key Point
- Stabilization of the elbow occurs primarily through static stabilizers of the ligament complexes and the intrinsic stability conferred by its osseous anatomy. Acute and chronic repetitive traumas are commonly encountered and have MR findings that vary with regard to skeletally maturity. Structural failure can be predicted with known mechanism of injury.

3.5 Tendons and Muscles

3.5.1 Tendons and Muscles: Normal Anatomy (Fig. 3.12)

The biceps tendon courses across the elbow anteriorly to insert on the radial tuberosity and is best seen in the axial plane. The bicipital aponeurosis (lacertus fibrosus) is a fascial extension from the short head of the biceps that extends
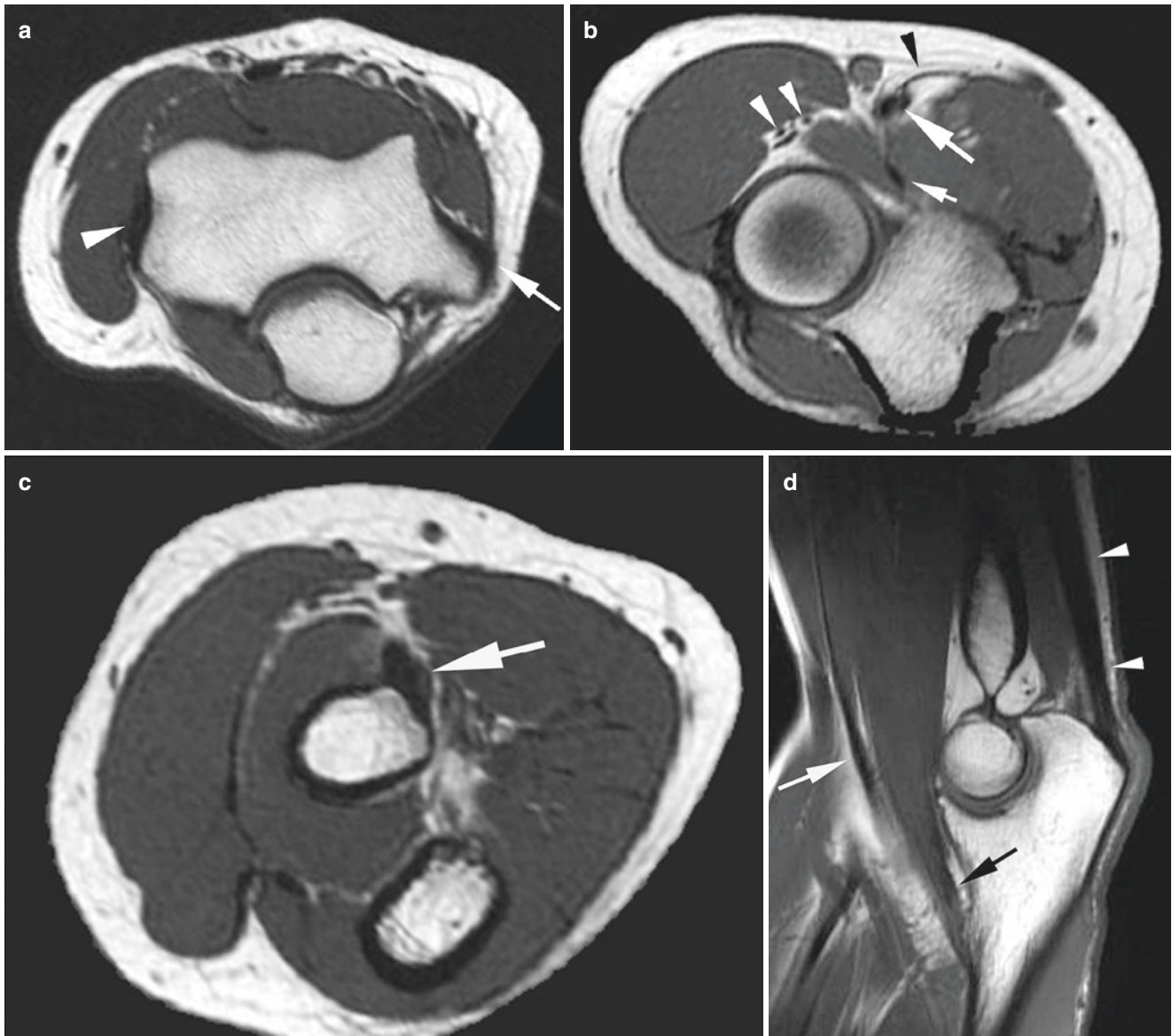
Fig. 3.12 Normal tendons. Axial T1-weighted images display (**a**) the common flexor/pronator (arrow) and common extensor (arrowhead) tendons, (**b**) the biceps tendon (large arrow), lacertus fibrosis/bicipital aponeurosis (black arrowhead), brachialis tendon (small arrow), branches of the radial nerve within the radial tunnel (white arrowheads), and (**c**) the distal biceps tendon at its insertion on the radial tuberosity (arrow). (**d**) Sagittal T1-weighted image again demonstrates the biceps (white arrow) and brachialis (black arrow) tendons as well as the triceps tendon (arrowheads). Used by permission of Springer Nature

over the biceps tendon and provides some tendon stability in this region. Immediately deep to the biceps lies the brachialis muscle and its very short tendon that attaches to the ventral aspect of the coronoid process of the ulna.

Posteriorly, the triceps tendon attaches along the dorsal aspect of the olecranon, distal to its tip, and can be divided into a thicker central tendon and a thinner lateral expansion. The small anconeus muscle lies along the posterolateral aspect of the elbow, arising from the posterior aspect of the lateral epicondyle and inserting along the proximal ulna. The anconeus epitrochlearis is an anomalous muscle, seen in approximately 10% of individuals, that lies along the medial aspect of the olecranon. While this is usually an asymptomatic normal variant, it may produce symptoms of ulnar neuropathy due to compression of the nerve within the adjacent cubital tunnel (see Fig. 3.17).

The flexor/pronator muscles of the forearm originate via a common tendon from the medial epicondyle, while the common extensor/supinator tendon originates on the lateral epicondyle.

3.5.2 Tendon and Muscles: Pathology

The classification of tendon injuries about the elbow can be organized by location, acuity, and degree of injury. Tendon injury related to a single isolated event is uncommon, although exceptions to this rule do occur. More commonly, tendon pathology in the elbow relates to chronic repetitive micro-trauma. MR imaging and ultrasound are particularly well suited to diagnose tendon pathology.

As elsewhere in the body, the tendons about the elbow should be smooth, linear structures of low signal intensity on MRI [19]. Abnormal morphology (attenuation or thickening) can be seen in tendinosis (also termed tendinopathy) or tear. If signal intensity becomes increased within the substance of a tendon on fluid-sensitive sequences, a tear is present. Tears can be further characterized as partial or complete.

3.5.2.1 Epicondylitis and Overuse Syndromes

Chronic stresses applied to the common flexor and extensor tendons result in medial and lateral "epicondylitis," though this is a misnomer since the underlying pathology relates to chronic degeneration and partial tendon tearing rather than an acute inflammatory reaction. The injury is believed to result from repetitive tensile overload of the tendon that produces microscopic tears that do not heal appropriately.

3.5.2.2 Lateral Epicondylitis

Lateral epicondylitis is associated with excessive, repetitive use of the wrist extensors and is the most common athletic injury in the elbow. It has been termed "tennis elbow," but this is somewhat misleading since the vast majority of cases of lateral epicondylitis occur in non-tennis players. The pathology most commonly affects the extensor carpi radialis brevis at the origin of the common extensor tendon.

The imaging findings of epicondylitis may include tendon thickening or attenuation with intrasubstance intermediate signal intensity (tendinosis) or partial- or full-thickness tears in which case fluid signal intensity will be seen within the tendon (Fig. 3.13). Close scrutiny of the underlying lateral ligaments is necessary to exclude concomitant pathology, especially in the lateral ulnar collateral ligament [20]. Underlying ligament involvement predisposes to a poorer

Fig. 3.13 Lateral epicondylitis. (**a**) Coronal fat-saturated T2-weighted image displays partial tearing of the proximal common extensor tendon at its humeral origin (arrow). (**b**) An adjacent image reveals partial tearing of the underlying humeral attachment of the radial collateral and lateral ulnar collateral ligaments (arrow)

response to conservative therapy and is an important finding for preoperative planning if surgical debridement of the common extensor tendon is contemplated.

3.5.2.3 Medial Epicondylitis

Medial "epicondylitis" involves a similar degenerative process affecting the common flexor tendon and results from repetitive valgus strain. It is associated primarily with golfing, pitching, and tennis. The pronator teres and flexor carpi radialis tendons are involved most frequently, resulting in pain and tenderness to palpation over the anterior aspect of the medial epicondyle and at the origin of the common flexor tendon. The imaging findings in this process are exactly those seen with lateral epicondylitis. As on the lateral side, when assessing the tendon, it is important to closely scrutinize the underlying collateral ligament complex to ensure its integrity.

3.5.2.4 Biceps Tendon

Rupture of the tendon of the biceps brachii muscle at the elbow constitutes less than 5% of all biceps tendon injuries with the most common injury in this region being complete avulsion of the tendon from the radial tuberosity [21]. The typical mechanism of injury relates to forced hyperextension applied to a flexed and supinated forearm, and the patient often describes sensing a "pop" and sharp pain in the antecubital fossa. Accurate clinical diagnosis is difficult in a partial tendon tear or in the case of a complete tear without retraction which can occur with an intact bicipital aponeurosis, which tethers the ruptured tendon to the pronator flexor muscle group.

Imaging of distal biceps tendon pathology becomes important in patients who do not present with the classic history or physical findings. It is critical that axial MR images extend distal to the radial tuberosity for accurate evaluation. MRI diagnosis of tendon pathology, as previously mentioned, is largely dependent on morphology, signal intensity, and the identification of areas of tendon discontinuity. The degree of partial tearing should be described and, in the case of a complete tear, the degree of tendon retraction and status of the bicipital aponeurosis. A useful indirect sign of biceps tendon pathology is the presence of radiobicipital bursitis (see below) (Fig. 3.14).

3.5.2.5 Triceps Tendon

Rupture of the triceps tendon is quite rare [22]. This most often results from an acute injury and is most common in weight lifters and other athletes. Partial tears are more common than complete tears, and both usually occur at its olecranon insertion. Associated findings may include olecranon bursitis, subluxation of the ulnar nerve, or fracture of the radial head (Fig. 3.15). The MRI features of a tear are similar to those associated with any other tendon.
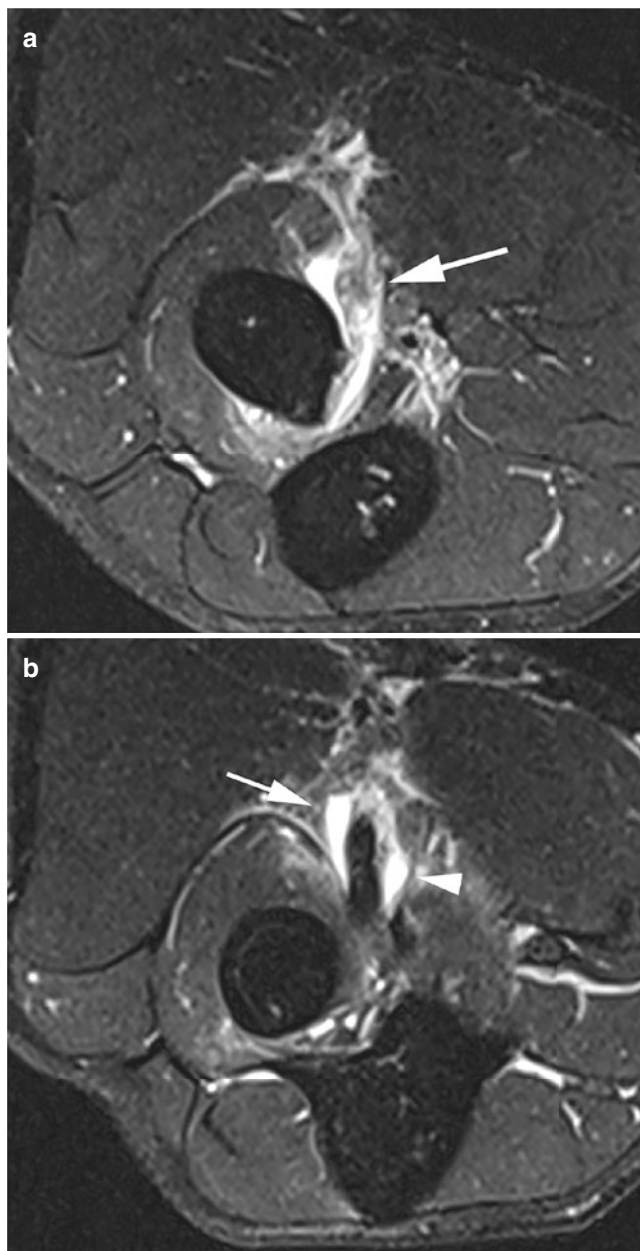
Fig. 3.14 Biceps tendon tear. (**a**) Axial fat-saturated T2-weighted image shows near complete tearing of the biceps tendon from the radial tuberosity (arrow). A more proximal image (**b**) demonstrates some associated distention of the radiobicipital bursa (arrow) and interosseous bursa (arrowhead)

3.6 Nerves

3.6.1 Nerves: Normal Anatomy (Fig. 3.16)

The ulnar nerve courses along the periphery of the medial head of the triceps muscle in the distal portion of the upper arm and into the cubital tunnel along the posteromedial elbow where it lies superficial to the posterior bundle of the UCL and deep to the cubital tunnel retinaculum.
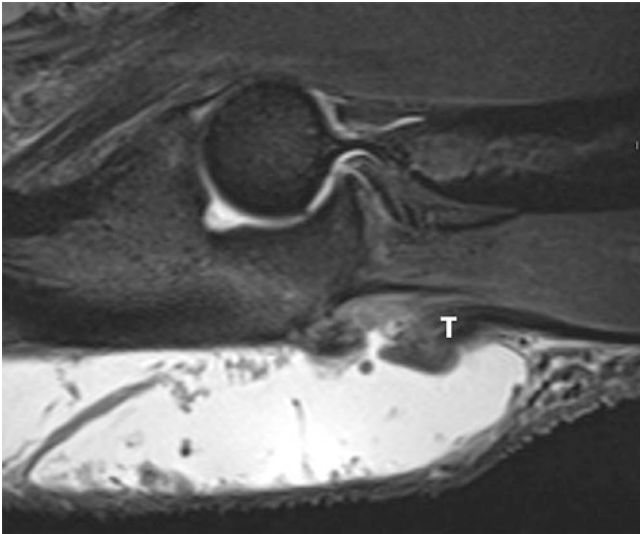
Fig. 3.15 Triceps tendon tear. Sagittal STIR image demonstrates partial tearing of the distal triceps tendon (T) and extensive fluid and synovial hypertrophy within the olecranon bursa

Fig. 3.16 Normal nerves. Axial T1-weighted image (MR arthrogram) demonstrates the ulnar nerve within the cubital tunnel (large arrow) and overlying cubital tunnel retinaculum (large arrowhead), the superficial and deep branches of the radial nerve within the radial tunnel (arrowheads), and the median nerve (small arrow). Used by permission of Springer Nature

After spiraling around the midhumeral shaft, the radial nerve courses through the radial tunnel, a space along the volar-lateral aspect of the elbow between the brachioradialis and brachialis muscles, where it divides into its deep and superficial branches. The deep branch then passes under the arcade of Froshe, pierces the supinator muscle, and continues as the posterior interosseous nerve.

The median nerve travels along the medial upper arm with the brachial vessels and then courses between the two heads of the pronator teres muscle and gives off the anterior interosseous nerve more distally.

3.6.2 Nerves: Pathology

Pathology involving the nerves of the upper extremity may result from nerve compression/entrapment or a "non-entrapment" etiology such as infection, polyneuropathy, acute trauma, or iatrogenic injury during arthroscopy [23]. Most types of nerve pathology will result in changes within the muscles they innervate: high signal intensity "edema" on T2W images with an acute process and high signal intensity on T1-weighted images, indicating fatty atrophy, with more chronic processes. In many cases, these muscle findings are more conspicuous on MR images than an abnormality of the nerve itself.

3.6.2.1 Ulnar Nerve

Ulnar nerve entrapment most commonly occurs in the cubital tunnel and may arise from a number of etiologies including a medial trochlear osteophyte, an anomalous anconeus epitrochlearis muscle, or an adjacent soft tissue mass (Fig. 3.17).

On MR imaging, ulnar neuritis should be considered when the nerve is enlarged, contains fascicles of varying size, and demonstrates increased signal intensity on T2W images, although this latter sign can be seen in asymptomatic patients and therefore must be correlated with other imaging and clinical information [24].

If the ulnar nerve is not seen within the cubital tunnel, it has likely been previously surgically transposed to the volar aspect of the elbow either deep or superficial to the proximal flexor muscles. To locate the nerve after transposition, it is easiest to identify it on T1-weighted images in the medial musculature of the proximal forearm where it is surrounded by bright fat and then trace its course proximally from there.

3.6.2.2 Median Nerve

Compression of the median nerve may occur at several sites. In patients with a supracondylar process emanating from the anterior cortex of the distal humerus, the nerve may become compressed by an associated ligament of Struthers (supracondylar process syndrome). The nerve may also become entrapped as it passes between the two heads of the pronator teres muscle or under the fibrous arch of the flexor digitorum profundus (pronator syndrome). More distally, the anterior interosseous nerve may be injured or compressed by an adjacent mass (anterior interosseous nerve syndrome).

Fig. 3.18 Radial nerve impingement. A 46-year-old female presenting with symptoms of posterior interosseous syndrome. Axial fat-saturated T2-weighted image shows a multilocular ganglion (arrowheads) displacing the deep branch of the radial nerve at that level (arrow)

patients. The nerve may also be compressed by an adjacent space-occupying mass (Fig. 3.18).

3.7   Synovial Processes

As a synovial joint, the elbow has a synovial membrane and joint capsule, separated by fat pads in some locations. Lubricating bursae, lined by synovium, are located superficial to the olecranon and surrounding the distal biceps tendon. The synovial anatomy is further complicated by the synovial plicae, folds of synovial tissue that represent embryonic remnants. Synovial inflammation can result from infectious, inflammatory, or post-traumatic conditions. Its appearance on MR imaging is nonspecific and includes T2-hyperintense joint fluid and synovial hypertrophy with enhancement if intravenous gadolinium is administered.

3.7.1   Bursae

The large olecranon bursa lies in the subcutaneous tissues overlying the dorsal aspect of the proximal ulna [25]. Two other bursae lie adjacent to the distal biceps tendon: the radiobicipital and interosseous bursae [26]. It is important to note that there is no tendon sheath at the level of the distal biceps tendon, so peritendinous fluid in this region indicates distention of one or both of these bursae.

Bursal inflammation may result from a number of etiologies which will be discussed below. MR imaging findings include bursal distention with high signal intensity fluid or,

Fig. 3.17 Ulnar neuritis. A 31-year-old male with elbow pain and symptoms of ulnar neuropathy. (**a**) Axial T1-weighted image reveals an anconeus epitrochlearis muscle (M) superficial to the ulnar nerve within the cubital tunnel. (**b**) Sagittal STIR image shows an increased signal intensity within a markedly enlarged ulnar nerve just proximal to the cubital tunnel (arrows) (E = medial epicondyle)

3.6.2.3   Radial Nerve

The radial nerve may be injured from direct trauma or may be compressed at various sites, the most common being where it penetrates the supinator muscle at the arcade of Frohse, a fibrous band found at that level in 30–50% of

Fig. 3.19 Olecranon bursitis. Sagittal fat-saturated T1-weighted image demonstrates marked synovial enhancement in a distended olecranon bursa. Used by permission of Springer Nature

in the case of infection or hemorrhage, more heterogeneous material on T2W images and pronounced synovial enhancement on T1-weighted images after the intravenous administration of gadolinium contrast (Fig. 3.19).

3.7.2 Plicae

Synovial plicae represent embryologic remnants that are commonly found within asymptomatic elbows. The most common of these synovial folds is the posterolateral plica, which is present in 86% of cadavers and up to 98% of asymptomatic patients on MR imaging; it has been implicated as a potential cause of lateral elbow pain known as the synovial fold syndrome [27]. This is thought to result from dynamic entrapment of the plica between the radial head and capitellum and often produces snapping, popping, or even locking of the elbow. The MR imaging findings of a plica measuring greater than 3 mm in thickness or covering more than one third of the articular surface of the radial head should raise suspicion for the diagnosis (Fig. 3.20).

3.7.3 Synovial Inflammation

Synovial inflammation can result from infectious, inflammatory, or post-traumatic conditions. The appearance on MR imaging is nonspecific and includes T2-hyperintense joint effusion, synovial hypertrophy, and synovial enhancement if intravenous gadolinium is administered [28] (Fig. 3.21).
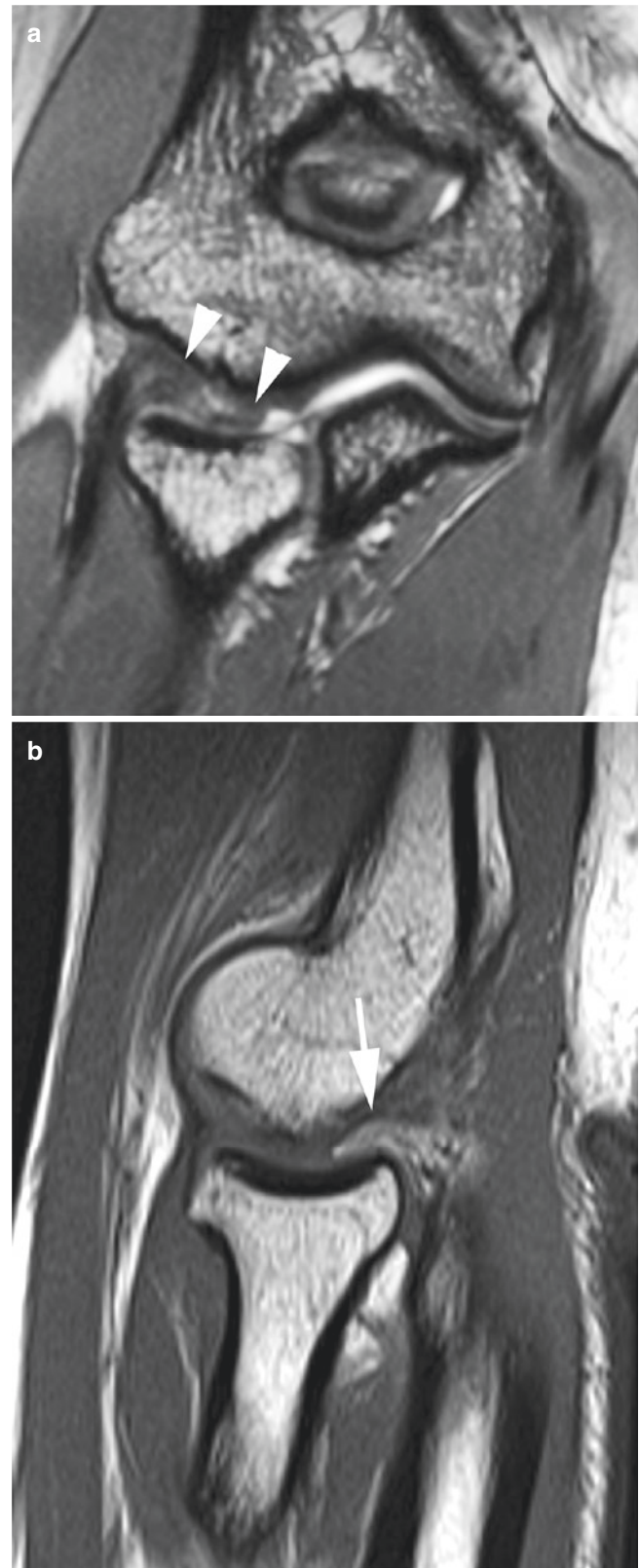
Fig. 3.20 Plica. An 18-year-old gymnast with pain in the region of the radiocapitellar joint. (**a**) Coronal gradient echo T2*-weighted image demonstrates a prominent radiocapitellar plica (arrowheads) which is also shown to be thickened and extending into the posterior joint on a corresponding sagittal T1-weighted image (**b**) (arrow)
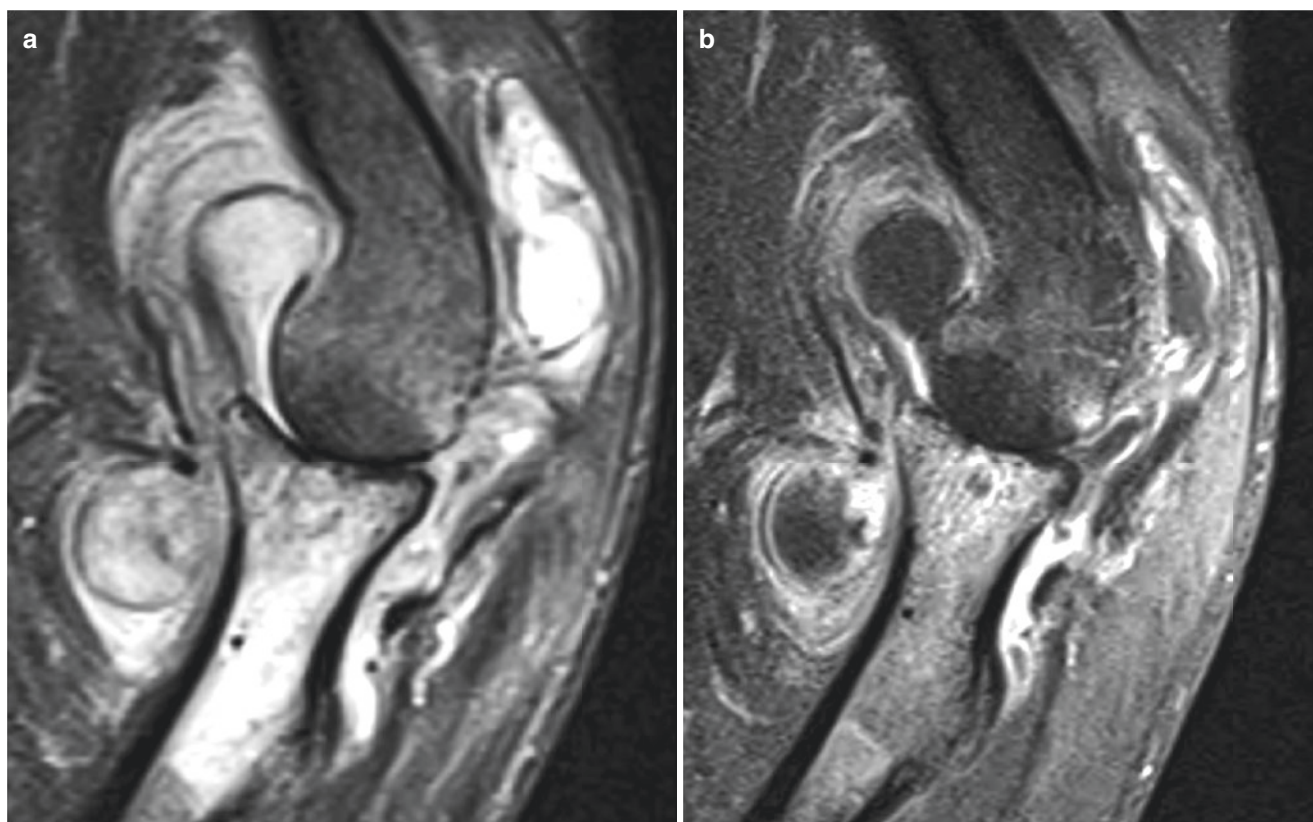
Fig. 3.21 Inflammatory synovitis. A 49-year-old female with a prior history of Lyme arthritis who developed an unspecified inflammatory polyarthropathy. (**a**) Sagittal fat-saturated T2-weighted image shows fluid and marked synovial hypertrophy distending the elbow joint, complete loss of articular cartilage, and prominent marrow edema in the proximal radius. (**b**) Corresponding sagittal fat-saturated T1-weighted image after intravenous gadolinium administration provides better delineation between low signal intensity fluid and enhancing synovium. Rheumatoid arthritis or a septic joint could demonstrate a similar MR appearance

3.7.3.1 Infectious Synovial Processes

Septic arthritis of the upper extremity is uncommon and often occurs in patients with existing comorbidities. The nonspecific nature of imaging findings emphasizes the need for accurate correlation with clinical and laboratory findings as well as joint aspiration when there is high clinical suspicion. Any destructive monoarticular process should be regarded as infection until proven otherwise.

The majority of olecranon bursitis results from an inflammatory cause with only 25% having an infectious etiology. Septic bursitis occurs due to bacterial penetration of microtrauma or hematogenous seeding. The olecranon bursal lining has been described as poorly vascularized, resulting in an increased propensity for transcutaneous spread of infection, even when no obvious wound is present [29].

3.7.3.2 Noninfectious Synovial Inflammatory Processes

Rheumatoid arthritis is among the disorders characterized by synovial inflammation. Although the elbow is not classically an initial site of involvement in rheumatoid arthritis, characteristic findings of synovial hypertrophy, altered marrow signal, and erosive changes are present on MRI. When it involves the olecranon bursa, inflammation with nodular involvement may be present. Gout is another rheumatologic disorder in which bursal involvement is characteristic. When sodium urate crystals are present within the bursa, low signal intensity on T1-weighted images with heterogeneous signal on fluid-sensitive sequences is noted. Radiographic correlation can be helpful to identify the cloud-like increased density seen with tophus formation. Seronegative spondyloarthropathies and calcium pyrophosphate dihydrate crystal deposition disease show MR findings of nonspecific synovial inflammation.

Pigmented villonodular synovitis (PVNS) is a rare, benign synovial proliferative process. It is an idiopathic process that most commonly affects the knee. While relatively uncommon in the elbow, the MR findings are quite characteristic. Clumps of hemosiderin-laden macrophage deposits demonstrate low signal on T1- and T2-weighted images. Gradient echo imaging enhances the magnetic susceptibility effects of the hemosiderin deposition. Joint effusion, osseous erosion, and extraarticular spread may also be seen [30].

5. Tomsick SD, Petersen BD. Normal anatomy and anatomical variants of the elbow. Semin Musculoskelet Radiol. 2010;14:379–3.
6. Major NM, Crawford ST. Elbow effusions in trauma in adults and children: is there an occult fracture? Am J Roentgenol. 2002;178:413–8.
7. Rosenberg ZS, Blutreich SI, Schweitzer ME, Zember JS, Fillmor K. MRI features of posterior capitellar impaction injuries. Am J Roentgenol. 2008;190:435–41.
8. Smith SR, Patel NK, White AC, Hadley CJ, Dodson CC. Stress fractures of the elbow in the throwing athlete: a systematic review. Orthop J Sports Med. 2018;6:1–8.
9. Ruchelsman DE, Hall MP, Youm T. Osteochondritis dissecans of the capitellum: current concepts. J Am Acad Orthop Surg. 2010;18:557–67.
10. Marshall KW, Marshall DL, Busch MT, Williams JP. Osteochondral lesions of the humeral trochlea in the young athlete. Skelet Radiol. 2009;38:479–91.
11. Jans LBO, Ditchfield M, Anna G, Jaremko JL, Verstraete KL. MR imaging findings and MR criteria for instability in osteochondritis dissecans of the elbow in children. Eur J Radiol. 2012;81:1306–10.
12. Acosta Batlle J, Cerezal L, López Parra MD, et al. The elbow: review of anatomy and common collateral ligament complex pathology using MRI. Insights Imaging. 2019;10:43. https://doi.org/10.1186/s13244-019-0725-7.
13. Anderson MW, Alford BA. Overhead throwing injuries of the shoulder and elbow. Radiol Clin N Am. 2010;48:1137–54.
14. Joyner PW, Bruce J, Hess R, Mates A, Mills FB, Andrews JR. Magnetic resonance imaging-based classification for ulnar collateral ligament injuries of the elbow. J Shoulder Elb Surg. 2016;25:L1710–6.
15. Wei AS, Khana S, Limpisvasti O, et al. Clinical and magnetic resonance imaging findings associated with little league elbow. J Pediatr Orthop. 2010;30:715–9.
16. Kheterpal AB, Bredella MA. Overuse injuries of the elbow. Radiol Clin N Am. 2019;57:931–42.
17. Potter HG, Weiland AJ, Schatz JA, Paletta GA, Hotchkiss RN. Posterolateral rotatory instability of the elbow: usefulness of MR imaging in diagnosis. Radiology. 1997;204:185–9.
18. Kani KK, Chew FS. Terrible triad injuries of the elbow. Emerg Radiol. 2019;26:341–7.
19. Chung CB, Chew FS, Steinbach L. MR imaging of tendon abnormalities of the elbow. Magn Reson Imaging Clin N Am. 2004;12:233–45.
20. Kwak AH, Lee S-J, Jeong HS, Do MU, Kuen TS. Subtle elbow instability associated with lateral epicondylitis. BMC Musculoskeletal Disord. 2018;19:136. https://doi.org/10.1186/s12891-2069-8.
21. Quach T, Jazayeri R, Sherman OH, Rosen JE. Distal biceps tendon injuries current treatment options. Bull NYU Hosp Jt Dis. 2012;68:103–11.
22. Keener JD, Sethi PM. Distal triceps tendon injuries. Hand Clin. 2015;31:641–50.
23. Andreisek G, Crook DW, Burg D, Marincek B, Weishaupt D. peripheral neuropathies of the median, radial, and ulnar nerves: MR imaging features. Radio Graph. 2006;26:1267–87.
24. Husarik DB, Saupe N, Pfirrmann CW, Jost B, Hodler J, Zanetti M. Elbow nerves: MR findings in 60 asymptomatic subjects—normal anatomy, variants, and pitfalls. Radiology. 2009;252(1):148–56.
25. Floemer F, Morrison WB, Bongartz G, Ledermann HP. MRI characteristics of olecranon bursitis. Am J Roentgenol. 2004;183:29–34.
26. Skaf AY, Boutin RD, Dantas RWM, et al. Bicipitoradial bursitis: MR imaging findings in eight patients and anatomic data from con-

3.8   Concluding Remarks

The elbow is a complex articulation from an anatomic and functional perspective. MR imaging has emerged as the primary tool for non-invasive evaluation of osseous and soft tissue structures, providing excellent resolution and contrast. Coupled with an understanding of disease process and mechanism of injury, MR imaging is a powerful tool for the diagnosis and characterization of disease.

> **Key Point**
> • Synovial inflammatory processes demonstrate nonspecific MR findings. In some entities, signal characteristics allow more specific diagnostic considerations. Correlation with other imaging studies, clinical presentation, and laboratory findings are important for accurate diagnosis.

> **Take Home Messages**
> • MR imaging of the elbow presents technical and diagnostic challenges that can be overcome through protocol optimization.
> • Detailed understanding of anatomy and mechanism of injury is crucial for accurate diagnosis and characterization of traumatic pathology.
> • Familiarity with the MR imaging appearance of osseous and soft tissue anatomy, as well as variations in anatomy, serves as the basis for improving diagnostic performance.

References

1. Johnson D, Stevens KJ, Riley G, Shapiro L, Yoshioka H, Gold GE. Approach to MR imaging of the elbow and wrist: technical aspects and innovation. Magn Reson Imaging Clin N Am. 2015;23:355–66.
2. Acosta Batlle J, Cerezal L, Márquez MV, et al. MRI of the normal elbow and common pathologic conditions. Radiographics. 2020;40:468–9.
3. Magee T. Accuracy of 3-T MR arthrography versus conventional 3-T MRI of elbow tendons and ligaments compared with surgery. Am J Roentgenol. 2015;204(1):W70–5.
4. Andreisek G, Froehlich JM, Hodler J, et al. Direct MR arthrography at 1.5 and 3.0 T: signal dependence on gadolinium and iodine concentrations—phantom study. Radiology 2008. 2008;247(3):706–16.

trast material opacification of bursae followed by routine radiography and MR imaging in cadavers. Radiology. 1999;212:111–6.

27. Cerezal L, Rodriguez-Sammartino M, Canga A, et al. Elbow synovial fold syndrome. Am J Roentgenol. 2013;201:W88–96.

28. Jbara M, Patnana M, Kazmi F, Beltran J. MR imaging: arthropathies and infectious conditions of the elbow, wrist, and hand. Radiol Clin N Am. 2006;44:625–42.

29. Blackwell JR, Hay BA, Bolt AM, Hay SM. Olecranon bursitis: a systematic overview. Shoulder Elbow. 2014;6:182–90.

30. Lu H, Chen Q, Shen H. Pigmented villonodular synovitis of the elbow with radial, median and ulnar nerve compression. Int J Clin Exp Pathol. 2015;8:14045–9.

Wrist and Hand

4

Omid Khalilzadeh, Clarissa Canella, and Laura M. Fayad

Learning Objectives
- A basic approach to radiologic interpretation of wrist and hand imaging.
- Review of common fractures affecting the wrist and hand.
- Review of common injuries to ligamentous, tendinous, and capsular structures of the hand and wrist.

4.1 Introduction

In this chapter, we will review some of the common traumatic injuries affecting the wrist and hand. The wrist is complex, with small bones and supporting soft tissue structures, which limits the diagnostic yield for radiologic assessment [1]. A practical ABCs (alignment, bones, chondral surfaces, and soft tissues) checklist for reviewing wrist and hand exams includes assessment of alignment, bones including cortical margins, bone trabecular pattern and bone marrow signal, chondral surfaces and joints, and the soft tissues and supporting structures. Wrist alignment can be assessed by radiographs: on the frontal view (Fig. 4.1), proximal and distal carpal rows form smooth and congruent arcs, and there is mild ulnar inclination of distal radius, while on the lateral view, there is mild volar tilt of the distal radius articular surface, and the lunate bone is aligned within 10 degrees of the capitate. Evaluation of the bones is achieved through radiography, CT, and MRI, as described for different inju-

O. Khalilzadeh · L. M. Fayad (✉)
The Russell H. Morgan Department of Radiology and Radiological Science, The Johns Hopkins School of Medicine, Baltimore, MD, USA
e-mail: omidk@jhmi.edu; lfayad1@jhmi.edu

C. Canella
Radiology Department, Clínica de Diagnóstico por Imagem (CDPI)/DASA, Rio de Janeiro, RJ, Brazil

Fig. 4.1 Three arcs drawn on the frontal radiograph of the wrist demonstrate normal alignment of the proximal and distal carpal rows

ries below, with the bones providing boundaries to the five different compartments of the wrist (distal radioulnar joint compartment, radiocarpal compartment, midcarpal compartment, common carpometacarpal compartment, and thumb carpometacarpal compartment). When performing a wrist arthrogram (Fig. 4.2), communication of the administered contrast between any of these compartments is usually suggestive of internal derangement due to ligamentous disruption. Arthrography techniques, including MRI, are also used for assessment of the chondral surfaces.

In the following sections, common traumatic injuries affecting the wrist and hand are reviewed.

Fig. 4.2 Wrist arthrogram images demonstrate injection of radiopaque contrast material within the midcarpal (left), radiocarpal (center), and distal radioulnar (left) compartments of wrist

4.2 Metacarpal and Phalangeal Fractures

Distal phalanx fractures are the most common fractures of the hand and are frequently seen in sports injuries, such as with the mallet finger and the jersey finger. Middle phalanx fractures are the least common fractures. Proximal phalanx fractures are the most common pediatric hand fractures and can be epiphyseal or shaft fractures.

Metacarpal fractures are common, with metacarpal shaft and neck fractures typically occurring as a result of axial loading, direct trauma, or torsional force. Specific names are given to fractures of the base of the thumb metacarpal (epibasal fractures of the thumb, Bennett fracture dislocation of the thumb, and Rolando fracture of the thumb) and little finger metacarpal (reverse Bennett fracture dislocation fracture and boxer fracture) [2].

Mallet finger: The mallet finger results from disruption of the terminal tendon contribution to the extensor mechanism of the finger at its attachment to the dorsal aspect of proximal phalangeal base, with or without bony avulsion [3]. These are the most common tendon injuries in sports, resulting from a combination of pulling force at the terminal tendon combined with extension of distal interphalangeal joint. Radiographs may show a tiny avulsed bone fragment, and ultrasound may show loss of real-time movement of the tendon.

Seymour fracture: This is a pediatric subtype of the mallet finger with distal phalanx physeal fracture and associated nail bed injury, most commonly occurring with ungual subluxation.

Jersey finger: The Jersey finger (Fig. 4.3) results from disruption of the flexor digitorum profundus at the volar base of distal phalanx, with or without a bony avulsion [4]. The avulsed tendon or bone fragment may be retracted proximally, most commonly up to the edge of the A2 pulley along

Fig. 4.3 Jersey finger with avulsion fracture of the volar base of distal phalanx and proximal retraction to the edge of A4 pulley

the proximal phalanx. It usually occurs in sports secondary to forceful hyperextension of a flexed finger during activity.

Bennett fracture dislocation: This is a two-piece fracture of the base of the thumb metacarpal with intra-articular extension and dorsolateral displacement. A small ulnar fragment of the thumb metacarpal, attached to the anterior oblique ligament of the thumb carpometacarpal bone, remains in place articulating with the trapezium.

Fig. 4.4 Fracture of fifth metacarpal neck compatible with boxer fracture

Rolando fracture dislocation: This can be categorized as a comminuted form of the Bennett fracture. This is a three-part, intra-articular fracture dislocation of the base of the thumb. The fracture line is typically a Y or T shape, and a volar fragment remains in articulation.

Epibasal fractures of the thumb: This is a two-piece fracture of the base of the thumb. These fractures are usually stable and often do not require surgery, in contrast to the above Bennett and Rolando fractures.

Boxer fracture: This is a fracture of fifth metacarpal neck (Fig. 4.4), commonly secondary to direct longitudinal trauma, such as boxing injury.

Reverse Bennett fracture dislocation: This is a fracture dislocation of the base of the fifth metacarpal.

Key Point
- Phalanx and metacarpal fractures are common and are usually seen with sports injuries. Intra-articular extension and injury to joint capsular ligaments, tendons, or physeal plates are commonly seen with these fractures.

4.3 Carpal Fractures

Carpal bone fractures can involve one or a combination of carpal bones, usually seen as part of carpal fracture dislocations [5]. Individual fractures include the following fractures:

Scaphoid fracture: This is the most common carpal bone fracture (Fig. 4.5) and may be occult on radiographs. Fractures are usually secondary to a fall on an outstretched hand and may involve the waist of the scaphoid (70–80%), distal pole of scaphoid tubercle (20%), or proximal pole (10%). Arterial supply to the scaphoid is from distal to proximal pole. Therefore, the more proximal the site of fracture, the higher likelihood of malunion/non-union, avascular necrosis of the proximal fragment, and long-term complications such as SNAC wrist (scaphoid nonunion advanced collapse) and SLAC wrist (scapholunate advanced collapse) (Fig. 4.6).

Triquetral fracture: This is the second most common carpal fracture after the scaphoid. The most common fracture of the triquetral bone is a dorsal avulsion fracture at the attachment of radiocarpal ligament, secondary to fall on an outstretched hand, best seen on lateral view. Triquetral body or volar avulsion fractures are less commonly seen fractures.

Lunate fracture: This fracture is usually secondary to axial loading and could involve the volar pole, dorsal pole, or body. Non-displaced transverse fractures through the body of the lunate have been known as a predisposing factor to avascular necrosis of lunate, particularly in patients with negative ulnar variance who receive more axial loading on the lunate through contact with the distal radius.

Hook of hamate fracture: This type of fracture (Fig. 4.7) may occur due to a direct trauma during sports or a fall and may result in Guyon's canal syndrome. A hook of hamate fracture is best identified on axial cross-sectional imaging, with MRI or CT, through the wrist.

Tubercle of trapezium fracture: The most common site of fracture is the tubercle of trapezium (Fig. 4.8) at its volar surface.

Trapezoid, pisiform, and capitate fractures: These fractures are less commonly seen in isolation.

Combination fractures: These fractures involve more than one carpal bone and may be associated with a dislocation [6].

4.3.1 Perilunate Injuries

Due to dynamic alignment and ligament support of the wrist, transmission of force through the carpus (usually via axial loading, dorsiflexion, ulnar deviation, and supination) can
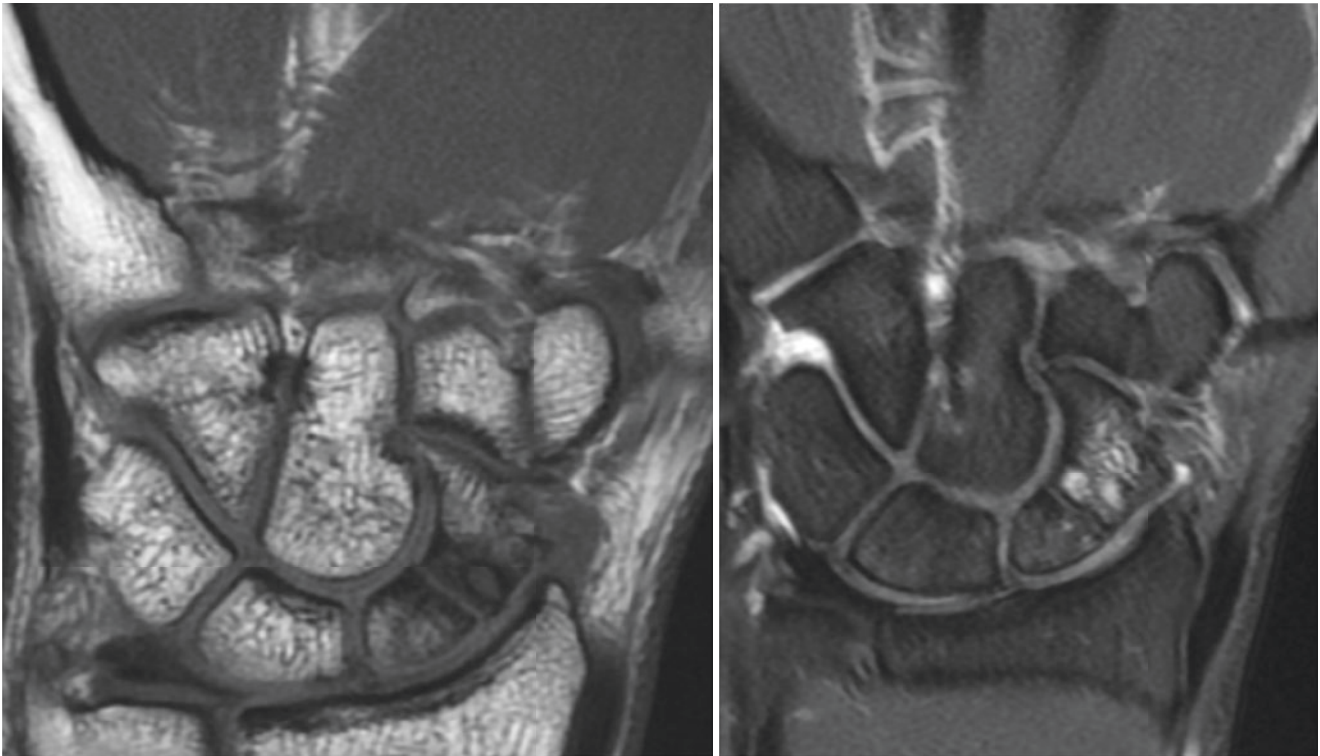
Fig. 4.5 Scaphoid fractures could be occult on radiographs. Coronal MR images through the wrist demonstrate a chronic appearing minimally displaced fracture of scaphoid wrist

Fig. 4.6 Severe case of scapholunate advanced collapse (SLAC), commonly known as SLAC wrist. Coronal fluid-sensitive MR image through the wrist demonstrates widening of the scapholunate interval compatible with scapholunate ligament tear, with associated proximal migration of capitate and advanced secondary degenerative changes of radioscaphoid articulation

cause a sequence of injuries through a perilunate *zone of vulnerability* in the wrist, as described by Mayfield et al. [7]. Two different sets of injuries can occur in the wrist "zone of vulnerability" (Fig. 4.9):

1. **Lesser arc injuries:** These are usually related to rapid transmission of force and are purely ligamentous.
2. **Greater arc injuries:** These are usually related to slower transmission of force and include fractures as well as ligament injuries.

Perilunate injuries can result in volar dislocation of the capitate with respect to the lunate which could progress from stage I **scapholunate dissociation** to stage II, dorsal **perilunate dislocation**; stage III, **midcarpal dislocation**; and finally stage IV, volar **lunate dislocation** (Fig. 4.10).

Lesser arc perilunate injuries occur in a sequence which is called progressive perilunate failure. These injuries start at the scapholunate joint, then proceed to the lunocapitate and lunotriquetral joints, and finally culminate in complete dislocation of the lunate.

Perilunate injury with associated fracture of one or more bones around the lunate (scaphoid, trapezium, capitate, hamate, or triquetrum) is called a greater arc injury. Greater arc injuries could have trans-radial, trans-scaphoid, trans-capitate, trans-triquetrum, or trans-ulnar styloid components in association.
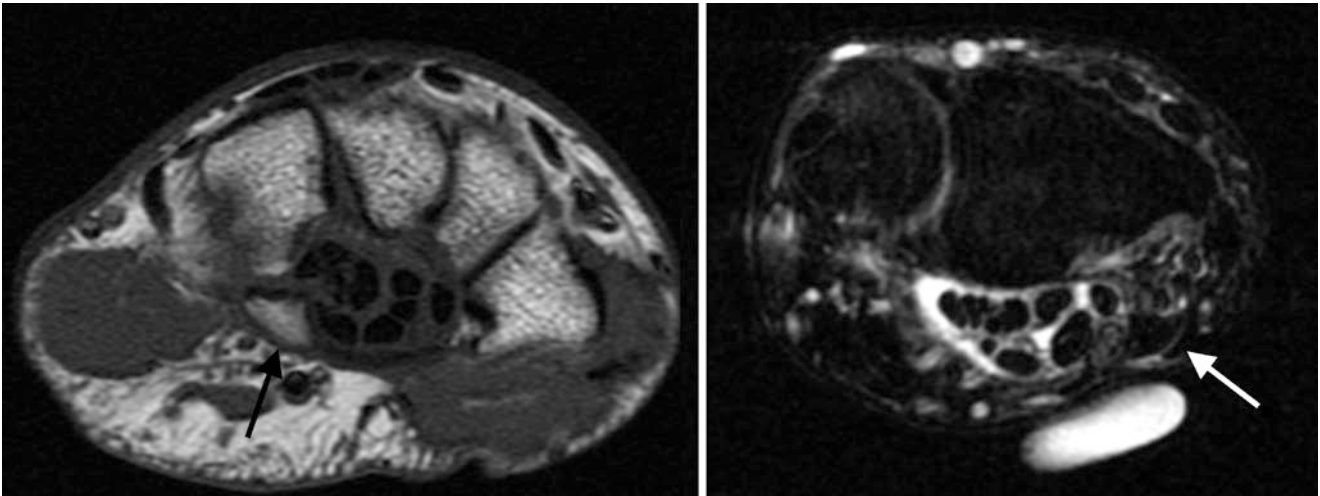
Fig. 4.7 Axial MR images demonstrate a mildly displaced fracture of hook of hamate. Lack of edema like signal and corticated margins are suggestive of a chronic fracture
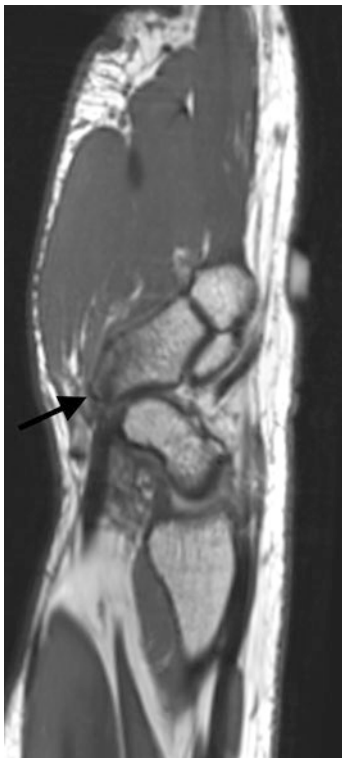
Fig. 4.8 Sagittal T1-weighted MR image demonstrates a non-displaced fracture of tubercle of trapezium

Key Point
- Carpal fractures may involve one individual bone or more than one carpal bone, as part of the commonly seen perilunate injuries through the zone of vulnerability. Perilunate injuries may be associated with dislocation.

Fig. 4.9 Wrist is vulnerable to injuries through a perilunate "zone of vulnerability" (red zone). Two different sets of injuries can occur along this zone, as depicted by dash lines: lesser arc injuries and greater arc injuries

4.3.2 Carpal Instability

By terminology, instability is a dynamic process and requires dynamic assessment of carpal bones in motion, often evaluated by dynamic fluoroscopy. What is commonly evaluated on static radiologic images is malalignment which is a manifestation of dynamic instability. Therefore, radiology
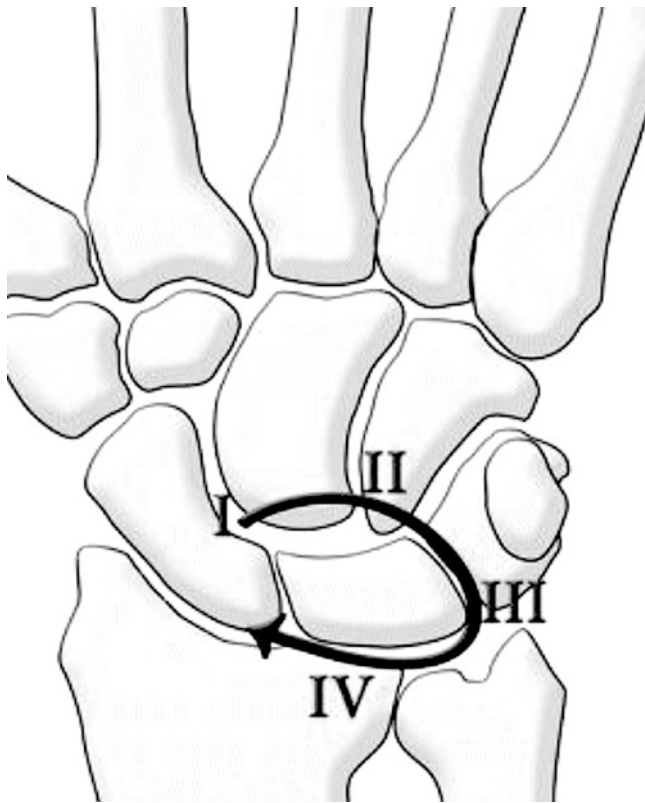
Fig. 4.10 Four stages of progressive perilunate injury: stage I, "scapholunate dissociation"; stage II, dorsal "perilunate dislocation"; stage III, "midcarpal dislocation"; and finally stage IV, volar "lunate dislocation"

reports describe the findings as "malalignment which is seen with a certain clinical pattern of carpal instability."

Different classifications have been suggested for carpal instability [8], as below:

The Mayfield classification of carpal instability: This classification system is also known as perilunate instability, which is focused on perilunate patterns of carpal instability [7]. Other forms of carpal instability such as adaptive instability secondary to an extracarpal factor are not included in this classification.

Under this classification, instability is divided into four stages:

– Stage I: scapholunate dissociation.
– Stage II: perilunate dislocation, with the lunate remaining normally aligned with the distal radius and the remaining carpal bones dislocated dorsally.
– Stage III: midcarpal dislocation, where neither the capitate nor the lunate is aligned with the distal radius.
– Stage IV: lunate dislocation, which is usually volar (Fig. 4.11).

The Mayo classification of carpal instability: This scheme offers a more comprehensive classification, divided into four categories [9].

- Dissociative (CID): dissociation of bones of the same carpal row, in the mediolateral direction.
  – Scapholunate dissociation, which is the most common cause of dorsal intercalated segment instability (DISI) (Fig. 4.12).
  – Lunotriquetral dissociation, which is the most common cause of volar intercalated segment instability (VISI).
  – Distal dissociative carpal instability.
- Non-dissociative (CIND): structural derangement between the proximal carpal row and the radius or the distal carpal row with a normal relationship of the carpal bones within that row. Typically, with CIND, there is dissociation in a direction other than mediolateral.
  – Radiocarpal instability, including ulnar or radial translocation, or radiocarpal dislocation.
  – Midcarpal instability, including volar or dorsal midcarpal instability.
- Complex (CIC): CID and CIND combined, including dorsal or volar perilunate dislocation or fracture dislocation, i.e., greater or lesser arc injury.
  – Axial dislocations (high energy trauma, e.g., peritrapezium or perihamate).
- Adaptive (CIA): Dissociation occurs secondary to extrinsic causes including proximal or distal causes such as distal radius fracture malunion or madelung deformity.

The articulations between the lunate and the surrounding four bones play the most important role in carpal stability. When evaluating carpal instability, attention should be focused on lunate articulations, including radiolunate, lunocapitate, lunotriquetral, and scapholunate. Each articulation should be assessed for signs of displacement or malrotation. Measurement of carpal angles between the lunate and other bones including radiolunate, scapholunate, and lunocapitate could be used as a hint to carpal malalignment. For example, malalignment at the radiolunate is seen with radiocarpal instability. Malalignment at the lunocapitate articulation is seen with midcarpal instability.

Please note that perilunate instability is not interchangeable with midcarpal instability. The former may include dissociation within the proximal carpal row. However, the latter is a non-dissociative instability. The key feature in midcarpal instability is lunocapitate malalignment which may or may not be seen in perilunate instability.

4.4   Tendon Injuries

Flexor tendon and extensor mechanism anatomy of the hand is demonstrated in Fig. 4.13. Common conditions involving the tendons of the hand and wrist include a trigger finger, tenosynovitis of the first through sixth dorsal extensor
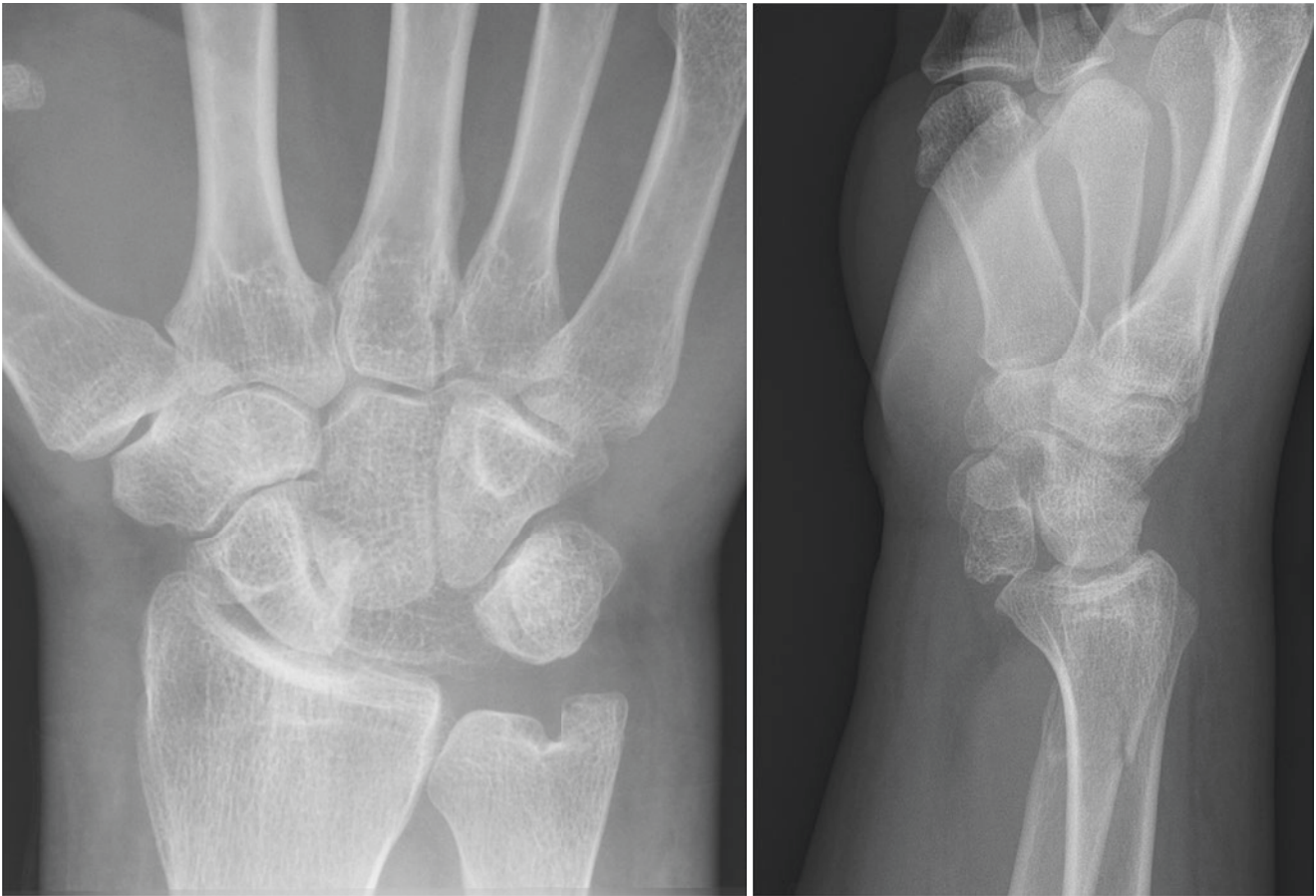
Fig. 4.11 Frontal and lateral radiographs demonstrate volar dislocation of lunate. Notice disruption of carpal arcs on the frontal view. Additional fracture of distal radius is visible on the lateral radiograph

compartments, and flexor carpi radialis tendonitis. Tendinosis is chronic degeneration of a tendon due to mechanical stress and repetitive trauma. Laceration followed by avulsion injuries is the main cause of traumatic injuries to tendons. Tenosynovitis is fluid expansion and synovitis of a tendon sheath, which could be due to degenerative, infectious, or inflammatory etiologies [10, 11].

4.4.1 Extensor Carpi Ulnaris Tendon (ECU) Injury

It is important to differentiate between ECU subluxation and normal dynamic variations in positioning. ECU position within the ulnar groove is dependent on wrist position. ECU is in ulnar position on pronation and in radial position in supination. ECU dislocation is secondary to ECU subsheath injury, including tears of the radial or ulnar roots of the ECU subsheath. ECU tendinosis and tear (Fig. 4.14) are the most common tendon pathologies of the hand and wrist.

Stenosis tenosynovitis: Stenosing tenosynovitis develops secondary to chronic repetitive microtrauma from frequent

movements of the tendons, through osseofibrous tunnels, such as with the overlying retinaculum or pulley [10].

De Quervain's tenosynovitis: This is a common form of stenosing tenosynovitis involving the first extensor tendon compartment (abductor pollicis longus (APL) and extensor pollicis brevis (EPB) tendons) of the wrist, typically at the radial styloid (Fig. 4.15). The most common etiology is thickening of the overlying extensor retinaculum at the radial styloid.

Trigger finger: This is a type of stenosing tenosynovitis involving the flexor digitorum superficialis at the level of the A1 pulley. Ultrasound can show real-time impingement of the tendon while gliding through its tunnel, and there is thickening of the overlying flexor pulley measuring >1–1.5 mm.

Intersection syndrome: At the crossing point of the first dorsal compartment (APL and EPB) and second dorsal compartment (ECRL, ECRB), tenosynovitis occurs and is known as proximal intersection syndrome. Tenosynovitis at the third compartment (extensor pollicis longus, EPL) and second dorsal compartment (ECRL, ECRB) crossing point is known as distal intersection syndrome.
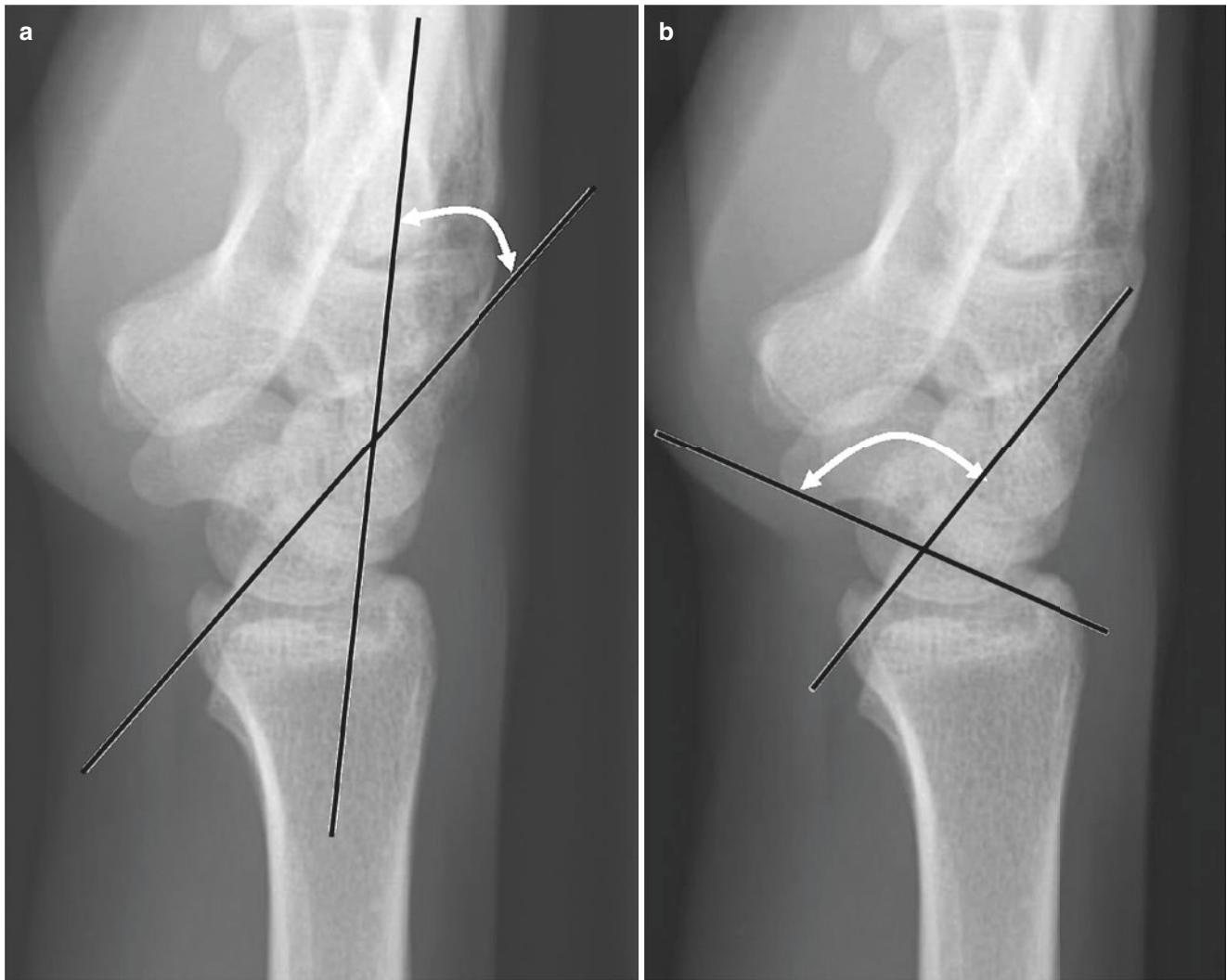
Fig. 4.12 Lateral radiographs demonstrate volar tilt of lunate with widening of capitolunate angle >30° and scapholunate angle >60° (**a** and **b**, respectively) compatible with malalignment seen with dorsal intercalated segment instability (DISI)

Pulley injuries: Pulleys are fibrous structures which wrap around the flexor tendon sheaths of the digits to form a supporting fibro-osseous tunnel (Fig. 4.16). Five such annular pulleys (A1–A5), together with three cruciate pulleys (C1–C3), form a fibro-osseous tunnel. Cruciate pulleys are difficult to find on imaging due to their thin size, and injuries are less commonly discussed. However, the A2 pulley is the most load bearing and most commonly injured pulley and can be identified by imaging, particularly axial non-fat-suppressed T1- or intermediate-weighted imaging. A1, A3, and A5 pulleys attach to volar plates at the level of metacarpophalangeal (MCP), proximal interphalangeal (PIP), and distal interphalangeal (DIP) joints and are less commonly torn. A2 and A4 pulleys attach to the periosteum at the proximal and middle phalanx. Pulley sprain or rupture can be associated with bowstringing of the flexor digitorum tendons, and increased bone-tendon distance is best detected on sagittal images.

Boutonniere deformity: "Boutonnière" is French for buttonhole. Increasing PIP joint flexion causes further extensor retinaculum damage resulting in "buttonholing" of the proximal phalanx between the lateral bands of the extensor tendon. Secondary DIP joint extension then occurs. Findings result from rupture of the central slip of the extensor mechanism from its attachment at the dorsal base of the middle phalanx or failure of the triangular ligament.

Key Point

- Common conditions involving the tendons of the hand and wrist include trigger finger, tenosynovitis of the first through sixth dorsal extensor compartments, and flexor carpi radialis tendonitis.
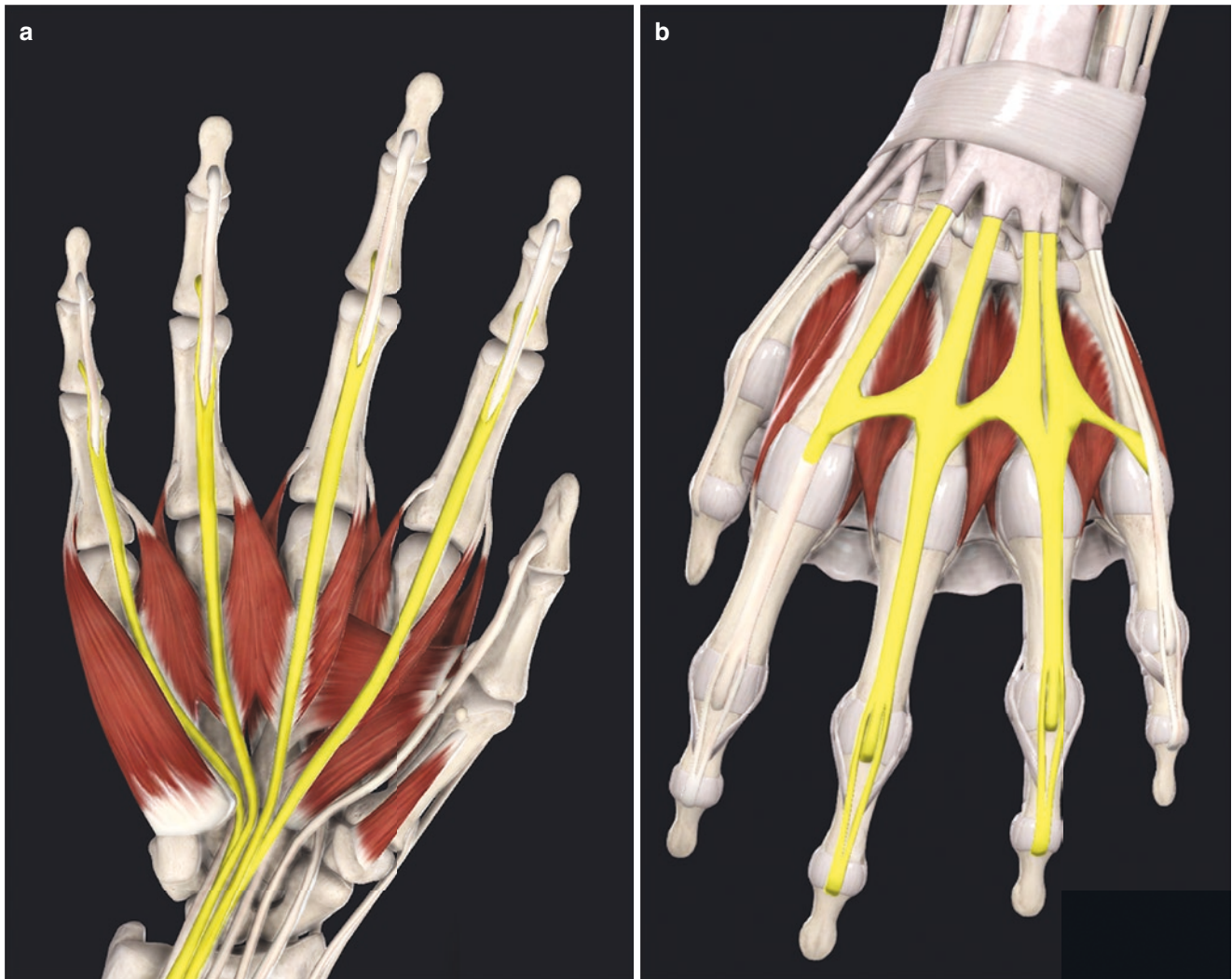
Fig. 4.13 Flexor (**a**) and extensor tendon (**b**) anatomy of the hand. Flexor digitorum superficialis (FDS) divides into two medial and lateral slips (yellow) and attaches to the base of the middle phalanx. Flexor digitorum profundus (FDP) attaches to the base of the distal phalanx.

The extensor hood forms a central slip, which attaches to the base of the middle phalanx, and two lateral bands join together to form a terminal tendon, which attaches to the base of distal phalanx

4.5   Ligaments and Capsular Injuries

Volar and dorsal plate injuries: The most commonly injured site is the volar plate of the PIP joints. A hyperextension injury may result in a ligament tear or an intra-articular avulsion fracture.

Collateral ligament injuries: Collateral ligaments have two components: main (proper) and accessory. Forced ulnar or radial deviation at any of the interphalangeal joints can cause collateral ligament tears, best detected by MRI.

Sagittal band injuries: Sagittal band rupture can be evaluated on axial slice T1-weighted or intermediate-weighted non-fat-suppressed images. Rupture of the sagittal band leads to medial or lateral dislocation of the extensor tendon at the level of the MCP joint.

Gamekeeper's thumb and Stener lesion: This is an avulsion or rupture of the ulnar collateral ligament of the thumb MCP joint. MRI plays a key role in differentiating a simple collateral ligament injury from a Stener lesion, which requires surgical treatment. In simple injury, the adductor pollicis aponeurosis remains superficial to the torn collateral ligament. In a Stener lesion (Fig. 4.17), the adductor pollicis aponeurosis is interposed between the torn end of the ulnar collateral ligament and the base of the proximal phalanx, interfering with the healing process and warranting a surgical intervention [12].

Injury to extrinsic and intrinsic carpal ligaments: Carpal ligaments (Fig. 4.18) play a vital role in stability of the wrist [13]. Carpal ligaments are classified as intrinsic (when only attached to carpal bones) and extrinsic (when
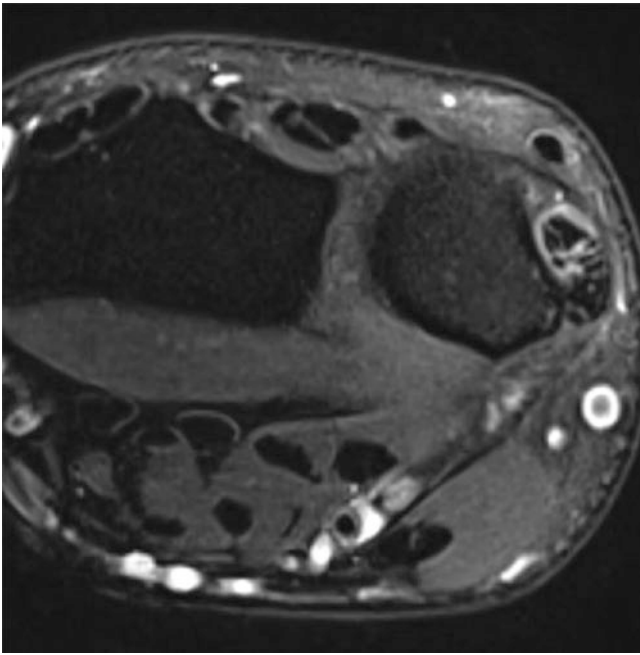
Fig. 4.14 Fluid-sensitive MRI images through the wrist demonstrate tendinosis and mild tenosynovitis of extensor carpi ulnaris with a superimposed partial thickness longitudinal tear
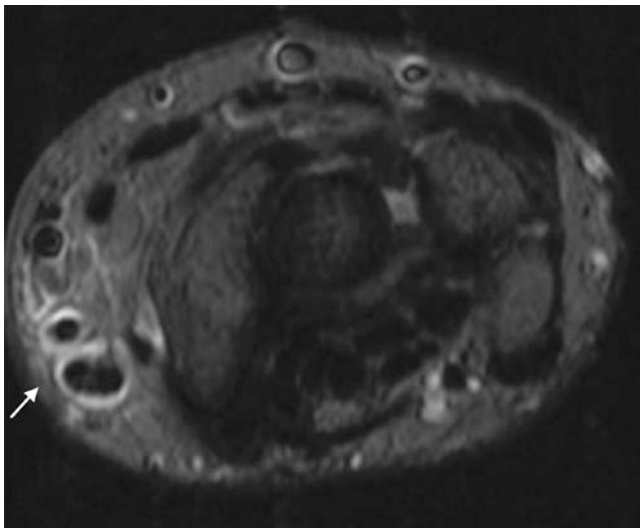
Fig. 4.15 Axial fluid-sensitive MR images demonstrate tenosynovitis of the first extensor compartment at the level of radial styloid process compatible with De Quervain's tenosynovitis

Fig. 4.16 Pulleys are fibrous structures which wrap around the flexor tendon sheaths of the digits to form a supporting fibro-osseous tunnel. Five such annular pulleys (A1–A5), together with three cruciate pulleys (C1–C3), form a fibro-osseous tunnel along each finger

attached to structures outside the carpus). Of the proximal interosseous ligaments, the scapholunate and lunotriquetral ligaments are the most important intrinsic carpal ligaments and are best assessed by MRI.

Scapholunate ligament injury: The scapholunate ligament is a U-shaped ligamentous complex with three compo-nents: dorsal, volar, and interosseous components. The dorsal component is the thickest component and is more commonly injured. Failure of this ligament results in rotary subluxation of the scaphoid, with volar rotation of the scaphoid and dor-sal rotation of the lunate (DISI instability as discussed above).

Lunotriquetral ligament injury: Lunotriquetral liga-ment is a U-shaped ligamentous complex with three compo-nents: dorsal, volar, and interosseous components. Volarly it blends with the ulnocarpal ligaments as part of the triangular fibrocartilage complex (TFCC). The volar component is the thickest component and is more commonly injured. Failure of this ligament results in volar rotation of the lunate (VISI instability as discussed above).

Fig. 4.17 Stener lesion. Coronal fluid-sensitive MRI images through the thumb demonstrate full-thickness tear of ulnar collateral ligament (white arrow) with the adductor pollicis aponeurosis interposed between the torn end of the ulnar collateral ligament and the base of the proximal phalanx (black arrow)
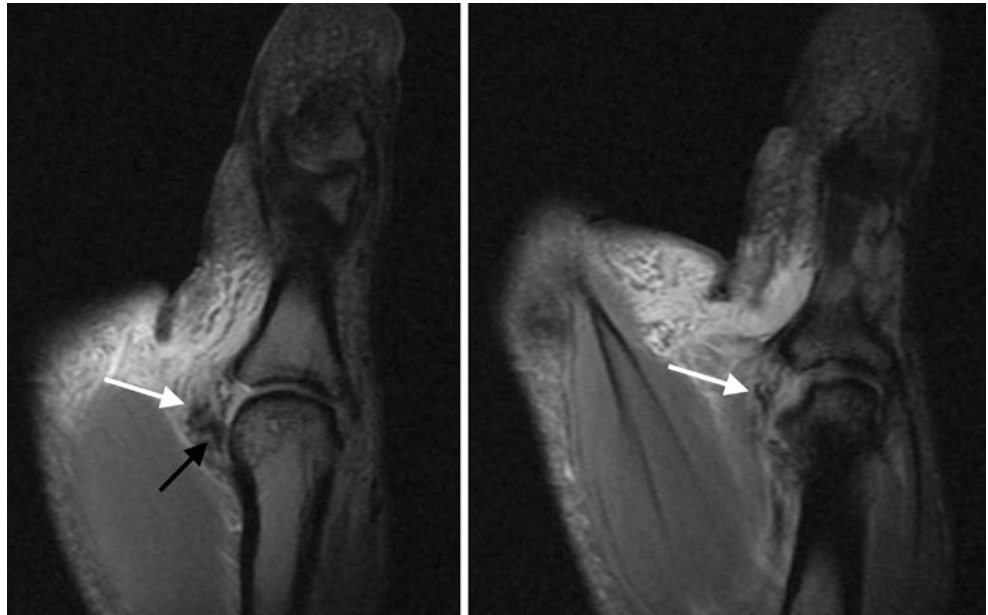
4.6 Miscellaneous Topics

Ulnar variance: Ulnar variance is measured in neutral wrist position on radiographs and refers to a relative distal projection of the distal ulnar articular surface with respect to the radius [14]. In a neutral variance wrist, approximately 80% of axial loading passes through the radius, and 20% passes through the ulna. A positive ulnar variance is associated with more axial loading through the ulna which results in ulnocarpal impaction and TFC wear and tear. A negative ulnar variance results in more axial loading through the radius to the lunate and scaphoid and may be associated with avascular necrosis of lunate.

Triangular fibrocartilage complex (TFCC) tear: TFCC is a complex structure (Fig. 4.19) with several components supporting a central triangular-shaped fibrocartilage, known as the TFC, or disk proper portion of TFCC. The TFC is attached dorsally and volarly to radioulnar ligaments supporting it on the sides like a hammock between the sigmoid notch and the ulnar styloid. The dorsal and volar radioulnar ligaments extend from the dorsal and volar edges of the ulnar styloid process to the dorsal and volar edges of the sigmoid notch of the distal radius, respectively. Dorsally, the dorsal radioulnar ligament blends with the ulnomeniscal homologue which extends ulnarly to form a meniscus-shaped styloid component. The styloid component extends distally and forms a collateral component which joins with the ulnar collateral ligament and ECU subsheath and attaches to triquetrum distally [15]. Dorsally, the dorsal radioulnar ligament, ulnomeniscal homologue, and ulnar collateral ligaments blend with the ECU subsheath. Volarly, the radiocarpal liga-

ment blends with the ulnocarpal ligaments. The TFC is attached to the ulna via two laminar attachment points which are in continuity with radioulnar ligaments: the proximal lamina, which connects to the fovea, and distal lamina which connects to the ulnar styloid. The fibers interposed between the proximal and distal lamina are referred to as the ligamentum subcruentum. Injuries to the TFCC have been described in the Palmer classification as traumatic or degenerative [16].

The blood supply for the TFC is from periphery to its central aspect. Therefore, its central aspect is most prone to degeneration and degenerative central perforation. The peripheral portion is more vascular and may repair following injury.

An acute TFCC injury may involve the TFC and any of the complex supporting components detailed above. Common patterns of acute TFCC injury include central perforation, peripheral or ulnar sided tear, distal tear or tear of ulnocarpal ligaments, and a radial disruption at sigmoid notch. TFCC tear is usually evaluated on coronal and sagittal fluid-sensitive pulse sequences of MRI.

A common pattern of chronic TFCC tear associated with degeneration is seen with ulnar impaction syndrome, as detailed below.

Ulnar impaction syndrome: Known as ulnar abutment or ulnocarpal impaction (Fig. 4.20), this syndrome results from impaction of the ulna on the proximal articular aspect of the lunate [17]. Etiologies include a positive ulnar variance associated with excessive axial loading. The spectrum of findings includes TFC complex wear and tear, lunotriquetral tear, ulnolunate cartilage disease, and ultimately secondary ulnocarpal degenerative joint disease.
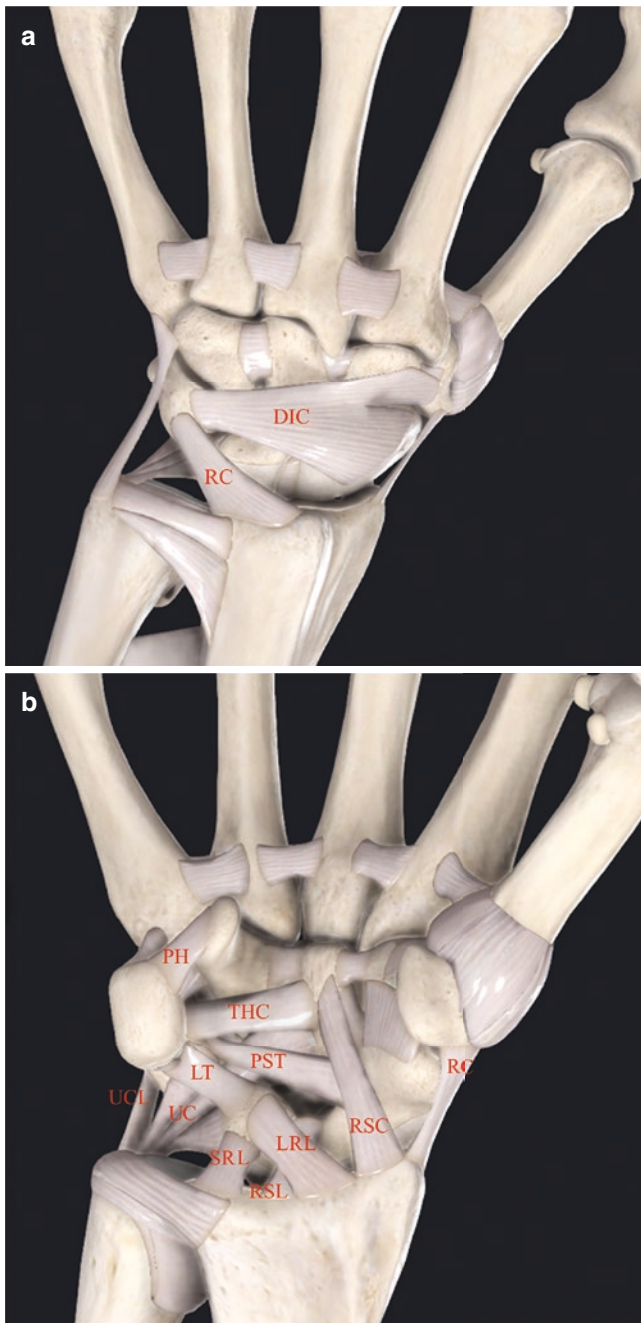
Fig. 4.18 Carpal ligaments. Major dorsal carpal ligaments (**a**) include dorsal intercarpal (DIC) ligament and dorsal radiocarpal ligament (DRC). Major volar carpal ligaments (**b**) include radioscaphocapitate (RSC), long radiolunate ligament (LRL) or radiolunotriquetral ligament, radioscapholunate (RSL), short radiolunate (SRL), and ulnocarpal (UC) ligaments. Triquetrohamocapitate (THC), radial collateral ligament (RC), ulnar collateral ligament (UCL), lunotriquetral (LT), palmar scaphotriquetral ligament (PST), and pisohamate (PH) are also demonstrated

Ulnar impingement syndrome: This syndrome results from a shortened distal ulna impinging on the distal radius proximal to the sigmoid notch, causing secondary degenera-

tive changes including surface remodeling, marginal osteophyte formation, and bone marrow edema [18]. Etiologies of this syndrome include negative ulnar variance, a madelung deformity, or surgical resection of the distal ulna.

Hamatolunate impaction: Secondary degenerative changes with chondral loss and subchondral bone marrow edema at the hamatolunate articulation occur in patients with type II lunate [19]. A type II lunate is the existence of a medial facet on the distal lunate for articulation with the hamate.

Avascular necrosis: Kienböck disease (Fig. 4.21) is the eponymous name given to avascular necrosis of the lunate. Post-traumatic avascular necrosis of the scaphoid is discussed above as well.

> **Key Point**
> - Ulnar variance should be assessed with wrist in neutral position. Positive and negative ulnar variance is associated with variation in the axial loading balance of the distal radius and ulna and may result in different conditions, including ulnar impingement, ulnar impaction, and TFCC wear.

4.6.1 Systemic Diseases

Many systemic diseases including rheumatologic conditions, inflammatory arthropathy, crystal arthropathy, and metabolic diseases demonstrate manifestations in the hands and wrists. Discussion of these entities is beyond the scope of this chapter. These disorders are associated with synovitis (Fig. 4.22) in the various compartments of the wrist as well as tenosynovitis (well depicted by MRI) and periarticular erosions, which lead to ligamentous injuries and various patterns of deformity, such as a SLAC wrist.

4.7 Concluding Remarks

This chapter reviews traumatic injuries of the hand and wrist, highlighting that chronic rheumatologic conditions can be associated with similar manifestations. Knowledge of anatomy is key to the diagnosis in wrist and hand imaging, and usually, a combination of different imaging modalities may be needed to effectively diagnose osseous and soft tissue injuries. Radiographs can show the overall alignment, margins at the matrix of osseous lesions, presence or absence of mineralization, and differentiation of ossific from calcific opacities, including avulsion fractures. Computed tomography can better assess radiographically occult fractures and
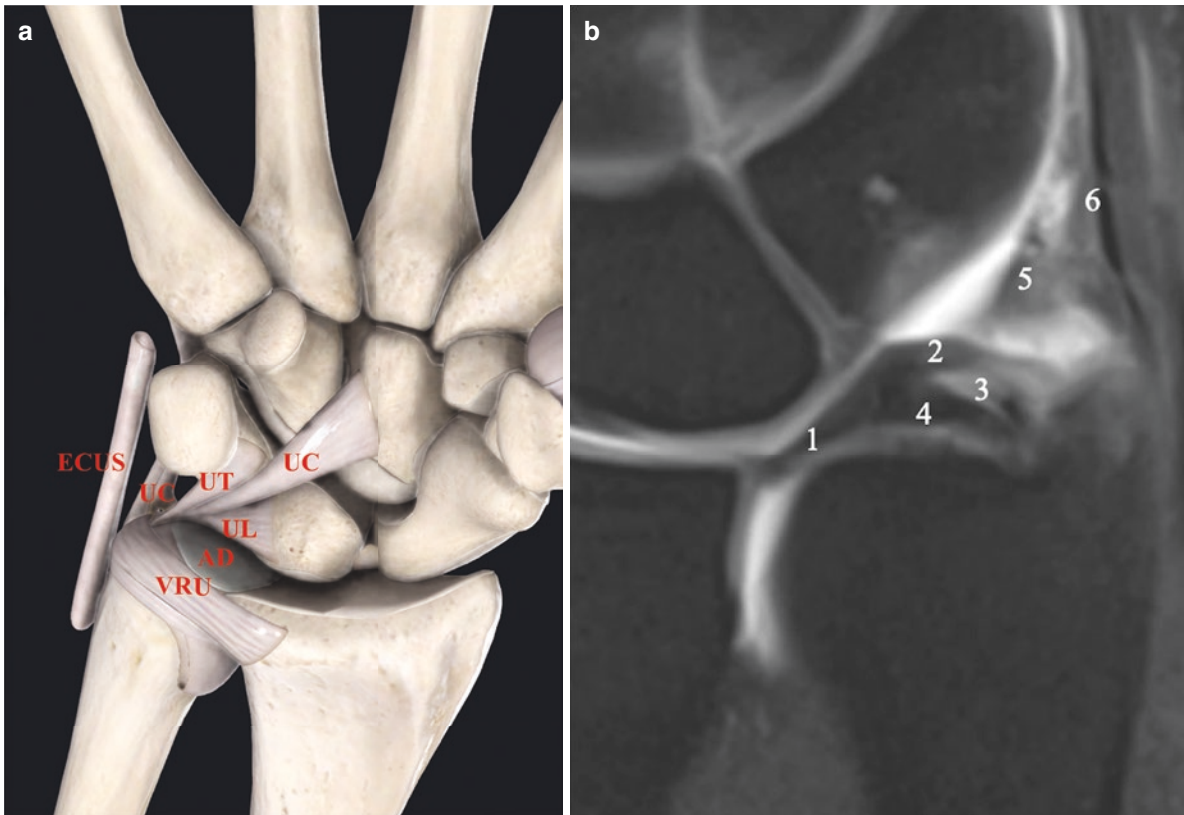
Fig. 4.19 Schematic (**a**) and coronal MR (**b**) images demonstrate some of the major components of the triangular fibrocartilage complex (TFCC), including articular disk (AD), volar radioulnar ligament (VRU), and ulnocarpal ligaments (UT, ulnotriquetral; UL, ulnolunate; and UC, ulnocapitate). Extensor carpi ulnaris subsheath (ECUS) and ulnar collateral ligament are also demonstrated. The numbers correspond to the following: (1) articular disc portion of TFCC; (2) proximal lamina; (3) ligamentum subcruentum; (4) distal lamina; (5) ulnomeniscal homologue; and [6] ulnar collateral ligament

Fig. 4.20 Coronal fluid-sensitive MR image demonstrates positive ulnar variance with associated degenerative central perforation of triangular fibrocartilage and subchondral cystic changes/bone marrow edema of the proximal articular aspect of lunate, compatible with ulnar abutment syndrome

show more details regarding bony alignment and the status of posttraumatic healing, osseous bridging, or complications related to fixation hardware. Magnetic resonance imaging best depicts the bone marrow signal and complex anatomy of the supporting soft tissue structures. And finally, ultrasound can add value as a method for real-time functional evaluation of the tendons and ligaments.

Take Home Messages
- Knowledge of wrist and hand anatomy is key to diagnosis. Some of the essential anatomic and clinical topics include topographic tendon anatomy of the wrist and hand, intrinsic and extrinsic carpal ligaments, collateral ligaments, triangular fibrocartilage complex, extensor mechanism, flexor tendon, and pulleys.
- Many systemic diseases including rheumatologic conditions, inflammatory arthropathy, crystal arthropathy, and metabolic diseases demonstrate manifestations in the hands and wrists. Differentiating an acute injury on a background of underlying disease may sometimes be challenging.

Fig. 4.21 Coronal MR images through the wrist demonstrate bone marrow edema-like signal and low signal sclerotic change involving the lunate compatible with avascular necrosis, Kienböck disease
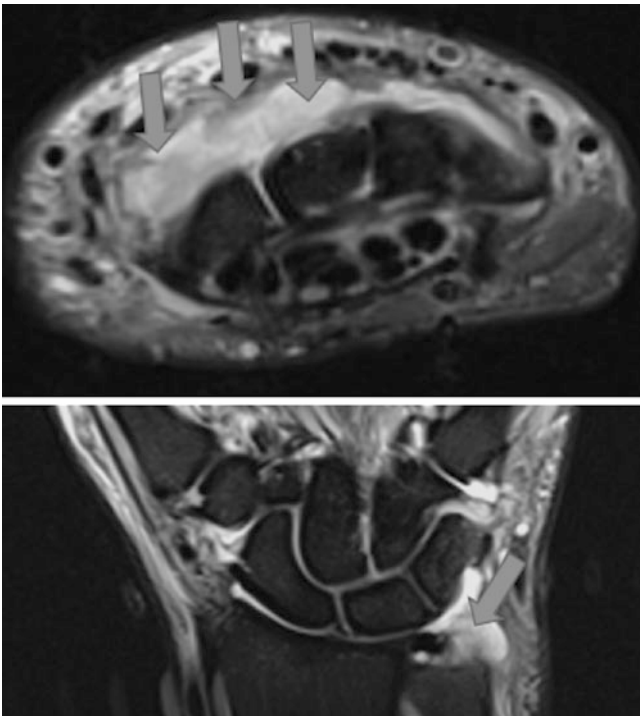
Fig. 4.22 Axial and coronal fluid-sensitive MR images demonstrate joint effusion and evidence of synovitis (arrows) involving the distal radioulnar joints and midcarpal joints compatible with inflammatory arthropathy

- Diagnosis is best made by a combination of imaging modalities, with radiography suited to defining alignment and osseous abnormalities. CT better depicts radiographically occult fractures, MRI best depicts the soft tissue support structures as well as abnormalities of the bone marrow, and ultrasound is suitable for a dynamic assessment of the tendons and ligaments.

References

1. Chang AL, Yu HJ, von Borstel D, Nozaki T, Horiuchi S, Terada Y, et al. Advanced imaging techniques of the wrist. Am J Roentgenol. 2017;209(3):497–510.
2. Taghinia AH, Talbot SG. Phalangeal and metacarpal fractures. Clin Plast Surg. 2019;46(3):415–23.
3. Lamaris GA, Matthew MK. The diagnosis and management of mallet finger injuries. Hand. 2017;12(3):223–8.
4. Elzinga KE, Chung KC. Finger injuries in football and rugby. Hand Clin. 2017;33(1):149–60.
5. Christie BM, Michelotti BF. Fractures of the carpal bones. Clin Plast Surg. 2019;46(3):469–77.
6. Scalcione LR, Gimber LH, Ho AM, Johnston SS, Sheppard JE, Taljanovic MS. Spectrum of carpal dislocations and fracture-dislocations: imaging and management. Am J Roentgenol. 2014;203(3):541–50.

7. Mayfield JK, Johnson RP, Kilcoyne RK. Carpal dislocations: pathomechanics and progressive perilunar instability. J Hand Surg Am. 1980;5(3):226–41.

8. Kani KK, Mulcahy H, Chew FS. Understanding carpal instability: a radiographic perspective. Skelet Radiol. 2016;45(8):1031–43.

9. Wright TW, Dobyns JH, Linscheid RL, Macksoud W, Siegert J. Carpal instability non-dissociative. J Hand Surg Br. 1994;19(6):763–73.

10. Saldana MJ. Trigger digits: diagnosis and treatment. J Am Acad Orthop Surg. 2001;9(4) Available from: https://pubmed.ncbi.nlm.nih.gov/11476534/

11. Adams JE, Habbu R. Tendinopathies of the hand and wrist. J Am Acad Orthop Surg. 2015;23(12):741–50.

12. Lark ME, Maroukis BL, Chung KC. The Stener lesion: historical perspective and evolution of diagnostic criteria. Hand. 2017;12(3):283–9.

13. Garcia-Elias M, Puig de la Bellacasa I, Schouten C. Carpal ligaments: a functional classification. Hand Clin. 2017 Aug;33(3):511–20.

14. Acott TR, Greenberg JA. Ulnar abutment syndrome in the athlete. Orthop Clin North Am. 2020;51(2):227–33.

15. Ko JH, Wiedrich TA. Triangular fibrocartilage complex injuries in the elite athlete. Hand Clin. 2012;28(3):307–21. viii

16. Kirchberger MC, Unglaub F, Mühldorfer-Fodor M, Pillukat T, Hahn P, Müller LP, et al. Update TFCC: histology and pathology, classification, examination and diagnostics. Arch Orthop Trauma Surg. 2015;135(3):427–37.

17. Tomaino MM, Elfar J. Ulnar impaction syndrome. Hand Clin. 2005;21(4):567–75.

18. Bell MJ, Hill RJ, McMurtry RY. Ulnar impingement syndrome. J Bone Joint Surg Br. 1985;67(1):126–9.

19. Cerezal L, del Piñal F, Abascal F, García-Valtuille R, Pereda T, Canga A. Imaging findings in ulnar-sided wrist impaction syndromes. Radiographics. 2002;22(1):105–21.

Imaging of the Hip

Reto Sutter and Donna G. Blankenbaker

Learning Objectives
- Understand different osseous pathologies of the hip joint.
- Know the key imaging findings of the different types of impingement of the hip joint.
- Explain typical patterns of intra-articular damage of the hip joint.

5.1 Introduction

In the last two decades, hip imaging has changed substantially. While hip joint damage was commonly evaluated in conditions such as developmental dysplasia of the hip or osteoarthritis, an additional condition for early onset hip osteoarthritis has been discovered since: femoroacetabular impingement (FAI). New biomechanical insights and improved techniques for hip preservation surgery have triggered the need for imaging evaluation of patients with suspected FAI [1].

Imaging technology has also changed quite a bit over these last two decades. Magnetic resonance imaging (MRI) sequences have become faster, and at the same time, the image resolution is much better than at the turn of the century, allowing for a more accurate evaluation of labrum and cartilage. And computed tomography (CT) datasets are now increasingly being used for preoperative 3D planning, e.g., with the use of patient-specific instruments modeled to the individual anatomical deformity.

R. Sutter (✉)
Department of Radiology, Balgrist University Hospital, University of Zurich, Zurich, Switzerland
e-mail: Reto.sutter@balgrist.ch

D. G. Blankenbaker
Musculoskeletal Imaging & Intervention, University of Wisconsin School of Medicine and Public Health, Madison, WI, USA
e-mail: dblankenbaker@uwhealth.org

5.2 Imaging Evaluation

The radiographic examination is a critical component in the diagnostic evaluation and treatment decision-making process and considered the first-line imaging technique in the evaluation of hip pain. Anteroposterior view of the pelvis is standard, and dedicated views of the symptomatic hip are often performed in the athletic hip which include cross-table lateral, frog-leg lateral, or Dunn lateral. According to the American College of Radiology Musculoskeletal Imaging Criteria [2], MRI is the next appropriate imaging method in those individuals with negative radiographs. For symptoms of generalized pain or nonspecific physical exam findings, imaging is best performed with conventional MRI of the pelvis and hip. If symptoms or clinical exam findings suggest intra-articular pathology, dedicated small field-of-view (FOV) MR arthrography of the hip is considered the imaging method of choice. Recently, high-resolution conventional MR imaging is replacing MR arthrography at many centers.

5.3 Osseous Disease

5.3.1 Stress Fractures

Stress injuries are due to a mismatch between native bone strength and chronic mechanical load applied on bone over time [3]. However, because stress injuries may progress to complete fracture and result in prolonged recovery or career-ending complications, it is imperative to identify these injuries early. Stress injuries are most commonly seen in endurance athletes, such as runners and military recruits, as well as recreational athletes with sudden increase in activity [4]. Stress fractures are classified as fatigue, resulting from normal bone being subjected to abnormal repetitive forces, and insufficiency, due to normal stress placed on abnormal bone [3].

The repetitive overloading stimulates bone remodeling, beginning with osteoclastic activity that is not matched by reparative osteoblastic activity and periosteal maturation, which lag 10–14 and 20 days, respectively. This causes temporary weakening of the marrow and cortical bone, leading to microtrabecular fractures (stress reaction) and cortical failure (stress fracture). Radiographs are not very sensitive in the identification of stress injuries of the femoral neck. Classic MRI features include ill-defined focal or diffuse high T2 bone marrow signal due to microtrabecular fractures and intramedullary edema, with or without corresponding low T1 signal and/or periosteal edema (Fig. 5.1). With any of these findings, one should carefully evaluate for a hypointense band in the marrow or focal cortical abnormality, indicating stress fracture and necessitating prolonged non-weight-bearing or rest from sporting activity. Because of the severe consequences of undiagnosed femoral neck stress fractures, the diagnosis is based on combined imaging findings of periosteal edema, endosteal edema, and high cortical signal, regardless of visible fracture line [4].

5.3.2 Osteonecrosis

Femoral head osteonecrosis (ON) is a common disease and potentially disabling disorder affecting mainly middle-aged adults that can lead to early osteoarthritis due to femoral head collapse and joint incongruity. It is estimated that the rate of symptomatic femoral head ON is 2–4.5 cases per

Fig. 5.1 Coronal T2 fat-suppressed MR image in a 40-year-old runner with hip pain shows edema along the medial femoral cortex and endosteal edema representing a stress fracture (arrow)

patient year, resulting in 10,000–20,000 new cases annually in the United States. However, this incidence markedly underestimates the true prevalence of ON, as the majority of patients are asymptomatic [5]. Various conditions have been associated with the development of ON, with idiopathic causes, trauma, corticosteroid use, and alcohol consumption implicated in most cases. Other causes include metabolic and hematologic disorders, marrow storage disorders, pancreatitis, radiation, drug therapy, occlusive vascular disease, infection, renal disease, Caisson disease, and rheumatologic conditions [5].

The initial phase of ON is cell death, interruption of cell enzymes, and loss of cell metabolic activity. The next pathologic phases represent a continuum of development of a reactive interface in an attempt to wall off and repair the area of ON. Over time, the reactive interface continues to develop and mature as a discrete zone at the margin of the area of ON. This reactive interface zone is essentially a vascularized granulation tissue attempting to repair the area of ON. Within the epiphysis, the junction of the reactive zone with the articular subchondral bone plate undergoes increased bone resorption which can lead to early fracture of the overlying cartilage at these locations and subsequent subchondral fracture. This is often the earliest manifestation of an impending articular collapse [6, 7]. Progressive fragmentation of the articular surface and secondary osteoarthritis are almost inevitable due to cortical flattening and collapse.

Diagnosis of femoral head ON depends on the combination of clinical symptoms and evaluation of radiographs and/or MRI (Fig. 5.2). Imaging has an important role in ON evaluation, allowing early detection, assessment of severity and prognosis, treatment options, and postoperative follow-up [7]. Radiographs are the initial imaging method in the evaluation of the patient with hip pain, however, are insensitive for early changes of ON [6]. In late stage ON, the radiographic features are often characteristic and usually do not require further imaging workup. At initial stages, nonspecific patchy areas of lucency and sclerosis can be identified on radiographs. As the disease progresses, a subchondral fracture with a crescentic appearance (crescent sign) may be visualized. Eventually this will lead to articular surface collapse and development of secondary osteoarthritis [6].

MR imaging is the most sensitive method for detecting early ON. There are two conditions involving the femoral head that can mimic ON leading to misdiagnosis and require imaging distinction: bone marrow edema syndrome (transient osteoporosis of the hip) and subchondral insufficiency fracture. A missed diagnosis and delay in appropriate treatment may result in disease progression and significant morbidity. Therefore, extra care in differentiating this process from other causes of femoral head or neck edema is important.
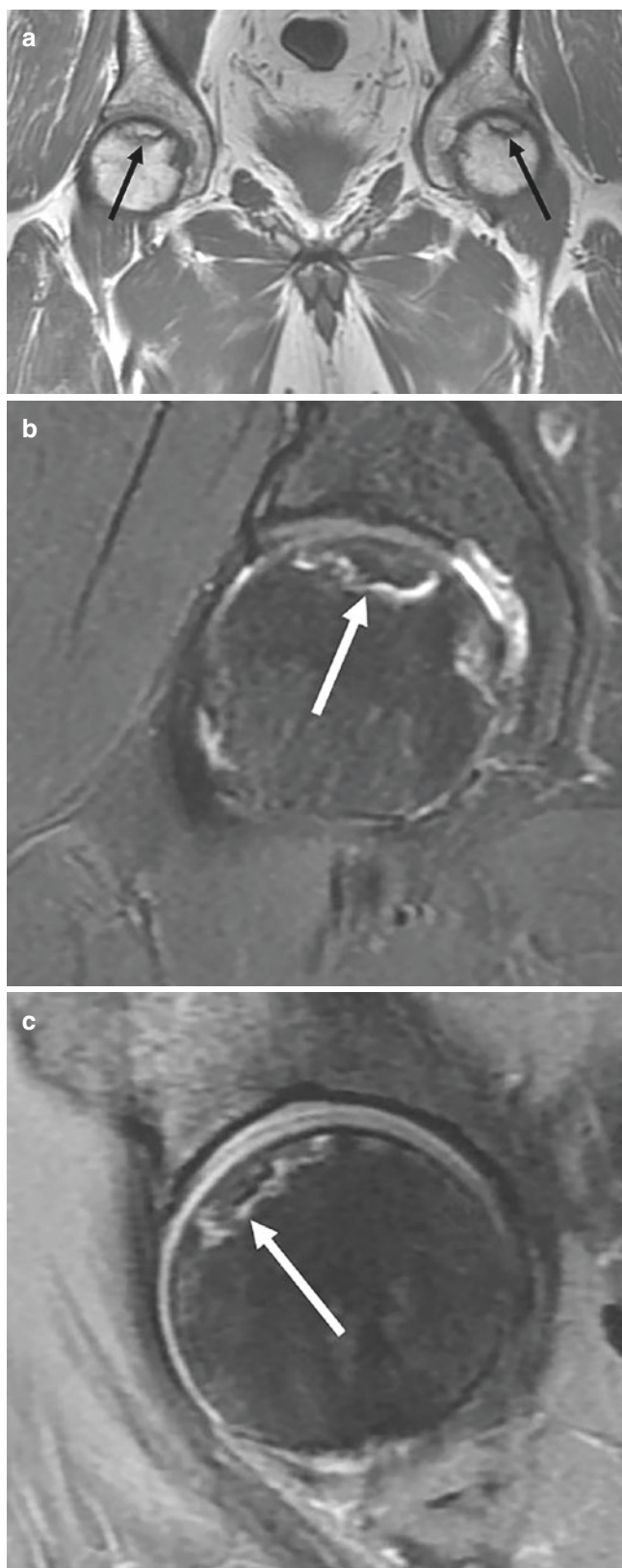
Fig. 5.2 Coronal T1 (**a**) MR shows bilateral femoral head serpentine low signal foci representing osteonecrosis in this 61-year-old man (arrows). Small field-of-view coronal T2 fat-suppressed (**b**) and sagittal PD fat-suppressed (**c**) images show the amount of involvement of the femoral head (arrows)

The MR appearance of ON is most commonly described as a geographic subchondral bone marrow signal abnormality, including band-like or linear T1 hypointensity representing the demarcation/transition zone [8]. The "double line sign" on T2-weighted images, described as a low-intensity outer rim with inner rim of hyperintense granulation tissue, is pathognomonic for this process [9]. Subchondral collapse, which is often underestimated on MR imaging, is not seen until late in the disease process and is a sign of poor prognosis. The continuous linear low signal abnormality with generally convex contour helps differentiate this entity from femoral head insufficiency fractures. Bone marrow edema is found with higher stages of ON and not considered an early finding [10]. The late stage imaging findings include edema around the transition zone, edema and/or sclerosis in the necrotic zone, subchondral fractures, collapse, and osteoarthritis. The edema has been shown to correlate with pain and more likely to progress to collapse [11].

Various staging systems have been developed for assessment of adult femoral head ON [12, 13]. All of these staging systems have in common progression from radiologically occult disease to positive imaging findings of ON to femoral head collapse and finally development of secondary osteoarthritis. The clinical significance of epiphyseal ON is almost entirely dependent on articular surface collapse [5]. The femoral head volume that is involved by ON appears to be the most important imaging predictor of subsequent articular collapse. ON affecting more than 25–50% of the femoral head is more likely to progress to articular collapse, while femoral head ON involving less than 25–30% of the femoral head is unlikely to progress to articular surface collapse [5].

5.3.3 Subchondral Insufficiency Fracture

Subchondral insufficiency fractures (SIF) of the femoral head are a cause of marked mechanical hip pain and typically occur in the older, osteoporotic population. These fractures may progress to advanced collapse and therefore should be recognized on imaging and distinguished from osteonecrosis [6]. The MR imaging findings of SIF are that of a low signal subchondral line that parallels the articular surface and extensive bone marrow edema of the femoral head/neck (Fig. 5.3). The presence of the typical band of low signal intensity in the subchondral bone, convex to the articular surface, has been suggested as specific for an insufficiency fracture, distinguishing it from the well-defined zonal pattern of signal abnormality found in osteonecrosis. Additionally, contrast-enhanced MR imaging may be helpful to distinguish SIF from osteonecrosis where hips with SIF will enhance proximal to the low signal intensity band in the femoral head, while osteonecrosis does not enhance proximally [14].
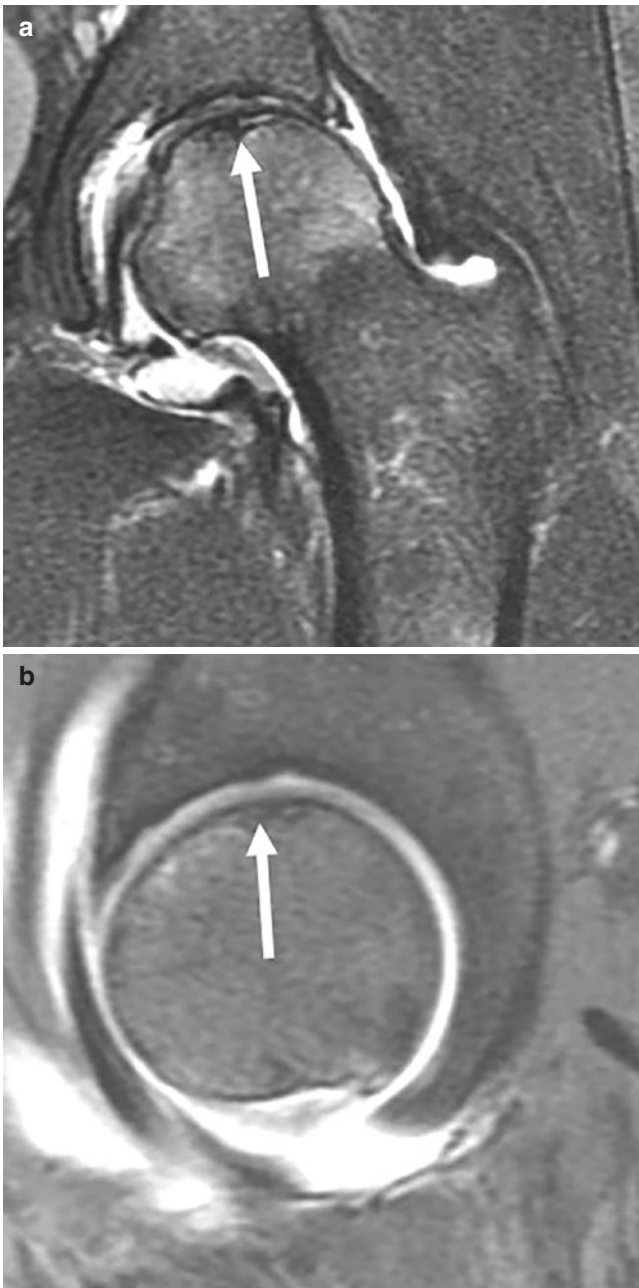
Fig. 5.3 Coronal T2 fat-suppressed (**a**) and sagittal PD fat-suppressed (**b**) MR images in a 51-year-old woman demonstrates subchondral insufficiency fracture (arrows). A subchondral linear band of low signal is present beneath the femoral head with surrounding bone marrow edema

5.3.4 Bone Marrow Edema Syndrome

The term transient bone marrow edema syndrome describes two clinical entities, transient osteoporosis of the hip (TOH) and regional migratory osteoporosis (RMO). Many consider this to be a "transient painful marrow edema." These conditions have basic characteristics which include sudden onset of pain in middle-aged men and in pregnant/post-partum
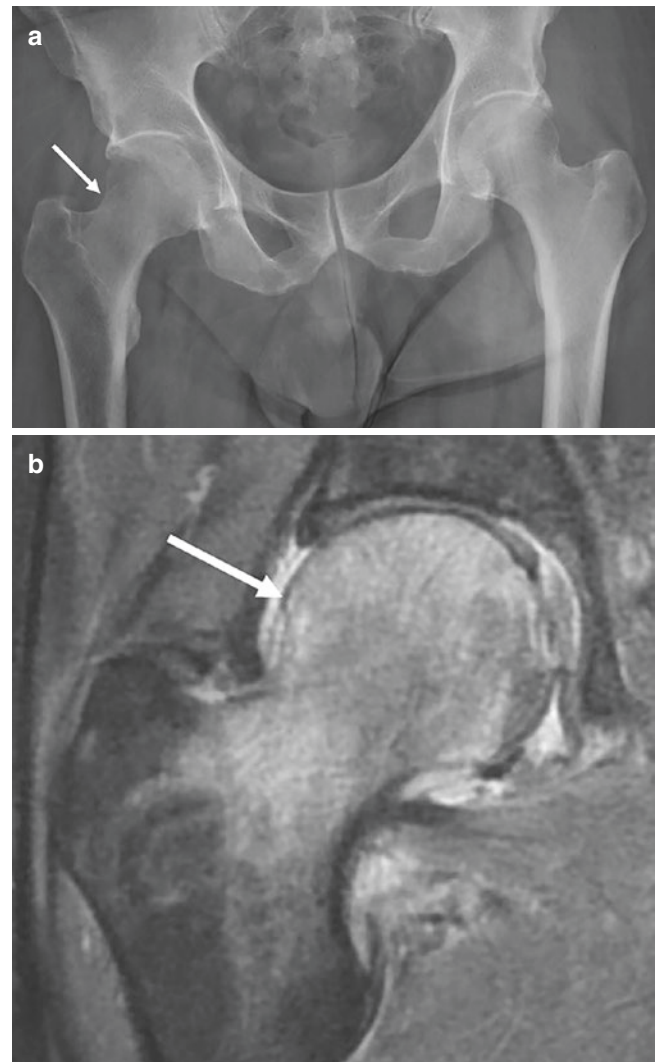
Fig. 5.4 Anteroposterior radiograph (**a**) of the pelvis in a 52-year-old man shows lucency of the right femoral head/neck (arrow). Coronal T2 fat-suppressed MR image (**b**) shows diffuse bone marrow edema within the femoral head/neck (arrow). There is no subchondral fracture line or findings of osteonecrosis

women, spontaneous with gradual resolution of symptoms with conservative treatment (6–8 months), and presence of bone marrow edema on MRI [6]. This is typically a unilateral process but, however, can involve the contralateral side. Radiographs may show severe osteopenia of the proximal femur and require at least 5 weeks from the onset of symptoms to become evident [15]. The MR imaging findings include bone marrow edema within the femoral head/neck and hip joint effusion (Fig. 5.4). There should not be a double line or demarcation sign as seen with osteonecrosis or subchondral changes. Insufficiency fractures may occur. Our recommendation is if you see diffuse edema on MR within the femoral head/neck, the patient may be vulnerable to insufficiency fracture. If a fracture line is present, just describe this as an insufficiency fracture.

5.4 Hip Impingement

There are several types of intra- and extraarticular impingement of the hip. While this chapter covers femoroacetabular impingement (FAI), abnormal femoral torsion, and subspine impingement, other types of extraarticular impingement exist, such as ischiofemoral impingement, greater trochanter impingement, or impingement due to extreme hip motion, such as in ballet dancers or kickboxers [16].

5.4.1 Biomechanical Concepts

Femoroacetabular impingement (FAI) is typically seen in young and athletic individuals who report hip or groin pain and present with reduced internal rotation of the hip joint [17]. At imaging there are two well-recognized osseous hallmarks of FAI: the cam deformity at the head-neck junction of the femur is the first hallmark (Fig. 5.5), and the second is an increased osseous coverage of the acetabulum known as pincer deformity, either due to a generally increased coverage or due to focal retroversion of the upper portion of the acetabulum. If these osseous deformities are present, a mechanical conflict may occur during internal rotation, with an increased mechanical impact between the proximal femur and the acetabular bone and subsequent damage to the acetabular labrum and to the articular cartilage of the hip.

There is however a third major osseous factor in the pathogenesis of FAI: femoral torsion, also termed femoral version, is the angle between the orientation of the femoral head and neck proximally versus the orientation of the femoral condyles distally, at the level of the knee. While increased femoral antetorsion has long been recognized as a part of the osseous deformities in developmental dysplasia of the hip, the discovery that abnormal femoral torsion plays a substantial role in the development of FAI is much more recent [18].

The three major osseous factors for the development of FAI are often seen in combination and not as isolated entities [19]. When evaluated individually, the literature shows that the risk of subsequent hip osteoarthritis is highest in the presence of a cam deformity, while this association is less well established for isolated pincer deformities and abnormal femoral antetorsion [1].

Key Point
- The three major osseous factors in the pathogenesis of femoroacetabular impingement (FAI) are the cam deformity, pincer deformity, and abnormal femoral antetorsion.
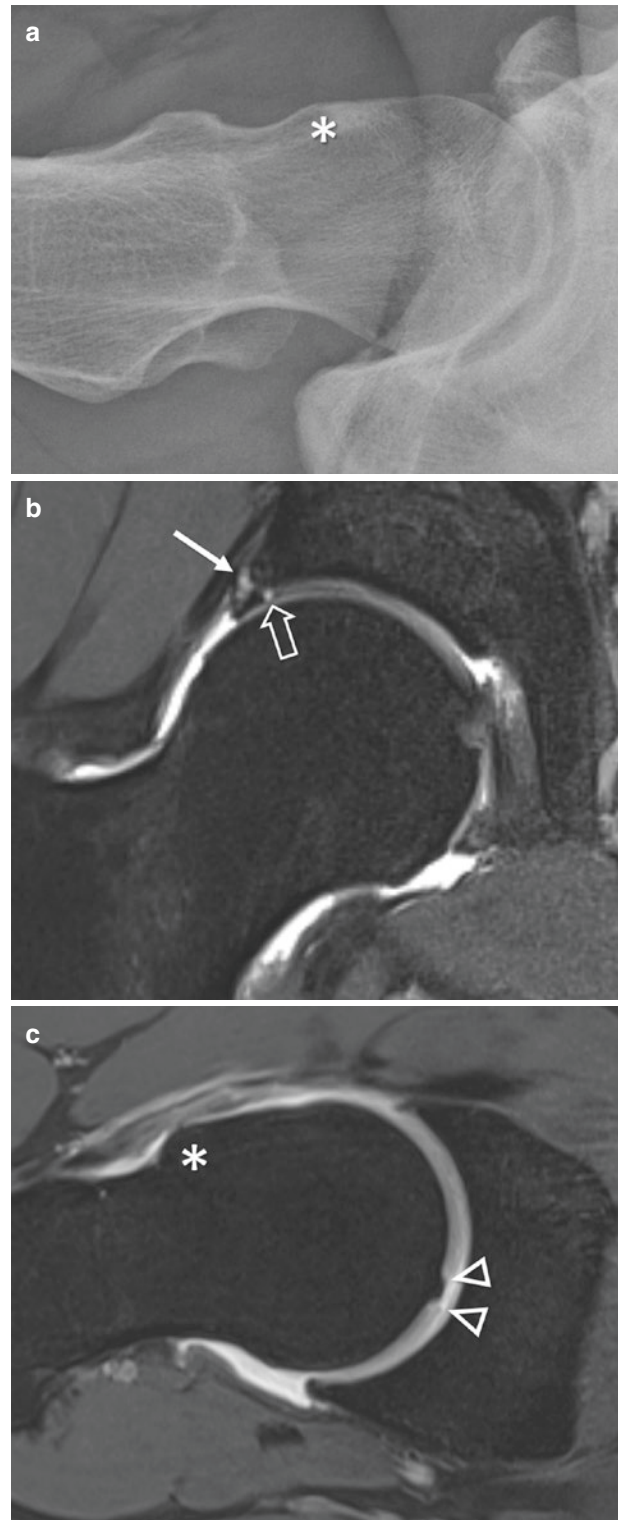
Fig. 5.5 Cross-table lateral radiograph (**a**) of the right hip in a 32-year old male competitive fencer with femoroacetabular impingement showing a large anterior cam deformity (asterisk). Coronal PD fat-suppressed (**b**) MR image demonstrates full-thickness labral tear with intra-substance ganglion (thin arrow) and adjacent peripheral defect of acetabular cartilage (outline arrow). Oblique axial T2 fat-suppressed (**c**) MR image shows an intra-cartilaginous osteophyte and adjacent central cartilage defects of the femur (arrowheads) as well as the cam deformity (asterisk)

5.4.2 Imaging Evaluation of FAI

After clinical examination, patients with suspected FAI are evaluated with radiographs as the first step of the imaging workup. On standard anteroposterior pelvic radiographs, the osseous coverage of the acetabulum is assessed, in order to detect the presence of a pincer morphology of the hip joint. A general increase of acetabular coverage is indicated by an increased lateral center edge (LCE) angle. An LCE angle of more than 40° indicates a deep acetabulum or coxa profunda. Alternatively, the depth of the acetabulum can be assessed visually, by identifying the presence or absence of an intersection between the acetabular fossa and the ilioischial line [20].

Apart from a generally increased osseous coverage, the orientation of the acetabulum can also be abnormal: if the acetabulum is retroverted, this results in an increased mechanical conflict between the femur and the acetabulum during internal rotation. Typically, it is the upper portion of the acetabulum where this retroversion occurs, which can be readily assessed on anteroposterior pelvic radiographs. The following three signs are indicative of acetabular retroversion: the crossover sign (or figure-of-eight sign), the posterior wall sign, and the ischial spine sign. While both the quantitative and qualitative assessment of pincer deformities on radiographs are easy to perform, it is important to know that to some degree these osseous deformities can also be detected in asymptomatic individuals. While the radiographic evaluation is an important part of the assessment of patients with FAI, there is no clear threshold that reliably allows identifying patients with pincer-type FAI [20].

Some cam deformities can be seen on radiographs, but typically MRI or CT with radial reformations is needed for the detection and assessment of cam deformities, especially in the location where they most commonly occur, the anterosuperior aspect of the femur. Over the years, many measurements have been proposed to assess cam-type deformities, such as the alpha-angle, femoral offset, and femoral distance measurements. The best-known measurement is the alpha-angle, which was introduced 20 years ago for assessing cam deformities at the anterior location of the femoral head. The initially proposed threshold for the alpha-angle was 55°, but later data showed that in a clinical setting, this results in a substantial number of false-positive cases [21, 22]. Raising the threshold to 60° or an even higher value reduces the rate of false positives but also substantially reduces the sensitivity of the measurement, as there is a large overlap in the presence of osseous deformities between asymptomatic healthy individuals and patients with FAI. There is no clear threshold that reliably allows identifying patients with cam-type FAI.

5.4.3 Assessing Joint Damage in FAI

An important part of the imaging evaluation in patients with suspected FAI is the assessment of any damage to the labrum and articular cartilage, which is described later in this chapter. Importantly, the assessment of joint damage allows accurate preoperative planning in those patients that need surgery. Moreover, in patients scheduled for surgery, the assessment of joint damage allows the stratification of patients into those with only minor and peripheral joint damage – these individuals can expect a good long-term outcome after arthroscopic surgery. Patients with more central lesions of the articular cartilage or widespread joint damage may choose to undergo surgery for pain relief, but the surgical procedure will not allow to prevent or delay osteoarthritis in those patients [1].

5.4.4 FAI Treatment

Exercise therapy is considered a good first option in patients with symptomatic FAI, with half of patients benefiting from a 12-week regimen of progressive exercise therapy. However, exercise therapy usually is not successful in patients with severe cam deformities, and in those patients, surgery is often advised [23]. Surgical treatment of symptomatic patients with FAI has a good success rate, with 80% of all patients reporting a good outcome and with a high rate of return to sport for professional athletes: in a recent meta-analysis, 94% of professional athletes returned to sports after arthroscopic hip surgery [17]. Those professional athletes with a shorter duration of symptoms before surgery had a significantly higher rate of return to sports than those with long-standing preoperative symptoms. The rate of conversion to hip arthroplasty after previous FAI surgery is 10% at 10-year follow-up, and patients with labral reattachment show a better clinical outcome than patients with a resected labrum, but without a difference in progression of osteoarthritis or conversion to hip arthroplasty [24].

5.4.5 Femoral Torsion

Decreased femoral antetorsion results in an additional mechanical impaction during internal rotation of the hip, worsening the symptoms of FAI patients with a cam or pincer deformity [18]. Femoral antetorsion tends to be lower in patients with cam-type FAI, but the range of femoral torsion seen in patients with FAI is large, with an average femoral torsion of 13° and a normal range of 4°–20°. Consequently, in some patients femoral torsion plays an important role in the development of FAI, while in other patients this factor is
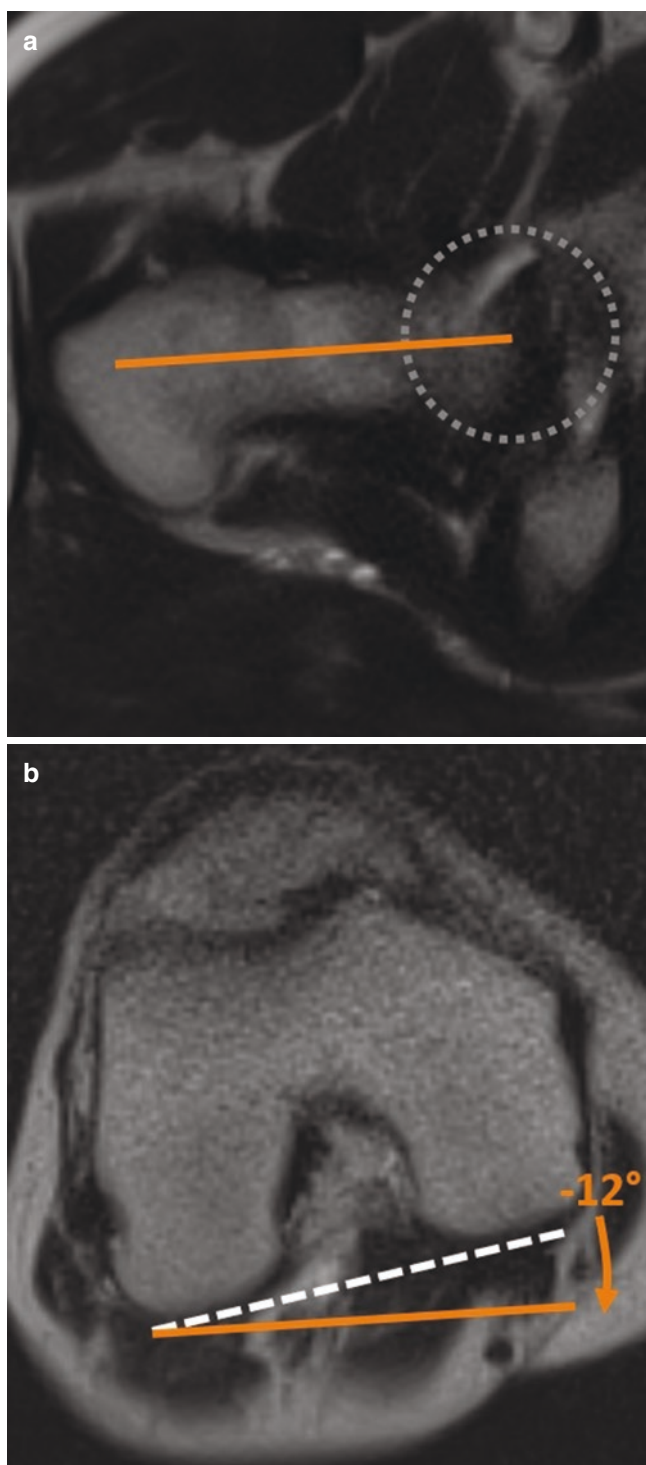
Fig. 5.6 Femoral retrotorsion in a 33-year-old man with hip pain. Axial T2 MR images over the proximal (**a**) and distal (**b**) femur show that the femoral neck axis (orange line in **a**) is oriented in 12° retroversion compared to the tangent at the femoral condyles (dashed white line in **b**). No cam or pincer deformities were seen in this patient

not relevant. On the other hand, abnormal femoral torsion (Fig. 5.6) can also cause symptoms in patients without cam or pincer deformities [16].

Femoral torsion needs to be measured at CT or MRI, because the clinical assessment of femoral torsion is notoriously unreliable [25]. Both CT and MRI are feasible for measuring femoral torsion, with MRI being the favored imaging method due to the lack of radiation.

> **Key Point**
> - Decreased femoral antetorsion results in increased mechanical impact during internal rotation of the hip, while increased femoral antetorsion can result in posterior extraarticular impingement.

Several reproducible measurement methods have been described, and it is advisable to use a consistent method that is both accepted by the radiologists and the surgeons or sport physicians treating the patient. Care should be taken however to employ only strictly axial images for femoral torsion measurements, as the use of axial oblique images results in divergent measurements [26]. While in most patients decreased femoral torsion is associated with reduced range of motion due to intra-articular impingement, in about a third of patients, reduced femoral torsion is associated with subspine impingement [27].

In FAI patients with abnormal femoral torsion, often the surgical removal of the cam deformity and acetabular rim trimming increase the range of motion of the hip joint sufficiently to also compensate for the abnormal femoral torsion. In patients with severe torsional abnormalities, or in patients with abnormal femoral torsion without concomitant FAI, a de-rotation osteotomy of the femur can be performed to normalize femoral torsion.

5.4.6 Subspine Impingement

Before the closure of the apophysis at the anterior inferior iliac spine (AIIS), apophyseal avulsion may occur in young athletes with repeated heavy loads on the hip such as soccer players (Fig. 5.7). Specifically, it is the origin of the rectus femoris tendon at the AIIS that is affected, either due to a single traumatic injury or due to repeated traction injuries [28].

The AIIS is typically enlarged in these patients, with a prominent osseous protrusion at the origin of the rectus femoris tendon. There is mechanical impaction between the AIIS and the proximal femur in these patients during hip flexion, and the disorder has been termed subspine impingement due to the impingement of soft tissues between the anterior inferior iliac spine and the femoral neck.

The apophyseal injuries of the AIIS typically affect adolescents, but the sequelae can persist into adulthood, as is
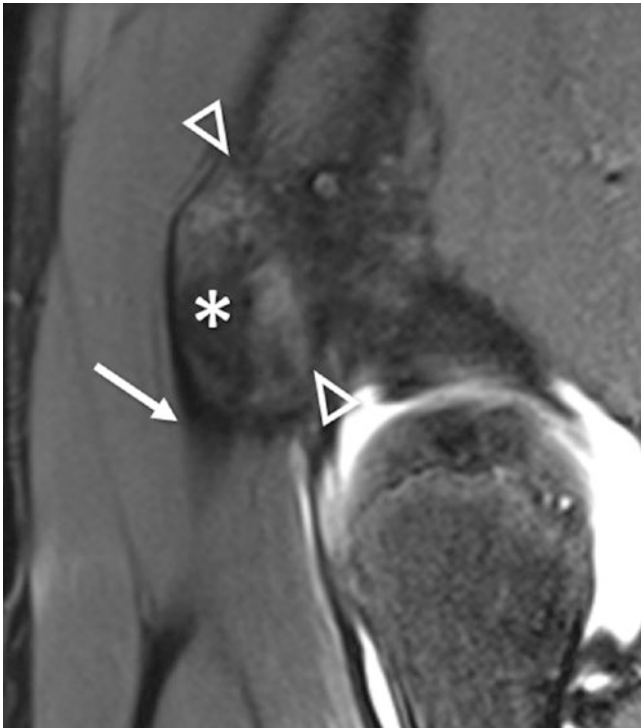
Fig. 5.7 Subspine impingement in a 14-year-old female soccer player with previous apophyseal avulsion. Sagittal PD fat-suppressed MRI shows widened and irregular aphophyseal gap (arrowheads) and displacement and enlargement of the anterior inferior iliac spine (asterisk). Note origin of the rectus femoris tendon (arrow)

evident in a recent report of patients who were surgically treated for subspine impingement at an average age of 43 years [29]. However, most patients respond well to conservative treatment.

> **Key Point**
> - Subspine impingement is a mechanical impaction between an enlarged anterior inferior iliac spine (AIIS) and the anterior aspect of the femoral neck in patients with previous apophyseal avulsion injury of the rectus femoris tendon.

Subspine impingement is often seen in patients who also suffer from FAI, possibly because both disorders are more commonly seen in athletes involved in high-level sports at a young age, just before the closure of the growth plates [30]. In adolescents, a widened and irregular growth plate may be seen at imaging, with adjacent bone marrow edema at MRI. In adult patients with long-standing subspine impingement, imaging signs in addition to an enlarged AIIS may include an osseous bump at the distal femoral neck and superior capsular edema adjacent to the AIIS. A distal location of

a cam deformity at the anterior aspect of the femoral neck is an independent risk factor for symptomatic subspine impingement [29].

5.5 Intra-articular Damage

5.5.1 Acetabular Labrum

The acetabular labrum is a fibrocartilaginous structure attached to the rim of the bony acetabulum. The transverse ligament creates a complete ring inferiorly, attaching to the anterior and posterior margins of the inferior labrum. Despite a limited vascular supply, there is an ample network of nerve endings with nociceptive and proprioceptive functions, explaining why labral tears may be painful [31]. The labrum is thought to increase stability at the hip joint, deepening the acetabulum which helps to resist lateral and vertical translation for the femoral head. The labrum also provides a seal for the joint, enhancing fluid lubrication, maintaining synovial fluid pressure, and preventing direct contact of the joint surfaces.

The shape of the labrum is triangular in the majority of individuals with the base attached to the bony acetabulum and acetabular cartilage [32], although it can have a rounded or irregular configuration. These variations from the expected triangular shape have been correlated with increasing age, suggesting typical degeneration. Labral hypoplasia or absence is described by some as a normal phenomenon, reportedly found in 1–10% of the population [32]. In general, however, absence of the labrum is more commonly seen in older individuals and is considered abnormal, likely due to degeneration or a chronic tear. The MR appearance of the normal labrum is triangular in morphology and hypointense on all pulse sequences. A normal transition zone of 1–3 mm between the labrum fibrocartilage and adjacent articular hyaline cartilage is important to recognize in MR interpretation so as not to confuse the appearance for a labral tear [33].

The etiology of labral tears includes trauma (posterior dislocation, twisting injury), underlying bony abnormality (hip dysplasia or FAI morphology), anterior capsule laxity, and idiopathic or age-related tears. Of these, the most important in athletes is the presence of FAI morphology. The relationship between FAI morphology and labral tears has been well documented in studies of many athletes, including rowers, football players, and dancers [34]. Thus, labral pathology should be considered in any athlete with radiographic bony morphologic abnormalities.

There are several surgical and MR-based classifications for description of labrum tears that have been proposed [33, 35]. Due to the lack of agreement between these classifications, the imaging assessment should instead focus on an accurate descriptive report including tears, size (extent),
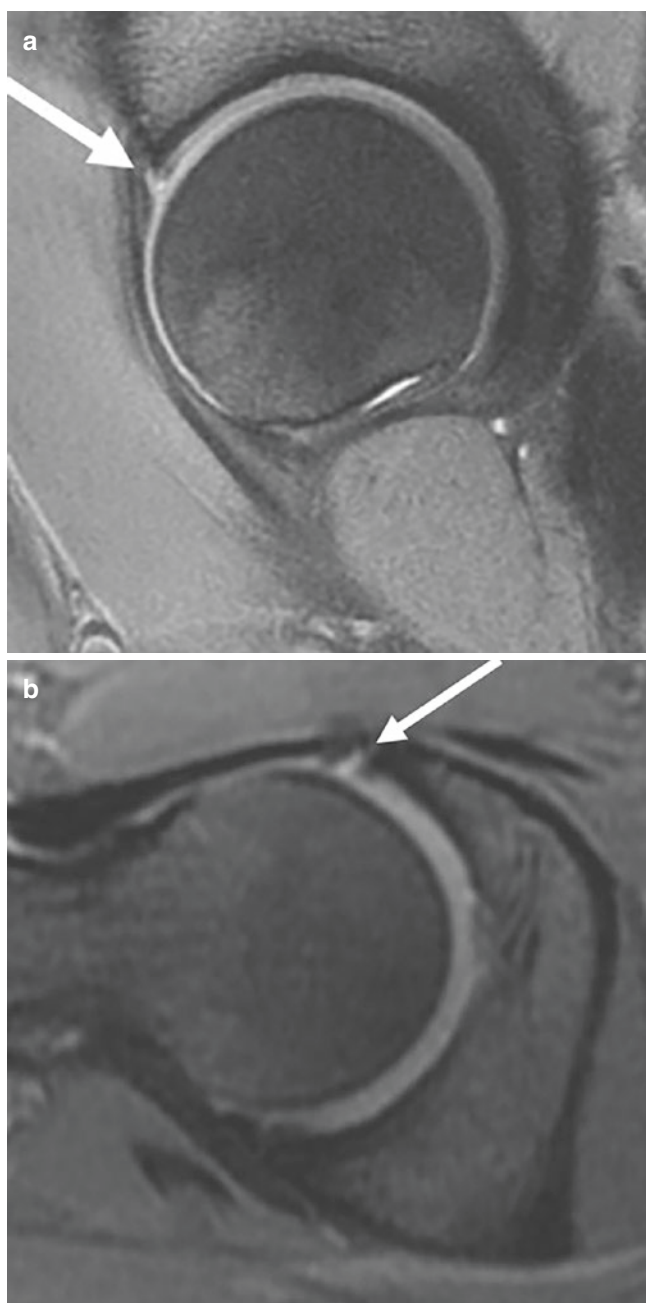
Fig. 5.8 Sagittal (**a**) and axial oblique (**b**) PD fat-suppressed MR images in a 22-year-old woman with hip pain shows linear high signal across the labral base representing labral injury (arrow)

and associated osseous changes at the acetabular rim. The MR imaging features of labral tears include contrast or high signal extending into the substance of the labrum, most often from the articular surface; blunting or irregularity of the labral apex or undersurface; or complete detachment from the acetabulum [35, 36] (Fig. 5.8). The description should include whether there is an intra-substance tear or detachment and whether there is a partial-thickness or full-thickness tear. Additional descriptions

may include frayed (irregular labrum margins without discrete tear), flap tear (contrast extending into or through labrum substance), thickened/distorted, or complex [35]. The extent of the tear can be determined using a clockface or quadrant localization. An associated secondary finding is a paralabral cyst, which is most common on the capsular surface of the labrum and may extend into the subchondral bone of the acetabulum.

> **Key Point**
> - Imaging assessment of the labrum should focus on tears and their extent; the description should differentiate between intra-substance tears or detachment and partial- or full-thickness tears. Possible additional features such as labrum fraying, flap tear, as well as associated osseous changes at the acetabular rim should also be described.

There are several anatomic variants that mimic labral pathology and may be mistaken for tears if not recognized. High signal at the chondrolabral junction is a commonly misinterpreted imaging finding. Mildly hyperintense signal at the articular surface of the labral base may be seen with cartilage undercutting and the previously described transition zone of the labral attachment to the articular cartilage. The hyaline cartilage has higher signal intensity than the labrum and may extend beneath the labral base, resulting in linear intermediate to hyperintense signal at the chondrolabral junction. This can be distinguished from a labral tear because the signal is hypointense to fluid or contrast and smoothly parallels the labral base and acetabular rim. Another cause of high signal at the chondrolabral junction may be due to a sublabral sulcus. This normal variant is located where the labrum meets the adjacent cartilage but is not directly attached at the articular surface. This sulcus is present in approximately 20–25% of the normal population and should not be confused with a labral tear [37]. A sublabral sulcus is a shallow, smooth defect at the labral base along the articular surface, involves less than 1/3 of the labral thickness, and often has a larger width than depth. The key to differentiating the normal variant sulcus from a tear includes its smooth contour, limited depth, and lack of secondary abnormalities, such as cartilage damage or paralabral cysts. Sublabral sulci are most commonly found at the posterior and anteroinferior labrum, but have been described in a variety of locations. Another smooth, shallow cleft at the chondrolabral base may be seen at the junction of the labrum and transverse ligament: labroligamentous sulcus. This is found in up to one third of normal, asymptomatic individuals [37].

5.5.2 Articular Cartilage

Unlike the fibrocartilage of the labrum, the articular cartilage of the acetabulum and femoral head is composed of hyaline cartilage, which is made up of predominantly water reinforced by chondrocytes and a type II collagen and proteoglycan matrix. The cartilage covers the majority of the femoral head, sparing only the fovea superomedially where the ligamentum teres attaches. The acetabular cartilage covers the osseous surface, except at the acetabular fossa. The articular cartilage is thickest at the superolateral acetabulum and anterosuperior femoral head, where there is greatest contact and need for load-bearing support.

Cartilage injuries are commonly found in combination with other abnormalities, specifically in association with labral tears and femoroacetabular impingement and following subluxations and dislocations [38]. Therefore, those who are predisposed to labral pathology, underlying FAI morphology, and subluxation or dislocation of the hip are also considered at risk for cartilage injury. Cartilage damage may be caused by shearing, impact, or routine wear on an incongruent joint. Because of its high water content, cartilage is generally hyperintense on T2-weighted images and intermediate signal on proton density images. On MR imaging cartilage injury manifests as generalized thinning, surface irregularity, fissures, delamination, chondral flaps, or full-thickness cartilage defects (Figs. 5.9 and 5.10). A specific, although not sensitive, sign for cartilage delamina-

tion is the presence of fluid or injected contrast material undermining the cartilage layer on MR arthrography [39]. Hypointense areas in the acetabular cartilage have been shown to correlate with cartilage delamination [40]. Most cartilage injuries involve the anterior acetabulum, followed by the superior and posterior acetabulum, and cartilage lesions are often accompanied by labral pathology, particularly when higher-grade cartilage damage is present. As the

Fig. 5.9 Coronal T2 fat-suppressed MR image in a 34-year-old man shows a focal cartilage defect near the labral base (arrow). Additionally, adjacent linear low signal may represent cartilage delamination. At arthroscopy, this was confirmed as delamination
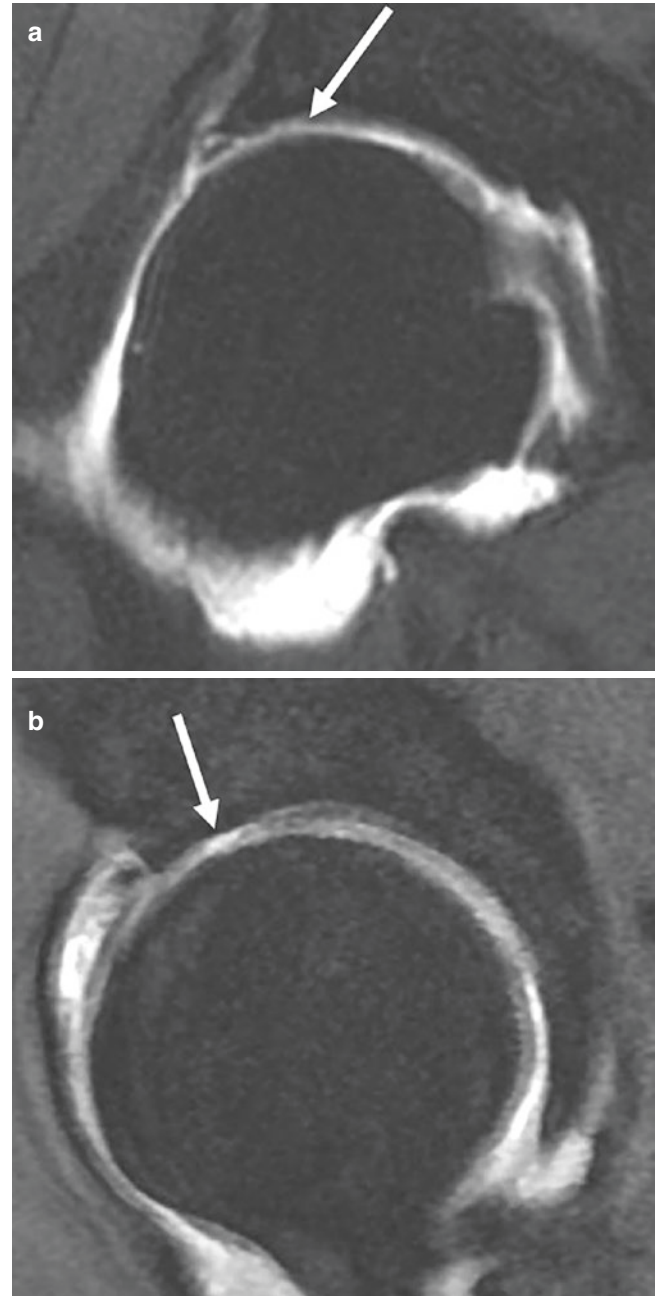
Fig. 5.10 Coronal (**a**) and sagittal (**b**) T1 fat-suppressed MR arthrogram images in a 43-year-old man show superficial and deep multifocal cartilage loss (arrows) predominantly involving the acetabulum. Note adjacent labral tear

cartilage status is considered to be one of the most important predictors for a favorable outcome of joint preserving hip surgery for hip dysplasia and FAI, close scrutiny and evaluation of the articular cartilage are key in the evaluation of the hip joint.

> **Key Point**
> - Articular cartilage lesions are important outcome predictors and can manifest as generalized thinning, surface irregularity, fissures, delamination, chondral flaps, or full-thickness defects; additionally, the exact location of cartilage defects at the acetabulum and femoral head should be given.

5.5.3 Ligamentum Teres

The ligamentum teres (LT) is an intra-articular ligament, comprised of two to three bands, connecting the fovea capitis of the medial femoral head and the transverse ligament of the inferior acetabular notch [41]. This ligament may have a role in stabilization of the adult hip and has been recognized as a potential source of pain and instability if torn [42]. The most common known etiology of ligamentum teres injury is trauma, ranging from dislocation to extreme abduction to relatively minor twisting or external rotation of the hip. Thus, sports with relatively high impact or twisting movements, including football, ice hockey, snow skiing, and dance, predispose athletes to LT injuries [42]. Symptoms of ligamentum teres tears are typically nonspecific, including deep anterior groin or hip pain, and often accompanied by mechanical snapping or catching sensations [42].

Noninvasive diagnosis of LT tears is challenging, not only because of a lack of specific symptoms but also due to poor visualization on imaging. Recent studies have shown that ligamentum teres abnormalities are detected in up to 51% of hip arthroscopies [43].

The normal appearance of the LT on MRI is a hypointense band on all sequences due to its fibrous nature and composition of tightly packed collagen bundles. Tears are most easily identified when complete, demonstrating absence when chronic and a redundant displaced band of tissue when acute. Other appearances of a torn LT include thickened, intermediate signal with degeneration or degenerative intrasubstance tearing, irregularity of the fibers with fraying, and disrupted fibers or fluid signal intensity within a distorted ligament with partial tears (Fig. 5.11). Even though there is limited accuracy, MR arthrography is still considered the best imaging method for diagnosis [43].
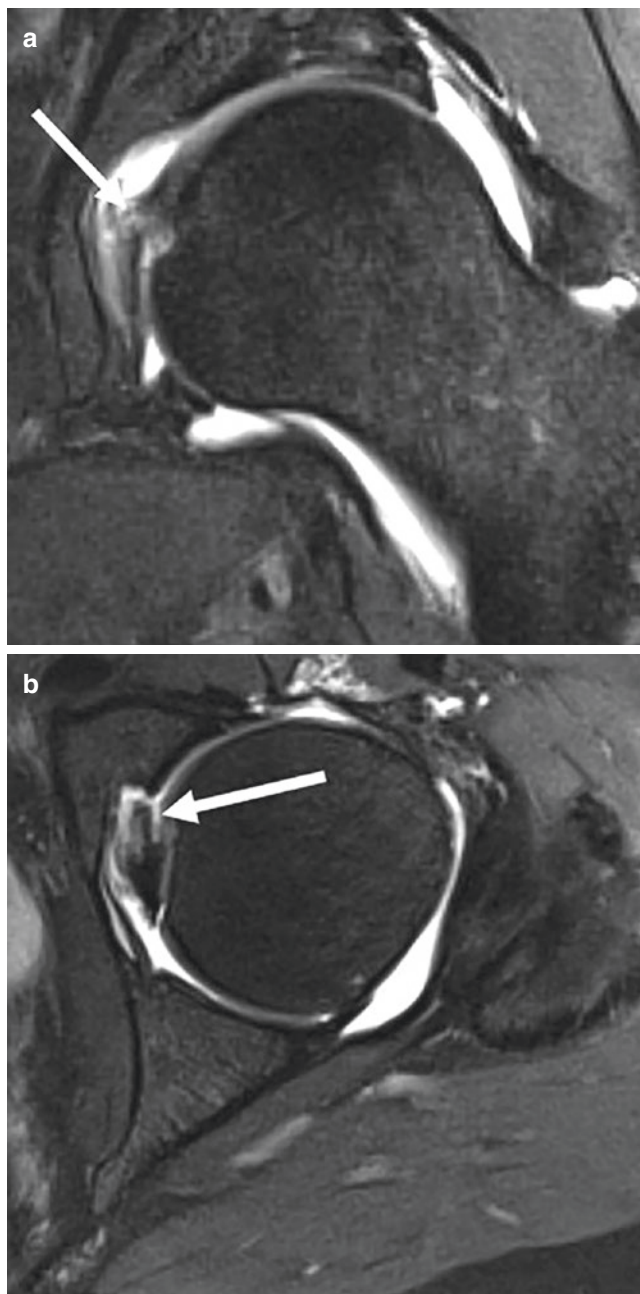
Fig. 5.11 Coronal (**a**) and axial (**b**) T2 fat-suppressed MR arthrogram images in a 42-year-old woman show irregular appearance and disruption of the proximal fibers of the ligamentum teres, near the fovea (arrows). This was a partial tear at arthroscopy and was subsequently debrided

5.6 Concluding Remarks

State-of-the art imaging of the hip joint allows good assessment of osseous and soft tissue damage of the hip joint. Knowledge of specific injury patterns aids in identifying damage to the labrum and articular cartilage lesions.

Take Home Messages

- Evaluation of the osseous morphology is the first cornerstone of hip imaging; this includes assessing diseases such as stress fractures or osteonecrosis, as well as detecting abnormal osseous morphology of the hip joint, such as seen in femoroacetabular impingement.
- Femoral torsion abnormalities are more common than previously thought and cannot only be seen in developmental dysplasia of the hip but also in patients with hip impingement; we recommend to acquire additional fast transverse MR sequences over the proximal and distal femur to measure femoral torsion and identify those patients with abnormal femoral antetorsion.
- Intra-articular damage of the labrum and cartilage can be readily assessed with MRI; the exact description of the localization and extent of any intra-articular damage is an important predictor for outcome, especially in patients with femoroacetabular impingement.

References

1. Domb BG, Annin S, Chen JW, et al. Optimal treatment of Cam morphology may change the natural history of femoroacetabular impingement. Am J Sports Med. 2020:363546520949541.
2. Expert Panel on Musculoskeletal I, Mintz DN, Roberts CC, et al. ACR Appropriateness Criteria((R)) chronic hip pain. J Am Coll Radiol. 2017;14(5S):S90–S102.
3. Anderson MW, Greenspan A. Stress fractures. Radiology. 1996;199(1):1–12.
4. Blankenbaker DG, De Smet AA. Hip injuries in athletes. Radiol Clin N Am. 2010;48(6):1155–78.
5. Murphey MD, Foreman KL, Klassen-Fischer MK, et al. From the radiologic pathology archives imaging of osteonecrosis: radiologic-pathologic correlation. Radiographics. 2014;34(4):1003–28.
6. Vassalou EE, Spanakis K, Tsifountoudis IP, et al. MR imaging of the hip: an update on bone marrow edema. Semin Musculoskelet Radiol. 2019;23(3):276–88.
7. Malizos KN, Karantanas AH, Varitimidis SE, et al. Osteonecrosis of the femoral head: etiology, imaging and treatment. Eur J Radiol. 2007;63(1):16–28.
8. Hong RJ, Hughes TH, Gentili A, et al. Magnetic resonance imaging of the hip. J Magn Reson Imaging. 2008;27(3):435–45.
9. Mitchell DG, Rao VM, Dalinka MK, et al. Femoral head avascular necrosis: correlation of MR imaging, radiographic staging, radionuclide imaging, and clinical findings. Radiology. 1987;162(3):709–15.
10. Meier R, Kraus TM, Schaeffeler C, et al. Bone marrow oedema on MR imaging indicates ARCO stage 3 disease in patients with AVN of the femoral head. Eur Radiol. 2014;24(9):2271–8.
11. Ito H, Matsuno T, Minami A. Relationship between bone marrow edema and development of symptoms in patients with osteonecrosis of the femoral head. Am J Roentgenol. 2006;186(6):1761–70.
12. Ficat P. Vascular pathology of femoral head necrosis (author's transl). Orthopade. 1980;9(4):238–44.
13. Steinberg ME, Hayken GD, Steinberg DR. A quantitative system for staging avascular necrosis. J Bone Joint Surg Br. 1995;77(1):34–41.
14. Miyanishi K, Hara T, Kaminomachi S, et al. Contrast-enhanced MR imaging of subchondral insufficiency fracture of the femoral head: a preliminary comparison with that of osteonecrosis of the femoral head. Arch Orthop Trauma Surg. 2009;129(5):583–9.
15. Bramlett KW, Killian JT, Nasca RJ, et al. Transient osteoporosis. Clin Orthop Relat Res. 1987;(222):197–202.
16. Sutter R, Pfirrmann CW. Atypical hip impingement. Am J Roentgenol. 2013;201(3):W437–42.
17. Memon M, Kay J, Hache P, et al. Athletes experience a high rate of return to sport following hip arthroscopy. Knee Surg Sports Traumatol Arthrosc. 2019;27(10):3066–104.
18. Sutter R, Dietrich TJ, Zingg PO, et al. Femoral antetorsion: comparing asymptomatic volunteers and patients with femoroacetabular impingement. Radiology. 2012;263(2):475–83.
19. Shin J, Adeyemi TF, Hobson T, et al. The bipolar hip: how acetabular and femoral pathomorphology affects hip motion in femoral acetabular impingement syndrome. Arthroscopy. 2020;36(7):1864–71.
20. Nepple JJ, Riggs CN, Ross JR, et al. Clinical presentation and disease characteristics of femoroacetabular impingement are sex-dependent. J Bone Joint Surg Am. 2014;96(20):1683–9.
21. Sutter R, Dietrich TJ, Zingg PO, et al. How useful is the alpha angle for discriminating between symptomatic patients with cam-type femoroacetabular impingement and asymptomatic volunteers? Radiology. 2012;264(2):514–21.
22. van Klij P, Reiman MP, Waarsing JH, et al. Classifying Cam morphology by the alpha angle: a systematic review on threshold values. Orthop J Sports Med. 2020;8(8):2325967120938312.
23. Casartelli NC, Bizzini M, Maffiuletti NA, et al. Exercise therapy for the management of femoroacetabular impingement syndrome: preliminary results of clinical responsiveness. Arthritis Care Res (Hoboken). 2019;71(8):1074–83.
24. Steppacher SD, Anwander H, Zurmuhle CA, et al. Eighty percent of patients with surgical hip dislocation for femoroacetabular impingement have a good clinical result without osteoarthritis progression at 10 years. Clin Orthop Relat Res. 2015;473(4):1333–41.
25. Maier C, Zingg P, Seifert B, et al. Femoral torsion: reliability and validity of the trochanteric prominence angle test. Hip Int. 2012;22(5):534–8.
26. Sutter R, Dietrich TJ, Zingg PO, et al. Assessment of femoral antetorsion with MRI: comparison of oblique measurements to standard transverse measurements. Am J Roentgenol. 2015;205(1):130–5.
27. Lerch TD, Boschung A, Todorski IAS, et al. Femoroacetabular impingement patients with decreased femoral version have different impingement locations and intra- and extraarticular anterior subspine FAI on 3D-CT-based impingement simulation: implications for hip arthroscopy. Am J Sports Med. 2019;47(13):3120–32.
28. Hetsroni I, Larson CM, Dela Torre K, et al. Anterior inferior iliac spine deformity as an extra-articular source for hip impingement: a series of 10 patients treated with arthroscopic decompression. Arthroscopy. 2012;28(11):1644–53.
29. Samim M, Walter W, Gyftopoulos S, et al. MRI Assessment of subspine impingement: features beyond the anterior inferior iliac spine morphology. Radiology. 2019;293(2):412–21.
30. Agricola R, Heijboer MP, Ginai AZ, et al. A cam deformity is gradually acquired during skeletal maturation in adolescent and young male soccer players: a prospective study with minimum 2-year follow-up. Am J Sports Med. 2014;42(4):798–806.
31. Kim YT, Azuma H. The nerve endings of the acetabular labrum. Clin Orthop Relat Res. 1995;320:176–81.
32. Lecouvet FE, Vande Berg BC, Malghem J, et al. MR imaging of the acetabular labrum: variations in 200 asymptomatic hips. Am J Roentgenol. 1996;167(4):1025–8.

33. Seldes RM, Tan V, Hunt J, et al. Anatomy, histologic features, and vascularity of the adult acetabular labrum. Clin Orthop Relat Res. 2001;(382):232–40.

34. Wenger DE, Kendell KR, Miner MR, et al. Acetabular labral tears rarely occur in the absence of bony abnormalities. Clin Orthop Relat Res. 2004;(426):145–50.

35. Blankenbaker DG, De Smet AA, Keene JS, et al. Classification and localization of acetabular labral tears. Skelet Radiol. 2007;36(5):391–7.

36. Ziegert AJ, Blankenbaker DG, De Smet AA, et al. Comparison of standard hip MR arthrographic imaging planes and sequences for detection of arthroscopically proven labral tear. Am J Roentgenol. 2009;192(5):1397–400.

37. Dinauer PA, Flemming DJ, Murphy KP, et al. Diagnosis of superior labral lesions: comparison of noncontrast MRI with indirect MR arthrography in unexercised shoulders. Skelet Radiol. 2007;36(3):195–202.

38. Philippon MJ, Kuppersmith DA, Wolff AB, et al. Arthroscopic findings following traumatic hip dislocation in 14 professional athletes. Arthroscopy. 2009;25(2):169–74.

39. Agten CA, Sutter R, Buck FM, et al. Hip imaging in athletes: sports imaging series. Radiology. 2016;280(2):351–69.

40. Pfirrmann CW, Duc SR, Zanetti M, et al. MR arthrography of acetabular cartilage delamination in femoroacetabular cam impingement. Radiology. 2008;249(1):236–41.

41. Cerezal L, Kassarjian A, Canga A, et al. Anatomy, biomechanics, imaging, and management of ligamentum teres injuries. Radiographics. 2010;30(6):1637–51.

42. Bardakos NV, Villar RN. The ligamentum teres of the adult hip. J Bone Joint Surg Br. 2009;91(1):8–15.

43. Shakoor D, Farahani SJ, Hafezi-Nejad N, et al. Lesions of ligamentum teres: diagnostic performance of MRI and MR arthrography—a systematic review and meta-analysis. Am J Roentgenol. 2018;211(1):W52–63.

Pelvis and Groin

Practical Anatomy, Injury Patterns, and Imaging Findings

Robert D. Boutin ⓘ and Philip Robinson ⓘ

The groin and pelvis represent a large anatomical region with disorders affecting a diverse array of osteoarticular, musculotendinous, gastrointestinal, and genitourinary structures. Clinically, it can be difficult to pinpoint a pain generator, and imaging often proves helpful for establishing a diagnosis – particularly if the imager is familiar with practical anatomy, common injury patterns, and high-yield imaging findings.

Anatomy is fundamental to understanding the key concepts in this chapter (Figs. 6.1 and 6.2). The groin and pelvis

are at the junction of the trunk and lower extremities and are subjected to prodigious compression, traction, and shearing forces. For example, even with an everyday activity like a "single leg stance," physiologic loading can be phenomenal: ~7.7 times the body weight (4653 N) [1]. In athletes, powerful muscle contractions and various "supra-physiologic" demands can cause biomechanical overloading from acute trauma or repetitive microtrauma.

Radiologists benefit from knowledge of anatomic target sites for biomechanical failure and common injury patterns. Injuries can occur across a life span in acute, chronic, and acute-on-chronic settings. While stress fractures can occur in both pediatric and adult patients, there are other types of injuries favoring particular age groups.

- In skeletally immature patients, a frequent "weak link" in the "kinetic chain" is the apophyseal physis (which is weaker than the adjacent bone and tendon). Apophyseal avulsions in the pelvis most commonly occur at the ischial tuberosity and anterior superior iliac spine; other characteristic sites include the anterior inferior iliac spine, iliac crest, and pubic symphysis (Figs. 6.3 and 6.4). Of note, prior to ossification of apophyses (e.g., typically from 13 to 15 years of age at the ischial tuberosity), avulsions are occult radiographically [2]. Apophysitis also can occur in this age group [3].
- In young adults, the myotendinous junction is a common point of biomechanical failure for acute non-contact injuries [4]. Particularly frequent sites of injury in young adult athletes include the myotendinous junction of the hamstrings and rectus femoris (Figs. 6.5–6.7). With repetitive microtrauma, often with muscle imbalances, overuse injuries often occur at the tendon (tendinopathy) with peritendinous edema (e.g., peritendinitis, enthesitis).
- In older adults, tendon degeneration is increasingly prevalent, with resultant weakening of the tendon. Imaging commonly showing tendinopathy and tendon tearing.

R. D. Boutin (✉)
Department of Radiology, Stanford University School of Medicine, Stanford, CA, USA
e-mail: boutin@stanford.edu

P. Robinson
Musculoskeletal Centre X-Ray Department, Leeds Teaching Hospitals Trust, Chapel Allerton Hospital, Leeds, UK

NIHR Leeds Biomedical Research Centre, Leeds Teaching Hospitals, NHS Trust, Leeds, UK
e-mail: Philip.robinson10@nhs.net
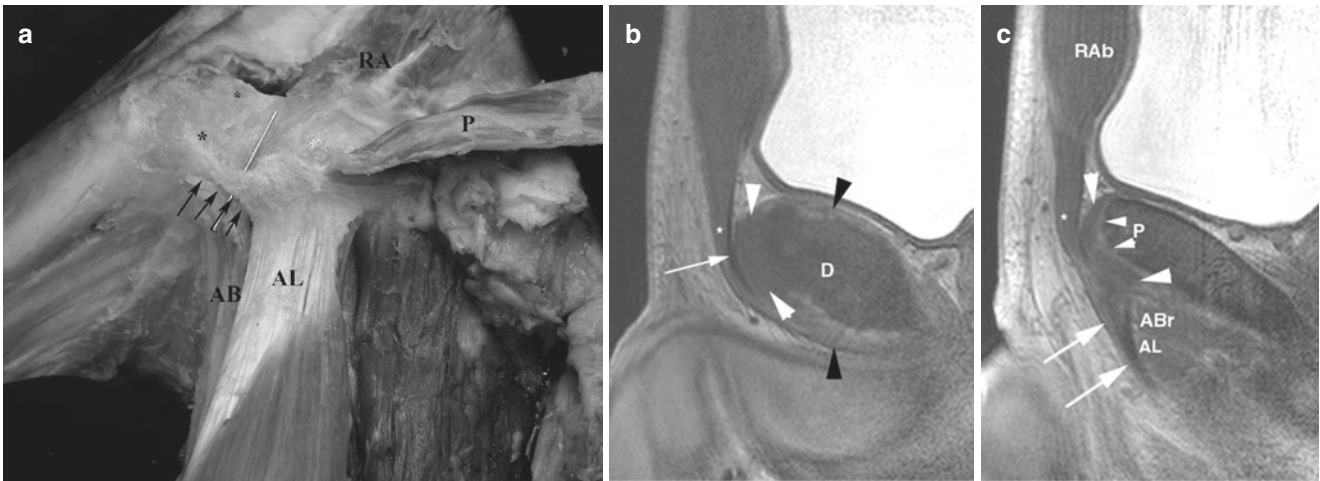
Fig. 6.1 (**a**) Normal anatomy, male cadaver dissection, anterolateral view. Asterisks mark the center of the symphysis pubis. The tendinous attachment of adductor longus (AL) to tissue overlying the anterior symphysis pubis is elevated by a pin and inferiorly outlined with arrows. Pyramidalis (P) is reflected to reveal rectus abdominis (RA). The medial margin of adductor brevis (AB) can be seen medial to adductor longus (AL). (**b**) Normal sagittal MRI anatomy. A 29-year-old male athlete (experienced previous pubalgia). Sagittal T1 FFE MR image shows edge of fibrocartilagenous disk (D), interdigitating hyaline cartilage and pubic bone (black arrowheads). Anteriorly, the capsular tissues (white arrowheads) merge with the disk (D) and rectus abdominis tendon (white arrow). Pyramidalis present anteriorly (asterisk). (**c**) Lateral to (a) pubic marrow and cortex (P) with thin layer of intermediate signal hyaline cartilage (small arrowheads) closely applied to the anterior capsular tissues (between large white arrowheads). Merging with this tissue are the rectus abdominis tendon (RAb), pyramidalis (asterisk), superficial adductor longus tendon (arrows), deeper muscle (AL), and adductor brevis (ABr) muscle. (Reproduced with permission from Robinson P, Salehi F, Grainger A, et al. Cadaveric and MRI Study of the Musculotendinous Contributions to the Capsule of the Symphysis Pubis. *American Journal of Roentgenology.* 2007;188(5):W440–W445.)
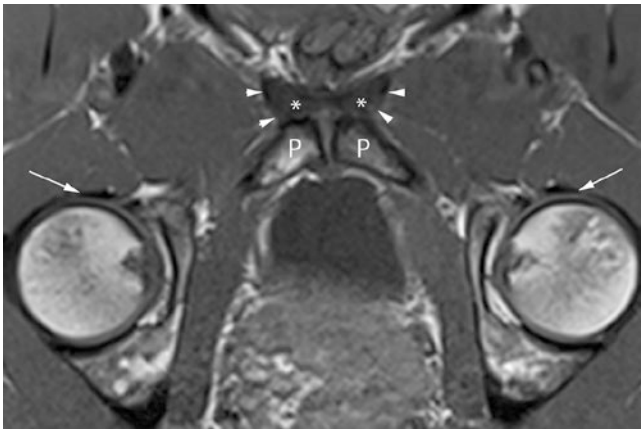
Fig. 6.2 Normal anatomy, MR imaging. Axial oblique T1 MR image shows pubic bodies (P) and the adductor group tendons (arrowheads) beginning to separate from the aponeurotic tissues (*). Normal iliopsoas tendons (small arrows). (Reproduced with permission from reference Madani H, Robinson P. Top-Ten Tips for Imaging Groin Injury in Athletes. *Semin Musculoskelet Radiol.* 2019;23(4):361–75.)

Although it can be difficult to pinpoint a precise pain generator clinically, patients often present with orthopedic complaints that are most severe in a particular region of the pelvis: *anterior*, *lateral*, *inferior*, or *posterior*. (Note: The hip joint is covered in a separate chapter.) In this chapter, we highlight the most important injury patterns in each of these four locations, with a special emphasis on the anterior pelvis.

6.1 Anterior Pelvis

6.1.1 Who Is Most Likely to Get Imaging for Anterior Pain?

At the anterior aspect of the pelvis, orthopedic imaging is often performed in athletes with pain. Athletic-related groin pain can occur with acute injuries, but commonly presents with an insidious onset owing to overuse. Sports that involve intense pivoting, twisting, and kicking are often implicated (e.g., soccer/football, rugby, hockey).

- In professional ice hockey players, for example, over half of all players experience groin and hip problems in a typical season, with almost one-third losing time from playing their sport [5].
- Other athletes also can experience groin pain, including dancers, swimmers, runners, and even unicyclists. In a recent study of 1304 unicyclists (who actively use adductor and other muscles), 17% complained of groin pain [6]!

6.1.2 What Is the Optimal Imaging Workup?

Radiography is the initial screening test of choice in many practices. Unfortunately, radiography is often insensitive and non-specific in patients with chronic groin pain.
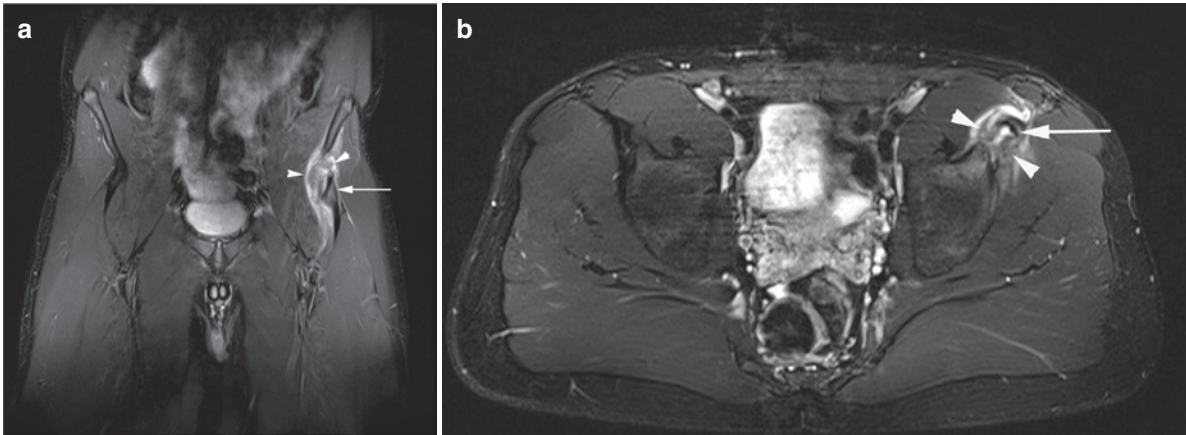
Fig. 6.3 Apophyseal injury. A 16-year-old rugby player with sudden anterior hip pain. (**a**) Coronal and (**b**) axial T2FS MR images show avulsion of the left anterior inferior iliac apophysis (arrow), hematoma (arrowheads), and intact indirect head of rectus femoris
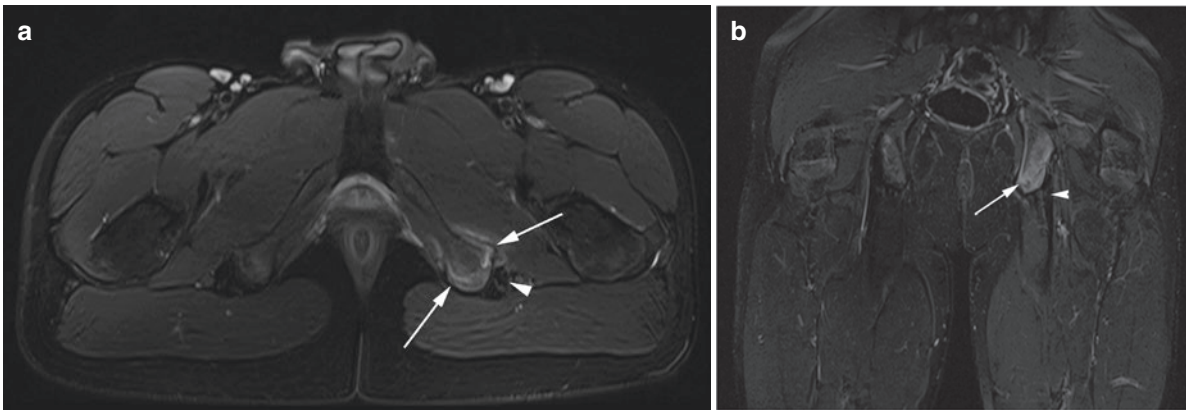
Fig. 6.4 Apophyseal injury. A 17-year-old soccer player with subacute hamstring pain. (**a**) Axial and (**b**) coronal T2FS MR images show left ischial apophysis edema, stress fracture and periosteal reaction (arrow), and normal hamstring tendons (arrowheads)
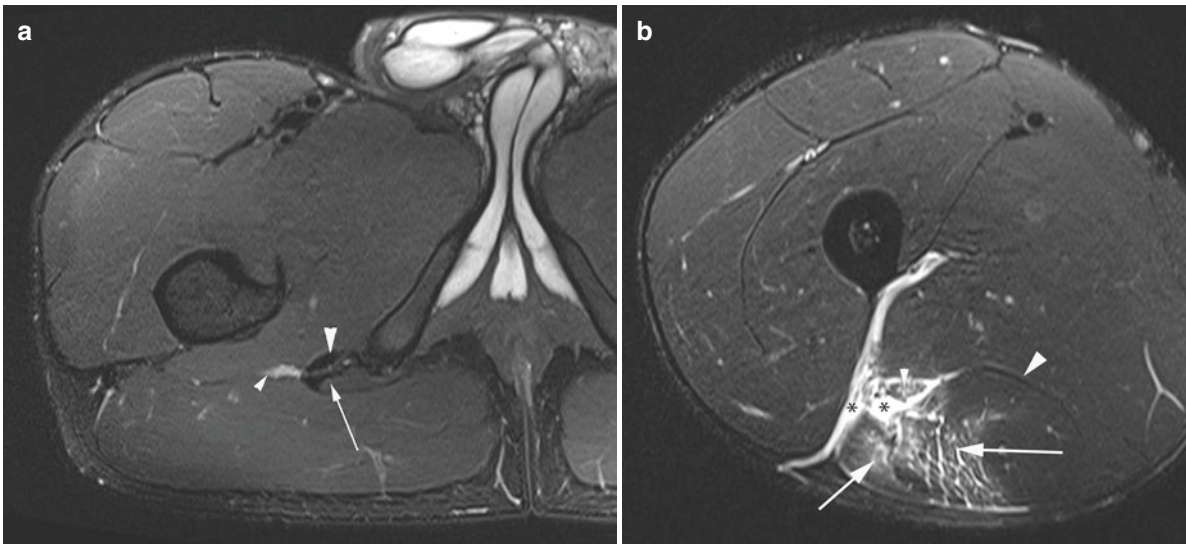
Fig. 6.5 Myotendinous injury. A 24-year-old soccer player with acute hamstring pain. Axial T2FS MR images show (**a**) right proximal thigh with normal conjoint tendon (arrow), semimembranosus (large arrowhead), and sciatic nerve (small arrowhead) and (**b**) semitendinosus and biceps femoris myotendinous tear with tendon involvement (arrows) with decompressed hematoma (asterisk) around the sciatic nerve (small arrowhead) and fascia. Normal semimembranosus (large arrowhead)
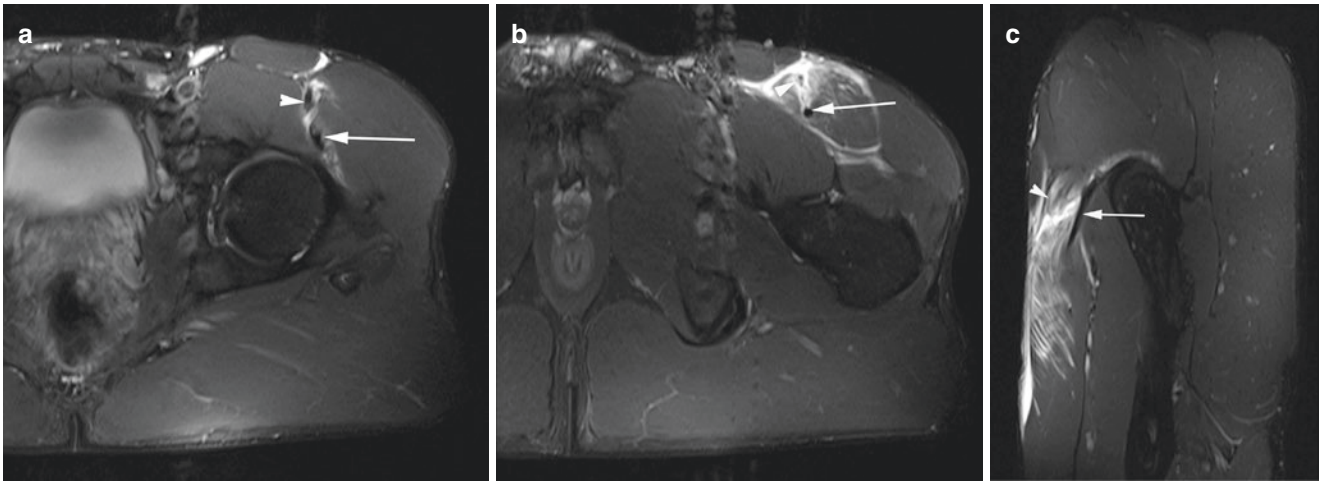
Fig. 6.6 Myotendinous injury. A 23-year-old soccer player with acute anterior hip pain. Axial and sagittal T2FS MR images show (**a**) left proximal thigh intact indirect head tendon (arrow), direct head tendon (arrowhead), and muscle edema. (**b**) and (**c**) Inferior to (**a**) show intact indirect head tendon (arrow), torn direct head tendon (arrowhead), and extensive muscle disruption
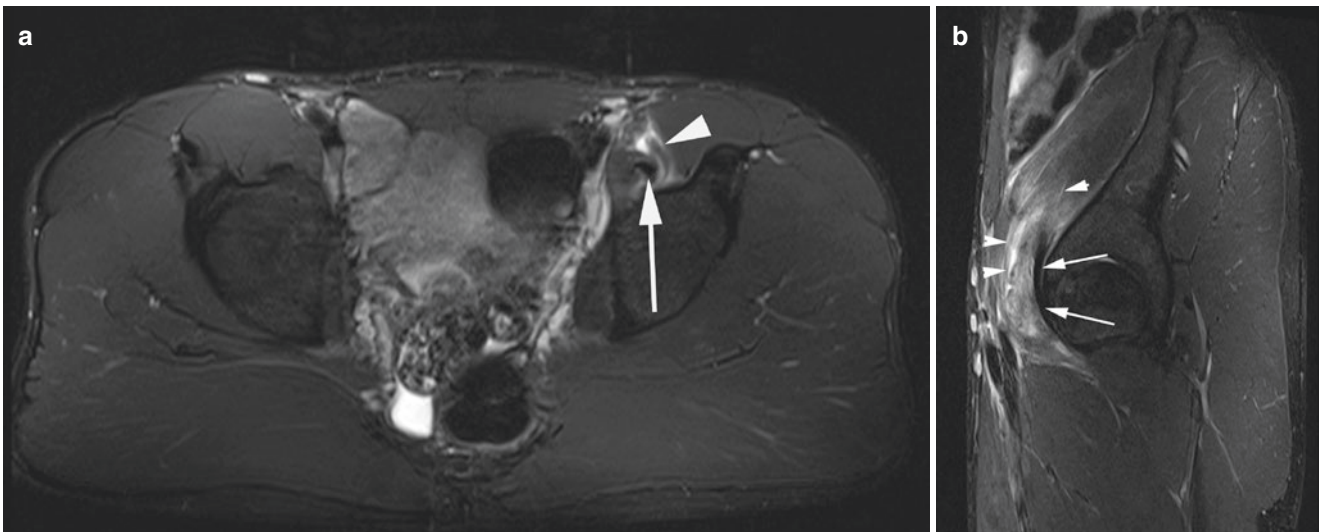
Fig. 6.7 Myotendinous injury. A 21-year-old soccer player with acute anterior hip pain. (**a**) Axial and (**b**) sagittal T2FS MR images show intact psoas major tendon (arrow) and myotendinous iliacus injury (arrowhead)

Indeed, sonography and MRI have become frontline tools in many practices owing to the low diagnostic yield of radiography, as well as concerns related to radiation exposure associated with radiography, CT, and scintigraphy in young athletes.

Sonography has numerous strengths, including point-of-care evaluation, dynamic assessment (e.g., for hernia [7], tendon snapping), real-time sonopalpation at the exact site of pain, and guiding percutaneous injections for diagnostic and therapeutic purposes [8, 9].

- Sonography is best performed with a systematic protocol [10, 11]. Using a high-frequency (e.g., ≥ 14 MHz) linear array transducer, the patient is positioned supine with the hips abducted and externally rotated. First, imaging is performed of the rectus abdominis/adductor aponeurosis (in the transverse and longitudinal planes) and the adductor longus attachment (in an oblique sagittal plane longitudinal to these fibers and in an orthogonal transverse plane). Then, dynamic imaging during Valsalva can be used assessing for an inguinal or femoral hernia [12], as well as the controversial finding of inguinal wall bulging believed by some to cause ilioinguinal nerve irritation. If indicated, additional evaluation of the iliopsoas and hip region also can be performed (e.g., for tendon snapping, iliopsoas bursitis, hip effusion).

MRI is better able to show soft tissue edema than sonography, as well as a wide spectrum of abnormalities within bones.

- MRI protocols commonly combine both a small and large field of view (FOV). The high spatial resolution images with a small FOV (e.g., 16–25 cm) have thin slices (e.g., 3 mm) and are generally performed in the sagittal plane and an oblique-axial plane (paralleling the anterior tilt of the pelvic brim). Additional images with a large FOV (e.g., 38–40 cm) have thicker slices (e.g., 4–5 mm) covering the pelvis, which allows screening of the hips, sacroiliac joints, spine, and pelvic viscera. This is particularly helpful because symptoms may radiate from another site or may not be localized [13]. No gadolinium is needed.

6.1.3 What Terminology Should Be Used?

Terminology has evolved over time. A multispecialty expert group consensus statement suggests the use of an umbrella term "groin pain in athletes" (a general description that cannot be misunderstood as a diagnostic term), rather than previously used terms with variable definitions (e.g., athletic pubalgia, sports hernia, sportsman's groin) [14]. Although this entity may be caused by a wide variety of derangements at the hip or elsewhere, groin pain in athletes is often classified into four categories related to location: *pubic*, *adductor*, *inguinal*, and *iliopsoas* [14]. Pubic- and adductor-related groin pain have overlapping features and are discussed together here.

6.1.4 Pubic and Adductor Groin Pain

Anatomy. The pubic symphysis is a cartilaginous joint supported by four capsular ligaments (superior, inferior, anterior, posterior) and numerous musculotendinous attachments. Of all the abdominal and adductor muscles that converge in this region, the most important stabilizers are the *rectus abdominis* and the *adductor longus*. The adductor longus can be identified as the most anterior of the adductor muscle group.

Injury Patterns. Acutely, muscle tears (partial or complete) or avulsion injuries can occur near the pubic symphysis. Such injuries frequently target the adductor longus (Fig. 6.8) [15–17].

In the non-acute setting, the most common areas of injury are the rectus abdominis/adductor aponeurosis and pubic symphysis capsular attachment site. Athletes are predisposed to injury when shear stresses are accentuated by muscle imbalances (typically stronger adductor muscles with anteroinferior tension versus weaker abdominal muscles with superior tension). This allows initial low-grade overuse injuries to propagate into overt tears at the musculoaponeurotic attachments.

Imaging Findings. Although pubic bone marrow edema (BME) may be seen in asymptomatic athletes owing to chronic loading, more severe and extensive BME is positively associated with pain. Pubic BME may be an isolated finding related to stress reaction, but it is crucial to look for additional abnormalities (Fig. 6.9). Three abnormalities associated with pubic BME are especially important to report: (1) stress fractures (typically with intense BME adjacent to a fracture line of low signal intensity), (2) apophysitis
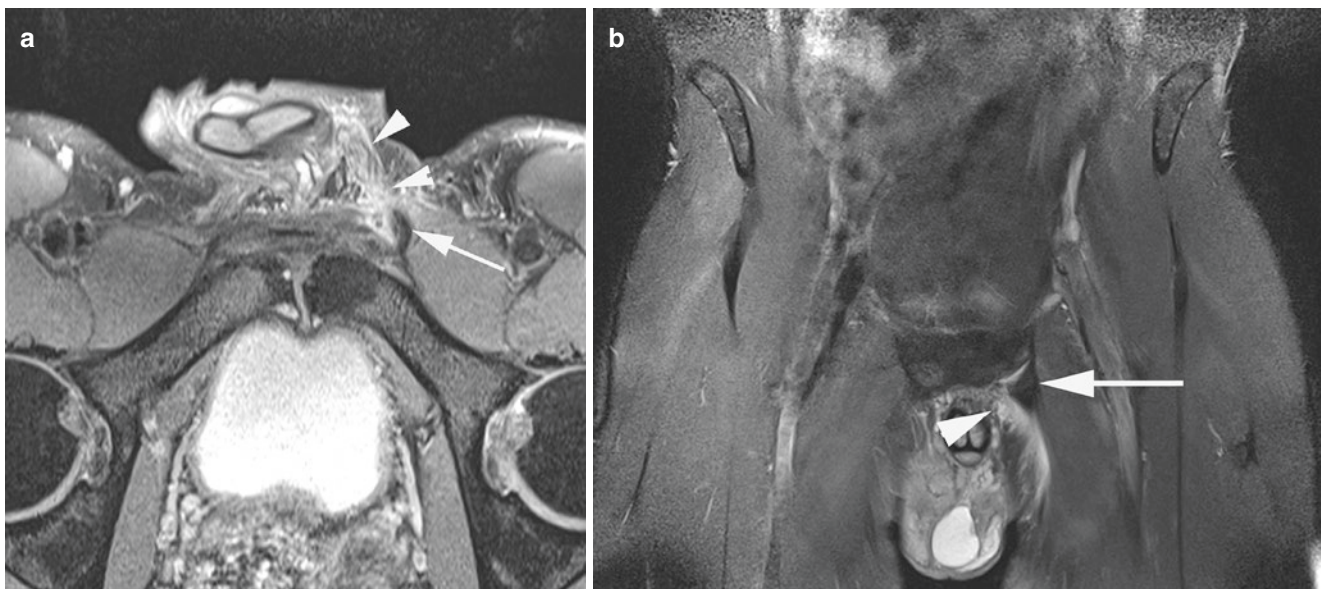
Fig. 6.8 Acute groin injury. A 26-year-old soccer player with acute left groin pain. (**a**) Oblique axial PDFS and (**b**) coronal T2FS MR images show left adductor longus and pectineus tendon avulsion (arrow) with soft tissue hemorrhage extending into the left inguinal canal due to acutely torn aponeurosis (arrowheads)
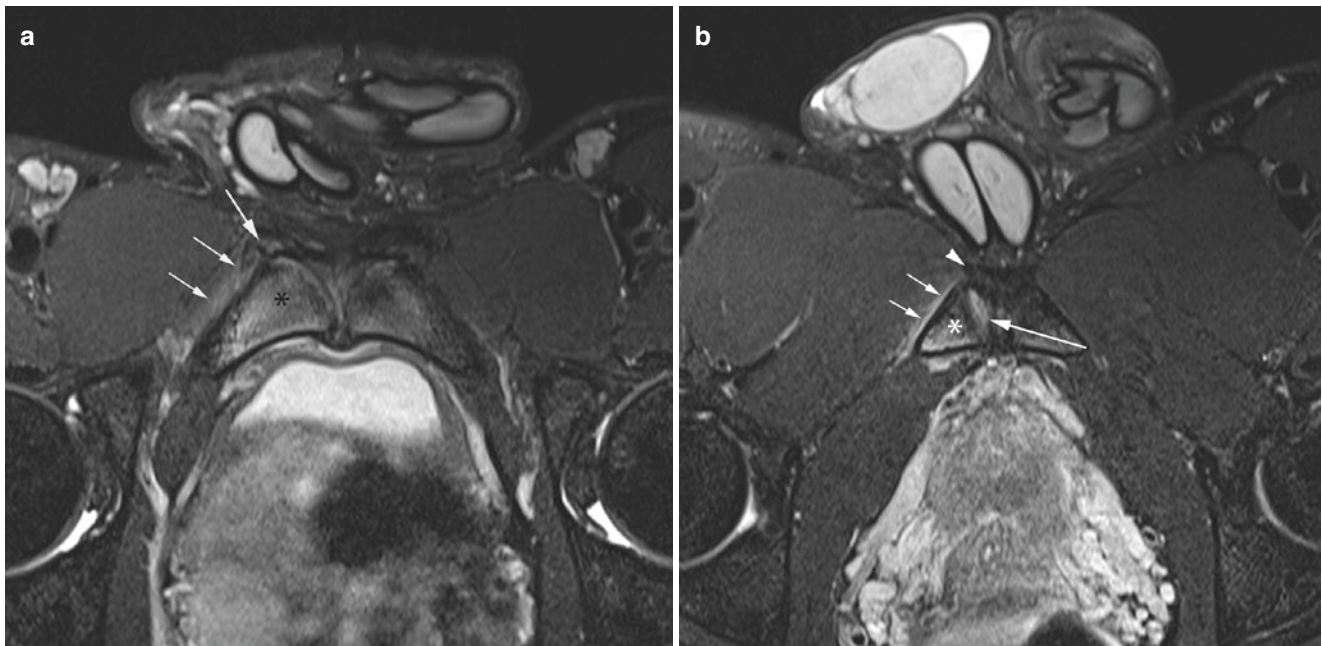
Fig. 6.9 Unilateral edema pubic capsule aponeurotic and bone marrow. A 22-year-old professional soccer player with right-sided symptoms. (**a**) and (**b**) Sequential axial oblique PDFS MR images show right-sided high signal with no definite tear (large white arrow) between the pubis and main aponeurotic tissue. There is also mild soft tissue edema adja-

cent to the pubic cortex (small arrows). The left side shows no tear and minimal edema. There is diffuse moderate bilateral bone marrow edema (*) more extensive on the right. (Reproduced with permission from reference Madani H, Robinson P. Top-Ten Tips for Imaging Groin Injury in Athletes. *Semin Musculoskelet Radiol*. 2019;23(4):361–75.)

(i.e., T2 hyperintensity at the pubic apophysis, anteromedially in young athletes) (Fig. 6.10), and (3) rectus abdominis/adductor aponeurosis injury (Fig. 6.11).

Rectus abdominis/adductor aponeurosis injury is among the most common imaging finding in athletes with chronic groin pain. Key MRI findings include edema or disruption at the aponeurosis or the capsular attachment. Such abnormalities go by variable names in the medical literature (e.g., "secondary cleft sign," "plate injury," "pubic aponeurotic defect," "overuse enthesitis"), and therefore objective reporting of anatomic location, signal intensity (e.g., mild to severe edema), and size is often recommended.

The most widely known MRI finding is the "secondary cleft sign" seen as fluid signal undermining the rectus abdominis/adductor aponeurosis attachment to the pubis (in communication with the pubic symphysis). Similar to BME, these MRI findings tend to be mild or absent in asymptomatic athletes, while more severe and extensive findings are positively associated with active injury. Tendinopathy in the adductors can also be sought, but imaging diagnosis of adductor tendinopathy has not been validated as highly reliable [18].

6.1.5 Inguinal Groin Pain

Anatomy. The inguinal canal is located superolateral to the pubic symphysis (above the medial half of the inguinal ligament) and is approximately 4 cm long. This tunnel transmits
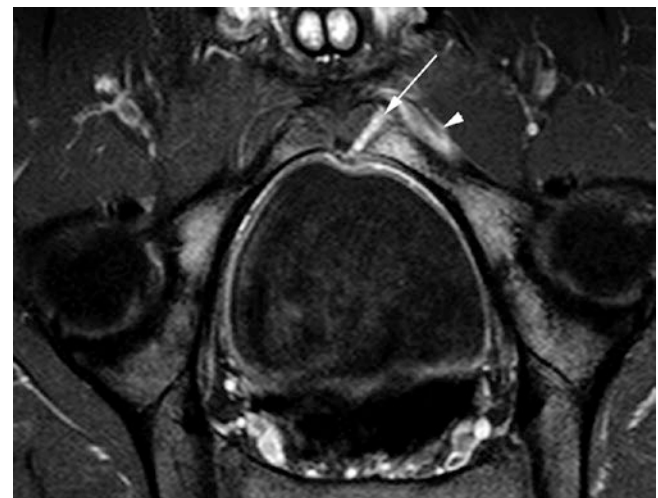
Fig. 6.10 Apophyseal injury. A 16-year-old soccer player with severe left-sided pain. Axial oblique T2FS MR image shows severe left pubic body and ramus bone marrow edema with adjacent soft tissue edema (arrowhead). The apophyseal junction is ill-defined, widened, and of high signal (arrow). (Reproduced with permission from reference Madani H, Robinson P. Top-Ten Tips for Imaging Groin Injury in Athletes. *Semin Musculoskelet Radiol*. 2019;23(4):361–75.)

the spermatic cord in men or the round ligament in women, as well as associated neurovascular structures.

The inguinal aponeurotic falx or "conjoint tendon" (the aponeurosis of both the internal oblique and transverse muscles of the abdomen) merges with the sheath of the rectus abdominis muscle at a variable distance from the symphysis
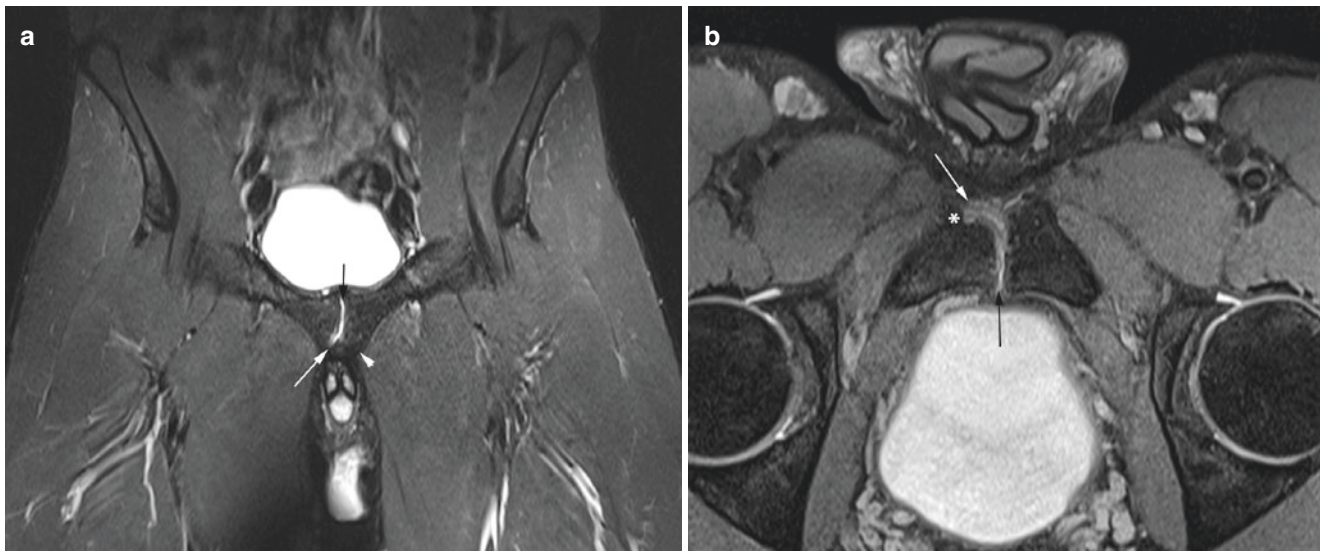
Fig. 6.11 Partial tear pubic capsule aponeurotic junction ("inferior cleft"). A 23-year-old professional rugby player with right-sided symptoms. (**a**) Coronal T2FS and (**b**) axial oblique PDFS images show normal joint (black arrow) and left soft tissue junction (white arrowhead) with right high signal tear (white arrow) between the pubis and main tubercle. Recent research suggests that a high insertion of the

aponeurotic tissue. No bone marrow edema is evident though there is chronic remodeling (*) present. (Reproduced with permission from reference Madani H, Robinson P. Top-Ten Tips for Imaging Groin Injury in Athletes. *Semin Musculoskelet Radiol*. 2019;23(4):361–75.)

conjoint tendon seen on MRI is associated with inguinal-related groin pain in athletes [19].

Injury Patterns. Pain with tenderness at the inguinal canal region aggravated by a Valsalva-type maneuver is widely reported in the medical literature. However, in the young athletic population, no true hernia is typically palpable at clinical examination or visible at imaging. When a true hernia is present in this region, it is classically described as "indirect" (i.e., abdominal contents exit through the inguinal canal) or "direct" (i.e., exists through the abdominal wall deep layers, thereby bypassing the inguinal canal).

Imaging Findings. Imaging evaluation for true inguinal and femoral hernias is best performed by sonography. For patients with inguinal-related pain but not true hernia, the posterior inguinal wall can be evaluated for laxity (incompetence) that may possibly irritate the ilioinguinal nerve. Unfortunately, these findings are regarded as subjective and have disappointing diagnostic reliability. MRI evaluation in these patients is generally normal.

6.1.6   Iliopsoas Groin Pain

Anatomy. The iliopsoas is formed by the confluence of the iliacus muscle (at the inner aspect of the iliac fossa) and the psoas muscle. The tendon slips from the two muscle bellies may or may not fuse together prior to insertion onto the lesser trochanter; a normal longitudinal division between these two components should not be misdiagnosed as a longitudinal tendon tear.

The iliopsoas bursa is located between the iliopsoas and the hip joint. This is the largest bursa in the human body and communicates with the hip joint normally in up to approximately 15% of adults.

Injury Patterns. The iliopsoas is considered the least common source of athletic groin pain. Injuries are more common with repetitive microtrauma than with a single traumatic event. Typical maneuvers causing pain include getting up from sitting or squatting, as well as sometimes resisted hip flexion.

Imaging Findings. Sonography can be useful in the evaluation of snapping (e.g., dynamic assessment as the iliopsoas passing over the iliopectineal eminence), iliopsoas bursitis (i.e., hypoechoic fluid along the iliopsoas tendon), and guiding percutaneous injections.

MRI provides for simultaneous assessment of iliopsoas edema, iliopsoas bursitis, and derangements in adjacent structures like the hip (Fig. 6.12). Peritendinous edema associated with the iliopsoas bursa can be seen in the setting of overuse or strain injuries, as well as in some cases of snapping hip ("coxa saltans interna").

Key Point
- The differential diagnosis of groin pain in athletes is broad and includes *pubic*, *adductor*, *inguinal*, and *iliopsoas* etiologies. Knowledge of the anatomy in each region allows for optimized diagnosis with sonography and MRI.
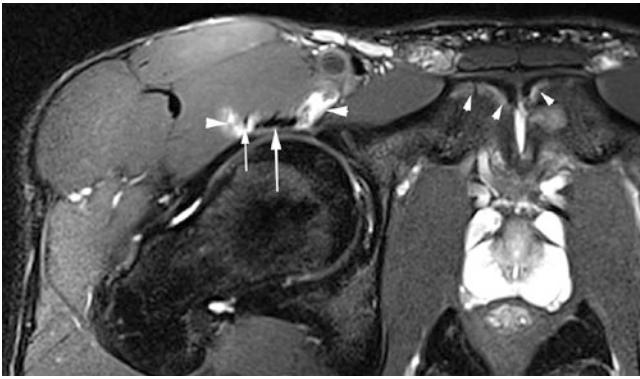
Fig. 6.12 Iliopsoas bursitis. A 23-year-old soccer player with right-sided pain. Axial T2FS MR image shows marked edema and bursitis (arrowheads) surrounding both the psoas (large arrow) and iliacus (small arrow) components of the iliopsoas tendon anterior to a normal hip joint. Note the normal pubic apophyses (small white arrowheads). (Reproduced with permission from reference Madani H, Robinson P. Top-Ten Tips for Imaging Groin Injury in Athletes. *Semin Musculoskelet Radiol.* 2019;23(4):361–75.)
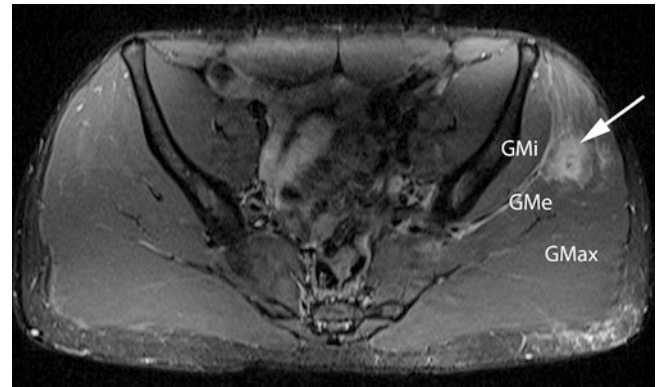
6.2 Lateral Pelvis

Anatomy. The abductor tendons evaluated most commonly are the gluteus minimus and gluteus medius. The gluteus minimus inserts predominantly onto the anterior facet of the greater trochanter, with some fibers also merging with the hip joint capsule. The gluteus medius has two insertion sites on the greater trochanter, with a thicker portion inserting at the superoposterior facet and a thinner portion inserting distally at the lateral facet [20]. Together, these two gluteal tendons are often referred to as "the abductor tendons" or "rotator cuff of the hip." Several bursae adjacent to the greater trochanter have been described, with the largest located superficial to the posterior facet (the trochanteric bursa).

At the lateral aspect of the pelvis, the iliotibial band (ITB) (anteriorly) and gluteal aponeurotic fascia (posteriorly) originate at the margin of the iliac crest, descending superficial to the gluteus medius and greater trochanter [21].

Injury Patterns. Trochanteric pain syndrome is generally caused by abnormalities involving the abductor tendons. Although peritrochanteric edema and bursal fluid are commonly present with trochanteric pain syndrome, they are generally not reliably associated with symptoms [22].

The ITB and gluteal aponeurotic fascia can be injured with trauma or repetitive microtrauma. In addition to apophyseal derangements in skeletally immature patients and enthesitis at the osseous attachment in adults, the proximal ITB is a characteristic site of overuse injuries (e.g., in runners).

Imaging Findings. Tendinopathy and tearing in the abductor tendons become increasingly prevalent with advanc-

Fig. 6.13 Myotendinous injury. A 23-year-old soccer player with acute buttock pain. Axial T2FS MR image shows left gluteus medius myotendinous tear (arrow). The distal tendon was normal and intact

ing age. As with rotator cuff tears in the shoulder, these tendon tears typically are located near the osseous insertion site and begin as partial-thickness tears (fiber discontinuity and T2 hyperintensity). Incomplete abductor tendon tears are most commonly reported at the distal-anterior fibers of the gluteus medius tendon [20]. Some tears are discovered as incidental, non-acute findings. Chronic tears associated with muscle atrophy and fatty infiltration have suboptimal surgical outcomes. Acute tears in the muscle belly of athletes are relatively uncommon but can occur (Fig. 6.13).

"Proximal ITB syndrome" typically occurs superolateral to the hip joint and may be overlooked at the margin of the MRI FOV. Characteristic findings include edema along the proximal ITB, often with subtle fiber thickening at the proximal attachment or a small area of ill-defined partial tearing.

> **Key Point**
> - At the *lateral* aspect of the pelvis, derangements may occur in the abductor tendons, ITB, and gluteal aponeurotic fascia. Partial abductor tears are most commonly reported at the distal-anterior gluteus medius tendon. Disorders at the ITB and gluteal aponeurotic fascia regions include apophysitis, enthesitis, and proximal iliotibial band syndrome.

6.3 Inferior Pelvis

Anatomy. The hamstring tendons originate at the ischial tuberosity, with the semimembranosus tendon anteriorly and the conjoined tendon of the biceps femoris (long head) and semitendinosus posteriorly. (*If you have difficulty remembering that it's the biceps femoris and semitendinosus that form the conjoined tendon, just remember that "best friends stick together"!*)

Ischiofemoral impingement is associated with a narrowed space between the ischial tuberosity and the femur. Predisposing factors may be developmental (e.g., pelvic morphology resulting in increased ischial and femoral neck angles [23], femoral morphology resulting in increased femoral version or coxa valga [24]) or acquired (e.g., heterotopic ossification, post-traumatic deformity).

Injury Patterns and Imaging Findings. In the acute setting, hamstring muscle eccentric contraction can result in strain-type injuries that usually involve the myotendinous junction and are treated non-operatively in young adult athletes (as shown in Fig. 6.5, above). Tendon ruptures at the proximal attachment are much less common in young adults but are important to recognize because they may be repaired surgically (particularly if at least two-thirds of the tendon fibers are ruptured and retracted) (Fig. 6.14).

In the chronic setting, hamstring tendon tears are associated with scarring that may tether the sciatic nerve and make delayed repair more difficult. In older adults, hamstring tendinopathy and attritional partial tears are extremely common (e.g., interstitial tearing or stripping at the conjoined tendon attachment). Hamstring tendinopathy with symptomatic peritendinous edema in the adjacent bone and soft tissues also can occur in young adult athletes owing to overuse (Fig. 6.15).

Ischiofemoral impingement on MRI is defined by narrowing of the ischiofemoral space (≤ 15 mm) or quadratus
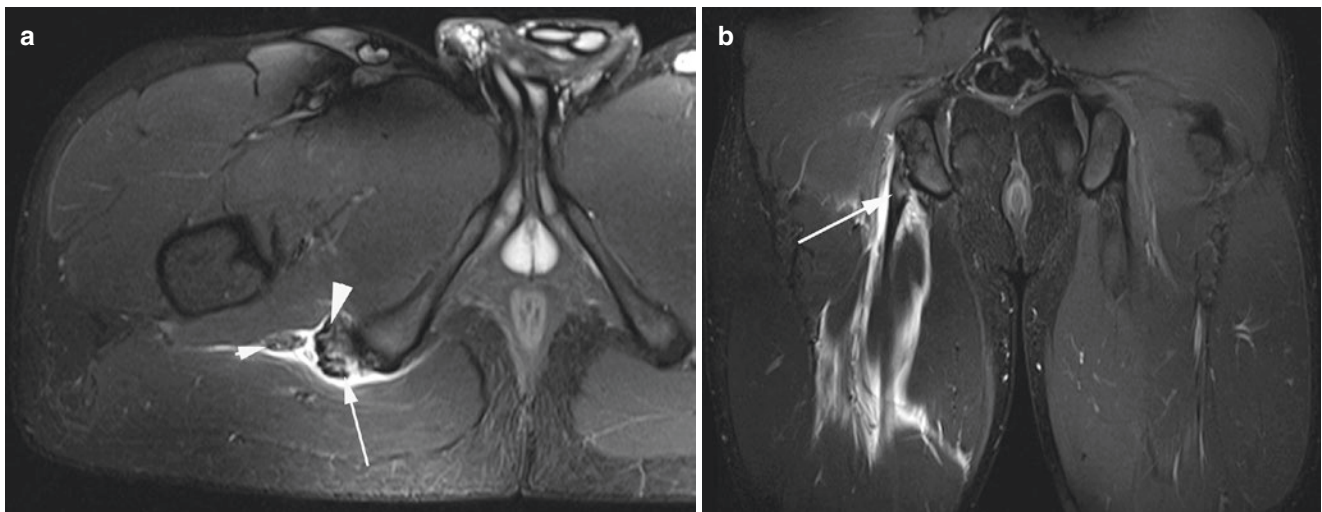
Fig. 6.14 Tendon injury. A 26-year-old soccer player with acute hamstring pain. (**a**) Axial and (**b**) coronal T2FS MR images show right conjoint tendon origin partial tear (arrow), edematous but grossly intact proximal semimembranosus tendon (large arrowhead). Adjacent sciatic nerve (small arrowhead) and extensive tracking fluid/hemorrhage
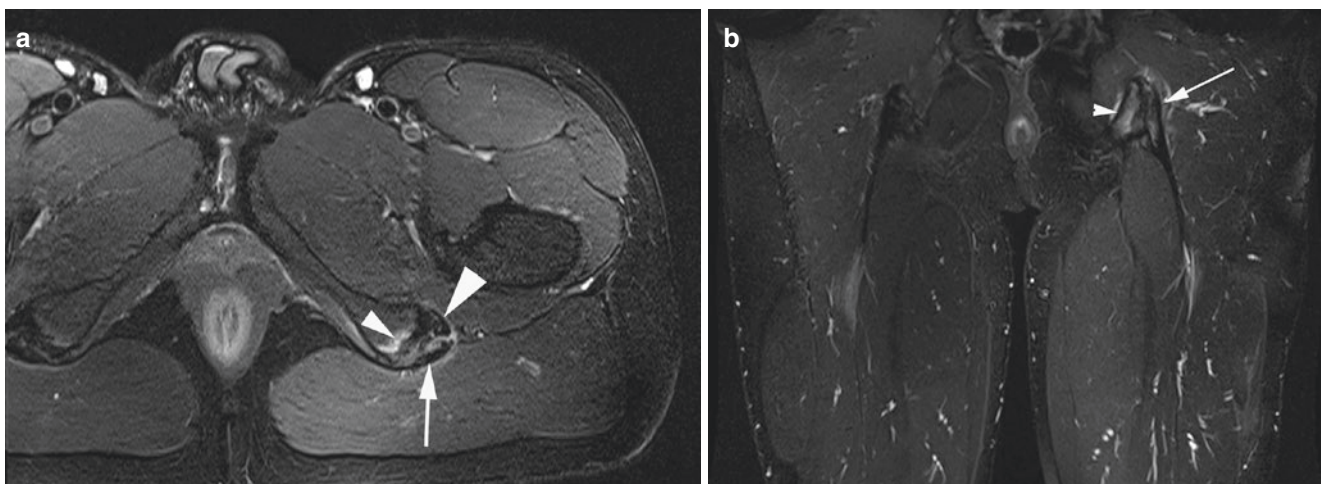
Fig. 6.15 Tendinopathy. A 25-year-old soccer player with subacute hamstring pain. (**a**) Axial and (**b**) coronal T2FS MR images show left ischial subcortical bone marrow edema (small arrowhead), paratenon edema, intrinsic conjoint tendon oedema (arrow), and normal semimembranosus tendon (large arrowhead)

femoris space (≤ 10 mm) with associated quadratus femoris edema or fatty infiltration/atrophy (Fig. 6.16). The ischiofemoral interval, however, varies with patient positioning. With active external rotation during kinematic MRI, for example, dynamic narrowing of the space occurs [25]. Interestingly, compared with matched controls, patients with ischiofemoral impingement have a higher prevalence of abductor tears and abductor muscle atrophy, suggesting to some investigators that abductor tears might be causally associated with ischiofemoral impingement [26].

Fig. 6.16 Ischiofemoral impingement. A 22-year-old female recreational athlete with chronic hip pain. Axial PDFS MR image shows diffuse edema in the quadratus femoris muscle (arrows) bridging between the ischium and lesser trochanter

> **Key Point**
> • At the *inferior* aspect of the pelvis, hamstring disorders and ischiofemoral impingement are well characterized by MRI.

6.4 Posterior Pelvis

Anatomy. The sacrum typically has five fused segments in adults, with four pairs of anterior and posterior foramina, as well as a normal opening ("sacral hiatus") posteriorly at the S4/S5 level [27].

The coccyx has four segments in ~75% of the population, but the number of segments varies from three to five. The intercoccygeal joints may or may not be fused and have highly variable alignment [27].

Injury Patterns and Imaging Findings. Both traumatic fractures and stress fractures occur in the sacrum (Fig. 6.17). These fractures may be described as involving the ala (zone I), the foraminal region (zone II), or the sacral spinal canal (zone III) [28]. In trauma patients, isolated zone I fractures are usually not associated with neurological deficits (< 10%) and are treated conservatively, while zone III fractures are more commonly associated with neurological deficits (> 50%) and surgical treatment (especially for displaced or unstable fractures) [28].

With acute trauma to the sacrum or coccyx, it has been recommended that radiography be eliminated. Radiography misses most sacral fractures, with a sensitivity often cited at 30% [29]. Consequently, even in the setting of known or sus-
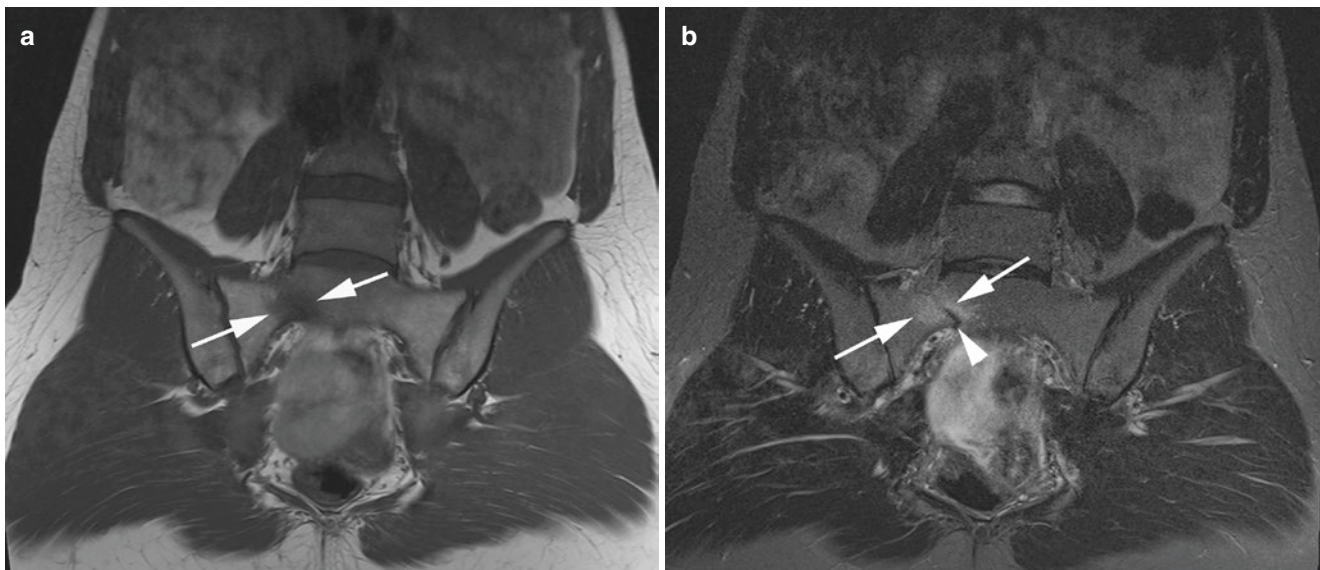
Fig. 6.17 Stress fracture. A 24-year-old male recreational athlete with subacute low back pain. Coronal (**a**) T1 and (**b**) T2FS MR images show right-sided focal sacral bone marrow edema (arrows) and fracture line (arrowhead)

pected trauma, radiography is *not* considered the initial diagnostic imaging test of choice in many settings. In the emergency department setting, for example, it has been recommended that radiography of the sacrum and coccyx be eliminated because it can actually result in increased wait times, delayed follow-up imaging, and substantial radiation exposure [29]. Rather, patients may benefit from being treated conservatively or receiving advanced imaging based on clinical parameters.

In geriatric patients with bilateral fragility fractures of the sacrum [30], fractures start with unilateral sacral disruption, followed by contralateral sacral alar fracture and then an interconnecting transverse fracture in at least half of all cases (more commonly at S1/S2 than S2/S3).

With chronic coccyx pain (coccydynia), radiography is controversial. Advocates believe that lateral radiography in the seated position can reveal excessive motion (compared to the standing position) (defined as > 25% posterior subluxation or > 25 degrees of flexion with sitting, compared to standing) [27]. Detractors of coccygeal radiography note the high pelvic radiation dose and the low diagnostic yield, including unreliable assessment for important abnormalities like fracture, neoplasm, and infection. On MRI, a small FOV technique in patients with coccydynia can show edema that is related to mechanical irritation and abnormal motion [27]. Depending on the etiology of coccydynia, the diverse menu of treatment options includes percutaneous injection (e.g., of the ganglion impar), cement augmentation (coccygeoplasty), extracorporeal shock wave therapy, neuromodulation of dorsal root ganglia, and coccygectomy.

> **Key Point**
> - At the *posterior* aspect of the pelvis, pain in the sacrum and coccyx is a common clinical complaint. Rather than routine radiography, patients may benefit from being treated conservatively or receiving advanced imaging based on clinical evaluation. In evaluation of small abnormalities, high spatial resolution cross-sectional imaging may help direct patient management.

6.5 Concluding Remarks

Pain in the groin and pelvis are common, but accurate clinical diagnosis can be challenging. Patients commonly localize orthopedic symptoms to the anterior, lateral, inferior, or posterior aspect of the pelvis. Each of these four locations has its own intricate anatomy, distinctive disorders, and treatment pathways. By optimizing our knowledge and imaging techniques in each location, we are able to add value by optimally "ruling in" and "ruling out" key diagnoses, thus optimizing patient management and outcomes.

> **Take Home Messages**
> - Although groin pain in athletes can originate at the hip or elsewhere, groin pain is often classified into four categories related to location: pubic, adductor, inguinal, and iliopsoas.
> - At the anterior aspect of the pelvis, the most important areas of injury in athletes include the pubic symphysis capsular ligaments and the rectus abdominis/adductor aponeurosis attachment sites.
> - At the lateral aspect of the pelvis, tendinopathy and tearing of the abductor tendons are common pain generators. Important injuries also may occur near the margin of the iliac crest, including proximal ITB syndrome.
> - At the inferior aspect of the pelvis, hamstring disorders and ischiofemoral impingement are frequently evaluated by MRI.
> - At the posterior aspect of the pelvis, derangements in the sacrum and coccyx are often missed with conventional radiography. Patients should be advanced to cross-sectional imaging in the appropriate clinical context.

References

1. Ricci PL, Maas S, Gerich T, Kelm J. Influence of pubic symphysis stiffness on pelvic load distribution during single leg stance. Int J Numer Methods Biomed Eng. 2020;36:e3319.
2. Meyers AB, Laor T, Zbojniewicz AM, Anton CG. MRI of radiographically occult ischial apophyseal avulsions. Pediatr Radiol. 2012;42:1357–63.
3. Sailly M, Whiteley R, Read JW, Giuffre B, Johnson A, Hölmich P. Pubic apophysitis: a previously undescribed clinical entity of groin pain in athletes. Br J Sports Med. 2015;49:828–34.
4. Serner A, Weir A, Tol JL, et al. Characteristics of acute groin injuries in the hip flexor muscles—a detailed MRI study in athletes. Scand J Med Sci Sports. 2018;28:677–85.
5. Wörner T, Thorborg K, Eek F. High prevalence of hip and groin problems in professional ice hockey players, regardless of playing position. Knee Surg Sports Traumatol Arthrosc. 2020;28:2302–8.
6. Kobayashi D, Kobayashi N, Oishi T, et al. Prevalence of groin pain in unicycle athletes: a nationwide questionnaire survey. J Orthop Surg (Hong Kong). 2020;28:2309499020934201.
7. Vasileff WK, Nekhline M, Kolowich PA, Talpos GB, Eyler WR, van Holsbeeck M. Inguinal hernia in athletes: role of dynamic ultrasound. Sports Health. 2017;9:414–21.
8. Brandon CJ, Jacobson JA, Fessell D, et al. Groin pain beyond the hip: how anatomy predisposes to injury as visualized by musculoskeletal ultrasound and MRI. Am J Roentgenol. 2011;197:1190–7.

9. Yeap PM, Robinson P. Ultrasound diagnostic and therapeutic injections of the hip and groin. J Belg Soc Radiol. 2017;101(Suppl 2):6.

10. Madani H, Robinson P. Top-ten tips for imaging groin injury in athletes. Semin Musculoskelet Radiol. 2019;23:361–75.

11. Morley N, Grant T, Blount K, Omar I. Sonographic evaluation of athletic pubalgia. Skeletal Radiol. 2016;45:689–99.

12. Gupta H, Subedi N, Robinson P. Effectiveness of sonography in detecting clinically occult femoral hernias. J Ultrasound Med. 2016;35:1675–9.

13. Robinson P, Grainger AJ, Hensor EMA, Batt ME, O'Connor PJ. Do MRI and ultrasound of the anterior pelvis correlate with, or predict, young football players' clinical findings? A 4-year prospective study of elite academy soccer players. Br J Sports Med. 2015;49:176–82.

14. Weir A, Brukner P, Delahunt E, et al. Doha agreement meeting on terminology and definitions in groin pain in athletes. Br J Sports Med. 2015;49:768–74.

15. Serner A, Roemer FW, Hölmich P, et al. Reliability of MRI assessment of acute musculotendinous groin injuries in athletes. Eur Radiol. 2017;27:1486–95.

16. Serner A, Weir A, Tol JL, et al. Associations between initial clinical examination and imaging findings and return-to-sport in male athletes with acute adductor injuries: a prospective cohort study. Am J Sports Med. 2020;48:1151–9.

17. Schilders E, Mitchell AWM, Johnson R, Dimitrakopoulou A, Kartsonaki C, Lee JC. Proximal adductor avulsions are rarely isolated but usually involve injury to the PLAC and pectineus: descriptive MRI findings in 145 athletes. Knee Surg Sports Traumatol Arthrosc. 2020; https://doi.org/10.1007/s00167-020-06180-5. Epub ahead of print. PMID: 32767053

18. Branci S, Thorborg K, Nielsen MB, Hölmich P. Radiological findings in symphyseal and adductor-related groin pain in athletes: a critical review of the literature. Br J Sports Med. 2013;47:611–9.

19. Bou Antoun M, Ronot M, Crombe A, Moreau-Durieux MH, Reboul G, Pesquer L. High insertion of conjoint tendon is associated with inguinal-related groin pain: a MRI study. Eur Radiol. 2020;30:1517–24.

20. Tsutsumi M, Nimura A, Akita K. The gluteus medius tendon and its insertion sites: an anatomical study with possible implications for gluteus medius tears. J Bone Joint Surg Am. 2019;101:177–84.

21. Huang BK, Campos JC, Michael Peschka PG, et al. Injury of the gluteal aponeurotic fascia and proximal iliotibial band: anatomy, pathologic conditions, and MR imaging. Radiographics. 2013;33:1437–52.

22. Blankenbaker DG, Ullrick SR, Davis KW, De Smet AA, Haaland B, Fine JP. Correlation of MRI findings with clinical findings of trochanteric pain syndrome. Skeletal Radiol. 2008;37:903–9.

23. Bredella MA, Azevedo DC, Oliveira AL, et al. Pelvic morphology in ischiofemoral impingement. Skeletal Radiol. 2015;44:249–53.

24. López-Royo MP, Valero-Tena E, Roca M. Anatomical analysis of the pelvis to identify any predisposing anatomical factors for ischiofemoral space pathology: a retrospective study. Br J Radiol. 2020;93:20190556.

25. Vicentini JR, Martinez-Salazar EL, Simeone FJ, Bredella MA, Palmer WE, Torriani M. Kinematic MRI of ischiofemoral impingement. Skeletal Radiol. 2020; https://doi.org/10.1007/s00256-020-03519-4.

26. Kheterpal AB, Harvey JP, Husseini JS, Martin SD, Torriani M, Bredella MA. Hip abductor tears in ischiofemoral impingement. Skeletal Radiol. 2020;49:1747–52.

27. Skalski MR, Matcuk GR, Patel DB, Tomasian A, White EA, Gross JS. Imaging coccygeal trauma and coccydynia. RadioGraphics. 2020;40:1090–106.

28. Rizkalla JM, Lines T, Nimmons S. Classifications in brief: the Denis classification of sacral fractures. Clin Orthop Relat Res. 2019;477:2178–81.

29. Hanna TN, Sadiq M, Ditkofsky N, et al. Sacrum and coccyx radiographs have limited clinical impact in the emergency department. Am J Roentgenol. 2016;206:681–6.

30. Mendel T, Ullrich BW, Hofmann GO, et al. Progressive instability of bilateral sacral fragility fractures in osteoporotic bone: a retrospective analysis of X-ray, CT, and MRI datasets from 78 cases. Eur J Trauma Emerg Surg. 2020; https://doi.org/10.1007/s00068-020-01480-4.

Knee

7

Marcelo Bordalo-Rodrigues and Lawrence M. White

Learning Objectives
- To recognize normal anatomy of the knee.
- To recognize abnormalities of main knee structures.
- To diagnose knee abnormalities on MRI.

7.1 Introduction

Imaging has a crucial role in detecting internal derangements of the knee, and knowledge of pathologic conditions has increased. Imaging aspects of meniscal, ligament, tendinous, and chondral lesions will be discussed in this chapter.

7.2 Menisci

7.2.1 Anatomy and Function

Menisci are fibrocartilaginous structures that serve to enlarge the articular surfaces of the femoral condyles and tibia, as well as promote shock absorption and load distribution across the joint [1, 2]. The menisci are composed of an anterior horn, a body, and a posterior horn and do not have identical morphologies. The lateral meniscus has a circular shape and a looser capsular attachment. Posteriorly the lateral meniscus is separated from the capsule by the popliteus tendon and sheath (popliteus hiatus). The anterior and posterior horns of the lateral meniscus have the same size. The medial meniscus has a semicircular shape

M. Bordalo-Rodrigues (✉)
Department of Radiology, University of Sao Paulo Medical School, Sao Paulo, SP, Brazil

L. M. White
Department of Medical Imaging, University of Toronto, Toronto, ON, Canada
e-mail: Lawrence.white@uhn.ca

and is firmly attached to the capsule and less mobile than the lateral meniscus. For that reason, it is more susceptible to tears. Its anterior horn is smaller than the posterior horn. Both menisci have anterior and posterior insertions at the tibia (meniscal roots) [2].

The transverse meniscal ligament connects and stabilizes the anterior horns of the menisci and can mimic a tear on sagittal MR images [3] (Fig. 7.1).

Meniscofemoral ligaments connect the posterior horn of the lateral meniscus to the inner aspect of the medial femoral condyle, with the anterior meniscofemoral ligament of Humphrey and posterior meniscofemoral ligament of Wrisberg denoted based on their course, anterior and posterior to the posterior cruciate ligament, respectively [4].

Popliteomeniscal fascicles are fibrous structures that connect the posterior horn of the lateral meniscus to the joint capsule around the popliteal tendon sheath and help form the popliteal hiatus [1, 2]. They stabilize the posterior horn of the lateral meniscus during knee motion. Lesions of these fascicles are highly associated with tears of the posterior horn of the lateral meniscus [5].

An oblique meniscomeniscal ligament is an uncommon variant with a reported prevalence of 1–4% consisting of a ligamentous connection between the anterior horn of one meniscus and the posterior horn of the opposite meniscus and can mimic a displaced meniscal fragment [6].

7.2.2 Anatomic Variants

Discoid meniscus is an enlarged meniscus with central extension onto the tibial articular surface. It is 10–20 times more common in the lateral meniscus [7]. There are four distinct variants of discoid meniscus, according to the percentage of tibial plateau coverage: (1) complete (covers entire tibial plateau), (2) partial (covers 80% or less of the tibial plateau), (3) Wrisberg (thickened posterior horn, lacking posterior meniscal attachments), and (4) ring-shaped variant
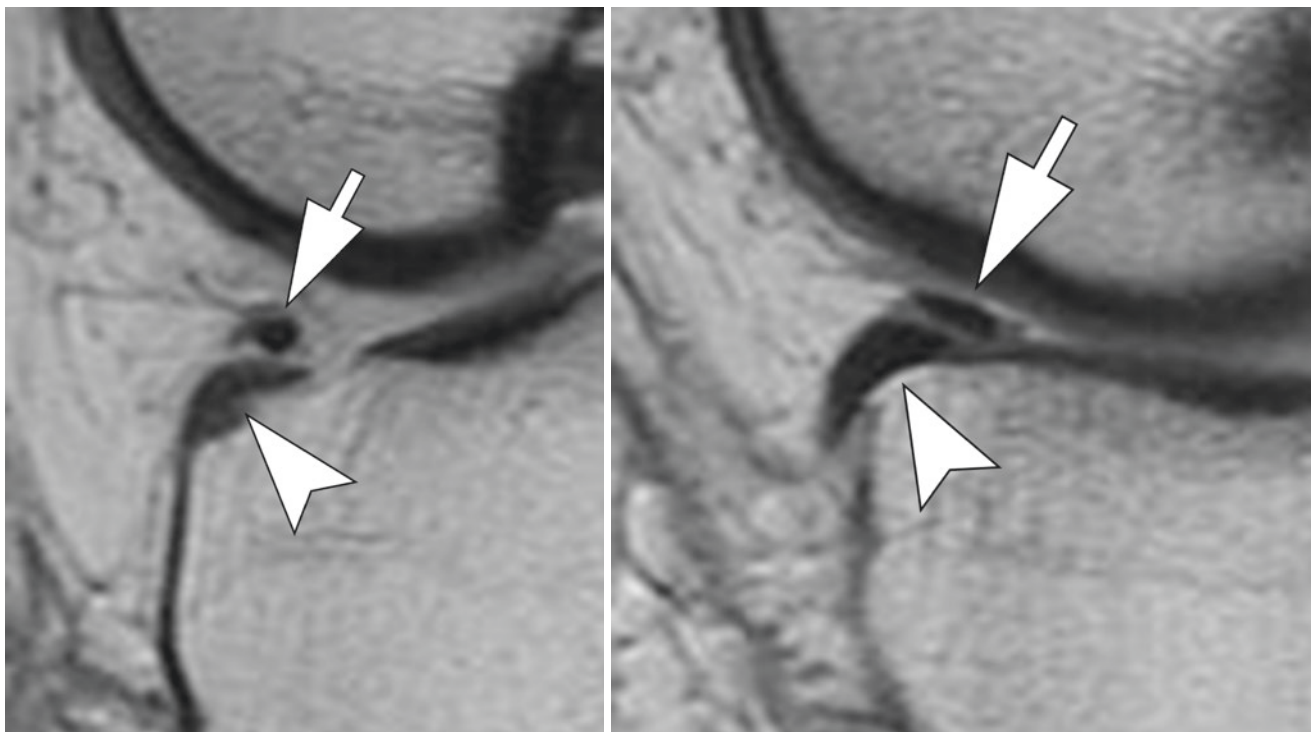
Fig. 7.1 Transverse meniscal ligament. Consecutive sagittal proton density (PD)-weighted images of the knee. The transverse meniscal ligament (arrows) inserting on the anterior horn of the medial meniscus (arrowheads), mimicking a tear

with connection between the anterior and posterior horns (can mimic a bucket-handle tear) [8, 9] (Fig. 7.2).

Meniscal flounce is a single symmetric fold along the free edge of the medial meniscus, secondary to flexion of the knee and physiologic redundancy of the free edge of the meniscus. It is not a tear; however, it may mimic a radial tear on coronal images [10, 11].

Meniscal ossicle is a rare developmental, degenerative, or post-traumatic variant, more common on the posterior horn of the medial meniscus. It may mimic an ossified loose body on radiographs and a tear on MRI.

7.2.3 Meniscal Tears

Meniscal tears are most common at the posterior horn of the medial meniscus; however, in young patients with acute injuries, lateral meniscal tears are common. There is an increased incidence of peripheral meniscal tears in cases of anterior cruciate ligament tears [12].

Normal menisci should have low signal on MR imaging. Linear or globular intrameniscal high signal is normally observed in children and at peripheral portions of the meniscus (red zone), due to high vascularization. MR accuracy for diagnosis of a meniscal tear is 90–95%, using arthroscopy as gold standard [12, 13]. MR imaging criteria for a meniscal tear are meniscal morphologic distortion (in absence of prior surgery) or intrameniscal high signal intensity extending to an articular surface, seen on two or more consecutive slices [13, 14]. If these criteria are seen in only one slice, the finding should be reported as a "possible tear" [15]. Increased intrameniscal high signal without articular surface extension should not be reported as tear and usually represents mucinous degeneration are acute intrasubstance contusion due to trauma [7].

Tears should be described accurately by radiologists in order to guide appropriate treatment. Most meniscal tear classification systems are based on the direction and location of the tear. **Longitudinal tears** run parallel to the long (circumferential) axis of the meniscus and perpendicular to tibial plateau. **Vertical longitudinal tears** are oriented in a superior-inferior direction and extend to one or both articular surfaces (Fig. 7.3). **Horizontal tears** also run parallel to the long axis of the meniscus but, however, are oriented parallel to the tibial plateau (Fig. 7.4). Typically, horizontal meniscal tears communicate with the free edge or articular surface of the meniscus. **Radial tears** are vertical meniscal tears which run perpendicular to the long axis of the meniscus and the tibial plateau. Typically, radial tears appear as linear signal changes perpendicular to the free/inner edge of the meniscus. Depending on the tear location and extent, unique MR signs may be present in the setting of a radial tear, including the "ghost meniscus" and the "truncated triangle" signs (Fig. 7.5). **A root tear** is typically a radial tear involving one
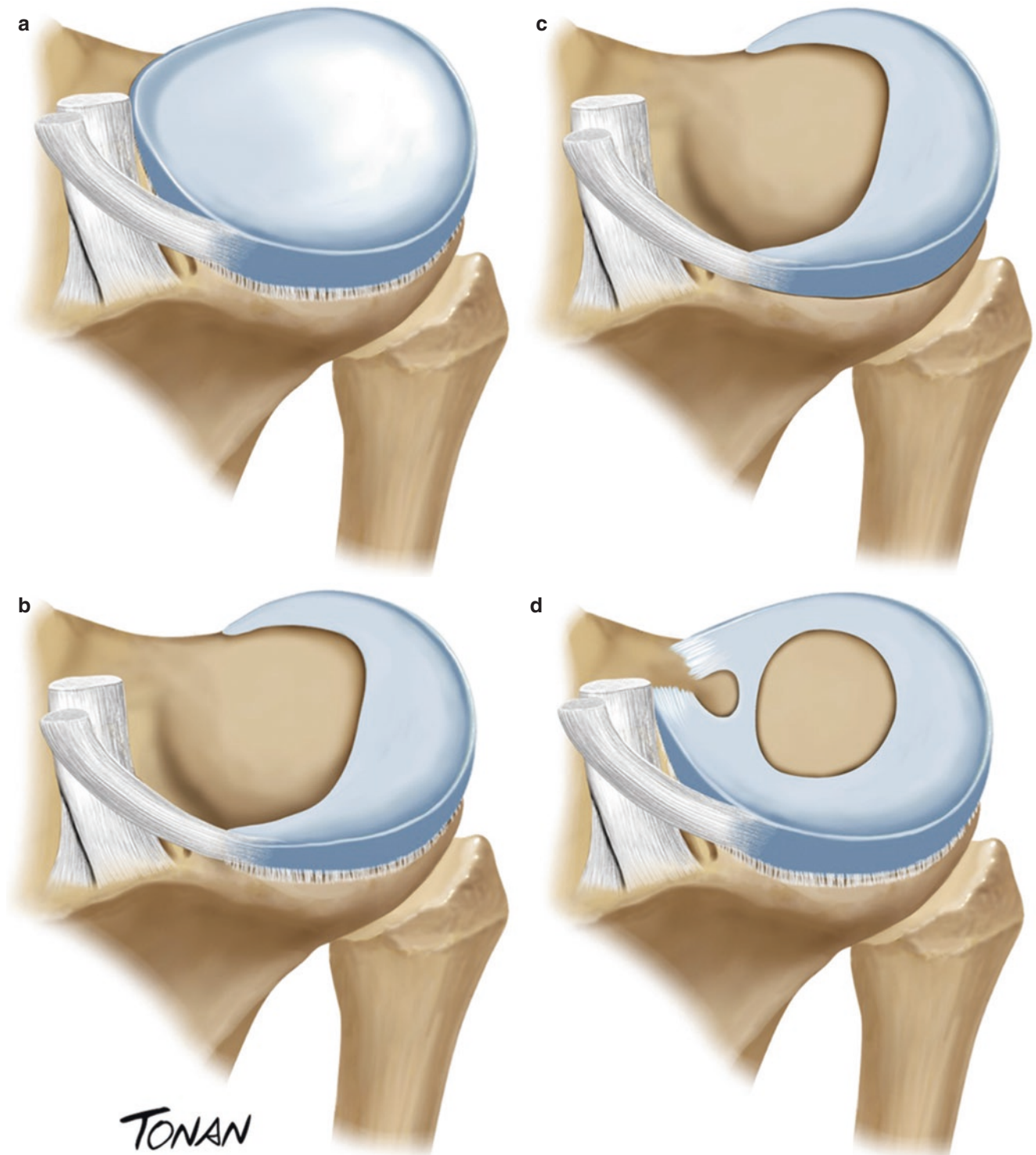
Fig. 7.2 Discoid meniscus variants. Schematic drawing demonstrates (**a**) complete discoid meniscus; (**b**) partial discoid meniscus; (**c**) Wrisberg variant (note absence of posterior meniscal attachments); and (**d**) ring-shaped discoid meniscus. (Reproduced with Permission by Rodrigo Tonan)

of the meniscal roots, most commonly the posterior root of the medial meniscus. Complete root tears are associated with meniscal extrusion and progressive femorotibial degenerative changes (Fig. 7.6). **Complex tears** are a combination of longitudinal, horizontal, and radial tear components (at least two) [7]. Meniscal tears which communicate with the periphery of the meniscus may be associated with the formation of a parameniscal cyst.

A **meniscal "ramp lesion"** is a longitudinal vertical meniscal tear at the peripheral attachment of the posterior horn of the medial meniscus [16]. It is strongly associated with ACL tears and reflective of traumatic injury of the meniscocapsular junction [17, 18]. MR findings of a ramp lesion are meniscocapsular separation (with or without intervening fluid-like signal), peripheral meniscal irregularities, and far peripheral longitudinal tearing of the medial meniscus [19] (Fig. 7.7).

A **zip lesion** or Wrisberg rip is a longitudinal vertical meniscal tear progressing from the distal insertion of the posterior meniscofemoral ligament (Wrisberg) through the posterior horn of the lateral meniscus, which may be seen in association with ACL tears [20–22] (Fig. 7.8).

Displaced meniscal tears include free fragments or flap lesions associated with a meniscal tear. Small meniscal displaced fragments may not be seen at arthroscopy; thus,

Fig. 7.3 Horizontal tear. Sagittal T2-weighted image of the knee with fat suppression. There is a horizontal tear of the mesial meniscus, extending to the free edge (arrow) and posterior capsular surface (arrowhead)
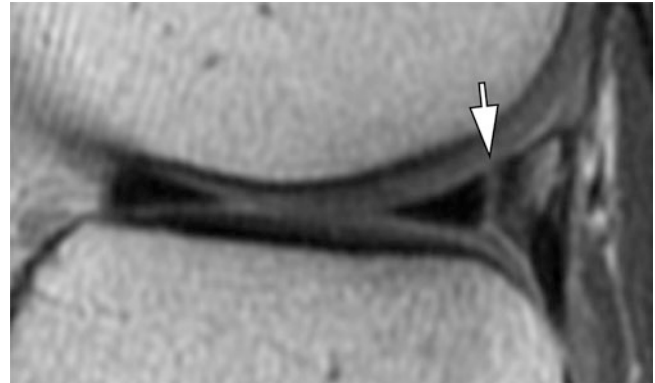
Fig. 7.4 Vertical tear. Sagittal PD-weighted image of the knee. A peripheral vertical tear extending to superior and inferior articular surfaces (arrow)
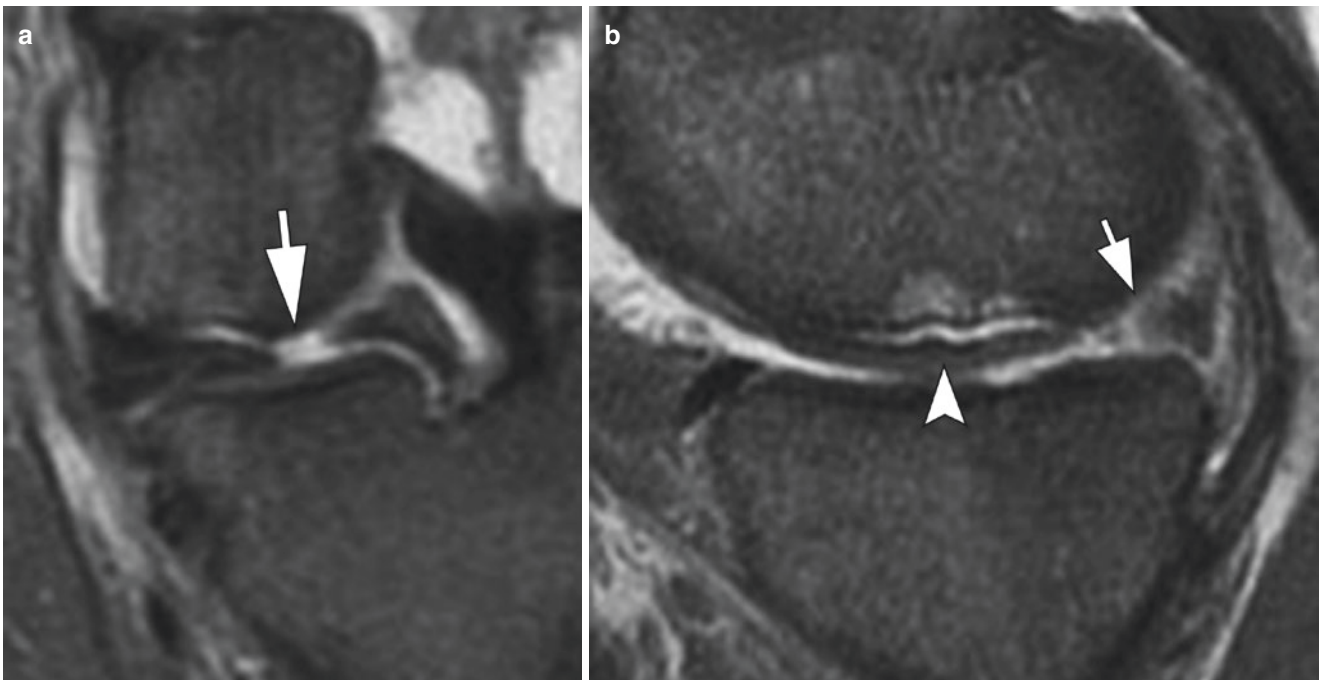
Fig. 7.5 Radial tear. (**a**) Coronal and (**b**) sagittal T2-weighted images of the knee with fat suppression. Linear tear of the posterior horn of the medial meniscus, perpendicular to free edge (white arrow). On the sagittal plane, the radial tear has a "truncated triangle" aspect (black arrow). There is also a subchondral fracture of the medial femoral condyle (arrowhead)
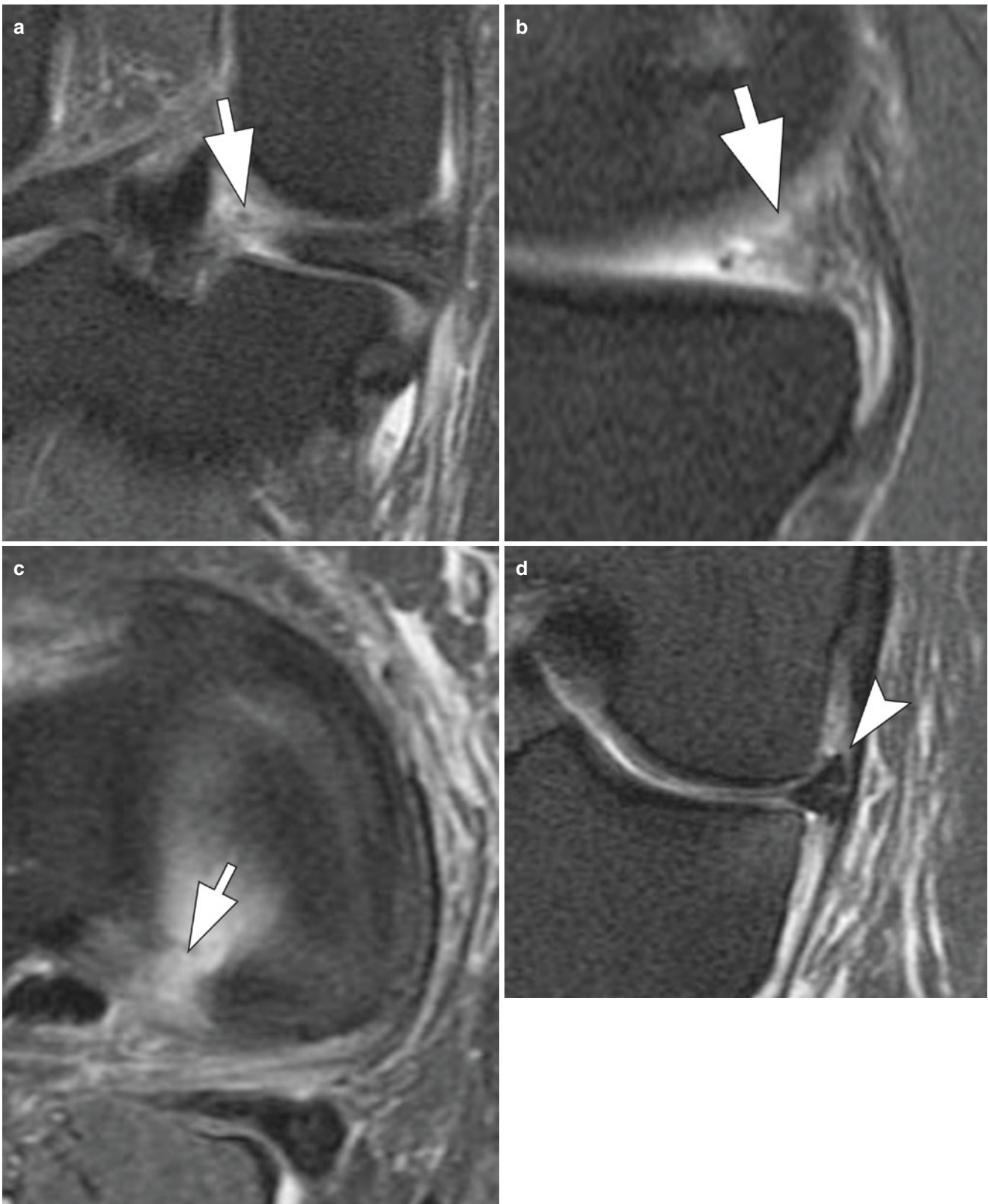
Fig. 7.6 Root tear. (**a**) Coronal; (**b**) sagittal; (**c**) axial; and (**d**) coronal T2-weighted images of the knee with fat suppression. There is a complete radial tear in the posterior root of the medial meniscus (arrows), with a "ghost meniscus" sign on the sagittal image (arrow in **b**). There is an associated extrusion of the body (arrowhead)

Fig. 7.7 Ramp lesion. Sagittal T2-weighted image of the knee with fat suppression. Vertical tear of the posterior meniscocapsular junction extending to the peripheral aspect of the medial meniscus (arrow)

identification on MR images can be of critical importance in patient management and preoperative planning. Fragments are more common arising from the medial meniscus and may be displaced around the PCL, in the intercondylar notch, or peripherally along the superior/inferior recesses of the joint. In absence of prior surgery, a diminutive morphology of the meniscus should alert the radiologist to search for a displaced meniscal flap (Fig. 7.9). A bucket handle tear is a displaced vertical longitudinal tear associated with central displacement of the inner part of the meniscus. Bucket handle tears are more common in the medial meniscus, and several imaging signs have been described associated with bucket handle meniscal tears at MR imaging including a double PCL sign, absent bow tie, double anterior horn, fragment in the notch, and small posterior horn [23, 24] (Fig. 7.10).

> **Key Point**
> - Signal abnormalities that extend to meniscal surface and displaced meniscal fragments are important features to be identified on MRI.
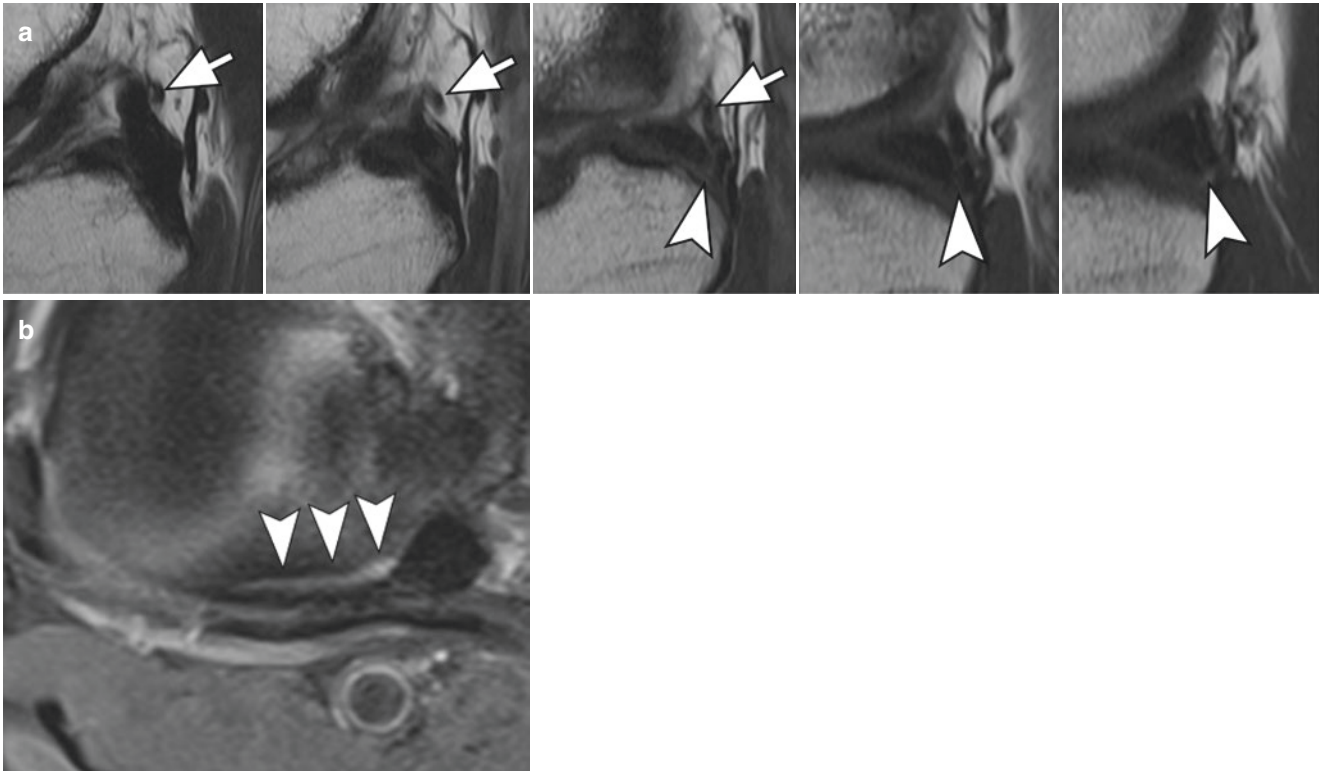
Fig. 7.8 Zip lesion. (**a**) Consecutive sagittal PD-weighted images and (**b**) axial T2-weighted image show the Wrisberg ligament inserting in the posterior horn of the lateral meniscus (arrows) and a peripheral vertical longitudinal tear of this meniscus (arrowheads)
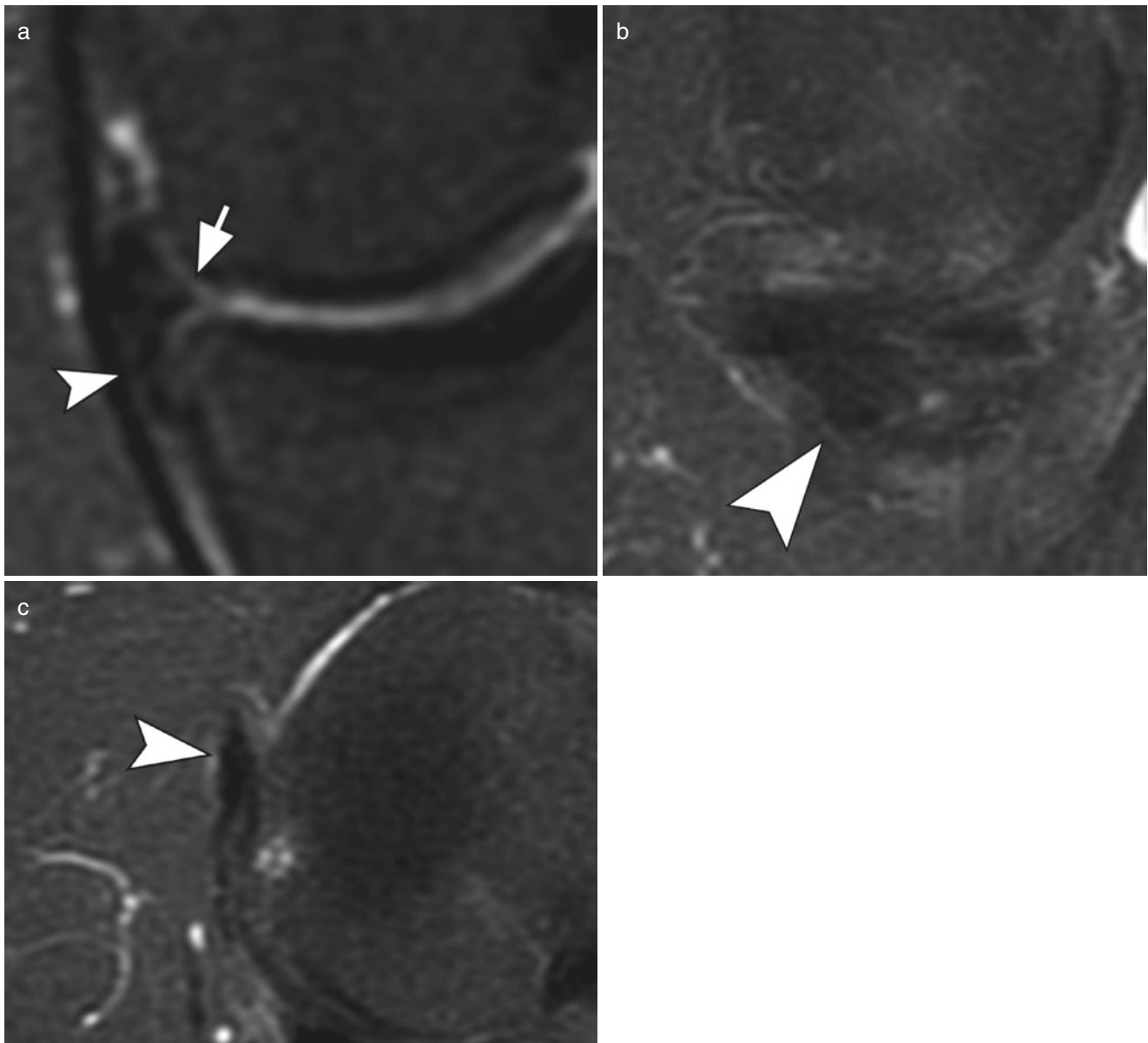
Fig. 7.9 Displaced meniscal tear. (**a**) Coronal; (**b**) sagittal; and (**c**) axial T2-weighted images of the knee with fat suppression. There is a complex tear at the body of medial meniscus with increase in size (arrow). A displaced inferior meniscal flap is associated with this tear (arrowheads)

7.3 Ligaments

7.3.1 Cruciate Ligaments

7.3.1.1 Anterior Cruciate Ligament
Anatomy and Function
The anterior cruciate ligament (ACL) is an intracapsular and extrasynovial structure that is proximally attached to the medial surface of the lateral femoral condyle and a distal attachment on the tibia, anterolateral to the tibial spines. The distal insertion of the ACL is stronger and broader than its proximal femoral attachment. The fascicles are anatomically divided into two bundles, the posterolateral and anteromedial bands. The anteromedial bundle is the main restraint to anterior translation of the tibia during knee flexion, and the posterolateral bundle is the predominant restraint to anterior tibial translation during knee extension and also serves as a restraint against internal rotation of the tibia. The bundles can be visualized as distinct bands along the middle to distal thirds of the ligament, especially on axial and coronal MR images. Increased intrasubstance linear signal intensity parallel to the long axis of the ligament may be seen within the
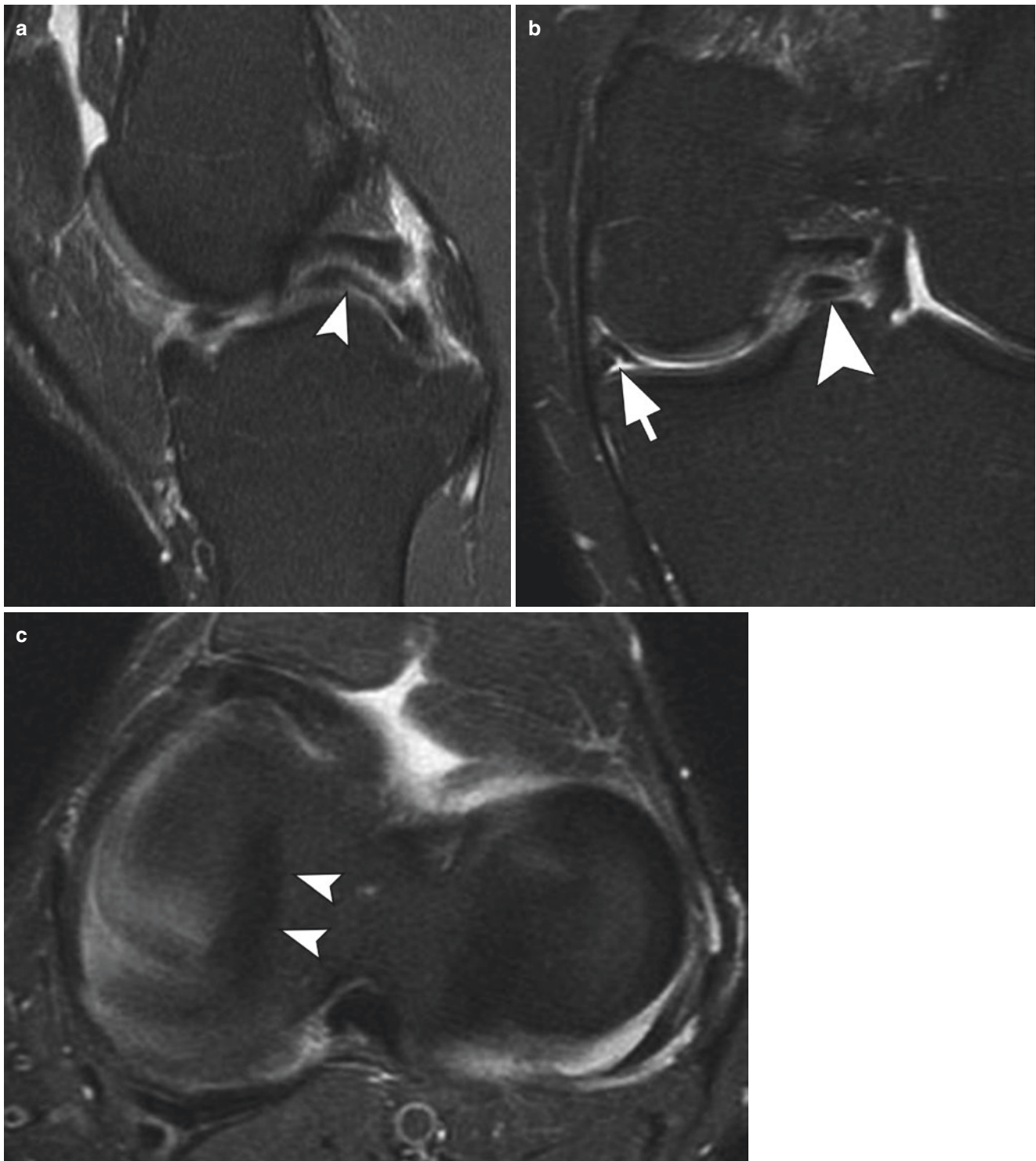
Fig. 7.10 Bucket handle tear. (**a**) Sagittal; (**b**) coronal; and (**c**) axial T2-weighted images of the knee with fat suppression. A complete longitudinal tear of the medial meniscus (arrow) with a displaced meniscal fragment to the intercondylar notch (arrowheads), with a double PCL sign (arrowhead in **b**)

distal ACL, presumably related to areas of fat and synovium between ligament fibers [2, 25]. Normal orientation of the ACL in the sagittal plane is parallel or within 9° to the roof of the intercondylar notch.

ACL Tears

Anterior cruciate ligament tears are the most common ligamentous injuries in the knee, alone or in combination with other injuries. The classic mechanism of injury involved in

Fig. 7.11 ACL tear – direct sign. Sagittal T2-weighted image of the knee with fat suppression. Complete acute tear of the ACL with increased signal at the expected location of the ligament

ACL injury is indirect trauma with pivoting stress. MR imaging examination includes evaluation of axial, coronal, and sagittal images and is highly sensitive and specific in the diagnosis of ACL tears, with an accuracy of 90–95% [26, 27].

Direct MR signs of an ACL tear are focal ligamentous discontinuity, diffuse or focal signal intensity abnormality, and mass-like appearance in the expected location of the ACL [28] (Fig. 7.11). Increased signal within the ligament may be also seen in the setting of mucoid degeneration of the ACL, with characteristic features of an intact continuous ligament fibers with internal striated intervening T2 fluid-like signal (Fig. 7.12). Abnormal orientation of the ACL including a horizontally oriented distal ACL (angle of less than 45° between the distal ACL and the tibia) or a vertically oriented proximal ACL (angle greater than 15° between the proximal ligament and the roof of the intercondylar notch) is an additional finding which may be seen following ACL injury [29]. Distal fibers of the ACL may flip anteriorly following ACL disruption [30].

Indirect MR findings of an ACL tear have additionally been described. Such indirect findings of ACL injury include subchondral bone marrow edema at the central aspect of the lateral femoral condyle (sulcus terminalis) and posterior aspect of the lateral tibial plateau, secondary to pivot shift translational osseous impaction injuries (Fig. 7.13). Osseous injury is commonly associated with meniscal injury in the same compartment [31]. Anterior translation of 5 mm or more of the posterior aspect of the lateral tibial plateau in relation to the posterior aspect of the lateral femoral condyle is another indirect finding seen in the setting of ACL disruption [32]. Other signs described in the setting of an ACL tear include uncovering of the posterior horn of the lateral meniscus and "buckling" of the PCL [28]. In chronic ACL tears, the ligament may scar, and MR may not depict true severity/extent of the prior ACL injury. Scarring of the ACL can occur to the PCL, to the roof of the intercondylar notch, to its anatomical femoral origin, or as end-to-end scarring across torn tendon margins [33].

Partial tears account for 30% of all ACL injuries [30]. Such partial ACL injuries include isolated complete tearing of either the anteromedial (more common) or posterolateral bundles of the ligament or most commonly partial injuries of both bundles [34, 35]. MRI illustrates lower accuracy rates in the detection of partial ACL tears, ranging from 25 to 53% [35]. MR signs of partial ACL tearing include attenuation of the ACL, increased intraligamentous T2 signal with partial disruption of ligamentous fibers, and posterior ACL bowing on sagittal acquisitions [34–36] (Fig. 7.14).

7.3.1.2 Posterior Cruciate Ligament
Anatomy and Function

The posterior cruciate ligament (PCL), similar to the ACL, is also an intracapsular and extrasynovial ligament. The proximal origin of the PCL is along the lateral surface of the medial femoral condyle and its distal insertion in the midline of the proximal tibia, posteroinferior to tibial articular surface. The PCL is the major restraint to tibial posterior translation and anatomically consists of anterolateral and posteromedial fiber bundles. On MR imaging, the PCL has a homogeneous low signal intensity on all pulse sequences, with a curved "comma-shaped" morphologic appearance well depicted on sagittal imaging.

PCL Tears

Posterior cruciate ligament tears are less frequent than ACL tears due to its strong fibrous structure. The most common mechanism of PCL injury is a force applied to the anterior aspect of the proximal tibia with the knee flexed, driving the tibia posteriorly. Motor vehicle accidents in which the flexed knee hits the dashboard or in a fall upon the knee with knee flexion and posterior tibial translation are typical injuries leading to PCL disruption. Multiligamentous injuries are more common than isolated PCL tears. MR signs of PCL tears include complete focal ligamentous discontinuity and
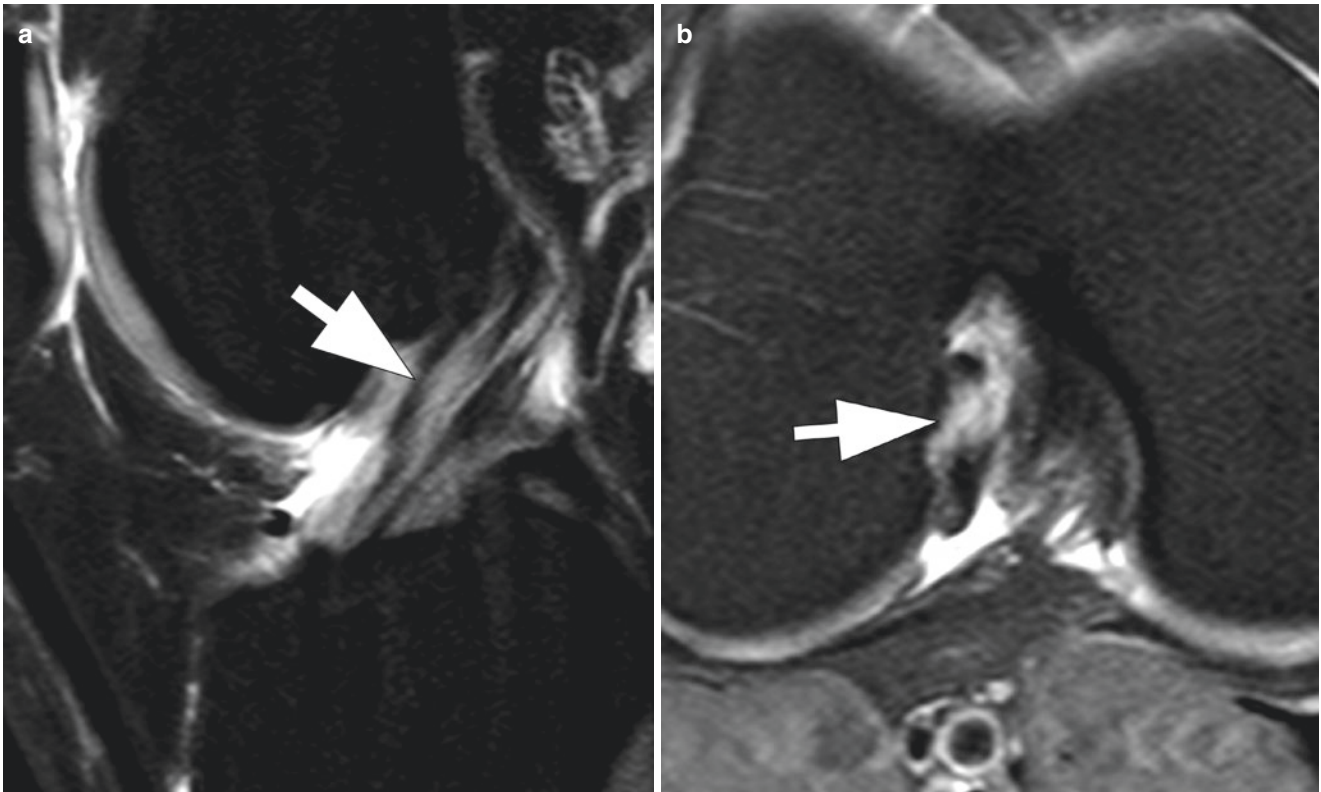
Fig. 7.12 ACL mucoid degeneration. (**a**) Sagittal and (**b**) axial T2-weighted images of the knee with fat suppression. There is increased signal within the ACL, with internal ligament striation preserved (arrows)
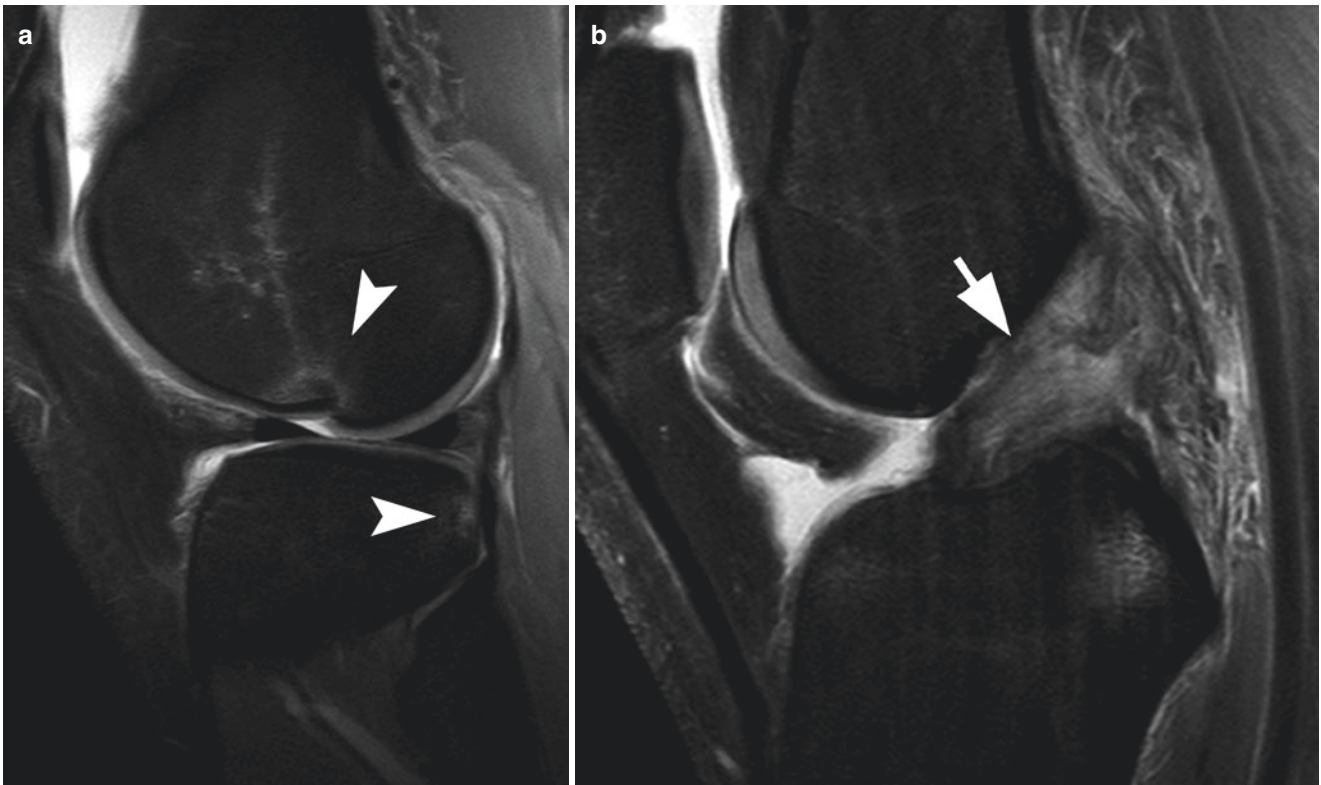
Fig. 7.13 ACL tear – indirect sign. (**a**) Sagittal T2-weighted image with fat suppression shows bone edema and impaction fractures at the central aspect of the lateral femoral condyle and posterior aspect of the lateral tibial plateau (arrowheads). (**b**) Sagittal T2-weighted image with fat suppression demonstrates the ACL tear (arrow)

Fig. 7.14 Partial ACL tear. Sagittal T2-weighted image of the knee with fat suppression shows increased thickening within the ACL with attenuation of ligamentous fibers (arrow)

Fig. 7.15 PCL tear. Sagittal PD-weighted image demonstrates PCL discontinuity with increased signal intensity (arrow)

increased T2 signal intensity of the PCL [37] (Fig. 7.15). Differentiation between complete and partial PCL tears is more difficult on MRI [38]. Mucoid degeneration of PCL can be suggested with a "tram-track" appearance, in which there is a peripheral rim of normal low signal intensity fibers [39] (Fig. 7.16). The PCL has a greater propensity to heal, when compared to ACL [40, 41]. Up to 28% of PCL tears can have a near normal MR appearance 6 months post injury [42]. Patients with combined PCL and posterolateral corner injuries and those with greater than 12 mm of posterior sub-luxation of the tibia on stress radiographs are less likely to demonstrate healing of PCL on follow-up MRI [40].

7.3.2 Medial Collateral Ligament

Anatomy and Function
The medial collateral ligament (MCL) serves as a primary stabilizer against valgus stress of the knee. It is composed of a superficial and a deep layer. The superficial layer or tibial collateral ligament is the strongest portion of MCL and most easily seen on MRI [43–45]. The deep layer is part of the joint capsule and composed of meniscofemoral and menis-cotibial ligament extensions. An MCL bursa is situated between the superficial and deep portions of the MCL [46]. The superficial and deep components of the MCL are fused posteriorly by the posterior oblique ligament [44]. The superficial MCL has a femoral origin located posterior to the medial epicondyle and anterior to the adductor tubercle and a tibial attachment located approximately 5 cm distal to the joint line and deep to the pes anserinus tendons [43, 47, 48]. Some authors describe a second tibial attachment of the superficial MCL along the anterior arm of the semimembra-nosus [49].

MCL Tears
Medial collateral ligament tears are most commonly located along the proximal MCL and can be classified in three types [50]:

– Grade I: microscopic injury; MR demonstrates periliga-
mentous edema, with normal hypointense signal of the
MCL (Fig. 7.17).
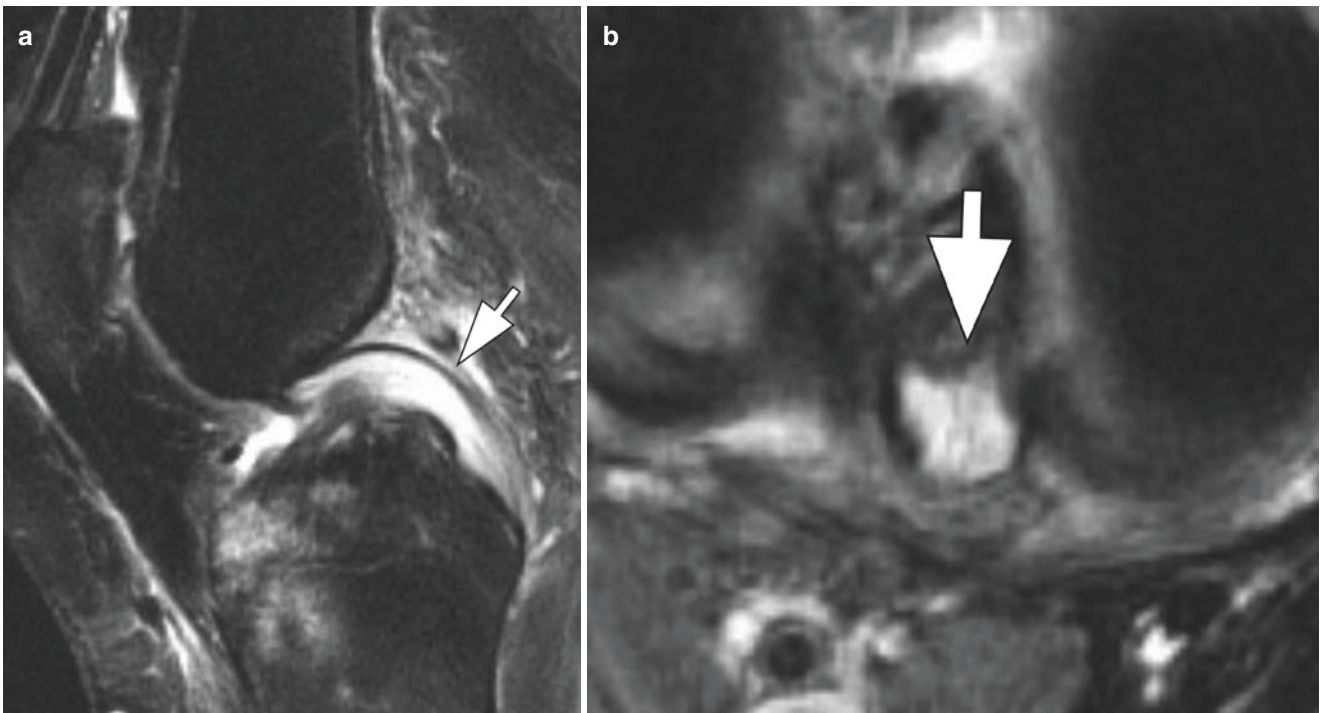
Fig. 7.16 PCL mucoid degeneration. (**a**) Sagittal and (**b**) axial T2-weighted images. There is increased signal within the PCL and a peripheral rim of intact fibers – "tram-trak" appearance (arrows)

Fig. 7.17 Grade I MCL tear. Coronal T2-weighted image with fat suppression. Edema surrounding the MCL (arrow)
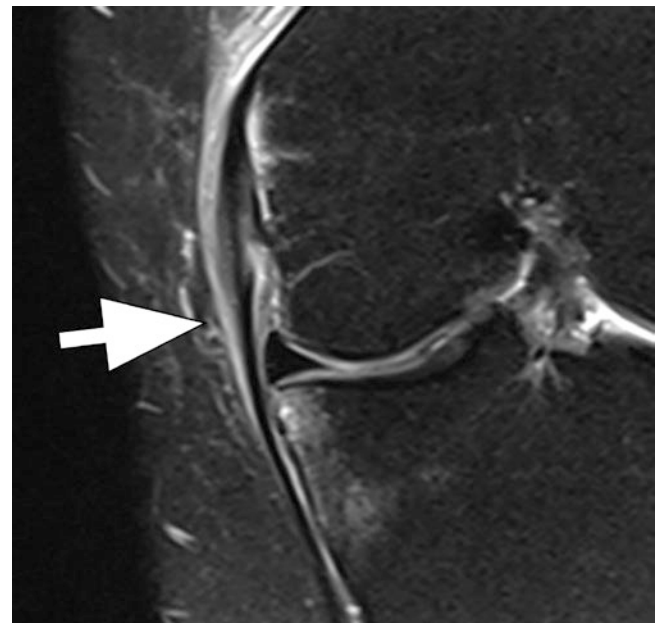
Fig. 7.18 Grade II MCL tear. Coronal T2-weighted image with fat suppression. Increased signal and thickening of the MCL (arrow)

- Grade II: partial tear; MR shows a thickened and edematous MCL with areas of increased intrasubstance signal, incomplete ligamentous disruption (Fig. 7.18).
- Grade III: complete tear; MR demonstrates complete discontinuity of superficial MCL.

Distal insertional tears of the superficial MCL are less common; however normal healing of far distal tears of the superficial MCL can be impaired due to poor blood supply and possible displacement of torn distal MCL ligament fibers. A "Stener-like" lesion of the distal superficial MCL occurs when there is ligament displacement superficial to the pes anserinus tendons [51]. A wavy morphologic appearance of the MCL without MCL disruption proximally is an imaging feature suggestive of a high-grade distal tear of the superficial MCL [52] (Fig. 7.19).

7.3.3 Posterolateral Corner

Anatomy and Function
The posterolateral corner structures are primary restraints of varus rotation and external tibial rotation and secondary restraints of anterior and posterior tibial translation.

The main stabilizers of the posterolateral corner complex are, from superficial to deep, include the lateral collateral ligament (or fibular collateral ligament), biceps femoris tendon, fabellofibular ligament, arcuate ligament, popliteofibular ligament, and popliteus tendon [53] (Fig. 7.20).

Lateral Collateral Ligament (Fibular Collateral Ligament)
The LCL is injured in about 23% of cases of posterolateral corner injury [54]. The lateral collateral ligament (LCL) or fibular collateral ligament is the primary stabilizer against
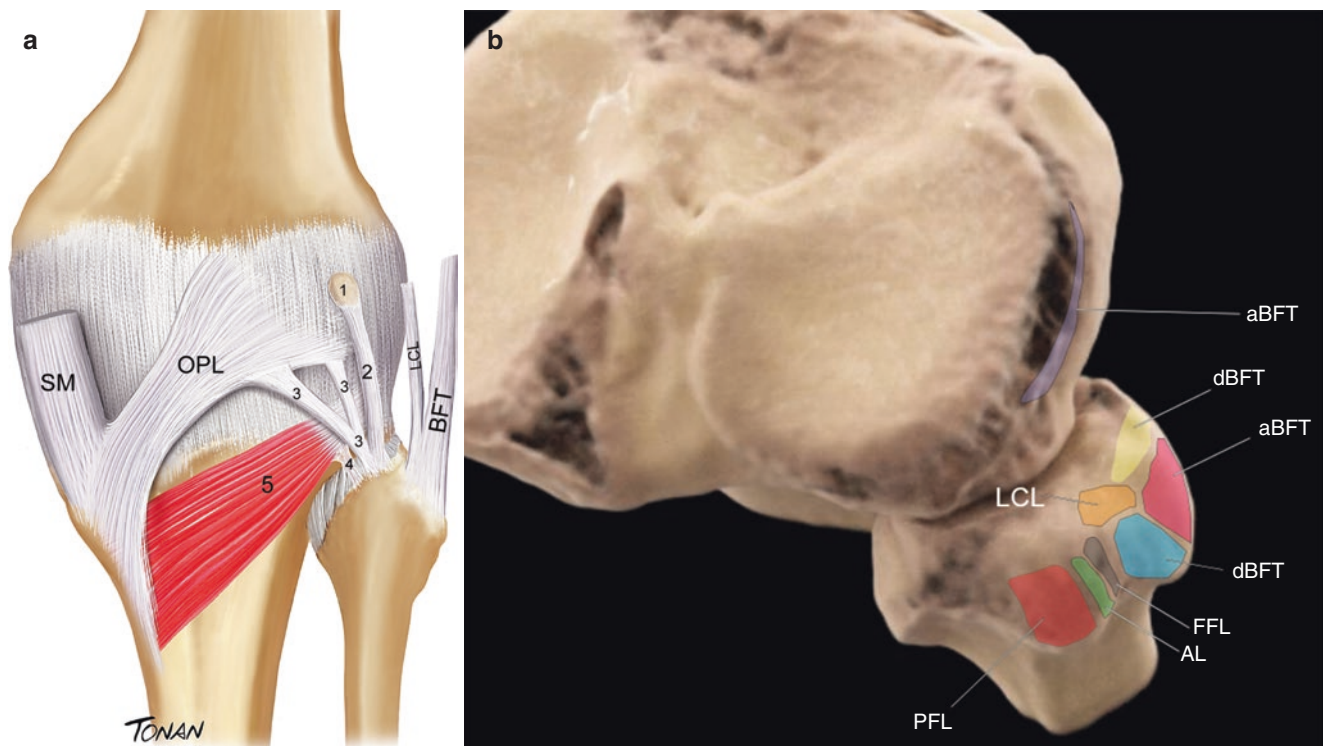
Fig. 7.20 Posterolateral corner anatomy. (**a**) Schematic drawing illustrating the posterolateral corner anatomy. *BFT* biceps femoris tendon, *LCL* lateral collateral ligament; (*1*), fabella; (*2*), fabellofibular ligament; (*3*), arcuate ligament; (*4*), popliteofibular ligament; and (*5*), popliteus muscle. Structures from the posteromedial corner are also demonstrated OPL, oblique popliteal ligament, and SM, semimembranosus tendon. (**b**) CT 3D reconstruction with posterolateral corner attachments. *aBFT* anterior arm of the biceps femoris tendon, *dBFT* direct arm of the biceps femoris tendon, *LCL* lateral collateral ligament, *FFL* fabellofibular ligament, *AL* arcuate ligament, *PFL* popliteofibular ligament. (Reproduced with Permission by Rodrigo Tonan)

Fig. 7.21 Lateral collateral ligament tear. Coronal T2-weighted image with fat suppression. Complete LCL tear (arrow)

varus stress of the knee and has a secondary role as a restraint to external rotation. It arises from the lateral femoral condyle and extends distally attaching to the lateral aspect of the fibular head, sometimes merging with the distal biceps femoris tendon to form a conjoined insertional tendon structure [55]. The lateral collateral ligament-biceps femoris bursa can be seen between these two structures [56].

Lateral collateral ligament tears can be classified as grades I (periligamentous edema), II (thickened and edematous LCL), and III (complete LCL disruption) (Fig. 7.21). Avulsion fracture of the fibular head by the LCL can be seen in the setting of an arcuate fracture [56, 57].

Biceps Femoris Tendon

The biceps femoris tendon descends posterior to the iliotibial tract and has two distal attachments identified on MRI: a direct arm (inserting on the posterolateral aspect of the fibular head) and an anterior arm (inserting to the anterior aspect of the fibular head and to the lateral tibial metaphysis) [55, 58, 59]. The biceps femoris tendon merges with the distal LCL and forms a conjoined insertional tendon. Injuries to the biceps femoris tendon include partial tears and tendinous and osseous avulsions from the fibular head.

Fabellofibular Ligament

The fabellofibular ligament is variably present but commonly seen when there is a bony fabella. The ligament runs from the fabella to the styloid process of the fibular head. When the fabella is absent, the ligament originates proximally to the posterior aspect of the supracondylar process of the femur [60]. The fabellofibular ligament may not be identified on MRI but when present is seen on coronal and sagittal planes posterior to genicular vessels and on axial plane anterior to the lateral head of the gastrocnemius tendon. Injuries include avulsions from the fibular head and partial−/complete-thickness tears.

Arcuate Ligament

The arcuate ligament is a thickening of the posterior joint capsule and has a Y shape. The medial limb attaches proximally to the oblique popliteal ligament, and the lateral limb attaches to the lateral femoral condyle. Distally, the medial and lateral limbs merge, attaching to the fibular styloid process, posterior to the insertion of the popliteofibular ligament. Identification of the arcuate ligament is variable on MRI, and when visualized the ligament is best depicted on axial and sagittal MR imaging acquisitions. Injury of the arcuate ligament is often implicated based on secondary MR imaging signs, especially edema and fluid/hemorrhage indicative of soft tissue injury immediately posterior to the popliteus tendon/hiatus [61] (Fig. 7.22). The presence of the arcuate sign (edema or avulsion fracture of the fibular head with intact LCL and biceps femoris tendon) is indicative of concurrent arcuate and popliteofibular ligament injuries [62].

Popliteofibular Ligament

The popliteofibular ligament is a major stabilizer of the posterolateral complex, originating at the popliteus tendon close to its myotendinous junction and inserting at the posterior aspect of the fibular styloid process [63]. MR visualization of this ligament is difficult, with improved visualization described with dedicated oblique coronal or isotropic volumetric sequences [64]. Injuries are common in a setting of posterolateral instability [65], although direct identification of popliteofibular ligament disruption can be challenging at MRI (Fig. 7.23).

Popliteus Tendon

The popliteus tendon and muscle provide primary resistance to external rotation and secondary resistance to posterior tibial translation at the knee. The popliteus tendon is located deep to arcuate and fabellofibular ligaments, enters the joint, and attaches to the popliteus sulcus of the lateral femoral condyle, deep and anterior to the femoral origin of the LCL. Popliteomeniscal fascicles connect the popliteus
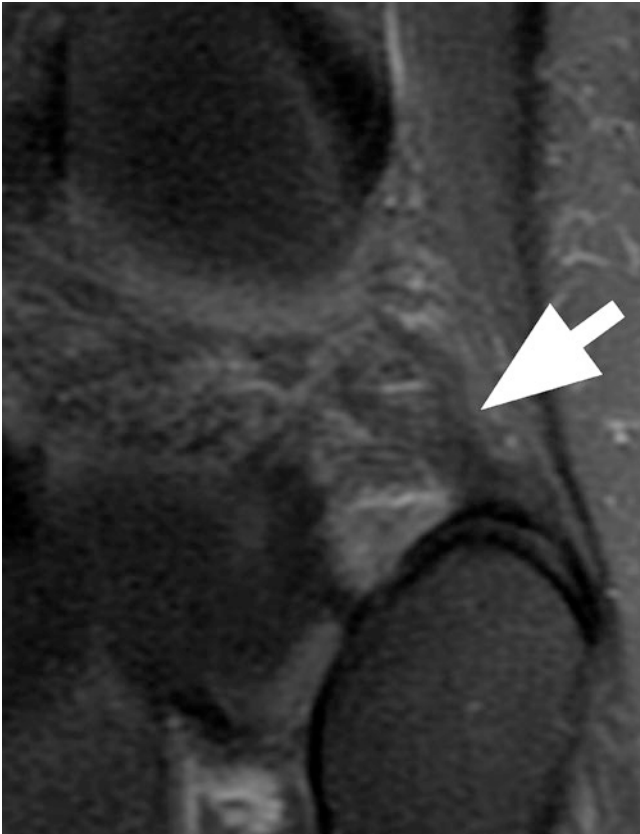
Fig. 7.22 Arcuate ligament strain. Coronal T2-weighted image with fat suppression. Increased signal and thickening of the arcuate ligament at its fibular attachment (arrow)

Fig. 7.23 Popliteofibular ligament strain. Sagittal T2-weighted image with fat suppression. Increased signal and thickening of the arcuate ligament at its fibular attachment (arrow)

tendon to the lateral meniscus, forming the popliteus hiatus. Popliteus injuries are more common at its myotendinous junction, although avulsions of the popliteus tendon at its femoral origin can occur (Fig. 7.24).

7.3.4 Posteromedial Corner

Anatomy and Function
The posteromedial corner structures are primary restraints to anteromedial rotatory instability and are composed of the posterior oblique ligament (POL), the oblique popliteal ligament (OPL), the semimembranosus tendon, and the meniscotibial ligament.

Posterior Oblique Ligament (POL)
The POL originates at the adductor tubercle, just posterior to the origin of the MCL, and extends distally composed of three arms: (1) central (or tibial) arm, attaching to the posteromedial aspect of the medial meniscus; (2) superior (or capsular) arm, attaching to the oblique popliteal ligament and capsule; and (3) distal arm, attaching to the semimembranosus tendon and tibia.

Fig. 7.24 Popliteus myotendinous strain. Axial T2-weighted image with fat suppression. Increased signal involving the popliteus myotendinous junction and muscle (arrow)

Oblique Popliteal Ligament (OPL)
The OPL is a broad ligamentous band that originates from the lateral aspect of the semimembranosus tendon and courses in a superolateral oblique direction across the
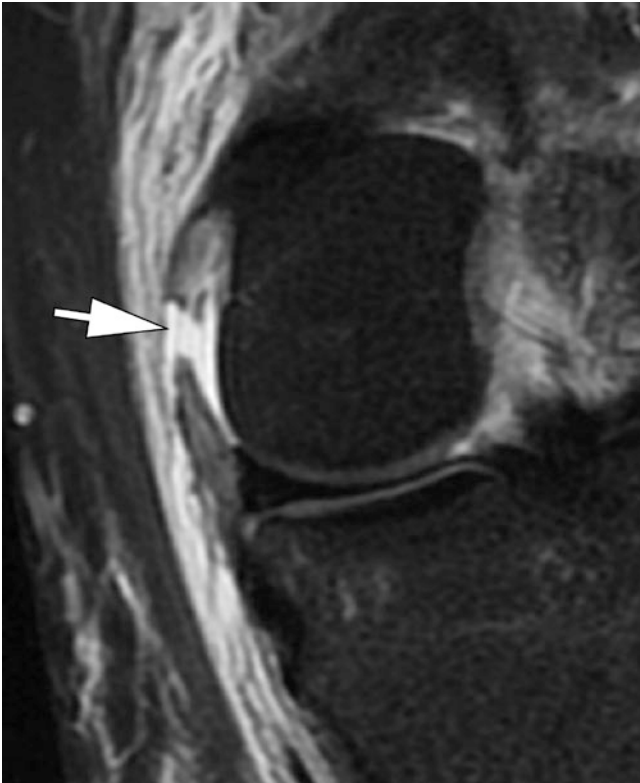
Fig. 7.25 Posterior oblique ligament tear. Coronal T2-weighted image with fat suppression. Complete tear of the POL (arrow) with exuberant surrounding edema

Fig. 7.26 Oblique popliteal ligament tear. Axial T2-weighted image with fat suppression. Increased signal and thickening of the OPL (arrow heads)

posterior aspect of the joint, forming part of the popliteal fossa and inserts at the fabella and posterolateral joint capsule (Fig. 7.20).

Semimembranosus Tendon
The distal semimembranosus tendon has five insertional arms: (1) direct arm (inserts at the posterior aspect of the medial tibial condyle), (2) capsular arm (merges with the capsular portion of the OPL), (3) anterior arm (courses anteriorly, deep to the POL, and inserts at the medial aspect of the tibia, deep to the MCL, (4) inferior arm (courses deep to MCL and POL and inserts proximal to tibial attachment of MCL, and (5) OPL extension. The semimembranosus is the main stabilizer of the posteromedial corner.

Injuries
Patients with anteromedial rotatory instability show injury of the POL in 99%, semimembranosus in 70%, and medial meniscus detachment in 30% of cases [66] (Figs. 7.25 and 7.26). There is an association between posteromedial corner injuries and ACL tears, although association between posteromedial and posterolateral corner injuries is uncommon. Adequate interpretation of these injuries is important, because posteromedial corner injury with anteromedial rotatory instability often requires surgical intervention.

7.3.5 Anterolateral Ligament

Anatomy and Function
The anterolateral ligament (ALL) originates posterior and proximal to the lateral femoral epicondyle and courses anteroinferiorly overlapping the LCL toward the anterolateral tibia. As it approaches the joint line, some fibers attach to the lateral meniscus and anterolateral capsule [67, 68]. The tibial insertion is just behind Gerdy's tubercle (Fig. 7.27). ALL is an important stabilizer of internal rotation of the tibia. The ALL is identified in 90–100% of MR examinations [69, 70].

Injuries
A Segond fracture represents a bony injury of the tibial ALL insertion [71, 72]. ALL injuries are generally associated with ACL lesions (Fig. 7.28). Identification of ALL injuries is difficult, and secondary signs such as bony avulsion and edema at the anterolateral tibia may be useful findings in support of possible ALL injury.

7.3.6 Iliotibial Tract

Anatomy and Function
The iliotibial tract is composed of contributions from the tensor fascia lata and gluteus maximus muscles and from fibers of the fascia lata [73]. The superficial layer of the iliotibial tract inserts onto the Gerdy tubercle at the anterolateral tibia. The deep layer attaches the superficial
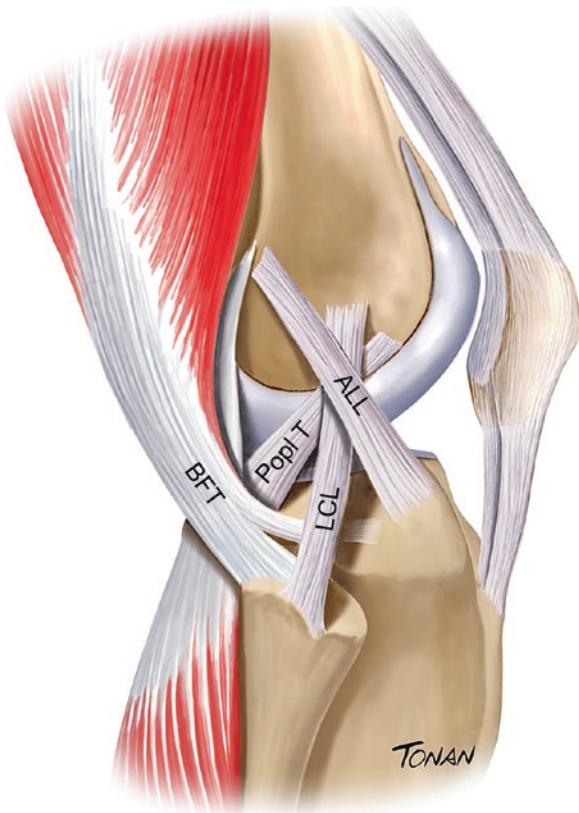
Fig. 7.27 Anterolateral ligament anatomy. Schematic drawing illustrating the anterolateral ligament anatomy and related structures. ALL, anterolateral ligament; LCL, lateral collateral ligament; Popl T, popliteus tendon; BFT, biceps femoris tendon. (Reproduced with Permission by Rodrigo Tonan)

layer to the supracondylar tubercle of the lateral femur with additional fibers inserting on lateral patellar retinaculum. The iliotibial tract provides anterolateral stability to the knee.

Iliotibial Band Syndrome

In general, iliotibial band syndrome or ilitotibial band friction syndrome is due to chronic overuse in activities such as cycling and running, with patients presenting with pain around the anterolateral femur due to repetitive friction between the iliotibial band and the underlying lateral femoral epicondyle. On MR, increased T2 soft tissue signal or a bursal fluid collection can be identified between the iliotibial tract and the lateral femoral condyle [73] (Fig. 7.29).

Injuries

In general, iliotibial tract tears occur in the setting of an acute knee trauma with other knee injuries, especially ACL tears and patellar dislocation. MRI demonstrates strains (edema superficial and deep to iliotibial tract) and partial (thickening and increased signal) and complete tears [74].

> **Key Point**
> - Adequate comprehension of detailed ligament anatomy is crucial to identify injuries on MRI.
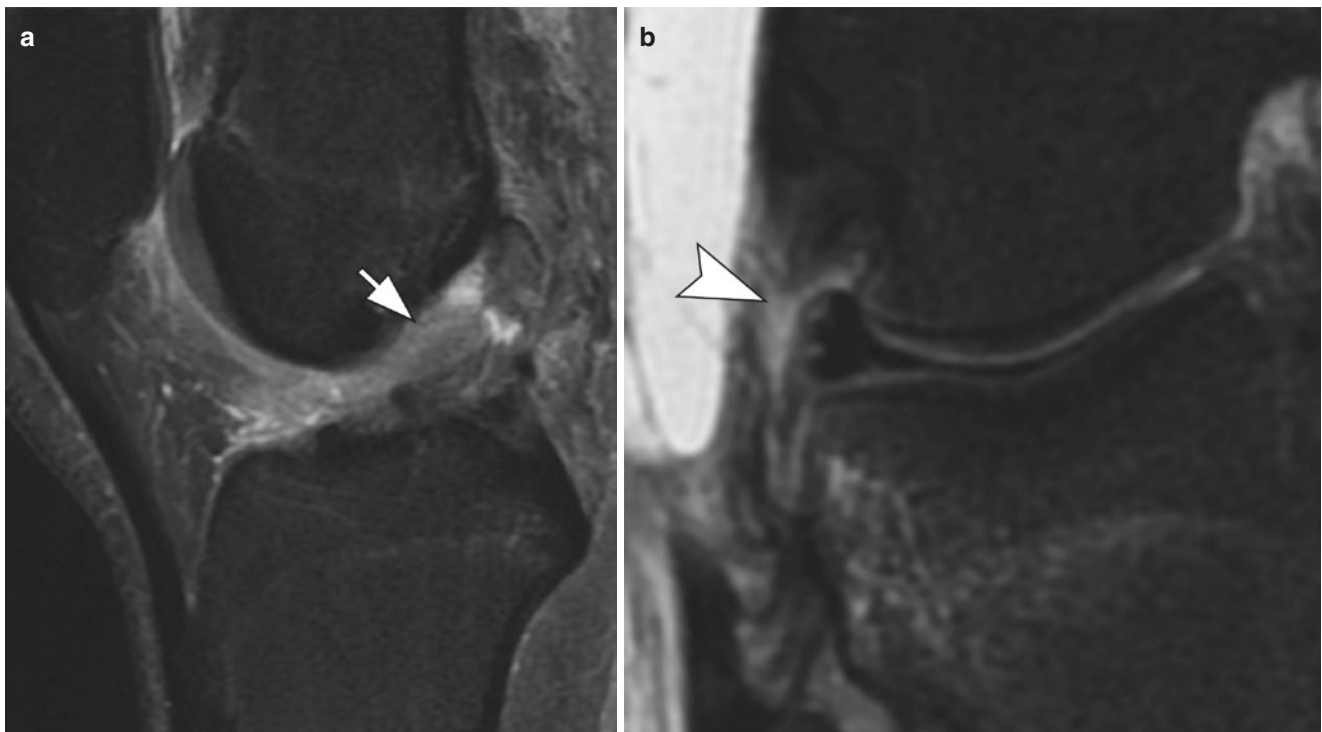
Fig. 7.28 Associated anterolateral and ACL tears. (**a**) Sagittal T2-weighted image with fat suppression showing an ACL tear (arrow). (**b**) Coronal T2-weighted image with fat suppression demonstrates a complete tear of the ALL (arrowhead)
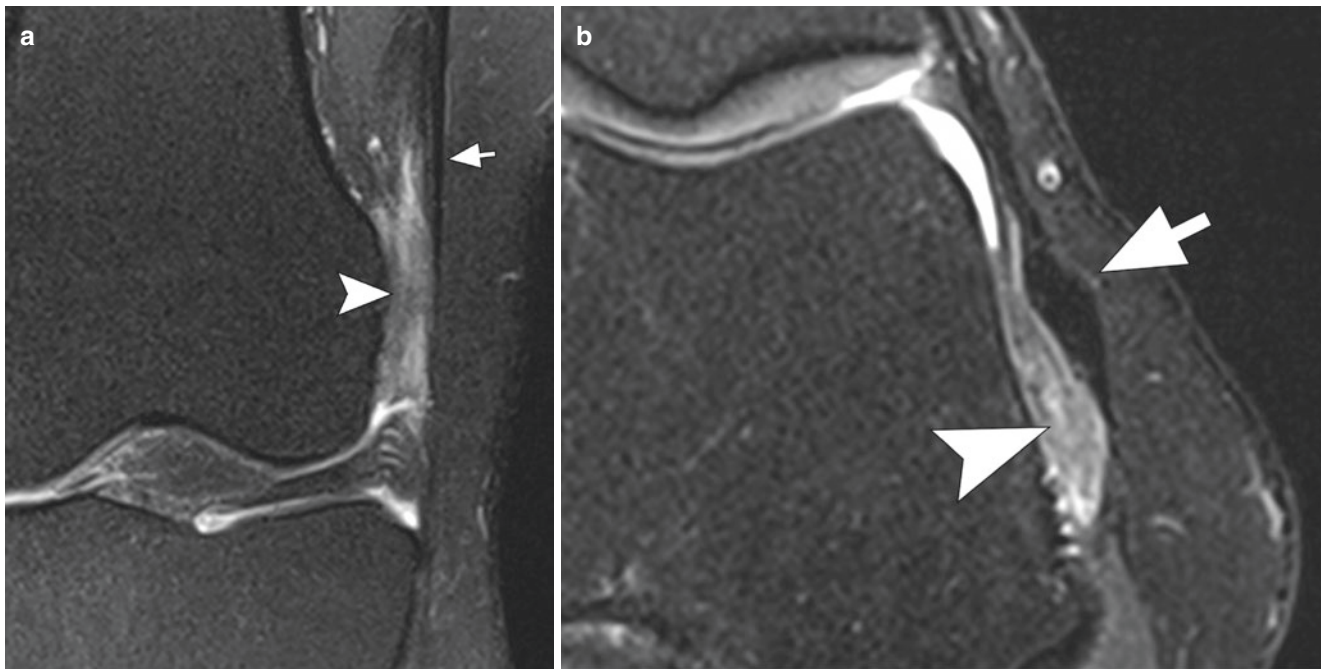
Fig. 7.29 Iliotibial band friction syndrome. (**a**) Coronal and (**b**) axial T2-weighted images with fat suppression demonstrate edema in the fat pad (arrowheads) between the lateral femoral condyle and the iliotibial band (arrows)

7.4 Tendons

7.4.1 Extensor Mechanism

Anatomy and Function

The extensor mechanism of the knee is composed of the quadriceps muscle group and tendon, the patella, the patellar retinaculum, and the patellar tendon. The tendons of the rectus femoris and vastus muscles converge distally to form the quadriceps tendon, inserting onto the superior pole of the patella. The quadriceps tendon has a tri-laminar appearance on MR imaging, with the rectus tendon forming the most superficial layer, the vastus medialis and lateralis forming the middle layer, and the vastus intermedius forming the deepest layer. Fat tissue interposes between the three tendon layers. The distal vastus medialis muscle has a longitudinal and an oblique portion, called the vastus medialis obliquus. Fascial extensions of the vastus medialis and lateralis form the patellar retinacula. Patellofemoral ligaments are focal thickening of the retinacula, similar to glenohumeral ligaments in the shoulder. The patellar tendon is composed by fibers of the rectus femoris and extends from the inferior pole of the patella to anterior tibial tuberosity.

Lateral Patellar Dislocation

Dynamic and anatomical conditions, including trochlear dysplasia and patella alta, can predispose to lateral patellar dislocation. In general, patellar dislocation is diagnosed on imaging retrospectively due to indirect findings on MRI: disruption of the medial retinaculum and medial patellofemoral ligament, typical bone marrow edema on the medial aspect of the patella and the anterolateral aspect of the lateral femoral condyle, osteochondral injuries (especially at the medial facet of the patella), and joint effusion/hemarthrosis [75] (Fig. 7.30).

> **Key Point**
> - Typical imaging features of lateral patellar dislocation are bone marrow edema at the medial aspect of the patella and anterolateral aspect of lateral femoral condyle, injury at the medial patellofemoral ligament, and joint effusion/hemarthrosis.

7.5 Cartilage

Hyaline cartilage is a fine connective tissue composed of a complex mesh of collagenous fibers, water, and proteoglycans. Chondral lesions include acute traumatic chondral or osteochondral injuries or chronic degenerative lesions which generally progress slowly with late clinical manifestations of disease.

MR imaging can provide information on chondral thickness, surface abnormalities, intrasubstance changes, and
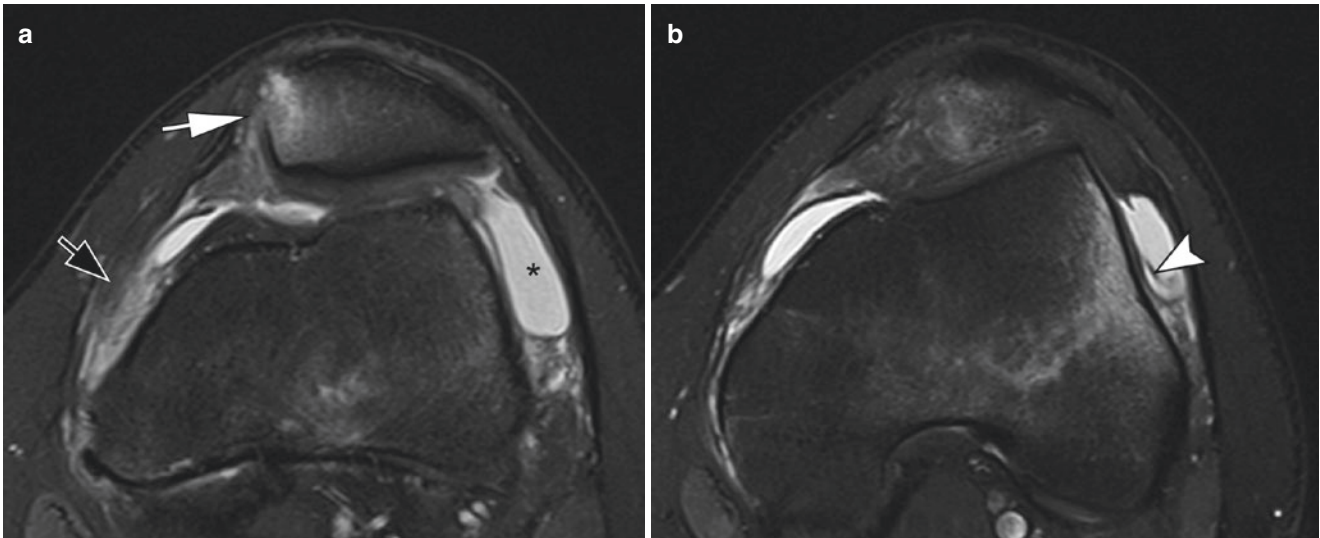
Fig. 7.30 Lateral patellar dislocation. Axial T2-weighted images of the knee with fat suppression. (**a**) Bone impaction with marrow edema at the medial facet of the patella (white arrow) and strain of the proxi-mal aspect of the medial patellofemoral ligament (black arrow). * joint effusion. (**b**) Bone impaction with marrow edema at the anterolateral aspect of the lateral femoral condyle (arrowhead)

7.5.1 Chondral Lesions

The accuracy of MRI for detecting chondral lesions can be variable depending on MRI hardware and technique used, patient factors, as well as the etiology, extent/depth, and location of the lesion itself. The accuracy of MRI in diagnosis of degenerative chondral lesions is greater in deeper lesions, particularly in those that present more than 50% loss of chondral substance, with accuracy results in the literature ranging from 73 to 96% [76].

Chondral lesions are characterized on MRI by thickness and morphological abnormalities of hyaline cartilage as well as intrasubstance increased signal on proton density, T2-weighted and gradient echo sequences. One prior study demonstrated that 70% of chondral lesions presented as areas of high signal in relation to normal cartilage on proton density acquisitions, while 20% of lesions illustrated signal similar to that of normal cartilage (lesions not identified on MRI) and 10% illustrating low signal [77].

Chondral tapering, loss of definition, and chondral surface irregularities are additional features of chondral lesions that can be characterized on MR imaging. It has been demonstrated that the most frequent locations for chondral lesions are the medial femoral condyle (on its most internal aspect) and the lateral tibial plateau (on its most posterior portion) [78].

To classify chondral lesions using MRI, a system based on arthroscopic classifications is used [79]. Grade I lesions are shown as abnormalities of intrasubstance cartilage signal, corresponding to softening of the cartilage seen on arthroscopy. Grade II lesions are shown as morphologic irregularities and abnormalities of the surface

Fig. 7.31 Three-layer pattern of normal cartilage. Axial PD-weighted image with fat suppression. The deep layer shows low signal intensity (white arrow); the intermediate layer has high signal (black arrow), and the superficial layer has low signal (arrowhead)

subchondral bone abnormalities. Through more recent techniques, MRI can provide information on the biochemical and physiological characteristics of hyaline cartilage.

By using MRI with high spatial resolution and good soft tissue contrast, a three-layer pattern can be observed in the hyaline cartilage: 1) surface layer with low-intensity signal; 2) intermediate layer with high-intensity signal; and 3) deep layer with low-intensity signal and a "palisade" transition into the intermediate zone (Fig. 7.31). This three-layer appearance is more evident in thicker chondral surfaces, such as the patellar and femoral trochlear cartilage.

Fig. 7.32 Chondral injury classification. (A, B, and C) Axial and (D) sagittal PD-weighted images with fat suppression. (**a**) Increased signal of the superficial layer of the hyaline cartilage of the lateral facet of the patella with irregularities (arrow), indicating grade I lesion. There is also a deep chondral erosion (>50% – grade III) in the medial facet (arrowhead). (**b**) Fissure involving less than 50% of the hyaline carti-

lage of the lateral facet of the patella (arrow) (grade II lesion). (**c**) Chondral fissure involving more than 50% of the hyaline cartilage of the medial facet of the patella (arrow) (grade III lesion). (**d**) Deep chondral erosion in the lateral femoral condyle (arrow), reaching the subchondral bone associated with adjacent bone marrow edema (arrowheads) (grade IV lesion)

signal, indicating fibrillation or erosion of less than 50% of the chondral thickness. In Grade III lesions, there is loss of more than 50% of the chondral substance, and there may be small areas in which the bone surface is reached. Grade IV lesions indicate extensive full-thickness chondral defects with subchondral bone marrow edema [79, 80] (Fig. 7.32).

Loss of cartilage integrity may lead to abnormalities in the underlying subchondral bone, such as cysts, sclerosis, and osteophytosis, which can be detected on MRI. Another frequently associated finding is subchondral bone marrow edema-like signal changes, which studies suggest may predate and progress to subchondral cysts over time [81].

Chronic chondral lesions with detachment of cartilaginous fragments into the joint lead to chronic irritation of the

synovium and may cause synovitis. In some cases, the synovial response can be very extensive and may take on a pseudotumoral appearance on imaging examinations (Fig. 7.33). Intraarticular loose bodies can be identified, especially in the suprapatellar recess, intercondylar notch, posterior to the femorotibial joint space and along the popliteal hiatus of the articulation (Fig. 7.34).

> **Key Point**
> • MRI underestimates size of chondral lesions. A complete description including cartilage, subchondral bone, and synovial abnormalities should be performed in a setting of chondral imaging.

Fig. 7.33 Pseudotumoral appearance of knee osteoarthrosis. Coronal T2-weighted image with fat suppression demonstrates complete and diffuse cartilage loss in the femorotibial compartments with large subchondral cysts, especially at the tibial plateau

7.6 Concluding Remarks

Knee abnormalities include meniscal, ligamentous, tendinous, bone, and chondral disorders. MRI is highly accurate and is the imaging method of choice to assess internal derangement of the knee. Several new information regarding anatomy and pathology of the menisci, tendons, and ligaments were published in the last years. Recognition of knee anatomy, normal variants, and imaging patterns of main disorders is pivotal for an accurate diagnosis.

Take Home Messages
- MR imaging criteria for a meniscal tear are meniscal morphologic distortion (in absence of prior surgery) or intrameniscal high signal intensity extending to an articular surface, seen on two or more consecutive slices.
- Direct MR signs of an ACL tear are focal ligamentous discontinuity, diffuse or focal signal intensity abnormality, and abnormal orientation of the ACL.

Fig. 7.34 Intraarticular loose body. Sagittal PD-weighted images with fat suppression. (**a**) A deep chondral lesion with sharp margins at the lateral femoral condyle (arrowhead), indicating an acute chondral detachment. (**b**) The chondral fragment is dislocated to the anterior aspect of the intercondylar notch (arrow)
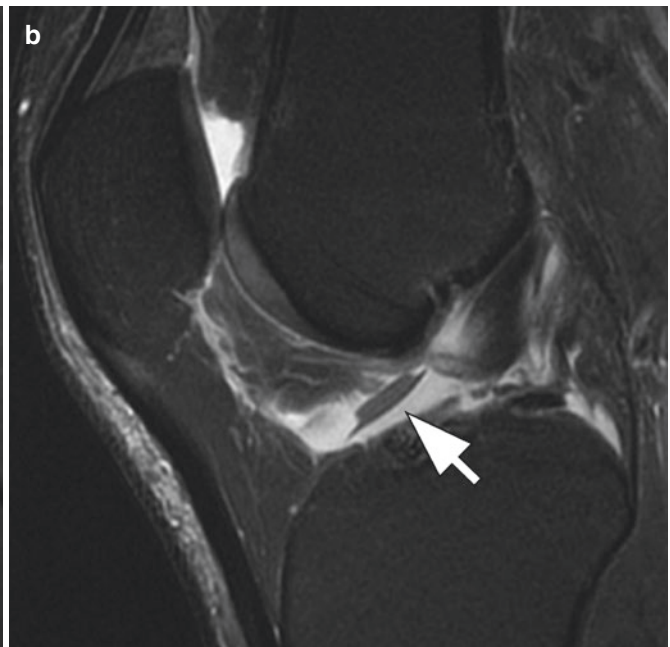
- Main structures involved in posterolateral corner stability are lateral collateral ligament, biceps femoris tendon, popliteus tendon, and popliteofibullar ligament.
- Chondral lesions are characterized on MRI by thickness and morphological abnormalities of hyaline cartilage as well as intrasubstance increased signal on fluid-sensitive sequences.

References

1. Scott WN, Diduch DR, Long WJ. Insall & Scott surgery of the knee. 6th ed. Philadelphia, PA: Elsevier; 2018. 2360 p
2. Resnick D. Diagnosis of bone and joint disorders. 4th ed. Philadelphia, PA: W.B. Saunders Company; 2002.
3. Marcheix PS, Marcheix B, Siegler J, Bouillet P, Chaynes P, Valleix D, et al. The anterior intermeniscal ligament of the knee: an anatomic and MR study. Surg Radiol Anat. 2009;31(5):331–4.
4. Cho JM, Suh JS, Na JB, Cho JH, Kim Y, Yoo WK, et al. Variations in meniscofemoral ligaments at anatomical study and MR imaging. Skelet Radiol. 1999;28(4):189–95.
5. De Smet AA, Asinger DA, Johnson RL. Abnormal superior popliteomeniscal fascicle and posterior pericapsular edema: indirect MR imaging signs of a lateral meniscal tear. Am J Roentgenol. 2001;176(1):63–6.
6. Sanders TG, Linares RC, Lawhorn KW, Tirman PF, Houser C. Oblique meniscomeniscal ligament: another potential pitfall for a meniscal tear--anatomic description and appearance at MR imaging in three cases. Radiology. 1999;213(1):213–6.
7. Nguyen JC, De Smet AA, Graf BK, Rosas HG. MR imaging-based diagnosis and classification of meniscal tears. Radiographics. 2014;34(4):981–99.
8. Monllau JC, León A, Cugat R, Ballester J. Ring-shaped lateral meniscus. Arthroscopy. 1998;14(5):502–4.
9. Yaniv M, Blumberg N. The discoid meniscus. J Child Orthop. 2007;1(2):89–96.
10. Chew FS. Medial meniscal flounce: demonstration on MR imaging of the knee. Am J Roentgenol. 1990;155(1):199.
11. Schnarkowski P, Tirman PF, Fuchigami KD, Crues JV, Butler MG, Genant HK. Meniscal ossicle: radiographic and MR imaging findings. Radiology. 1995;196(1):47–50.
12. De Smet AA, Graf BK. Meniscal tears missed on MR imaging: relationship to meniscal tear patterns and anterior cruciate ligament tears. Am J Roentgenol. 1994;162(4):905–11.
13. Crues JV, Mink J, Levy TL, Lotysch M, Stoller DW. Meniscal tears of the knee: accuracy of MR imaging. Radiology. 1987;164(2):445–8.
14. De Smet AA, Norris MA, Yandow DR, Quintana FA, Graf BK, Keene JS. MR diagnosis of meniscal tears of the knee: importance of high signal in the meniscus that extends to the surface. Am J Roentgenol. 1993;161(1):101–7.
15. De Smet AA, Tuite MJ. Use of the "two-slice-touch" rule for the MRI diagnosis of meniscal tears. Am J Roentgenol. 2006;187(4):911–4.
16. Chahla J, Dean CS, Moatshe G, Mitchell JJ, Cram TR, Yacuzzi C, et al. Meniscal ramp lesions: anatomy, incidence, diagnosis, and treatment. Orthop J Sports Med. 2016;4(7):2325967116657815.
17. Hatayama K, Terauchi M, Saito K, Aoki J, Nonaka S, Higuchi H. Magnetic resonance imaging diagnosis of medial meniscal ramp lesions in patients with anterior cruciate ligament injuries. Arthroscopy. 2018;34(5):1631–7.
18. Balazs GC, Greditzer HG, Wang D, Marom N, Potter HG, Marx RG, et al. Ramp lesions of the medial meniscus in patients undergoing primary and revision ACL reconstruction: prevalence and risk factors. Orthop J Sports Med. 2019;7(5):2325967119843509.
19. Nguyen JC, Bram JT, Lawrence JTR, Hong S, Leska TM, Ganley TJ, et al. MRI criteria for ramp lesions of the knee in children with anterior cruciate ligament tears. Am J Roentgenol 2020.
20. Savoye PY, Ravey JN, Dubois C, Barbier LP, Courvoisier A, Saragaglia D, et al. Magnetic resonance diagnosis of posterior horn tears of the lateral meniscus using a thin axial plane: the zip sign--a preliminary study. Eur Radiol. 2011;21(1):151–9.
21. de Abreu MR, Chung CB, Trudell D, Resnick D. Meniscofemoral ligaments: patterns of tears and pseudotears of the menisci using cadaveric and clinical material. Skelet Radiol. 2007;36(8):729–35.
22. Saad SS, Gorbachova T, Meniscal Tears SM. Scanned, scoped and sculpted. Radiographics. 2015;35(4):1138–9.
23. Magee TH, Hinson GW. MRI of meniscal bucket-handle tears. Skelet Radiol. 1998;27(9):495–9.
24. Dorsay TA, Helms CA. Bucket-handle meniscal tears of the knee: sensitivity and specificity of MRI signs. Skelet Radiol. 2003;32(5):266–72.
25. Hodler J, Haghighi P, Trudell D, Resnick D. The cruciate ligaments of the knee: correlation between MR appearance and gross and histologic findings in cadaveric specimens. Am J Roentgenol. 1992;159(2):357–60.
26. Fitzgerald SW, Remer EM, Friedman H, Rogers LF, Hendrix RW, Schafer MF. MR evaluation of the anterior cruciate ligament: value of supplementing sagittal images with coronal and axial images. Am J Roentgenol. 1993;160(6):1233–7.
27. Lee JK, Yao L, Phelps CT, Wirth CR, Czajka J, Lozman J. Anterior cruciate ligament tears: MR imaging compared with arthroscopy and clinical tests. Radiology. 1988;166(3):861–4.
28. Robertson PL, Schweitzer ME, Bartolozzi AR, Ugoni A. Anterior cruciate ligament tears: evaluation of multiple signs with MR imaging. Radiology. 1994;193(3):829–34.
29. Gentili A, Seeger LL, Yao L, Do HM. Anterior cruciate ligament tear: indirect signs at MR imaging. Radiology. 1994;193(3):835–40.
30. Naraghi A, White LM. MR imaging of cruciate ligaments. Magn Reson Imaging Clin N Am. 2014;22(4):557–80.
31. Kijowski R, Sanogo ML, Lee KS, Muñoz Del Río A, McGuine TA, Baer GS, et al. Short-term clinical importance of osseous injuries diagnosed at MR imaging in patients with anterior cruciate ligament tear. Radiology. 2012;264(2):531–41.
32. Vahey TN, Hunt JE, Shelbourne KD. Anterior translocation of the tibia at MR imaging: a secondary sign of anterior cruciate ligament tear. Radiology. 1993;187(3):817–9.
33. Nakase J, Toratani T, Kosaka M, Ohashi Y, Tsuchiya H. Roles of ACL remnants in knee stability. Knee Surg Sports Traumatol Arthrosc. 2013;21(9):2101–6.
34. Tjoumakaris FP, Donegan DJ, Sekiya JK. Partial tears of the anterior cruciate ligament: diagnosis and treatment. Am J Orthop (Belle Mead NJ). 2011;40(2):92–7.
35. Van Dyck P, De Smet E, Veryser J, Lambrecht V, Gielen JL, Vanhoenacker FM, et al. Partial tear of the anterior cruciate ligament of the knee: injury patterns on MR imaging. Knee Surg Sports Traumatol Arthrosc. 2012;20(2):256–61.
36. Busch MT, Fernandez MD, Aarons C. Partial tears of the anterior cruciate ligament in children and adolescents. Clin Sports Med. 2011;30(4):743–50.
37. Sonin AH, Fitzgerald SW, Hoff FL, Friedman H, Bresler ME. MR imaging of the posterior cruciate ligament: normal, abnormal, and associated injury patterns. Radiographics. 1995;15(3):551–61.
38. Patten RM, Richardson ML, Zink-Brody G, Rolfe BA. Complete vs partial-thickness tears of the posterior cruciate ligament: MR findings. J Comput Assist Tomogr. 1994;18(5):793–9.
39. McMonagle JS, Helms CA, Garrett WE, Vinson EN. Tram-track appearance of the posterior cruciate ligament (PCL):

correlations with mucoid degeneration, ligamentous stability, and differentiation from PCL tears. Am J Roentgenol. 2013;201(2):394–9.

40. Mariani PP, Margheritini F, Christel P, Bellelli A. Evaluation of posterior cruciate ligament healing: a study using magnetic resonance imaging and stress radiography. Arthroscopy. 2005;21(11):1354–61.

41. Shelbourne KD, Jennings RW, Vahey TN. Magnetic resonance imaging of posterior cruciate ligament injuries: assessment of healing. Am J Knee Surg. 1999;12(4):209–13.

42. Jung YB, Jung HJ, Yang JJ, Yang DL, Lee YS, Song IS, et al. Characterization of spontaneous healing of chronic posterior cruciate ligament injury: Analysis of instability and magnetic resonance imaging. J Magn Reson Imaging. 2008;27(6):1336–40.

43. Warren LF, Marshall JL. The supporting structures and layers on the medial side of the knee: an anatomical analysis. J Bone Joint Surg Am. 1979;61(1):56–62.

44. De Maeseneer M, Van Roy F, Lenchik L, Barbaix E, De Ridder F, Osteaux M. Three layers of the medial capsular and supporting structures of the knee: MR imaging-anatomic correlation. Radiographics. 2000;20 Spec No:S83–9.

45. Wen DY, Propeck T, Kane SM, Godbee MT, Rall KL. MRI description of knee medial collateral ligament abnormalities in the absence of trauma: edema related to osteoarthritis and medial meniscal tears. Magn Reson Imaging. 2007;25(2):209–14.

46. De Maeseneer M, Shahabpour M, Van Roy F, Goossens A, De Ridder F, Clarijs J, et al. MR imaging of the medial collateral ligament bursa: findings in patients and anatomic data derived from cadavers. Am J Roentgenol. 2001;177(4):911–7.

47. Liu F, Yue B, Gadikota HR, Kozanek M, Liu W, Gill TJ, et al. Morphology of the medial collateral ligament of the knee. J Orthop Surg Res. 2010;5:69.

48. Saigo T, Tajima G, Kikuchi S, Yan J, Maruyama M, Sugawara A, et al. Morphology of the insertions of the superficial medial collateral ligament and posterior oblique ligament using 3-dimensional computed tomography: a cadaveric study. Arthroscopy. 2017;33(2):400–7.

49. LaPrade RF, Engebretsen AH, Ly TV, Johansen S, Wentorf FA, Engebretsen L. The anatomy of the medial part of the knee. J Bone Joint Surg Am. 2007;89(9):2000–10.

50. Schweitzer ME, Tran D, Deely DM, Hume EL. Medial collateral ligament injuries: evaluation of multiple signs, prevalence and location of associated bone bruises, and assessment with MR imaging. Radiology. 1995;194(3):825–9.

51. Keyhani S, Mardani-Kivi M. Anatomical repair of Stener-like Lesion of medial collateral ligament: a case series and technical note. Arch Bone Jt Surg. 2017;5(4):255–8.

52. Boutin RD, Fritz RC, Walker REA, Pathria MN, Marder RA, Yao L. Tears in the distal superficial medial collateral ligament: the wave sign and other associated MRI findings. Skelet Radiol. 2020;49(5):747–56.

53. Watanabe Y, Moriya H, Takahashi K, Yamagata M, Sonoda M, Shimada Y, et al. Functional anatomy of the posterolateral structures of the knee. Arthroscopy. 1993;9(1):57–62.

54. LaPrade RF, Terry GC. Injuries to the posterolateral aspect of the knee. Association of anatomic injury patterns with clinical instability. Am J Sports Med. 1997;25(4):433–8.

55. Sanchez AR, Sugalski MT, LaPrade RF. Anatomy and biomechanics of the lateral side of the knee. Sports Med Arthrosc Rev. 2006;14(1):2–11.

56. Rosas HG. Unraveling the posterolateral corner of the knee. Radiographics. 2016;36(6):1776–91.

57. Geiger D, Chang EY, Pathria MN, Chung CB. Posterolateral and posteromedial corner injuries of the knee. Magn Reson Imaging Clin N Am. 2014;22(4):581–99.

58. Moorman CT, LaPrade RF. Anatomy and biomechanics of the posterolateral corner of the knee. J Knee Surg. 2005;18(2):137–45.

59. LaPrade RF, Gilbert TJ, Bollom TS, Wentorf F, Chaljub G. The magnetic resonance imaging appearance of individual structures of the posterolateral knee. A prospective study of normal knees and knees with surgically verified grade III injuries. Am J Sports Med. 2000;28(2):191–9.

60. Terry GC, LaPrade RF. The posterolateral aspect of the knee. Anatomy and surgical approach. Am J Sports Med. 1996;24(6):732–9.

61. Recondo JA, Salvador E, Villanúa JA, Barrera MC, Gervás C, Alústiza JM. Lateral stabilizing structures of the knee: functional anatomy and injuries assessed with MR imaging. Radiographics. 2000;20 Spec No:S91–S102.

62. Lee J, Papakonstantinou O, Brookenthal KR, Trudell D, Resnick DL. Arcuate sign of posterolateral knee injuries: anatomic, radiographic, and MR imaging data related to patterns of injury. Skelet Radiol. 2003;32(11):619–27.

63. Maynard MJ, Deng X, Wickiewicz TL, Warren RF. The popliteofibular ligament. Rediscovery of a key element in posterolateral stability. Am J Sports Med. 1996;24(3):311–6.

64. Rajeswaran G, Lee JC, Healy JC. MRI of the popliteofibular ligament: isotropic 3D WE-DESS versus coronal oblique fat-suppressed T2W MRI. Skelet Radiol. 2007;36(12):1141–6.

65. Collins MS, Bond JR, Crush AB, Stuart MJ, King AH, Levy BA. MRI injury patterns in surgically confirmed and reconstructed posterolateral corner knee injuries. Knee Surg Sports Traumatol Arthrosc. 2015;23(10):2943–9.

66. Sims WF, Jacobson KE. The posteromedial corner of the knee: medial-sided injury patterns revisited. Am J Sports Med. 2004;32(2):337–45.

67. Claes S, Vereecke E, Maes M, Victor J, Verdonk P, Bellemans J. Anatomy of the anterolateral ligament of the knee. J Anat. 2013;223(4):321–8.

68. Helito CP, Demange MK, Helito PV, Costa HP, Bonadio MB, Pecora JR, et al. Evaluation of the anterolateral ligament of the knee by means of magnetic resonance examination. Rev Bras Ortop. 2015;50(2):214–9.

69. Helito CP, Helito PV, Costa HP, Bordalo-Rodrigues M, Pecora JR, Camanho GL, et al. MRI evaluation of the anterolateral ligament of the knee: assessment in routine 1.5-T scans. Skelet Radiol. 2014;43(10):1421–7.

70. Caterine S, Litchfield R, Johnson M, Chronik B, Getgood A. A cadaveric study of the anterolateral ligament: re-introducing the lateral capsular ligament. Knee Surg Sports Traumatol Arthrosc. 2015;23(11):3186–95.

71. Claes S, Luyckx T, Vereecke E, Bellemans J. The Segond fracture: a bony injury of the anterolateral ligament of the knee. Arthroscopy. 2014;30(11):1475–82.

72. Helito PVP, Bartholomeeusen S, Claes S, Rodrigues MB, Helito CP. Magnetic resonance imaging evaluation of the anterolateral ligament and the iliotibial band in acute anterior cruciate ligament injuries associated with segond fractures. Arthroscopy. 2020;36(6):1679–86.

73. Flato R, Passanante GJ, Skalski MR, Patel DB, White EA, Matcuk GR. The iliotibial tract: imaging, anatomy, injuries, and other pathology. Skelet Radiol. 2017;46(5):605–22.

74. Mansour R, Yoong P, McKean D, Teh JL. The iliotibial band in acute knee trauma: patterns of injury on MR imaging. Skelet Radiol. 2014;43(10):1369–75.

75. Sonin AH, Fitzgerald SW, Bresler ME, Kirsch MD, Hoff FL, Friedman H. MR imaging appearance of the extensor mechanism of the knee: functional anatomy and injury patterns. Radiographics. 1995;15(2):367–82.

76. Azer NM, Winalski CS, Minas T. MR imaging for surgical planning and postoperative assessment in early osteoarthritis. Radiol Clin N Am. 2004;42(1):43–60.

77. Vande Berg BC, Lecouvet FE, Poilvache P, Jamart J, Materne R, Lengele B, et al. Assessment of knee cartilage in cadavers with

dual-detector spiral CT arthrography and MR imaging. Radiology. 2002;222(2):430–6.

78. Vande Berg BC, Lecouvet FE, Malghem J. Frequency and topography of lesions of the femoro-tibial cartilage at spiral CT arthrography of the knee: a study in patients with normal knee radiographs and without history of trauma. Skelet Radiol. 2002;31(11):643–9.

79. Outerbridge RE. The etiology of chondromalacia patellae. J Bone Joint Surg Br. 1961;43-B:752–7.

80. Brittberg M, Winalski CS. Evaluation of cartilage injuries and repair. J Bone Joint Surg Am. 2003;85-A(Suppl 2):58–69.

81. Carrino JA, Blum J, Parellada JA, Schweitzer ME, Morrison WB. MRI of bone marrow edema-like signal in the pathogenesis of subchondral cysts. Osteoarthr Cartil. 2006;14(10):1081–5.

Ankle and Foot

8

Soterios Gyftopoulos and Klaus Woertler

> **Learning Objectives**
> - To understand the importance of profound anatomic knowledge for analyzing radiologic examinations of the ankle and foot.
> - To get an insight into important ankle and foot pathologies.

8.1 Tendon Pathology

8.1.1 Anatomy and Pathophysiology

Tendons have one of the highest tensile strengths of all soft tissues but can get injured secondary to both acute and chronic trauma [1–5]. Tendon pathology occurs along a spectrum, beginning with peritendinous inflammatory change. This then can progress to tendinosis, which represents progressive degeneration of the tendon fibers with incomplete healing secondary to chronic stress. Tendinosis sets the stage for tearing, which comes in two variants: partial and complete thickness.

Ankle tendons and any associated pathology can be easily evaluated on imaging, most commonly MR imaging and ultrasound. On MR imaging, a normal tendon appears as an ovoid or circular low signal structure with intact margins. Peritendinous inflammatory change appears as increased T2-weighted signal surrounding portions of the tendon. In instances where a tendon sheath is present, this abnormal signal is consistent with tenosynovitis or sheath inflammation.

In these cases, you may see associated thickening of the tendon sheath and/or thickened regions of synovium interspersed in the increased T2 signal. Tendinosis will appear as abnormal thickening of the tendon with possible associated regions of intermediate increased intrasubstance signal. With partial thickness tears, you will see a defect or fluid-like increased T2-weighted signal region within a portion of the tendon that does not involve the entire cross-sectional area of the tendon. Patients with complete tears have a defect or abnormal increased T2-weighted signal throughout the entire cross-sectional area of the tendon.

On ultrasound, the normal tendon will have a hyperechoic fibrillar appearance [6]. Tendinosis will appear similar to MR imaging with abnormal thickening of the tendon with possible associated regions of intrasubstance hypoechogenicity. With partial-thickness tears, you will see a defect or defined hypoechoic region within a portion of the tendon that does not involve the entire cross-sectional area of the tendon. Patients with complete tears have a defect or hypoechogenicity throughout the entire cross-sectional area of the tendon.

8.1.2 Ankle Tendon Compartments

There are four ankle/foot tendon compartments.

Anteriorly, you will find the anterior tibialis, extensor hallucis, and extensor digitorum tendons (a.k.a. anterior extensor tendons). The anterior tibialis tendon is the largest, strongest, and most commonly injured of the three anterior tendons (Fig. 8.1). Acute injuries can occur in normal anterior tibialis tendons secondary to penetration or laceration injuries from a sharp object such as a hockey boot blade [3]. Acute injuries more commonly occur in the setting of chronic tendinosis, typically in older patients in the 60–70 age range [3]. In certain instances, these patients can present to imaging to rule out neoplasm with a mass-like lesion along the anterior aspect of the ankle, which represents the torn, retracted tendon.

S. Gyftopoulos
Departments of Radiology and Orthopedic Surgery, NYU Langone Health, New York, NY, USA
e-mail: Soterios.Gyftopoulos@nyulangone.org

K. Woertler (✉)
Department of Radiology, Technische Universität München, Munich, Bavaria, Germany
e-mail: klaus.woertler@tum.de
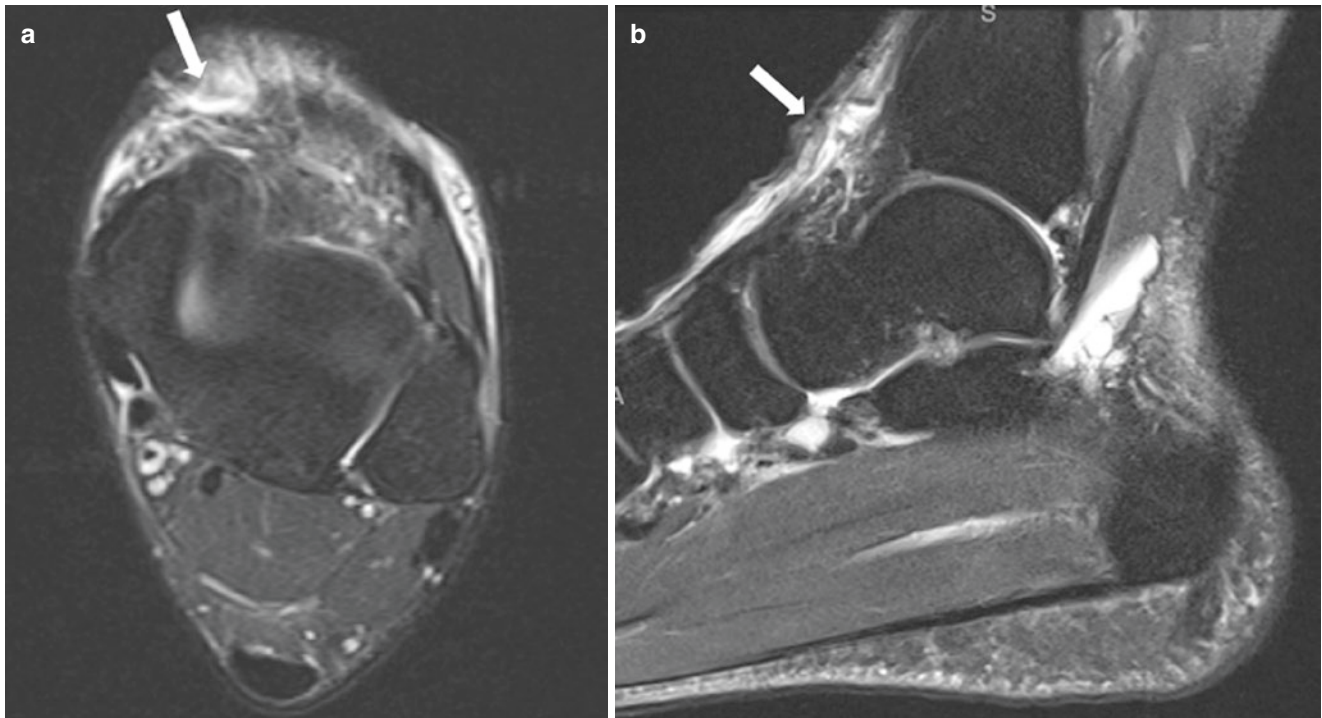
Fig. 8.1 Anterior tibialis tendon tear. Axial (**a**) and sagittal (**b**) fat-suppressed T2-weighted MR images of the right ankle demonstrate a full-thickness tear of the anterior tibialis tendon (*arrows*) secondary to a recent laceration injury

Medially, you will find the posterior tibialis, flexor digitorum, and flexor hallucis tendons (a.k.a. medial flexor tendons). The posterior tibialis tendon is the most commonly injured tendon along the medial ankle, typically in middle-aged and elderly women [2]. The spectrum of injuries ranges from tenosynovitis to complete tearing and is commonly associated with flat foot deformity [2]. Partial-thickness tearing of the posterior tibialis tendon can also appear as thinning or atrophy of the tendon [2]. It is important to note that the posterior tibialis tendon can be dysfunctional without evidence of tearing on imaging [2]. The flexor hallucis longus tendon is the second most commonly injured medial tendon, classically seen in dancers.

Posteriorly, you will find the Achilles tendon. The Achilles tendon is most commonly injured 2–6 cm proximal to its calcaneal insertion, related to the low vascularity in this portion of the tendon (a.k.a. Watershed region) [4]. Injuries are typically posttraumatic in nature with acute tearing superimposed on chronic tendinosis. There are different types of Achilles tendinosis, most commonly hypoxic and mucoid [4]. The insertional portion of the tendon is interposed between the retrocalcaneal bursa (anteriorly) and subcutaneous bursa (posteriorly). These bursae can get inflamed, along with the tendon, in the setting of Haglund's disease (Fig. 8.2) [4].

Laterally, you will find the peroneal tendons: brevis and longus. Peroneal tendon pathology can occur in the acute setting, secondary to ankle sprains, as well as in the chronic setting, in the form of tendinosis from repetitive stress, impingement from displaced fractures of the calcaneus or

Fig. 8.2 Haglund's syndrome. Sagittal fat-suppressed T2-weighted MR image of the right ankle demonstrates insertional Achilles tendinosis (*white arrow*) with adjacent retrocalcaneal bursitis (*gray arrow*) and an enlarged posterosuperior calcaneal margin (*curved arrow*) in a ballet dancer with chronic posterior ankle pain

distal fibula, or inflammatory arthroplasty [5]. Stenosing tenosynovitis can be seen along the peroneal tendons, secondary to chronic friction along the tendons related to
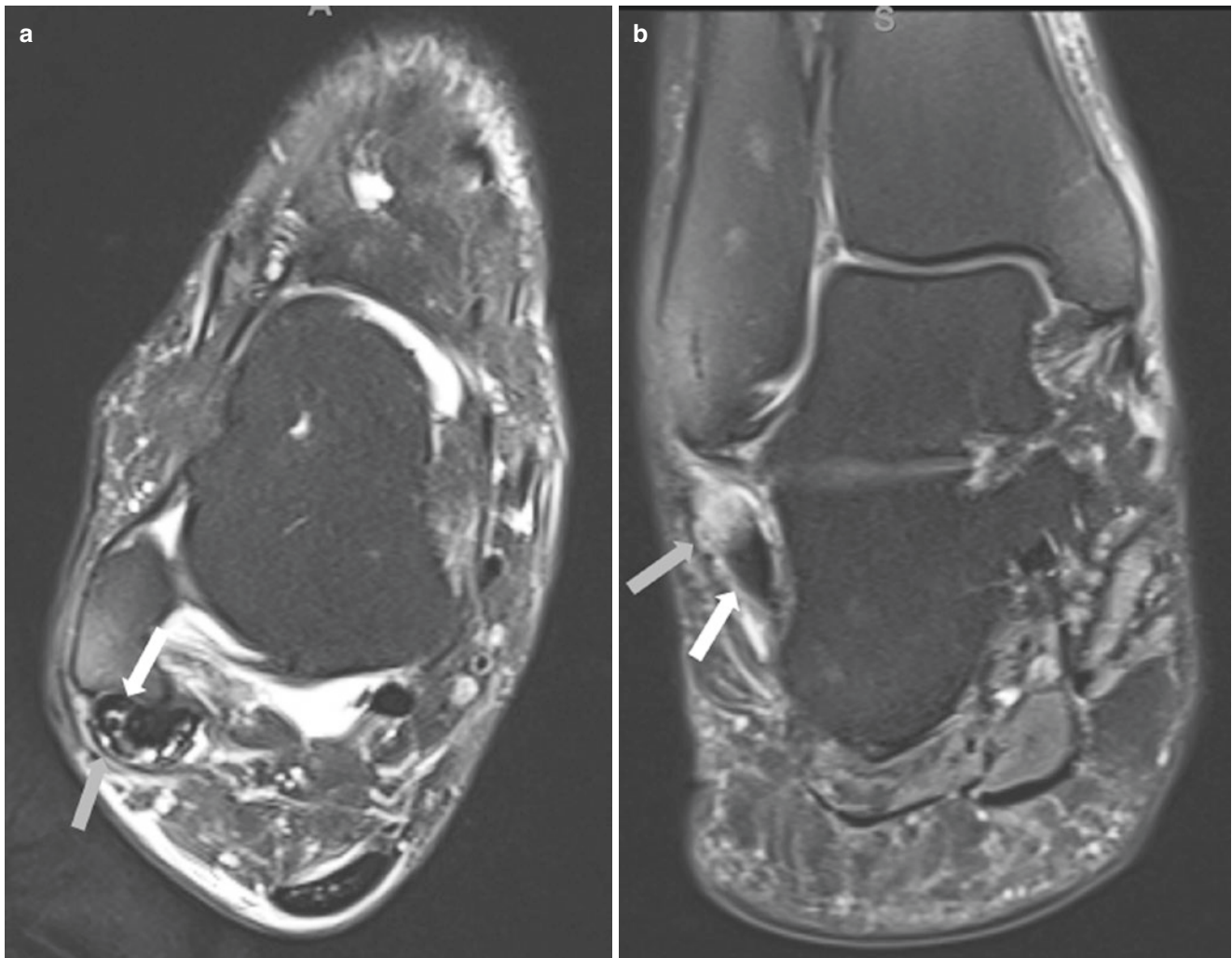
Fig. 8.3 Peroneal stenosing tenosynovitis. Axial (**a**) and coronal (**b**) fat-suppressed T2-weighted MR images of the right ankle demonstrate peroneus brevis and longus tendinosis with partial-thickness tearing (*white arrows*), surrounding tendon sheath thickening and scarring (*gray arrows*)

tendinosis, thick inferior retinaculum, and/or a narrowed inferior osteofibrous tunnel (Fig. 8.3). Peroneal tendon instability can also be seen on imaging, typically related to superior peroneal retinacular injuries [5]. While displaced tendons can be seen on MR imaging, ultrasound can nicely demonstrate the unstable tendons during imaging.

Key Point
- Systematic evaluation of the ankle tendons on MR imaging and ultrasound is crucial in both the acute and chronic pain settings. The spectrum of important tendon pathology ranges from tendinosis to partial-thickness tearing to full-thickness tearing. Tenosynovitis is another important imaging finding to report.

8.2 Bone Injuries

Bone injuries are commonly seen at the ankle and foot, especially in the athletic population. The most common class of bone injuries diagnosed on imaging are stress fractures, which occur in two varieties [7–9]. There are fatigue-type stress fractures which result from chronic abnormal stress on normal bone. There are also insufficiency-type stress fractures which result from normal stress on abnormal bone. The imaging algorithm for stress fracture typically begins with radiographs which may appear normal or show early signs of fracture including early callus formation, endosteal sclerosis, and/or fracture line [8]. MR imaging is the most sensitive imaging modality for this pathology, with findings including periosteal and endosteal edema, hypointense fracture line, and/or hypointense callus formation [8].
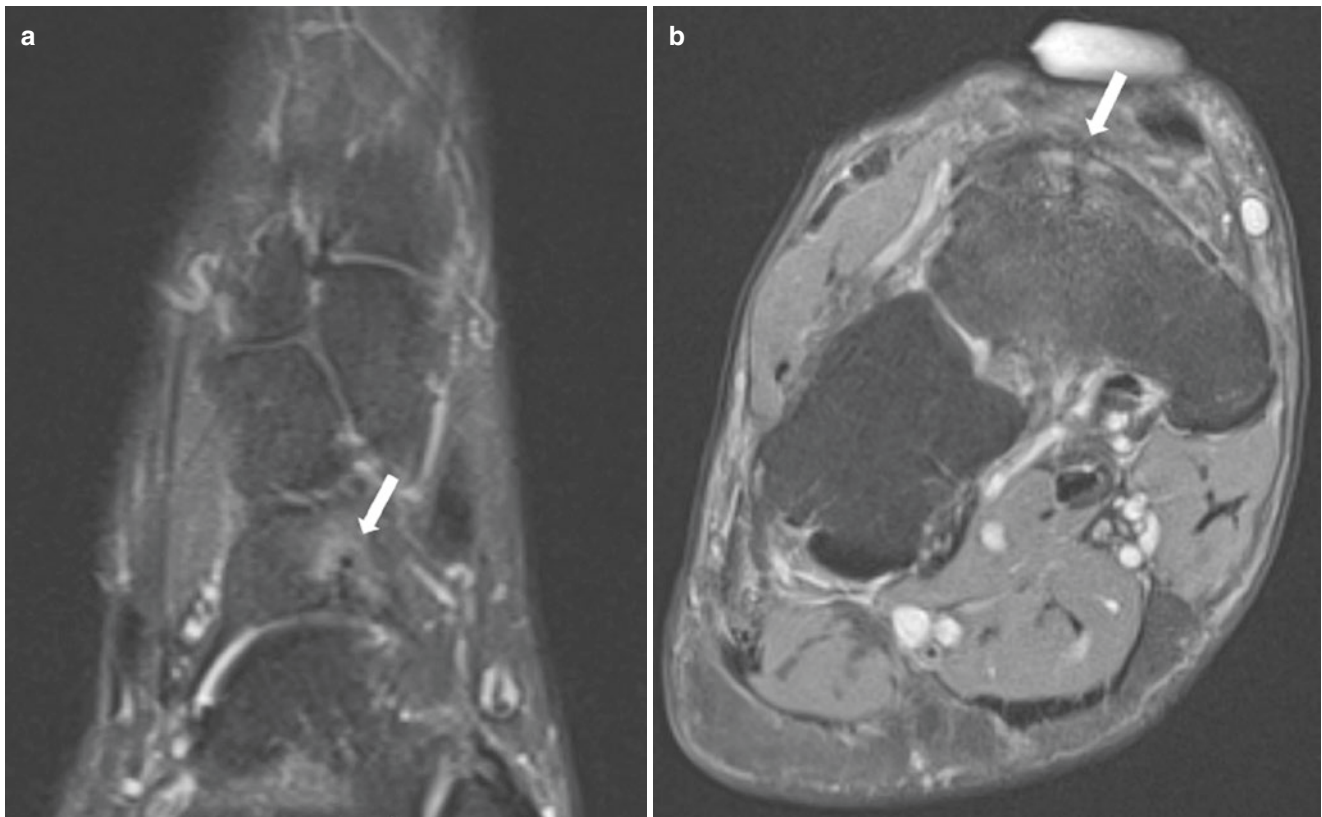
Fig. 8.4 Navicular stress fracture. Axial (**a**) and coronal (**b**) fat-suppressed T2-weighted MR images of the left foot demonstrate an incomplete stress fracture with surrounding bone marrow edema along the dorsal aspect of the navicular (*arrows*)

Common locations for stress fractures at the ankle and foot include metatarsal diaphysis, tarsal navicular, calcaneus, sesamoids, distal tibia, and distal fibula (Figs. 8.4 and 8.5). These injuries are most commonly seen in distance runners but can also be seen in other types of sports including basketball, gymnastics, and ballet [8]. Ultrasound, nuclear medicine, and CT imaging can also be used to diagnose these injuries, although less commonly than radiographs and MR imaging.

> **Key Point**
> • Stress fractures are common and important patholo-gies to diagnose on radiographs and MR imaging. Familiarity with the most common locations for stress fractures increases your chances for accurate diagnosis.

8.3 Lisfranc Joint Injuries

The Lisfranc joint complex compromises three separate compartments: medial, central, and lateral [10]. The medial compartment is made up of the first tarsometatarsal joint, while the central compartment is composed of the second and third tarsometatarsal joints. The lateral compartment is composed of the articulations of the fourth and fifth tarso-metatarsal joints. These articulations along with the surrounding capsules and ligaments provide stability to the Lisfranc joint complex.

The most important ligament is the Lisfranc ligament which is found along the medial aspect of the midfoot [10, 11]. The Lisfranc ligament has three components [12]. The strongest and most important component is the interosseous component, which extends from the medial cuneiform to the second metatarsal base [11, 12]. The second strongest component is the plantar component, which extends from the medial cuneiform to the plantar aspects of the second and third metatarsals. The weakest component is the dorsal component, which is found dorsally and extends from the medial cuneiform to the second metatarsal base.

The imaging algorithm for Lisfranc injury typically begins with radiographs. While gross disruption of the tarsometatarsal joints can be easily seen in the setting of a Lisfranc fracture dislocation injury secondary to high-energy trauma, special attention should be placed on the first and second tarsometatarsal joints in more subtle low-energy trauma cases [13]. One should carefully evaluate the middle cunei-form and second metatarsal base articulation for offset, the
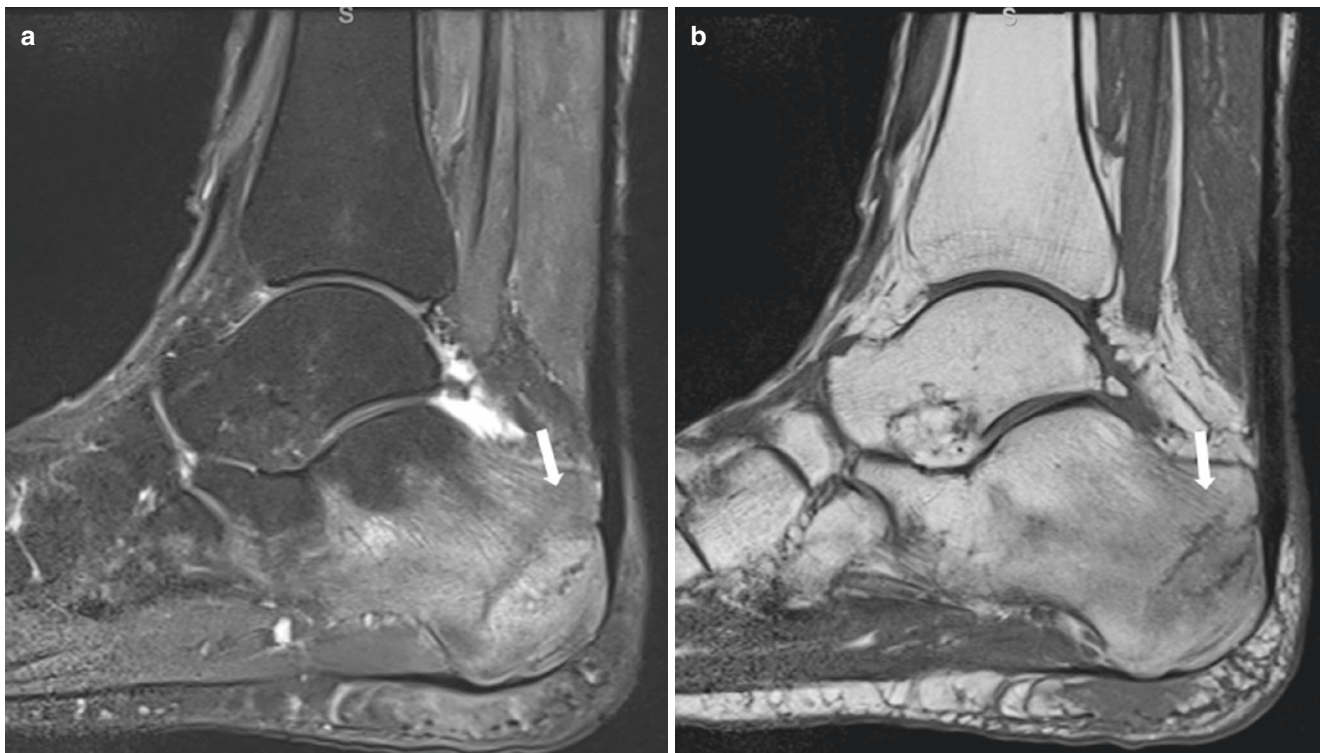
Fig. 8.5 Calcaneal stress fracture. Sagittal fat-suppressed T2- (**a**) and proton density weighted (**b**) MR images of the left ankle demonstrate incomplete stress fractures with surrounding bone marrow edema within the posterior third of the calcaneus (*arrows*)

first and second tarsometatarsal joint interval for abnormal widening (> 2 mm), and avulsion fracture at the second metatarsal base. If possible, weight-bearing radiographs should be obtained as these radiographic findings are more likely to be seen in this imaging setting.

MR imaging is typically the second imaging modality utilized for the evaluation of Lisfranc ligament injury if radiographs are inconclusive and/or more information is needed to make a treatment decision. The main advantage of MR imaging is the ability to visualize each component of the Lisfranc ligament [12]. The normal interosseous component is a thick low signal structure that is best seen on the long-axis and short-axis MR imaging planes extending from the medial cuneiform to the second metatarsal base. This ligament can appear striated, especially on 3 T imaging, which is a normal variant and should not be confused with pathology [12]. The plantar component is best seen on short-axis imaging as a low signal structure extending from the medial cuneiform to the plantar aspects of the second and third metatarsals. The dorsal component is also best seen on short-axis imaging as a thin low signal structure extending along the dorsal aspects of the medial cuneiform and second metatarsal base.

MR imaging signs of ligament injury include abnormal increased T2-weighted signal within and/or along the margins of the Lisfranc ligament components, disrupted liga-

ment fibers, and avulsion of the ligament from one of its osseous attachments (Fig. 8.6). While all three components should be evaluated, special attention to the interosseous component should be made as the state of this component most directly guides treatment decisions. Bone injuries, including bone contusions and/or fractures, along the margins of the first and second tarsometatarsal joints should bring your attention to the Lisfranc ligament complex in order to assess for possible injury. Focal osseous avulsion fragments can be easily missed on MR imaging; correlation with radiographs or CT would be useful in these settings. CT is also useful, and typically the second imaging modality utilized, in the setting of Lisfranc fracture dislocation injuries.

> **Key Point**
> - High suspicion for Lisfranc ligament injury is crucial in the setting of foot trauma. On radiographs, the reader should pay careful attention to the middle cuneiform-second metatarsal base articulation and the first and second tarsometatarsal joint interval. On MR imaging, the reader should carefully evaluate the interosseous component as this is the most important portion of the Lisfranc ligament complex.
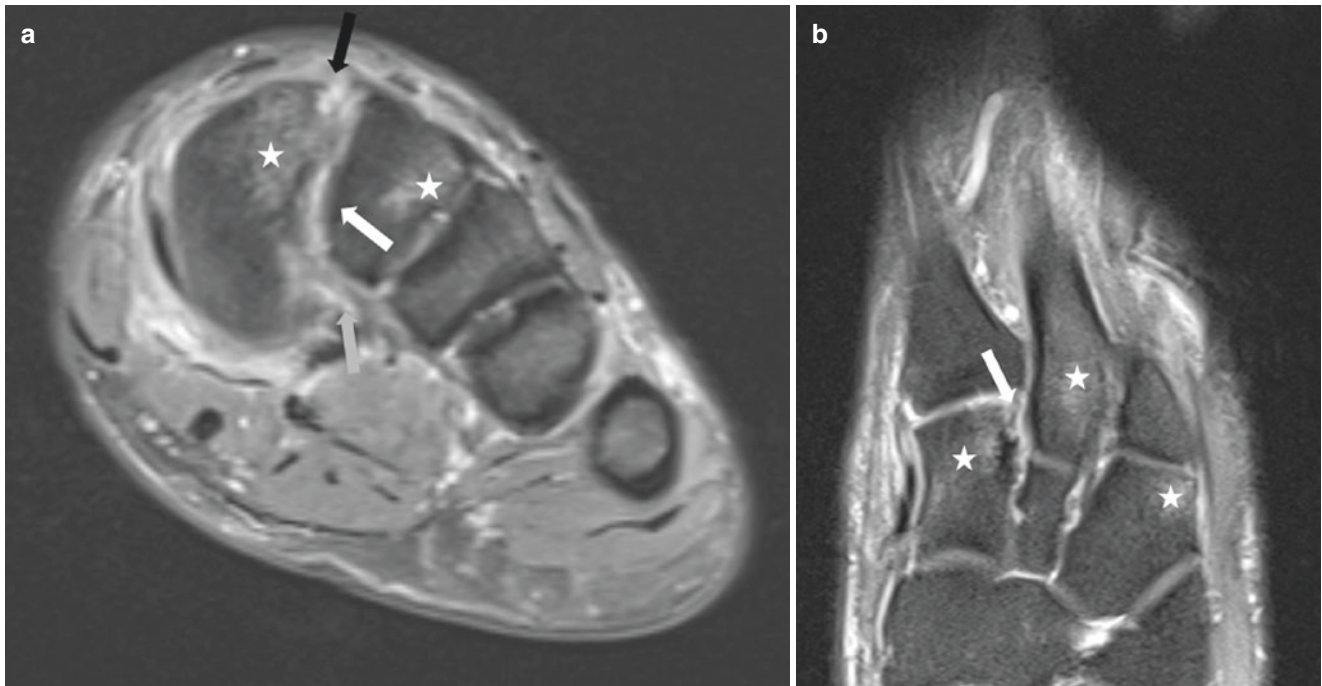
Fig. 8.6 Lisfranc ligament tear. Coronal (**a**) and axial (**b**) fat-suppressed T2-weighted MR images of the left midfoot demonstrate tearing of the interosseous (*white arrows*), plantar (*gray arrow*), and dorsal (*black arrow*) components of the Lisfranc ligament and adjacent bone contusions (*stars*)

8.4 Turf Toe/Plantar Plate Injuries

The plantar plates at the metatarsophalangeal (MTP) joints are common locations of pathology in the forefoot [11, 14, 15]. Plantar plate pathologies are typically divided into two categories: first MTP (great toe) injuries and second through fifth (lesser toe) injuries. Both categories of pathology can be evaluated with either MRI or ultrasound, although MR imaging is the preferred modality.

The first ray and MTP joint, in particular, play an important role in foot mechanics [14]. Thus, injuries to the first MTP joint can have important and potentially devastating consequences. The plantar aspect of the first MTP joint is composed of several components which make up what is referred to as the plantar plate complex. This complex provides both dynamic and static joint stability, while providing protection to the articular surfaces of the first MTP joint.

The plantar plate complex has three main parts: osseous, ligamentous, and musculotendinous [14]. The osseous component is comprised of the medial and lateral sesamoids, which serve as attachment sites for important adjacent soft tissue structures, as well as the proximal phalanx and metatarsal head articular surfaces. The ligamentous part has multiple components. There is a fibrocartilaginous pad which surrounds the sesamoids and is inseparable from paired sesamoid phalangeal ligaments, intersesamoid ligament, and paired metatarsosesamoid ligaments. On imaging, each normal ligament appears as a thin structure that extends from the sesamoids to a surrounding structure. Sagittal (ultrasound, long axis) and coronal (ultrasound, short axis) imaging planes are typically the most useful. The most important structures are the sesamoid phalangeal ligaments as they are the most common location for pathology, typically in the setting of hyperextension injury [14]. The musculotendinous part compromises the medial and lateral heads of the flexor hallucis brevis, flexor hallucis longus, adductor hallucis, and abductor hallucis tendons.

Injuries to the first MTP plantar plate complex can occur in the acute (trauma) or chronic (degenerative) setting [14]. Acute injuries, referred to as Turf toe, occur along a spectrum [11, 14]. Mild (grade I) injuries represent sprains and present with abnormal increased T2-weighted signal along the ligament components, most commonly the sesamoid phalangeal, as well as the sesamoids, and/or musculotendinous structures. Grade II injuries represent partial-thickness tearing of the plantar plate complex, most commonly the sesamoid phalangeal, with associated intrasubstance and surrounding abnormal increased T2-weighted signal. Grade III injuries represent complete tearing of the plantar plate complex ligamentous structures and/or fracture or diastasis of the sesamoids. Grade I–III injuries are typically treated conservatively with a positive correlation between injury
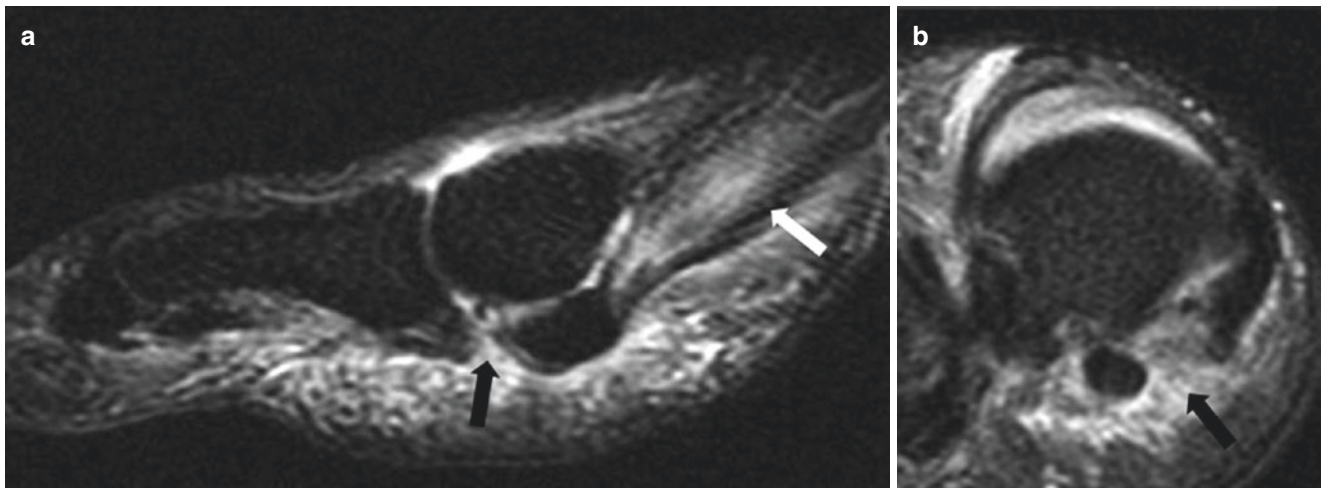
Fig. 8.7 Plantar plate tear (great toe). Sagittal (**a**) and coronal (**b**) fat-suppressed T2-weighted MR images of the right forefoot demonstrate tearing of the medial sesamoid phalangeal ligament (*black arrows*) and strain of the abductor hallucis muscle (*white arrow*)
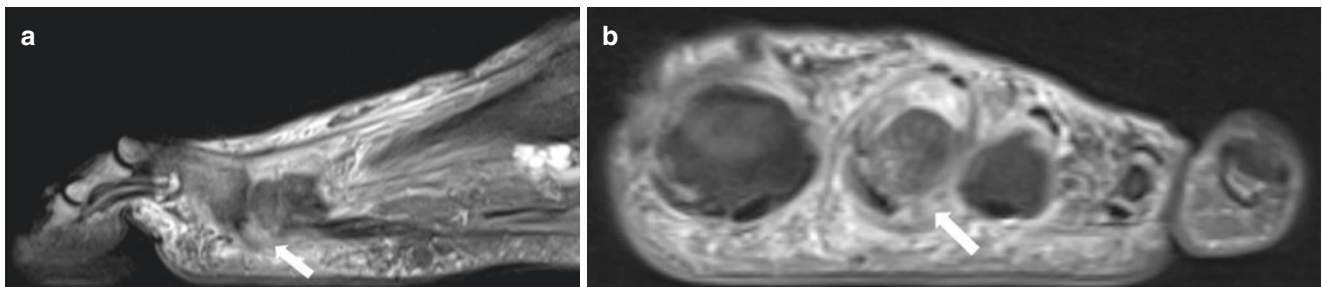
Fig. 8.8 Plantar plate tear (lesser toes). Sagittal (**a**) and coronal (**b**) fat suppressed T2-weighted MR images of the left forefoot demonstrate tearing of the second metatarsophalangeal plantar plate along its lateral aspect (*white arrows*)

grade and recovery time [14]. Marked first MTP joint instability may be an indication for surgery in certain cases [14].

Osteochondral injuries are common and typically involve the sesamoids [14]. Sesamoid pathologies include sesamoiditis (stress reaction), fractures, osteonecrosis, and diastasis of a bipartite sesamoid. Acute injuries along the proximal phalanx and metatarsal head articular surfaces can also occur but are less common. Chronic first MTP plantar plate injuries are typically seen in the setting of osteoarthritis and hallux valgus deformities.

Unlike the first MTP, the plantar plates of the lesser toes consist of a single fibrocartilaginous plate that extends from the metatarsal head (thinnest portion of the plate) to the proximal phalanx base (thickest portion of the plate) at each joint [11, 15]. Similar to the first MTP joint, the lesser toe plantar plates provide joint stability and articular surface protection. On imaging, the plate appears as a well-defined structure extending from the metatarsal head to the phalanx base. Sagittal (long axis) and coronal (short axis) imaging planes are typically the most useful. The second and third MTP plantar plates are most commonly injured with the

spectrum of pathology ranging from degeneration to partial-thickness tearing to complete tearing [11]. Plantar plate degeneration appears as thickening of the plate, while tearing typically presents as a defect at the plate insertion (Figs. 8.7 and 8.8). The medial phalanx insertion is the most common initial site for plantar plate pathology. Care should be taken to not confuse the synovitis that can occur adjacent to plantar plate tearing with a Morton neuroma [11].

Key Point
- Understanding of the plantar plate anatomy is essential for the accurate diagnosis of pathology on imaging. The sesamoid phalangeal ligaments are the most common location for pathology at the first MTP joint. The second and third MTP plantar plates are most commonly injured in the lesser toes with the spectrum of pathology ranging from degeneration to partial-thickness tearing to complete tearing.

8.5 Ankle Ligament Injuries

8.5.1 Lateral Collateral Ligament Complex

The lateral collateral ligament complex of the ankle is composed of three main structures: the anterior talofibular ligament (ATFL), the calcaneofibular ligament (CFL), and the posterior talofibular ligament (PTFL). The ATFL, as the weakest of these ligaments, originates from the tip of the distal fibula, takes an almost horizontal intra-articular course, and inserts to the talar neck. The CFL is vertically oriented and extra-articular and extends from the lateral malleolar tip to the trochlear eminence of the calcaneus, lying deep to the peroneal tendons. Both the ATFL and the CFL are seen as linear structures of low signal intensity on MR imaging. The PTFL takes an almost horizontal course from the fibular malleolar fossa to the posterior talus. It has an intra-articular but extra-synovial location and blends with the posterior capsule. On MR imaging, it appears as a strong, often fan-shaped structure with a striated appearance due to fibrofatty composition [16–18].

The lateral ligaments are the most commonly injured structures of the ankle. Approximately 85% of all ankle sprains result in damage to the lateral ligamentous complex. Inversion injuries most often lead to isolated tears of the ATFL or combined tears of the ATFL and CFL. Isolated tears of the CFL are rare, and injuries of the PTFL almost never occur unless following gross dislocation of the ankle. Typical sites of ATFL and CFL tears are the mid-substance of the ligaments or their insertions to the talus and calcaneus [16, 17].

On MR imaging, thickening and increased T1- and T2-weighted signal intensity associated with surrounding edema suggest a partial ligament tear. Complete tears are characterized by discontinuity and retraction of the ligament (Fig. 8.9). Osseous avulsion can be overlooked, in particular if the bony fragment is small, and therefore, correlation with conventional radiography is mandatory. Associated injuries can include osteochondral lesions of the talus; injury to the medial collateral ligament complex, the tibiofibular syndesmosis, the bifurcate ligament, and the ligaments of the tarsal sinus; and peroneal tendon lesions, as well as fractures [16–18].

8.5.2 Medial Collateral Ligament Complex

The medial collateral ligament complex has a superficial and a deep layer. The superficial layer crosses two joints and is composed of the tibiocalcaneal ligament (TCL), the tibio-
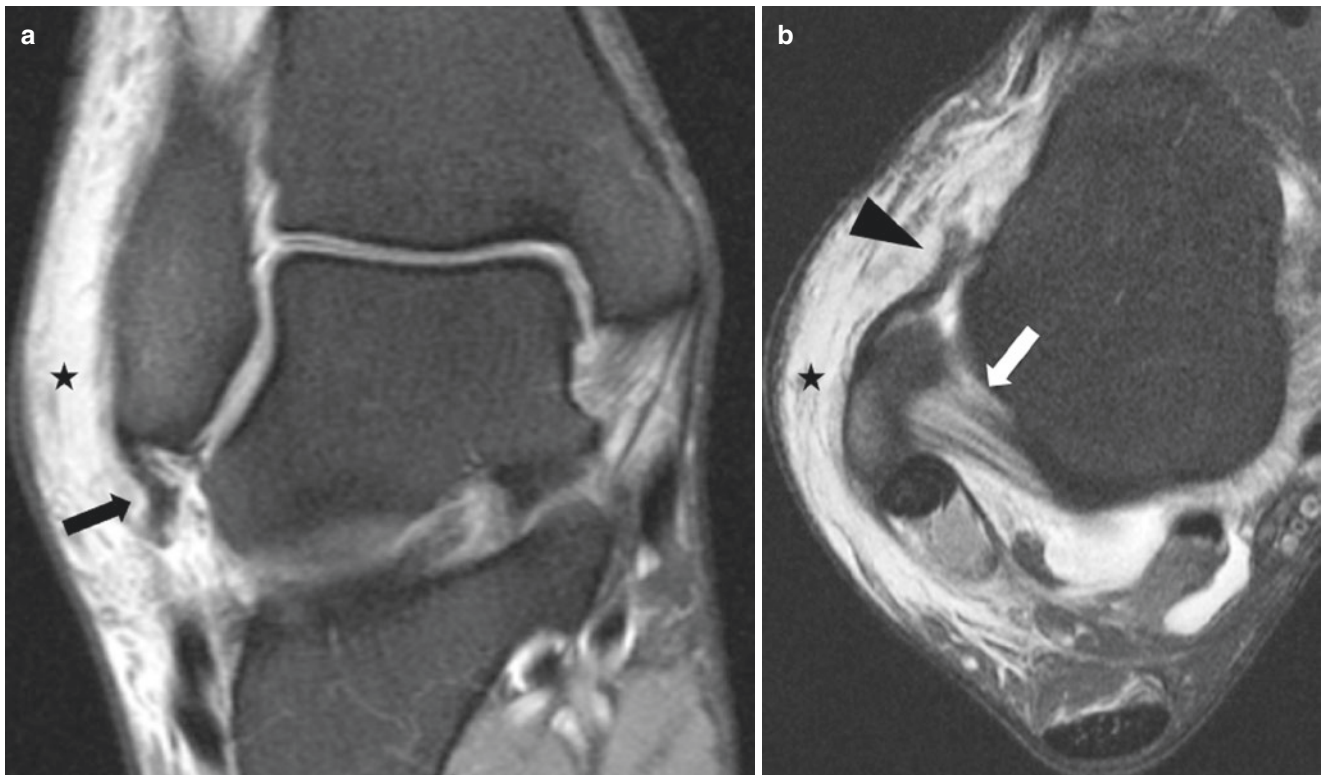
Fig. 8.9 Lateral collateral ligament complex tear. Coronal (**a**) and axial (**b**) fat-suppressed intermediate weighted MR images obtained after a right ankle sprain show complete tearing of the calcaneofibular (*black arrow*) and anterior talofibular (*black arrowhead*) ligaments with discontinuity and retraction. Note intact posterior talofibular ligament (*white arrow*) with typical striated appearance. Posttraumatic hematoma is seen in the lateral subcutaneous tissue (*stars*)

spring ligament (TSL), and the tibionavicular ligament (TNL). The deep layer crosses only one joint and is formed by the posterior tibiotalar ligament (pTTL) and the anterior tibiotalar ligament (aTTL). Not all of these five components may always be visualized on routine MR images; the pTLL, TCL, and TNL can however be identified in most cases. The pTTL is the thickest of the medial ligaments and differs from the others by usually showing a striated appearance [19, 20].

Overall, the medial collateral ligament complex is more resistant to trauma than the lateral one, and therefore, the strength of the medial complex may lead to medial malleolar fracture without rupture of the ligaments. Injury to the medial ligaments is seen in only 5–15% of all ankle sprains. In more than half of these cases, both superficial and deep components of the medial complex are involved. Most medial collateral ligament injuries occur in combination with lateral ligament tears, malleolar fractures, and syndesmotic tears. Isolated injuries are rare. MR imaging criteria for the diagnosis of partial and complete tears of the different components of the medial complex are identical to those described with lateral ligament injuries. Loss of striation is an additional sign suggesting injury of the pTTL [19–21].

8.5.3 Tibiofibular Syndesmosis

The tibiofibular syndesmosis maintains integrity between the distal tibia and fibula and resists axial, rotational, and translational forces. It is formed anteriorly by the anteroinferior tibiofibular ligament (AITFL) and the interosseous ligament (IL) and posteriorly by the posteroinferior tibiofibular ligament (PITFL) and the transverse tibiofibular ligament (TrTFL). The AITFL is often referred to as the anterior syndesmosis, and the PITFL and TrTFL as the posterior syndesmosis. The syndesmotic ligaments have an oblique course, and therefore, some authors recommend oblique axial images for MR imaging. In most cases the tibiofibular syndesmosis can however be sufficiently evaluated by analyzing standard images in all three orthogonal planes. The normal AITFL, PITFL, and TrTFL typically show a fascicular morphology on MR images with T2 contrast [17, 21, 22].

Syndesmotic tears comprise approximately 10% of all ankle injuries and are often overlooked at initial presentation. They can occur in isolation or in combination with other ligament ruptures. Tearing of the tibiofibular syndesmosis is evident in approximately 50% of Weber B and the vast majority of Weber C ankle fractures. A Maisonneuve-type fracture should be ruled out in case of a seemingly isolated syndesmotic injury. In high ankle sprains, the anterior syndesmosis is often ruptured, whereas the posterior syndesmosis remains intact. Posterior syndesmotic injuries are more often bony avulsions from the tibial insertion

(Volkmann fracture) than ligament tears. They commonly occur if all components of the syndesmosis are involved and in combination with ankle fractures [17, 18, 21–23].

Injuries of the tibiofibular syndesmosis can be diagnosed by MR imaging with a high sensitivity and specificity. Partial ligament tears are characterized by thickening, increased signal intensity, and loss of fascicular appearance as well as adjacent soft tissue swelling. Frank discontinuity, a wavy or curved ligament contour, and bony avulsion represent criteria of a complete tear (Fig. 8.10) [22, 23]. Since rupture of the AITFL at its fibular insertion is common, linear high signal intensity on the anterior cortex of the fibula seen on sagittal intermediate or T2-weighted images with fat suppression represents a secondary sign of an anterior syndesmotic tear.

> **Key Point**
> - Evaluation of the ligamentous structures on MR images obtained after ankle sprains is crucial. All components of the lateral and medial collateral complex and the tibiofibular syndesmosis should be routinely checked. Partial tears typically lead to thickening and increased signal intensity of the involved ligaments, whereas complete tears are characterized by discontinuity and retraction. Bony avulsion might be overlooked on MR imaging.

8.6 Osteochondral Lesions of the Ankle

Osteochondral lesions (OCL) of the talus (OLT) are most often diagnosed in young adults as sequels of acute or recent trauma. They are estimated to occur in 6–7% of all inversion injuries, but their true incidence is probably higher. Regarding all sports injuries of the ankle, OLT can be found as associated findings in up to 50% of the cases. OCL of the tibial plafond are less frequent [21, 24, 25].

OLT following inversion trauma of the ankle can involve the medial or lateral shoulder of the talar dome. Whereas medial lesions are thought to be caused by compression forces, lateral lesions are more likely initiated by shearing forces. Medial OLT therefore often represent sequels of (osteo)chondral contusions or compression fractures, and lateral OLT are caused by cartilage delamination or (osteo)chondral fractures. All staging systems for OLT are more or less based on the classic publication by Berndt and Harty [26], who classified the appearance of traumatic transchondral fractures: stage 1 describes an area of subchondral compression with intact overlying cartilage, stage 2 a partially detached osteochondral fragment, stage 3 a completely detached osteochondral fragment, and stage 4 a displaced fracture with intra-articular loose body. A stage 5 describing
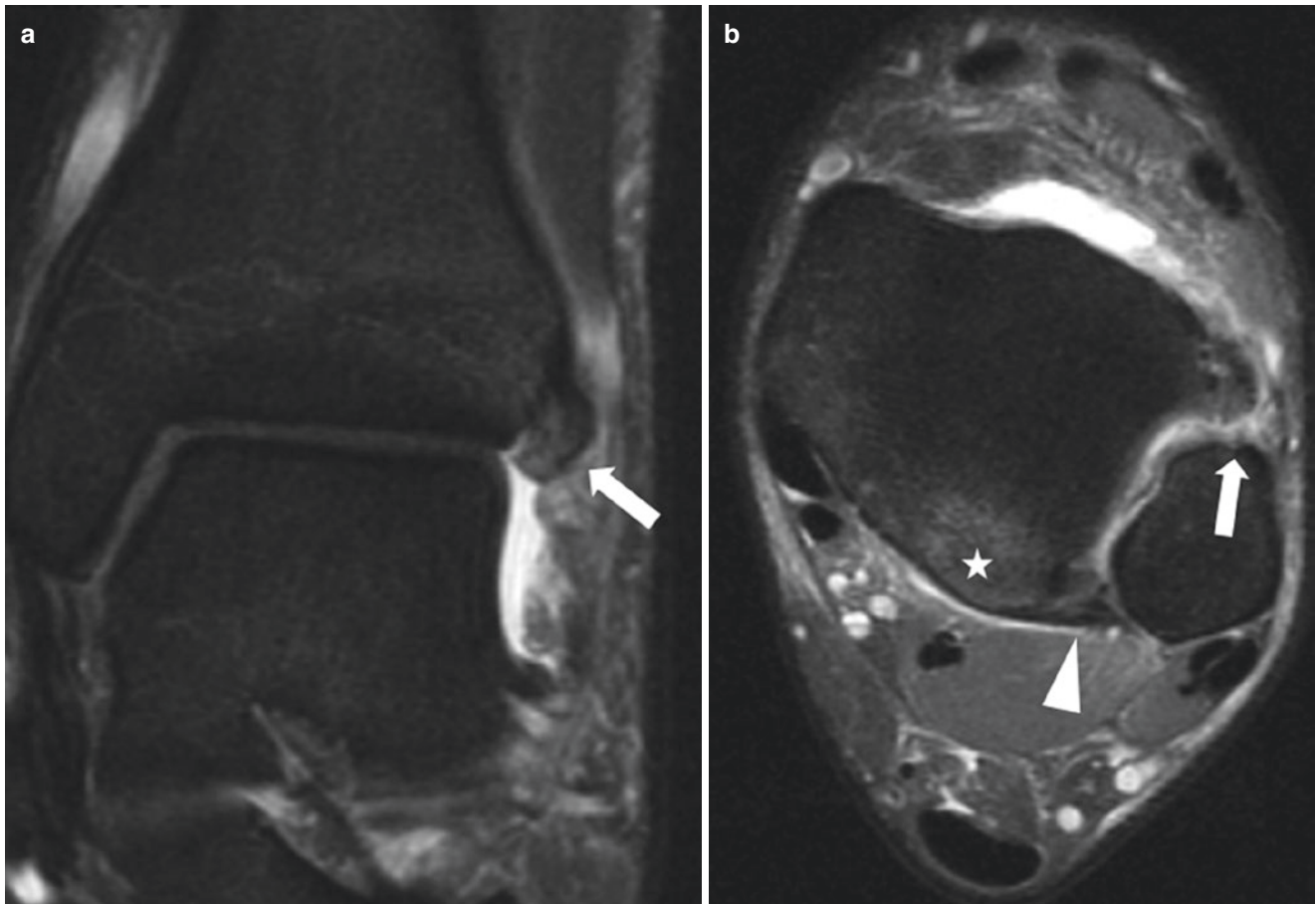
Fig. 8.10 Anterior syndesmotic tear. Coronal (**a**) and axial (**b**) fat-suppressed intermediate weighted MR images of the left ankle demonstrate a tear of the anteroinferior tibiofibular ligament at its fibular insertion (*white arrows*). The posteroinferior tibiofibular ligament (*white arrowhead*) has remained intact. Bone marrow edema without evidence of a fracture line is seen in the posterior tibial plafond (*star*)

formation of a subchondral "cyst" (fibrous defect) was later added by Loomer [21, 24, 26, 27].

In addition to radiographs, conventional MR imaging is usually sufficient to detect and classify OCL of the ankle joint after acute trauma (Fig. 8.11). Chronic lesions are often difficult to characterize on MR imaging due to secondary changes developing in and adjacent to the initially damaged area. In this setting, CT arthrography has proved to be a useful tool to accurately depict cartilage and bone defects of the ankle with an impact on therapeutic decisions [25]. Important criteria for surgical treatment include the integrity of articular cartilage overlying the talar as well as the opposite tibial joint surface, the presence of subchondral "cysts," and the stability and viability of the osteochondral fragment.

> **Key Point**
> • The evaluation of chronic osteochondral lesions of the ankle by MR imaging is challenging. CT arthrography represents a valuable technique for further analysis.

8.7 Ankle Impingement Syndromes

Impingement syndromes of the ankle are characterized by painful soft tissue encroachment most often due to posttraumatic changes following ankle injuries, usually sprains. The diagnosis is largely clinical and may be supported by imaging findings, including the depiction of morphologic bone and soft tissue changes, localized synovitis, and predisposing anatomic conditions [28, 29]. Anterolateral, anterior, and posterior ankle impingement represent the most important clinical entities. Anteromedial and posteromedial impingement syndromes are less common [28].

8.7.1 Anterolateral Impingement Syndrome

Anterolateral impingement is caused by entrapment of abnormal soft tissue in the anterolateral recess (anterolateral gutter) of the ankle, usually subsequent to an inversion sprain with persistent anterolateral pain and swelling. The abnormal soft tissue can represent posttraumatic scar tissue ("meniscoid lesion") or, more rarely, hypertrophy of the
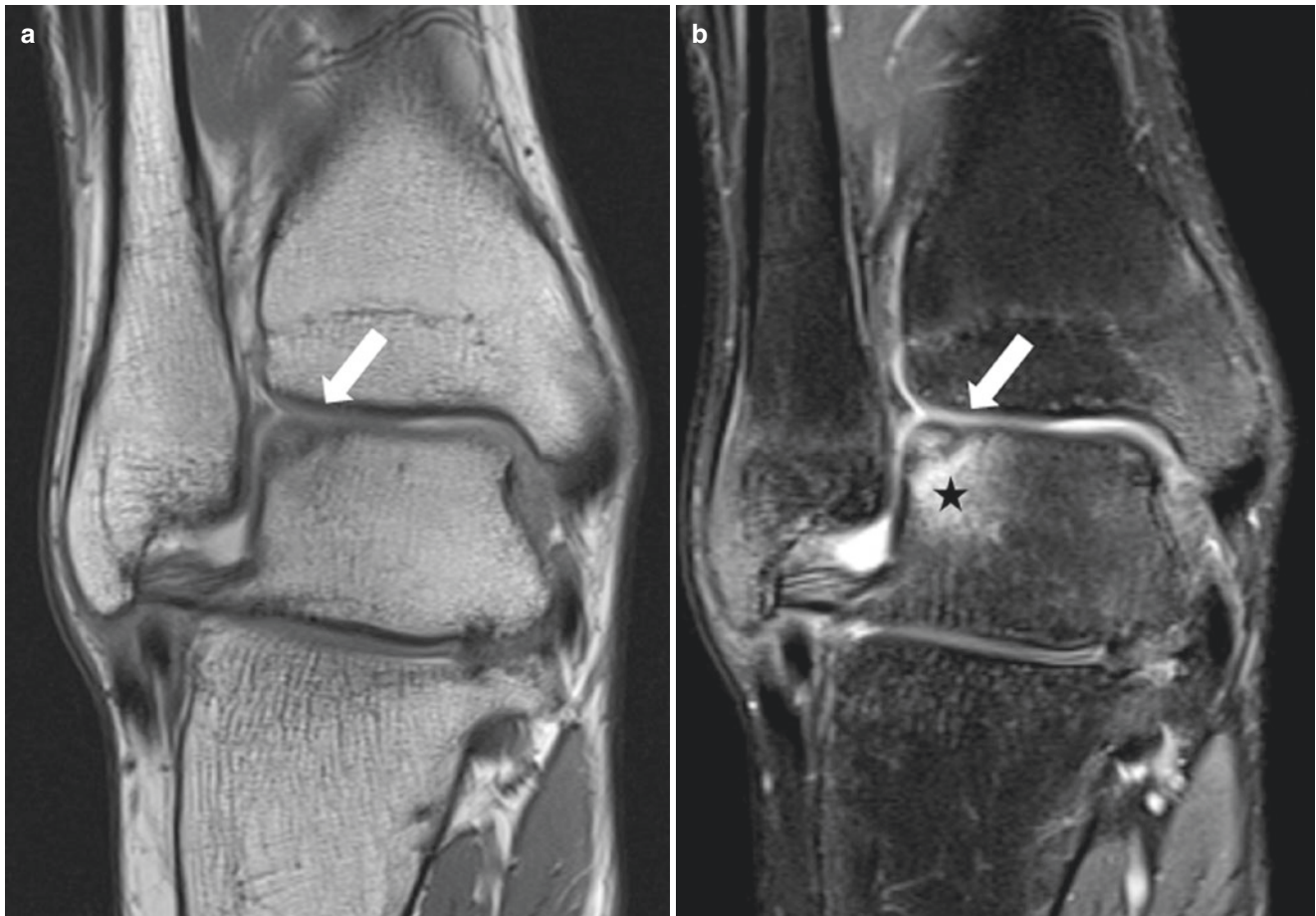
Fig. 8.11 Osteochondral lesion (OCL) of the talus. Coronal T1-weighted MR image with DRIVE pulse (**a**) and corresponding fat-suppressed intermediate weighted image (**b**) obtained eight weeks after inversion injury of the right ankle show non-displaced osteochondral fracture at the lateral shoulder of the talus (*arrows*) with adjacent bone marrow edema (*star*)

Bassett ligament. On MR imaging, scar tissue or synovial hypertrophy can be seen obscuring the anterolateral recess. These findings may be more easily identified on MR arthrography. MR images obtained after intravenous contrast administration can show synovitis exclusively confined to the anterolateral recess [28–31].

8.7.2 Anterior Impingement Syndrome

Anterior impingement is relatively common in soccer players, ballet dancers and runners. Tibiotalar spur formation in the anterior joint recess, hypertrophy of capsular tissue, and painful soft tissue entrapment are thought to be induced by repetitive trauma. Conventional radiographs are usually sufficient to identify the underlying bony changes at the distal tibia and the anterior process of the talus. MR imaging can demonstrate bone marrow edema, cartilage loss, capsular thickening, and synovitis in the anterior recess [28, 30].

8.7.3 Posterior Impingement Syndrome

Posterior ankle impingement is typically seen in athletes who execute repetitive plantar hyperflexion, such as ballet dancers and soccer players. The underlying mechanism is compression of bone and soft tissue structures between the tibia and the calcaneus during forced plantar flexion of the foot. Predisposing conditions include the presence of an os trigonum, an elongated Stieda process, and a fractured lateral tubercle of the talus. A more downsloping articular surface of the tibia, a prominent posterior process of the calcaneus, and a posterior intermalleolar ligament may also contribute. Conventional radiography allows for identification of the abovementioned variants and changes of osseous anatomy. MR images can show bone marrow edema in all involved osseous structures, fluid within a non-united fracture, thickening of the posterior capsule, synovitis in the posterior joint recess, as well as tenosynovitis of the flexor hallucis longus and soft tissue edema (Fig. 8.12). An abnormal intermalleolar ligament may also be visualized [28, 30].
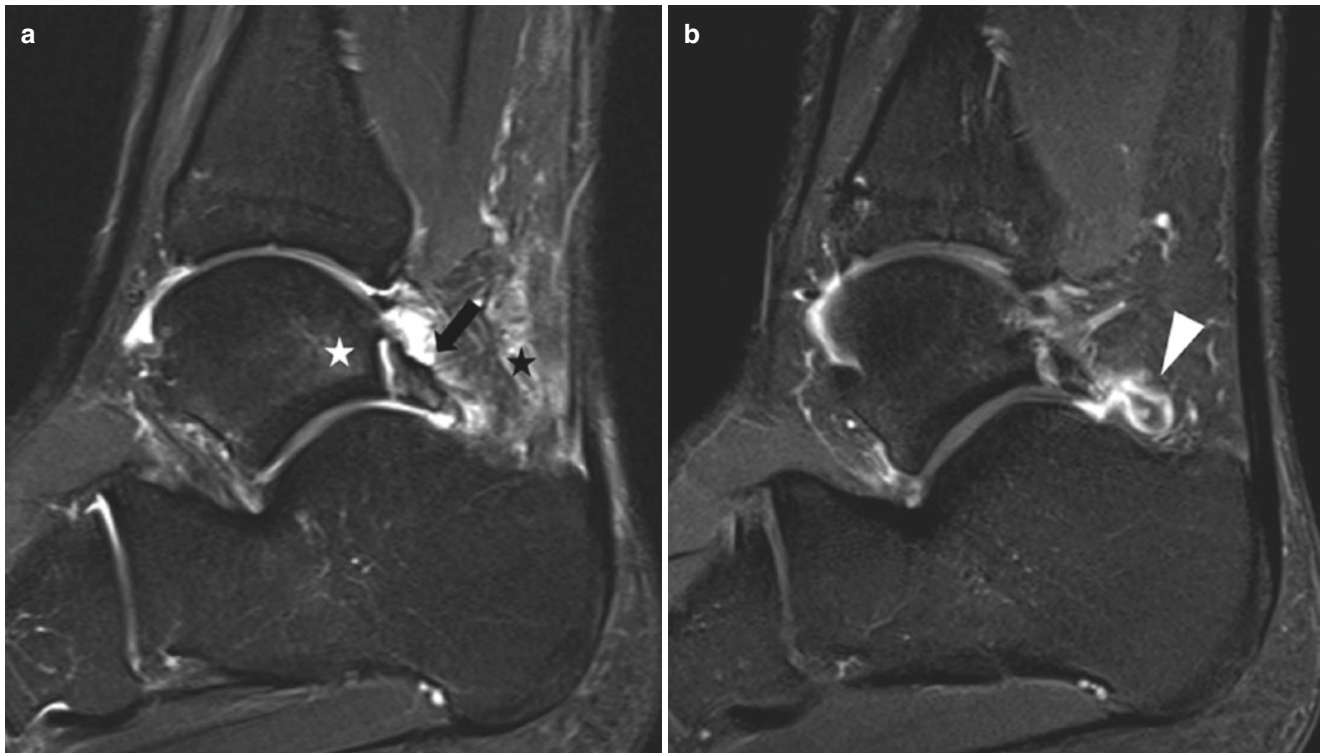
Fig. 8.12 Posterior ankle impingement (os trigonum syndrome). Sagittal fat-suppressed intermediate weighted MR image of the ankle (**a**) demonstrates os trigonum with bone marrow edema separated from the talus by interposed fluid (*black arrow*), bone marrow edema in the posterior talus (*white star*), and retroachillear soft tissue edema (*black star*) in a soccer player with clinical symptoms of posterior impingement. Corresponding fat-suppressed T1-weighted image after contrast administration (**b**) shows localized synovitis in the posterior joint recess (*white arrowhead*)

> **Key Point**
> • Ankle impingement is a clinical and not a radiological diagnosis.

8.8 Nerve Entrapment

8.8.1 Tarsal Tunnel Syndrome

Tarsal tunnel syndrome is caused by compression of the posterior tibial nerve and its branches in the tarsal tunnel, a fibro-osseous canal extending from the posteromedial ankle to the plantar aspect of the foot. Possible clinical symptoms include pain and paresthesia at the medial heel and/or the medial and plantar aspect of the foot and toes, positive Tinel's sign, and weakness of the plantar muscles. Entrapment of the nerve can occur due to trauma or repetitive stress (athletes), foot deformity, ankle instability, spur formation, and space-occupying masses (ganglia, nerve sheath tumors, accessory muscles). MR imaging may show morphologic changes of the posterior tibial nerve, denervation edema of the plantar muscles, a soft tissue mass (Fig. 8.13), (teno)synovitis, or diffuse contrast enhancement of the tarsal tunnel [32–34].

8.8.2 Baxter Neuropathy

The inferior calcaneal nerve (Baxter nerve) is a mixed sensory and motor nerve, which arises from the lateral plantar nerve within the tarsal tunnel. It takes a vertical course between the abductor hallucis and quadratus plantae muscles and then makes a horizontal turn, coursing laterally beneath the calcaneus to innervate the abductor digiti minimi muscle. Baxter neuropathy due to stretching of the inferior calcaneal nerve is a common problem in runners, ballet dancers, and gymnasts, who experience heel pain and burning sensations radiating along the lateral foot. Other causes include a hypermobile pronated foot, hypertrophy of the abductor hallucis muscle, inferior calcaneal spurs, and plantar fasciitis. A classic sign of affection of the Baxter nerve on MR imaging is denervation edema or fatty infiltration of the abductor digiti minimi muscle [32–34].

8.8.3 Jogger's Foot

Entrapment of the medial plantar nerve between the abductor hallucis muscle and the plantar crossover of the flexor digitorum longus and flexor hallucis longus tendons ("knot of Henry") is classically described in runners, typically with hyperpronation and heel valgus. Clinical symptoms are radiating medial foot pain, tenderness, and dysesthesia along the

plantar aspect of the first and second toes. MR imaging can confirm the diagnosis by demonstrating denervation edema or fatty atrophy of the abductor hallucis, flexor digitorum brevis, flexor hallucis brevis, and first lumbrical muscles [32–34].

8.8.4 Morton Neuroma

Morton neuroma represents perineural fibrosis of a plantar digital nerve due to chronic entrapment. The lesion is most commonly found in the second or third intermetatarsal space at the level of the metatarsal heads deep to the transverse ligament. Clinical symptoms include numbness and forefoot pain radiating into the toes or leg. MR imaging shows a round or dumbbell-shaped mass extending from the involved intermetatarsal space in a plantar direction, typically exhibiting low T1- and T2-weighted signal intensity (Fig. 8.14). Lesion conspicuity can be increased by examination of the foot in prone position [33–35].

> **Key Point**
> • The diagnosis of nerve entrapment is based on clinical and imaging findings. MR images should be searched for morphologic changes of the involved nerve, signs of nerve compression, and muscle denervation.

8.9 Concluding Remarks

The complex anatomy and wide spectrum of pathology in the ankle and foot region present a significant challenge to the radiologist. Familiarity with the normal anatomy, anatomic variants, various clinical conditions, and their appearance on imaging is essential for accurate diagnosis.

Fig. 8.13 Tarsal tunnel syndrome caused by a ganglion. Coronal fat-suppressed intermediate weighted MR image of the left ankle shows cystic mass (*arrow*) with surrounding soft tissue edema entrapping the tibial nerve (*arrowhead*) in the posterior tarsal tunnel. The patient experienced typical clinical symptoms of tarsal tunnel syndrome

Fig. 8.14 Morton neuroma. Coronal T1- (**a**) and T2-weighted (**b**) MR images of the left forefoot obtained at the level of the metatarsal heads reveal a dumbbell-shaped soft tissue mass of low signal intensity pro-truding from the third intermetatarsal space into the plantar soft tissues (*arrows*)

Findings as the Reference Standard. AJR Am J Roentgenol. 2017;209:W100–8.

Take Home Message

- This short article can only give a rough overview on selected anatomic features and pathologies of the ankle and foot. Broaden your knowledge by studying major textbooks, book chapters, review articles, and scientific publications.

References

1. Albano D, Martinelli AD, Bianchi MN, et al. Posterior tibial tendon dysfunction: Clinical and magnetic resonance imaging findings having histology as reference standard. Eur J Radiol. 2018;99:55–61.

2. Flores DV, Gomez CM, Hernando MF, et al. Adult Acquired Flatfoot Deformity: Anatomy, Biomechanics, Staging. and Imaging Findings Radiographics. 2019;39:1437–60.

3. Ng JM, Rosenberg ZS, Bencardino JT, et al. US and MR imaging of the extensor compartment of the ankle. Radiographics. 2013;33:2047–64.

4. Schweitzer ME, Karasick D. MR imaging of disorders of the Achilles tendon. AJR Am J Roentgenol. 2000;175:613–25.

5. Taljanovic MS, Alcala JN, Gimber LH, et al. High-resolution US and MR imaging of peroneal tendon injuries--erratum. Radiographics. 2015;35:651.

6. De Maeseneer M, Marcelis S, Jager T, et al. Sonography of the normal ankle: a target approach using skeletal reference points. AJR Am J Roentgenol. 2009;192:487–95.

7. Greaser MC. Foot and Ankle Stress Fractures in Athletes. Orthop Clin North Am. 2016;47:809–22.

8. Marshall RA, Mandell JC, Weaver MJ, et al. Imaging Features and Management of Stress, Atypical, and Pathologic Fractures. Radiographics. 2018;38:2173–92.

9. Spitz DJ, Newberg AH. Imaging of stress fractures in the athlete. Magn Reson Imaging Clin N Am. 2003;11:323–39.

10. Tafur M, Rosenberg RS, JBencardino JTMR. Imaging of the Midfoot Including Chopart and Lisfranc Joint Complexes. Magn Reson Imaging Clin N Am. 2017;25:95–12.

11. Linklater JM. Imaging of sports injuries in the foot. AJR Am J Roentgenol. 2012;199:500–8.

12. Castro M, Melao L, Canella C, et al. Lisfranc joint ligamentous complex: MRI with anatomic correlation in cadavers. AJR Am J Roentgenol. 2010;195:W447–55.

13. Raikin SM, Elias I, Dheer S, et al. Prediction of midfoot instability in the subtle Lisfranc injury. Comparison of magnetic resonance imaging with intraoperative findings. J Bone Joint Surg Am. 2009;91:892–9.

14. Hallinan J, Statum SM, Huang B, et al. High-Resolution MRI of the First Metatarsophalangeal Joint: Gross Anatomy and Injury Characterization. Radiographics. 2020;40:1107–24.

15. Yamada AF, Crema MD, Nery MD, et al. Second and Third Metatarsophalangeal Platar Plate Tears: Diagnostic Performance of Direct and Indirect MRI Features Using Surgical

16. Hur ES, Bohl DD, Lee S. Lateral ligament instability: review of pathology and diagnosis. Curr Rev Musculoskelet Med. 2020;13:494–500.

17. Perrich KD, Goodwin DW, Hecht PJ, Cheung Y. Ankle ligaments on MRI: appearance of normal and injured ligaments. AJR. 2009;193:687–95.

18. Zoga AC, Schweitzer ME. Imaging sports injuries of the foot and ankle. Magn Reson Imaging Clin N Am. 2003;11:295–310.

19. Mengiardi B, Pinto C, Zanetti M. Medial collateral ligament complex of the ankle: MR imaging anatomy and findings in medial instability. Semin Musculoskelet Radiol. 2016;20:91–103.

20. Lee S, Lin J, Kamran JL, Bohl DD. Deltoid ligament rupture in ankle fracture: diagnosis and management. J Am Acad Orthop Surg. 2019;27:e648–58.

21. Linklater J. Ligamentous, chondral and osteochondral ankle injuries in athletes. Semin Musculoskelet Radiol. 2004;8:81–98.

22. Sharif B, Welck M, Saifuddin A. MRI of the distal tibiofibular joint. Skelet Radiol. 2020;49:1–17.

23. Oae K, Takao M, Maito K, et al. Injury of the tibiofibular syndesmosis: value of MR imaging for diagnosis. Radiology. 2003;227:155–61.

24. O'Loughlin PF, Heyworth BE, Kennedy JG. Current concepts in the diagnosis and treatment of osteochondral lesions of the ankle. Am J Sports Med. 2010;38:392–404.

25. Kirschke J, Braun S, Baum T, et al. Diagnostic value of CT arthrography for evaluation of osteochondral lesions at the ankle. Biomed Res Int. 2016;3594253:2016.

26. Berndt AL, Harty M. Transchondral fractures (osteochondritis dissecans) of the talus. JBJS Am. 1959;41:988–1020.

27. Loomer R, Fisher C, Lloyd-Smith R, Sisler J, Cooney T. Osteochondral lesions of the talus. Am J Sports Med. 1993;21:13–9.

28. Sellon E, Robinson P. MR imaging of impingement and entrapment syndromes of the foot and ankle. Magn Reson Imaging Clin N Am. 2017;25:145–58.

29. Huh YM, Suh JS, Lee JW, Song HT. Synovitis and soft tissue impingement of the ankle: assessment with enhanced three-dimensional FSPGR MR imaging. J Magn Reson Imaging. 2004;19:108–16.

30. Cerezal L, Abascal F, Canga A, et al. MR imaging of ankle impingement syndromes. Am J Roentgenol AJR. 2003;181:551–9.

31. Robinson P, White LM, Salonen DC, Daniels TR, Ogilvie-Harris D. Anterolateral ankle impingement: MR arthrographic assessment of the anterolateral recess. Radiology. 2001;221:186–90.

32. Default EM, Demondion X, Bieganski A, Thiron MC, Mestdagh H, Cotton A. Imaging of foot and ankle nerve entrapment syndromes: from well-demonstrated to unfamiliar sites. Radiographics. 2003;23:613–23.

33. Ferkel E, Davis WH, Ellington JK. Entrapment neuropathies of the foot and ankle. Cin Sports Med. 2015;34:791–801.

34. Beltran LS, Bencardino J, Ghazikhanian V, Beltran J. Entrapment neuropathies III: lower limb. Semin Musculoskelet Radiol. 2010;14:501–11.

35. Woertler K. Tumors and tumor-like lesions of peripheral nerves. Semin Musculoskelet Radiol. 2010;14:547–58.

Postoperative Knee and Shoulder

Ara Kassarjian and David A. Rubin

Learning Objectives
- Learn normal and abnormal imaging findings on postoperative knee MRI.
- Learn normal and abnormal imaging findings on postoperative shoulder MRI.

Key Points
- Interpretation of postoperative MRIs of the knee and shoulder can be challenging.
- Knowledge of the details of the original lesion, surgery performed, timing of surgery, and expected normal postoperative findings is crucial for the correct interpretation of postoperative MRIs.
- Knowledge of the common complications of each type of surgery and their appearance on MRI is crucial for the correct interpretation of postoperative MRIs.

9.1 Postoperative MRI of the Knee

Common knee operations address abnormalities of the ligaments, menisci, and articular cartilage. Because most procedures are performed arthroscopically, the first challenge for interpretation of a postoperative MRI examination is recog-

A. Kassarjian (✉)
Elite Sports Imaging, SL, Pozuelo de Alarcón, Madrid, Spain

Corades, LLC, Brookline, MA, USA

D. A. Rubin
All Pro Orthopedic Imaging Consultants, LLC,
St. Louis, MO, USA

Radsource, Brentwood, TN, USA

NYU Grossman School of Medicine, New York, NY, USA

nition that prior surgery has occurred. Horizontally oriented, low-signal-intensity fibrotic scarring from arthroscopic portals in Hoffa's fat pad or adjacent to the patellar tendon may be the only clue to prior surgery, especially when no implants or grafts were used (Fig. 9.1a) [1].

9.2 Ligament Surgery

The knee ligament injuries that most commonly require operative management are tears of the anterior cruciate ligament (ACL) and medial patellofemoral ligament (MPFL). Nonoperative care is typical for isolated tears of the medial collateral or posterior cruciate ligament. Posterolateral corner and combined ligament injuries are less common but usually require surgery.

9.2.1 Anterior Cruciate Ligament

Rarely a proximal ACL tear or avulsion with relatively preserved tissue quality will be treated with primary repair, using suture anchors or pull-out buttons. Postoperatively, the MRI appearance of a repaired ligament should closely mimic a native intact ACL; a tibial tunnel may be visible if augmentation with fiber tape was employed [2]. Most ACL tears are managed with graft reconstruction, using autograft harvested from the patellar or hamstring tendons. The graft is passed through tunnels drilled in the distal femur and proximal tibia and then anchored by bioabsorbable or metal fixation. Some surgeons use two tunnels and grafts to replace the anteromedial and posterolateral bundles separately [3], although clinical outcomes and stability are similar for single- and double-bundle reconstructions [4].

Hamstring grafts are typically stripped from the distal semitendinosus and gracilis and then quadrupled, resulting in a multi-fascicle appearance. The resected tendons can appear attenuated or regenerate and appear relatively
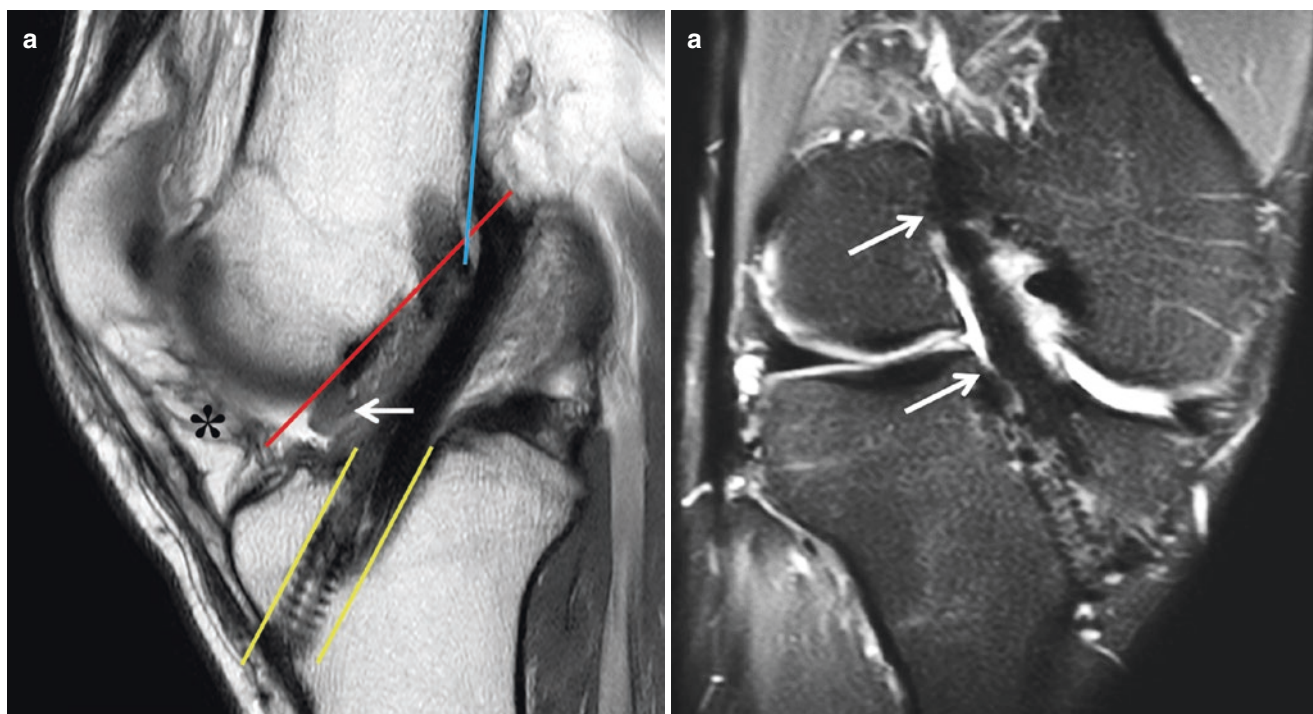
Fig. 9.1 A 27-year-old man with expected findings after anterior cruciate ligament reconstruction. (**a**) Sagittal proton-density-weighted image shows low-signal-intensity intact taut graft in intercondylar notch. Femoral tunnel is near intersection of intercondylar roof (Blumensaat's line, *red line*) and posterior femoral cortex (*blue line*), while tibial tunnel (*yellow lines*) lies in anterior half of tibia but entirely posterior to Blumensaat's line. Note mild linear scarring in Hoffa's fat pad (*aster-isk*) from arthroscopy. Small cyclops lesion (*arrow*) was asymptomatic. (**b**) Coronal fat-suppressed intermediate-weighted sequence was reconstructed slightly obliquely to demonstrate graft course and tunnels (*arrows*) on a single image. Opening of femoral tunnel is at 11:00 position (right knee). Tibial tunnel aperture is in midline

normal after several years [5, 6]. Patellar tendon grafts come from the middle or medial third of the tendon together with attached bone blocks from the inferior patella and tibial tubercle. Postoperatively, a sagitally oriented defect in the residual tendon may persist or heal with hypertrophied scar tissue [7]. Donor site complications are infrequent, with anterior knee pain the most common occurring in approximately 17% of reconstructions using a patellar tendon graft [8]. Patellar fractures are rare. Both a recent prospective series and a 2003 meta-analysis found a higher graft failure rate for hamstring compared with patellar tendon grafts [8, 9].

Tunnel position affects outcomes and should be evaluated on postoperative MRI. On sagittal images the femoral tunnel exits near the junction of the roof of the intercondylar notch (Blumensaat's line) and the posterior femoral cortex [10]. The normal tunnel aperture in the coronal plane is between 10:00 and 11:00 for a right knee and between 1:00 and 2:00 for a left knee [7, 10]. The intra-articular opening of the tibial tunnel belongs midline on coronal images, while on sagittal images it should be just anterior to the midpoint of the tibia but posterior to Blumensaat's line (Fig. 9.1) [10, 11]. Tunnels

that are located more anteriorly can predispose to graft impingement and rupture, while tunnel positions that create a nearly vertical graft may result in a lax graft and instability [12, 13]. Tunnel widening, with or without intra-tunnel cyst formation, typically occurs in the first 6 months after surgery and later stabilizes or partly reverses [14]. These intraosseous changes are more common after hamstring reconstructions and within the tibial tunnel and do not affect graft function, but may influence plans for future revisions; cysts can extend into the pretibial soft tissues as a mass [15, 16].

The MRI signal within an ACL graft follows a predictable time course [7]. Initially tendon grafts are avascular and will appear dark on all pulse sequences for the first 3–4 months. Thereafter, vascular ingrowth and "synovialization" increase the signal intensity on both T1- and T2-weighted images; at this point diagnosis of a recurrent tear may be difficult, and close correlation between imaging findings and clinical examination is needed for correct assessment. Maturation ("ligamentization") of the graft by 12–18 months results in predominantly low signal intensity, although small foci of increased signal intensity on intermediate and T2-weighted images can be seen within normally functioning grafts even
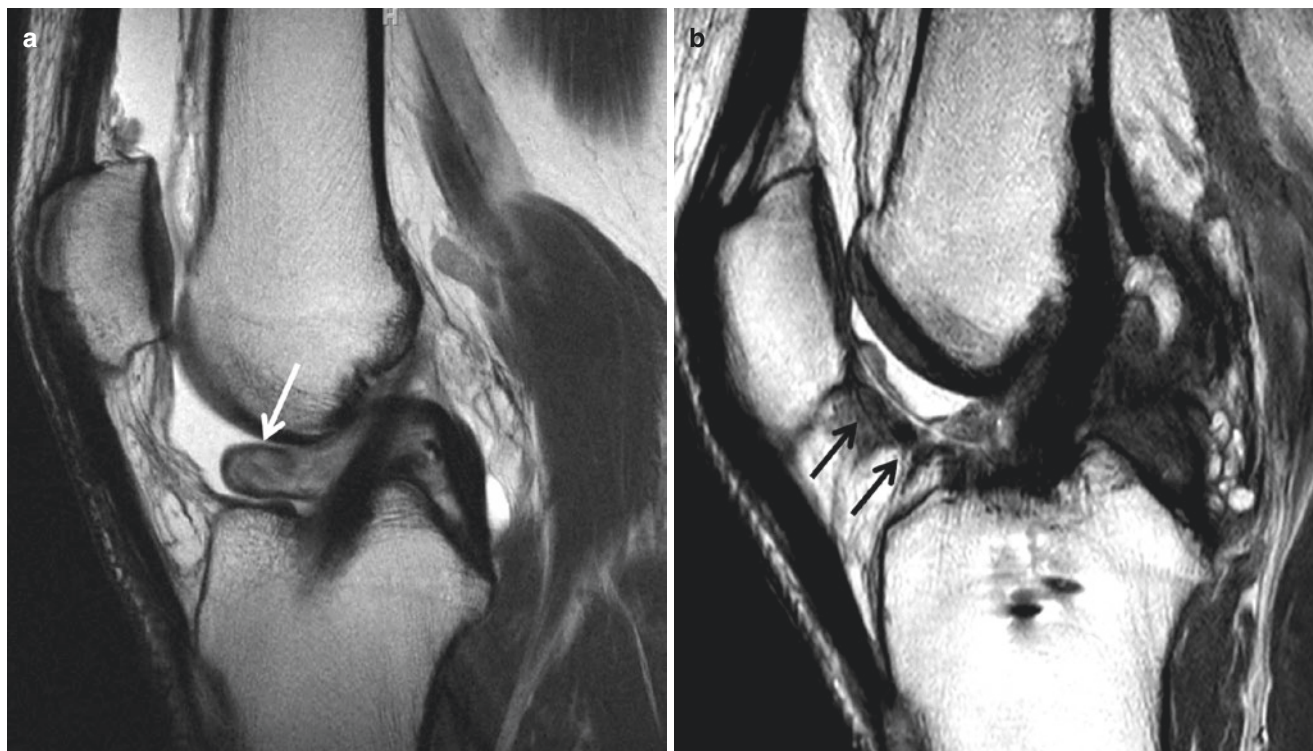
Fig. 9.2 Focal and diffuse arthrofibrosis following anterior cruciate ligament reconstruction on sagittal T2-weighted images. (**a**) Intra-articular cyclops lesion (*arrow*) anterior to graft in a 28-year-old man with painful, limited knee extension. (**b**) A 51-year-old woman with severe knee stiffness due to generalized arthrofibrosis. Note band of low-signal-intensity fibrotic scar in anterior interval (*arrows*), extending along posterior margin of Hoffa's fat pad to inferior patella and associated patella infera

several years after reconstruction [17]. Additionally, linear high-signal-intensity bands oriented between the layers of a hamstring tendon allograft are normal [10]. An impinged graft may show a distorted course with indistinctness of the distal fiber contour and focally increased signal intensity [7, 18]. Graft impingement may limit knee extension and predispose to graft failure [10, 19].

Postoperative stiffness affects approximately 3% of patients, more commonly women [20]. One contributor is arthrofibrosis (Fig. 9.2). The focal form results in a synovial-based soft tissue nodule (a "cyclops" lesion) anterior to the distal graft of varying signal intensity [21]. Lesions greater than 5 mm in diameter occur in approximately 25% of patients 6 months after ACL reconstruction; however, the presence and size do not correlate with clinical outcomes through the first 2 years after surgery [22]. In cases where a cyclops lesion contributes to pain or limited motion, arthroscopic resection is indicated [23]. Diffuse arthrofibrosis appears as thick, low-signal-intensity bands within the posterior aspect of Hoffa's fat pad [24]. In severe cases fibrotic scar tissue can involve the entire anterior interval of the knee, extending from the intercondylar synovium to the inferior pole of the patella, resulting in patella infera, severely limited knee motion, and accelerated patellofemoral osteoarthritis [25]. Treatment consists of active motion and physical therapy; failures may undergo manipulation under anesthesia or arthroscopic lysis of adhesions [26].

Graft rupture occurs in 3–8% of cases, usually due to repeat trauma after a patient has returned to activity [7]. The primary signs of a failed graft are similar to those for a native ACL—namely, graft discontinuity, abnormal orientation, or absence of visible fibers (Fig. 9.3) [11, 27]. Acutely, joint effusion, edema within and surrounding the graft, and typical bone contusions may also occur. Accuracy of MRI for diagnosing torn grafts is lower when failure is insidious compared to cases with an acute re-injury [28]. Secondary findings of laxity such as anterior tibial subluxation have low positive predictive value after ACL reconstruction, limiting clinical usefulness [29]. Fractured or migrated fixation implants may contribute to graft failures.

9.2.2 Other Ligaments

Recurrent lateral patellofemoral instability may require operative management. The medial patellofemoral ligament (MPFL) is the most biomechanically important component of the medial patellar retinaculum [30, 31]. In cases where the MPFL is acutely avulsed from the patella, primary suture repair with or without augmentation is possible [32]. When
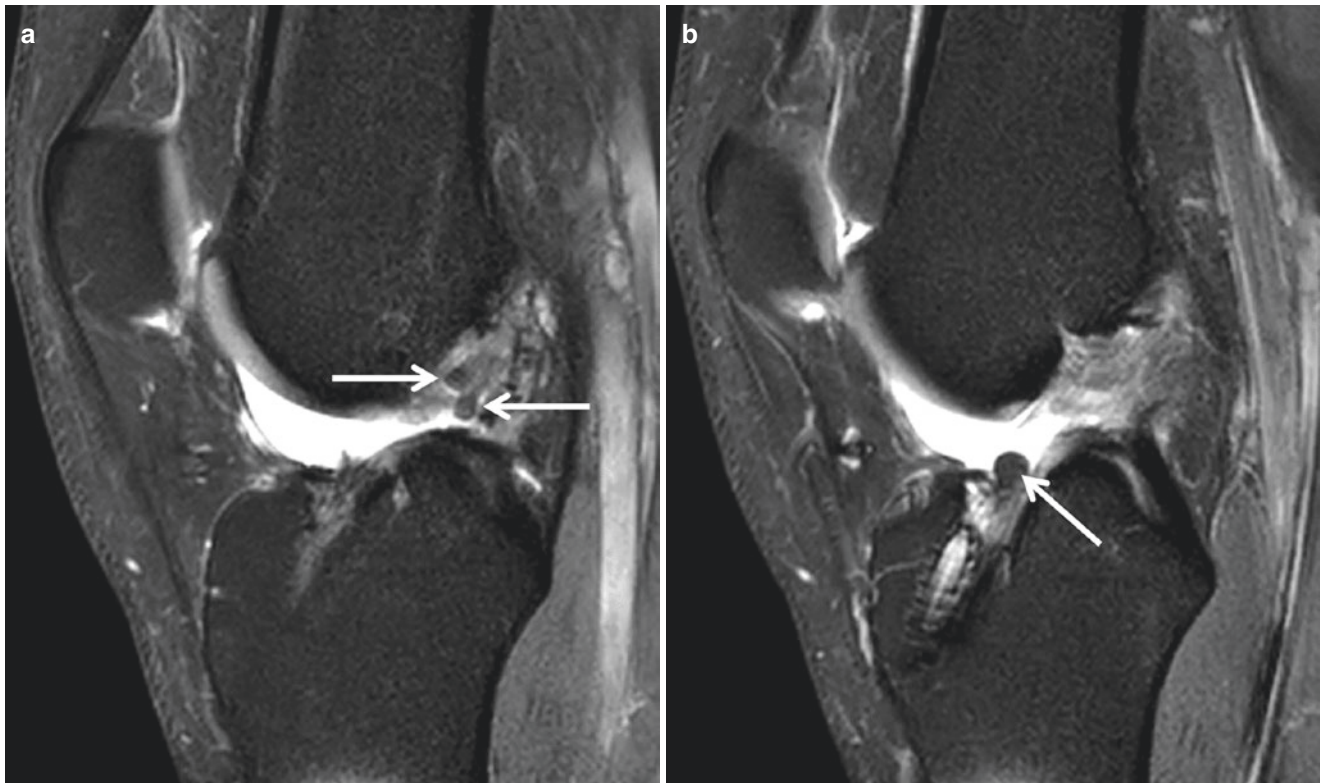
Fig. 9.3 Graft rupture 3 years after anterior cruciate ligament reconstruction in A 25-year-old man. Sagittal fat-suppressed T2-weighted images show discontinuous (**a**) proximal and (**b**) distal graft fibers (*arrows*). Note presence of multiple strands in this hamstring autograft

the ligament is disrupted in other locations or is chronically torn, formal reconstruction with a tendon graft can be performed [30]. Postoperative MRI evaluation is similar to that for ACL reconstructions: the tendon graft signal will evolve over time, but the graft should be taut and continuous. Usually there will be two patellar anchor sites, located within 1 cm of each other in mid and upper part of the bone. The femoral tunnel should be located just caudal and anterior to the adductor tubercle [33]. Complications include fracture around the tunnel or anchor sites, graft laxity, graft rupture, and recurrent patellar dislocation [33, 34].

The same principles outlined above for the ACL and MPFL apply when imaging reconstructions of the less commonly injured ligaments like the posterior cruciate or lateral collateral [35–37]. Bone anchor sites and tunnels should be located so that the single or multiple bundle tendon grafts approximate the native ligament orientations and positions. The anterolateral ligament (ALL), which originates just cranial and posterior to the lateral femoral epicondyle and extends to the lateral tibial rim posterior to Gerdy's tubercle, is a secondary stabilizer to the ACL. ALL reconstruction is sometimes done to augment primary or revision ACL reconstructions, for patients at high risk of ACL graft failure [38, 39].

9.3 Meniscal Surgery

Treatment of meniscal tears continues to evolve. For symptomatic meniscal tears, the current operative approach is to preserve as much meniscal tissue as possible ideally by primary repair. New surgical techniques have expanded the spectrum of which tears may be repaired, including some meniscal root avulsions. Nonrepairable tears typically require limited resections. Unsalvageable menisci may be replaced by transplantation. Each of these interventions alters the imaging appearance of the meniscus. An understanding of the expected postoperative appearances, the limitations of MRI after meniscal surgery, and the imaging criteria that can be used is necessary for accurate postoperative interpretation.

9.3.1 Partial Meniscectomy and Meniscal Repair

During partial meniscectomy the surgeon resects as little of the torn meniscus as possible in order to leave a stable residual component, because both radiographic and functional results are worse when more meniscus is resected
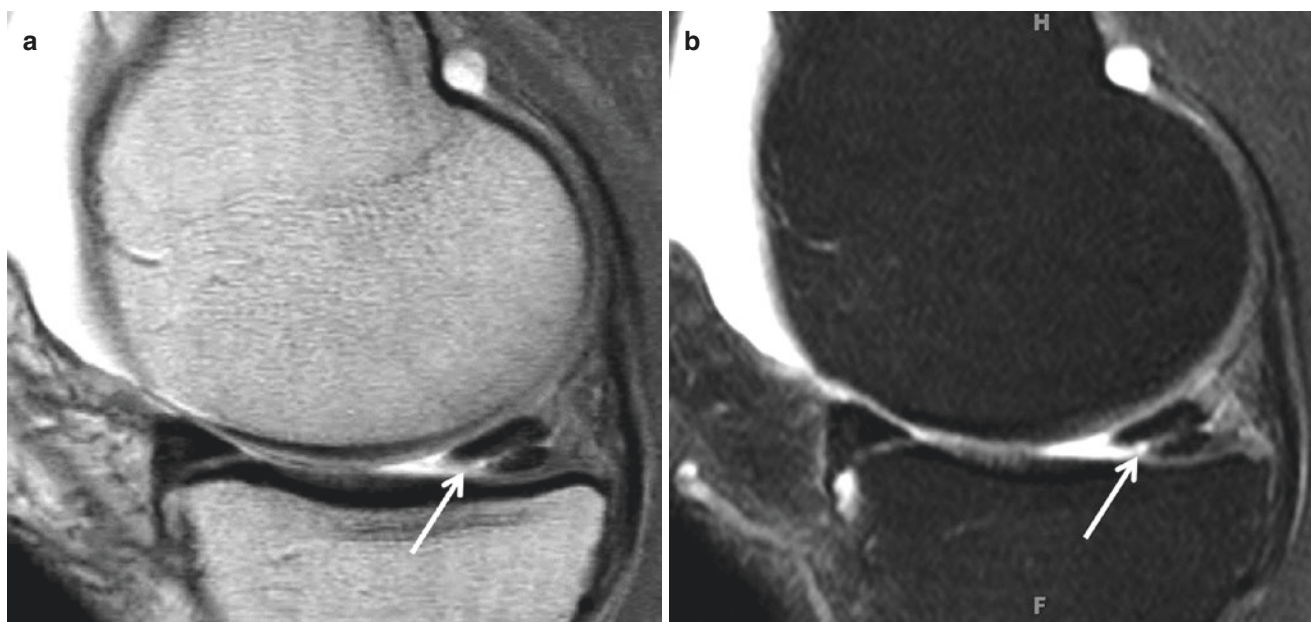
Fig. 9.4 Recurrent meniscal tear following partial meniscectomy in a 39-year-old woman. (**a**) Sagittal proton-density-weighted image shows truncation of inner meniscal margin and intrameniscal signal extending to articular surface (*arrow*), findings diagnostic for tear in native menisci, but unreliable when more than 25% of meniscus has been resected. (**b**) On T2-weighted image, surfacing high signal intensity (*arrow*) indicates recurrent meniscal tear

[40]. Partial resection truncates the normal triangular meniscal cross section, invalidating one of the chief MRI criteria used for diagnosing tears in native menisci. The altered shape can both simulate and obscure a recurrent meniscal tear [41]. Furthermore, partial excision may allow normal internal signal that was not part of the original tear to now contact the new meniscal surface on a proton-density-weighted image, which invalidates the other major criteria for meniscal tear [42]. If less than 25% of the meniscal width is resected, applying the standard rules for meniscal tears still work well; however, when more meniscus is removed, accuracy decreases [43]. A tear in a new location (if a preoperative MR is available to show the original tear location), displaced meniscal fragments, or a fluid-filled cleft extending into the meniscus on a T2-weighted image remain reliable but insensitive signs of a recurrent meniscal tear, even when greater than 25% of the meniscus is removed (Fig. 9.4) [44, 45].

Primary repair using suture, darts, or other anchors is the preferred treatment for menisci that have the potential to heal. Reparable tears are primarily vertical longitudinal ones near the vascularized meniscal periphery (the "red" zone) [46]. Tears heal with granulation and scar tissue, which may continue to demonstrate high signal intensity, even years later (Fig. 9.5) [47]. Thus, a healed meniscus will frequently fulfill the signal criteria for a meniscal tear, decreasing the specificity for diagnosing a persistent (unhealed) or recurrent tear. When the repaired meniscus shows no signal on any sequence, the meniscus is healed; however, only surfacing signal isointense to fluid on a T2-weighted sequence is reliable for diagnosing a residual or recurrent tear [48]. Approximately 14% of meniscal repairs develop a meniscal cyst, which may be asymptomatic. In contrast to cysts that occur in native menisci, those presenting after meniscal repair do not necessarily indicate an underlying tear [49].

MR arthrography (MRA), most often performed after direct intra-articular injection of a dilute gadolinium mixture, is a useful adjunct in postoperative knees. The primary sign of a tear in a postoperative meniscus is injected contrast (confirmed on a T1-weighted imaging) entering the substance of the residual meniscal fragment or repaired meniscus (Fig. 9.5) [50]. Some practices use indirect MRA by injecting gadolinium intravenously, exercising the knee, and allowing contrast to diffuse from the synovium into the joint. However, intravenous contrast injection does not produce joint distention (limiting sensitivity for nondisplaced tears) and enhances granulation tissue (decreasing specificity after meniscal repair) [51]. Accuracy for residual or recurrent tears increases from 57–80% with non-contrast MRI to 85–93% with direct MRA [46]; the added value persists even when conventional MRI is acquired using a 3-T magnet [52].
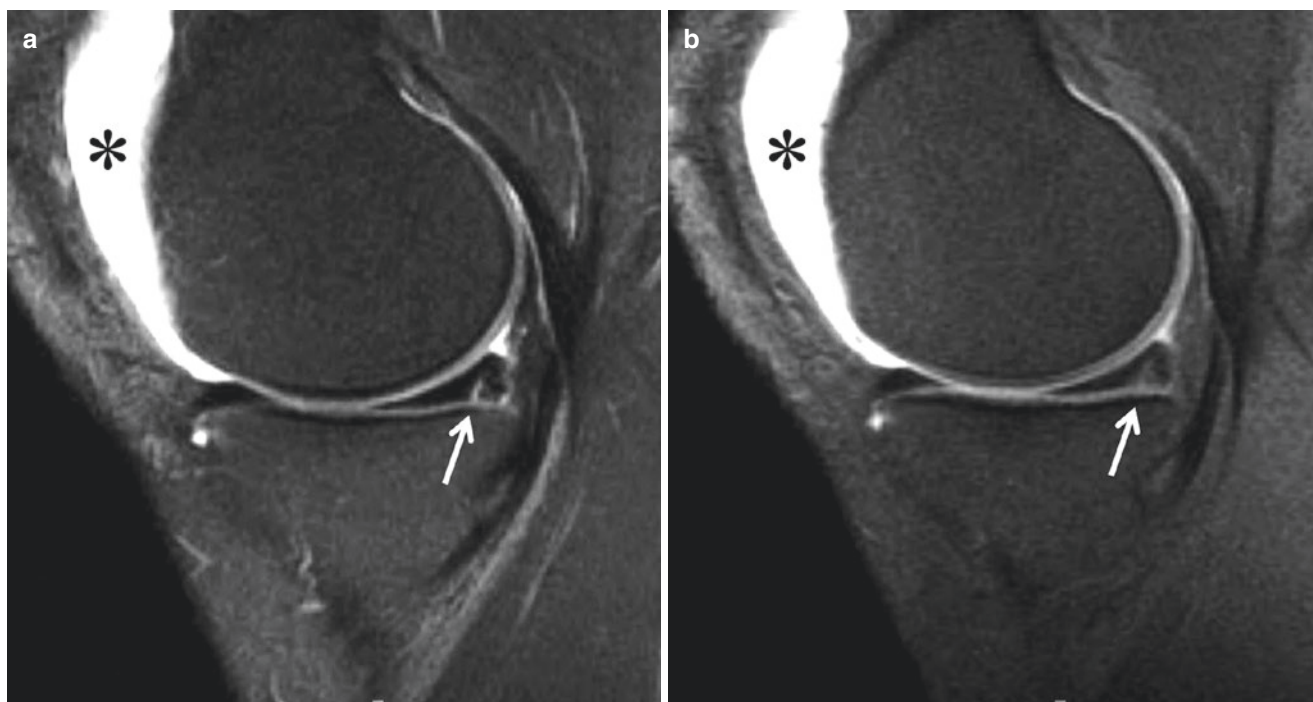
Fig. 9.5 A 32-year-old man with healed meniscal tear, repaired 7 years previously. (**a**) Sagittal fat-suppressed T2-weighted image shows persistent signal (*arrow*) contacting meniscal surface at site of previously repaired peripheral longitudinal tear. Abnormality is bright but less intense than fluid (*asterisk*) in knee joint. (**b**) Fat-suppressed T1-weighted image from direct MR arthrogram shows no contrast extending into meniscus (*arrow*). Compare to gadolinium in joint (*asterisk*). No tear was found at subsequent arthroscopy

9.3.2 Root Repair and Meniscal Transplant

Newer surgical procedures now offer meniscal preservation for a broader range of meniscal injuries. Rupture of the posterior root that anchors the meniscus to the tibia is a devastating condition, rendering the meniscus unable to distribute contact forces [53] predisposing to accelerated osteoarthritis, subchondral insufficiency fracture, and osteonecrosis in the affected compartment. Partial meniscectomy in these knees is associated with progressive osteoarthritis, but in some cases, repair can restore normal biomechanics and lessen the negative impact [54]. The torn root is usually reattached by drawing sutures through a transosseous tunnel and then anchoring the construct in the tibia [55]. Cadaveric replacement is an option in stable knees with relatively normal articular cartilage that have essentially nonfunctional menisci (due to prior subtotal meniscectomy or recurrent, nonrepairable tears). The allograft meniscus is harvested with bone plugs or a bone bridge attached to the anterior and posterior roots, and the osseous components are fixated to the recipient tibia through drilled tunnels or a trough. The periphery of the transplanted meniscus is then sutured to the joint capsule [56].

No standardized criteria have been validated for imaging evaluation of meniscal root repairs. A completely healed repair should show continuous tissue from the posterior root through the drilled tunnel. The tissue may be intermediate in signal intensity on proton-density-weighted sequences, but fluid intensity signal on a T2-weighted image or fragment displacement at the repair site indicates operative failure (Fig. 9.6) [55]. New tears may also develop separate from the repaired root. Studies have found both reduced and increased degrees of meniscal extrusion after root repair, with a meta-analysis showing no overall change in extrusion and varying degrees of progressive degenerative arthritis [57]. However, the short-to-medium term clinical improvement seems to be independent of these MRI findings [58].

Imaging after a meniscal allograft procedure is challenging. Normal, functioning grafts can shrink (especially if graft was fresh as opposed to frozen) or may demonstrate extrusion, but neither imaging finding is associated with clinical outcomes [57]. After 4 years, knees with >3 mm extrusion of the allograft do show significantly more joint space narrowing compared to those with non-extruded grafts, but the clinical results in the two groups do not differ [59]. At least for the first year, signal intensity of the transplanted meniscus is higher compared to native menisci (especially in the anterior horn) [60]. A systemic review of meniscal allografts found an 11% average failure rate at approximately 5 years [61]. Failure mechanisms include fracture of the native tibia
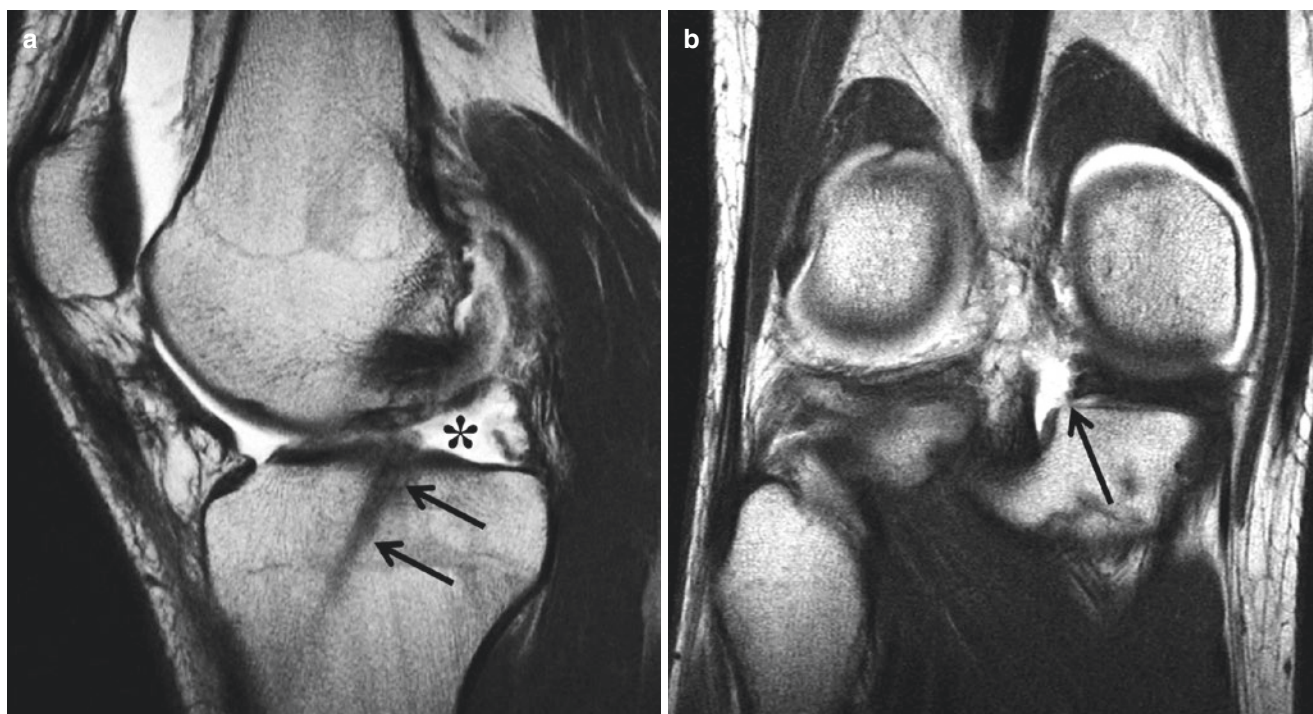
Fig. 9.6 Failed posterior medial meniscal root repair in a 23-year-old man. (**a**) Sagittal T2-weighted image shows transtibial tunnel (*arrows*) drilled for suture passage without attached meniscal tissue (*asterisk*).

(**b**) Coronal T1-weighted image from MR arthrogram demonstrates re-torn meniscal root (*arrow*) separated from anchor site

around the fixation, new tears within the meniscal substance, and peripheral separation at the meniscocapsular junction. In these latter cases, the meniscus may displace like a bucket handle tear into the intercondylar notch [46].

9.4   Articular Cartilage Surgery

Articular cartilage is avascular, which limits its ability to self-repair or for surgically reattached chondral fragments to heal. Simple debridement of symptomatic focal cartilage defects ("chondroplasty") leads to formation of reparative fibrous or fibrocartilaginous tissue that lacks the gliding and protective qualities of normal hyaline cartilage and breaks down in a few years. Nevertheless, recovery after chondroplasty is rapid, and patients may get short-term relief, so it is used in high-end athletes [62]. Procedures that aim to create more functional hyaline-like cartilage include techniques to stimulate the underlying bone marrow, replace the cartilage surface by transplanting intact osteochondral fragments, or implant new cartilage cells and substrate into a defect. The choice of procedure depends on the patient age and physical demands, the size of the lesion, and concomitant abnormalities of the knee ligaments, menisci, and alignment. Procedures can also be combined with each other or with bone grafting, especially when a chondral defect is associated with extensive bone loss [63].

9.4.1   Marrow Stimulation

During microfracture, the surgeon debrides the chondral lesion and then repeatedly punctures the underlying subchondral bone plate with an awl, pick, or drill, allowing blood and marrow stem cells to fill the cartilage crater. The resultant blood clot later differentiates into fibrous tissue or fibrocartilage. Patients may get short-term relief, but the reparative tissue typically fails by 5 years, with poorer outcomes in athletes [62, 64]. On postoperative MRI, the signal of the fibrocartilage is initially brighter than surrounding normal hyaline cartilage [65, 66]. The amount of the defect that is ultimately filled correlates with clinical success [67]. Ideally the new articular surface will be congruent by 1–2 years (Fig. 9.7). Overgrowth of the subchondral bone including osteophyte formation at the base of the lesion increases the risk of failure by a factor of 10× [68]. Underlying bone marrow edema is common and decreases over time; marrow edema persisting beyond 2 years can be associated with treatment failure and should be noted [69].

9.4.2   Osteochondral Grafting

In osteochondral transfer, the articular surface is reconstructed by implanting one or more cylinders composed of a bone core and overlying hyaline cartilage into a chondral
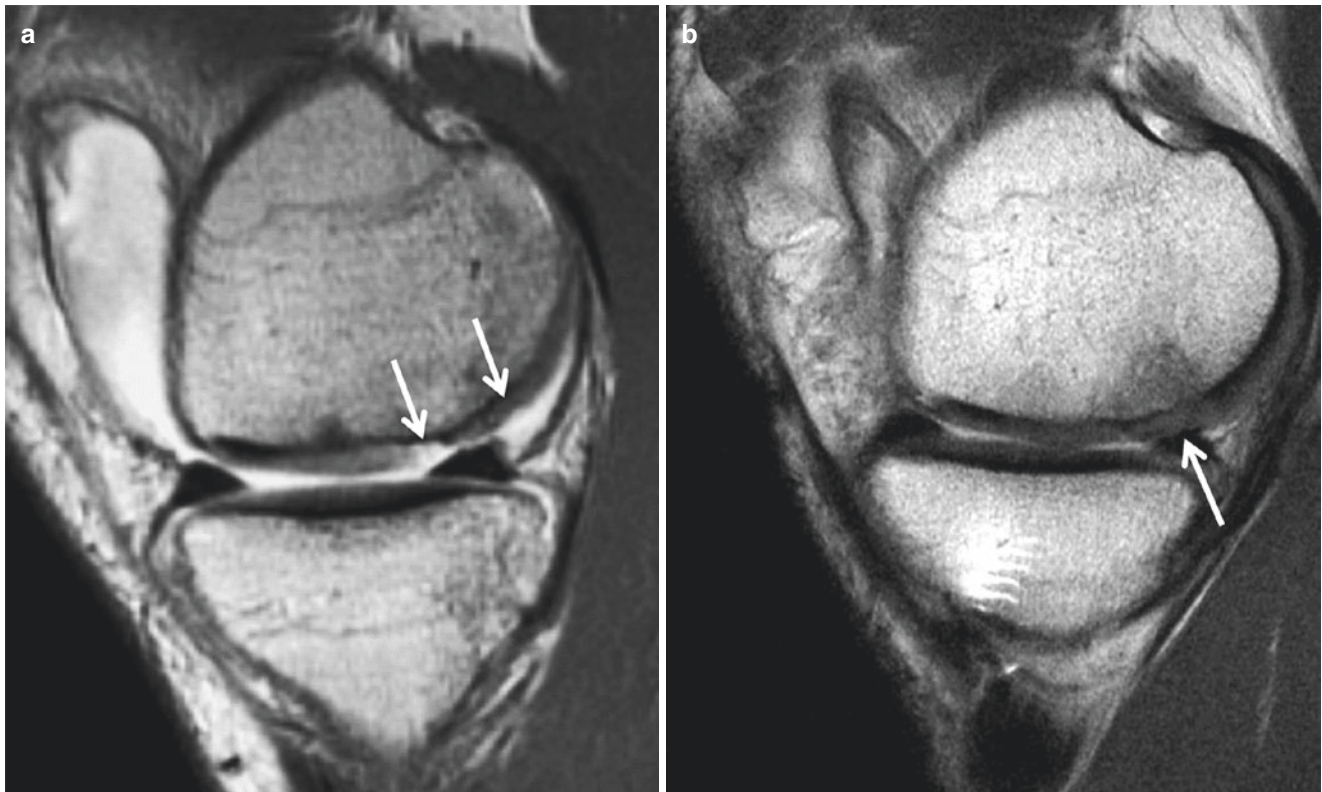
Fig. 9.7 A 39-year-old man with medial femoral condyle cartilage lesion managed by microfracture. (**a**) Initial sagittal T2-weighted image shows areas of partial- and full-thickness cartilage loss (*arrows*). (**b**) Three years after procedure reparative fibrocartilage remains slightly hyperintense compared to normal hyaline cartilage but fills defect and demonstrates smooth articular surface (*arrow*)

defect (Fig. 9.8). The graft may come from a relatively low-stress surface in the patient's knee (an autograft, sometimes called Mosaicplasty™ or OATS™) or from a cadaver donor (an allograft). Ideally the deep (ossified) portion will integrate with the surrounding bone, while the overlying cartilage will remain viable and merge with the bordering healthy cartilage [70]. Results of osteochondral autograft procedures are better compared to microfracture, especially for small lesions in young patients [64, 71]. Allografts are typically used for larger defects, with extensive bone loss, or for revision after other failed procedures [72].

The postoperative imaging appearance after osteochondral grafting can be deceptive—a step-off may be present between of the donor and recipient subchondral bone plates due to different thicknesses in the overlying cartilage [69]. The surgeon places the graft(s) to create a smooth articular surface, which should be evident on postoperative imaging [24]. For autografts, the MRI signal in the overlying cartilage is variable and does not correlate with outcomes. Marrow edema in the graft and underlying bone is common and can persist normally for up to 3 years [73]. However, cyst formation at the base of the graft is a sign indicating poor integration [69]. Underfilling of the original defect is weakly associated with clinical failures. Osteonecrosis of a graft can occur without clinical manifestations [73]. The harvest site typically heals with bone and fibrocartilage (Fig. 9.8b), but donor site morbidity (typically patellofemoral pain or crepitus) occurs in approximately 6% of procedures [74].

Imaging findings following allograft reconstruction are similar. One difference is that extensive marrow edema in the host bone, graft, and interface can be associated with an immunologic reaction against the donor's bone [75]. MRI signs portending failure at 1 year include persistent marrow edema deep to the transplant, cysts or fluid at the bone interface, and collapse of the articular surface [65, 66, 72].

9.4.3 Cellular Repair

Autologous chondrocyte implantation (ACI) is usually a multi-step procedure, initially harvesting a sample of the patient's own cartilage cells, then growing them in vitro as a cell culture or embedded in a collagen scaffolding (the later for third generation, matrix-assisted chondrocyte transplantation, M-ACI), and finally implanting them into the original debrided defect during a second operation. In first-generation
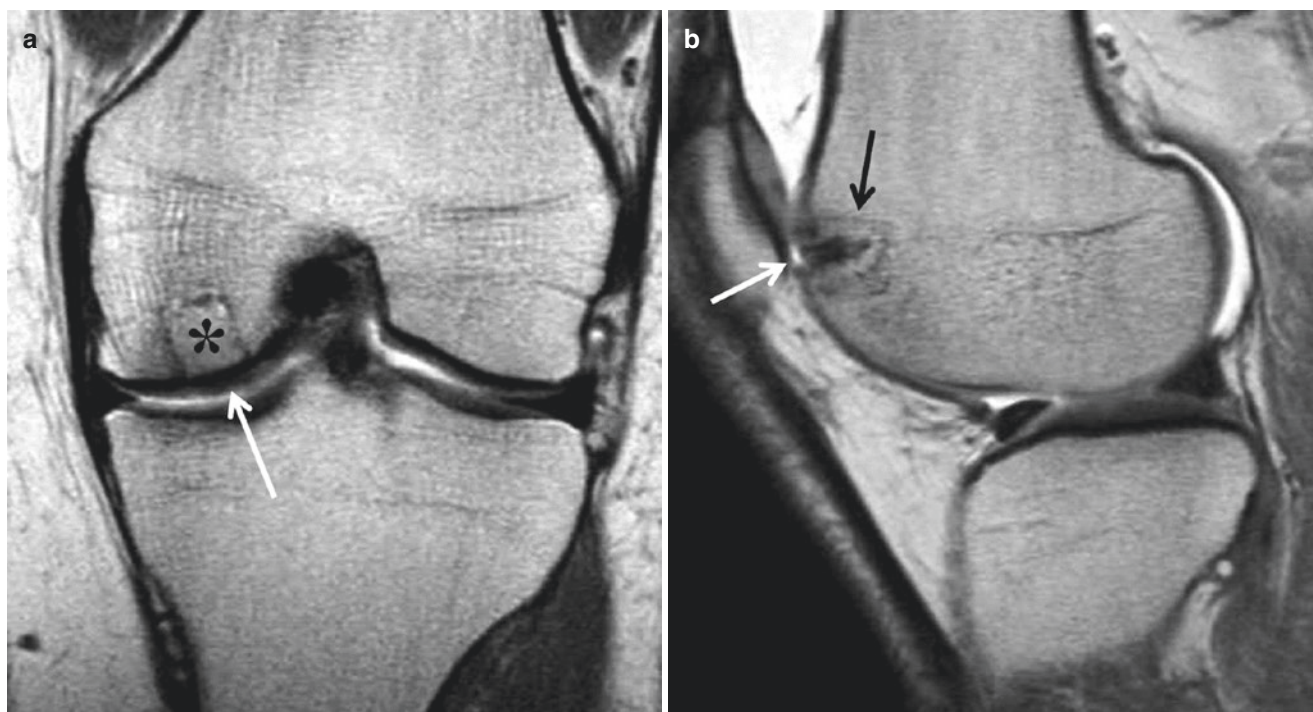
Fig. 9.8 Osteochondral autograft for medial femoral condyle chondral defect in a 26-year-old man. (**a**) Coronal T1-weighted image from MR arthrogram shows complete incorporation of osseous (*asterisk*) and cartilage (*arrow*) portions of graft. (**b**) On sagittal T2-weighted image, harvest site in lateral femoral trochlea is nearly refilled with bone (*black arow*). Thin layer of high-signal-intensity fibrocartilage (*white arrow*) covers the donor site

ACI, the cultured cells are injected under a periosteal or similar membrane that is sewn over the lesion. For M-ACI a plug of the new cells together with the ancillary supporting tissues are shaped to fit the lesion [66]. Reported outcomes are similar to those for microfracture and osteochondral grafting at 2 years and equivalent or better than microfracture at 5 years [76, 77].

Postoperatively the transplanted cells are initially hyperintense compared to native hyaline cartilage and then begin to normalize at approximately 1 year [65]. Complete filling of the chondral defect is expected after first-generation ACI [78]. Lesions can appear initially underfilled with M-ACI, which improves over time (Fig. 9.9). Graft hypertrophy may be symptomatic and require debridement [66, 69]. Most findings on conventional MRI sequences (including lesion underfilling, bone marrow edema for up to 3 years, and the signal intensity of the transplanted tissue) do not necessarily correlate with clinical outcomes [69, 79]. First-generation procedures can fail by sudden delamination of the covering membrane with or without the underlying cells. Delamination typically occurs in the first few months and appears as a fluid-filled cleft beneath the graft [66]. Adhesions develop in 5–10% of patients and may cause knee stiffness; on MRI adhesions may be difficult to appreciate but appear as relatively low-signal-intensity intra-articular bands extending to the graft [80].

Fig. 9.9 Trochlear cartilage defect in a 34-year-old man managed with matrix-assisted autologous chondrocyte implantation. Sagittal proton-density-weighted image 14 months postoperatively shows implanted cartilage slightly underfilling defect (*white arrow*). Thin strands of tissue extending to articular surface (*black arrow*) may represent small adhesions

9.5 Postoperative MRI of the Shoulder

Shoulder arthroscopy is one of the most commonly performed arthroscopic procedures. Most radiologists are familiar with the interpretation of preoperative shoulder MRI as it is one of the most commonly performed joint MRI examinations. However, when interpreting postoperative shoulder MRIs, certain factors must be considered given the associated alterations in anatomy and signal intensity of tissues.

The following chapter will focus on postoperative MRI of the shoulder following rotator cuff surgery, labral/instability surgery, and long head biceps tendon surgery, some of the most commonly performed arthroscopic procedures of the shoulder.

9.6 MRI Technique

In most cases, routine MR sequences can be used in imaging of the postoperative shoulder. However, gradient recalled echo (GRE) sequences may be distorted due to susceptibility artifact depending on the type of surgery and materials used. As such, these sequences are often less useful in imaging the postoperative shoulder. In addition, if there is inhomogeneous fat suppression, frequency-selective fat suppression can be replaced with metal artifact reduction sequences or STIR sequences to achieve more homogeneous fat suppression (Fig. 9.10). Following rotator cuff repair surgery, conventional non-arthrographic proto-

cols are usually sufficient. Following labral or instability surgery, and in cases of equivocal results following non-arthrographic MRI following rotator cuff surgery, direct MR arthrography or CT arthrography can be used. Finally, in the setting of instability surgery, imaging in the ABER position may prove beneficial.

9.7 Imaging Following Rotator Cuff Repair

As in most fields of arthroscopy, the indications and techniques for arthroscopic surgery for rotator cuff pathology continue to evolve. The most common procedures include rotator cuff repair and rotator cuff debridement, with the latter being performed in the setting of partial-thickness tears. When a rotator cuff repair is performed, the rotator cuff tendon or tendons are fixated to the greater tuberosity of the humerus with the use of screws, anchors, and/or sutures. Depending on the morphology and concomitant pathology of the acromioclavicular joint, acromioplasty and/or distal clavicular resection (Mumford procedure) may also be performed.

9.7.1 Normal MRI Findings After Rotator Cuff Repair

When only debridement has been performed for small articular surface partial-thickness tears, postoperative MR
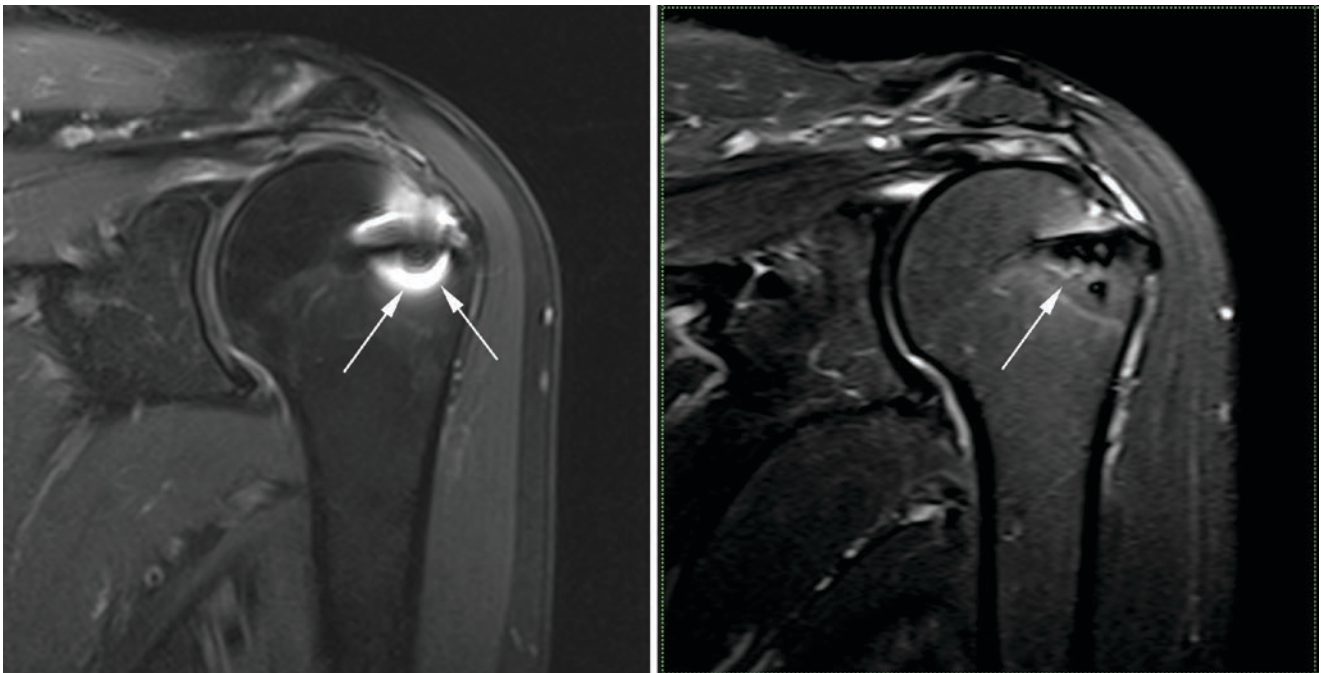
Fig. 9.10 Coronal oblique fat-saturated proton-density (FS PD)-weighted image (left, arrows) demonstrates inhomogeneous fat suppression and susceptibility artifact adjacent to a screw after rotator cuff repair. Coronal oblique short tau inversion recovery (STIR) image (right, arrow) in the same patient on the same day demonstrated minimal artifact and excellent homogenous fat suppression
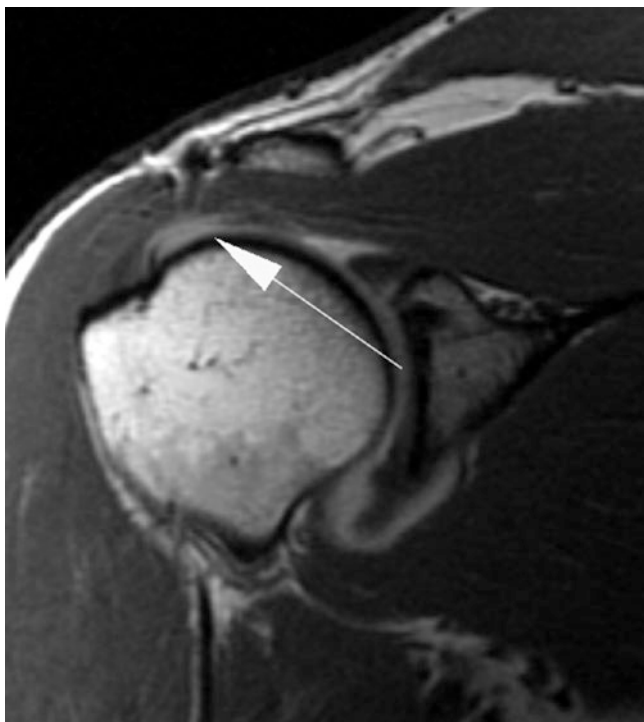
Fig. 9.11 Coronal oblique PD-weighted image demonstrates a smooth articular surface defect (arrow) along the undersurface of the supraspinatus following debridement of a small articular surface tear. Note that the defect is wider than deep, a common finding following debridement/shaving

imaging may have an appearance which is quite similar to if not identical to a small partial-thickness articular surface tear (Fig. 9.11). In these instances, it is imperative to know the size and location of the original tear and the extent of debridement. It has been reported that the region of debridement may show a defect that is wider than it is deep [81]. However, this is not always clearly evident at MRI. In general, the role of postoperative imaging in these settings is to assess for complications of the debridement or extension of the tear into a larger partial-thickness tear or full-thickness tear.

When a rotator cuff repair is performed, the resulting repair may not be watertight. As such, a small usually vertically oriented cleft of fluid (or contrast in the setting of direct MR arthrography) traversing the tendon and communicating with the subacromial-subdeltoid bursa may be present and may represent a small normal postoperative finding (Fig. 9.12) [82]. Within the greater tuberosity, a small amount of edema-like signal near the anchors may persist for months following surgery [83]. If an acromioplasty was performed, there will be flattening of the undersurface of the acromion, diminution of the size of the acromion, and, in more extensive acromioplasties and Mumford procedures, widening of the acromioclavicular joint.
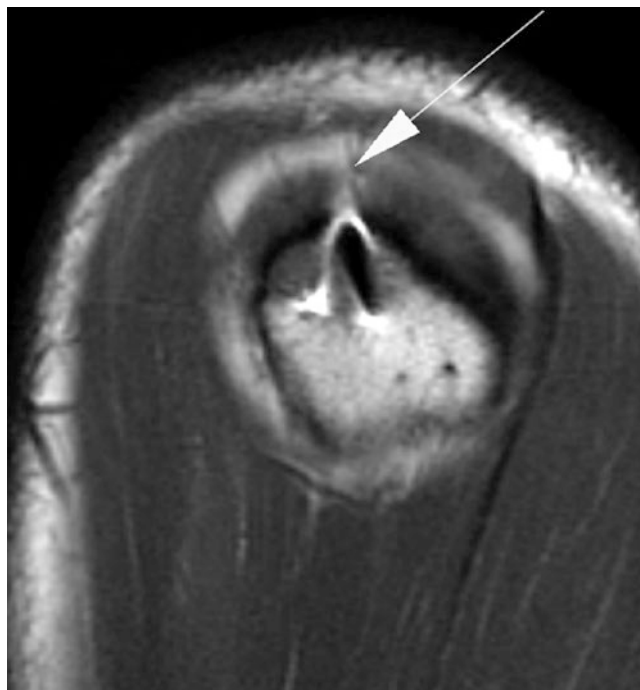
Fig. 9.12 Sagittal oblique T1-weighted image from direct MR arthrogram demonstrates a thin vertical full-thickness cleft (arrow) following rotator cuff repair. This can be a normal finding as the repairs are often not watertight

9.7.2   Abnormal MRI Findings After Rotator Cuff Repair

Abnormal findings following rotator cuff repair include a discreet gap within the tendon, tendon retraction, and new regions of tendon delamination (Fig. 9.13). Occasionally, a recurrent tendon tear may be masked due to fibrous tissue and scarring filling the tendon gap (Fig. 9.14) [84]. If there is new or worsening atrophy of the rotator cuff muscles, the integrity of the tendon repair should again be closely scrutinized to assess for recurrent tear. In these instances, close attention should be paid to the location of the myotendinous junction. Typically, the myotendinous junction of the supraspinatus will be medially displaced and closer to the superior glenoid rim. This can be a secondary sign of a recurrent tendon tear with retraction.

Less common complications following rotator cuff surgery include dislodged or displaced sutures, anchors and screws, deltoid dehiscence following acromioplasty, and, rarely, chondrolysis and septic arthritis.

9.8   Imaging Following Superior Labral Surgery

Depending on the location and configuration of labral tears, labral debridement or labral repair may be performed.
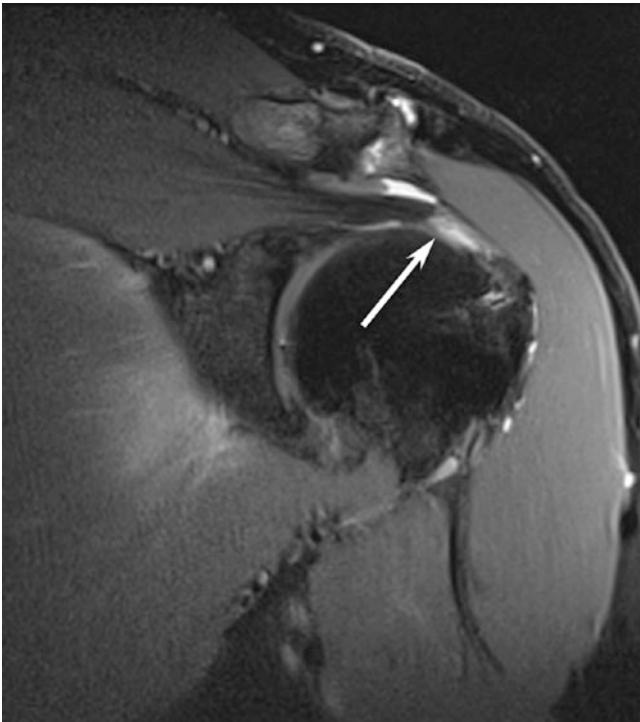
Fig. 9.13 Coronal oblique FS PD-weighted image demonstrates a recurrent full-thickness tear of the supraspinatus with retraction (arrow) and a fluid-filled gap
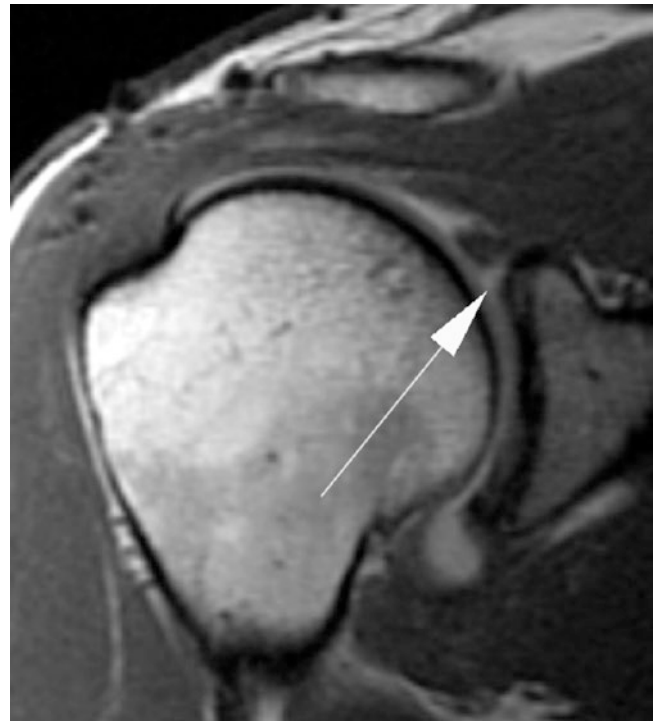
Fig. 9.15 Coronal oblique T1-weighted image from direct MR arthrogram shows a normal small smooth cleft (arrow) partially undercutting the superior labrum after SLAP repair. The labral repair was intact at second look arthroscopy

In the superior labrum, degenerative fraying and degenerative tearing are commonly found in middle-aged and older patients. If there is no associated extension of the labral tearing into the proximal portion of the tendon of the long head biceps brachii and if there is no significant instability of the origin of the long head biceps, these are often treated with simple debridement and shaving of the frayed portion of the labrum. If there is significant extension of the tear into the biceps tendon and/or associated instability of the origin of the biceps tendon (biceps anchor), then a superior labral repair may be performed.

9.8.1 Normal MRI Findings After Superior Labral Surgery

If only shaving and debridement of the labrum are performed, postoperative MR imaging may demonstrate increased signal within the superior labrum, often indistinguishable from the original preoperative MRI if minimal debridement was performed. With more extensive debridement and shaving, the postoperative superior labrum may appear blunted or truncated [85]. If a superior labral tear is repaired, a persistent cleft undercutting the labrum may be present on postoperative imaging (Fig. 9.15) [86].

Fig. 9.14 Coronal oblique T2-weighted image demonstrates intermediate signal scarring/fibrosis (arrow) filling the gap at the site of a recurrent supraspinatus tear. Another clue to the presence of a tear with retraction is the medial displacement of the myotendinous junction of the supraspinatus (arrowheads) nearly to the level of the glenoid

Fig. 9.16 Coronal oblique FS T1-weighted image from direct MR arthrogram demonstrates a recurrent SLAP tear with contrast undercutting the entire thickness of the labrum in an irregular fashion (arrow)

9.8.2 Abnormal MRI Findings After Superior Labral Surgery

Differentiating residual cleft from a residual or recurrent tear can be challenging. In order to make a confident diagnosis of a residual or recurrent superior labral tear, high signal should be clearly seen extending to and through the base of the labrum and/or involving a portion of the labrum which was normal on preoperative imaging (Fig. 9.16). If conventional MR is inconclusive, MR arthrography can be performed to better assess the status of the postoperative superior labrum. Imaging in slightly exaggerated external rotation will put additional traction on the biceps tendon and thus make superior labral tears more conspicuous [87].

9.9 Imaging Following Instability Surgery

Tears of the anterior inferior labrum are typically seen in the setting of anterior shoulder instability. These are the so-called Bankart lesions and their associated variants. The goal of arthroscopic surgery is to recreate the "bumper" of the labrum along the glenoid rim, thereby reducing the chance of humeral head displacement over the edge of the rim and resultant humeral head subluxation or dislocation. Depending on the size and configuration of the original Bankart lesion
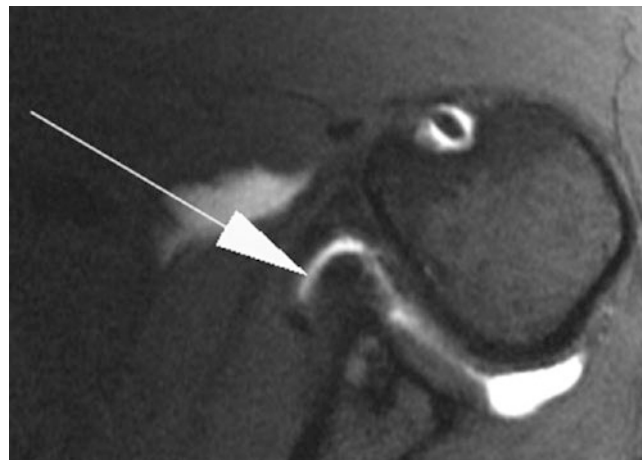
Fig. 9.17 Axial FS T1-weighted image from direct MR arthrogram demonstrates a normal postoperative globular anterior inferior labrum (arrow) following soft tissue Bankart repair. Note how the anterior glenoid "bumper" has been restored, and no contrast is seen undercutting the labrum

and the presence or absence of associated involvement of the osseous glenoid rim, operative techniques may be limited to a soft tissue repair/reconstruction including a capsular shift versus associated osseous repair/augmentation including bone grafting or a Latarjet procedure whereby a portion of the coracoid is transferred to the glenoid rim for osseous augmentation.

If there is a large Hill-Sachs lesion, this may be elevated/reduced or augmented with a remplissage technique.

9.9.1 Normal MRI Findings After Instability Surgery

If a soft tissue Bankart repair has been performed, postoperative imaging should show restoration of the anterior inferior bumper along the glenoid rim. This can be low to intermediate signal intensity but should be clearly visible as a labral-like structure along the osseous rim, although it often has a more rounded appearance (Fig. 9.17). Imaging in the ABER position is highly recommended following Bankart repair to assess for small nondisplaced recurrent tears [88].

If an osseous Bankart repair has been performed, whether with reattachment of the bone fragment, augmentation with bone graft, or a Laterjet procedure, a prominent anterior inferior glenoid rim should be present with or without associated overlying soft tissue depending on the repair technique. Again, the goal of the repair is to re-create a prominence or bumper along the anterior inferior glenoid rim to prevent the humeral head from dislocating out of the concave portion of the glenoid.
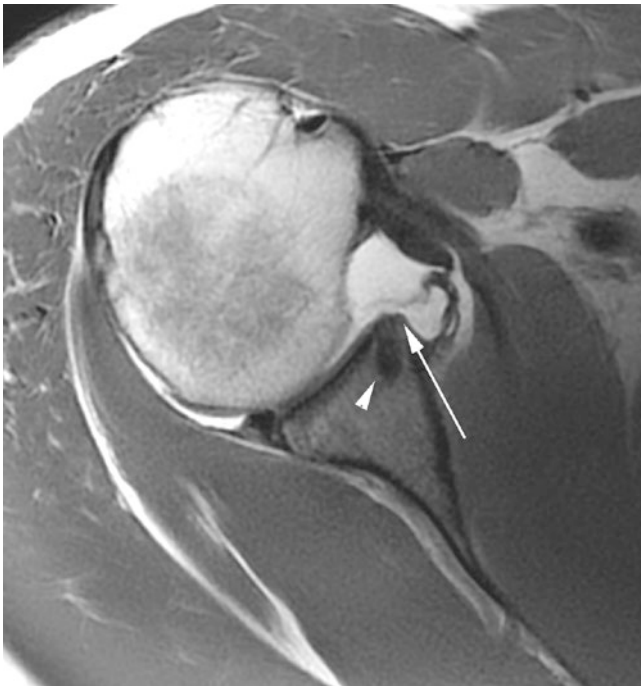
Fig. 9.18 Axial T1-weighted image from direct MR arthrogram demonstrates a failed Bankart repair with a missing antero-inferior labrum (arrow) and lack of the "bumper" along the glenoid rim. Note artifact from prior repair (arrowhead)

9.9.2 Abnormal MRI Findings After Instability Surgery

Abnormal findings following instability surgery include absence of the soft tissue prominence along the anterior inferior glenoid rim (bumper), detachment of the labrum or labro-ligamentous complex, and detachment or displacement or failure or consolidation/union of the osseous augmentation (Fig. 9.18). In addition, if there has been over-tightening of the anterior capsule, the shoulder may be prone to posterior subluxation or dislocation, thereby resulting in a posterior labral tear. The use of direct MR arthrography and imaging in the ABER position are often preferred as they better delineate the intra-articular structures and help in the detection of subtle nondisplaced anterior inferior labro-ligamentous tears (Fig. 9.19) [89].

9.10 Imaging After Biceps Tenotomy and Tenodesis

Pathology of the intra-articular portion and, to a lesser degree, the extra-articular portion of the tendon of the long head biceps brachii is commonly seen when imaging the shoulder. In many cases, it is an incidental finding in patients with rotator cuff pathology. However, symptomatic biceps

Fig. 9.19 Oblique coronal FS T1-weighted image in the ABER position from direct MR arthrogram demonstrates a recurrent tear of the antero-inferior labrum (arrow) following a Bankart repair

tendonopathy either in isolation or in combination with rotator cuff pathology or labral pathology, particularly superior labral pathology, may undergo surgical treatment. In advanced cases of symptomatic tendonopathy, a biceps tenotomy, with or without tenodesis, may be performed. When tenotomy alone is performed, the tendon is allowed to retract distally into the upper arm. The short head of the biceps ensures at least partial maintenance of the function of the biceps brachii. If tenodesis is performed, the tendon of the long head of the biceps is secured to the proximal humeral diaphysis with a screw or other fixation device.

9.10.1 Normal MRI Findings After Biceps Tenotomy and Tenodesis

When biceps tenotomy is performed, the tendon of the long head of the biceps is severed at its origin along the superior aspect of the glenoid (the supra-glenoid tubercle) at its junction with the superior labrum. If there is concomitant superior labral pathology, that is also addressed in the form of repair or shaving. At MRI, the tendon of the long head of the biceps will not be visible within the glenohumeral joint. No significant tendon stump should be visible along the superior glenoid rim. Depending on the degree of distal retraction, a portion of the tendon may or may not be visible within the bicipital groove. If a tenodesis has been performed, the actual point of fixation of the tendon onto the humeral diaphysis may be below the level of the axial images and thus may only be seen on the oblique coronal and oblique sagittal images. Depending on the fixation device used, the actual point of tenodesis may be difficult to appreciate unless there is
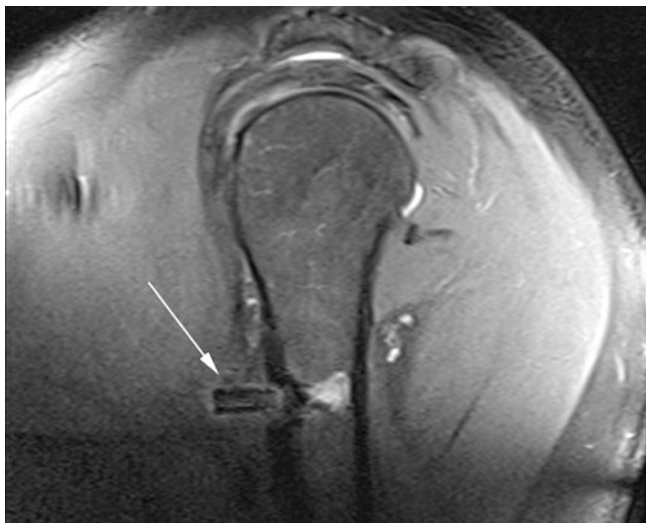
Fig. 9.20 Sagittal oblique FS T1-weighted image from direct MR arthrogram demonstrated a dislodged interference screw (arrow) following biceps tenodesis

susceptibility artifact. If an interference screw has been used, the screw may be slightly "proud" and protrude beyond the cortex of the humerus. This is a normal finding [90].

9.10.2 Abnormal MRI Findings After Biceps Tenotomy and Tenodesis

Complications specific to biceps tenotomy are rare since it is a straightforward procedure that merely involves releasing the tendon origin. Rarely, a residual stump is present along the glenoid rim and appears as a small protuberance of low signal tissue at the origin of the tendon. If a tenodesis has been performed, the most common anatomical complication is dislodgement of the interference screw and/or detachment/failure at the fixation site (Fig. 9.20) [91]. As mentioned above, a slightly proud interference screw is a normal finding. However, significant protuberance or dislodgement is abnormal. Rarely, intra-osseous ganglia may form, similar to ganglia that may form in the tibial tunnel following anterior cruciate ligament repair.

9.11 Concluding Remarks

Interpretation of postoperative MRI of the knee and shoulder can be challenging due to the variety of surgical techniques. Detailed knowledge of the original lesion, surgical technique employed, time since surgery, and potential postoperative complications is critical to the proper interpretation of the imaging findings. Following most types of knee surgery, rotator cuff surgery and biceps tendon surgery, high-quality

non-arthrographic MRI is usually sufficient. Following meniscal repair, shoulder instability surgery, and possibly SLAP repair, direct MR arthrography (with ABER positioning in the shoulder) should be considered.

> **Take Home Message**
> • Detailed knowledge of the original lesion, surgical technique employed, time since surgery, and potential postoperative complications is critical to the proper interpretation of postoperative MRIs of the knee and shoulder.

References

1. Discepola F, Park JS, Clopton P, Knoll AN, Austin MJ, Le HB, et al. Valid MR imaging predictors of prior knee arthroscopy. Skelet Radiol. 2012;41:67–74.
2. Daniels SP, van der List JP, Kazam JJ, DiFelice GS. Arthroscopic primary repair of the anterior cruciate ligament: what the radiologist needs to know. Skelet Radiol. 2018;47:619–29.
3. Kiekara T, Jarvela T, Huhtala H, Paakkala A. MRI of double-bundle ACL reconstruction: evaluation of graft findings. Skelet Radiol. 2012;41:835–42.
4. Xu Y, Ao YF, Wang JQ, Cui GQ. Prospective randomized comparison of anatomic single- and double-bundle anterior cruciate ligament reconstruction. Knee Surg Sports Traumatol Arthrosc. 2014;22:308–16.
5. Ahlen M, Liden M, Bovaller A, Sernert N, Kartus J. Bilateral magnetic resonance imaging and functional assessment of the semitendinosus and gracilis tendons a minimum of 6 years after ipsilateral harvest for anterior cruciate ligament reconstruction. Am J Sports Med. 2012;40:1735–41.
6. Rispoli DM, Sanders TG, Miller MD, Morrison WB. Magnetic resonance imaging at different time periods following hamstring harvest for anterior cruciate ligament reconstruction. Arthroscopy. 2001;17:2–8.
7. Tsifountoudis I, Karantanas AH. Current concepts on MRI evaluation of postoperative knee ligaments. Semin Musculoskelet Radiol. 2016;20:74–90.
8. Freedman KB, D'Amato MJ, Nedeff DD, Kaz A, Bach BR Jr. Arthroscopic anterior cruciate ligament reconstruction: a metaanalysis comparing patellar tendon and hamstring tendon autografts. Am J Sports Med. 2003;31:2–11.
9. Rousseau R, Labruyere C, Kajetanek C, Deschamps O, Makridis KG, Djian P. Complications after anterior cruciate ligament reconstruction and their relation to the type of graft: a prospective study of 958 cases. Am J Sports Med. 2019;47:2543–9.
10. Meyers AB, Haims AH, Menn K, Moukaddam H. Imaging of anterior cruciate ligament repair and its complications. AJR Am J Roentgenol. 2010;194:476–84.
11. Bencardino JT, Beltran J, Feldman MI, Rose DJ. MR imaging of complications of anterior cruciate ligament graft reconstruction. Radiographics. 2009;29:2115–26.
12. Marchant BG, Noyes FR, Barber-Westin SD, Fleckenstein C. Prevalence of nonanatomical graft placement in a series of failed anterior cruciate ligament reconstructions. Am J Sports Med. 2010;38:1987–96.
13. Walz DM. Postoperative imaging of the knee: meniscus, cartilage, and ligaments. Radiol Clin N Am. 2016;54:931–50.

14. Zhang S, Liu S, Yang L, Chen S, Chen S, Chen J. Morphological changes of the femoral tunnel and their correlation with hamstring tendon autograft maturation up to 2 years after anterior cruciate ligament reconstruction using femoral cortical suspension. Am J Sports Med. 2020;48:554–64.

15. Ghazikhanian V, Beltran J, Nikac V, Feldman M, Bencardino JT. Tibial tunnel and pretibial cysts following ACL graft reconstruction: MR imaging diagnosis. Skelet Radiol. 2012;41:1375–9.

16. Wilson TC, Kantaras A, Atay A, Johnson DL. Tunnel enlargement after anterior cruciate ligament surgery. Am J Sports Med. 2004;32:543–9.

17. Saupe N, White LM, Chiavaras MM, Essue J, Weller I, Kunz M, et al. Anterior cruciate ligament reconstruction grafts: MR imaging features at long-term follow-up—correlation with functional and clinical evaluation. Radiology. 2008;249:581–90.

18. Bedi A, Maak T, Musahl V, Citak M, O'Loughlin PF, Choi D, et al. Effect of tibial tunnel position on stability of the knee after anterior cruciate ligament reconstruction: is the tibial tunnel position most important? Am J Sports Med. 2011;39:366–73.

19. Howell SM, Clark JA. Tibial tunnel placement in anterior cruciate ligament reconstructions and graft impingement. Clin Orthop Relat Res. 1992;283:187–95.

20. Wang B, Zhong JL, Xu XH, Shang J, Lin N, Lu HD. Incidence and risk factors of joint stiffness after anterior cruciate ligament reconstruction. J Orthop Surg Res. 2020;15:175.

21. Bradley DM, Bergman AG, Dillingham MF. MR imaging of cyclops lesions. AJR Am J Roentgenol. 2000;174:719–26.

22. Facchetti L, Schwaiger BJ, Gersing AS, Guimaraes JB, Nardo L, Majumdar S, et al. Cyclops lesions detected by MRI are frequent findings after ACL surgical reconstruction but do not impact clinical outcome over 2 years. Eur Radiol. 2017;27:3499–508.

23. Wang J, Ao Y. Analysis of different kinds of cyclops lesions with or without extension loss. Arthroscopy. 2009;25:626–31.

24. Sanders TG. Imaging of the postoperative knee. Semin Musculoskelet Radiol. 2011;15:383–407.

25. Yoon KH, Tak DH, Ko TS, Park SE, Nam J, Lee SH. Association of fibrosis in the infrapatellar fat pad and degenerative cartilage change of patellofemoral joint after anterior cruciate ligament reconstruction. Knee. 2017;24:310–8.

26. Bodendorfer BM, Keeling LE, Michaelson EM, Shu HT, Apseloff NA, Spratt JD, et al. Predictors of knee arthrofibrosis and outcomes after arthroscopic lysis of adhesions following ligamentous reconstruction: a retrospective case-control study with over two years' average follow-up. J Knee Surg. 2019;32:536–43.

27. Collins MS, Unruh KP, Bond JR, Mandrekar JN. Magnetic resonance imaging of surgically confirmed anterior cruciate ligament graft disruption. Skelet Radiol. 2008;37:233–43.

28. Waltz RA, Solomon DJ, Provencher MT. A radiographic assessment of failed anterior cruciate ligament reconstruction: can magnetic resonance imaging predict graft integrity? Am J Sports Med. 2014;42:1652–60.

29. Naraghi AM, Gupta S, Jacks LM, Essue J, Marks P, White LM. Anterior cruciate ligament reconstruction: MR imaging signs of anterior knee laxity in the presence of an intact graft. Radiology. 2012;263:802–10.

30. Kyung HS, Kim HJ. Medial patellofemoral ligament reconstruction: a comprehensive review. Knee Surg Relat Res. 2015;27:133–40.

31. Weber AE, Nathani A, Dines JS, Allen AA, Shubin-Stein BE, Arendt EA, et al. An algorithmic approach to the management of recurrent lateral patellar dislocation. J Bone Joint Surg Am. 2016;98:417–27.

32. Puzzitiello RN, Waterman B, Agarwalla A, Zuke W, Cole BJ, Verma NN, et al. Primary medial patellofemoral ligament repair versus reconstruction: rates and risk factors for instabil-

ity recurrence in a young, active patient population. Arthroscopy. 2019;35:2909–15.

33. Torabi M, Wo S, Vyas D, Costello J. MRI evaluation and complications of medial patellofemoral ligament reconstruction. Clin Imaging. 2015;39:116–27.

34. Meyers AB, Laor T, Sharafinski M, Zbojniewicz AM. Imaging assessment of patellar instability and its treatment in children and adolescents. Pediatr Radiol. 2016;46:618–36.

35. Alcala-Galiano A, Baeva M, Ismael M, Argueso MJ. Imaging of posterior cruciate ligament (PCL) reconstruction: normal postsurgical appearance and complications. Skelet Radiol. 2014;43:1659–68.

36. Parkar AP, Alcala-Galiano A. Rupture of the posterior cruciate ligament: preoperative and postoperative assessment. Semin Musculoskelet Radiol. 2016;20:43–51.

37. Naraghi A, Pearce DH, Whelan DB, Chahal J. Imaging of the postoperative condition of posterolateral corner injuries. Semin Musculoskelet Radiol. 2018;22:413–23.

38. Sonnery-Cottet B, Vieira TD, Ouanezar H. Anterolateral ligament of the knee: diagnosis, indications, technique, outcomes. Arthroscopy. 2019;35:302–3.

39. Kraeutler MJ, Welton KL, Chahla J, LaPrade RF, McCarty EC. Current concepts of the anterolateral ligament of the knee: anatomy, biomechanics, and reconstruction. Am J Sports Med. 2018;46:1235–42.

40. Higuchi H, Kimura M, Shirakura K, Terauchi M, Takagishi K. Factors affecting long-term results after arthroscopic partial meniscectomy. Clin Orthop Relat Res. 2000:161–8. https://doi.org/10.1097/00003086-200008000-00022.

41. Smith DK, Totty WG. The knee after partial meniscectomy: MR imaging features. Radiology. 1990;176:141–4.

42. Sciulli RL, Boutin RD, Brown RR, Nguyen KD, Muhle C, Lektrakul N, et al. Evaluation of the postoperative meniscus of the knee: a study comparing conventional arthrography, conventional MR imaging, MR arthrography with iodinated contrast material, and MR arthrography with gadolinium-based contrast material. Skelet Radiol. 1999;28:508–14.

43. Magee T, Shapiro M, Rodriguez J, Williams D. MR arthrography of postoperative knee: for which patients is it useful? Radiology. 2003;229:159–63.

44. Cordle AC, Williams DD, Andrews CL. The postoperative meniscus: anatomical, operative, and imaging considerations. Semin Musculoskelet Radiol. 2018;22:398–412.

45. Chapin R. Imaging of the postoperative meniscus. Radiol Clin N Am. 2018;56:953–64.

46. Baker JC, Friedman MV, Rubin DA. Imaging the postoperative knee meniscus: an evidence-based review. AJR Am J Roentgenol. 2018;211:519–27.

47. Eggli S, Wegmuller H, Kosina J, Huckell C, Jakob RP. Long-term results of arthroscopic meniscal repair. An analysis of isolated tears. Am J Sports Med. 1995;23:715–20.

48. Miao Y, Yu JK, Ao YF, Zheng ZZ, Gong X, Leung KK. Diagnostic values of 3 methods for evaluating meniscal healing status after meniscal repair: comparison among second-look arthroscopy, clinical assessment, and magnetic resonance imaging. Am J Sports Med. 2011;39:735–42.

49. Nishino K, Hashimoto Y, Nishida Y, Terai S, Takahashi S, Yamasaki S, et al. Incidence and risk factors for meniscal cyst after meniscal repair. Arthroscopy. 2019;35:1222–9.

50. Vives MJ, Homesley D, Ciccotti MG, Schweitzer ME. Evaluation of recurring meniscal tears with gadolinium-enhanced magnetic resonance imaging: a randomized, prospective study. Am J Sports Med. 2003;31:868–73.

51. White LM, Schweitzer ME, Weishaupt D, Kramer J, Davis A, Marks PH. Diagnosis of recurrent meniscal tears: prospective eval-

uation of conventional MR imaging, indirect MR arthrography, and direct MR arthrography. Radiology. 2002;222:421–9.

52. Magee T. Accuracy of 3-tesla MR and MR arthrography in diagnosis of meniscal retear in the post-operative knee. Skelet Radiol. 2014;43:1057–64.

53. Allaire R, Muriuki M, Gilbertson L, Harner CD. Biomechanical consequences of a tear of the posterior root of the medial meniscus. Similar to total meniscectomy. J Bone Joint Surg Am. 2008;90:1922–31.

54. Kim SB, Ha JK, Lee SW, Kim DW, Shim JC, Kim JG, et al. Medial meniscus root tear refixation: comparison of clinical, radiologic, and arthroscopic findings with medial meniscectomy. Arthroscopy. 2011;27:346–54.

55. Palisch AR, Winters RR, Willis MH, Bray CD, Shybut TB. Posterior root meniscal tears: preoperative, intraoperative, and postoperative imaging for Transtibial pullout repair. Radiographics. 2016;36:1792–806.

56. Elattar M, Dhollander A, Verdonk R, Almqvist KF, Verdonk P. Twenty-six years of meniscal allograft transplantation: is it still experimental? A meta-analysis of 44 trials. Knee Surg Sports Traumatol Arthrosc. 2011;19:147–57.

57. Chung KS, Ha JK, Ra HJ, Kim JG. A meta-analysis of clinical and radiographic outcomes of posterior horn medial meniscus root repairs. Knee Surg Sports Traumatol Arthrosc. 2016;24:1455–68.

58. Feucht MJ, Kuhle J, Bode G, Mehl J, Schmal H, Sudkamp NP, et al. Arthroscopic transtibial pullout repair for posterior medial meniscus root tears: a systematic review of clinical, radiographic, and second-look arthroscopic results. Arthroscopy. 2015;31:1808–16.

59. Lee SM, Bin SI, Kim JM, Lee BS, Lee CR, Son DW, et al. Long-term outcomes of meniscal allograft transplantation with and without extrusion: mean 12.3-year follow-up study. Am J Sports Med. 2019;47:815–21.

60. Lee DH, Lee BS, Chung JW, Kim JM, Yang KS, Cha EJ, et al. Changes in magnetic resonance imaging signal intensity of transplanted meniscus allografts are not associated with clinical outcomes. Arthroscopy. 2011;27:1211–8.

61. Smith NA, MacKay N, Costa M, Spalding T. Meniscal allograft transplantation in a symptomatic meniscal deficient knee: a systematic review. Knee Surg Sports Traumatol Arthrosc. 2015;23:270–9.

62. Scillia AJ, Aune KT, Andrachuk JS, Cain EL, Dugas JR, Fleisig GS, et al. Return to play after chondroplasty of the knee in National Football League athletes. Am J Sports Med. 2015;43:663–8.

63. Ogura T, Merkely G, Bryant T, Winalski CS, Minas T. Autologous chondrocyte implantation "Segmental-Sandwich" technique for deep osteochondral defects in the knee: clinical outcomes and correlation with magnetic resonance imaging findings. Orthop J Sports Med. 2019;7:2325967119847173.

64. Goyal D, Keyhani S, Lee EH, Hui JH. Evidence-based status of microfracture technique: a systematic review of level I and II studies. Arthroscopy. 2013;29:1579–88.

65. Choi YS, Potter HG, Chun TJ. MR imaging of cartilage repair in the knee and ankle. Radiographics. 2008;28:1043–59.

66. Guermazi A, Roemer F, Alizai H, Winalski CS, Welsch G, Brittberg M, et al. State of the art: MR imaging after knee cartilage repair surgery. Radiology. 2015;277:23–43.

67. Kreuz PC, Steinwachs MR, Erggelet C, Krause SJ, Konrad G, Uhl M, et al. Results after microfracture of full-thickness chondral defects in different compartments in the knee. Osteoarthr Cartil. 2006;14:1119–25.

68. Mithoefer K, Venugopal V, Manaqibwala M. Incidence, degree, and clinical effect of subchondral bone overgrowth after microfracture in the knee. Am J Sports Med. 2016;44:2057–63.

69. Liu YW, Tran MD, Skalski MR, Patel DB, White EA, Tomasian A, et al. MR imaging of cartilage repair surgery of the knee. Clin Imaging. 2019;58:129–39.

70. Hangody L, Fules P. Autologous osteochondral mosaicplasty for the treatment of full-thickness defects of weight-bearing joints: ten years of experimental and clinical experience. J Bone Joint Surg Am. 2003;85-A(Suppl 2):25–32.

71. Lynch TS, Patel RM, Benedick A, Amin NH, Jones MH, Miniaci A. Systematic review of autogenous osteochondral transplant outcomes. Arthroscopy. 2015;31:746–54.

72. Alparslan L, Winalski CS, Boutin RD, Minas T. Postoperative magnetic resonance imaging of articular cartilage repair. Semin Musculoskelet Radiol. 2001;5:345–63.

73. Link TM, Mischung J, Wortler K, Burkart A, Rummeny EJ, Imhoff AB. Normal and pathological MR findings in osteochondral autografts with longitudinal follow-up. Eur Radiol. 2006;16:88–96.

74. Andrade R, Vasta S, Pereira R, Pereira H, Papalia R, Karahan M, et al. Knee donor-site morbidity after mosaicplasty—a systematic review. J Exp Orthop. 2016;3:31.

75. Sirlin CB, Brossmann J, Boutin RD, Pathria MN, Convery FR, Bugbee W, et al. Shell osteochondral allografts of the knee: comparison of MR imaging findings and immunologic responses. Radiology. 2001;219:35–43.

76. Na Y, Shi Y, Liu W, Jia Y, Kong L, Zhang T, et al. Is implantation of autologous chondrocytes superior to microfracture for articular-cartilage defects of the knee? A systematic review of 5-year follow-up data. Int J Surg. 2019;68:56–62.

77. Kraeutler MJ, Belk JW, Purcell JM, McCarty EC. Microfracture versus autologous chondrocyte implantation for articular cartilage lesions in the knee: a systematic review of 5-year outcomes. Am J Sports Med. 2018;46:995–9.

78. Wuennemann F, Rehnitz C, Weber MA. Imaging of the knee following repair of focal articular cartilage lesions. Semin Musculoskelet Radiol. 2018;22:377–85.

79. Niethammer TR, Valentin S, Gulecyuz MF, Rossbach BP, Ficklscherer A, Pietschmann MF, et al. Bone marrow edema in the knee and its influence on clinical outcome after matrix-based autologous chondrocyte implantation: results after 3-year follow-up. Am J Sports Med. 2015;43:1172–9.

80. Marlovits S, Striessnig G, Resinger CT, Aldrian SM, Vecsei V, Imhof H, et al. Definition of pertinent parameters for the evaluation of articular cartilage repair tissue with high-resolution magnetic resonance imaging. Eur J Radiol. 2004;52:310–9.

81. Bancroft LW, Wasyliw C, Pettis C, Farley T. Postoperative shoulder magnetic resonance imaging. Magn Reson Imaging Clin N Am. 2012;20(2):313–25, xi. https://doi.org/10.1016/j.mric.2012.01.010. Epub 2012 Feb 11.

82. Woertler K. Multimodality imaging of the postoperative shoulder. Eur Radiol. 2007;17(12):3038–55. https://doi.org/10.1007/s00330-007-0649-3. Epub 2007 May 22.

83. Spielmann AL, Forster BB, Kokan P, Hawkins RH, Janzen DL. Shoulder after rotator cuff repair: MR imaging findings in asymptomatic individuals—initial experience. Radiology. 1999;213(3):705–8. https://doi.org/10.1148/radiology.213.3.r99dc09705.

84. Zlatkin MB. MRI of the postoperative shoulder. Skelet Radiol. 2002;31(2):63–80. https://doi.org/10.1007/s00256-001-0460-1. Epub 2002 Jan 8.

85. Beltran LS, Bencardino JT, Steinbach LS. Postoperative MRI of the shoulder. J Magn Reson Imaging. 2014;40(6):1280–97. https://doi.org/10.1002/jmri.24570. Epub 2014 Feb 6.

86. Pierce JL, Nacey NC, Jones S, Rierson D, Etier B, Brockmeier S, Anderson MW. Postoperative shoulder imaging: rotator cuff, labrum, and biceps tendon. Radiographics. 2016;36(6):1648–71. https://doi.org/10.1148/rg.2016160023.

87. Boutin RD, Marder RA. MR imaging of SLAP lesions. Open Orthop J. 2018;12:314–23. https://doi.org/10.2174/1874325001812010314.

88. Tian CY, Cui GQ, Zheng ZZ, Ren AH. The added value of ABER position for the detection and classification of anteroinferior labroligamentous lesions in MR arthrography of the shoulder. Eur J Radiol. 2013;82(4):651–7. https://doi.org/10.1016/j.ejrad.2012.11.038. Epub 2013 Jan 1.

89. Van der Woude HJ, Vanhoenacker FM. MR arthrography in glenohumeral instability. JBR-BTR. 2007;90(5):377–83.

90. Salata MJ, Bailey JR, Bell R, Frank RM, McGill KC, Lin EC, Kercher JS, Wang VM, Provencher MT, Mazzocca AD, Verma NN, Romeo AA. Effect of interference screw depth on fixation strength in biceps tenodesis. Arthroscopy. 2014;30(1):11–5. https://doi.org/10.1016/j.arthro.2013.08.033. Epub 2013 Oct 31.

91. Nho SJ, Reiff SN, Verma NN, Slabaugh MA, Mazzocca AD, Romeo AA. Complications associated with subpectoral biceps tenodesis: low rates of incidence following surgery. J Shoulder Elb Surg. 2010;19(5):764–8. https://doi.org/10.1016/j.jse.2010.01.024. Epub 2010 May 14.

Adult Tumors of Soft Tissue, Bone, and Bone Marrow: What the Clinician Wants to Know

10

Hillary W. Garner and Mark D. Murphey

Learning Objectives
- To gain knowledge and understanding of what clinicians want to know from imaging of soft tissue, bone, and bone marrow tumors.
- To understand how the key imaging features of tumors impact their diagnosis, staging, and treatment options.
- To illustrate examples of report templates for the comprehensive and clear reporting of imaging studies obtained for evaluation of soft tissue, bone, and bone marrow tumors.

Adult tumors of soft tissue, bone, and bone marrow encompass a broad range of histopathologies with varying immunohistochemical and molecular properties, but the tenets of imaging for these tumors and their value to clinicians and patients are consistent regardless of tumor type. Demonstrating an understanding of the relevance and influence of the patient's history and addressing the important imaging features of a tumor in a consistent and concise manner in the radiology report elevate the perceived worth of the radiologist's input into patient care. In this chapter, we focus on magnetic resonance imaging (MRI) findings and provide guidance on what clinicians want to know and how to report this information using a clear and uniform approach.

10.1 Introduction

The function of imaging in the setting of a soft tissue, bone, or bone marrow tumor hinges on the capacity to accurately characterize, localize, and quantitate the abnormality. A radiologist's interpretation and reporting of these key imaging findings allow for a differential diagnosis, can add specificity and confidence in diagnosis, and allow for a determination regarding the need for biopsy and a shared platform from which the clinical team and patient can discuss further diagnostic management and an initial treatment plan. In addition, the appropriate characterization of a tumor can often provide insight into the potential staging of the tumor and guide the need for additional imaging prior to biopsy.

10.2 Soft Tissue Tumors

Although the majority of soft tissue tumors (STT) are benign, the morbidity and mortality associated with soft tissue sarcoma (STS) are significant and warrant that radiologists have a fundamental knowledge of their imaging presentations and treatment methods and goals. Radiographs, ultrasound, computed tomography (CT), and positron emission tomography (PET)/CT can all often provide useful information for differential diagnosis of a STT. The purpose of radiographs for the evaluation of STT is often underestimated, but they can provide highly valuable information, such as the identification and characterization of associated mineralization and osseous lesion origin and the identification of underlying cortical involvement, which can influence the differential diagnosis. Therefore, radiographs should be routinely performed during the workup of STT and are an appropriate initial imaging study. For superficial STT, either radiographs or ultrasound is appropriate initially [1]. If the STT requires further characterization after radiographic or ultrasound evaluation, MRI is the imaging technique of choice [2–4] as it often allows for a limited differential diagnosis. For example, the most common myxoid lesions, soft tissue myxoma,

H. W. Garner (✉)
Department of Radiology, Mayo Clinic, Jacksonville, FL, USA
e-mail: garner.hillary@mayo.edu

M. D. Murphey
American Institute for Radiologic Pathology,
Silver Spring, MD, USA

Department of Radiology and Nuclear Medicine, Uniformed
Services University of the Health Sciences, Bethesda, MD, USA
e-mail: mmurphey@acr.org

myxoid liposarcoma, and myxofibrosarcoma (Fig. 10.1), can usually be distinguished by their imaging characteristics in the vast majority of cases on MRI [5–7]. An understanding of the relevance of the MRI features favoring a benign versus malignant diagnosis is paramount to making a determination of radiology-pathology concordance or discordance and making appropriate recommendations for next steps in management. For STS in particular, the key MRI features that help predict its behavior and potentially impact surgical management are the tumor's anatomical site (intramuscular, intermuscular, subcutaneous, intraarticular, extensive/multifocal), size, depth, margin, and morphological/enhancement complexity. Specific locations can also improve diagnostic accuracy, such as deep to the scapular tip for elastofibroma and hand/foot for fibromatosis. Reporting of associated inflammatory edema-like signal or hemorrhage in the surrounding soft tissues or associated fascial enhancement extending from the tumor (fascial tails) is also crucial because these areas can contain tumor cells and needs to be addressed in the treatment plan to maximize local control.

Several recent studies have incorporated the numerous

> **Key Point**
> - Knowledge of the key imaging features that predict tumor behavior is critical to providing a comprehensive imaging report.

elemental constituents of these key MRI features into MRI radiomics models in an effort to better grade [8] and stage [9] STS as well as predict specific histopathology [4], treatment response [10], and overall survival [11]. Therefore, each of these key MRI features should be specifically described in the radiology report. Of note, in the setting of an aggressive-appearing or otherwise indeterminate STT, it behooves radiologists, particularly those practicing outside the tertiary care setting, to clearly and specifically recommend in the final impression of the imaging report that the patient be referred to an orthopedic oncologist prior to biopsy. An

example of a structured MRI report for a soft tissue sarcoma is provided in Fig. 10.2.

In addition to an appreciation of the importance of the key MRI features, an understanding of the staging methods for STS is relevant. The most commonly used staging system for almost all histological subtypes of STS is the American Joint Committee on Cancer (AJCC) staging system [12], which incorporates extent of tumor (T), lymph node status (N), presence of metastasis (M), and tumor grade (G). In the most recent 8th edition of the AJCC staging system published in 2017 [13], the anatomical site of STS became a more relevant staging parameter, with different staging systems now employed based on whether the STS is located in the trunk/extremity, retroperitoneum, head and neck, or thoracic/abdominal visceral organs [12, 13]. In the musculoskeletal radiology realm, we are primarily involved in the assessment of STS of the trunk/extremity, so specific knowledge of the staging system for this anatomical site is useful. The tumor grade in the AJCC staging system is based on the French Federation of Cancer Centers (FNCLCC) grading system, which includes tumor differentiation, presence of necrosis, and mitotic count in its analysis. Radiologists can provide insight on the histological grade of a STS by identifying and reporting necrosis during image interpretation and including areas of necrosis within biopsy specimens. Of note, a few aspects of the AJCC trunk/extremity staging system are controversial, including the designation of regional nodal metastasis as stage IV disease, the exclusion of tumor depth as an independent prognostic factor, and the division of tumors greater than 10 cm into two separate T categories rather than just one category (T3, >10 cm ≤ 15 cm; T4, >15 cm) [14]. Given these controversies and the broad non-uniformity in STS types and behaviors, tumor genomics likely plays a greater role, if not a central role, in future prognostication. In the interim, clinicians rely on clinical examination and the information gleaned from the MRI interpretation to plan treatment.

The mainstay of treatment for STS is wide surgical resection with the primary goal being a balance between achieving local control and preserving patient function. Additional MRI features that are essential to report in an effort to help surgeons best achieve this balance, particularly in the setting

Fig. 10.1 Examples of common pathologically proven myxoid lesions on MRI. Coronal T1-weighted (**a**), coronal T2-weighted fat-saturated (**b**), and coronal T1-weighted fat-saturated post-contrast (**c**) MR images of the proximal right thigh demonstrating a <5 cm circumscribed intramuscular mass with homogeneous T1 signal isointense to muscle and a thin rim of perilesional fat (arrowheads in **a**), homogeneous extremely bright T2 signal with perilesional edema at the superior and inferior margins (arrows in **b**), and whorl-like areas of mild enhancement internally. There is no enhancement extending away from the mass. **These MRI features are most compatible with a soft tissue myxoma.** Coronal T1-weighted (**d**), coronal T2-weighted fat-saturated (**e**), and coronal T1-weighted fat-saturated post-contrast (**f**) MR images of the proximal right thigh demonstrating a >5 cm fat-containing heterogeneous mass with irregular perilesional edema and enhancement. **These MRI features are most compatible with a myxoid liposarcoma.** Coronal T1-weighted (**g**), coronal T2-weighted fat-saturated (**h**), and coronal T1-weighted fat-saturated post-contrast (**i**) MR images of the proximal right thigh demonstrating a >5 cm heterogeneous mass avid irregular peripheral enhancement, central necrosis, and irregular perilesional edema and enhancement. **These MRI features are most compatible with a myxofibrosarcoma**
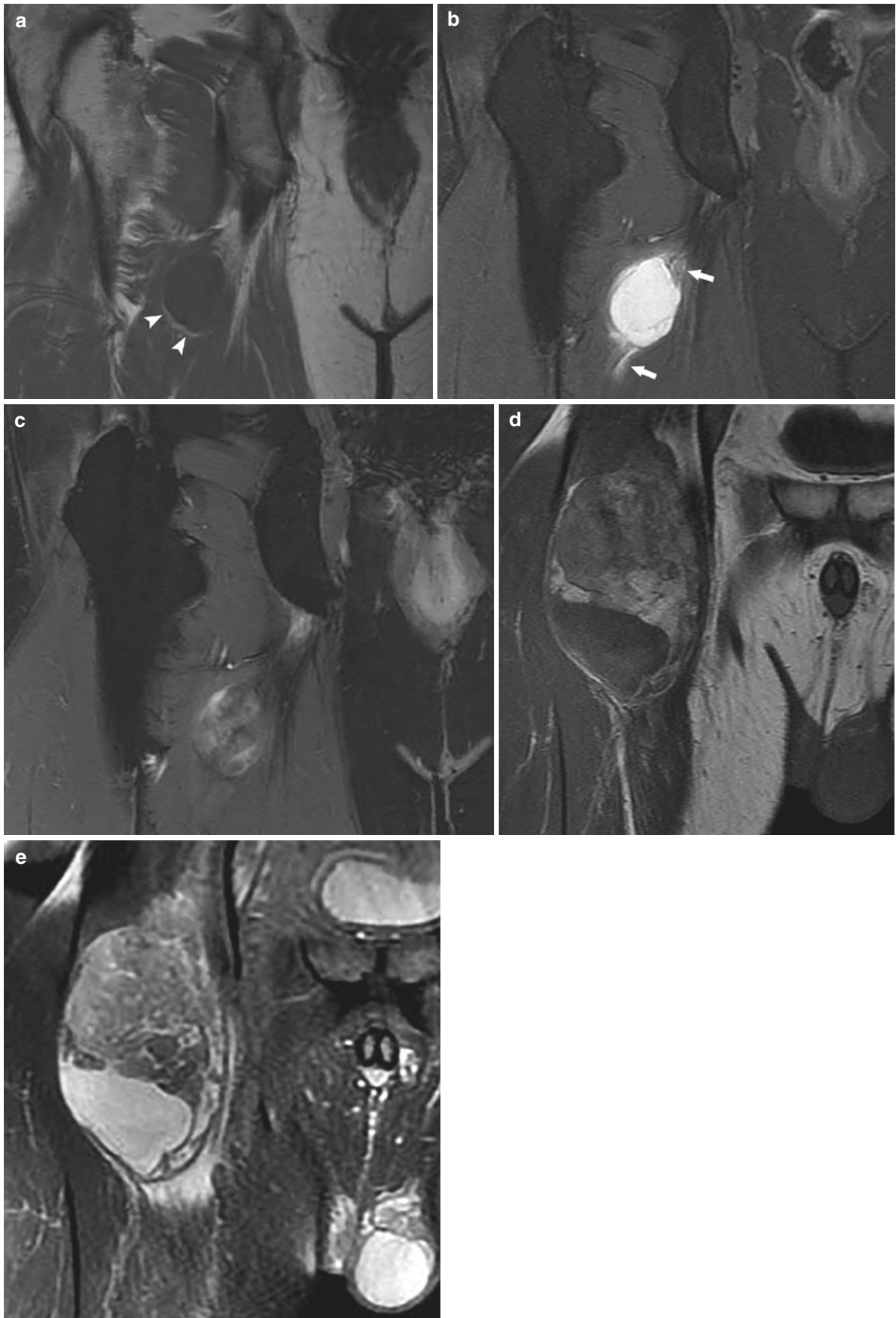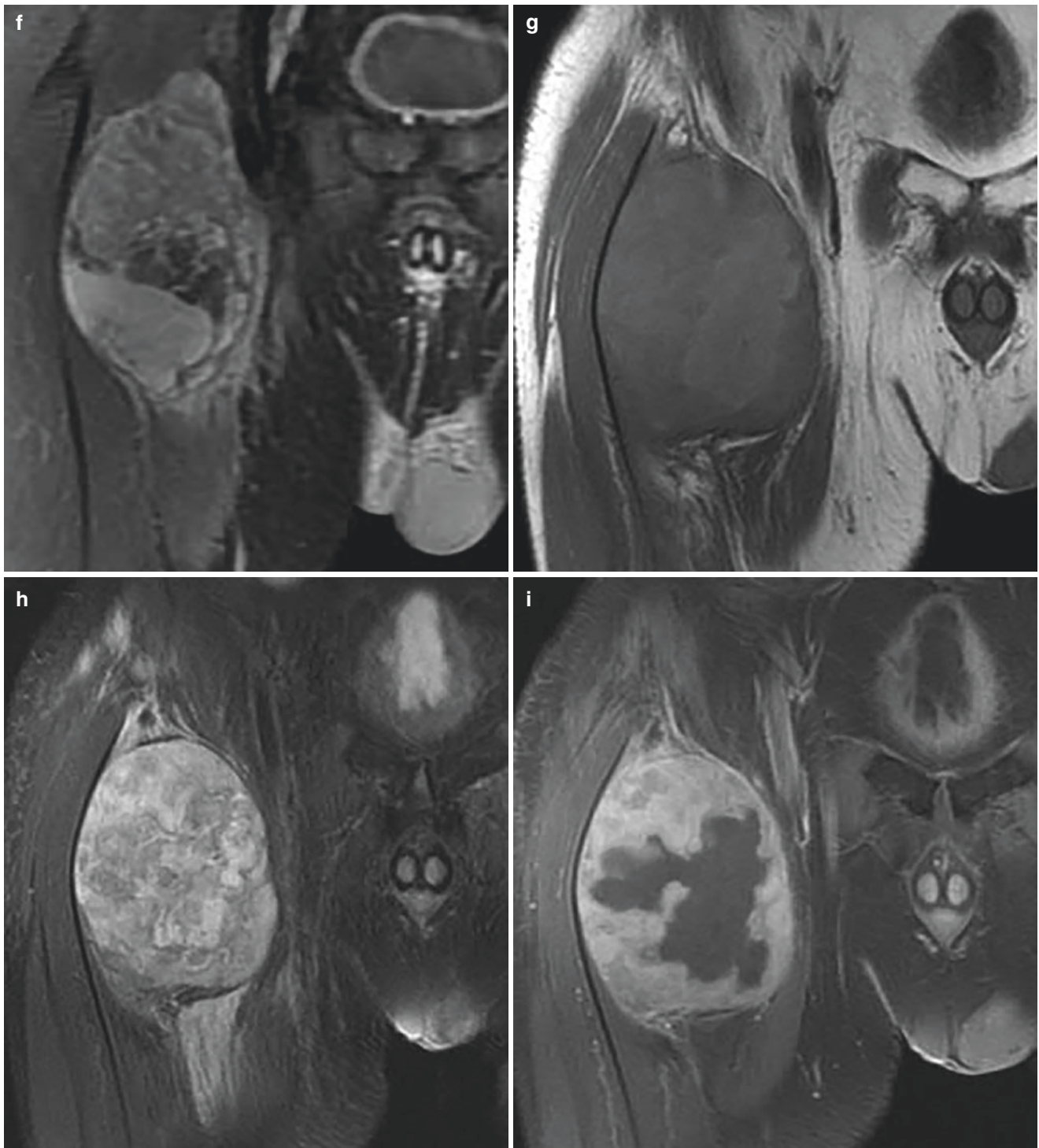
Fig. 10.1 (continued)

of an aggressive-appearing STT, are the presence or absence of muscular compartmental breaching, neurovascular involvement (Fig. 10.3), organ invasion, or bone invasion. This information often dictates the treatment plan, including whether to pursue neoadjuvant therapies prior to resection or to proceed with primary surgical intervention. In the case of neurovascular or organ involvement, the orthopedic oncol-

ogy team requires operative assistance by other surgical specialties. Furthermore, if the STT is situated within an anatomically complex region such as the pelvis, the need for three-dimensional (3D) printing for surgical planning can be anticipated.

Another crucial element to the report which often receives less attention from radiologists is a description of the

EXAM: MRI [ANATOMICAL SITE] WO + W/CON

Technique: Multiplanar multisequence MR imaging of the [anatomical site] was performed before and after the uneventful intravenous administration of [x] mL [contrast agent].

History: xx-year-old man/woman presented to an outside physician 1 month ago for evaluation of a slowly enlarging painless mass at the anterior aspect of the [anatomical site] which was first noticed approximately 2 years ago. Outside ultrasound demonstrated a solid vascular mass that was reported as worrisome for malignancy. The patient has no other health concerns.

Comparisons: Radiographs of the [anatomical site] obtained earlier today.

FINDINGS:

Mass characteristics:

    Location:

        Anatomical site:

        Tissue depth/location (subcutaneous,fascial,intra-/intermuscular,intraarticular, multifocal):

    Size:

    Margin (circumscribed/irregular):

    Morphology and T1/T2 signal characteristics:

    Enhancement characteristics (avid/heterogeneous/central/peripheral):

    Most aggressive portion for biopsy target:

    Necrosis (None vs <50% vs >50%):

    Radiographic appearance (mineralization/cortical involvement):

    Sonographic appearance (solid vs cystic/echogenicity/vascularity):

Status of surrounding tissues:

    Edema (peritumoral/fascial):
    Hemorrhage:
    Neurovascular involvement:
    Bone involvement:
    Other:

Other findings:

Staging information:

    Longest diameter of tumor (T):

    Lymph node (L): may be unknown at time of MRI; report expected date of staging CT

    Metastasis (M): may be unknown at time of MRI; report expected date of staging CT

    Necrosis:

FINAL IMPRESSION:

Fig. 10.2 Example of a structured MRI report for soft tissue sarcoma

patient's history. Accurately and thoroughly addressing the patient's history relevant to the STT directly in the report, particularly in the setting of treated soft tissue sarcoma, gives the referring clinician and the patient confidence in the care that the radiologist is providing. For example, if the patient has a history of an undifferentiated pleomorphic sarcoma, specifically reporting in chronological order the date of initial biopsy diagnosis, the histologic grade, the incorporation of radiation with dates of initiation and conclusion and total dosage, the incorporation of chemotherapy, and the date of any surgeries, whether non-oncologic or oncologic is extremely helpful for bringing together a common language for all involved in the patient's care. Also, a key piece of information that should be sought when interpreting follow-up MRI after STS resection is the surgical margin status as it is the primary influence on risk of local recurrence [15].
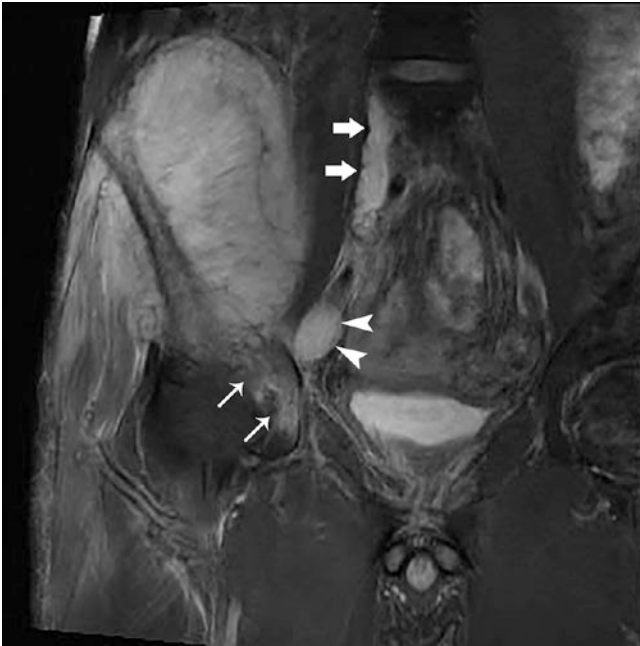
Fig. 10.3 A 36-year-old man with osteosarcoma of the right ilium. Coronal T2-weighted fat-saturated image of the pelvis demonstrates the large primary tumor with invasion into the right hip joint (skinny arrows), a right external iliac lymph node metastasis (arrowheads), and tumor thrombus in the right common iliac vein (fat arrows)

Fortunately, much of this information is now available in the electronic medical record. Other alternatives to obtaining this information could be providing a questionnaire to the patient at the time of check-in for imaging or contacting the patient directly.

> **Key Point**
> • Inclusion of a detailed patient history in the imaging report confirms to the patient and the other members of the healthcare team the investment of the radiologist in helping maximize patient care and outcome.

10.3   Bone Tumors

Similar principles guiding the imaging reporting of STT can be applied to bone tumors. Although radiographs are highly valuable in the setting of a STT even when negative, in the setting of extremity bone tumors, accurate characterization of an extremity bone tumor relies heavily on the radiographic appearance. Therefore, radiographs in at least two orthogonal planes are imperative and should be employed as the initial imaging modality. Given that the location of a bone lesion in combination with the patient age allows for a limited differential of two or three diagnoses in most cases, the radio-

graphic report should initially include a clear description of the specific location within the bone, whether epiphyseal, metaphyseal, or diaphyseal and whether intramedullary, cortical, or surface. Other key features to analyze and report are the size, zone of transition (narrow or wide), pattern of bone destruction (geographic, moth-eaten, permeative), periosteal reaction (aggressive or nonaggressive), and internal characteristics of the lesion (lucent/lytic, sclerotic, mixed, osteoid/chondroid matrix). For indeterminate or aggressive-appearing lesions, it is vital to also report on the status of the cortex and soft tissues and assess for risk of pathologic fracture.

> **Key Point**
> • Radiographic evaluation of a bone tumor is imperative. MRI interpretation of a bone lesion without comparison to the corresponding radiographs raises the risk of misdiagnosis and mistreatment.

When radiographs confirm the presence of an aggressive or indeterminate bone lesion in the extremity or pelvis, the modality of choice for further imaging evaluation is MRI, which should be protocoled to include sequences of the entire compartment with the associated proximal and distal joints [16]. Of note, the corresponding radiographs should always be reviewed concurrently during the MRI interpretation, and this direct correlation should be stated in the report. For non-extremity bone lesions, CT is typically used as the primary imaging modality [16], but MRI is also advantageous as a subsequent test as it can better define tissue planes between tumor and surrounding structures. The same features of the lesion described radiographically should similarly be addressed in the MRI and/or CT report. Additionally, the morphological/enhancement complexity can be better defined with these advanced modalities. Other highly important potential findings to identify and describe include physeal transgression, articular invasion, and soft tissue/organ/neurovascular involvement (Fig. 10.3). Each of these features has implications for diagnosis, staging, biopsy planning, and treatment planning. Therefore, as stated above for STT, radiologists in a non-tertiary care setting can best serve their patients by clearly and specifically recommending in the final impression of the report a referral to an orthopedic oncologist prior to biopsy.

> **Key Point**
> • Patients with high-risk musculoskeletal tumors should only undergo biopsy following consultation with the treating orthopedic oncologist.

Similar to STS, there are controversies surrounding the available staging systems for bone sarcoma, which include the AJCC 8th edition, Musculoskeletal Tumor Society, and Vanderbilt staging systems. In particular, these staging systems have variable accuracies for predicting overall survival in the three most common types of primary bone sarcoma, which are osteosarcoma, Ewing sarcoma, and chondrosarcoma [17, 18]. However, radiologists can benefit from the knowledge that histologic grade and the presence and location of metastatic disease are key factors for staging in all of these lesions. Although combining these three most common bone sarcoma types into one staging system simplifies the clinical approach, it may be a disservice to patients who would more likely benefit from individualized prognostic information. Therefore, a greater focus on tumor-type specific genomics is expected to play more of a role in the staging of bone sarcomas in the future. As radiologists, keeping up to date as the staging systems for these tumors evolve over time is important to maintain a common multidisciplinary language.

MRI or CT reports obtained for evaluation of a bone tumor need to include a thorough description of all relevant patient history associated with the bone tumor, particularly in the post-treatment setting. For example, the general treatment strategies for osteosarcoma and Ewing sarcoma incorporate both neoadjuvant and adjuvant chemotherapy, but radiation is usually reserved for anatomical locations where complete surgical resection is difficult or impossible [16]. Therefore, the knowledge that a patient with osteosarcoma or Ewing sarcoma was treated with radiation is helpful in that it alerts the radiologist to the potential of a higher risk of local recurrence. An example of a structured report template for bone sarcoma following treatment is provided in Fig. 10.4.

EXAM: MRI [ANATOMICAL SITE] WO + W/CON

Technique: Multiplanar multisequence MR imaging of the [anatomical site] was performed before and after the uneventful intravenous administration of [x] mL [contrast agent].

History: xx-year-old man/woman with history of grade 2 chondrosarcoma of the [anatomical site] initially diagnosed on [date] from CT guided biopsy specimen. The patient was treated with wide oncologic resection on [date], resulting in wide negative margins > 3 cm. Immediate reconstruction was achieved with allograft prosthetic composite, tendon reconstruction, myocutaneous flap, and skin grafting. This is the patient's 4th follow-up MRI (performed every 6 months) with no evidence of tumor recurrence in the interval since surgery.

Comparisons: Initial pre-treatment radiographs from [date] and initial pre-treatment MRI from [date]. Multiple other post-treatment radiographs and MRI examinations were also compared, the most recent from [date].

FINDINGS:

Nodular signal abnormality/enhancement: None. There is no evidence of local tumor recurrence.

Postoperative change:

       Prostheses/Fixation:
       Myocutaneous flap:
       Fluid collection:

Postradiation change:

       Subcutaneous tissues:
       Muscle:
       Bone marrow:

Other findings:

       Lymph nodes:
       Neurovascular structures:
       Myotendinous structures:
       Joint findings:

FINAL IMPRESSION:

Fig. 10.4 Example of a structured MRI report for post-treatment follow-up of bone sarcoma

10.4 Bone Marrow Tumors

Primary bone marrow tumors (BMT) include myeloma, leukemia, and lymphoma. Radiographs, CT, PET/CT, and MRI are all used in the evaluation of these tumors. As with bone tumors, radiographs are the most appropriate initial imaging test when the clinical presentation is that of localized unremitting atraumatic bone pain. However, if the clinical presentation of a BMT is instead based on laboratory abnormalities, the historical practice of using skeletal survey for initial evaluation is now considered suboptimal. Currently, low-dose CT, PET/CT, or whole-body MRI are considered acceptable initial imaging modalities today. The primary advantages of low-dose CT are that it is more sensitive than skeletal survey and has short acquisition time and wide availability. However, CT relies on the presence of trabecular and/or cortical destruction for detection of focal disease [19]. PET/CT can also detect focal bone lesions and has been used for assessment of treatment response and for monitoring, but its sensitivity is lower than that of MRI. Comparatively, whole-body MRI with diffusion weighted imaging is the most sensitive for BMT and allows for the earliest detection of focal disease in the form of cellular infiltration, even before trabecular or cortical destruction [19]. Unfortunately, there remain barriers to whole-body MR's wide implementation into routine clinical practice due to its cost, acquisition time, and challenges with billing and reimbursement [20]. If whole-body MRI is not available, MRI of the spine and pelvis is considered a suitable alternative [19].

When assessing BMT with imaging, the key elements of disease to report are the disease distribution (focal or diffuse), associated soft tissue components, nodal/organ involvement, and the presence of fracture or predicted fracture risk. In regard to focal disease, the International Myeloma Working Group has provided guidance on size measurements using thresholds of 5 and 10 mm. For lesions ≤5 mm, documentation of the abnormality is recommended to facilitate continued surveillance, but an exact measurement is not necessary. Lesions that are >5 mm but <10 mm should be interpreted as unequivocally active myeloma, but again an exact measurement is not necessary [19]. Focal lesions larger than 10 mm should be reported with associated measurements. If the imaging findings are instead indicative of diffuse disease, this should be identified in the report. In addition, analysis of burden of disease in the posteromedial aspects of the ilia, which are the most commonly used sites for bone marrow aspiration and biopsy, would be helpful to ensure optimal tissue sampling of the most abnormal area or to suggest an alternate site. Reporting of ADC values is also recommended, but only for lesions where diffusion weighted imaging demonstrates water signal. Radiologists can benefit their referring clinicians and patients by following the structured reporting recommendations provided by the Myeloma Response Assessment and Diagnosis System (MY-RADS), which was created under the guidance of the International Myeloma Working Group and the National Institute for Clinical Excellence in the United Kingdom [19]. Although a similar system has not been specifically devised for other BMT such as leukemia or lymphoma, a similar approach to image analysis and reporting is recommended.

> **Key Point**
> - The use of structured reporting in the setting of myeloma allows for clear and consistent communication between the radiologist and other members of the healthcare team.

10.5 Concluding Remarks

In this review, we have highlighted what clinicians want to know from the imaging of soft tissue, bone, and bone marrow tumors and how the key imaging features influence their diagnosis, staging, and treatment. We have stressed the importance and value of providing a detailed patient history in the imaging report and of explicitly stating the need for referral to an orthopedic oncologist if a sarcoma is suspected. An accurate and quality imaging report that demonstrates investment in the patient's care can elevate the perceived worth of radiologists to the healthcare team.

> **Take Home Messages**
> - Clearly and consistently report the key imaging features that may impact the diagnosis, staging, and treatment of soft tissue, bone, and bone marrow tumors.
> - Provide a detailed patient history regarding the tumor in the imaging report.
> - Do not hesitate to recommend referral to an orthopedic oncologist in the final impression of the report if an aggressive tumor is suspected.

References

1. Kransdorf MJ, Murphey MD, Wessell DE, et al. American College of Radiology. ACR Appropriateness Criteria®: soft-tissue masses. 2020. Available at: https://acsearch.acr.org/docs/69434/Narrative/. Accessed 30 Sept 2020.
2. Kransdorf MJ, Murphey MD. Radiologic evaluation of soft-tissue masses: a current perspective. AJR Am J Roentgenol. 2000;175:575–87.

3. Manaster BJ. Soft-tissue masses: optimal imaging protocol and reporting. AJR Am J Roentgenol. 2013;201:505–14.

4. Zhang Y, Zhu Y, Shi X, et al. Soft tissue sarcomas: preoperative predictive histopathological grading based on radiomics of MRI. Acad Radiol. 2019;26(9):1262–8.

5. Murphey MD, McRae GA, Fanburg-Smith JC, Temple HT, Levine AM, Aboulafia AJ. Imaging of soft-tissue myxoma with emphasis on CT and MR and comparison of radiologic and pathologic findings. Radiology. 2002;225(1):215–24.

6. Murphey MD, Acara LK, Fanburg-Smith JC. From the archives of the AFIP: imaging of musculoskeletal liposarcoma with radiologic-pathologic correlation. Radiographics. 2005;25(5):1371–95.

7. Baheti AD, Tirumani SH, Rosenthal MH, et al. Myxoid soft-tissue neoplasms: comprehensive update of the taxonomy and MRI features. AJR Am J Roentgenol. 2015;204(2):374–85.

8. Peeken JC, Spraker MB, Knebel C, et al. Tumor grading of soft tissue sarcomas using MRI-based radiomics. EBioMedicine. 2019;48:332–40.

9. Vallières M, Freeman CR, Skamene SR, El Naqa I. A radiomics model from joint FDGPET and MRI texture features for the prediction of lung metastases in soft-tissue sarcomas of the extremities. Phys Med Biol. 2015;60:5471–96.

10. Spraker MB, Wootton LS, Hippe DS, et al. MRI radiomic features are independently associated with overall survival in soft tissue sarcoma. Adv Radiat Oncol. 2019;4:413–21.

11. Crombé A, Périer C, Kind M, et al. T2-based MRI Delta-radiomics improve response prediction in soft-tissue sarcomas treated by neoadjuvant chemotherapy. J Magn Reson Imaging. 2019;50:497–510.

12. Gilbert NF, Cannon CP, Lin PP, Lewis VO. Soft-tissue sarcoma. J Am Acad Orthop Surg. 2009;17(1):40–7.

13. Amin MB, Edge S, Greene F, et al., editors. AJCC cancer staging manual. 8th ed. Cham: Springer International Publishing; 2017.

14. Cates JMM. The AJCC 8th edition staging system for soft tissue sarcoma of the extremities or trunk: a cohort study of the SEER database. J Natl Compr Cancer Netw. 2018;16(2):144–52.

15. Spolverato G, Callegaro D, Gronchi A. Defining which patients are at high risk for recurrence of soft tissue sarcoma. Curr Treat Options Oncol. 2020;21(56):1–18.

Bone Tumors

16. Casali PG, Bielack S, Abecassis N, et al. Bone sarcomas: ESMO-PaedCan-EURACAN clinical practice guidelines for diagnosis, treatment and follow-up. Ann Oncol. 2018;29(Suppl 4):iv79–95.

17. Compton ML, Cates JMM. Evidence-based tumor staging of skeletal chondrosarcoma. Am J Surg Pathol. 2020;44(1):111–9.

18. Cates JMM. Simple staging system for osteosarcoma performs equivalently to the AJCC and MSTS systems. J Orthop Res. 2018;36(10):2802–8.

19. Messiou C, Hillengass J, Delorme S, et al. Guidelines for acquisition, interpretation, and reporting of whole-body MRI in myeloma: myeloma response assessment and diagnosis system (MY-RADS). Radiology. 2019;291(1):5–13.

20. Feldhaus JM, Garner HW, Wessell DE. Society of skeletal radiology member utilization and performance of whole-body MRI in adults. Skelet Radiol. 2020;49(11):1731–6.

Arthritis

11

Andrew J. Grainger and Charles S. Resnik

Learning Objectives
- To understand the most common arthritides seen in clinical practice and have an overview of their pathophysiology.
- To develop a logical and systematic approach to the assessment of arthritides using conventional radiographs.
- To understand the characteristic features of common arthritides seen on imaging.
- To recognize the role advanced imaging modalities play in the diagnosis and management of common arthritides.

11.1 Overview of Arthritis

A wide variety of conditions affect the joints of the body, but for this chapter we will focus on the most common conditions seen and their imaging features. We will look at arthritides in three main categories: osteoarthritis, inflammatory arthritides (rheumatoid arthritis and spondyloarthritis), and crystal arthritides.

11.1.1 Osteoarthritis

Osteoarthritis (OA) is the most common arthritis encountered and is seen in the majority of people at some stage

A. J. Grainger (✉)
Department of Radiology, Cambridge University Hospital, Cambridge, UK
e-mail: andrewgrainger@nhs.net

C. S. Resnik
Department of Diagnostic Radiology, University of Maryland School of Medicine, Baltimore, MD, USA
e-mail: cresnik@umm.edu

in their lives. Despite being so common, its etiology is still poorly understood and the subject of considerable research, much of it involving imaging studies. The disease can be considered to arise primarily from a failure of the normal transmission of forces across a joint. This may come about through trauma to bones or ligaments or through altered ability of the tissues of the joint to transmit forces, for instance, alterations in the composition of cartilage in ochronosis or ligaments in some collagen disorders. However, OA has a complex etiology with multiple factors playing a part including genetics, race and ethnicity, obesity, age, and gender.

The term primary generalized OA refers to OA when it occurs without an apparent underlying cause. This is more common in women and carries a genetic predisposition. It most typically affects the hands, thumb bases, hips, knees, and first metatarsophalangeal joints in the feet. In contrast, secondary OA describes cases where an underlying cause exists. A wide variety of causes are recognized, but the radiological features at any joint may be identical to those of primary generalized OA (Table 11.1). It is important to realize that OA can co-exist with other forms of joint disease.

Table 11.1 Causes of secondary osteoarthritis [1]

Trauma	Acute
	Chronic repetitive
Systemic/metabolic	Hemochromatosis
	Wilson's disease
	Ochronosis
Endocrine	Acromegaly
	Hypothyroidism
	Hyperparathyroidism
	Diabetes mellitus
Other forms of arthritis	Calcium pyrophosphate deposition disease
	Gout
	Rheumatoid arthritis
Other	Paget's disease
	Bone and joint dysplasia

Erosive OA represents a subset of OA characterized by prominent inflammatory features including destructive joint changes in the form of osseous erosions. While large joint disease may rarely be seen with this form of OA, it typical affects only the distal and proximal interphalangeal joints of the hands. There may be clues to the inflammatory nature of the disease from the clinical assessment, but the diagnosis of erosive OA is based on the imaging findings. Erosive OA primarily occurs in postmenopausal women.

11.1.2 Rheumatoid Arthritis

Rheumatoid arthritis (RA) is an example of an inflammatory arthritis associated with joint inflammation characterized by synovitis. Extra-articular inflammation, including tenosynovitis, soft tissue (rheumatoid) nodules, and multisystem involvement outside the musculoskeletal system (such as rheumatoid lung disease) may also be seen. This autoimmune condition is mediated through inflammatory pathways, and its treatment has changed greatly in recent years with the advent of disease-modifying anti-rheumatic drugs (DMARDs) based on biologic therapies. These can induce remission and prevent the severe joint destruction that was commonly seen prior to their introduction. To achieve such remission, DMARDs need to be introduced early in the treatment pathway before structural joint damage occurs. This has led to an increased role for advanced imaging modalities such as MRI and ultrasound, both for earlier diagnosis and for monitoring the response to treatment.

Joint damage, including cartilage loss and osseous erosion, is thought to be mediated through synovitis; there is strong evidence that synovitis is a predictor of future joint structural damage [2]. The diagnosis of RA is based on clinical findings, along with laboratory assessment (inflammatory and immunological markers) and radiological assessment. It is recognized that both ultrasound and MRI are more sensitive than clinical assessment for identifying synovitis [3].

RA is more common in women and typically begins in the small joints in the hands and feet, usually with a fairly symmetrical distribution. Large joint involvement is seen later in the disease.

11.1.3 Spondyloarthritis

The spondyloarthritides are a group of inflammatory arthritides which share certain common features. One of the most characteristic features of these diseases is the presence of inflammatory change at entheses, the sites where tendons and ligaments insert on to the bone. These diseases are also characterized by:

- Axial skeleton and typically sacroiliac joint (SIJ) involvement (sacroiliitis).
- Presence of the human leukocyte antigen B27 (HLA-B27), although the presence of this histocompatibility antigen is not a pre-requisite for diagnosis of these conditions.
- Absence of serum rheumatoid factor.

Like RA, these diseases are increasingly treated aggressively with biological DMARDs to achieve remission and prevent structural joint damage. This means early diagnosis is important, and given the propensity for spinal and SIJ involvement, this frequently includes MRI. While synovitis is a feature of these diseases, osteitis identified as bone edema-like signal is typically the earliest imaging finding. Diagnosis of spondyloarthritis is based on specific criteria, and MRI now forms a component of the diagnostic pathway as outlined in the Assessment of Spondyloarthritis International Society (ASAS) classification criteria for axial spondyloarthritis [4] (Table 11.2).

Four diseases are generally considered under the heading of spondyloarthritis (SpA). However, it is important to recognize that it is often not possible to classify a patient as having a specific type of SpA despite clear clinical criteria for a diagnosis of SpA being present. These patients form a large subgroup referred to as "undifferentiated spondyloarthritis." Some of these patients may go on to develop more specific features allowing them to be reclassified.

11.1.3.1 Ankylosing Spondylitis (AS)

Ankylosing spondylitis is a multisystem disease which characteristically affects the axial skeleton and typically presents with inflammatory back pain. Sacroiliitis is a characteristic feature of the disease and is typically bilateral and symmetrical. This is frequently seen in association with spinal involvement. Peripheral joint involvement is present in

Table 11.2 Criteria for the diagnosis of spondyloarthritis (SpA) [4]

Imaging pathway	Clinical pathway	SpA features
Sacroiliitis on imaging	HLA B27 positive	– Inflammatory back pain
– MRI or radiograph		– Dactylitis
		– Enthesitis
One or more SpA features – From column 3	Two or more other SpA features – From column 3	– Family history of SpA
		– Good NSAID response
		– Uveitis
		– Psoriasis
		– IBD
		– HLA B27 positive
		– Elevated CRP

up to 30% of patients; the hip followed by the shoulder is the most common peripheral joint involved [5]. Unchecked, the disease will progress to joint ankylosis and spinal fusion.

11.1.3.2 Psoriatic Arthritis (PsA)

There is a complicated relationship between cutaneous psoriasis and arthritis, including an increased incidence of seropositive RA in patients with psoriasis. However, the association is strongest if RA is not considered, at which point 20% of patients with seronegative arthritis will be found to have psoriasis [6]. In patients with psoriasis, the presence of nail involvement is a significant risk factor for developing arthritis.

Five typical subgroups of patients with PsA can be identified:

- An erosive arthritis affecting distal interphalangeal (DIP) joints in an asymmetrical distribution often seen with dactylitis
- An arthritis which is similar to RA
- An oligoarthritis involving any of the synovial joints with an asymmetrical distribution
- A pattern of disease involving the axial skeleton and large joints resembling AS
- A severely destructive arthritis typically involving the small joints of the hands and feet (arthritis mutilans)

11.1.3.3 Reactive Arthritis

Reactive arthritis is typically triggered by an extra-articular infection (most commonly gastrointestinal or genitourinary) and usually manifests as an asymmetrical arthritis involving joints of the lower limb and the axial skeleton. Appearances resemble those of PsA, except axial involvement is less common and upper limb involvement is extremely unusual. It is classically associated with soft tissue inflammation in the form of urethritis, conjunctivitis, and mucocutaneous lesions in the oropharynx, tongue, glans penis, and skin.

11.1.3.4 Enteropathy-Associated Arthritis

Arthritis is associated with inflammatory bowel disorders, most commonly Crohn's disease and less frequently ulcerative colitis. It occurs infrequently in other inflammatory gastrointestinal disorders such as celiac disease and primary biliary cirrhosis. Typically, the associated arthritis closely resembles AS, with sacroiliitis and spinal involvement. Peripheral joint disease is uncommon, although patients may experience transient arthritis comprising joint effusion and synovitis in the peripheral joints. These often occur during flare up of the inflammatory bowel disease.

11.1.4 Metabolic Joint Disease

Gout and calcium pyrophosphate dihydrate-related arthritis are both associated with the deposition of crystals in and around joints.

11.1.4.1 Gout

Gout is a condition associated with the buildup of uric acid in the body (hyperuricemia) that gives rise to intense joint inflammation with the potential to progress to an extremely destructive arthritis. Although any synovial joint can be involved, the disease has a particular propensity for the first metatarsophalangeal joints. The sodium urate crystals formed in a state of hyperuricemia characteristically deposit in the synovial membranes, joint fluid, tendon sheaths, bursae, subcutaneous tissues, and kidneys. Asymptomatic hyperuricemia is reported in around 19% of individuals in the USA and UK with only a small percentage of these going on to develop clinical gout [7]. Uric acid is an end product of purine metabolism, and hyperuricemia results from reduced renal excretion of urate or, less commonly, its increased production. A complicated interaction of multiple factors determines a person's propensity for developing gout, including genetic, racial, and dietary characteristics. Comorbidities also predispose to gout, including renal impairment and failure, cardiovascular disease, obesity, and diabetes. Gout is much more common in men than women, although the incidence among women increases following menopause. Gout usually initially presents as an acute intermittent inflammatory arthritis giving rise to severe pain, erythema, and swelling of the affected joint. Similar presentations may be seen in tendon sheaths and bursae. Aspiration of the affected joint will allow the identification of urate crystals under the microscope. This is frequently undertaken in the workup of this disease as septic arthritis is an important differential diagnosis. Between episodes of acute gout attacks (which may be triggered by trauma or other factors), the patient usually becomes asymptomatic.

Longer-term gout sufferers may go on to develop a chronic arthritis where the symptoms fail to settle between attacks. There is chronic deposition of sodium urate crystals in the joint and soft tissues (including tendons) leading to joint effusion, synovitis, and destructive changes in the form of erosions. Although small joints of the hands and feet are most commonly affected, large joint involvement is frequently seen, particularly in the knees and ankles. A characteristic feature of chronic gout is the development of soft tissue deposits know as tophi presenting as soft tissue masses most commonly seen in the hands and feet and on the extensor surfaces of the elbows and knees. Tendon deposition is also seen with the development of tendon nodules.

11.1.4.2 Calcium Pyrophosphate Dihydrate (CPPD) Deposition Disease

CPPD deposition disease is most commonly seen in the middle aged and elderly. Many people identified as having CPPD crystal deposition in joints will be asymptomatic. Deposition of CPPD crystals occurs in hyaline cartilage, fibrocartilage, synovium, and ligaments. If the crystals are then shed into the joint, an acute attack of inflammatory arthritis which resembles acute gout can develop, known as pseudogout. This is a clinical diagnosis which can be confirmed by identification of the crystals on microscopy in a joint aspirate. A second more chronic pattern of joint disease which resembles OA on imaging is also recognized, although this too can have inflammatory features [8]. Aging forms the main risk factor for CPPD arthritis, but there are associations with metabolic conditions including hemochromatosis, Wilson's disease, hyperparathyroidism, hypomagnesemia, and hypophosphatasia [8].

It is important to recognize that the presence of chondrocalcinosis itself does not imply a diagnosis of CPPD arthropathy and an absence of chondrocalcinosis does not rule out the diagnosis.

11.2 Imaging in Arthritis

11.2.1 Conventional Radiography

Conventional radiographs remain fundamental to the diagnosis of joint disease, and an understanding of the typical appearances of different arthritides on the radiograph is vital to the diagnosis of these conditions. A review of the radiograph requires attention to be paid to:

- The joint space between bones
- The soft tissues around the joint
- The appearance of the bones forming the articulation
- The alignment of the bones at the joint
- The distribution of the disease

11.2.1.1 Joint Space

Joint space narrowing is an important feature of many arthritides, resulting from loss of the radiolucent cartilage which normally provides the gap seen between the bones on the radiograph. It is helpful to identify the pattern of joint space loss, in particular whether it is even across the whole of the joint (symmetrical) or just involves part of the visualized joint space (asymmetrical). Inflammatory arthritides tend to show joint space loss which is uniform across the joint, while OA shows a more uneven pattern of joint space loss (Fig. 11.1).

Just as valuable is the identification of arthritides such as gout and PsA, where joint space is preserved even where joint damage is significant. In some cases, arthritis will lead to ankylosis of the joint and complete loss of joint space. This is a characteristic feature of the spondyloarthritides.

11.2.1.2 Soft Tissues

Soft tissue swelling is an early feature of disease in the inflammatory arthritides and may be due to synovitis, joint effusion, and/or soft tissue edema. Soft tissue swelling is also a feature of gout as a result of tophus formation around the joint. The radiographic appearance of tophi is much more irregular and "lumpy" than the swelling associated with synovitis or effusion that causes capsular distention (Fig. 11.2).

In addition to swelling, calcifications may be observed in the soft tissue around the joint (for instance, in cases of CPPD), with or without the presence of chondrocalcinosis.

11.2.1.3 Bones

A variety of changes may be seen in the bones at articulations affected by arthritis. These include change in bone density (sclerosis or osteopenia), cyst formation, and bone erosion. New bone formation can also occur in the form of osteophyte, enthesophyte, and periosteal reaction.

Osteophytes are the hallmark of OA and represent new bone forming around the site of the cartilage degeneration associated with this disease. Osteophytes are most commonly found at the margins of joints, although central osteophytes occurring within the joint space are also recognized (Fig. 11.3). Enthesophytes are a feature of enthesitis and, in contrast to osteophytes, have a finer wispier appearance. Periosteal new bone (periostitis) may be seen in patients with spondyloarthritis, particularly in association with the peripheral joint disease seen in PsA and reactive arthritis.

Subchondral sclerosis and cyst formation are typical features of OA but may also be seen in association with inflammatory and metabolic arthritides. Cysts are often prominent in patients with CPPD arthropathy (Fig. 11.4).
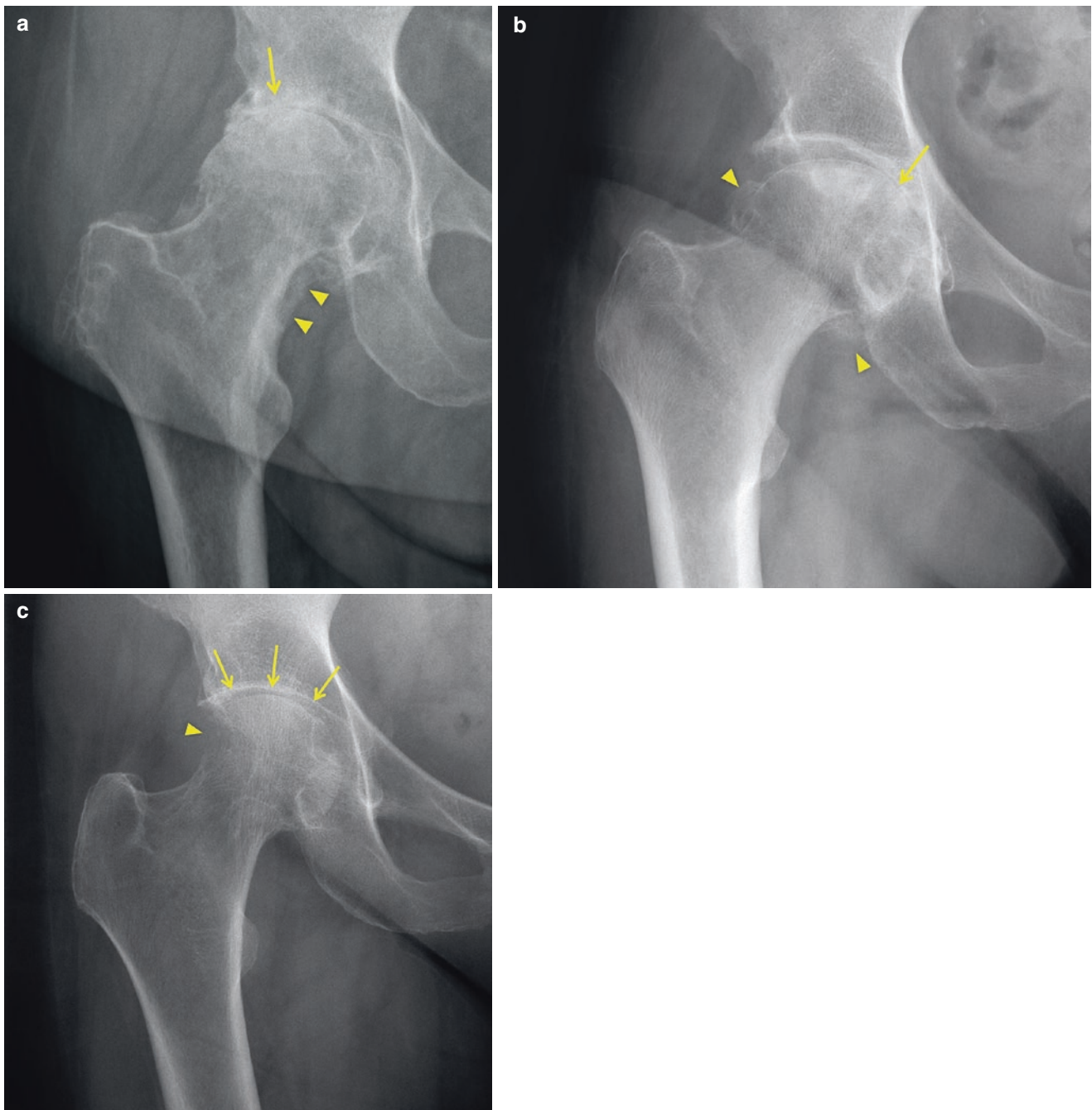
Fig. 11.1 (**a**) Osteoarthritis, showing superior joint space loss associated with subchondral cyst formation and sclerosis (arrow). Note also the bone proliferation along the medial femoral neck, known as buttressing (arrowheads). (**b**) Osteoarthritis, showing medial joint space loss with subchondral sclerosis (arrow). Prominent osteophytes are seen at the margins of the articular cartilage (arrowheads). (**c**) Rheumatoid arthritis, showing more uniform narrowing of joint space (arrows). Note also the absence of subchondral cyst and sclerosis and the large erosion (asterisk)
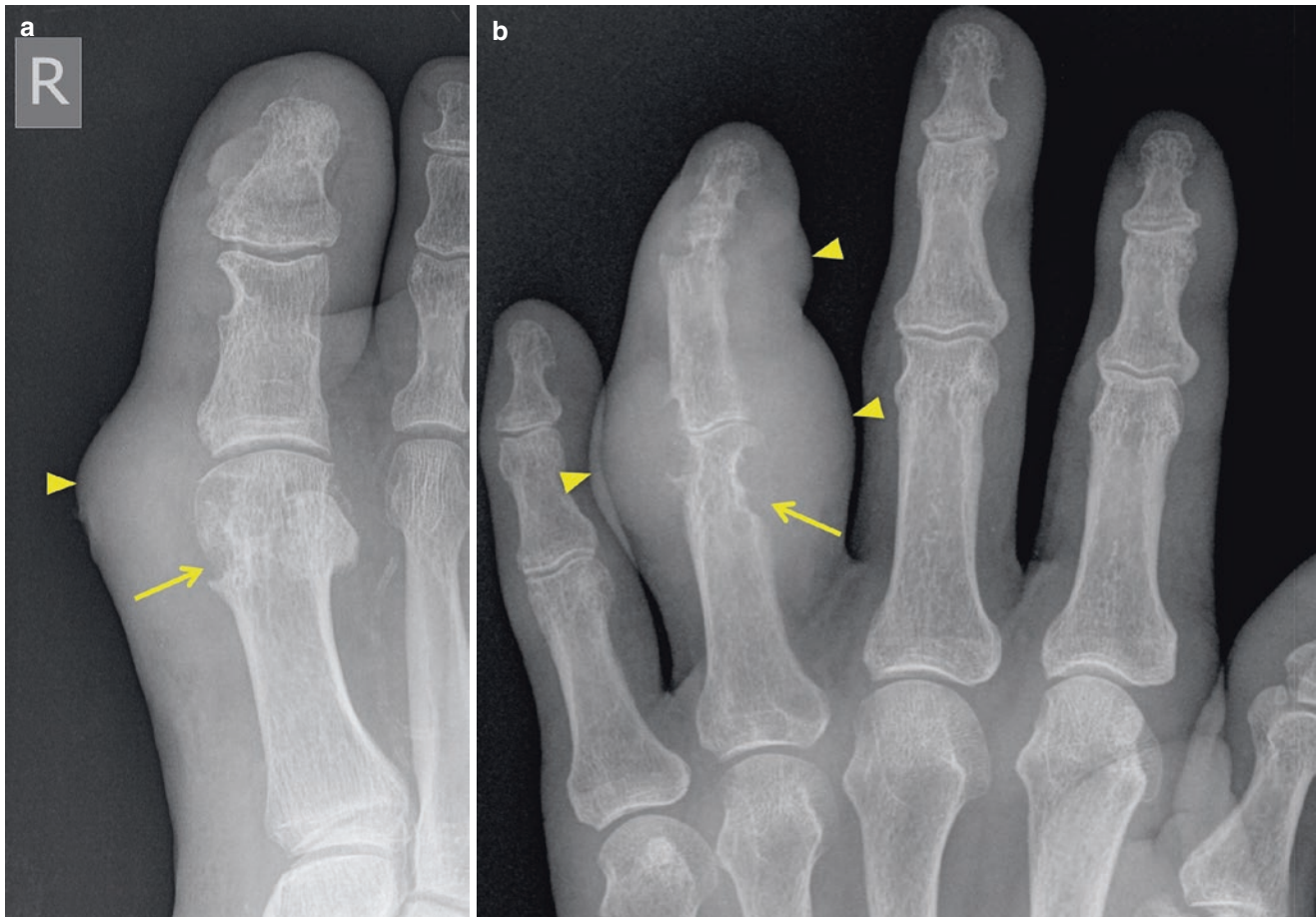
Fig. 11.2 Great toe (**a**) and hand (**b**), showing typical radiographic features of gout. Note the irregular soft tissue swelling (arrowheads) and punched out erosions, some of which occur more remotely from the joint (arrows). Despite the destructive changes, joint spaces are well preserved

Juxta-articular osteopenia is a feature of some arthritides such as RA but can be challenging to identify, particularly if there is extensive joint involvement and if normal joints for comparison are not visible on the radiograph. Gout, spondylarthritis, and OA typically show preservation of bone density.

Bone erosion is a well-recognized feature of the inflammatory arthritides. On conventional radiographs, erosive change can be subtle, and care must be taken not to miss the earliest features of erosion.

11.2.1.4　Joint Alignment

Joint malalignment resulting from arthritis has a variety of causes and usually represents a late feature of the disease. Besides resulting from bone and cartilage loss, joint malalignment may also result from tendon and ligament disruption and dysfunction.

11.2.1.5　Distribution of Joint Disease

When reviewing hand and foot radiographs in a patient with peripheral arthritis, the pattern of joint involvement is an invaluable clue to the underlying nature of the arthritis. Certain arthritides have a predilection for certain joints. Some of the more commonly observed patterns of joint involvement are illustrated in Fig. 11.5.

11.2.2　CT

CT shows similar features in joint disease to conventional radiographs. However, its ability to image bone in fine detail and its cross-sectional and multiplanar capabilities make it more sensitive than radiographs and other cross-sectional imaging techniques for the identification of erosive change. This is particularly true for deep-lying joints with complex 3D anatomy and those joints not aligned to the standard planes viewed in radiography such as the sacroiliac joints (Fig. 11.6). Despite these advantages CT is less commonly used clinically in arthritis imaging, as both MRI and ultrasound are also more sensitive than radiographs for identifying erosive change and offer other advantages in their ability to assess joint disease.
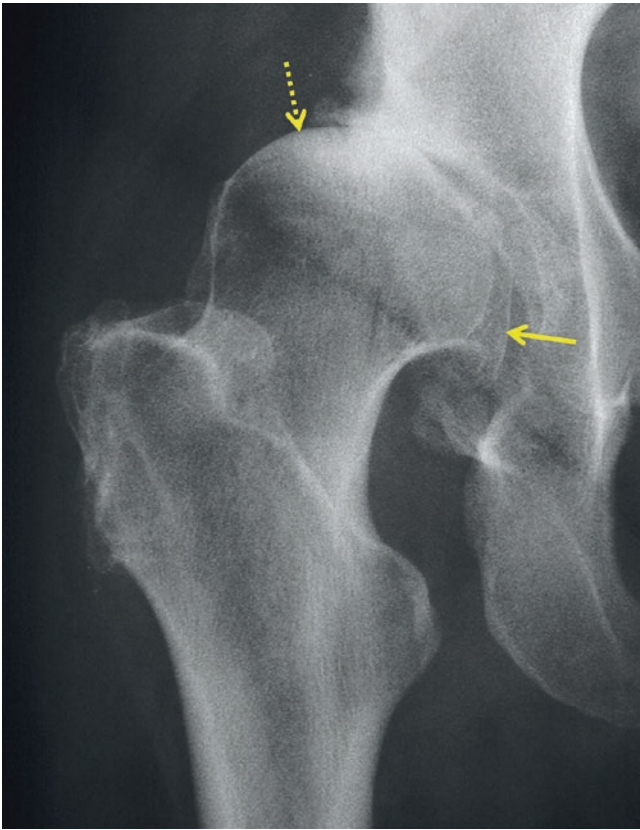
Fig. 11.3 Osteoarthritis of the hip. In addition to the superior joint space loss and subchondral sclerosis, there is central osteophyte (arrow). This is causing lateral subluxation and exposure of the femoral head (dotted arrow)

In recent years, dual energy CT has become increasingly available and has found a particular use in the assessment of patients with gout. The ability of this technique to identify urate deposits in joints and soft tissues with high specificity has made it valuable in clinical practice for diagnosing gout non-invasively [9]. This technique is also able to quantify the volume of urate deposits and therefore shows promise for assessing response to treatment [10].

11.2.3 Ultrasound

The ready availability of ultrasound and its ability to assess multiple joints in a relatively short time frame, along with its dynamic capabilities, ability to guide diagnostic and therapeutic injection/aspiration, and high level of acceptability to patients make it an excellent modality for assessing joint disease [11]. However, ultrasound does have disadvantages:

1. Its assessment of bone is confined to the cortical surface, so while erosions, osteophytes, and enthesophytes are visualized, subchondral cysts and sclerosis and bone inflammation (osteitis) are not demonstrated.
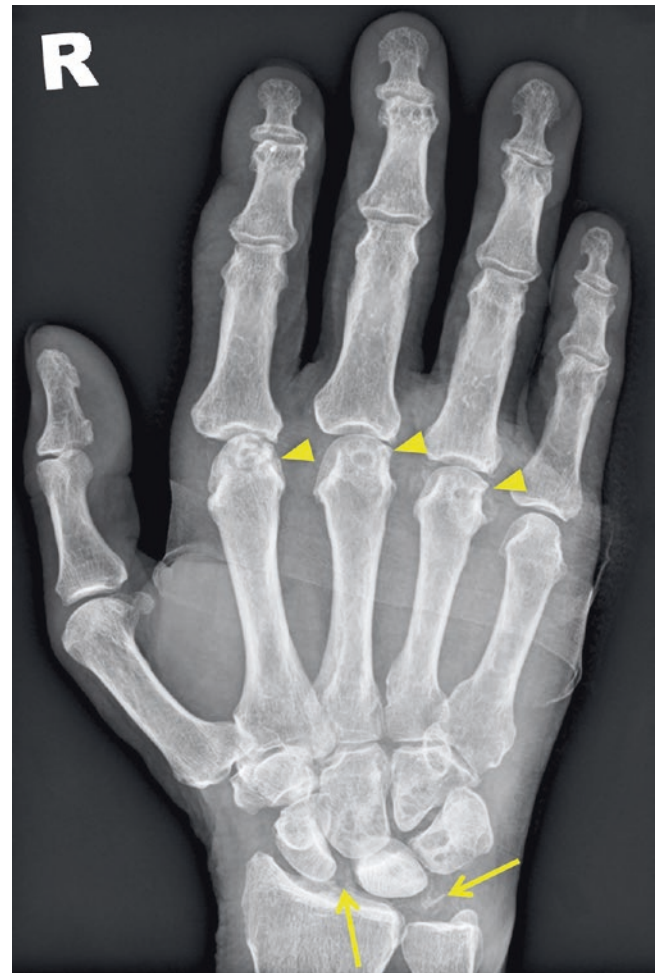
Fig. 11.4 Calcium pyrophosphate crystal arthropathy. In addition to affecting DIP joints, there is MCP (arrowheads) and wrist involvement with prominent cystic change. There is chondrocalcinosis and synovial/ligamentous calcification seen in the proximal wrist joint (arrows). Osteophyte formation is minimal, and the distribution involving MCP joints is typical. Scapholunate dissociation is also evident, a feature of CPPD arthropathy at the wrist

2. Because ultrasound cannot "see" through bone, its ability to assess the interior of a joint is limited to those parts of the joint in the sonographic window, and views of internal joint structures such as articular cartilage and menisci are limited.
3. Deeper joints, such as the sacroiliac joints, allow only very limited assessment, and access to parts of some joints (for instance, parts of some MCP and MTP joints) is limited by the anatomy.

Ultrasound readily identifies features of inflammatory arthritis such as erosion, synovitis, and effusion and can also assess the presence of osteophytes and enthesophytes. It can also be useful for assessing extra-articular disease such as soft tissue rheumatoid nodules, gout tophi, and tendon and tenosynovial disease. While not usually used to assess articu-
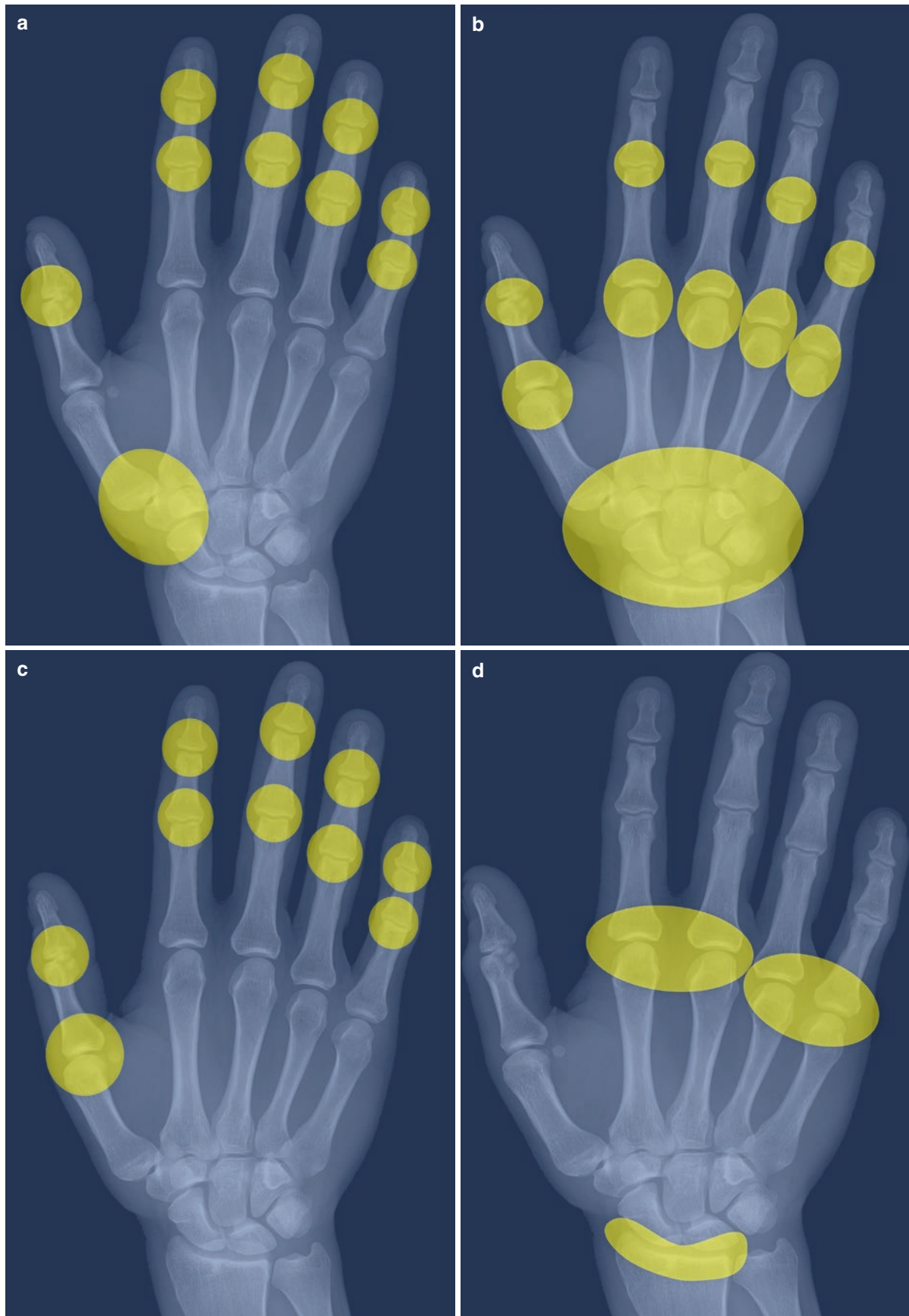
Fig. 11.5 Typical patterns of typical joint involvement in the hand in different arthritides. (**a**) Osteoarthritis, (**b**) rheumatoid arthritis, (**c**) psoriatic arthritis, (**d**) calcium p/yrophosphate deposition arthropathy

Fig. 11.6 Axial CT. Both sacroiliac joints (arrows) show subchondral erosions and sclerosis typical for chronic sacroiliitis
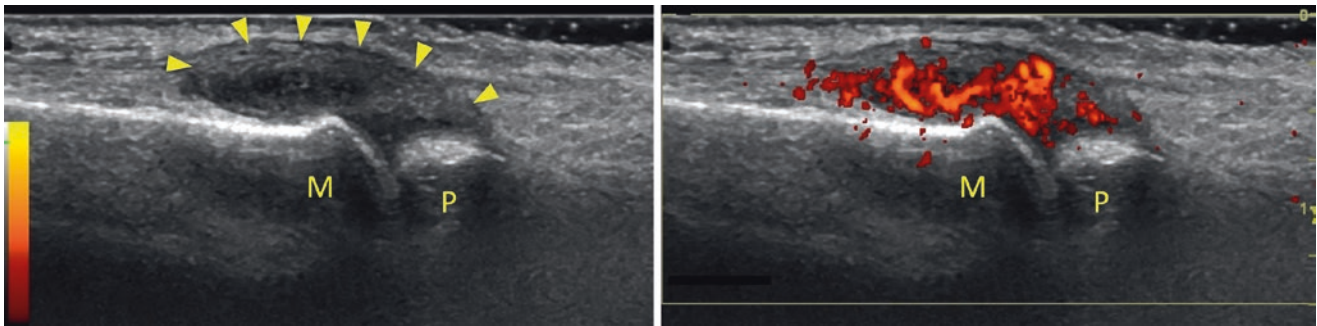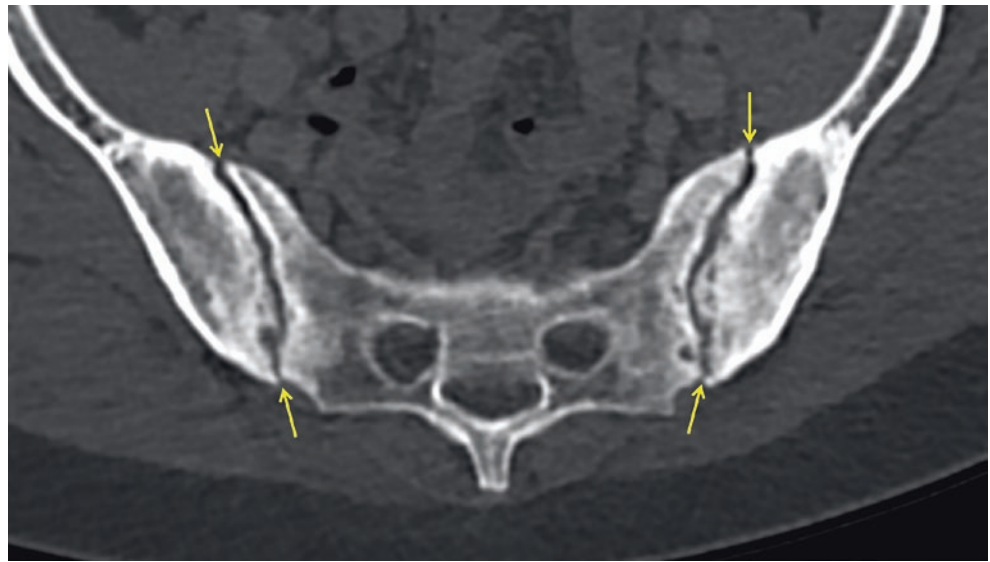
Fig. 11.7 Index metacarpal joint in a patient with synovitis due to rheumatoid arthritis. Longitudinal ultrasound of the dorsum of the joint. M, metacarpal head; P, proximal phalangeal base. The B-mode image on the left demonstrates hypoechoic synovitis in the joint bulging the dorsal joint capsule (arrowheads). The synovitis shows marked vascularity demonstrated on the power Doppler duplex image on the right

lar cartilage in OA and inflammatory arthritides, ultrasound can provide useful information relating to the crystal arthritides, which will be discussed in Sect. 11.3.

11.2.3.1 Synovitis and Effusion

Ultrasound has been shown to be more sensitive than clinical assessment and radiographs for assessing synovitis (soft tissue swelling) and is comparable to MRI [12]. Synovitis appears as hypoechoic intra-articular material that is non-displaceable and may exhibit Doppler signal (Fig. 11.7) [13]. While the degree of Doppler signal detected is variable, its presence, along with the non-compressibility of synovitis, is a useful feature to distinguish synovium from joint fluid on ultrasound. The extent of blood flow in the synovium detected by ultrasound provides a measure of disease activity in the inflammatory arthritides, and several scoring systems have been described [14].

11.2.3.2 Erosion

Erosions are identified on ultrasound as a discontinuity of the bone surface, but it is important that these are identified in two planes to avoid confusion with normal surface contours

[13, 14]. While ultrasound has superior ability to conventional radiographs in assessing the presence of erosions [15], it has disadvantages to other cross-sectional techniques as not all parts of a joint necessarily fall within the sonographic window (for instance, the radial and ulnar aspects of the middle finger metacarpophalangeal joint). This means that MRI is arguably more sensitive to erosive change.

11.2.3.3 Other Bone Changes

Both osteophytes and enthesophytes appear as bone outgrowths on ultrasound. Enthesophytes appear finer compared to the generally coarse nature of osteophytes. However, the distinction is ultimately dependent on the clinical context along with the location of an enthesophyte relative to an enthesis and the presence of other features of enthesitis, such as thickening and low-reflective change in the inserting tendon or ligament, and associated erosive change [13, 14]. Increased Doppler signal can be seen at sites of active enthesitis. Ultrasound does appear more sensitive than radiographs for the detection of osteophytes in the hands and feet [16, 17].

11.2.3.4 Extra-Articular Soft Tissue Features

Tenosynovitis appears as hypoechoic or anechoic thickened tissue with or without fluid in the tendon sheath and is readily identified on ultrasound [13]. Ultrasound can also demonstrate tendon rupture and may even show an osteophyte or bone prominence causing tendon attrition. Enthesitis is associated with thickening of inserting tendons and ligaments along with hypoechogenicity and loss of the normal echotexture. Vascularity may also be identified within and around the inserting soft tissue structure at sites of enthesitis on Doppler imaging.

Rheumatoid nodules appear as hypoechoic mass lesions often with a well-defined hypo- to anechoic center representing necrosis [18]. Gout tophi can appear very poorly defined on ultrasound but are usually hyperechoic, often with a hypoechoic rim (Fig. 11.8). Depending on their composition, especially the presence or absence of calcification, they may also show posterior acoustic shadowing.

11.2.4 MRI

The role of MRI has been increasing in recent years as evidence has grown for its role in the diagnosis and assessment
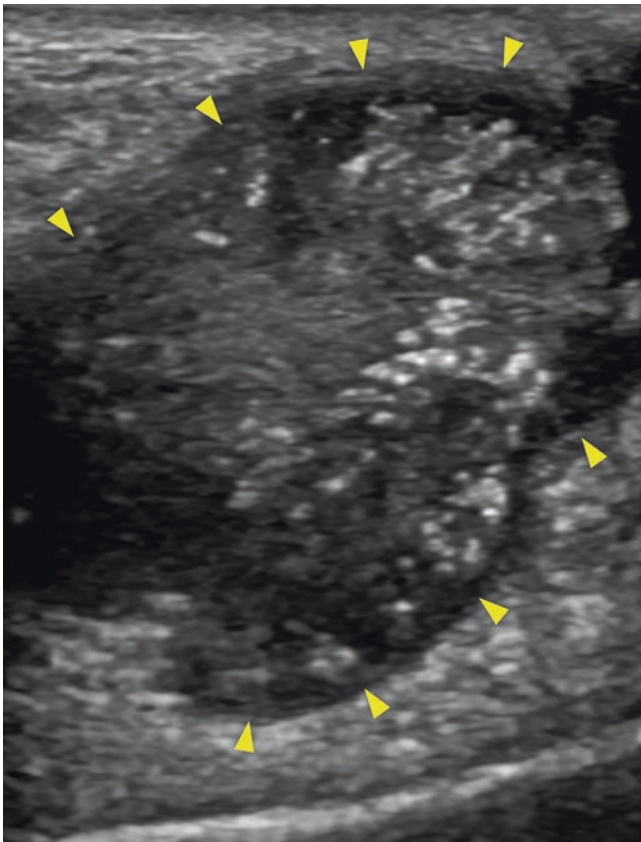
Fig. 11.8 Longitudinal ultrasound showing gout tophus with typical hyperechogenicity and a lower reflective rim. Bright echogenic foci representing crystal aggregates are seen within the tophus

of arthritides, particularly the inflammatory arthritides. As highlighted in Sect. 11.1.3, MRI now plays a fundamental role in the diagnosis and management of patients with suspected axial spondyloarthritis. Like ultrasound, MRI is sensitive to the assessment of synovitis and erosions and can identify osteophytes and extra-articular disease manifestations. However, MRI also enables an assessment of articular cartilage and the subchondral and medullary bone. MRI techniques have been integral to research that has provided a much greater understanding of the pathophysiology of many arthritides. Despite the many advantages of MRI, there are disadvantages such as cost, and MRI may be contraindicated in some patients, for instance, patients with some types of implantable devices. Other recognized weaknesses include:

1. It is very time-consuming to image multiple joints. While multiple joints can be scanned in a single examination with whole-body MRI, this necessitates an acceptance of decreased resolution.
2. To reliably assess synovitis, the administration of intravenous gadolinium contrast is normally required.
3. Patient tolerance can be poor.

The identification of both synovitis and erosions usually requires assessment in two planes, both to confirm location and to ensure that the abnormality is not due to partial volume averaging or a normal anatomical feature. It is often helpful, particularly with small joint disease, to employ 3D sequences with isotropic resolution to permit multiplanar reconstruction. When serial imaging over time is employed, the added ability to reconstruct also makes it easier to compare timepoints if imaging has not been acquired in precisely the same plane.

11.2.4.1 Synovitis

Synovitis on MRI is defined by the Outcome Measures in Rheumatology (OMERACT) as an area in the synovial compartment that shows above normal post-gadolinium enhancement of a thickness greater than the width of normal synovium [19]. This recognizes that normal synovium may show some enhancement and indeed implies that synovium may be seen in a normal joint, but in practice the distinction between synovium and synovitis is rarely difficult [20]. While the use of gadolinium complicates the examination, current thinking is that gadolinium contrast is required, particularly for distinguishing synovitis from effusion. In addition, the rate of gadolinium uptake by the synovium can also provide useful information as it relates to disease activity in both inflammatory arthritides and OA and may even play a role in distinguishing between different types of arthritis [21–24]. However, research into imaging techniques which allow accurate assessment of synovitis without the use of contrast medium is still ongoing.

11.2.4.2 Erosion and Structural Bone Changes

Erosions are readily shown on MRI as sharply marginated bone lesions visible in at least two planes with a cortical break seen in at least one plane [19]. The OMERACT definition also specifies that the erosion shows "typical signal characteristics," which in practice usually means a loss of the normal high signal from the marrow on T1-weighted imaging. Enhancing synovium will be frequently seen in the erosion on post-gadolinium imaging. MRI is sensitive to erosion detection but may identify erosion like lesions in normal control subjects, especially in older patients.

Osteophytes are generally well demonstrated on MRI, and in the hand MRI has been shown to be more sensitive to their detection than conventional radiographs [25]. Unlike ultrasound, MRI is also able to detect osteophytes which occur in the central portions of the articular space and are associated with severe cartilage damage (central osteophyte).

The thin and delicate nature of enthesophytes and syndesmophytes, frequently occurring without the presence of high T1 signal bone marrow, can make MRI relatively insensitive to their presence, particularly because they are usually seen in association with tendon and ligament and cortical bone, all of which also appear low signal on conventional MRI sequences.

11.2.4.3 Bone Marrow Changes

Edema-like signal in the bone marrow is a feature of OA and inflammatory arthritis and typically appears as high T2 signal on fat-suppressed imaging (Fig. 11.9). In RA and spondyloarthritis, this appearance represents an inflammatory
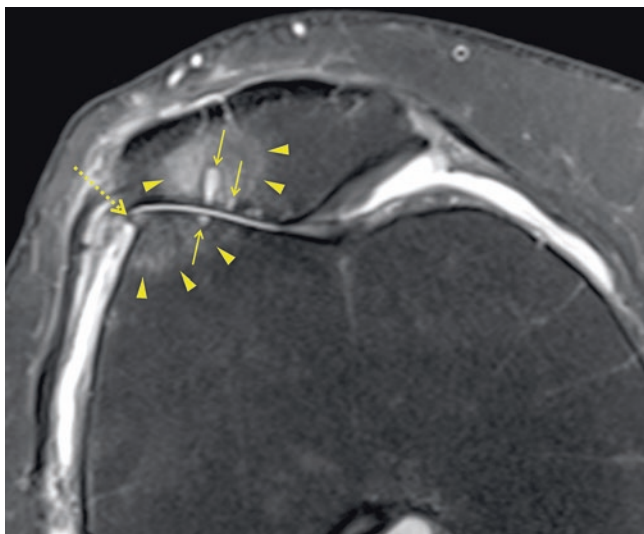
Fig. 11.9 Patellofemoral osteoarthritis. Axial intermediate weighted MRI with fat suppression. There is full-thickness cartilage loss on both sides of the lateral patellofemoral joint associated with subchondral bone marrow lesions, showing an edema pattern (arrowheads) surrounding subchondral cyst-like lesions (arrows). A small osteophyte is also seen (dotted arrow)

process within the bone (osteitis). However, it is evident that the nature of these lesions in OA is not the same, although the actual underlying pathophysiology remains poorly understood and a topic of ongoing research. Subchondral cysts are also demonstrated by MRI in OA (Fig. 11.9), corresponding to the cysts described on conventional radiographs. However, even these may not be all that they seem since studies show they frequently demonstrate full or partial contrast enhancement, which would not be expected with pure fluid-filled cysts [26].

11.2.4.4 Articular Cartilage

The ability of MRI to directly image articular cartilage and demonstrate cartilage loss and cartilage defects is one of the great advantages of this modality over other imaging techniques. Cartilage visualization requires visual contrast between the cartilage and underlying bone and between the cartilage and overlying joint fluid. A variety of sequences may be employed to achieve this, including both gradient echo and fast spin-echo techniques. An early advantage of gradient echo (GRE) imaging for articular cartilage visualization was the ability to undertake 3D sequences with high-resolution thin slices. In recent years, the advent of 3D fast spin-echo (FSE) sequences has allowed optimized visual contrast from spin-echo sequences in addition to thin slices similar to GRE imaging. In clinical practice, FSE proton-density-weighted images with fat suppression provide accurate depiction of the articular cartilage. Imaging techniques which provide information about cartilage composition have now become available and continue to be an area of research. The object of these sequences is to identify compositional changes in cartilage at a stage before cartilage damage becomes apparent in the form of morphological change. These techniques, which include T2 mapping, T1 rho imaging, delayed gadolinium enhanced imaging (DGEMRIC), sodium imaging, and magnetization transfer contrast-based techniques, are currently primarily used in the research environment and are beyond the scope of this chapter.

11.2.4.5 Soft Tissue Features

Like ultrasound, MRI is able to identify tendon and ligament abnormalities associated with arthropathy, including tendon rupture, tenosynovitis, and changes within tendons and ligaments in association with enthesitis. In cases of enthesitis, thickening of the inserting tendon with increased intrasubstance signal on short and long TE sequences becomes apparent.

Tophaceous gout deposits are also shown with MRI, although their signal characteristics are dependent on their composition, including the degree of calcification. The majority of tophi are isointense to muscle on T1 imaging and intermediate to low signal on proton density and T2 imaging. Rheumatoid nodules are seen on MRI with variable and nonspecific signal characteristics.

Key Point

- Conventional radiographs remain fundamental to the imaging workup of patients with arthritis and provide valuable information relating to the assessment of joint space, periarticular soft tissues, bone (including erosions and osteophytes), joint alignment, and the distribution of the arthritis. However, these changes often represent late and irreversible features of the disease. Because of this, more advanced imaging modalities are increasingly used in the investigation of joint disease. In particular, ultrasound and MRI allow sensitive assessment of synovitis and erosions, with MRI also able to identify bone marrow changes including osteitis along with articular cartilage changes.

11.3 Imaging Findings in Specific Arthritides

11.3.1 Osteoarthritis

11.3.1.1 Radiographic Appearances

OA shows very characteristic features on conventional radiographs regardless of the joint affected. However, it should be remembered that the severity of the patient's symptoms correlates poorly with the extent of radiographic change in the joint. Also, OA frequently coexists with other arthritides, and features of more than one type of arthritis may be seen. In cases of OA occurring secondary to trauma, features of the injury may be apparent.

- *Joint space*: Cartilage thinning and therefore joint space loss are a feature of OA. Typically, this occurs in an asymmetric pattern across the joint leading to uneven areas of joint space loss. This is a helpful discriminator from other causes of arthropathy. For instance, in the knee, loss of joint space in one compartment, most commonly the medial femorotibial, will often predominate, and in the hip, joint space loss will often be limited to the superior or superolateral portion (Fig. 11.1a). Generally, the degree of joint space loss relates to the severity of other changes seen.
- *Soft tissues*: Synovitis, giving rise to soft tissue swelling, is variably seen in OA. In the finger joints, clinically apparent nodules may be due solely to prominent osteophytes, but focal synovial/capsular hyperplasia may accentuate the soft tissue prominence.
- *Bones*: Osteophytes are a key feature of OA and represent new bone generally formed at the joint margins at the edge of the cartilage. Central osteophytes developing in the subchondral bone are a less common feature of the

disease. When present, central osteophytes can contribute to joint malalignment (Fig. 11.3). In the hip, a particularly characteristic feature of OA is the development of osseous hypertrophy along the inferomedial femoral neck, known as buttressing (Fig. 11.1a).

Additional features of OA are subchondral cyst formation and sclerosis. These changes may progress to subchondral collapse and remodeling.

- *Alignment*: Malalignment of joints is typical in OA, arising from focal cartilage loss, subchondral collapse, and ligamentous dysfunction. In the elderly, reduced proprioception and muscle tone are also thought to be important factors. At the knee, joint space narrowing predominating in the medial femorotibial compartment may lead to varus deformity.
- *Joint distribution*: In primary OA of the hands, a distal pattern involving DIP and PIP joints is typical. In the wrist, OA is usually confined to a "trapeziocentric" distribution involving the scaphotrapeziotrapezoid (STT) joint and thumb carpometacarpal joint. Large joint involvement typically involves the hips and knees, while in the feet, the first MTP joint is typically affected. Bilateral OA may be symmetrical or asymmetrical.

Erosive OA

Erosive OA is usually confined to the hands with a similar distribution to the pattern of disease seen in generalized primary OA. While marginal erosions may occur, central erosions in the subchondral bone are characteristic, giving rise to a "seagull wing" pattern of erosion (Fig. 11.10). Ankylosis may eventually occur, a distinguishing feature from non-erosive OA.

Osteoarthritis in the Spine

OA (degenerative disease) of the spine typically occurs in the cervical and lumbar regions and is associated with disk degeneration (evident as loss of disk height) and prominent osteophyte formation. The vertebral endplate will show irregularity and sclerosis with advancing disease. Typically, the facet joints (synovial joints) are also involved. OA changes in the spine lead to ligamentous laxity and intervertebral subluxation in the form of anterior or posterior subluxation of a vertebra on its more caudal neighbor (antero- and retrolisthesis).

11.3.1.2 Advanced Imaging

In clinical practice, imaging of OA is usually confined to conventional radiography. However, osteophytes, synovitis, and joint effusion are readily seen on ultrasound and MRI. MRI also offers additional advantages in being able to directly assess the articular cartilage and visualize the subchondral bone (Fig. 11.9). In addition to subchondral cysts, MRI frequently identifies edema-like signal in the subchondral bone. This does not represent true edema, and such foci are often referred to simply as bone marrow lesions.
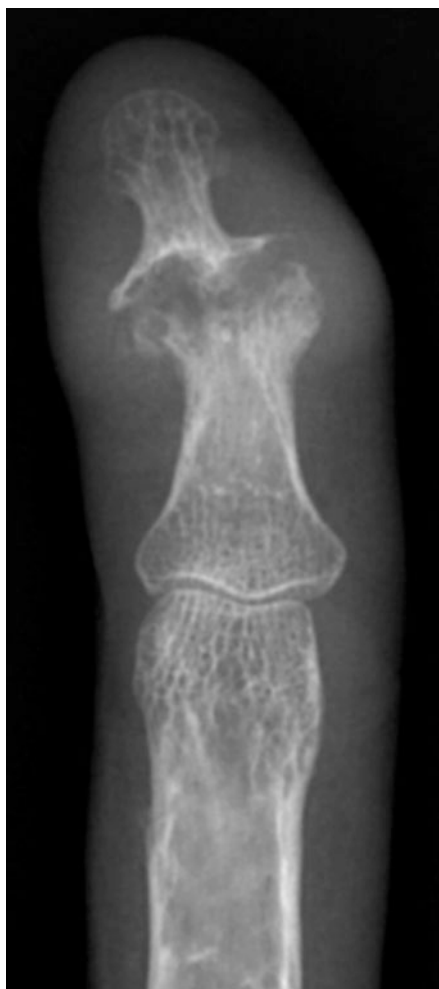
Fig. 11.10 Typical central erosive change with seagull configuration to the distal phalangeal base in a patient with erosive osteoarthritis

Key Point
- Key radiographic features of OA are uneven (asymmetric) joint space loss, osteophytes, and subchondral bone changes. Involvement in the hands and wrists is typically seen at DIP and PIP joints and at the thumb base. Erosive OA is associated with central joint erosion.

11.3.2 Rheumatoid Arthritis

11.3.2.1 Radiographic Appearances

- *Joint space*: Joint space narrowing in RA tends to be more uniform than in OA as cartilage loss is evenly spread across the joint (Fig. 11.1c). It should be noted that joint space loss does not always precede bone erosion.
- *Soft tissues*: Soft tissue swelling at joints is an early feature of rheumatoid arthritis. At MCP and PIP joints in the hands, this is seen as smooth fusiform swelling about the joints. Swelling as a result of effusion and/or synovitis may produce a thickened suprapatellar stripe at the knee or displaced fat pads at the elbow.
- *Bones*: Another early feature of RA is the development of periarticular osteopenia (Fig. 11.11). However, its detection can be very subjective, particularly where multiple joints are involved and there are no normal joints for comparison.

  The erosions seen in RA are typically marginal in location, occurring at the edge of the joint where intra-capsular bone is unprotected by overlying cartilage, the so-called bare area. Erosions are more commonly seen in the small joints of the hands, wrists, and feet rather than large joints, and early sites of erosion are the radial side of the metacarpal heads in the hands (especially on the index and middle metacarpals) and the ulnar aspect of the wrists, characteristically the ulnar styloid process (Fig. 11.11). Involvement in the foot is often seen first on the lateral aspect of the fifth metatarsal head. The earliest evidence of erosion is seen as subtle discontinuities in the cortex of the bone with underlying osteopenia, before larger areas of bone destruction become apparent.

  Osteophytes and enthesophytes are not features of RA.
- *Alignment*: Joint malalignment occurs as a result of tendon and ligament dysfunction and erosive change. Ulnar deviation of the fingers at the MCP joints and radial deviation at the wrist are characteristic. In the fingers, swan neck (flexion at the DIP and extension at the PIP) and boutonnière (extension at the DIP and flexion at the PIP) deformities are also characteristic.
- *Joint distribution*: RA typically begins in the peripheral joints, usually the MCP and PIP joints, the wrists, and the MTP joints, with a predominantly symmetrical left/right distribution. This more proximal distribution in the hands and wrists with sparing of the DIP joints (Fig. 11.5b) is a useful distinguishing feature compared to OA and PsA. Large joint involvement is a later feature of RA.

11.3.2.2 Advanced Imaging

Many of the radiographic features of RA, such as erosion and joint space loss, constitute structural changes to the joint which are largely irreversible. Effective therapy needs to be commenced prior to these occurring, and the use of advanced imaging modalities to detect disease earlier is now commonplace.

Both ultrasound and MRI are routinely used to detect subclinical synovitis in the early stages of RA and to monitor its response to therapy (Figs. 11.7 and 11.12). Both modalities also detect erosive changes and extra-articular features of the disease, such as tenosynovitis and rheumatoid nodules (Fig. 11.12). Unique to MRI is its ability to assess the bone marrow and identify osteitis. The presence of osteitis is strongly predictive of the development of erosions [27].

Fig. 11.11 Dorsopalmar radiograph of both hands in a patient with rheumatoid arthritis. There is typical involvement of the MCP joints with joint space narrowing and marginal erosions, most markedly seen on the radial side of the metacarpal heads (arrows). Subluxation is evident at the index MCP joints. Note erosions also seen at the ulnar styloid processes (arrowheads). Periarticular osteopenia is seen at several sites, for instance, at the fifth metacarpal bases (dotted arrows)
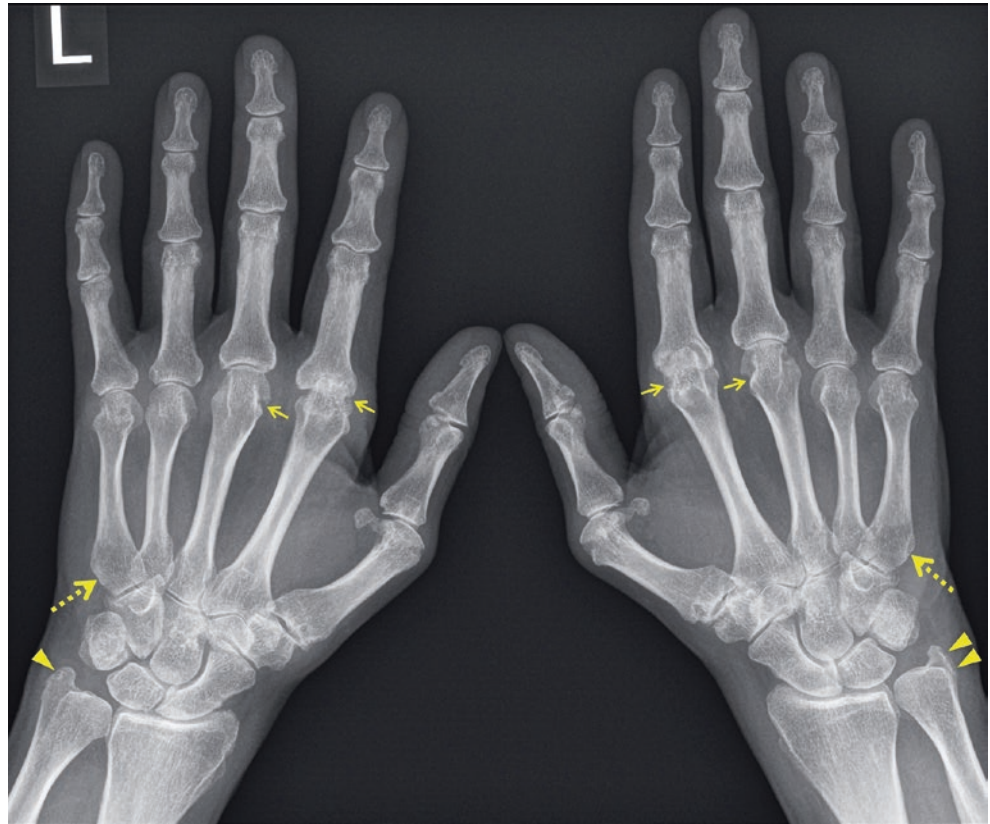
Fig. 11.12 Axial MPR of 3D fat-suppressed spoiled gradient echo (SPGR) MRI post-gadolinium, just proximal to MCP joints in a patient with rheumatoid arthritis. There is extensive enhancing synovitis seen around the metacarpal heads (arrows) associated with erosion in the ring finger metacarpal head (arrowhead). Note also enhancing tenosynovitis around the ring finger flexor and middle finger extensor tendons (dashed arrows)
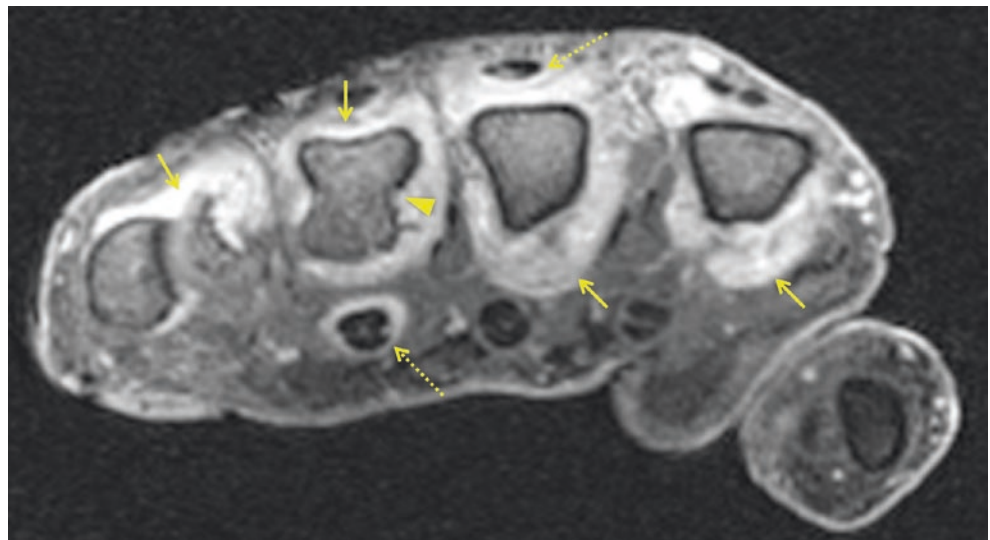
Key Point

- The radiographic features of RA are characterized by marginal erosions and joint space narrowing, with involvement typically seen at the PIP, MCP, and wrist joints. These features are relatively late findings in the disease process, and increasingly MRI and ultrasound are used to detect early abnormalities, including synovitis and osteitis. Both modalities detect erosions with higher sensitivity than radiographs.

11.3.3 Spondyloarthritides

While PsA and reactive arthritis typically involve the small joints of the hands and feet, AS more usually involves the large peripheral joints. However, all of the spondyloarthritides are characterized by frequent axial involvement of the spine and sacroiliac joints. These conditions also involve enthesis sites throughout the body.

11.3.3.1 Radiographic Appearances

- *Joint space*: Joint space loss is a common feature of SpA and is characteristically pan-articular as with RA. However, a feature of SpA is apparent preservation of or even increase in joint space due to the formation of fibrous tissue within the joint. For instance, interphalangeal joint involvement in PsA can lead to large spaces between bone ends despite extensive osseous destruction. In later stages of SpA, joints may progress to ankylosis.
- *Soft tissues*: Soft tissue swelling is a feature of inflamed joints in SpA. A particular characteristic of PsA is inflammation of all joints in entire digits in the hands and feet, with diffuse soft tissue swelling, known as "sausage digit." Bursitis at sites of enthesitis, such as the retrocalcaneal bursa at the Achilles enthesis, along with tendon thickening may be seen as radiographic soft tissue swelling.
- *Bones*: Periarticular osteopenia is not a feature of peripheral SpA. However, bone erosion seen in the hands and feet is typically closely related to ligamentous and capsular enthesis sites and is associated with fluffy new bone formation (enthesophyte) (Fig. 11.13). At sites remote from joints, such as the Achilles tendon and plantar fascial insertions, enthesitis gives rise to similar patterns of erosion along with fluffy enthesophyte formation. A characteristic finding in the hands and feet of patients with PsA is the so-called "pencil in cup" appearance, with both extensive bone destruction and maintenance or even widening of apparent joint space. Bone loss may also be seen to involve the terminal phalangeal tufts, which can be useful in discriminating PsA from erosive OA.
- *Alignment*: Involvement of the hands and feet in PsA can result in "arthritis mutilans" with severe resorption of bone from the digits leading to telescoping of the overlying soft tissues and resulting alignment deformity.
- *Joint distribution*: Involvement of the small joints of the hands and feet is typical in PsA. This tends to be distally distributed with relative sparing of the wrist and MCP joints until later in the disease (Fig. 11.5c). The absence of trapeziocentric thumb base involvement is helpful in distinguishing PsA from OA, which otherwise shows similar joint distribution. In PsA and reactive arthritis, involvement of the MTP and interphalangeal joints of the foot is typical. Conversely, hip and shoulder involvement is relatively common in AS. In all types of SpA, a careful review of visualized enthesis sites is helpful to look for signs of enthesitis (soft tissue swelling, erosion, and fluffy enthesophytes) remote from the joints themselves.

11.3.3.2 Advanced Imaging

Both ultrasound and MRI have roles in imaging peripheral SpA with their ability to demonstrate synovitis, tenosynovitis, and articular cartilage. Dactylitis is associated with flexor tenosynovitis and thickening of the soft tissues, joint effusion, and synovitis on ultrasound, while MRI will also show bone and soft tissue edema.

The two modalities have a valuable role in the detection of enthesitis. Both techniques will identify erosive change and enthesophyte formation at enthesis sites with soft tissue changes of tendon/ligament thickening and signal/echogenicity change. Ultrasound may show increased vascularity, while MRI may show osteitis (bone edema) at enthesis sites. In large joints, the presence of bone edema at characteristic enthesis sites on MRI may point to the underlying etiology of the inflammatory joint changes.

11.3.3.3 Sacroiliitis

Sacroiliitis is evident on conventional radiographs as subchondral sclerosis and erosive change. Erosion may lead to apparent widening of the joint, but ultimately the natural history of the disease is progression to ankylosis. CT is more sensitive to the detection of sacroiliitis than conventional radiographs, but the features seen are similar (Fig. 11.6). In AS and enteropathic SpA, involvement of the sacroiliac joints is usually bilateral and fairly symmetrical; this contrasts with sacroiliitis associated with PsA and reactive arthritis where involvement is often more asymmetrical. MRI has become fundamental in the diagnosis and assessment of sacroiliitis. While the erosive findings

Fig. 11.13 Dorsoplantar radiograph showing the toes in a patient with psoriatic arthritis. There is erosive change at the base of the distal phalanx of the second toe, associated with fluffy new bone formation (enthesophyte). Further new bone formation is evident on the lateral aspect of the phalanx (dashed arrow). There is also early resorption of the phalangeal tuft (arrowhead)

Fig. 11.14 Coronal oblique STIR image through the sacroiliac joints in a patient with acute on chronic sacroiliitis. In addition to the subchondral bone edema (osteitis) seen bilaterally on both sides of the joint, there is periarticular soft tissue/ligamentous edema (arrows). Erosive change is also evident (arrowheads)
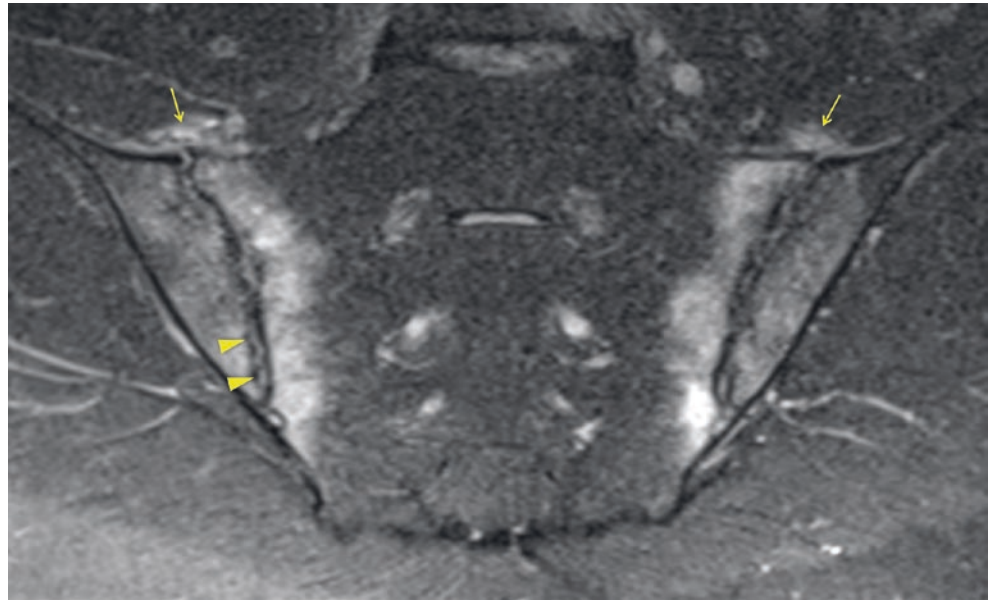
and subchondral changes seen with radiographs and CT are evident on MRI, these represent later changes. The earliest feature of sacroiliitis seen on MRI is osteitis in the subchondral bone, which has become an important feature in the classification of SpA (Table 11.2) (Fig. 11.14). However, sacroiliac subchondral bone edema is not specific to the diagnosis of SpA and is well recognized in healthy subjects, especially those participating in sports such as running; it is a prominent feature of infective arthritis. In chronic sacroiliitis, sites of subchondral bone edema eventually become replaced with high T1 signal fat.

11.3.3.4 Spinal Involvement in Spondyloarthritis

Involvement of the discovertebral unit and the posterior elements of the vertebral column in patients with SpA may precede sacroiliac involvement. The early features of spinal spondyloarthritis are the result of enthesitis, in particular at the attachment sites of the annulus fibrosus and ligaments. On conventional radiographs sclerosis becomes evident at these insertion points, classically seen at the corners of vertebral endplates, known as Romanus lesions. Erosive change at these sites is hard to detect on conventional radiographs, but associated ossification of the anterior longitudinal ligament results in a squared off appearance to the anterior vertebral body. Although these constitute the earliest features seen on conventional radiographs, they are late features of the disease. MRI will show bone edema at these same enthesis sites much earlier, giving rise to a characteristic appearance of high T2 signal corners to the vertebral bodies on water-sensitive sagittal imaging (Fig. 11.15). Edema at other sites of ligamentous insertion may also be apparent, for instance, at the costovertebral joints and at ligamentous attachments to the spinous processes (Fig. 11.15). Later in the disease, fat marrow signal may develop at these enthesis sites similar to the sacroiliac joints.

Proliferative new bone formation that develops later can be hard to appreciate on MRI, especially early in its development, as the low-signal syndesmophytes contrast poorly against adjacent bone cortex and ligaments. However, syndesmophytes become progressively coarser as the disease advances and are readily seen on CT and radiographs. Ultimately, vertebral fusion involving anterior and posterior elements may result in the characteristic appearance of a "bamboo spine." While the syndesmophyte formation seen in AS and enteropathic spondylitis typically has a fine appearance and involves the spine at each level in a symmetrical distribution, the bone proliferation in PsA and reactive arthritis tends to appear more coarse, with a more asymmetrical distribution.

It should be remembered that a fused inflexible spine is particularly susceptible to fracture and a transverse fracture through a fused spine is highly unstable and a potentially catastrophic event.

> **Key Point**
> - As with rheumatoid arthritis, the radiographic features of axial and peripheral spondyloarthritis are late findings of the disease. A characteristic finding of spondyloarthritis is enthesitis including erosive change and enthesophytes. On MRI this is associated with osteitis in the subchondral bone at the sacroiliac joints and in characteristic entheseal locations in the spine.
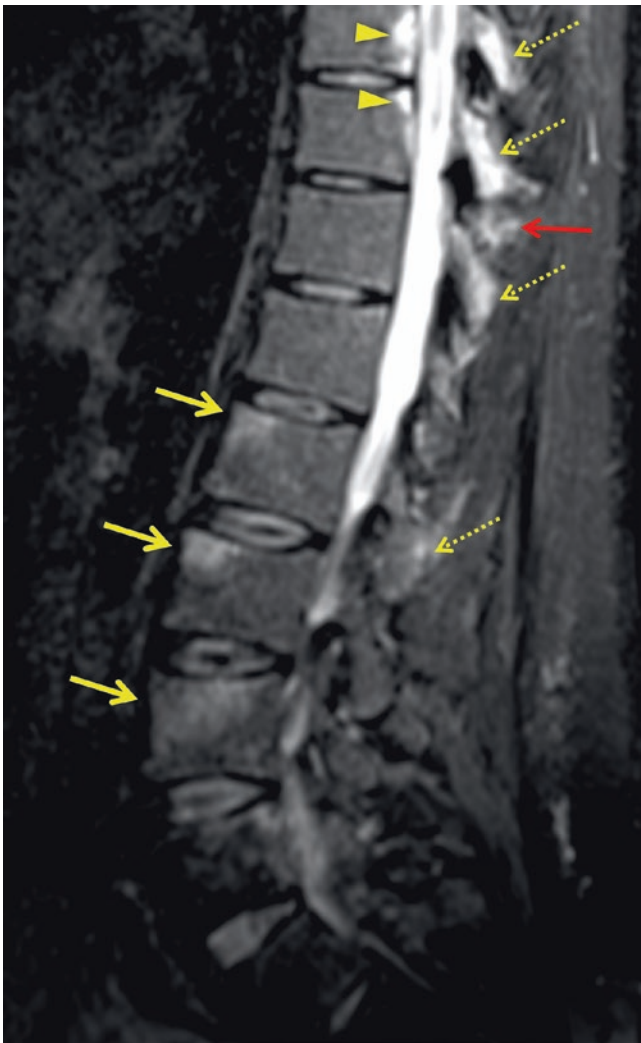
Fig. 11.15 Sagittal T2 fat-suppressed image of the lower thoracic and lumbar spine in a patient with ankylosing spondylitis. There are typical foci of high T2 signal (osteitis) in the anterior corners of the vertebral bodies (yellow arrows). Note the normal disks helping distinguish the appearances from reactive (Modic type) endplate change. There are similar findings in the posterior vertebral bodies more cranially (arrowheads) and in the posterior spinal elements (dashed arrows). There is also inflammatory edema in the posterior soft tissues (red arrow)

11.3.4 Metabolic Joint Disease

11.3.4.1 Gout

Gout can be highly destructive, and the conventional radiographic appearances in the later stages of the disease are very characteristic. However, in the earlier stages of the disease characterized by acute inflammatory episodes, imaging abnormalities may only be observed with more advanced imaging modalities.

Radiographic Appearances

- *Joint space*: Even in advanced chronic tophaceous gout with extensive bone erosion, joint space may be maintained; this is a useful distinguishing feature from other forms of arthritis (Fig. 11.2).
- *Soft tissues*: Urate crystal deposition in chronic tophaceous gout leads to irregular and eccentric soft tissue swelling, a characteristic feature of gout. Tophi sometimes show significantly increased density compared to the surrounding soft tissues due to the variable deposit of microcalcifications within the urate deposit, often associated with renal disease (Fig. 11.2).
- *Bones*: Loss of normal bone mineral density is not a common feature of gout. However, bone erosion is frequent in the chronic stages of the disease. The erosions have a characteristic round or oval configuration with sclerotic margins and sharp overhanging edges of bone. Erosions may be seen centrally, at the joint margin, or at some distance from the joint, often beneath soft tissue nodules (Fig. 11.2).
- *Alignment*: Deformity of joints affected by gout occasionally results from the extensive bone destruction that accompanies chronic disease, producing a severe mutilating arthritis.
- *Joint distribution*: In the majority of cases, the first MTP joint is initially affected; tarsometatarsal joint and carpometacarpal joint involvement is also common. However, disease progression leads to involvement of multiple joints typically with an asymmetrical distribution. Although any joint can be involved, the elbow, knee, and ankle are the most common large joints affected. The joints of the axial skeleton are rarely affected.

Advanced Imaging

Acute presentation of gout, before the chronic manifestations are apparent, involves synovitis and joint effusion. Both ultrasound and MRI will demonstrate these features. One feature of acute gout is the presence of crystal aggregates or "microtophi" within the synovitis and effusion. On ultrasound these can appear as bright reflective foci which may also be seen in gout tophi (Fig. 11.8). In the effusion, this a poor discriminator, since this appearance may be caused by fibrin deposits in rheumatoid arthritis and some types of septic arthritis including tuberculous arthritis. However, in the synovium, these fine reflective foci are more suggestive of acute gout and may even be seen in asymptomatic joints in patients with known gout [28]. On ultrasound, microaggregates may also be seen on the surface of cartilage giving

rise to the so-called "double contour" sign. Both ultrasound and MRI are able to demonstrate the soft tissue deposits and erosions of chronic gout. The characteristic "punched out" appearance to the erosions seen on radiographs is similar on these modalities. Gout tophi have an ill-defined, generally hyperechoic appearance on ultrasound, but this is dependent on the amount of calcification present (Fig. 11.8). Both ultrasound and MRI will also demonstrate gout involvement of tendons, tendon sheaths, and peritendinous tissues.

Dual energy CT, with its ability to characterize urate crystals in soft tissues, is becoming widely used in clinical practice, with high sensitivity and specificity.

11.3.4.2   Calcium Pyrophosphate Deposition Disease

Acute pseudogout is generally a clinical diagnosis supported by crystal analysis from aspirated fluid. However, as with gout, MRI and ultrasound will demonstrate effusion and synovitis.

Radiographic Appearances

- *Joint space*: CPPD arthropathy is associated with joint space narrowing as cartilage is lost. Calcium pyrophosphate deposited in the articular cartilage and, where present, fibrocartilage (chondrocalcinosis) will be visible within the joint (Fig. 11.4). In fibrocartilage, particularly in the knee menisci, the calcification has a coarse irregular appearance, while in hyaline cartilage, the calcification appears as a thin, linear density paralleling the subchondral bone margin.
- *Soft tissues*: CPPD crystal deposition may also be evident in the synovium and joint capsule. Although less frequent, ligament and tendon calcifications can occasionally be seen.
- *Bones*: The radiographic appearances of CPPD arthropathy resemble those of osteoarthritis, with subchondral sclerosis, cyst formation, and osteophytosis. However, characteristic findings include large cysts, often associated with collapse of the bone in the later stages of the disease, and less prominent osteophytes than would be expected for the degree of arthropathy seen (Fig. 11.4).
- *Alignment*: As with osteoarthritis, joint deformity is largely the result of subchondral collapse and cartilage loss. At the wrist, it is not uncommon for ligamentous dysfunction to lead to scapholunate disassociation (Fig. 11.4).
- *Joint distribution*: Along with crystal deposition, the unusual distribution compared to OA is the most characteristic feature of CPPD arthropathy. In particular, involvement of the index and middle MCP joints in the hand is very typical of CPPD arthropathy, along with radiocarpal and midcarpal wrist involvement (Fig. 11.5d). At the knee, a common feature is predominant or even isolated patellofemoral joint involvement. Hemochromatosis-related

arthropathy, which is associated with pyrophosphate deposition, frequently involves all of the MCP joints and may be associated with prominent hook-like osteophytes at the metacarpal heads.

Advanced Imaging

The deposition of pyrophosphate crystals in hyaline cartilage, synovium, and joint fluid can be demonstrated on ultrasound. CPPD crystal deposition in the substance of the cartilage may be distinguished from urate crystal deposition on the surface of the cartilage in gout, but the double contour sign described in gout may also be seen with pyrophosphate chondral deposition and, despite early reports, seems not to be specific for gout [29, 30].

On MRI, calcium deposition in fibrocartilage is not detected because of its similar low signal characteristics. However, in hyaline cartilage, MRI may sometimes depict chondrocalcinosis as punctate or linear hypointense signal.

> **Key Point**
> - Radiographic features of chronic tophaceous gout include irregular soft tissue swelling, preservation of joint space, and characteristic punched out erosions. Ultrasound can demonstrate aggregates of urate crystals in synovium and on the surface of articular cartilage. Tophi are readily identified with MRI and ultrasound. CPPD arthropathy, associated with chondrocalcinosis and crystal deposition in synovium and capsular tissues, is characterized by radiographic appearances similar to OA, but in atypical locations.

11.4   Concluding Remarks

While recognizing that there are many other causes of joint disease with characteristic findings, this review has concentrated on some of the most common arthritides seen in clinical practice. The fundamental role conventional radiographs continue to play in the diagnosis and management of these conditions has been emphasized, and a logical method of reviewing the radiograph assessing joint space, soft tissues, bones, alignment, and joint distribution has been suggested. Increasingly, advanced imaging modalities are playing an important part in assessing patients with arthritis, with ultrasound and MRI both playing roles in identifying early disease before radiographic findings become apparent. These advanced imaging modalities continue to contribute to our understanding of the pathophysiology of joint disease and enable the early instigation of treatment.

Take Home Messages

- Conventional radiographs remain fundamental to the imaging workup of patients with arthritis and provide valuable information relating to the assessment of joint space, periarticular soft tissues, bone (including erosions and osteophytes), joint alignment, and the distribution of the arthritis.
- Ultrasound and MRI allow sensitive assessment of synovitis and erosions in rheumatoid arthritis and the spondyloarthritides, with MRI also able to identify bone marrow changes including osteitis, along with articular cartilage changes.
- OA findings of uneven (asymmetric) joint space loss, osteophytes, and subchondral bone changes are typically seen at DIP and PIP joints and at the thumb base, whereas CPPD arthropathy characteristically involves the index and middle MCP joints along with radiocarpal and midcarpal wrist involvement.
- RA is characterized by marginal erosions and joint space narrowing typically seen at the PIP, MCP, and wrist joints, whereas spondyloarthritis is characterized by erosive change, enthesophytes, and osteitis at the sacroiliac joints and in characteristic entheseal locations in the spine.
- While gout shows an asymmetric distribution of irregular and eccentric soft tissue swelling, maintained joint space and bone erosions with a characteristic round or oval configuration, and sclerotic margins with sharp overhanging edges of bone on conventional radiographs, advanced imaging modalities, in particular ultrasound and dual energy CT, have an increasingly important role in characterizing the disease.

References

1. Rowbotham EL, Grainger AJ, O'Connor P. Arthritis. In: Adam A, Dixon AK, Gillard JH, Schaefer-Prokop CM, editors. Grainger & Allison's diagnostic radiology. 7th ed. Edinburgh: Elsevier; 2020. p. 1116–41.
2. Arend WP. Physiology of cytokine pathways in rheumatoid arthritis. Arthritis Rheum. 2001;45(1):101–6.
3. Colebatch AN, Edwards CJ, Østergaard M, Van Der Heijde D, Balint PV, D'Agostino M-A, et al. EULAR recommendations for the use of imaging of the joints in the clinical management of rheumatoid arthritis. Ann Rheum Dis. 2013;72(6):804–14.
4. Rudwaleit M, van der Heijde D, Landewe R, Listing J, Akkoc N, Brandt J, et al. The development of Assessment of Spondyloarthritis International Society classification criteria for axial spondyloarthritis (part II): validation and final selection. Ann Rheum Dis. 2009;68(6):777–83.
5. Resnick D. Patterns of peripheral joint disease in ankylosing spondylitis. Radiology. 1974;110(3):523–32.
6. Baker H. Prevalence of psoriasis in polyarthritic patients and their relatives. Ann Rheum Dis. 1966;25(3):229–34.
7. Mikuls T, Farrar J, Bilker W, Schumacher H, Fernandes S, Allison J, et al. The treatment of asymptomatic hyperuricemia: results from the population-based general practice research database (GPRD). Arthritis Rheum. 2003;48(9):S612.
8. Miksanek J, Rosenthal AK. Imaging of calcium pyrophosphate deposition disease. Curr Rheumatol Rep. 2015;17(3):20.
9. Nicolaou S, Liang T, Murphy DT, Korzan JR, Ouellette H, Munk P, Dual-energy CT. a promising new technique for assessment of the musculoskeletal system. AJR Am J Roentgenol. 2012;199(5 Suppl):S78–86.
10. Shi D, Xu J-X, Wu H-X, Wang Y, Zhou Q-J, Yu R-S. Methods of assessment of tophus and bone erosions in gout using dual-energy CT: reproducibility analysis. Clin Rheumatol. 2015;34(4):755–65.
11. Karim Z, Wakefield R, Conaghan P, Lawson C, Goh E, Quinn M, et al. The impact of ultrasonography on diagnosis and management of patients with musculoskeletal conditions. Arthritis Rheum. 2001;44(12):2932–3.
12. Szkudlarek M, Narvestad E, Klarlund M, Court-Payen M, Thomsen HS, Ostergaard M. Ultrasonography of the metatarsophalangeal joints in rheumatoid arthritis: comparison with magnetic resonance imaging, conventional radiography, and clinical examination. Arthritis Rheum. 2004;50(7):2103–12.
13. Wakefield RJ, Balint PV, Szkudlarek M, Filippucci E, Backhaus M, D'Agostino MA, et al. Musculoskeletal ultrasound including definitions for ultrasonographic pathology. J Rheumatol. 2005;32(12):2485–7.
14. Rowbotham EL, Wakefield RJ, Grainger AJ. The technique and application of ultrasound in the diagnosis and management of inflammatory arthritis. Semin Musculoskelet Radiol. 2012;16(5):360–6.
15. Wakefield RJ, Gibbon WW, Conaghan PG, O'Connor P, McGonagle D, Pease C, et al. The value of sonography in the detection of bone erosions in patients with rheumatoid arthritis: a comparison with conventional radiography. Arthritis Rheum. 2000;43(12):2762–70.
16. Camerer M, Ehrenstein B, Hoffstetter P, Fleck M, Hartung W. High-resolution ultrasound of the midfoot: sonography is more sensitive than conventional radiography in detection of osteophytes and erosions in inflammatory and non-inflammatory joint disease. Clin Rheumatol. 2017;36(9):2145–9.
17. Keen HI, Wakefield RJ, Grainger AJ, Hensor EM, Emery P, Conaghan PG. Can ultrasonography improve on radiographic assessment in osteoarthritis of the hands? A comparison between radiographic and ultrasonographic detected pathology. Ann Rheum Dis. 2008;67(8):1116–20.
18. Nalbant S, Corominas H, Hsu B, Chen LX, Schumacher HR, Kitumnuaypong T. Ultrasonography for assessment of subcutaneous nodules. J. Rheumatol. 2003;30(6):1191–5.
19. Ostergaard M, Peterfy C, Conaghan P, McQueen F, Bird P, Ejbjerg B, et al. OMERACT rheumatoid arthritis magnetic resonance imaging studies. Core set of MRI acquisitions, joint pathology definitions, and the OMERACT RA-MRI scoring system. J Rheumatol. 2003;30(6):1385–6.
20. Rubin DAMRI. ultrasound of the hands and wrists in rheumatoid arthritis. I. Imaging findings. Skelet Radiol. 2019;48(5):677–95.
21. Hodgson RJ, O'Connor PJ, Ridgway JP. Optimizing MRI for imaging peripheral arthritis. Semin Musculoskelet Radiol. 2012;16(5):367.
22. Gait A, Hodgson R, Parkes M, Hutchinson C, O'Neill T, Maricar N, et al. Synovial volume vs synovial measurements from dynamic contrast enhanced MRI as measures of response in osteoarthritis. Osteoarthritis Cartil. 2016;24(8):1392–8.

23. Schwenzer NF, Kötter I, Henes C Jr, Schraml C, Fritz J, Claussen CD, et al. The role of dynamic contrast-enhanced MRI in the differential diagnosis of psoriatic and rheumatoid arthritis. Am J Roentgenol. 2010;194(3):715–20.

24. Wenham CY, Balamoody S, Grainger AJ, Hensor EM, Draycott S, Hodgson R, et al. The responsiveness of novel, dynamic, contrast-enhanced magnetic resonance measures of total knee synovitis after intra-articular corticosteroid for painful osteoarthritis. Osteoarthritis Cartil. 2014;22(10):1614–8.

25. Haugen IK, Boyesen P, Slatkowsky-Christensen B, Sesseng S, Bijsterbosch J, van der Heijde D, et al. Comparison of features by MRI and radiographs of the interphalangeal finger joints in patients with hand osteoarthritis. Ann Rheum Dis. 2012;71(3):345–50.

26. Crema MD, Roemer FW, Marra MD, Niu J, Lynch JA, Felson DT, et al. Contrast-enhanced MRI of subchondral cysts in patients with or at risk for knee osteoarthritis: the MOST study. Eur J Radiol. 2010;75(1):e92–6.

27. McQueen FM. Bone marrow edema and osteitis in rheumatoid arthritis: the imaging perspective. Arthritis Res Ther. 2012;14(5):224.

28. Howard RG, Pillinger MH, Gyftopoulos S, Thiele RG, Swearingen CJ, Samuels J. Reproducibility of musculoskeletal ultrasound for determining monosodium urate deposition: concordance between readers. Arthritis Care Res. 2011;63(10):1456–62.

29. Ogdie A, Taylor WJ, Neogi T, Fransen J, Jansen TL, Schumacher HR, et al. Performance of ultrasound in the diagnosis of gout in a multicenter study: comparison with monosodium urate monohydrate crystal analysis as the gold standard. Arthritis Rheumatol. 2017;69(2):429–38.

30. Loffler C, Sattler H, Peters L, Loffler U, Uppenkamp M, Bergner R. Distinguishing gouty arthritis from calcium pyrophosphate disease and other arthritides. J Rheumatol. 2015;42(3):513–20.

Metabolic-Endocrine

12

Miriam A. Bredella and Bruno C. Vande Berg

Learning Objectives

- To understand the normal imaging appearance of bone marrow and bone marrow manifestations of metabolic and endocrine disorders.
- To understand the limitations of medical imaging in detecting metabolic bone disorders.
- To understand the imaging findings observed in symptomatic complications associated with metabolic bone disorders.

Table 12.1 Metabolic disorders of the musculoskeletal system

Muscles	Sarcopenia, drug-induced myopathies (statins), necrosis (diabetes mellitus), fat atrophy (steroids)
Tendons	Chondrocalcinosis, hypercholesterolemia, hyperuricemia, hypervitaminosis A, drug-induced tendinopathy (quinolones)
Cartilage	Chondrocalcinosis, hyperuricemia, recurrent hemorrhage, hemochromatosis, ochronosis
Synovium	Hyperuricemia, amyloidosis
Bone	Osteopenia, osteoporosis, rickets, osteomalacia, renal osteodystrophy, hyperparathyroidism, thyroid acropachy, acromegaly, drug-induced disorders
Bone marrow	Hemosiderosis, marrow aplasia, anemias, serous atrophy, fatty atrophy, drug-induced disorders

12.1 Introduction

All components of the musculoskeletal system can be involved with metabolic disorders (Table 12.1) as a result of endocrine diseases, genetic alterations, and environmental or nutritional aspects, with important worldwide variations in prevalence and severity. Early detection of these disorders is crucial because of the efficacy of preventive measures and availability of treatments. The current chapter will focus on the imaging appearance of metabolic disorders of bone marrow and of the mineralized skeleton. Marrow and bone disorders in athletes, the elderly, and individuals with eating disorders will be reviewed.

12.2 Metabolic Marrow Disorders

12.2.1 Structure, Function, and Development of Bone Marrow

The marrow cavity is divided into compartments by bony trabeculae. There are two types of marrow, red or hematopoietic marrow and yellow or fatty marrow.

Red (hematopoietic) marrow is hematopoietically active and is composed of various hematopoietic stem cells, lymphocytes, and lymphoid nodules, supported by reticulum cells and fat cells. Red marrow contains approximately 40% water, 40% fat, and 20% protein [1]. Blood supply is through centrally located nutrient arteries. Bone marrow lacks lymphatic channels [1].

Yellow (fatty) marrow is composed predominantly of fat and contains approximately 15% water, 80% fat, and 5% protein. Marrow adipose tissue has been increasingly recognized as an active and dynamic endocrine organ that responds to changes in nutrition and environmental milieu and can function as a biomarker for skeletal integrity and bone strength [2].

M. A. Bredella (✉)
Department of Radiology, Massachusetts General Hospital and Harvard Medical School, Boston, MA, USA
e-mail: mbredella@mgh.harvard.edu

B. C. Vande Berg
Department of Radiology, Cliniques Universitaires Saint Luc, Université Catholique de Louvain, Brussels, Belgium
e-mail: Bruno.vandeberg@uclouvain.be

12.2.1.1 Normal Development of Bone Marrow

The normal distribution and MR appearance of bone marrow changes with age. It is important to be familiar with the appearance of bone marrow during aging to be able to determine whether processes represent a disease or normal variations of marrow. Bone marrow and related disorders are best assessed using MRI [3].

12.2.1.2 Red to Yellow Marrow Conversion

At birth, hematopoietic marrow is present throughout the entire skeleton including the epiphyses. Normal physiologic conversion of red to yellow marrow occurs in a predictable fashion. It begins in the hands and feet progressing to the peripheral (appendicular) and then the central (axial) skeleton. In the peripheral skeleton, this process begins in the epiphyses, followed by the diaphyses, the distal metaphyses, and then the proximal metaphyses. Marrow conversion is typically complete by 25 years of age. However, residual red marrow can be present in the metaphyses of long bones in the adult, and in some cases subchondral red marrow can be seen in the proximal epiphyses of the humerus and femur. Although distribution of red marrow varies from person to person, it is usually symmetric in the same person [3] (Fig. 12.1).

12.2.1.3 Reconversion of Yellow to Red Marrow

Reconversion from yellow to red marrow is triggered by demand for increased blood cell production and can be seen in anemia, smoking, obesity, athletes, high altitude, or with certain treatments. It occurs in the mirror-opposite sequence of red to yellow marrow conversion. In the axial skeleton, the proximal metaphyses convert first, followed by the distal metaphyses, and the diaphyses, while the epiphyses usually only convert to red marrow in severe cases. The extent of reconversion depends on the duration and severity of the initiating cause [3–5] (Fig. 12.1).
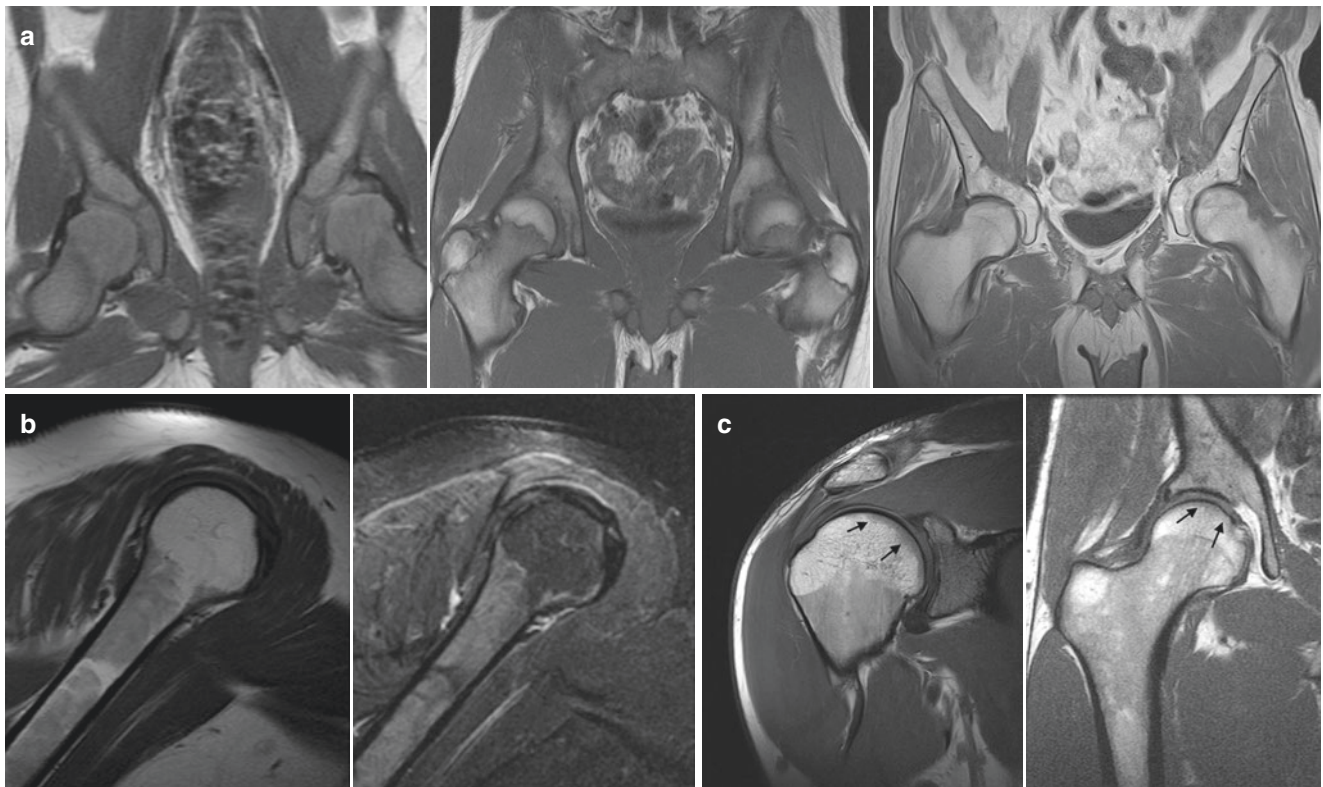
Fig. 12.1 Normal appearance of bone marrow. (**a**) T1-weighted MR images of the pelvis showing normal physiologic conversion of red (hematopoietic) to yellow (fatty) marrow. At birth, marrow is red and diffusely hypointense. During adolescence, physiologic conversion from red to yellow marrow occurs, involving first the epiphyses and epiphysis equivalents, such as the greater trochanters, and diaphyses, while the metaphyses still contain red marrow. In adulthood, there is nearly complete conversion to fatty marrow. (**b**) Marrow reconversion in an athlete. Sagittal T1-weighted and sagittal fat-suppressed T2-weighted MR images show red marrow in the proximal humeral metaphysis and the diaphysis. Red marrow is of intermediate signal and higher in signal than muscle on the T1-weighted image. (**c**) Normal appearance of residual red marrow in the humeral and femoral heads. The curvilinear subchondral distribution of red marrow involving the humeral and femoral heads (arrows) is a normal finding. (**d**) Chemical shift MR imaging of normal marrow in a woman with obesity showing red marrow on the in-phase image and normal signal drop on the out-of-phase image
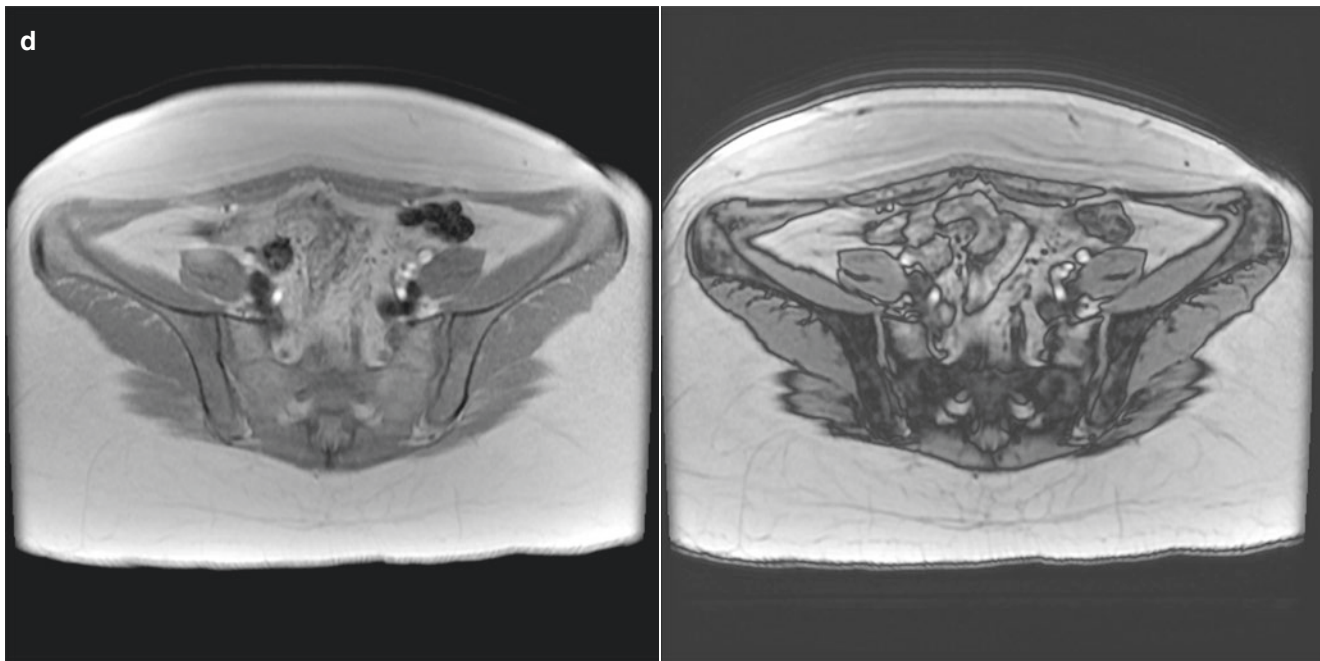
Fig. 12.1 (continued)

Key Points
- Normal physiologic conversion of red to yellow marrow occurs in a predictable fashion starting in the epiphyses, followed by the diaphysis, and the metaphyses.
- Residual red marrow can be found in the metaphyses and subchondral location of the epiphyses of the humeral head and femoral head of adults.
- Marrow reconversion from yellow to red marrow occurs in the reverse order as does conversion from red to yellow marrow.
- Although distribution of red marrow varies from person to person, it is usually symmetric in the same person.

12.2.2 Magnetic Resonance Imaging of Bone Marrow

12.2.2.1 Anatomic Imaging

The major determinants of the MRI appearance of bone marrow are its fat and water content. T1-weighted spin-echo or fast spin-echo/proton density-weighted sequences are most suitable to evaluate bone marrow. Bone marrow is typically hyperintense on T1-weighted images and follows the signal intensity of subcutaneous fat. On fat-suppressed or fluid-sensitive sequences (fat-suppressed T2-/proton density-weighted or short tau inversion recovery (STIR) sequences) bone marrow signal is hypointense. Red marrow demonstrates low signal intensity on T1-weighted images, reflecting its increased water content, and intermediate sig-

nal intensity with progressive T2 weighting. On T1-weighted images, normal red marrow is equal to or higher in signal intensity than adjacent muscle or intervertebral disks [1, 3, 4] (Fig. 12.1).

12.2.2.2 Chemical Shift Imaging

Chemical shift imaging also known as water-fat imaging, or Dixon method, represents a MRI-based method that generates water and fat images. Separation of water and fat signal is based on the chemical shift difference between water and fat resonance frequencies and can provide a quantitative measurement of the signal fraction of both water and fat [6]. This property is used to develop water and fat images by emphasizing in-phase or out-of-phase tissue properties, thus suppressing fat or water signal. Chemical shift imaging can be used as a problem solver to distinguish between benign and malignant etiologies of focal bone marrow abnormalities if conventional anatomic MR images are equivalent. Malignant processes are associated with the replacement of normal bone marrow resulting in a lack of signal intensity loss in the opposed-phase images compared to the in-phase images. Previous studies have calculated a cutoff of 0.75–0.8 for the ratio of opposed-phase signal to the in-phase signal in order to differentiate between malignant and benign processes [6, 7] (Fig. 12.1).

12.2.2.3 Proton MR Spectroscopy

Single-voxel proton magnetic resonance spectroscopy (^{1}H-MRS) can provide both quantitative and qualitative information of bone marrow and is typically used in research investigations. Point-resolved spectroscopy (PRESS) and stimulated echo acquisition mode (STEAM) single-voxel ^{1}H-MRS pulse sequences can be employed to obtain fat spectra at

various skeletal sites. The signal within a voxel is divided into two major peaks, a lipid and a water peak which can be determined to assess the lipid-to-water ratio or fat fraction of bone marrow. The amount of marrow adipose tissue by ^{1}H-MRS in combination with bone mineral density by dual-energy X-ray absorptiometry has been found to be a biomarker for bone health and bone strength, being more valuable than either parameter alone in evaluating skeletal integrity [8, 9].

> **Key Point**
> - Normal red marrow demonstrates T1 signal that is equal to or higher than adjacent muscle or intervertebral disks.

12.2.3 Bone Marrow Changes in Athletes

The hematologic responses to physical training are multifactorial. Endurance athletes often have expanded plasma volume and red blood cell mass. Moreover, many endurance athletes have elevated erythropoietin levels, probably due to hypoxia during exercise. Erythropoietin causes increased erythropoiesis and elevated red cell mass. Depleted iron reserves or increased hematopoiesis with elevated erythropoietin levels and reticulocyte count can contribute to the development of hematopoietic hyperplasia in this population. Hematopoietic bone marrow hyperplasia of the spine

and extremities has been identified on MRI in endurance athletes [4, 5] (Fig. 12.1).

12.2.3.1 Female Athlete Triad

The female athlete triad refers to a constellation of three clinical entities that are often observed in physically active girls and women. The female athlete triad involves any one of the three components: (1) low energy availability with or without disordered eating, (2) menstrual dysfunction, and (3) low bone mineral density. Energy availability directly affects menstrual status, and in turn, energy availability and menstrual status directly influence bone health [10, 11]. It is important to identify adolescents who exhibit subclinical abnormalities of the female athlete triad and thus allow for early intervention to prevent fractures later in life. Adolescence is a crucial time of maximal bone accrual toward attainment of peak bone mass, which is a key determinant of future fracture risk. Processes that affect bone health in adolescence are likely to be permanent, leading to increased fracture risk later in life [10].

Imaging findings of the female athlete triad include paucity of body fat and high marrow adipose tissue, low bone mineral density, and impaired bone microarchitecture [12]. Women with the female athlete triad are at high risk for stress fractures and often have higher MRI grades of stress injuries compared with eumenorrheic athletes and injuries being associated with a prolonged time to return to sport [13] (Fig. 12.2).
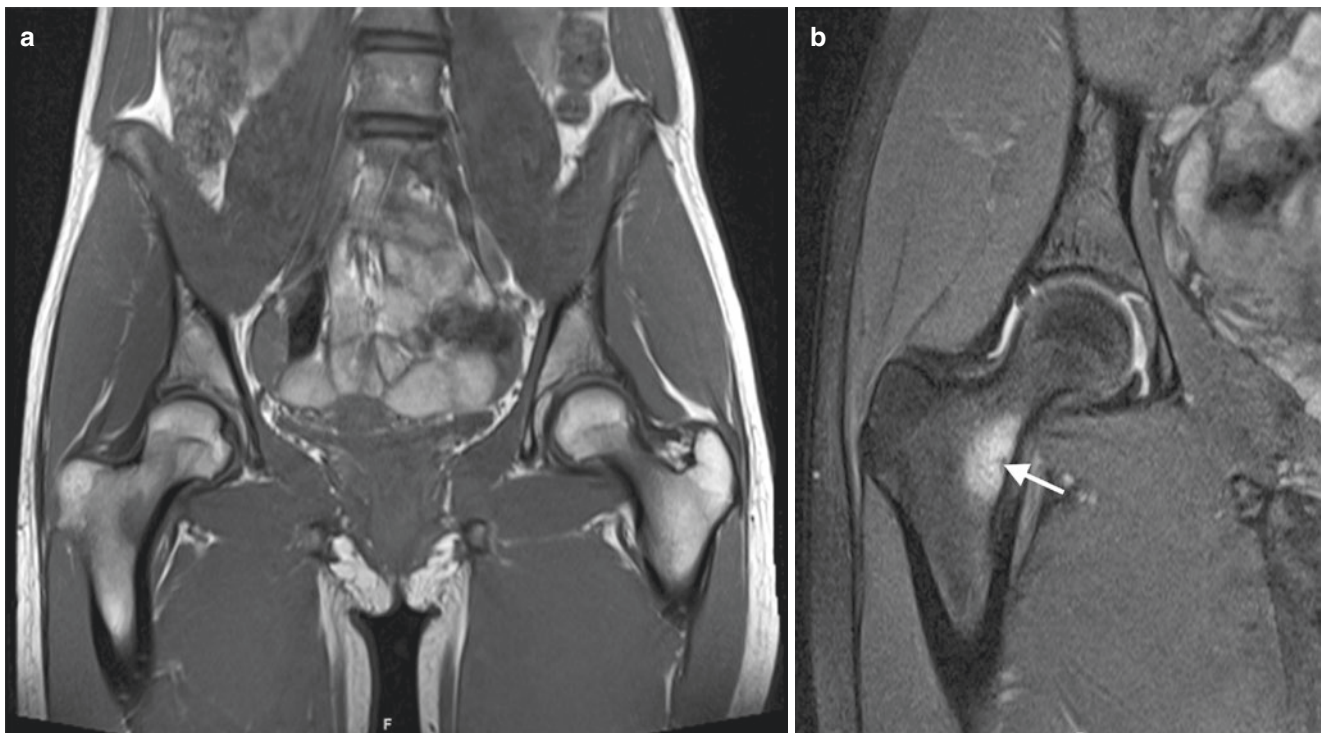
Fig. 12.2 MRI of a 19-year-old runner with the female athlete triad and right-sided hip pain. (**a**) Coronal T1-weighted MR image of the pelvis demonstrates paucity of body fat and signal abnormality of the right femoral neck. (**b**) Coronal fat-suppressed T2-weighted MR image shows a stress fracture of the right femoral neck (arrow). (**c**) MRI of the lower leg 6 months after the pelvic MRI demonstrates tibial stress reaction with periosteal and endosteal edema (arrows)
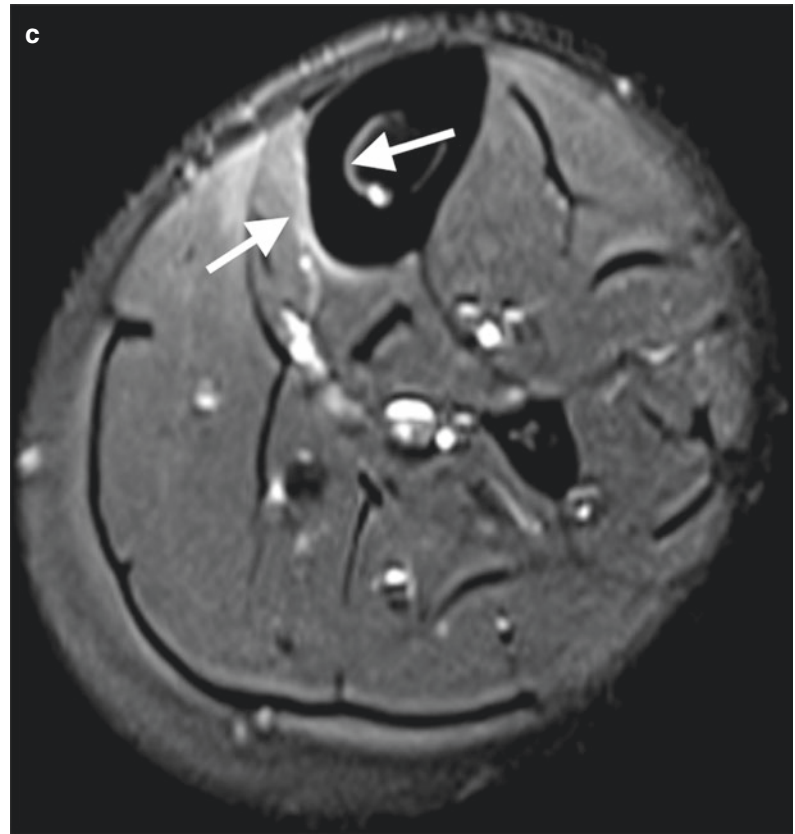
Key Point
- Young female athletes with paucity of body fat and stress fracture on MRI should be evaluated for the female athlete triad.

12.2.4 Bone Marrow Changes in Eating Disorders

Bone marrow can respond to nutritional challenges and might serve as a biomarker for bone quality. Patients with anorexia nervosa often develop marrow changes that can include decreased marrow cellularity with an increase in fat content or a reduction in both fat and hematopoietic cells with an increase in extracellular material, rich in hyaluronic acid, referred to as gelatinous transformation of bone marrow or serous atrophy. In cases of undernutrition (phase II of starvation), body fat can be metabolized with a paradoxical increase in fatty marrow. Bone marrow is relatively resistant to lipolysis and metabolism until other available fat depots have been utilized. During the late phase of starvation (stage III), marrow fat can be metabolized and replaced by hyaluronic acid-rich mucopolysaccharides, leading to gelatinous transformation or serous atrophy of bone marrow in which there is a significant decrease in the number and size of adipocytes ("atrophy") and hematopoietic cells [14].

On MRI, early fat conversion produces increased signal intensity on T1-weighted images, while late-stage serous atrophy is characterized by water-like signal intensity (i.e., decreased signal intensity on T1-weighted images and increased signal intensity on T2-weighted images) [14, 15]. Other etiologies of serous atrophy of bone marrow include cachexia, rapid weight loss following bariatric surgery, AIDS, endocrine disorders, and scurvy. Due to bone weakening, insufficiency fractures are common but are often obscured on MRI by the signal abnormalities associated with serous atrophy, often requiring radiographs of CT to detect the fracture [14] (Fig. 12.3). Of note, in a multicenter study examining the MRI appearance of serous atrophy, almost one fourth of cases were misinterpreted as technical error requiring unnecessary repeat imaging [14].

Key Points
- Serous atrophy of bone marrow is often associated with fractures which can be obscured by abnormal MRI signal, requiring radiographs or CT to identify fractures.
- The abnormal MRI signal of serous atrophy of bone marrow is often misinterpreted as technical error requiring unnecessary repeat imaging.

Fig. 12.3 Serous atrophy of bone marrow in a woman with anorexia nervosa referred for MRI of the ankle to rule out stress fracture. (**a**) Sagittal T1-weighted MR image shows diffusely hypointense marrow signal and paucity of subcutaneous fat with similar abnormal hypointense signal. No signal abnormality to suggest fracture. (**b**) Sagittal short tau inversion recovery (STIR) MR image shows diffuse abnormal hyperintense signal of bone marrow and subcutaneous fat. No findings to suggest insufficiency fracture. (**c**) Radiograph of the ankle demonstrates calcaneal stress fractures (arrows), which were obscured on the MRI by the abnormal marrow signal from serous atrophy

12.3 Metabolic Bone Disorders

12.3.1 Structure, Function, and Development of Bone

Bone is a specialized connective tissue made up of a matrix of collagen fibers, mucopolysaccharides, and inorganic crystalline mineral matrix (calcium hydroxyapatite) that are distributed along the length of the collagen fibers.

Bone remains metabolically active throughout life (bone remodeling) at a variable degree (bone turnover) with bone being constantly resorbed by osteoclasts (osteoclastic activity) and accreted by osteoblasts (osteoblastic activity) [16]. Since bone turnover mainly takes place on bone surface, trabecular bone, which has a greater surface-to-volume ratio than compact bone, is consequently some eight times more metabolically active than cortical bone.

The amount of bone in the skeleton at any moment is entirely dependent on the peak bone mass attained during the third decade of life and on the balance between bone resorption and formation. Bone turnover is under the influence of general factors including age and hormones but is also locally modified by many factors such as physical forces.

Key Points
- Bone remains metabolically active throughout life (bone remodeling) at a variable degree (bone turnover). Trabecular bone is more metabolically active than cortical bone.
- In adults, the amount of bone depends on the peak bone mass attained after adolescence and on bone turnover that is under the influence of systemic and local factors.

12.3.2 Osteoporosis

Osteoporosis, by far the most common metabolic bone disease in Western countries, is a systemic skeletal disease characterized by reduction in bone mass (amount of mineralized bone per volume unit) and by altered trabecular structure due to a loss of trabeculae interconnectivity with a consequent increase in bone fragility and susceptibility to fracture [17] (Fig. 12.4).

Fracture risk increases with advancing age and progressive loss of bone mass. The incidence of hip fracture has doubled over the past three decades and is predicted to continue to grow beyond what one would have predicted from increased longevity. At 1 year after hip fracture, 40% of patients are unable to walk independently, 60% have difficulty with one essential activity of life, 80% are restricted in other leaving activity, and 27% will be admitted to a nursing home for the first time [17]. Questionnaires are available to evaluate fracture risk (FRAX).

Generalized osteoporosis is associated with many diseases and can be either primary or secondary [17]. Presence of a vertebral fracture is a powerful predictor of future fracture, and the accurate identification and clear reporting of vertebral fracture by radiologists have a crucial role to play in the diagnosis and appropriate management of the patient [17].

Several quantitative techniques including dual-energy X-ray absorptiometry (DXA), quantitative computed tomography (QCT), and quantitative ultrasonography (QUS) enable accurate and precise assessment of mineral bone density [2]. Artificial intelligence is likely to play a role in the detection of osteoporosis and assessment of fracture risk by using radiographs and CT examinations [18].

Radiography is relatively insensitive in detecting early bone loss, and 30–40% loss of bone tissue usually remains occult on radiographs. Radiographic bone density is also affected by patient characteristics and technical parameters used to obtain the radiographs.

The main radiographic features of generalized osteoporosis include disappearance of the trabecular network and cortical thinning. Resorption and thinning of trabeculae initially affect secondary trabeculae that are parallel to the biomechanical stresses, and the primary trabeculae that are perpendicular to the biomechanical stresses may appear more prominent because they are affected at a later stage. Cortical thinning occurs as a result of endosteal, periosteal, or intracortical (cortical tunnelling) bone resorption. Intracortical tunnelling generally occurs in disorders with rapid bone turnover such as diffuse osteoporosis and reflex sympathetic osteodystrophy. Subperiosteal bone resorption on radiographs is specific for hyperparathyroidism.

Osteoporosis remains occult on MR images although an inverse relationship between trabecular bone density and marrow fat has been reported in some forms of osteoporosis. In the absence of trauma, the presence of multiple vertebral fractures including acute (with bone marrow edema-like changes) and healed (with increased marrow fat) fractures suggests increased bone fragility and, hence, osteoporosis.

Key Points
- Osteoporosis is characterized by a reduction in bone mass and by altered bone architecture with a consequent increase in bone fragility and susceptibility to fracture.
- Radiographs are not sensitive for the detection of osteoporosis, but disappearance of the trabecular network and cortical thinning can be seen in severe osteoporosis.
- Osteoporosis remains occult at MRI.
- Accurate identification and clear reporting of vertebral fractures by radiologists have a crucial role to play in the diagnosis and appropriate management of patient with undiagnosed osteoporosis.

Fig. 12.4 Second metacarpal bones from three patients with (**a**) normal bone, (**b**) osteoporosis, and (**c**) osteomalacia. Osteopenia is characterized by quantitative bone abnormality with decreased bone density and cortical thinning (arrows in **b**). Osteomalacia is characterized by qualitative bone abnormality with intracortical lucencies (arrows in **c**)

12.3.3 Rickets and Osteomalacia

Rickets (in children) and osteomalacia (in adults) are characterized by inadequate or delayed mineralization of osteoid substance in cortical and trabecular bone (Fig. 12.4) [19].

Looser's zone, the radiological hallmark of osteomalacia, corresponds to a relatively large and ill-delimited linear cortical lucency (the fracture). It typically involves the ribs, the superior and inferior pubic rami, and the inner margins of the proximal femora or lateral margin of the scapula.

Widened physeal growth plate and metaphyseal cupping and fraying are the radiological signs of rickets that are best seen at rapidly growing ends of bone such as distal femur and radius or anterior ends of ribs.

Additional radiological findings of rickets/osteomalacia include bone deformities, osteopenia, or a coarsened pattern of the cancellous bone [19].

At MRI, no specific findings for osteomalacia can be found. Presence of multiple trabecular bone fractures with variable appearance on fluid-sensitive sequences could suggest osteomalacia but is also observed in patients under steroid therapy (Fig. 12.5). Looser's zones are difficult to detect on MR images.
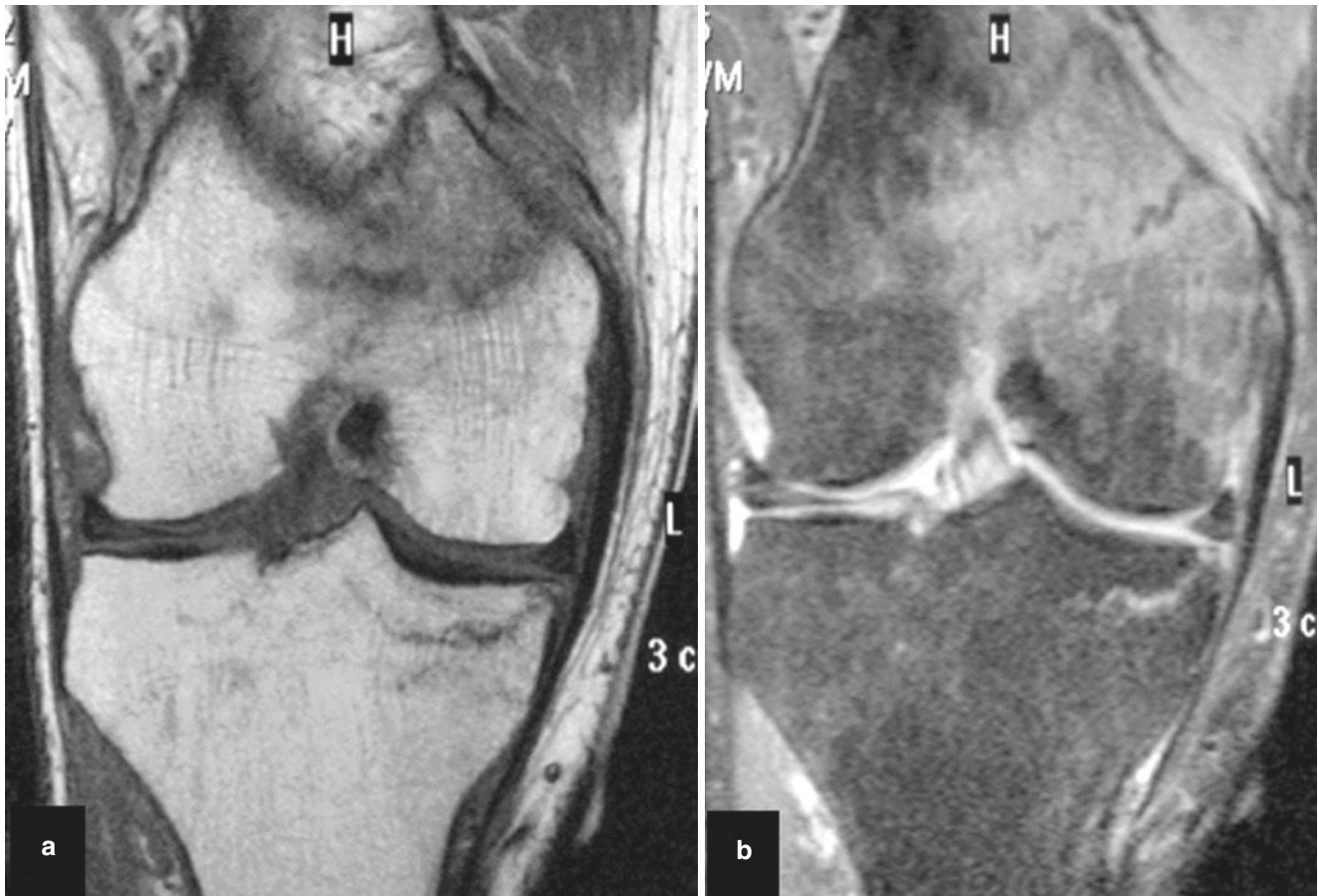
Fig. 12.5 Osteomalacia. Coronal (**a**) T1-weighted and (**b**) fat-suppressed proton density-weighted MR images of the left knee of a 70-year-old man with drug-induced osteomalacia. Multiple trabecular insufficiency fractures (low signal intensity bands) with variable amount of bone marrow edema-like changes are well depicted

---

Key Point
- Rickets (in children) and osteomalacia (in adults) are characterized by inadequate or delayed mineralization of osteoid substance.

12.3.4 Renal Osteodystrophy and Hyperparathyroidism

Renal osteodystrophy refers to all musculoskeletal manifestations associated with chronic renal failure including osteoporosis, osteomalacia, secondary hyperparathyroidism, and soft tissue calcifications.

The radiographic sign specific for hyperparathyroidism is subperiosteal bone resorption that occurs everywhere but is best visible on the radial side of the second finger phalanges and/or phalangeal tufts [19].

Marginal erosions mimicking synovial disorders can also develop in small joints, most likely due to traction at capsular insertions. They are usually discrete and radiological joint space is preserved. Osteoclastoma or brown tumors are lytic bone lesions associated with chronic hyperparathyroidism. Osteosclerosis may also be encountered in renal osteodystrophy. It is commonly appreciated in the vertebrae, pelvis, ribs, and metaphyses of long tubular bones. In vertebrae, sclerosis is frequently confined to the end plates, producing a characteristic appearance of alternating bands of different density (the "rugger jersey" spine).

Soft tissue calcifications may develop anywhere, in the vessel walls but also in the muscles and tendons. Massive amorphous calcification can develop in the soft tissue around articulations and probably reflect poorly controlled renal osteodystrophy.

Key Points
- Renal osteodystrophy refers to all musculoskeletal manifestations associated with chronic renal failure.
- Subperiosteal bone resorption bets appreciated on the radial aspect of the index phalanges is specific for hyperparathyroidism.

Presence of chondrocalcinosis (knees and wrists) in patients younger than 50 years of age should raise the possibility of hypercalcemia, but hemochromatosis may also present with osteoporosis.

12.3.5 Insufficiency Fractures

Insufficiency fractures result from a normal or slightly increased stress on diffusely weakened bones (Table 12.2). Medical imaging plays a crucial role in the diagnosis of insufficiency and pathological fractures because of the lack of a suggestive clinical history. The distinction between these two conditions can be challenging or even impossible as in patients with multiple myeloma.

Imaging findings of insufficiency fractures depend on the predominantly involved bone (trabecular or cortical bone) and on the time delay between fracture and imaging (acute, subacute, chronic) [20, 21].

Insufficiency fractures generally result from normal compressive forces associated with weight-bearing and are therefore perpendicular to the weight-bearing trabeculae. Due to the absence of trauma, bone deformity and soft tissue swelling can be limited.

Early radiographic diagnosis of insufficiency fractures is difficult and periosteal, and cortical callus formation accounts for their delayed detection on radiographs (Table 12.3). Trabecular callus is typically linear and perpendicular to the dominant trabecular network as a result of compressive forces.

Bone marrow edema (BME)-like change is the predominant MR feature of trabecular insufficiency fractures with unclear distinction between stress-induced and fracture-associated changes (Table 12.4).

Table 12.2 Classification of fractures

	Bone strength	Applied forces	Clinical clues
Traumatic fracture	Normal	Increased, acute	History
Fatigue fracture	Normal	Increased, chronic	History
Insufficiency fracture	Diffuse decrease	Normal	None
Pathological fracture	Focal decrease	Normal	None

Table 12.3 Radiologic appearance of trabecular and cortical insufficiency fractures

Radiographs/ CT	Acute	Chronic	Healed
Trabecular #	Normal	Mild sclerosis	Normal
Cortical #	Cortical interruption	Periosteal reaction	Cortical thickening

Table 12.4 MR appearance of trabecular and cortical insufficiency fractures

MR imaging	Acute	Chronic	Healed
Trabecular #	Extensive edema	Band, edema	Normal
Cortical #	Subtle marrow and soft tissue edema	Subtle marrow and soft tissue edema Periosteal callus	Normal

In trabecular insufficiency fractures, low signal intensity bands within BME-like changes are important to detect for diagnostic accuracy. Their conspicuity depends on imaging plane and sequences.

In cortical insufficiency fractures, cortical interruption is barely visible on routine MR images. Edema-like changes on the inner and outer sides of the cortex may suggest cortical fractures but tumors or infection should also be considered. Ultra-short TE MR images or CT may contribute to a specific diagnosis by depicting cortical interruption.

12.3.5.1 Vertebral Insufficiency Fractures

Spontaneous vertebral insufficiency fractures predominantly involve the thoracolumbar spine and never occur above T3 level. The anterior and central midportion of the vertebral body withstands compression forces less well than the posterior and outer ring element of the vertebrae, resulting in wedge or end plate fractures or, less commonly, crush fractures.

Vertebral deformity is the radiographic hallmark of vertebral body fracture on radiographs. BME-like changes adjacent to the vertebral end plate and sparing the posterior elements can be seen on MR images of acute fracture.

The low signal bands located a few millimeters underneath the vertebral end plate are important to detect as their presence adds specificity and contributes to narrow the large differential diagnosis associated with vertebral body BME (Fig. 12.6).

12.3.5.2 Pelvic Bone Insufficiency Fractures

Pelvic bone insufficiency fractures predominate in the pubic and ischiatic rami and sacral wings [22]. There is an increased prevalence of these lesions in patients with previous radiation therapy (importance of differential diagnosis with metastases).

MR imaging is the best imaging modality for sacral and supra-acetabular fractures. CT may contribute to the diagnosis by demonstrating cortical interruption or callus formation in trabecular fractures (sacrum).

12.3.5.3 Femoral and Tibial Insufficiency Fractures

Early recognition of femoral insufficiency fractures is extremely important because of possible progression to frac-
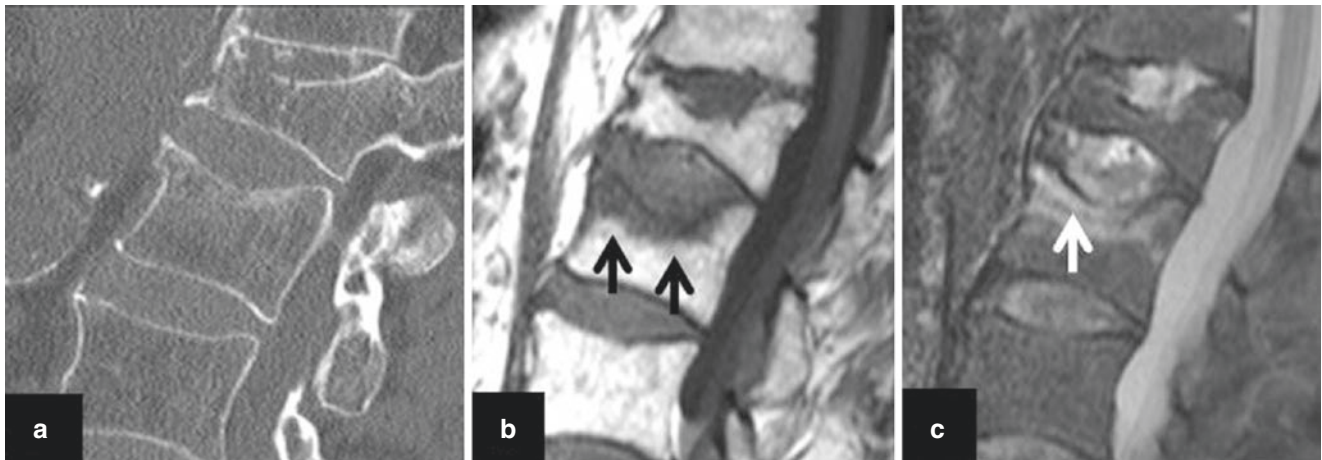
Fig. 12.6 Osteoporosis and vertebral fracture in an 82-year-old woman. (**a**) Sagittal reformatted CT image of the upper lumbar spine shows L1 and L2 vertebral fractures. (**b**) Corresponding T1-weighted MR image shows decreased signal intensity of L2 (recent fracture) (arrows in **b**) and normal signal intensity of L1 (healed fracture). (**c**) On the corresponding sagittal short tau inversion recovery (STIR) image, a low signal intensity band (arrow in **c**) indicates the fracture plane within the bone marrow edema-like signal intensity changes

ture displacement with subsequent increased morbidity. Any region of the femur and of the tibia can be involved.

Atypical insufficiency fracture of the femoral shaft has gained particular attention as they occur in patients with long-standing bisphosphonate therapy for osteoporosis (Fig. 12.7) [23]. These chronic uncomplete cortical fractures can be multiple and bilateral; they involve preferentially the lateral femoral cortex. Transverse cortical lucencies with periosteal beaking can be seen on radiographs or CT reformations. Lesions are barely visible at MRI, because of the limited amount of edema due to lesions chronicity and the limited conspicuity of cortical changes at MRI [24, 25]. Similar fractures occur in the lateral or anterior aspect of the diaphysis in femurs with Paget's disease and in the medial aspect of femurs in patients with osteomalacia.

Longitudinal insufficiency fractures are associated with extensive medullary and soft tissue edema [26]. Cortical interruption, a key diagnostic finding, is visible on short-axis MR or better CT images (with optimal bone settings). The lesion may be confused with infection or tumor at MR imaging because of the longitudinal extent of marrow infiltration.

12.3.5.4 Subchondral Insufficiency Fractures

Subchondral insufficiency fractures generally involve the convex epiphyses of the weight-bearing bones (femoral head and condyles, talar dome, and metatarsal heads) [22, 27–30] (Fig. 12.8).

Radiographs are generally normal but may show subtle subchondral sclerosis. MR imaging reveals BME-like changes that predominate near the subchondral cortical bone of the involved epiphysis. Subtle deformity of the bone contours and low signal intensity bands located at a few millimeters from the subchondral bone plate are generally present.

The differential diagnosis of subchondral BME-like changes is large and includes bone and articular disorders.

12.3.6 Complications of Insufficiency Fractures

12.3.6.1 Displacement of Insufficiency Fractures

Insufficiency fractures usually heal normally with appropriate conservative therapy.

Partial cortical insufficiency fractures of the long bones may progress to overt displaced fractures if not recognized in part because the causative stresses (torsion, compression, traction) favor displacement.

Delayed secondary displacement of trabecular fractures may occur due to persistent compression stresses. Sequelae due to bone deformity can be important, mainly in the spine.

12.3.6.2 Delayed Union and Nonunion

Delayed union and subsequent nonunion of trabecular insufficiency fractures may occur if immobilization is difficult to achieve, if vasculature is sparse, or if the bone metabolism is altered (radiation therapy, steroids).

Progressive collapse of the vertebral body or the epiphysis may occur in association with nonunion. In the past, this condition was known as "spontaneous osteonecrosis" because of the analogy with systemic osteonecrosis (associated with steroid, alcohol, and others) as both conditions may display intraosseous cleft with or without vacuum phenomenon and do not heal. The so-called spontaneous osteonecrosis of the knee (SONK) (Fig. 12.9) is the best known of these conditions, but some authors consider that this term is a misnomer and should not be used [27, 28].

Vertebral osteonecrosis may lead to spinal cord compression, a very uncommon feature in vertebral insufficiency fractures.

Distinction between "spontaneous osteonecrosis" and "subchondral insufficiency fracture" remains important for therapeutic purpose. Spontaneous osteonecrosis will not heal, whereas subchondral insufficiency fractures may heal. Several MR features may contribute to the recognition of subchondral insufficiency fractures that are more likely to progress to osteonecrosis [29, 30].

> **Key Points**
> - Medical imaging plays a crucial role in the diagnosis of insufficiency fractures because of the lack of a suggestive clinical history.
> - Imaging findings of insufficiency fractures depend on the involved bone (trabecular or cortical bone) and on their age (acute, subacute, chronic).
> - Bone marrow edema-like changes are a predominant but nonspecific finding in recent trabecular insufficiency fractures. Additional low signal intensity bands are important for a specific diagnosis but may be absent.
> - Diagnosis of cortical insufficiency fractures is challenging at MRI because of inherent limitations in detecting cortical interruption that can be seen at CT.

Fig. 12.7 Atypical femoral shaft fractures in a 78-year-old woman with history of long-standing bisphosphonate therapy for osteoporosis. Magnified radiograph of the femoral shaft shows a transverse linear cortical lucency with chronic periosteal reaction (white arrows) on the lateral cortex of the subtrochanteric femur indicative of a partial and chronic fracture of the lateral cortex. Other similar lesions are also visible inferiorly

Fig. 12.8 Subchondral insufficiency fracture of the femoral head in a 57-year-old man. (**a**) Coronal T1-weighted MR image of the left hip demonstrates extensive ill-delimited bone marrow edema-like signal changes in the proximal femur that predominate in the subchondral area. (**b**) Sagittal fat-suppressed proton density-weighted image demonstrates a subchondral low signal intensity band (arrows) in the femoral head suggestive of an acute trabecular fracture. (**c**) A follow-up MR image demonstrates complete healing of the lesion
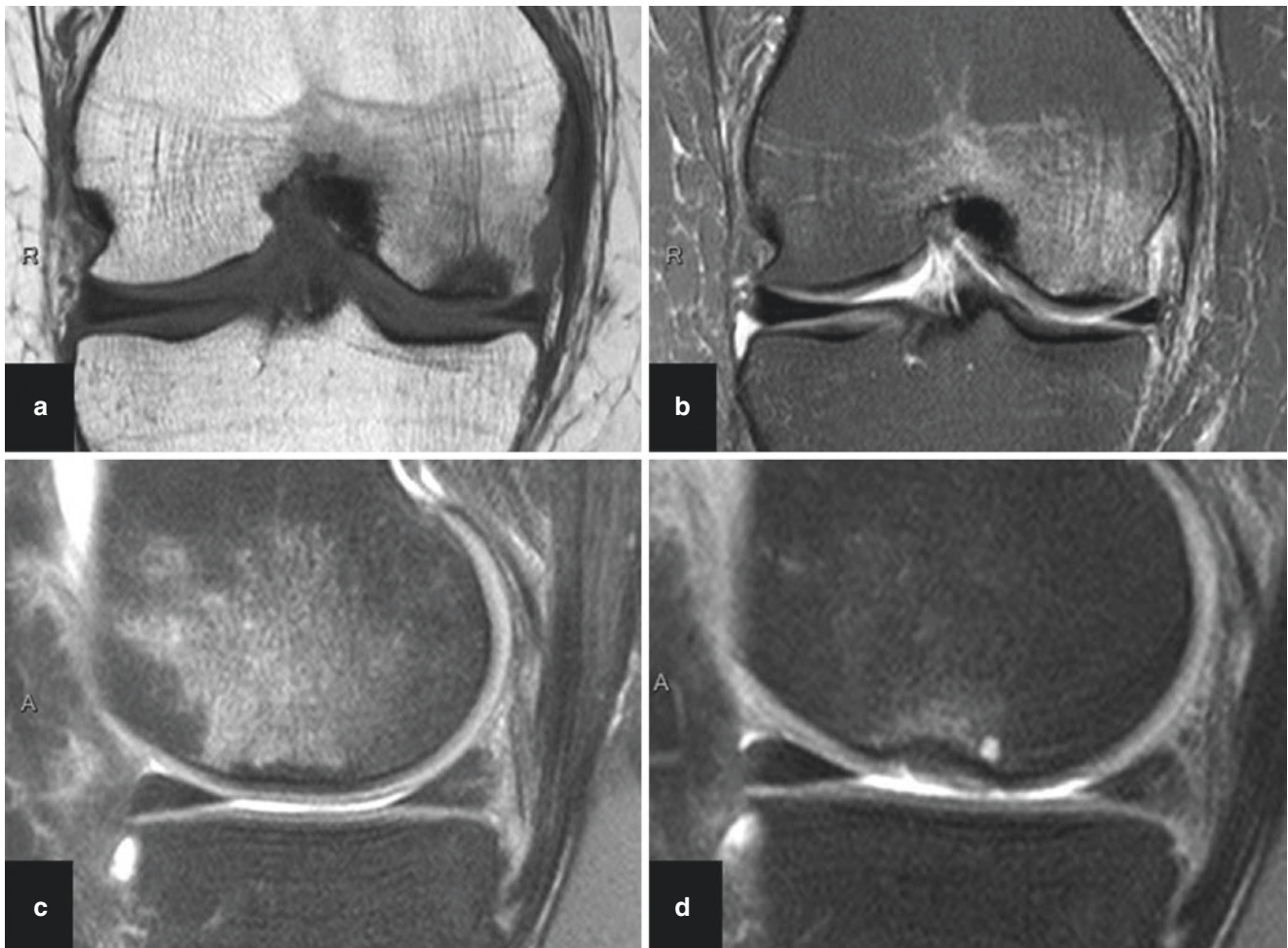
Fig. 12.9 Subchondral insufficiency fracture of the medial femoral condyle in a 65-year-old woman. (**a**) Coronal T1-weighted (**a**) and fat-suppressed proton density-weighted (**b**) MR images demonstrate bone marrow edema-like changes of the medial femoral condyle. On the sagittal fat-suppressed proton density-weighted MR image (**c**), a crescent-shaped low signal intensity line is depicted in the subchondral area with normal bone contour. (**d**) Fat-suppressed proton density-weighted MR image obtained 6 months later demonstrates focal collapse of the condyle and cyst-like bone changes which required subsequent unicompartmental joint replacement

12.4 Concluding Remarks

All components of the musculoskeletal system can be involved by metabolic disorders as a result of endocrine diseases, genetic alterations, and environmental or nutritional aspects with important worldwide variations in prevalence and severity. Early detection of these disorders is crucial because of the availability of efficient therapies and preventive measures. Metabolic disorders are usually clinically silent until complications do occur including mechanical failure (bone fracture, tendon tear), necrosis, and inflammation (arthritis). Imaging plays an important role in detecting complications of metabolic disorders but has limited value in their quantification. MR imaging is the method of choice in assessing bone marrow, with T1-weighted imaging being most helpful.

Take Home Messages
- Metabolic disorders can involve all components of the musculoskeletal system.
- Early detection of metabolic disorders is crucial to guide therapy.
- Osteoporosis, the most common metabolic bone disorder, is characterized by a reduction in bone mass and by altered bone architecture with increased fracture risk.
- Musculoskeletal complications of metabolic disorders include mechanical failure (bone fracture, tendon tear), necrosis and inflammation (arthritis).
- MR imaging is the method of choice in assessing bone marrow and insufficiency fractures.

References

1. Vogler JB 3rd, Murphy WA. Bone marrow imaging. Radiology. 1988;168(3):679–93.
2. Rosen CJ, Bouxsein ML. Mechanisms of disease: is osteoporosis the obesity of bone? Nat Clin Pract Rheumatol. 2006;2(1):35–43.
3. Moore SG, Dawson KL. Red and yellow marrow in the femur: age-related changes in appearance at MR imaging. Radiology. 1990;175(1):219–23.
4. Caldemeyer KS, et al. Hematopoietic bone marrow hyperplasia: correlation of spinal MR findings, hematologic parameters, and bone mineral density in endurance athletes. Radiology. 1996;198(2):503–8.
5. Shellock FG, et al. Hematopoietic bone marrow hyperplasia: high prevalence on MR images of the knee in asymptomatic marathon runners. AJR Am J Roentgenol. 1992;158(2):335–8.
6. Karampinos DC, et al. Quantitative MRI and spectroscopy of bone marrow. J Magn Reson Imaging. 2018;47(2):332–53.
7. Yoo HJ, et al. Measurement of fat content in vertebral marrow using a modified dixon sequence to differentiate benign from malignant processes. J Magn Reson Imaging. 2017;45(5):1534–44.
8. Schellinger D, et al. Bone marrow fat and bone mineral density on proton MR spectroscopy and dual-energy X-ray absorptiometry: their ratio as a new indicator of bone weakening. AJR Am J Roentgenol. 2004;183(6):1761–5.
9. Singhal V, Bredella MA. Marrow adipose tissue imaging in humans. Bone. 2019;118:69–76.
10. Ackerman KE, Misra M. Bone health and the female athlete triad in adolescent athletes. Phys Sportsmed. 2011;39(1):131–41.
11. De Souza MJ, et al. 2014 female athlete triad coalition consensus statement on treatment and return to play of the female athlete triad: 1st international conference held in San Francisco, California, May 2012 and 2nd international conference held in Indianapolis, Indiana, may 2013. Br J Sports Med. 2014;48(4):289.
12. Singhal V, et al. Regional fat depots and their relationship to bone density and microarchitecture in young oligo-amenorrheic athletes. Bone. 2015;77:83–90.
13. Nattiv A, et al. Correlation of MRI grading of bone stress injuries with clinical risk factors and return to play: a 5-year prospective study in collegiate track and field athletes. Am J Sports Med. 2013;41(8):1930–41.
14. Boutin RD, et al. MRI findings of serous atrophy of bone marrow and associated complications. Eur Radiol. 2015;25(9):2771–8.
15. Vande Berg BC, et al. Anorexia nervosa: correlation between MR appearance of bone marrow and severity of disease. Radiology. 1994;193(3):859–64.
16. Pathria MN, Chung CB, Resnick DL. Acute and stress-related injuries of bone and cartilage: pertinent anatomy, basic biomechanics, and imaging perspective. Radiology. 2016;280:21–38. https://doi.org/10.1148/radiol.16142305.
17. Adams J. Osteoporosis. In: Pope TL, et al., editors. Imaging of the musculoskeletal system. 1st ed. Philadelphia: Saunders; 2008. p. 1489–508.
18. Yasaka K, et al. Prediction of bone mineral density from computed tomography: application of deep learning with a convolutional neural network. Eur Radiol. 2020;30:3549–57. https://doi.org/10.1007/s00330-020-06677-0.
19. Sundaram M, Schils J. Hyperparathyroidism, renal osteodystrophy, osteomalacia and rickets. In: Pope TL, et al., editors. Imaging of the musculoskeletal system. 1st ed. Philadelphia: Saunders; 2008. p. 1509–23.
20. Vande Berg BC, et al. Transient epiphyseal lesions in renal transplant recipients: presumed insufficiency stress fractures. Radiology. 1994;191(2):403–7.
21. Vande Berg BC, Malghem J, Lecouvet FE, Maldague B. Magnetic resonance imaging and differential diagnosis of epiphyseal osteonecrosis. Semin Musculoskelet Radiol. 2001;5(1):57–67.
22. Cabarrus MC, Ambekar A, Lu Y, Link TM. MRI and CT of insufficiency fractures of the pelvis and the proximal femur. AJR Am J Roentgenol. 2008;191(4):995–1001.
23. Shane E, et al. Atypical subtrochanteric and diaphyseal femoral fractures: report of task forces of the American Society for Bone and Mineral Research. J Bone Miner Res. 2010;25:2267–94.
24. Chan SS, Rosenberg ZS, Chan K, Capeci C. Subtrochanteric femoral fractures in patients receiving long-term alendronate therapy : imaging features. AJR Am J Roentgenol. 2010;194:1581–6.
25. Haworth AE, Webb J. Skeletal complications of bisphosphonate use: what the radiologist should know. Br J Radiol. 2012;85(1018):1333–42.
26. Feydy A, et al. Longitudinal stress fractures of the tibia: comparative study of CT and MR imaging. Eur Radiol. 1998;8(4):598–602.
27. Yamamoto T, Schneider R, Bullough PG. Subchondral insufficiency fracture of the femoral head: histopathologic correlation with MRI. Skelet Radiol. 2001;30:247–54.
28. Yamamoto T, Bullough PG. Spontaneous osteonecrosis of the knee: the result of subchondral insufficiency fracture. J Bone Joint Surg Am. 2000;82(6):858–66.
29. Vande Berg BC, et al. Idiopathic bone marrow edema lesions of the femoral head: predictive value of MR imaging findings. Radiology. 1999;212(2):527–35.
30. Lecouvet FE, et al. Early irreversible osteonecrosis versus transient lesions of the femoral condyles: prognostic value of subchondral bone and marrow changes on MR imaging. AJR Am J Roentgenol. 1998;170(1):71–7.

Spine Trauma

13

Connie Y. Chang and Mini N. Pathria

Learning Objectives
- To describe common and important traumatic lesions of the spine, emphasizing different injuries that take place in different spinal segments.
- To illustrate the typical imaging appearance of spinal injuries on radiographs, computed tomography (CT), and magnetic resonance imaging (MRI).
- To introduce radiologists to the most widely used scoring systems used by orthopedic surgeons and neurosurgeons for classifying spinal trauma and selecting management.

Spine trauma is a common indication for diagnostic imaging, and the use of advanced imaging for assessment of spinal injury has become routine at major trauma centers. Injuries of the spine are best understood by considering it as five distinct anatomic regions, each with its own unique anatomy and patterns of injury. These regions consist of the cervicothoracic, low cervical, thoracic, thoracolumbar, and low lumbar segments of the spine, with the majority of injuries occurring in the low cervical and thoracolumbar areas.

13.1 Craniocervical Junction (CCJ)

The craniocervical junction includes three bones (occipital base, C1, and C2), two joints (atlantooccipital and atlantoaxial), and several extrinsic and intrinsic ligaments, allowing for the delicate balance of flexibility while protecting the

C. Y. Chang (✉)
Massachusetts General Hospital, Boston, MA, USA
e-mail: cychang@mgh.harvard.edu

M. N. Pathria
UCSD Health System, San Diego, CA, USA
e-mail: mpathria@ucsd.edu

cranial blood supply, brainstem, and cranial nerves [1]. Careful description of each injured component and the degree of distraction is important, because these details determine stability and management [1, 2]. In this section, we will focus on C2 fractures, which account for 17–20% of cervical spine fractures [3, 4]. There are three main C2 fracture types: odontoid fractures, traumatic spondylolysis, and, less commonly, vertebral body/lateral mass fractures [2, 3].

Key Point
- Odontoid fractures are the most common C2 fractures, followed by traumatic spondylolisthesis; both fracture types have clinically relevant classification schemes.

Approximately 59% of C2 fractures involve the odontoid process [3, 4]. Mortality of C2 fractures in patients 65 years and older is substantial—approximately 15% at 30 days and 34% and 1 year [5]. The most common mechanism is motor vehicle accident, but in older patients even low energy trauma can result in odontoid process fractures [5]. There are three types of odontoid fractures as classified by Anderson and D'Alonzo (Fig. 13.1) [2, 6]. Type I (1–3%) fractures are through the odontoid tip and are likely due to alar ligament avulsion [3, 4, 6]. Because it is high in the odontoid, type I fractures are considered stable and typically heal with immobilization [3]. Type II (54–60%) fractures are at the junction of the odontoid and the vertebral body, and fractures with >6 mm displacement, comminution, and/or concomitant ligamentous injury have a greater risk of nonunion and likely require surgical management [3, 7, 8]. Hadley et al. also proposed a type IIA odontoid fracture with additional chip fracture fragments at the dens base, either anteriorly or posteriorly (Fig. 13.2) [8]. These fractures are unstable and tend toward nonunion [8]. Patients older than 50 years are at greater risk
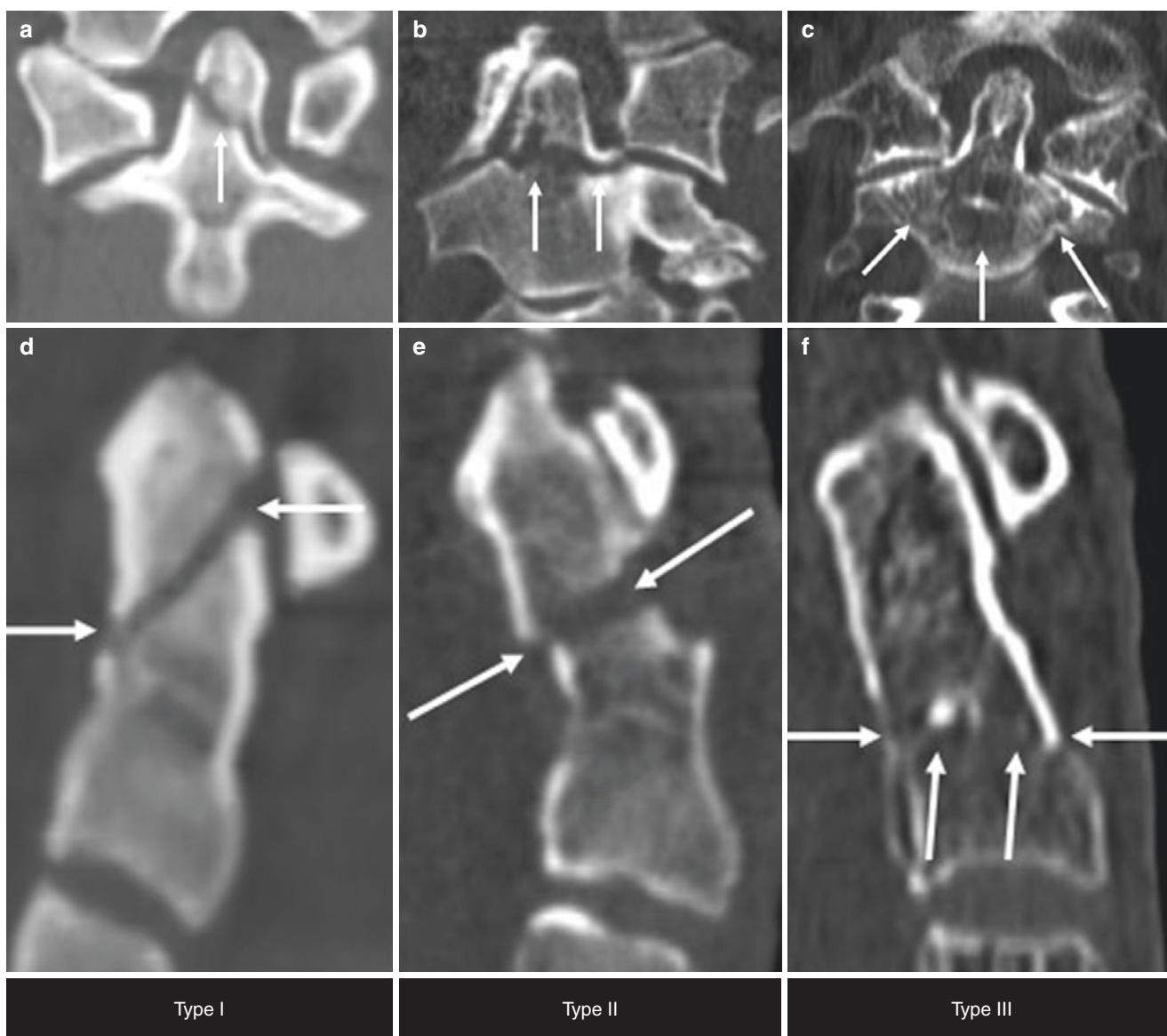
Fig. 13.1 Odontoid fracture classification. (**a**, **b**) A 39-year-old male injured in motor vehicle accident. Coronal (**a**) and sagittal (**b**) images of the C2 vertebral body demonstrate a fracture through the tip of the C1 vertebral body, consistent with a type I odontoid fracture. (**c**, **d**) A 69-year-old man who fell in the bathroom. Coronal (**c**) and sagittal (**d**) images of the C2 vertebral body demonstrate a fracture with less than 6 mm of displacement at the junction of the odontoid and C2 vertebral body, consistent with a type II odontoid fracture. The patient was neurologically intact and managed nonoperatively. (**e**, **f**) A 76-year-old woman with osteogenesis imperfecta who fell while transferring to a commode. Coronal (**e**) and sagittal (**f**) images of the C2 vertebral body demonstrate an oblique fracture through the cancellous portion of the C2 vertebral body (arrows), consistent with a type III odontoid fracture. This fracture was stable and healed with nonoperative management

for nonunion [9]. Type III (39–42%) fractures are through the cancellous bone of the vertebral body [4, 6]. They are generally stable and heal with halo immobilization [3, 4].

Traumatic spondylolisthesis is the second most common C2 fracture (approximately 38%) [1]. This fracture is commonly called the "hangman's fracture," although forensic research suggests that this fracture occurred in less than 10% of judicial hangings; currently it is most commonly due to motor vehicle accidents [10, 11]. There are five injury patterns as originally defined by Effendi and later revised by

Levine and Starr (Fig. 13.3) [12]. The degree of distraction and anterior translation should be described, as these determine fracture stability [12]. Type I (65–72%) fractures are the most common, followed by type II (27–28%) (Fig. 13.4) and type III (1–7%) fractures [3, 13]. Type I and type II may appear similar on supine imaging, and upright radiographs may reveal distraction [1, 14]. Type IIA has more distraction than translation and therefore a greater degree of kyphosis when compared with type II [1, 14]. Neurologic injury is uncommon and only occurs if there is spinal canal narrowing,
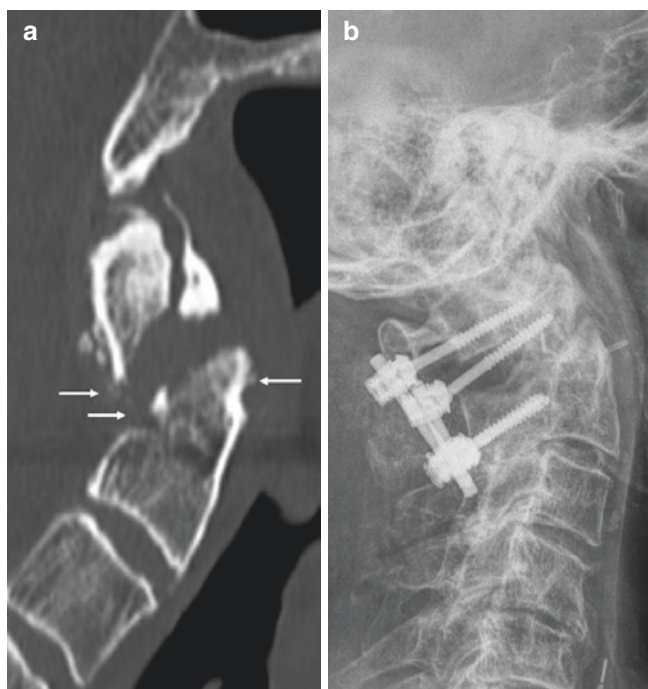
Fig. 13.2 An 85-year-old man with neck pain after unwitnessed fall. (**a**) Sagittal CT image demonstrates a displaced fracture through the base of the odontoid process, with more than 6 mm of displacement and small chip fragments anteriorly and posteriorly (arrows), consistent with a type IIA fracture. This fracture is unstable and requires surgical management. (**b**) Subsequent lateral radiograph demonstrates posterior C1–C2 spinal fusion

which may occur in type IA (33%) or type III (60%) injuries [1]. The other fracture types generally result in spinal canal widening [1].

Vertebral body/lateral mass fractures (22%) are the least common, and the vast majority are managed nonoperatively with good result [3]. C2 body fractures are difficult to detect on radiographs, and Pellei described a useful finding called the "fat" C2 sign to improve sensitivity (Fig. 13.5) [15]. The C2 vertebral body appears "fat" (increased anteroposterior diameter) when there is a displaced vertebral body fracture fragment and suggests that the fracture is unstable requiring further imaging. This sign may be the result of any fracture involving the C2 vertebral body, including a type III dens fracture or an atypical traumatic spondylolysis.

13.2 Mid to Lower Cervical

Mid to lower cervical spine (subaxial) injuries represent 65% of cervical spine fractures and are classified based on mechanism of injury: flexion compression, extension compression, vertical compression, flexion-distraction, extension-distraction, and lateral flexion or rotation [12]. The Subaxial Injury Classification and Scoring (SLIC) system incorporates imaging (CT and MRI) and clinical findings into a single score, placing the patient in nonsurgical (total SLIC

	Type I	**Type IA**	**Type II**	**Type IIA**	**Type III**
Forces	Hyperextension Axial loading	+ Lateral bending	+ Flexion	+ Flexion and distraction	
Displacement	< 3 mm		> 3 mm		
Associated injuries		Vertebral body	C2-C3 intervertebral disc Posterior longitudinal ligament		
					C2-C3 facet dislocation
Un/Stable	Stable	Unstable	Unstable	Unstable	Unstable
Management	Ambulatory immobilization	Ambulatory immobilization	Halo Immoblization	Surgical	Surgical

Fig. 13.3 Traumatic spondylolisthesis classification
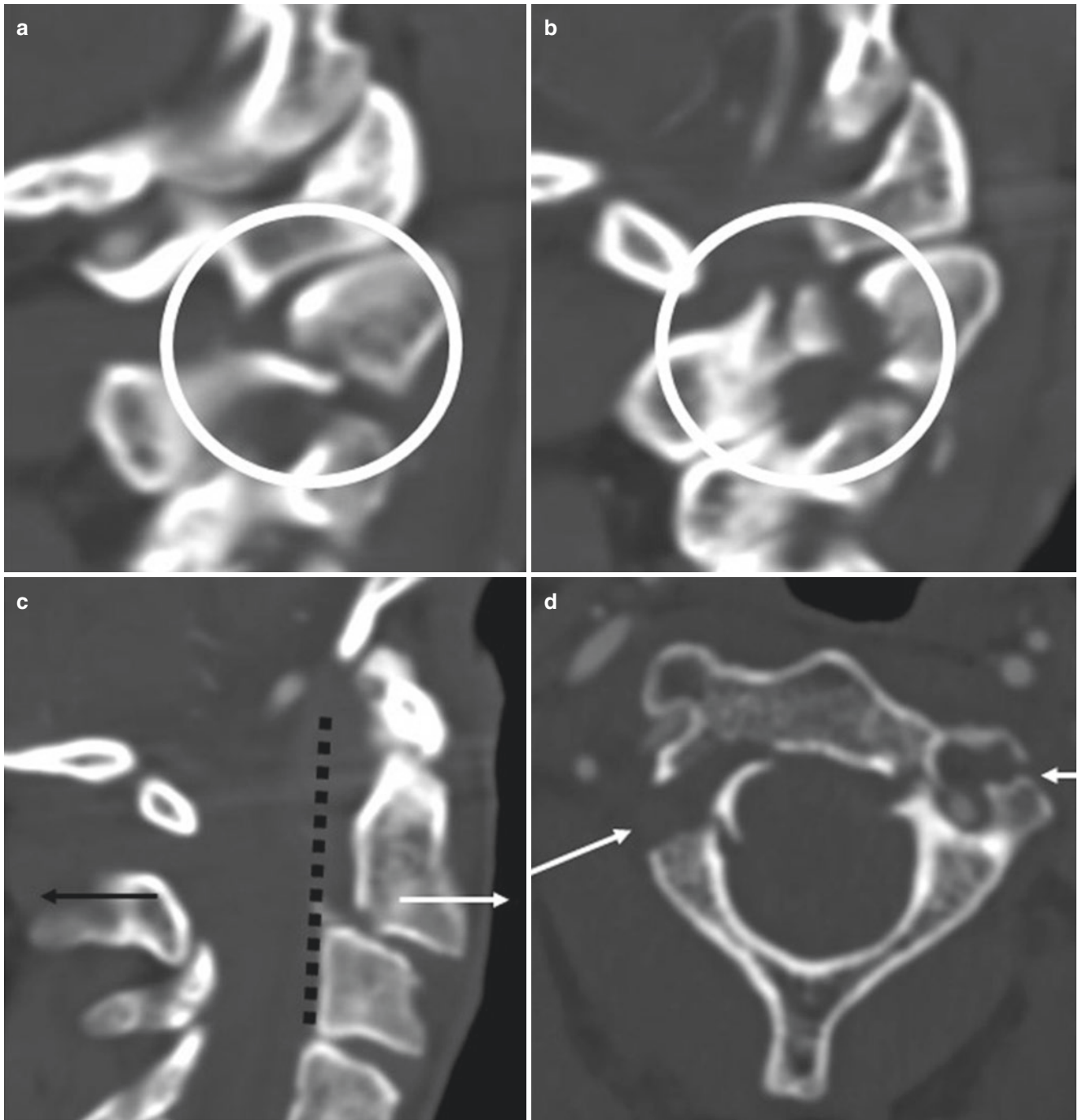
Fig. 13.4 A 62-year-old woman with multiple sclerosis who presents status post fall. (**a**, **b**) Sagittal CT images of the cervical spine demonstrate bilateral C2 pars interarticularis fractures. (**c**) Sagittal CT image of the cervical spine demonstrates anterolisthesis (white arrow) and posterior displacement of the C2 posterior elements (black arrow). (**d**)

Axial CT image of the cervical spine demonstrates bilateral comminuted fractures extending into the vertebral foramina. There was no evidence for vertebral artery injury. This fracture is atypical, but most closely approximates by a type II fracture
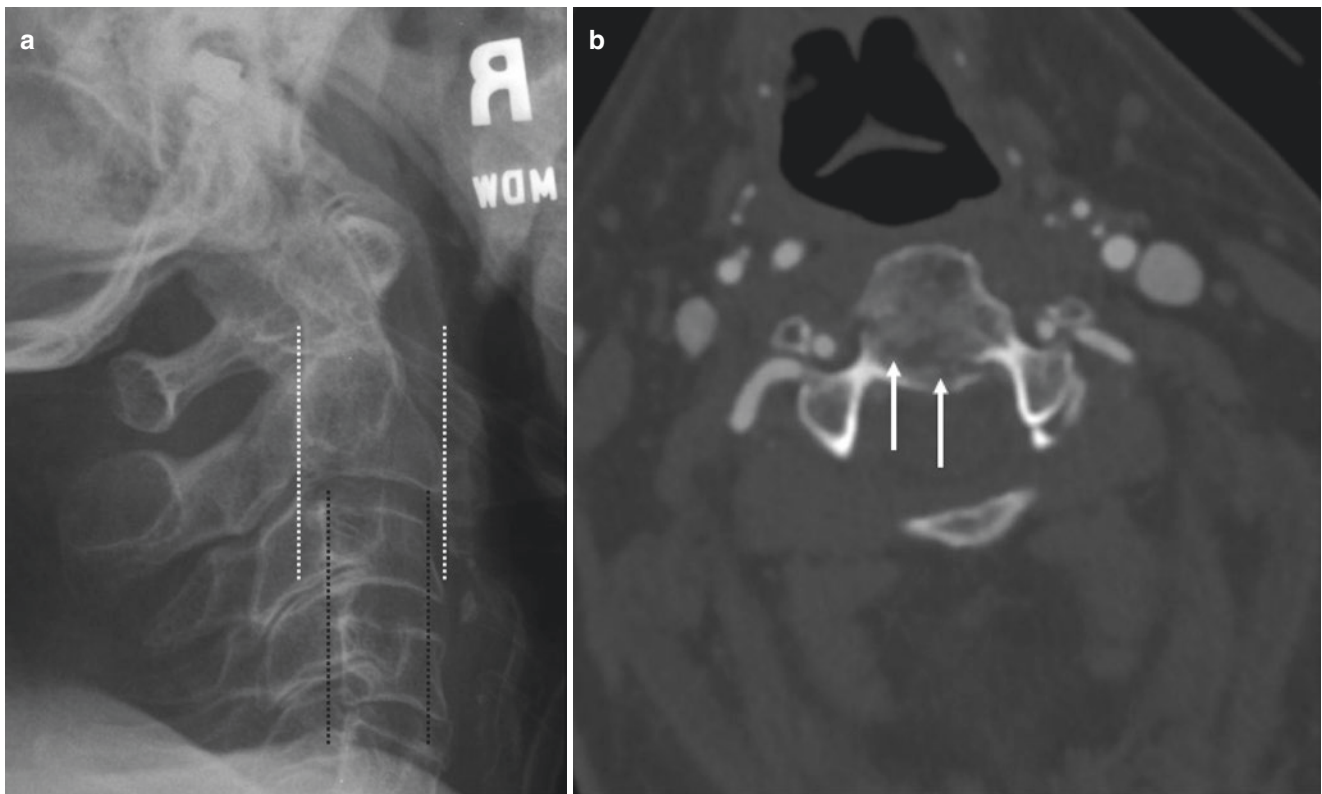
Fig. 13.5 A 79-year-old woman who was T-boned in a motor vehicle accident. (**a**) Lateral radiograph of the cervical spine demonstrates wider anterior-posterior (AP) diameter of the C2 vertebral body (white dotted line) compared to the AP diameter of the C3 vertebral body (black dotted line). (**b**) Axial CT image through the level of C2 demonstrates a mildly displaced vertebral body fracture

score ≤3), indeterminate (=4), or surgical (≥5) management categories (Table 13.1) [12]. Each injured level receives a separate score. The abnormality with the highest score is used for the scoring system, i.e., fractures with distraction and translation are scored as translation [16, 17].

> **Key Point**
> - The Subaxial Injury Classification and Scoring (SLIC) system is helpful for framing evaluation of mid to lower cervical spinal injuries.

Familiarity with this scoring system is important for radiologists interpreting these studies, because communication of findings using this terminology enhances communication with the trauma surgeons. Patients with a high SLIC score typically require surgical management to relieve cord compression and stabilize the spine (Fig. 13.6). Conversely, patients with a low SLIC score can be managed conservatively (Fig. 13.7).

Table 13.1 Subaxial Injury Classification and Scoring (SLIC) system [2, 35]

Category	Score
Neurologic status	
Intact	0
Root injury	1
Complete cord injury	2
Incomplete cord injury	3
Incomplete cord injury with ongoing cord compression	4
Morphology	
No abnormality	0
Compression	1
Burst	2
Distraction (facet diastasis >2 mm, facet subluxation with <50% overlap, posterior disk space widening and >11° angulation)	3
Rotation (anterolisthesis >3.5 mm but <50% of caudal vertebral body anterior-posterior (AP) dimension) *or* translation (anterolisthesis >3.5 mm and >50% of caudal vertebral body anterior-posterior (AP) dimension)	4
Discoligamentous complex	
Intact	0
Indeterminate	1
Disrupted	2
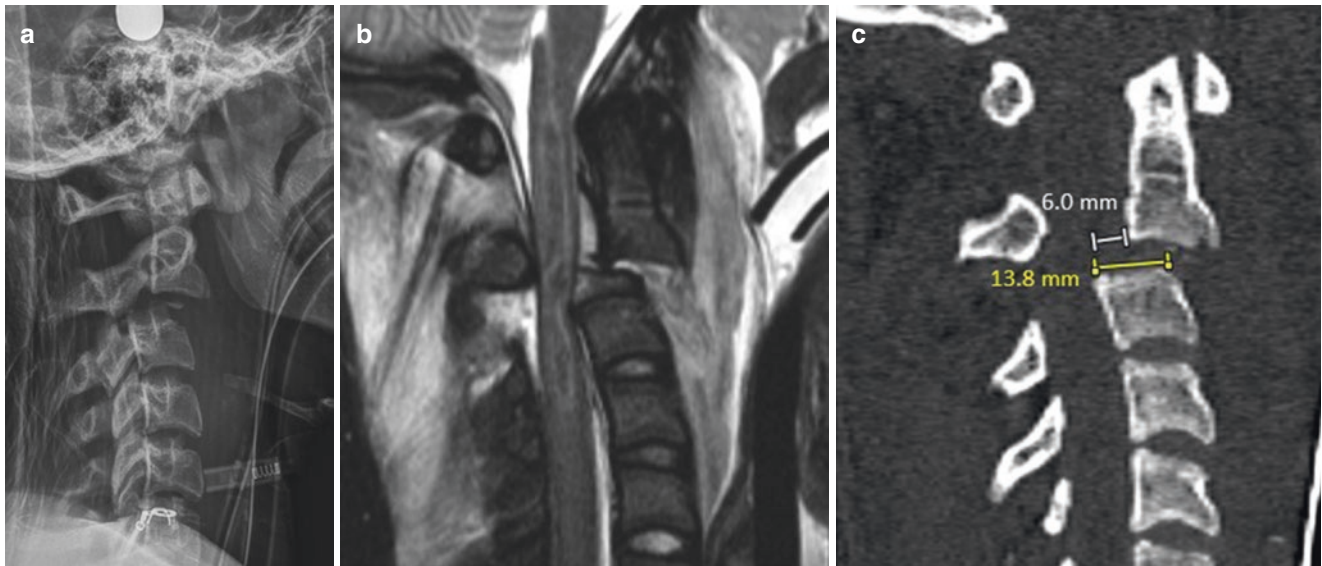
Fig. 13.6 An 18-year-old man who was a restrained passenger in a motor vehicle accident, where his car collided with another vehicle and rolled into a ditch. Unfortunately, the patient did not survive the accident and passed away several days later. (**a**) Lateral radiograph demonstrates anterolisthesis of the widened C2–C3 disk space, comminuted fracture fragments in the disk space, probably from the C3 superior endplate, and bilateral perched facets. (**b**) Sagittal T2 fat-suppressed image through the midline of the upper cervical spine demonstrates complete separation of the C2 inferior endplate from the C2–C3 intervertebral disk, anterior longitudinal and posterior longitudinal ligament injury, and interspinous ligament injuries. There is extensive anterior and posterior soft tissue hemorrhage. There is also hemorrhage within the swollen spinal cord, with ongoing compression of the cord by the C3 vertebral body. The patient's clinical examination was consistent with complete cord injury, but given the ongoing cord compression, the SLIC neurologic status score is 4. (**c**) Sagittal CT image through the midline of the upper cervical spine demonstrates anterolisthesis >3.5 mm but less than 50% of the C3 vertebral body. For the morphology category, the facets are subluxated >50% of the articular surfaces; however, there is also >3.5 mm anterolisthesis, which is <50% of the caudal vertebral body AP dimension, resulting in a SLIC morphology score of 4. The discoligamentous complex is disrupted, consistent with a SLIC score of 2. The total SLIC score is 10, which would warrant surgical management for the fracture

Fig. 13.7 A 70-year-old man status post fall with head strike against a wall. Sagittal CT image demonstrates a comminuted C7 vertebral body fracture with compression (arrows). The fracture does not extend to the vertebral body posterior margin. There is bilateral facet subluxation (only one side shown; circle). There is no listhesis (dotted line). The patient had no neurologic deficits (SLIC neurologic status score 0). The facet joints are subluxated bilaterally, but there is no facet diastasis or posterior disk space widening to indicate discoligamentous description. There is compression of the vertebral body, consistent with a SLIC morphology score of 1. The total SLIC score is low and the patient was successfully treated with conservative management

13.3 Upper Thoracic

The T1–T10 vertebrae are relatively immobile as they are stabilized by a ring formed by the spine, ribs, and sternum so traumatic injuries of this region are less common than at the more mobile cervical and thoracolumbar regions. In young adults, less than 25% of all thoracic fractures affect T1–T10, typically following a fall, motor vehicle accident or seizure [18]. The most common fracture pattern is superior endplate compression resulting in paraspinal swelling, anterior height loss, and disruption of the anterior cortex and subchondral bone, without posterior height loss, retropulsed bone, or malalignment. Mild height loss alone lacks specificity as it can be physiologic or due to Scheuermann disease, which is associated with disk height loss, Schmorl nodes, and kyphosis [19]. Impacted subchondral trabecular bone is more specific, appearing as a transverse zone of sclerosis paralleling the endplate that becomes more apparent as the fracture heals. Mild compression fractures are stable, but those with greater than 40% height loss can result in delayed kyphotic deformity, particularly if there are multiple contiguous fractures [20].

While fractures of the upper thoracic spine in young patients are typically the result of significant force, upper thoracic fractures in elderly osteoporotic patients often result from trivial injury and can be challenging to visualize on

radiographs. Osteoporotic thoracic fractures are common; 18% of white women older than 50 and 78% of white women older than 90 years have at least one thoracic compression fracture, typically in conjunction with additional fractures in the lumbar region [21]. Bone fragility allows the fracture to propagate easily to the posterior vertebral body margin, resulting in greater height loss and retropulsion of bone into the canal.

In elderly patients, distinguishing osteoporotic fractures from pathologic fractures can be challenging. Findings sug-

gesting underlying neoplasia include isolated fractures above T7, preferential posterior height loss or bulging of the posterior cortex, cortical erosion of the vertebral body or posterior elements, soft tissue mass, and diffuse replacement of the vertebral body fat signal, whereas a simple transverse fracture line with band-like partial marrow replacement limited to the upper or lower half of the vertebral body and the presence of a linear cleft of fluid or gas favor a benign process [22] (Fig. 13.8). MR techniques that identify regions of restricted diffusion within neoplastic tissue and phase imag-

Fig. 13.8 A 74-year-old male with history of prostate cancer. Sagittal CT (**a**) and T1-weighted MR (**b**) of the thoracic spine show a pathologic fracture at T10 (arrows) and a benign osteoporotic compression fracture at T12. The CT shows subtle increased density at T10 and cortical blurring of the edges of the spinous process. The MR shows complete marrow replacement of the T10 vertebral body and spinous process at T10, mild height loss and a convex contour at the posterior vertebral margin, and encroachment on the posterior epidural space by soft tissue extension from the posterior elements resulting in stenosis. In contrast, the chronic osteoporotic fracture at T12 shows normal fatty marrow signal, a more angular deformity of the superior endplate, and an intact posterior margin

ing to identify microscopic fat within benign lesions are useful in equivocal cases though some fractures remain indeterminate, requiring biopsy [23].

Key Point
- Upper thoracic fractures in elderly osteoporotic patients can be difficult to distinguish from pathologic fractures. Morphologic features of the fracture and adjacent soft tissues are augmented by advanced MR imaging techniques to help determine if the fracture is benign or malignant.

Severe upper thoracic injuries such as burst fractures with retropulsed bone, anterior and posterior distraction injuries, and fracture-dislocation are uncommon. Fracture-dislocation of the upper thoracic spine is the result of combined hyperflexion, axial loading, and rotary/shear forces resulting in extensive ligament disruption, complex fractures, and spinal malalignment including translation, rotation, and telescoping of vertebrae [23] (Fig. 13.9). In such injuries, the disproportionately small ratio of the spinal canal to the cord in the upper thoracic region leads to a high risk of neurologic deficit. Soft tissue hemorrhage and associated visceral and mediastinal injuries are common [18]. CT and MR are needed to fully characterize
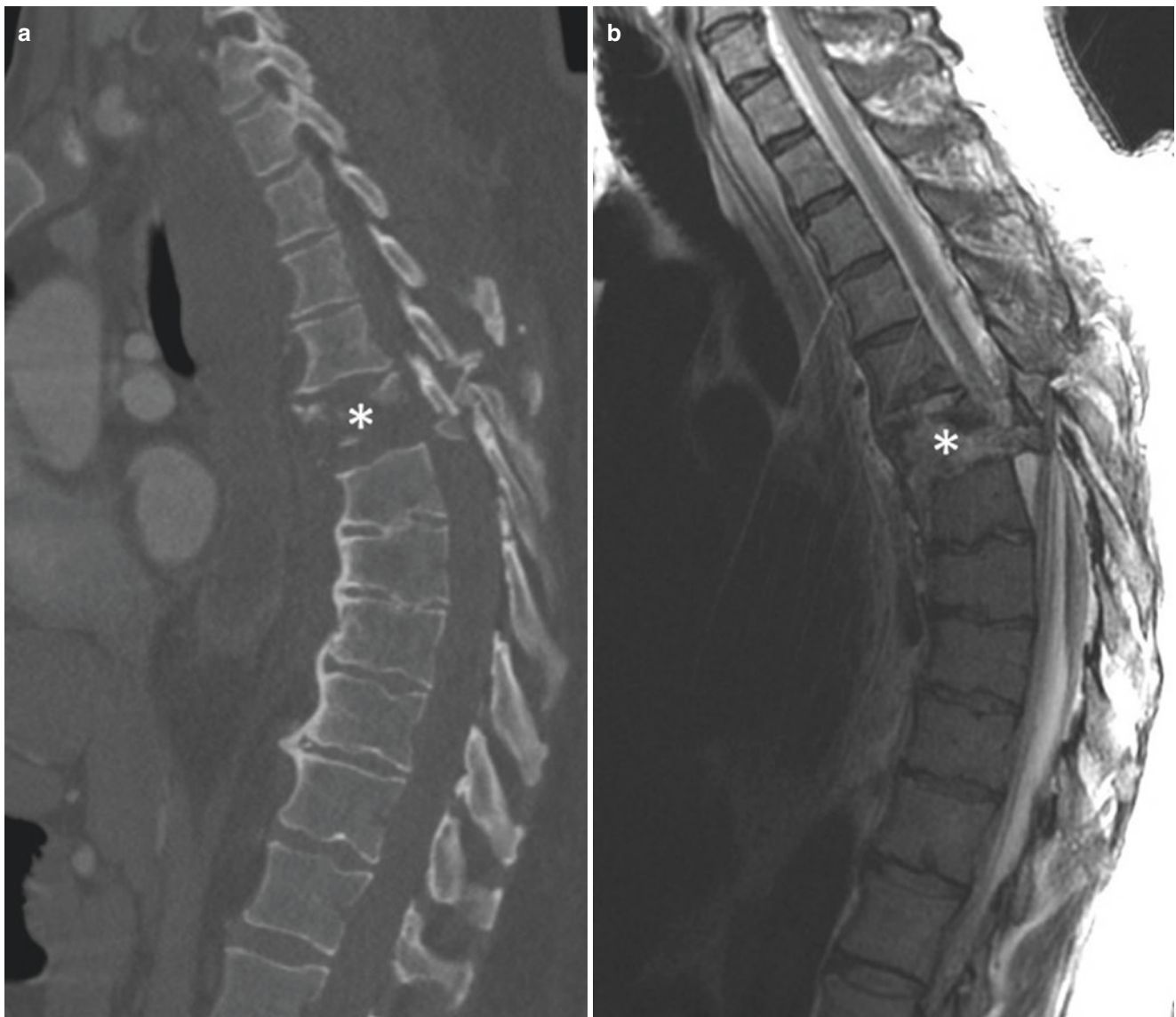
Fig. 13.9 A 56-year-old involved in all-terrain vehicle accident with fracture-dislocation of the upper thoracic spine resulting in paraplegia. Sagittal CT (**a**) of the thoracic spine illustrates multiple upper thoracic fractures with comminution of the T6 body (asterisk), malalignment with anterior shift of T5 relative to T7, disruption of the posterior elements with facet dislocation, and large bone fragments encroaching on the spinal canal. (**b**) The corresponding T2-weighted sagittal MR shows disruption of the thoracic cord at the injury level

these complex injuries, affording detailed assessment of fractures, ligaments, neural elements, and paraspinal soft tissues.

13.4 Thoracolumbar

The thoracolumbar region is commonly injured, representing the second most common site of spinal trauma following the lower cervical spine. Modern classification systems of spinal injury are based on systems initially developed to organize thoracolumbar injuries according to injury mechanism, using fracture morphology and degree of displacement to assess stability and plan management. The initial system widely used was the Denis classification that divided the spine into anterior, middle, and posterior columns, emphasizing the role of the middle column (posterior vertebral margin, posterior longitudinal ligament, and posterior annulus) in maintaining stability [24]. Denis classified thoracolumbar injuries into (1) compression fracture limited to the anterior column; (2) burst fracture involving anterior and middle columns; (3) seat belt injury resulting from distraction of the middle and posterior columns from distraction; and (4) fracture-dislocation with disruption of all three columns. This classification was based on radiographs and did not account for many spinal injuries, particularly those where the anterior spine was compressed while the posterior ligaments failed by distraction, a pattern well appreciated on MR imaging. Current classification systems have expanded Denis' system to offer a more comprehensive classification and account for more injury patterns and also include clinical parameters. Currently, the most widely used thoracolumbar injury classification is based on combining features of the AO-Magerl classification (Arbeitsgemeinschaft für Osteosynthesefragen) and TLICS (Thoracolumbar Injury Classification and Severity Score) system [16, 20]. The AO/TLICS system, based on a consensus of international spine surgeons, classifies fracture morphology into three main patterns: type A (compression), type B (tension band disruption, either anterior or posterior), and type C (displacement/translation) with several subtypes in the first two categories. The grading of morphology relies on accurate assessment of both bone and ligament injury and emphasizes the utility of CT and MRI for assessment of thoracolumbar trauma [25].

> **Key Point**
> - The AO/TLICS classification of thoracolumbar injuries is based on fracture morphology as defined by imaging, categorizing fractures into those caused by compression, distraction, or translation.

The fracture morphology score is combined with a grading of neurologic status and a description of patient-specific modifiers that affect the likelihood of surgery to help select management [16]. This classification has similar considerations as the SLIC grading system of cervical trauma previously discussed.

13.4.1 Type A: Compression Injuries

The most common injury mechanism is compression which produces a range of fracture morphologies that include superior and inferior endplate impaction, anterior wedging of varying severity, burst fractures, and sagittal splitting of the vertebral body. Similar to the remainder of the spine, mild compression fractures result in anterior height loss, buckling of the cortex, and endplate comminution producing band-like sclerosis adjacent to the fractured endplate. On CT, these appear as an arc of irregular bony fragments displaced circumferentially at the level of the endplate. Posterior vertebral and intervertebral disk height are preserved and there is no listhesis. Compression fractures with greater than 40% height loss, particularly in the setting of multiple contiguous fractures and posterior ligament sprain may require prolonged bracing [26]. Severe compression fractures showing with greater than 70% height loss may require posterior stabilization to avoid kyphotic deformity. Unlike simple compression fractures, burst fractures involve the posterior vertebral body margin, leading to posterior vertebral height loss and retropulsed bone in the spinal canal. The thoracolumbar region is the most common site of spinal burst fractures, and such injuries make up 16% of all spinal injuries encountered at a trauma center. CT scanning is the most efficient method for characterizing the fracture, identifying associated posterior element fractures and evaluating bone encroaching on the spinal canal (Fig. 13.10).

13.4.2 Type B: Distraction (Tension Band) Injuries

The vast majority of distraction injuries of the thoracolumbar spine results from flexion with the resulting tensile force, leading to purely osseous, purely ligamentous, or combined bony and soft tissue injury starting at the posterior spine allowing separation between the posterior elements, followed by anterior soft tissue injury or vertebral fracture. The classic horizontally oriented Chance fracture is one example of a distraction injury, but there is a broad spectrum of distraction injury patterns depending on whether the injury is primarily ligamentous or osseous and whether distraction affects the entire spine or only the posterior elements. Distraction injuries are associated with variable amounts of
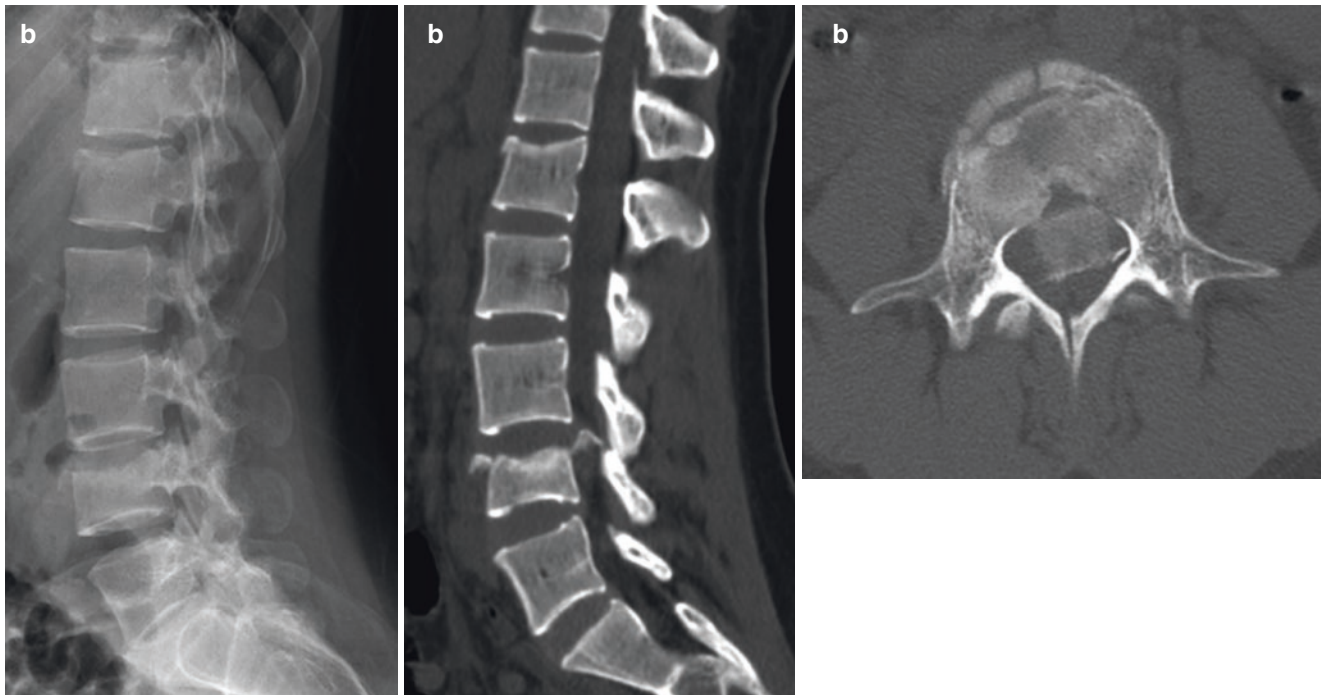
Fig. 13.10 A 28-year-old male with spinal injury after falling downstairs while intoxicated. The lateral radiograph (**a**) shows a mild superior endplate compression fracture of L1 with anterior cortical disruption and minimal height loss. Note the sclerosis below the superior endplate. The L4 vertebral body shows a burst fracture with height loss extending to the posterior vertebral margin. Sagittal CT (**b**) shows the fractures well and demonstrates a large rotated fragment of retropulsed bone within the spinal canal at L4. Axial CT (**c**) at L4 shows comminution of the vertebral body and a large fragment encroaching on the canal and neural elements. There is a sagittal split fracture through the posterior arch

splaying of the posterior elements, which can be overlooked on radiographs and CT, particularly if the patient is recumbent [27]. In practice, many posterior tension band injuries with vertebral body fractures are easily confused for simple compression or burst fractures without MR imaging, which should be obtained whenever posterior ligament injury is suspected (Fig. 13.11). Anterior tension band injuries caused by hyperextension are far less common. The typical injury pattern is a horizontal fracture through the vertebral body or through an ossified disk in an elderly patient with underlying degenerative spinal fusion, leading to increased vertebral or disk height and lordosis [28].

13.4.3 Type C: Displacement/Dislocation

The most severe pattern of injury consists of displacement injuries with translation and/or rotation due to disruption of all the spinal ligaments, typically in association with fractures at both the anterior and posterior vertebra. Rib fractures and costotransverse dislocations often accompany these injuries.

Thoracolumbar displacement/dislocation injuries are associated with a high rate of neurologic deficit, with 50–90% of patients developing a permanent neurologic deficit.

13.5 Lower Lumbar

Pars interarticularis fracture or spondylolysis is a stress fracture of the bony arch connecting the upper and lower facet joints and occurs primarily at the L5 (85–95%) and L4 (5–15%) levels [29, 30]. The prevalence is approximately 6%, and many are asymptomatic, but spondylolysis can cause pain in athletes with high lower back stress (football, wrestling, dancing, weight lifting), particularly in the adolescent and preadolescent population [31, 32]. Diagnosis on radiographs is best made on the oblique view, but radiographs have low sensitivity for stress injury and nondisplaced stress fractures (Fig. 13.12) [30, 33]. Flexion and extension views can detect motion and instability in the case of spondylolisthesis, which occurs in 50–81% of patients with spondylolysis [29, 31, 33].

Fig. 13.11 A 39-year-old female injured during motor vehicle accident. Sagittal CT (**a**) and T2-weighted MR (**b**) images of the lumbar spine show a fracture of the L1 vertebral body (asterisk) with height loss and a small bulge of retropulsed bone arising from the posterior margin of the upper endplate. An MR was obtained because of focal posterior pain and swelling and shows disruption of the supraspinous ligament (arrow), as well as edema in the T12/L1 interspace and loss of low signal at the ligamenta flava, indicating a tension band injury disrupting the posterior ligaments

A low threshold for obtaining a CT or MRI in patients with a suspicious clinical history and physical examination is recommended, because early detection and appropriate treatment (primarily rest and pain management) is important to prevent progression and more aggressive intervention [29]. CT has the highest sensitivity for fracture detection, while MRI has the advantage of detecting edema in early-stage injury (Fig. 13.13) [29]. Most patients are successfully managed conservatively, with surgery reserved for the 9–15% of cases that remain symptomatic after conservative care [29]. Because the condition can be asymptomatic, diagnostic steroid and anesthetic injection can be helpful to confirm the spondylolysis as the source of the patient's pain prior to surgery [34].
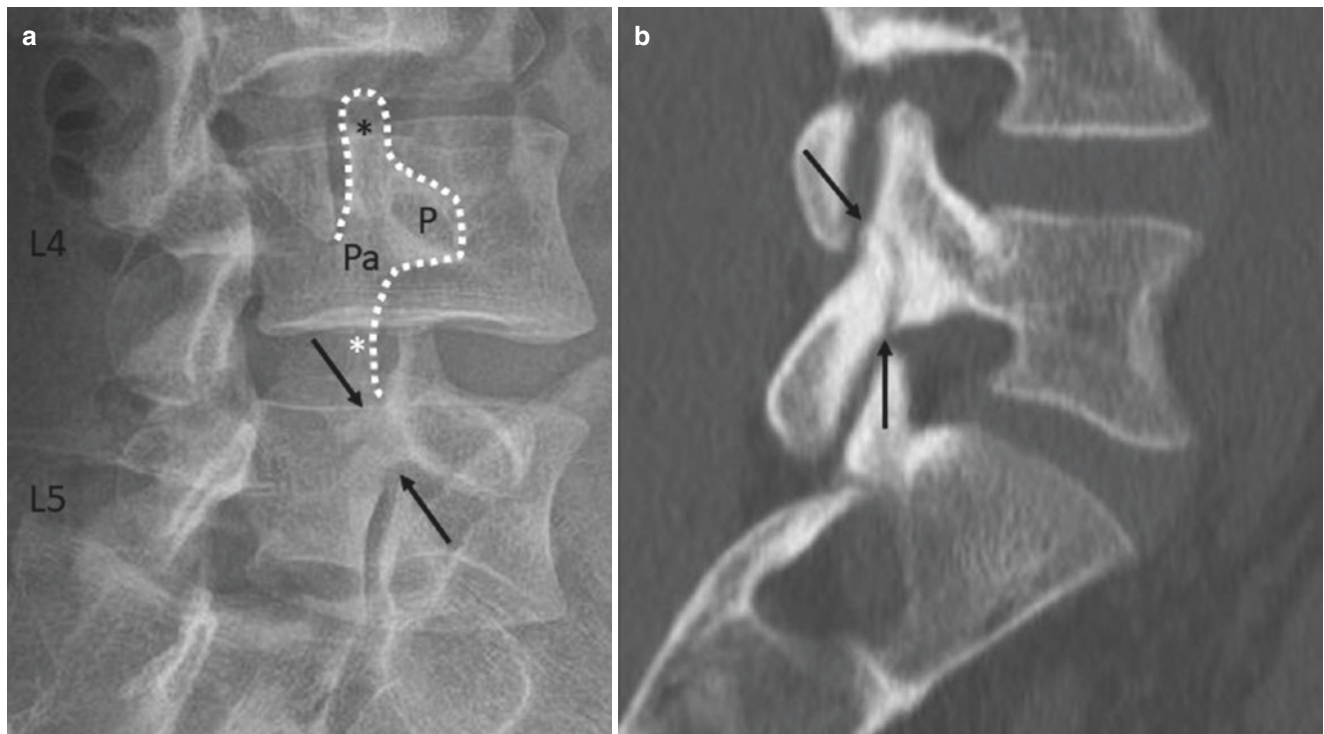
Fig. 13.12 A 24-year-old baseball player with acute on chronic unilateral left-sided lower back pain. (**a**) Oblique radiograph of the spine demonstrates the "Scottie dog" appearance of the vertebrae, outlined at the L4 level (dotted white line). P = pedicle, Pa = pars interarticularis, black * = superior articular facet, white * = inferior articular facet. There is a resorption of the cortices and thinning of the pars interarticularis at L5; the fracture line is only partially visualized (arrows). (**b**) Sagittal CT image demonstrates a nondisplaced fracture of the left L5 pars interarticularis (arrows). There is surrounding sclerosis
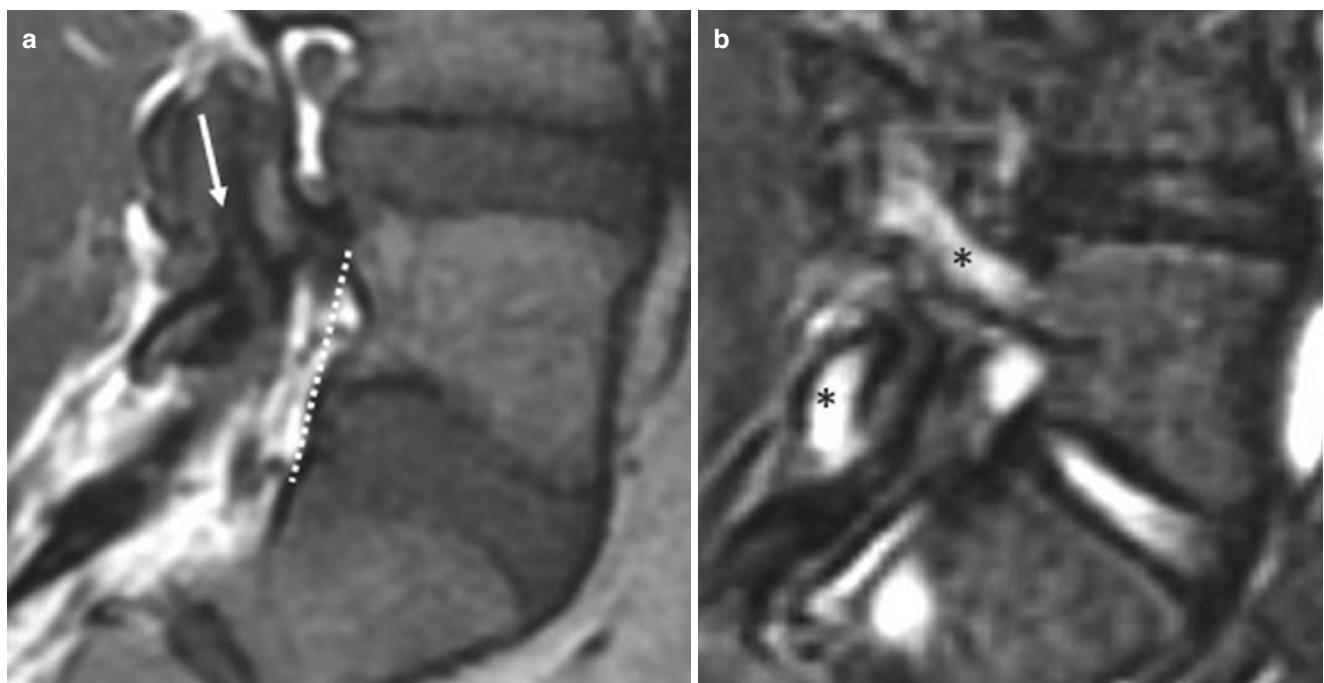
Fig. 13.13 An 18-year-old multisport collegiate athlete with acute on chronic left lower back pain since elementary school. (**a**) Sagittal T1 MRI image demonstrates nondisplaced left L5 pars interarticularis fracture (arrow). There is no anterolisthesis (dotted line). (**b**) Sagittal T2 FS MRI image demonstrates marrow edema around the nondisplaced left L5 pars interarticularis fracture (*)

13.6 Concluding Remarks

Diagnostic imaging plays a critical role in identifying and classifying spinal injury. Understanding the unique features of each spinal segment and relevant classification systems can help the radiologist both with injury detection and with generating clinically relevant reports to help guide management.

> **Take Home Messages**
> - Injury affects different regions of the spine in different ways as a result of their unique anatomy and physiology. The most commonly injured regions are the lower cervical and thoracolumbar segments.
> - Modern imaging and classification of spine trauma rely on cross-sectional imaging for diagnosis and classification of suspected spinal injury.
> - Current classifications (SLIC and AO/TLICS) of spinal fractures are based on injury morphology as defined by imaging, combined with clinical parameters, to select suitable management.

References

1. Bransford RJ, Alton TB, Patel AR, Bellabarba C. Upper cervical spine trauma. J Am Acad Orthop Surg. 2014;22:718–29.
2. Dreizin D, Letzing M, Sliker CW, Chokshi FH, Bodanapally U, Mirvis SE, Quencer RM, Munera F. Multidetector CT of blunt cervical spine trauma in adults. Radiogr Rev Publ Radiol Soc N Am Inc. 2014;34:1842–65.
3. Greene KA, Dickman CA, Marciano FF, Drabier JB, Hadley MN, Sonntag VK. Acute axis fractures. Analysis of management and outcome in 340 consecutive cases. Spine. 1997;22:1843–52.
4. Pryputniewicz DM, Hadley MN. Axis fractures. Neurosurgery. 2010;66:68–82.
5. Shafafy R, Valsamis EM, Luck J, Dimock R, Rampersad S, Kieffer W, Morassi GL, Elsayed S. Predictors of mortality in the elderly patient with a fracture of the odontoid process. Bone Jt J. 2019;101-B:253–9.
6. Anderson LD, D'Alonzo RT. Fractures of the odontoid process of the axis. J Bone Joint Surg Am. 1974;56:1663–74.
7. Hadley MN, Browner C, Sonntag VK. Axis fractures: a comprehensive review of management and treatment in 107 cases. Neurosurgery. 1985;17:281–90.
8. Hadley MN, Browner CM, Liu SS, Sonntag VK. New subtype of acute odontoid fractures (type IIA). Neurosurgery. 1988;22:67–71.
9. Lennarson PJ, Mostafavi H, Traynelis VC, Walters BC. Management of type II dens fractures: a case-control study. Spine. 2000;25:1234–7.
10. James R, Nasmyth-Jones R. The occurrence of cervical fractures in victims of judicial hanging. Forensic Sci Int. 1992;54:81–91.
11. Ferro FP, Borgo GD, Letaif OB, Cristante AF, Marcon RM, Lutaka AS. Traumatic spondylolisthesis of the axis: epidemiology, management and outcome. Acta Ortop Bras. 2012;20:84–7.
12. Riascos R, Bonfante E, Cotes C, Guirguis M, Hakimelahi R, West C. Imaging of atlanto-occipital and atlantoaxial traumatic injuries: what the radiologist needs to know. Radiogr Rev Publ Radiol Soc N Am Inc. 2015;35:2121–34.
13. Effendi B, Roy D, Cornish B, Dussault RG, Laurin CA. Fractures of the ring of the axis. A classification based on the analysis of 131 cases. J Bone Joint Surg Br. 1981;63-B:319–27.
14. Levine AM, Edwards CC. The management of traumatic spondylolisthesis of the axis. J Bone Joint Surg Am. 1985;67:217–26.
15. Pellei DD. The fat C2 sign. Radiology. 2000;217:359–60.
16. Vaccaro AR, Hulbert RJ, Patel AA, et al. The subaxial cervical spine injury classification system: a novel approach to recognize the importance of morphology, neurology, and integrity of the disco-ligamentous complex. Spine. 2007;32:2365–74.
17. Patel AA, Dailey A, Brodke DS, Daubs M, Anderson PA, Hurlbert RJ, Vacccaro AR, Spine Trauma Study Group. Subaxial cervical spine trauma classification: the subaxial injury classification system and case examples. Neurosurg Focus. 2008;25:E8.
18. Splendiani A, Bruno F, Patriarca L, Barile A, Di Cesare E, Masciocchi C, Gallucci M. Thoracic spine trauma: advanced imaging modality. Radiol Med (Torino). 2016;121:780–92.
19. Palazzo C, Sailhan F, Revel M. Scheuermann's disease: an update. Joint Bone Spine. 2014;81:209–14.
20. Magerl F, Aebi M, Gertzbein SD, Harms J, Nazarian S. A comprehensive classification of thoracic and lumbar injuries. Eur Spine J. 1994;3:184–201.
21. Gerdhem P. Osteoporosis and fragility fractures: vertebral fractures. Best Pract Res Clin Rheumatol. 2013;27:743–55.
22. Mauch JT, Carr CM, Cloft H, Diehn FE. Review of the imaging features of benign osteoporotic and malignant vertebral compression fractures. AJNR Am J Neuroradiol. 2018;39:1584–92.
23. Geith T, Schmidt G, Biffar A, Dietrich O, Duerr HR, Reiser M, Baur-Melnyk A. Quantitative evaluation of benign and malignant vertebral fractures with diffusion-weighted MRI: what is the optimum combination of b values for ADC-based lesion differentiation with the single-shot turbo spin-echo sequence? AJR Am J Roentgenol. 2014;203:582–8.
24. Denis F. The three column spine and its significance in the classification of acute thoracolumbar spinal injuries. Spine. 1983;8:817–31.
25. Khurana B, Sheehan SE, Sodickson A, Bono CM, Harris MB. Traumatic thoracolumbar spine injuries: what the spine surgeon wants to know. Radiogr Rev Publ Radiol Soc N Am Inc. 2013;33:2031–46.
26. Raniga SB, Skalski MR, Kirwadi A, Menon VK, Al-Azri FH, Butt S. Thoracolumbar spine injury at CT: trauma/emergency radiology. Radiogr Rev Publ Radiol Soc N Am Inc. 2016;36:2234–5.
27. Bernstein MP, Mirvis SE, Shanmuganathan K. Chance-type fractures of the thoracolumbar spine: imaging analysis in 53 patients. AJR Am J Roentgenol. 2006;187:859–68.
28. Balling H, Weckbach A. Hyperextension injuries of the thoracolumbar spine in diffuse idiopathic skeletal hyperostosis. Spine. 2015;40:E61–7.
29. Symrou E, Tsitsopoulos PP, Marinopoulos D, Tsonidis C, Anagnostopoulos I, Tsitsopoulos PD. Spondylolysis: a review and reappraisal. Hippokratia. 2010;14:17–21.
30. Standaert CJ, Herring SA. Spondylolysis: a critical review. Br J Sports Med. 2000;34:415–22.
31. Hu SS, Tribus CB, Diab M, Ghanayem AJ. Spondylolisthesis and spondylolysis. Instr Course Lect 57:431–445. JBJS. 2008;90:656–71.

32. McTimoney CAM, Micheli LJ. Current evaluation and manage-ment of spondylolysis and spondylolisthesis. Curr Sports Med Rep. 2003;2:41–6.
33. Scavone JG, Latshaw RF, Weidner WA. Anteroposterior and lat-eral radiographs: an adequate lumbar spine examination. AJR Am J Roentgenol. 1981;136:715–7.
34. Kershen LM, Nacey NC, Patrie JT, Fox MG. Accuracy and efficacy of fluoroscopy-guided pars interarticularis injections on immediate and short-term pain relief. Skelet Radiol. 2016;45:1329–35.
35. Dvorak MF, Fisher CG, Fehlings MG, Rampersaud YR, Oner FC, Aarabi B, Vaccaro AR. The surgical approach to subaxial cervical spine injuries: an evidence-based algorithm based on the SLIC clas-sification system. Spine. 2007;32:2620–9.

Spine Degeneration and Inflammation

14

David J. Wilson and Marcelo de Abreu

Learning Objectives
- To understand how degenerative disorders of the spine develop and exhibit themselves on imaging.
- To understand how inflammatory disorders of the spine develop and exhibit themselves on imaging.
- To recognize inflammatory and degenerative disorders in the differential diagnosis of spinal disease.

14.1 Degenerative Diseases of the Spine

At some point in our lives, almost all of us will suffer from back pain. The clear majority will have degenerative disease of the discs or facet joints. A small minority will have tumours, insufficiency fractures, inflammatory joint disease or infection. Differentiation of these conditions is clearly critical for management. In this syllabus, we will cover degeneration and inflammatory joint disease and describe how imaging and image-guided intervention are important in precise diagnosis and planning therapy. Brief mention will be made of the alternative diagnoses.

14.1.1 Anatomy

The spine consists of segments comprising a vertebral body, articulations with adjacent vertebrae and in the thoracic region with ribs. The sacrum is a specialized segment where vertebrae are embryologically fused and the whole structure acts as a part of the pelvic ring. These articulations are at risk from degenerative and inflammatory disorders.

D. J. Wilson (✉)
St Luke's Radiology Oxford Ltd., Oxford, UK
e-mail: david@slro.co.uk

M. de Abreu
Radiology, Hospital Mãe de Deus, Porto Alegre, RS, Brazil

Ligaments and muscles bridge vertebral segments and allow flexion, extension, tilt and rotation. It is useful to think of a mechanical segment as comprising the vertebra and its attachments.

The intervertebral disc's function is to allow the above movements at the same time as maintaining transverse stability. The disc sits at the division of a mechanical segment and is subject to considerable physical load. The joints between vertebrae must slide and rotate to allow movement. The annulus fibrosis is bound to the edge of the vertebral body and comprises 15–25 concentric layers. Within the disc, the nucleus pulposus is soft and very hydrated. It transmits hydrostatic pressure and acts as a buffer between the end plates.

The spine will experience compression, tensile force, shear force, bending movement and torsional movement. Normal function of joints, ligaments and muscle spreads these loads across many segments. However, when disease intervenes, focal load will increase at adjacent segments which must move more dramatically to compensate for less movement at diseased levels. It is therefore common that symptoms in one part of the spine precipitate pain and dysfunction throughout the vertebral column.

We should not consider the vertebral body to be a simple building block. It has a trabecular internal structure which responds to load applied in different ways. The discs distribute load across the vertebral body, and when they become degenerate, point pressures may become very much higher than in the young person's spine. In older patients, the bone mineral quantity is reduced often considerably, and these two processes combine to cause catastrophic collapse presenting as insufficiency fracture. The combination of osteoporosis and degenerative disease with mechanical dysfunction are major factors in this very common disorder.

Ligamentous attachments in the spine are extensive and complex. Some ligaments restrain the spinal segment from excessive motion, but others provide integral stability binding vertebra to disc, most particularly the posterior and anterior longitudinal ligaments. It is easy to underestimate the

complexity of the ligamentous structures around the sacroiliac region; there are anterior and posterior complexes with deep and superficial layers posteriorly. These envelop the articulation of the sacrum to the pelvis. The sacroiliac joint has both fibrous and synovial components and is therefore at risk in patients with systemic inflammatory disease of joints.

This concept of mechanical activity is very important when considering disease; it is easy to view the spine as a solid static structure, but observation and the above descriptions should make it clear that movement is a primary function and the one that is most frequently lost in patients who present with pain and dysfunction. Imaging is currently based on a static description of morphology, and abnormalities of function are more difficult to determine [1] (Figs. 14.1 and 14.2).
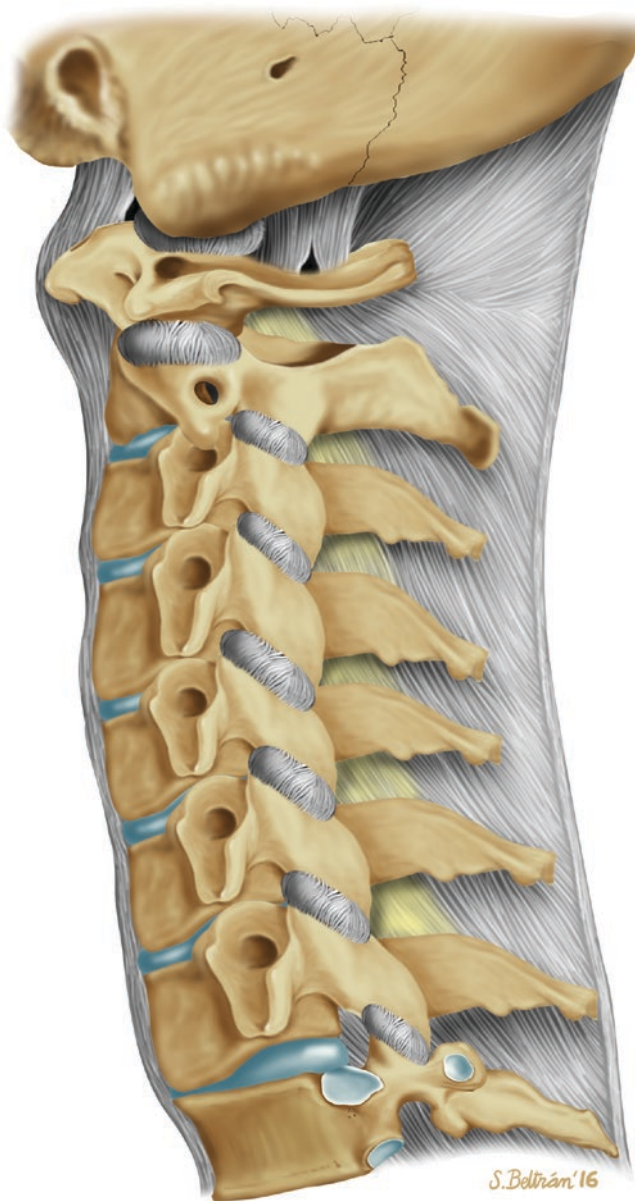
Fig. 14.1 Diagram of morphology of the vertebral supports

> **Key Point**
> - The static anatomy must be understood in detail, and those interpreting images must recognize that the spine is a flexible and movable structure, and conventional imaging does not include dynamic studies.

14.1.2 Degenerative Disease

The degenerative process seems to be an inevitable consequence of ageing. The changes may be observed in the third decade and progress throughout life. The mechanisms are:

1. Relatively poor blood supply to the intervertebral discs
2. Multiple micro injuries to discs
3. Cartilage wear in the joints
4. Reduction in the number of chondrocytes
5. Vascular ingrowth into the disc
6. Marginal osteophytes on vertebral bodies and joints
7. Herniation of discs
8. Osteopenia and osteoporosis
9. Biomechanical overload due to disease at other segments

There is a genetic element to the speed of progress of degeneration probably related to the proteoglycan binding of collagen fibres. More linkages mean stiffer collagen which is more brittle; fewer linkages mean softer collagen which is more likely to tear and displace.

The microtrauma element of degeneration is accelerated by impact and multiple minor traumatic incidents and therefore has an occupational and sporting association.

14.1.2.1 Manifestations of Degenerative Disease

14.1.2.2 Discs

Small tears within the disc lead to annular tears. A tear may be seen as a defect in the annulus, containing soft tissue material which may take on an increased water content. There is considerable debate as to whether these tears with high signal material are a cause of localized back pain [2–4]. Tears with scar tissue and repair produce low MRI signal. There is also considerable debate over alterations in water content in the annulus; some regard this as the main cause of reduced MRI signal on all sequences, but others believe that scar tissue from microtrauma is a major element. The consequence of all these changes is reduction in pliability and tension within the annulus and a tendency for disc height reduction. This in turn leads to buckling of the longitudinal ligaments. Less commonly described in imag-
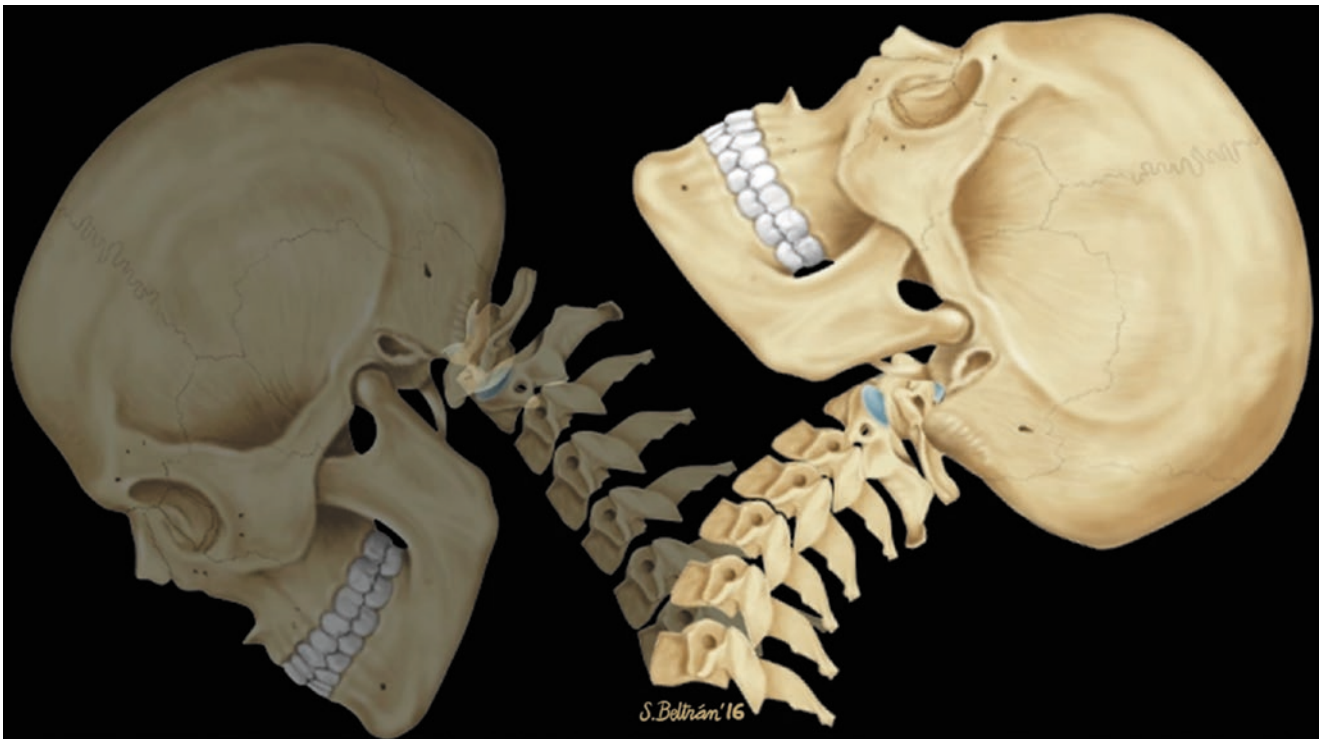
Fig. 14.2 Diagram to demonstrate spine movement

ing interpretation but probably a much more important factor in morbidity is mechanical instability due to loss of tension within the annulus and laxity of the margins of the disc. Frank herniation of disc material through tears in the annulus fibrosis may not only compress adjacent nerve roots but also releases several chemical irritants including prostaglandin, tumour necrosis factor alpha (TNFα) and interleukins [5]. These chemicals may be part of the localized pain response and are potentially toxic to the adjacent nerves.

The loss of height in an intervertebral disc will in turn create mechanical instability, and this will lead to osteophytes that may impinge on adjacent nerves [6] (Fig. 14.3).

14.1.2.3 Facet Joints

As for all synovial joints, articular cartilage wear and mechanical instability lead to osteoarthritis with localized pain and osteophytes. New bone formation around the joint may considerably limit movement which in turn places additional load on adjacent segments. As degeneration is inevitably widespread and extremely common, it may be very difficult to determine the origin of pain as the presence of facet joint arthropathy does not predict that pain arises from this area. Synovial cysts may arise from the joint and may compress nerve roots. Haemorrhage into the cysts may increase the pressure. The fundamental problem is that facet joint disease is very common, and we have no imaging technique that scans for the origin of pain. The presence of facet
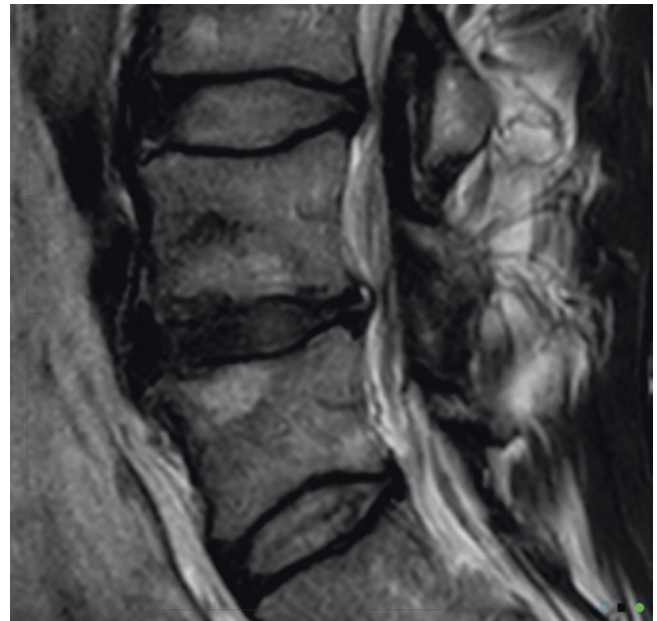
Fig. 14.3 MRI of annular tear

joint changes does not necessarily indicate an origin of pain; similarly, joints that look relatively normal may be the source of symptoms. Systems are closely interrelated, and there is association between muscle atrophy and facet joint disease; it may be that spine instability is exacerbated by this connection [7] (Figs. 14.4 and 14.5).
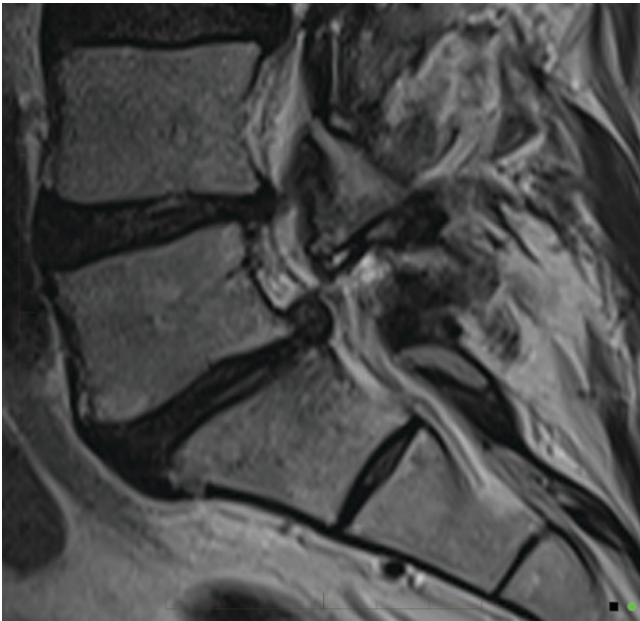
Fig. 14.4 Facet joint arthritis with a synovial cyst, disc prolapse and grade 1 spondylolisthesis leading to spinal stenosis

Fig. 14.5 Severe facet joint arthrosis with resultant instability and retrolisthesis of L1 and L2 beginning to impinge on the cauda equina. This image was taken in the supine position, and the changes will be worse when the patient stands

14.1.2.4 End Plates

Scheuermann (1877–1960) a Danish surgeon serving in Copenhagen in 1921 described a condition that he called osteochondritis deformans [8]. It comprises a deformity of the end plates, presenting in adolescence, which is now recognized to be a genetic autosomal dominant end plate dys-

plasia [9]. The main candidate genes are COL2A1 and COL9A3. It is sometimes called osteochondrosis. It causes irregularity of the end plates which become prominent when the vertebral body reaches sufficient maturity, normally in adolescence. It is uncommon but a potential cause of thoracic pain. This may be a factor in later facet joint arthritis and segmental instability [10] (Fig. 14.6).

14.1.2.5 Pars Interarticularis

Degenerative disorders are uncommon in young people. However, it might be argued that stress fractures are a form of degeneration. They are caused by repetitive mechanical stress. Pars interarticularis stress fractures are common in young people. Typically, they occur in adolescents who are undertaking sport or physical activity that places repeated stress on bone which is not yet mature. MRI demonstrates bone oedema for some weeks before a stress fracture occurs. Whilst this is easy to identify in an MR image, it does require that the observer look specifically at the pars interarticularis for signal change on either a STIR sequence or a T2-weighted fat-suppressed sequence (STIR sequences are more sensitive). This is an important diagnosis to make because even a few days of additional activity may irretrievably fracture the bone. This can lead to a lifetime of back pain and disability. Strict exercise limitation for 6 weeks followed by a careful rehabilitation can lead to complete and permanent healing of the stress response (Figs. 14.7 and 14.8).

Stress of the end plate may lead to the changes described by Modic et al. which may be characterized by their MRI signal as bone oedema, fatty infiltration and sclerosis. There is some evidence that end plate stress changes particularly those with oedema are linked to back pain [11, 12], but there is poor evidence to show that lumbar surgery results are related to the stage of end plate change.

14.1.2.6 Spinal Stenosis

Individuals are born with spinal canals of differing dimension. Those with narrow canals need very little disc protrusion or osteophytes formation to cause pressure on the cord or cauda equina. Spinal stenosis is when the spinal canal is rendered too narrow due to disc or joint disease for normal blood supply to reach the neural structures. Patients will typically complain of back and leg pain which comes on after walking (spinal claudication, named after the Emperor Claudius of Rome who had walking difficulties); this eases after several minutes' rest. The disease is progressive and rarely undergoes spontaneous resolution. Therefore, surgery is an important treatment method, and imaging is essential in plotting the extent and severity. There is considerable literature on the efficacy of surgery, but a recent Cochrane review suggested that fusion plus decompression was no better than conventional decompression alone [13] (Fig. 14.9).
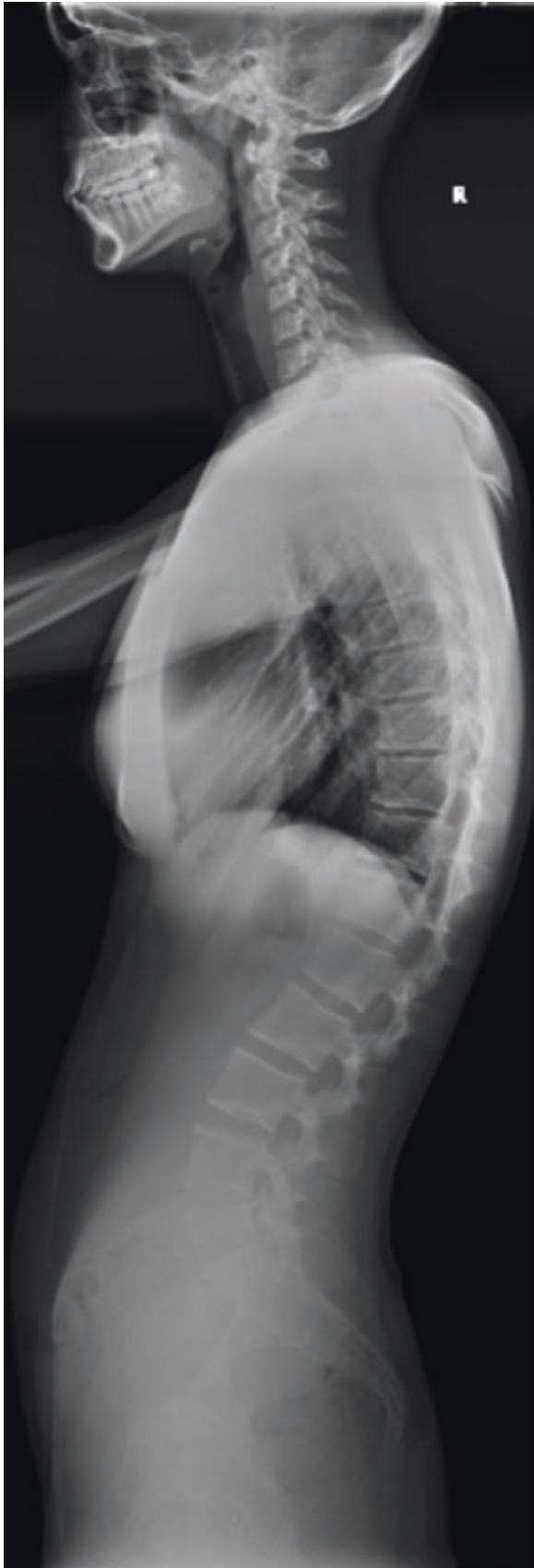
Fig. 14.6   Scheuermann's disease with irregular endplates in the lower thoracic spine
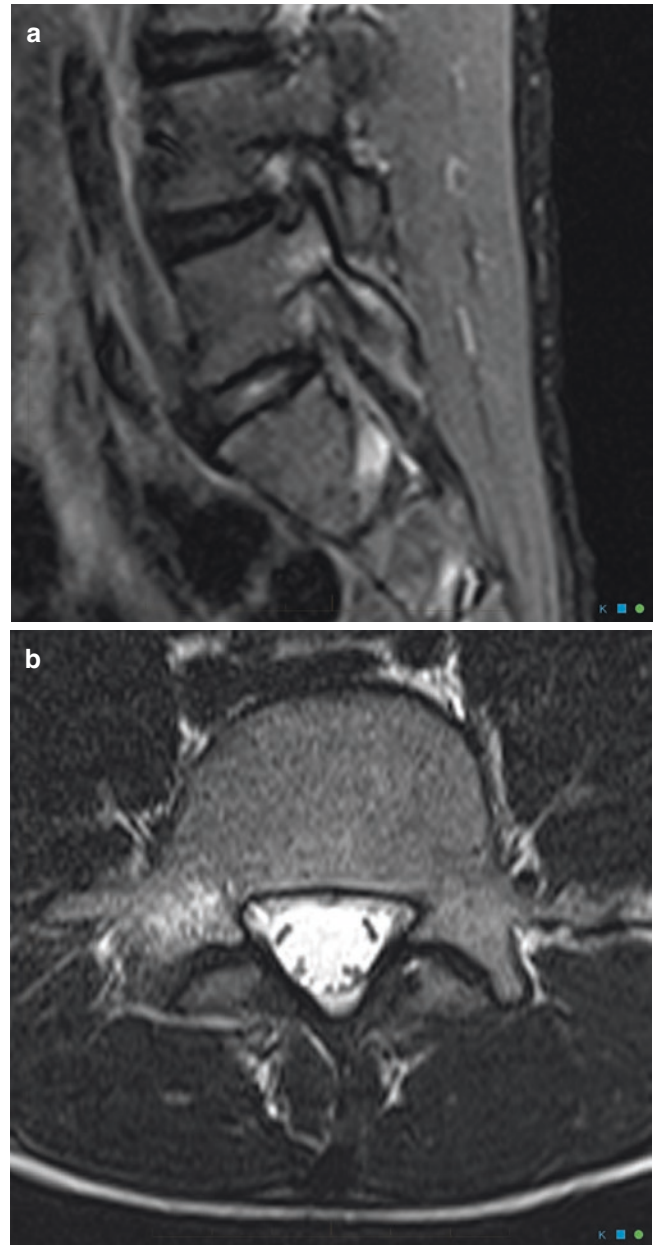
Fig. 14.7   (a, b) Unilateral stress response in the right pars interarticularis in a 15-year-old athlete

14.1.3   Imaging

14.1.3.1   Conventional Radiographs

Conventional radiographs of the spine have a principal role in assessing patients with trauma. This includes patients suspected of insufficiency fracture. However, it is now well recognized that they have limited if any value in the assessment of patients with back pain and are of minimal value in judging whether degenerative changes are affecting the patient in a way that might require interventional techniques. The appearances of advanced anky-
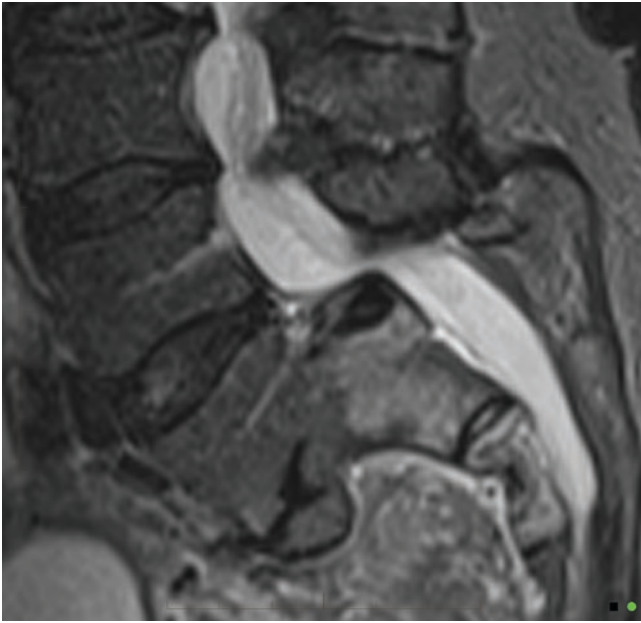
Fig. 14.8 Severe spondylolisthesis with surgical fusion. This is what happens when we miss stress response in teenagers

losing spondylitis are typical, but it might be argued that if you are trying to assess the disease at this stage, you are far too late. National guidance of the United Kingdom now states that conventional radiographs are not indicated for the investigation of back pain.

14.1.3.2 Computed Tomography

CT is the ideal method of assessing complex fractures and detecting destructive tumours. It will not demonstrate inflammatory changes at the early stage when they would be best treated, and it will not show bone oedema. It is much less effective than MRI at judging nerve root compression but can be used as an alternative when MRI is impossible.

14.1.3.3 Magnetic Resonance Imaging

MRI is the workhorse for the assessment and diagnosis of spinal disease. It is the preferred imaging for patients with back pain that fails to respond to conservative measures and those patients who have adverse clinical features or signs that might suggest infection, tumour or insufficiency frac-
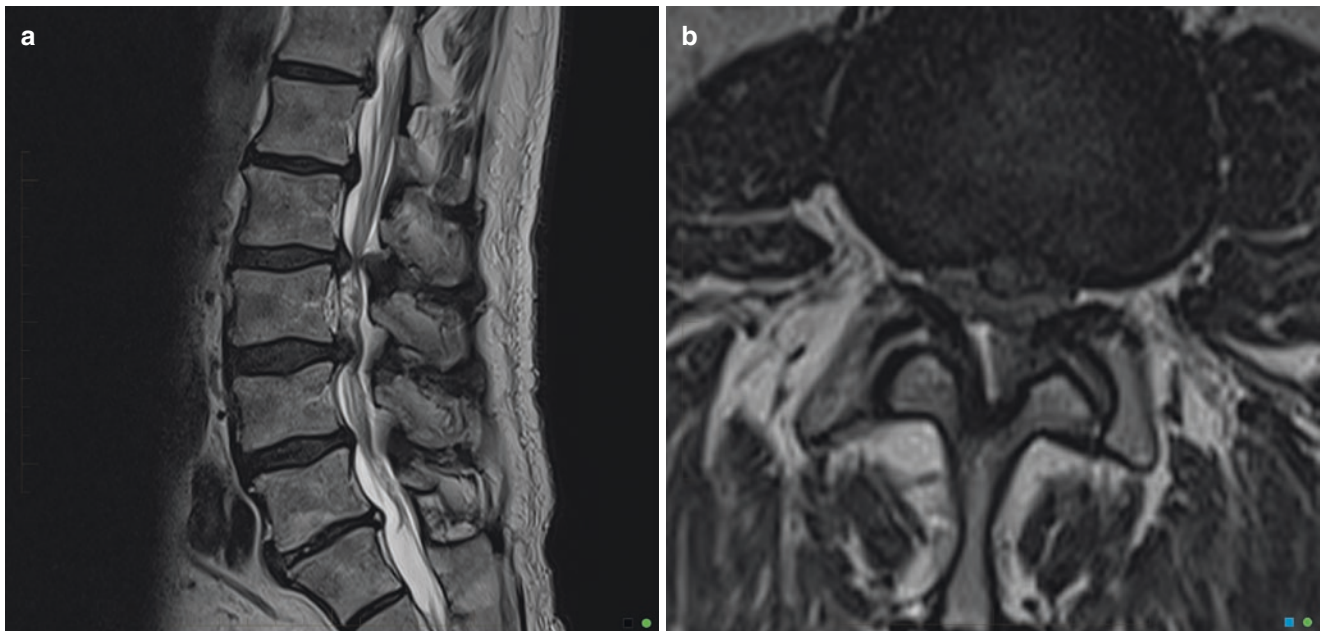
Fig. 14.9 (**a**) MRI spinal stenosis. Disc disease and facet joint hypertrophy lead to severe spinal canal stenosis at L2/L3 and moderate spinal stenosis at L3/L4. (**b**) Shows that the CSF has been completely effaced from the spinal canal or the nerves of the cauda equina are squeezed together

ture. It is without doubt the best technique for assessing nerve root compression. Perhaps the only weakness is when there is metal implanted surgically and despite newer metal artefact suppression techniques, the image will be distorted at the level of the metal. MRI has particular strength in assessing for bone oedema and haemorrhage in acute subtle fractures.

14.1.3.4 Isotope Bone Scintigraphy and White Cell Scintigraphy

These techniques have a particular use in patients where pain is unexplained by MRI or when there are so many abnormalities found using MRI that it is uncertain which is the origin. Increased metabolic activity or white cell accumulation at a particular site may point to this as the most likely origin of symptoms. The radiation dose and the nonspecificity of the techniques are sufficient to make this a second-line test rather than a primary investigation.

14.1.3.5 Interventional Techniques

In the assessment of patients with degenerative arthropathy, disc degeneration and nerve root irritation, local anaesthetic blocks optionally with the use of steroids may allow the examiner to determine the exact origin of pain. 12 hours of complete relief after a 1 mL injection of bupivacaine clinches the origin of the symptoms. Therapeutic interventions include anaesthetic and steroid blocks to joints or nerve roots, radiofrequency rhizolysis to denervate facet joints, laser and radiofrequency disc ablation for disc-generated pain and percutaneous annuloplasty for symptomatic disc protrusion and are all potential techniques in the spine. Sacroiliac joint injections and sacroiliac ligament injections may help to determine whether the joint or the surrounding tissues are the origin of pain. Radiofrequency denervation of the sacroiliac joint may be useful [14] (Fig. 14.10).

> **Key Point**
> - Whilst MRI is the primary investigation for many of those with spine disorders, it is not without its limitations; conventional radiographs, CT and bone scintigraphy have an important role as secondary investigations.

Fig. 14.10 Fusion imaging-guided nerve root block

14.2 Inflammatory Disorders of the Spine

Noninfective inflammation of the spine is a frequent cause of back pain. It may be caused by spondyloarthropathy (SpA), rheumatoid arthritis (RA) or other less frequent inflammatory diseases. Inflammatory spondyloarthropathy is often overlooked on routine reporting. The modern management of inflammatory properties depends on early diagnosis and treatment with anti-inflammatory drugs or biologic agents, and a careful imaging strategy is important to avoid misdiagnosis and delayed treatment.

Magnetic resonance imaging (MRI) is the best method of assessing inflammatory disorders of the spine because it has high sensitivity and specificity. Conventional radiography, computed tomography (CT) and scintigraphy can also be employed to assess some of the inflammatory sites within both the axial skeleton and have specific secondary indications.

Key Point
- Early imaging is key to determining effective treatment.

14.2.1 Imaging Methods in Evaluation of Inflammatory Spine

14.2.1.1 Conventional Radiographs

Conventional radiographs of the spine will demonstrate bone morphology, calcification, ossification, large erosions and spine alignment. However, all of those are late-stage findings of inflammatory disorders. Consequently, conventional radiographs have limited value in the initial diagnostic assessment. It is useful for the clinical follow-up to detect complications and record progress.

14.2.1.2 Computed Tomography (CT)

CT will not demonstrate inflammatory changes at the early stage when they would be best treated. Joint erosions, subchondral sclerosis and bony ankylosis are easily detected by CT examination which for this purpose is far superior to conventional radiographs. CT is the ideal method of assessing complex fractures, bone lesions, spinal canal stenosis and articular joints osteoarthritis (facet joints, costovertebral joints, manubriosternal joints).

14.2.1.3 Magnetic Resonance Imaging (MRI)

MRI is very effective in the early diagnosis of SpA, RA and also any inflammation of the spine. MRI-specific protocols for inflammation should be employed, using fluid-sensitive sequences such as STIR (short Tau inversion recovery) or T2 weighted with fat suppression techniques in sagittal and coronal planes, with adequate signal-to-noise ratio and adequate field homogeneity. In most high field scanners, a STIR sequence demonstrates better performance over a T2 weighted sequence. Areas of increased signal on those fluid-sensitive sequences correlate with oedema or vascularized fibrous tissue, termed bone marrow oedema (BME).

BME refers to nonspecific MR signal increase of the marrow cavity on fluid-sensitive sequences. Depending on cause, histological examination may demonstrate interstitial haemorrhage, organizing granulation tissue, necrosis, fibrosis, cellular infiltrate or reparative microcallus [15, 16]. Alternative terms include BME pattern, BME-like signal and oedema-like marrow signal. On T1-weighted images, marrow fat can be effaced but not entirely replaced, differentiating BME from malignancy. BME has a similar MR appearance in traumatic, degenerative, inflammatory, neoplastic, ischaemic and idiopathic conditions. In RA, SpA, SAPHO (synovitis, acne, pustulosis, hyperostosis, osteitis) and CRMO (chronic recurrent multifocal osteomyelitis), BME indicates inflammation (osteitis, enthesitis).

MRI may also demonstrate sites of old bone marrow inflammation, when the bone marrow turns into yellow marrow with high signal intensity on T1-weighted sequences, a finding encountered with frequency at anterior vertebral corners or at sacroiliac joints.

MRI may fail to demonstrate ossification and fusion of other spinal elements such as the apophyseal joints, paraspinal ligaments and interspinous ligaments, and it may not fully identify syndesmophytes. A further weakness of MRI is that implanted metal will distort the image. This effect may be minimized with utilizing novel MRI sequences with artefact reduction capability.

14.2.1.4 Isotope Bone Scintigraphy and White Cell Scintigraphy and FDG PET/CT

FDG (fluorodeoxyglucose) PET (positron emission tomography)/CT (computed tomography) and other methods of scintigraphy have a specific use in patients where pain is unexplained by MRI or when there are so many abnormalities using MRI that it is uncertain which is important. The increased metabolic activity or white cell accumulation at a

particular site suggests that this is the most likely origin of symptoms. The radiation dose and the non-specificity of the techniques are sufficient to make this a second line test rather than a primary investigation.
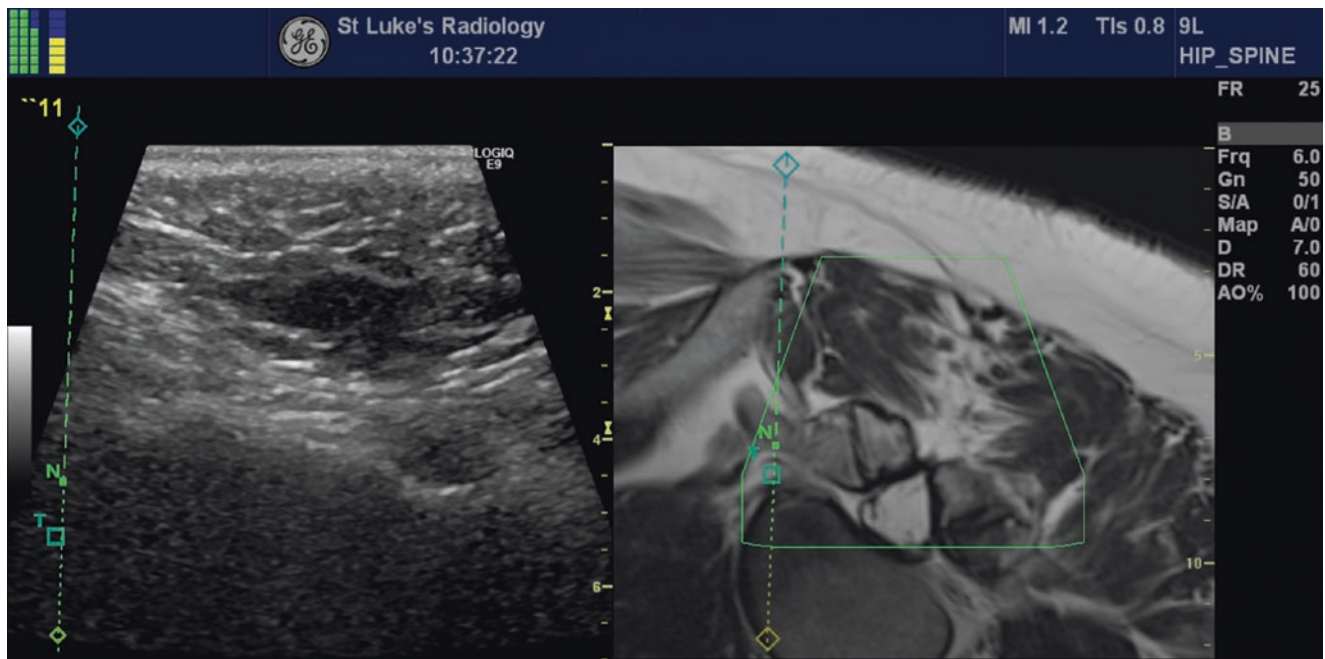
14.2.2 Inflammatory Diseases of the Spine

14.2.2.1 Rheumatoid Arthritis (RA)

Rheumatoid arthritis affects the cervical spine primarily. When that occurs, patients frequently develop anterior atlantoaxial subluxation. Abnormalities in the thoracic and lumbar spine are relatively rare. Disease onset is most frequent between the ages of 35 and 50 years [17].

Imaging Findings of RA

Features of spinal involvement in rheumatoid arthritis include erosive synovitis, ligamentous subluxation and osteopenia. Synovitis can be well detected with MRI as it demonstrates increased joint fluid at synovial joints (facet joints); in addition inflammatory osteitis may be observed when BME is present. Erosions are better detected with CT than by MRI or conventional radiography [18, 19].

14.2.2.2 Spondyloarthropathies (SpA)

Spondyloarthropathies are considered autoimmune disease mediated by antigen/antibody reactions that usually take place at the attachment of ligaments to bone (enthesis). The term enthesitis is reserved for rheumatological disorders that cause primary entheseal and osseous inflammation which are hallmarks of spondyloarthropathy [19]. In the spine, this process occurs where the collagen of the ligaments (especially the longitudinal ligaments) or intervertebral disc annulus enters bone directly. The cause of the inflammatory process is the generation of cytokines which results in oedema, bone erosion, disorganization of bone and ligament structure which in turn promotes a reactive osteitis and eventually ossification of the ligaments starting at the enthesis interface.

SpA include ankylosing spondylitis, psoriatic arthritis, reactive arthritis, enteropathic SpA and undifferentiated SpA. The seronegative spondyloarthropathies can be further categorized based on the imaging findings correlated with the clinical features and laboratory findings. Early diagnosis is key as disease-modifying drugs and physical therapy should be commenced as early as possible.

14.2.2.3 Ankylosing Spondylitis (AS)

This inflammatory disorder is the most frequent seronegative inflammatory spinal disease in adults and the prototype for other members of the spondyloarthropathies [20]. The prevalence of this disorder is estimated at 0.1–0.2% in the general population. Ankylosing spondylitis primarily affects young males, with a male-to-female ratio between 4:1 and 10:1. The mean age of presentation is 26 years. The HLA-B27 gene (human leukocyte antigen B27) is present in 95% of patients, but only a small percentage of all individuals positive for HLA-B27 actually develop the disorder [21].

AS typically begins in the sacroiliac joints and then affects the thoracolumbar and lumbosacral regions of the spine. Eventually, the spine becomes completely rigid, with loss of its normal curvatures and movement. Untreated, the disease will progress to bony ankylosis of joints which renders the spine at risk of transverse fractures following relatively minor injury. In the late stage, squaring of the vertebral bodies is a characteristic feature of AS and is caused by a combination of corner erosions and periosteal new bone formation along the anterior aspect of the vertebral body. Further inflammation is associated with formation of syndesmophytes: ossifications of the outer fibres of the annulus fibrosus that form bony bridges between the inflamed corners of adjacent vertebrae. Ossification also occurs within the fibres of the adjacent paravertebral connective tissue and of the posterior interspinous ligaments. Complete fusion of the vertebral bodies by syndesmophytes and related ossification produces the "bamboo spine" where the bone mimics a bamboo cane with segments of thickening. Fractures in AS usually occur at the thoracolumbar and cervicothoracic junctions where the biomechanical load is greatest. Spinal fractures are characteristically transverse (i.e., horizontal) rather than vertical or oblique and are called "chalk stick" or "banana" fractures. This is because these items will break transversely if bent.

There is considerable confusion in the literature about the difference between pseudarthrosis and discovertebral lesions. The Andersson lesion occurs where there is inflammatory involvement of the intervertebral disc; this may resemble disc infection. Excessive movement may occur at this level of destruction. This condition may develop spontaneously without any trauma. An advanced Andersson lesion is sometimes termed pseudarthrosis. However, pseudarthrosis may also occur when there has been a transverse fracture through bone and failure to unite. There are therefore three different groups of pseudarthrosis:

1. Localized lesions that always are of inflammatory origin and affect the disc space.
2. Extensive lesions without a fractured posterior element due to a combination of inflammatory and mechanical factors; they always are trans-discal and are associated with unfused facet joints.
3. Extensive lesions with fractured posterior elements resulting from mechanical fractures which may be trans-discal or trans-vertebral.

On balance, the term pseudarthrosis is best reserved for ununited unstable transverse fractures of bone, whilst Andersson lesions (discovertebral lesions) are potentially unstable disc spaces that do not involve the osseous skeleton.

14.2.2.4 Psoriatic Arthritis

This is a unique inflammatory arthritis associated with psoriasis. Among patients with psoriasis, the prevalence of inflammatory arthritis varies from 6% to 42% [22].

14.2.2.5 Reactive Arthritis (Reiter Syndrome)

This is an acute non-purulent seronegative arthritis that complicates an infection elsewhere in the body and can also be associated with the HLA-B27, but this gene is not always present in affected individuals. The peak onset is between 15 and 35 years. An estimated 1–3% of all patients with a nonspecific urethritis develop an episode of arthritis. Chronic arthritis or sacroiliitis occurs in 15–30% of patients [23]. The knee is most commonly affected followed by the ankle, small peripheral joints and sacroiliac joints. Some patients develop enthesitis (especially the calcaneus at attachment sites of the Achilles tendon and plantar fascia), dactylitis, urethritis and conjunctivitis. Diagnosis is based on clinical and laboratory findings. In chronic reactive arthritis (>6 months), radiographs may show signs of inflammatory arthritis or sacroiliitis. In earlier stages, MR and US (ultrasound) demonstrate nonspecific synovitis, asymmetric sacroiliitis and calcaneal enthesitis.

14.2.2.6 Enteropathic SpA

This condition occurs in patients with inflammatory bowel diseases (IBDs) and other gastrointestinal diseases, such as Whipple's disease (WD), celiac disease (CD) and intestinal bypass surgery [24].

14.2.2.7 Undifferentiated SpA

This term used to describe symptoms and signs of spondylitis in someone who does not meet the criteria for a definitive diagnosis of AS or a related disease.

14.2.2.8 Juvenile SpA

A term used to classify both differentiated and undifferentiated forms of SpA disorders that begin at 16 years of age or younger.

14.2.3 Imaging Findings of Spondyloarthropathy

14.2.3.1 Spondylitis

Inflammation of the vertebral body (spondylitis) is due to enthesitis at the insertion of the **annulus fibrosus** on the **ring apophysis** of the vertebral end plate predominantly at the anterior attachment where there are usually the more florid manifestations. Erosions with reactive sclerosis in the vertebral corners are seen radiographically and have been referred to as "Romanus lesions" when viewed as erosions, and "shiny corners" when the erosion is associated with sclerosis. The Romanus lesions resolve by producing syndesmophytes (ossification of the outer fibres of the annulus fibrosus). When it progresses to involve multiple segments, it can produce the characteristic "bamboo spine". The same inflammatory process results in ossification of the longitudinal ligaments which insert onto the vertebral bodies producing squaring of the vertebral body as the fusion progresses.

MRI is the most sensitive diagnostic tool for the identification of discovertebral inflammatory disease when BME is present. The Romanus lesions are identified on the sagittal sequences and characterized by a triangular pattern of BME at the corners of the vertebral end plates highlighted by low T1 signal and high T2 fat-sat and STIR sequence appearance. The small erosion may be overlooked when compared with the areas of BME. After the acute Romanus lesion phase subsides, the chronic lesions are identified by a fatty marrow replacement at the sites of enthesis inflammation within the vertebral bodies, highlighted by a high T1 signal and a low signal on STIR and T2-weighted fat-saturated sequences. The intervertebral disc in cases of long-term spinal fusion can also undergo changes with high T1 signal, due to the presence of calcification or ossification. Contrast agent-enhanced MRI studies and diffusion-weighted MRI sequences can be useful in cases where the STIR images are equivocal but is usually unnecessary when STIR or T2-weighted fat saturation are well performed [25] (Fig. 14.11).

14.2.3.2 Spondylodiscitis (Aseptic)

Primary Spondylodiscitis (Andersson Type A Lesions)

This disorder resembles Schmorl's nodes exhibiting a rim of oedema within the vertebral body, a focal end plate defect
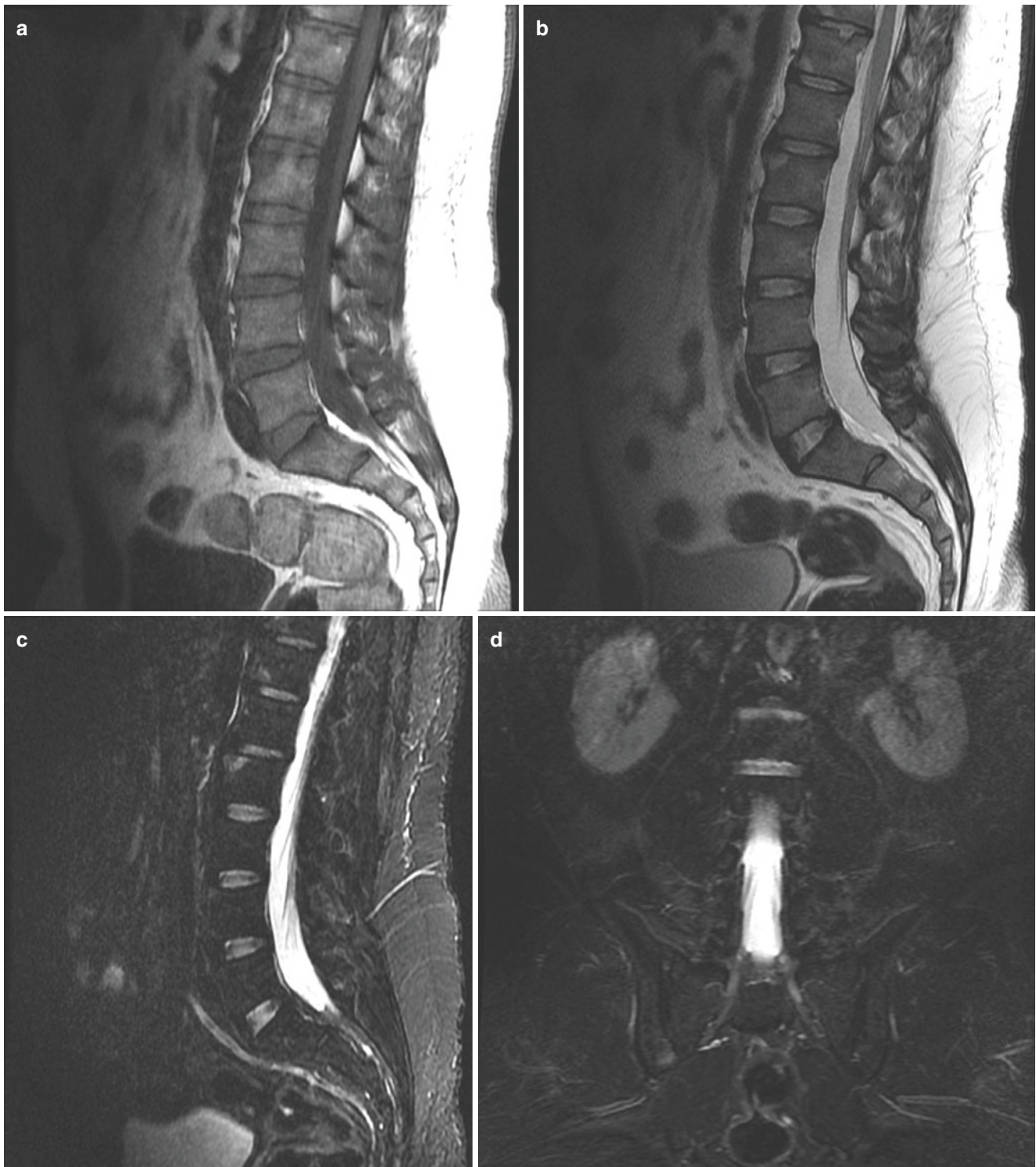
Fig. 14.11 (**a**) Sagittal T1-weighted MR image demonstrating Romanus lesions at L2 and T12 vertebral bodies, with low and high signal, respectively. (**b**) Sagittal T2-weighted MR image demonstrating both high signal Romanus lesions. (**c**) STIR sagittal MR image demonstrating high signal of Romanus lesions with active inflammation. (**d**) Coronal STIR sequence demonstrating signs of bilateral asymmetric active inflammatory sacroiliitis

and enhancement of the marrow oedema. Anderson type A lesions are usually a sign of early discovertebral involvement with a stable spinal status.

Secondary Spondylodiscitis (Andersson Type B Lesion)

This condition shows more extensive and florid discovertebral disease and destruction. These are particularly well demonstrated on CT and MRI. The degree of vertebral destruction is usually mild, but there is often extensive bony oedema and bony sclerosis, and in long established cases the end plates can be completely destroyed on both sides of the intervertebral disc. In Andersson type B lesions, the spine is unstable at the site of involvement due to increased mobility. This increased mobility could be at a level between fused segments or be associated with deficiency of the posterior elements where there is a pseudoarthrosis due to a fracture [25] (see above Hardy pseudarthrosis versus discovertebral disease) (Fig. 14.12).

Costovertebritis

This is a very typical finding of spondyloarthropathy usually starting in the lower thoracic spine. The inflammatory process with soft tissue oedema and bone oedema is seen in the costovertebral joints best seen on sagittal images. These are often overlooked when reporting MRI examinations because the slices showing the disease process are at the margin of the vertebral column.

Sacroiliitis

Sacroiliitis is a hallmark of all spondyloarthropathies. In AS and enteropathic SpA, it is usually bilateral and symmetrical, whilst in psoriatic spondyloarthropathy and reactive arthritis, it may be bilateral or unilateral. Involvement of the axial skeleton is not unusual in the absence of sacroiliitis, especially with the use of high-quality fluid-sensitive sagittal STIR and T2-weighted fat saturation sequences.

Conventional radiography has low sensitivity and relatively high false-negative rate in early disease. Early inflam-
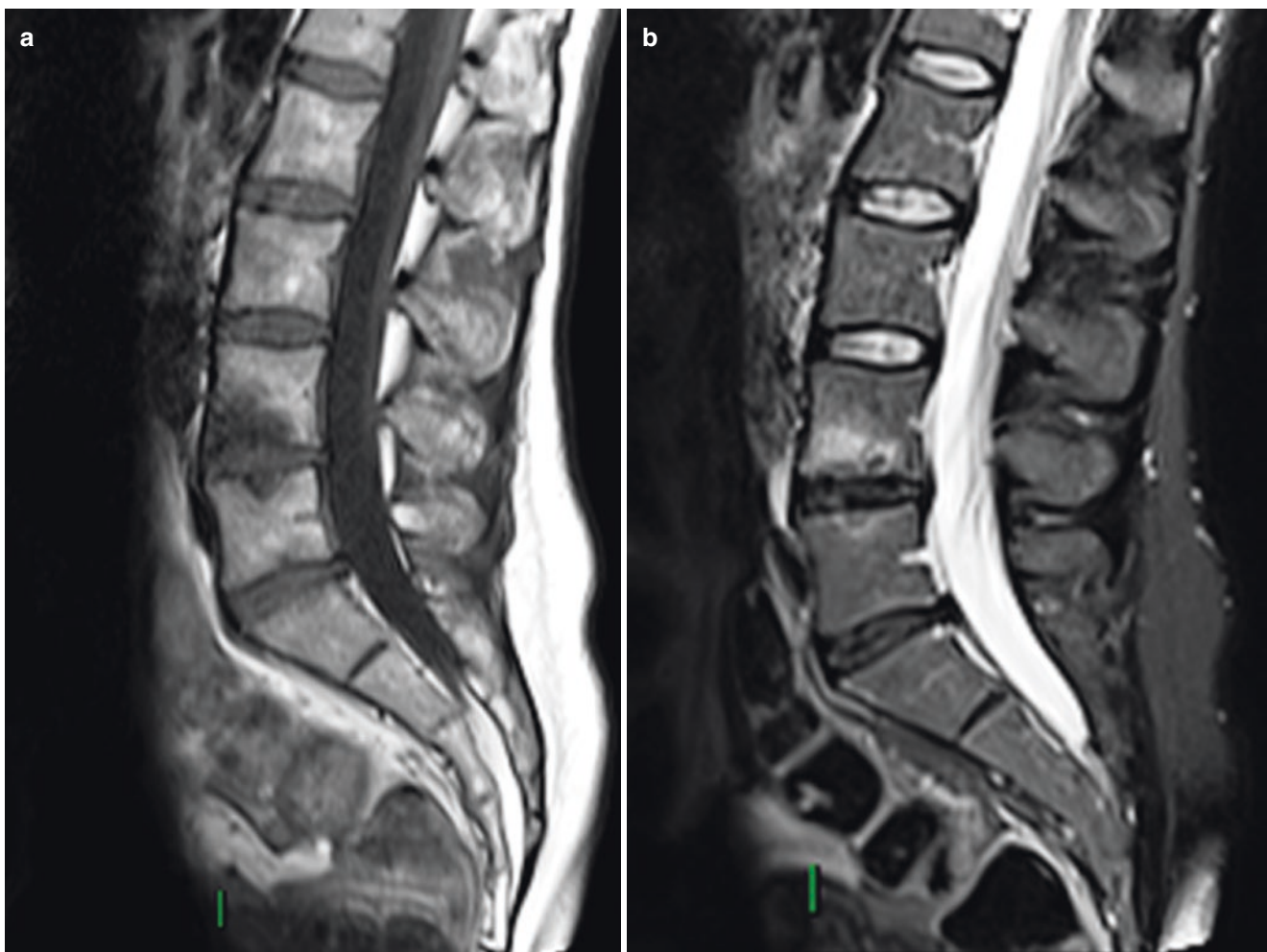
Fig. 14.12 (**a**) Sagittal T1-weighted MR image demonstrating Andersson lesions at L4–L5 level, with low signal. (**b**) Sagittal STIR demonstrating BME of Anderson inflammatory spondylitis

matory sacroiliitis is very difficult to access. Sclerosis of the subchondral bone on either side of the joint is fairly diagnostic in established disease and is more pronounced on the iliac side unlike infection of the sacroiliac joint which affects both sides equally. In established disease, the sacroiliac joint may also exhibit loss of sharpness due to ossification across the joint leading to ankylosis. The relatively late development of radiographic changes in ankylosing spondylitis is one reason for delay in diagnosis.

MR imaging has revolutionized the early diagnosis of sacroiliitis. This is primarily dependent on osteitis, an important feature of ankylosing spondylitis, which produces BME which is easily detected upon sensitive sequences such as T2-weighted sequences with fat suppression or the STIR sequence. The T1-weighted spin-echo sequences are better at depicting articular erosions. The degree of the oedema may vary ranging from florid, fairly extensive areas of periarticular oedema to more focal and localized zones of oedema paralleling the joint line. It is usually the inferior iliac portion of the joint that is involved in the early stages of sacroiliac inflammatory change as this is the sign of your component of the sacroiliac joint early commitment. Contrast agent enhancement can be useful if the oedema-sensitive sequence (STIR) is equivocal. CT is preferred for the detection of very early erosions of the sacroiliac joints and their early ankylosis.

> **Key Point**
> - Comprehensive imaging is an essential element of the diagnosis, but the conclusion will depend on the combination of imaging, clinical history and laboratory investigations.

14.2.4 Complications of Inflammatory Joint Disease

The most important spinal complications in ankylosing spondylitis are *osteoporosis*, *fracture*, *instability*, *cauda equina syndrome* and *spinal stenosis*.

Osteoporosis increases in prevalence directly with increased patient age, increased severity of spinal involvement, increased disease duration and peripheral arthritis. Bone fragility associated with osteoporosis obviously increases the chances of vertebral compression fractures, posterior element fractures, pseudoarthrosis and unstable fractures from relatively minor trauma. The treatment of inflammatory arthropathy may accelerate osteoporosis.

Fractures of the cervical spine may occur after a minor fall or injury to the head and neck. Typically, the conventional radiographs show a chalk stick type of break either through the disc or the vertebral body anteriorly and horizontally

through the posterior fused elements. A common spinal location for fracture is the thoracolumbar and cervicothoracic and lastly the lumbosacral junction. Any ankylosing spondylitis patient suffering minor trauma who complains of pain should have advanced imaging preferably by CT, as this will be most sensitive in detecting what are often very subtle but grossly unstable injuries. There should be a very low threshold for performing CT examinations with ankylosing conditions of the spine even after very mild trauma (Fig. 14.13).

Cauda equina syndrome is a rare but specific complication following long-standing ankylosing spondylitis. It invariably occurs in a fused spine and is most common in the lumbar region. Dural ectasia is common, resulting in erosions of primarily the posterior neural arch. This is best assessed by CT or MRI. MRI will show enlargement of the spinal canal with arachnoid diverticulae, erosion of the laminae and adherent nerve roots.

Spinal stenosis can be observed with ossification of the longitudinal ligament and the ligamentum flavum. Neurological deficit in patients with AS could have a number of causes, but C1–C2 subluxation, fracture, pseudoarthrosis, ligamentous ossification and cauda equina syndrome are the most common.

> **Key Point**
> - In ankylosing spondyloarthropathy, fractures may occur with minor trauma and are frequently severely unstable. Early cross-sectional imaging is essential in these cases which may be very difficult to interpret.

14.2.5 Other Inflammatory Diseases That Could Affect the Spine

14.2.5.1 SAPHO

SAPHO syndrome represents a rare inflammatory disorder involving the bone, joints and skin. The acronym refers to synovitis, acne, pustulosis, hyperostosis and osteitis. Although the aetiology is probably autoimmune, *Cutibacterium acnes* infection may activate the process in some cases. Cultures are usually negative, and biopsy shows sterile, nonspecific osteitis without sequestrum formation. SAPHO has been associated with axial spondyloarthropathy and CRMO, a childhood variant of chronic nonbacterial osteomyelitis (CNO). In adults, commonly involved sites include the sternocostoclavicular complex followed by the spine and sacroiliac joints. Radiographs and CT demonstrate erosive costoclavicular ankylosis, osteosclerosis and thick periosteal reaction of the clavicle and first rib. Bone scintigraphy shows the "bull's head sign" (avid uptake of
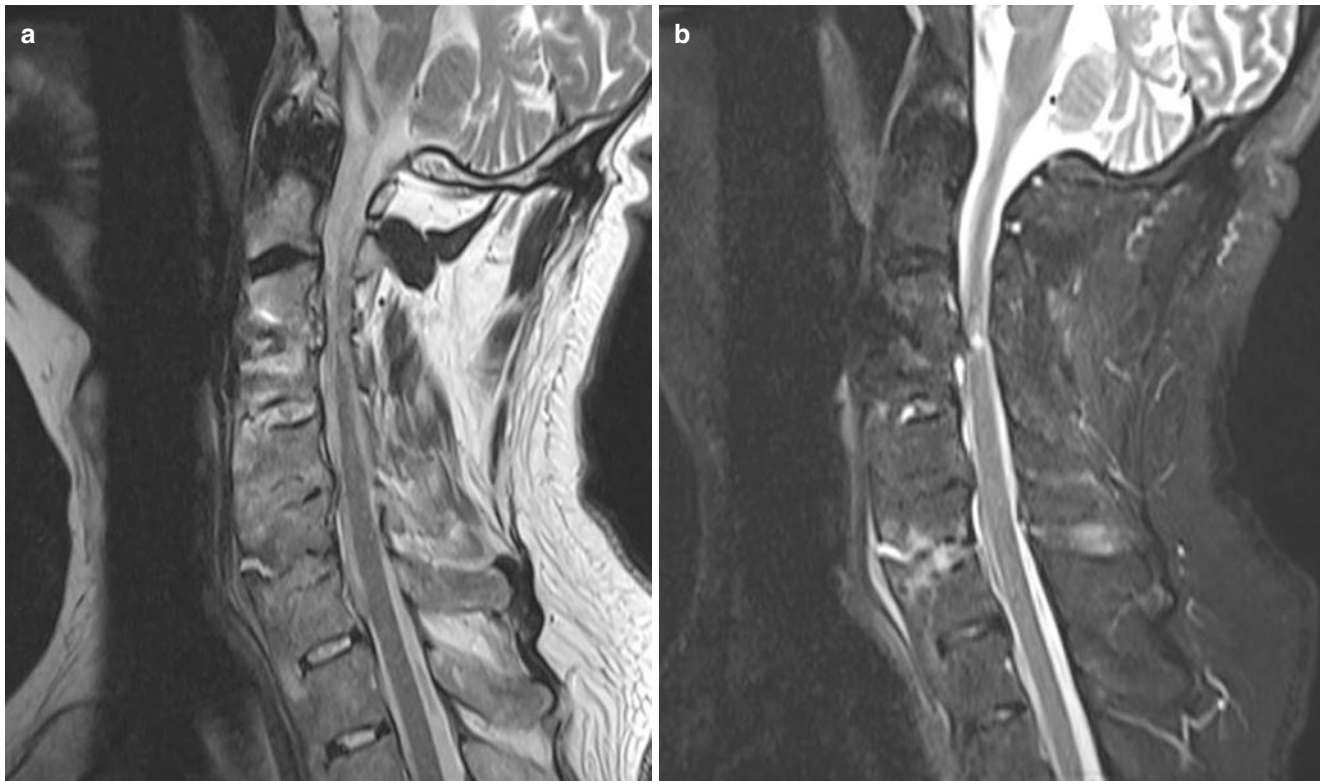
Fig. 14.13 (**a**) Sagittal T2-weighted MR image of cervical spine demonstrating multiple levels of bone fusion by AS from C3 to C6 with ossification demonstrated as low signal at disc space and spinal stenosis at C3–C4. (**b**) STIR sagittal MR image demonstrating myelopathy at C3–C4 level and high signal of active inflammation (Anderson lesion) of spondylitis process, as well as thick and increase signal of the anterior longitudinal ligament

99mTc-methylene diphosphonate by the sternomanubrial and bilateral sternocostoclavicular regions). In polyostotic disease, bone scintigraphy, PET and whole-body MRI are valuable for skeletal screening to identify sites of active osteitis. MRI can demonstrate early osteitis, synovitis, enthesitis, spondylodiscitis and sacroiliitis. In children and adolescents, long bone metaphases are commonly involved. Differential diagnosis includes osteomyelitis and malignancy.

14.2.5.2   Sarcoidosis

Sarcoidosis is a systemic granulomatous disease of unknown cause that has been shown to affect nearly every body system. Osseous involvement occurs in 1–13% of patients, typically in the small tubular bones of the hands and feet. Sarcoidosis is usually treated with corticosteroid [26].

14.2.5.3   Crystal Deposition Disorders

In crystal deposition disease, collections of crystal may be found in musculoskeletal tissues in asymptomatic individuals. In others these deposits may produce severe pain and profound symptoms. This systemic disease associated with some crystal disorders may be occult, and musculoskeletal deposits may be the presenting feature.

The common crystal-related deposition disorders are calcium pyrophosphate dihydrate (CPPD), hydroxyapatite and monosodium urate deposition. MRI and CT examination features include (a) location (discs, hyaline cartilage and fibrocartilage, ligaments, bone, synovial membrane), (b) morphology (size, soft tissue signal characteristics), (c) surrounding tissue signal change and (d) arthritis (bone, synovial membrane). There are different patterns with individual diseases.

CPPD crystal deposit can be found with a high frequency in older people in the discs, hyaline cartilage and ligaments. Calcification in the spinal ligaments especially around the odontoid process is common. Focal calcifications forming conglomerates around joints like tophaceous gout may be also seen. It is often seen in women >80 years old ("disease of octogenarians"). Intervertebral disc CPPD crystal deposits can be found in asymptomatic individuals but in some more rare cases can cause destructive disc disease.

Calcium hydroxyapatite crystals (HA) deposits also can be found in the spine in asymptomatic individuals, often intradiscal. At high calcium concentrations (above 30–40%), MRI susceptibility defects and decreases in proton density dominate, leading to signal intensity reduction. However, T1 shortening defects resulting in hyperintensity on T1-weighted images may also be present. They have been attributed to surface interaction of protons with calcified tissue. At lower concentrations of calcium, T1 shortening effect dominates, resulting in isointensity or even hyperintensity. Gradient echo sequences best show these calcific foci, but the gold standard confirmation is made with CT. The deposition of HA may mimic an acute inflammation (Figs. 14.14 and 14.15).
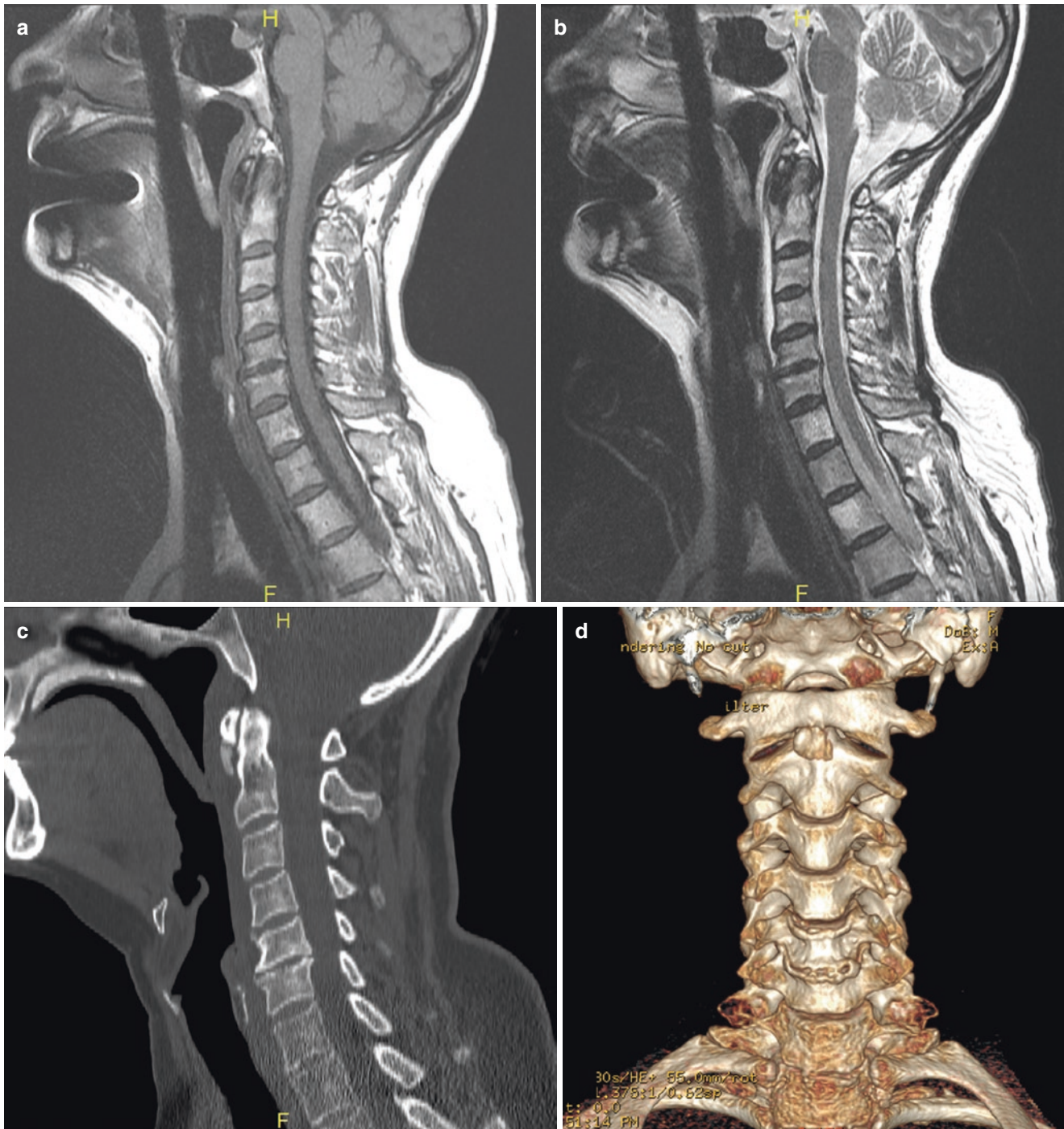
Fig. 14.14 Longus colli muscle insertion calcification by hydroxyapatite crystal deposition demonstrated with (**a**) sagittal T1-weighted MR image, (**b**) sagittal T2-weighted MR image, (**c**) CT sagittal CT reformat and (**d**) CT 3D reconstruction
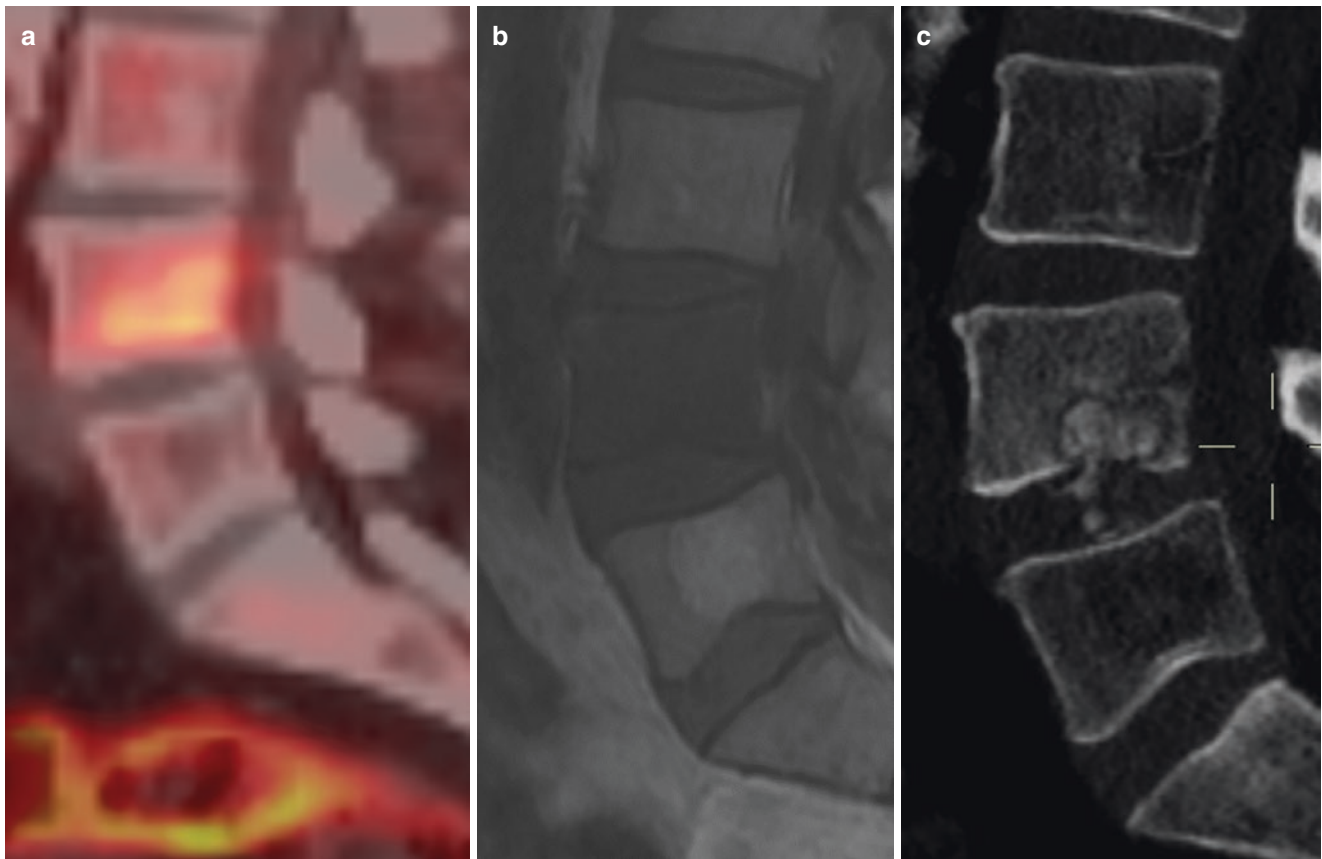
Fig. 14.15 Migration of hydroxyapatite crystal deposition into vertebral body of L4 causing spondylitis demonstrated with (**a**) FDG PET/CT, (**b**) sagittal T1-weighted MR image and (**c**) CT sagittal CT reformat

Monosodium urate monohydrate crystals or uric acid deposits into tissues may cause gout. It happens when hyperuricemia is above 6–7 mg/dL. Gout is the most common inflammatory arthritis in men over the age of 30 year but is uncommon in the spine. The radiographic findings of gout do not occur until the disease has been present for at least 6 or more years. In the acute phase, MRI findings are joint effusion and synovial thickening although these are nonspecific signs. Gouty tophi can be found in rare cases in the spine arising from facet joints. They are mostly of low or intermediate signal intensity on T1-weighted images with variable gadolinium enhancement. The imaging findings of tophi on T2-weighted images are variable. Calcification, fibrosis or hemosiderin can occur within the tophi. With dual source computed tomography, the uric acid deposits can be differentiated with considerable accuracy and high imaging contrast.

> **Key Point**
> • Inflammatory disease of the spine is not confined to ankylosing spondylitis.

14.3 Concluding Remarks

Degenerative and inflammatory disease of the spine may overlap in their signs and symptoms. There is a wide range of disorders, and radiologists must have a comprehensive knowledge of the presentation of these diseases. Imaging is now key in the critical stages of management, for example, in assessing spinal stability and helping to determine treatment with powerful anti-inflammatory drugs. MRI is the primary investigation in many spine disorders, but conventional radiographs and CT are more important first-line techniques in trauma. There will be occasions when a combination of imaging is required to make a precise and safe diagnosis.

> **Take Home Message**
> • Those who undertake reporting of spinal disorders using any imaging technique must have a comprehensive knowledge of disease processes, their symptoms and imaging signs.

References

1. Adams MA, Bogduk N, Burton K, Dolan P. The biomechanics of back pain. 3rd ed. Edinburgh: Elsevier Churchill Livingstone; 2013.
2. Bogduk N, Aprill C. On the nature of neck pain, discography and cervical zygapophysial joint blocks. Pain. 1993;54:213–7.
3. Aprill C, Bogduk N. High-intensity zone: a diagnostic sign of painful lumbar disc on magnetic resonance imaging. Br J Radiol. 1992;65:361–9.
4. Jha SC, Higashino K, Sakai T, et al. Clinical significance of high-intensity zone for discogenic low back pain: a review. J Med Investig. 2016;63:1–7.
5. Goupille P, Mulleman D, Valat JP. Radiculopathy associated with disc herniation. Ann Rheum Dis. 2006;65:141–3.
6. An HS, Masuda K, Inoue N. Intervertebral disc degeneration: biological and biomechanical factors. J Orthop Sci. 2006;11:541–52.
7. Sebro R, O'Brien L, Torriani M, Bredella MA. Assessment of trunk muscle density using CT and its association with degenerative disc and facet joint disease of the lumbar spine. Skelet Radiol. 2016;45:1221–6.
8. Scheuermann HW. The classic: kyphosis dorsalis juvenilis. Clin Orthop Relat Res. 1977;128:5.
9. Zaidman AM, Zaidman MN, Strokova EL, et al. The mode of inheritance of Scheuermann's disease. BioMed Res Int. 2013;2013:973716.
10. Palazzo C, Sailhan F, Revel M. Scheuermann's disease: an update. Joint Bone Spine. 2014;81:209–14.
11. Maatta JH, MacGregor A, Karppinen J, Williams FM. The relationship between Modic changes and intervertebral disc degeneration. BMC Musculoskelet Disord. 2016;17:371.
12. Xu L, Chu B, Feng Y, Xu F, Zou YF. Modic changes in lumbar spine: prevalence and distribution patterns of end plate oedema and end plate sclerosis. Br J Radiol. 2016;89:20150650.
13. Machado GC, Ferreira PH, Yoo RI, et al. Surgical options for lumbar spinal stenosis. Cochrane Database Syst Rev. 2016;11:CD012421.
14. Pope TL, Bloem HL, Beltran J, Morrison WB, Wilson DJ. Musculoskeletal imaging. 2nd ed. Philadelphia, PA: Elsevier Saunders; 2015.
15. Hiryayi WA, Thiryayi SA, Freemont AJ. Histopathological perspective on bone marrow oedema, reactive bone change and haemorrhage. Eur J Radiol. 2008;67(1):62–7.
16. Zanetti M, Bruder E, Romero J, Hodler J. Bone marrow edema pattern in osteoarthritic knees: correlation between MR imaging and histologic findings. Radiology. 2000;215(3):835–40.
17. Calleja M, Hide G. Rheumatoid arthritis, spine. Available at http://www.emedicine.com/radio/topic836.htm. Last updated 28 Mar 2006. Accessed 30 Jun 2007.
18. Hermann KG, Bollow M. Magnetic resonance imaging of the axial skeleton in rheumatoid disease. Best Pract Res Clin Rheumatol. 2004;18:881–907.
19. Selmi C, Gershwin ME. Diagnosis and classification of reactive arthritis. Autoimmun Rev. 2014;13:546–9.
20. Bollow M, Enzweiler C, Taupitz M, et al. Use of contrast enhanced magnetic resonance imaging to detect spinal inflammation in patients with spondyloarthritides. Clin Exp Rheumatol. 2002;20(Suppl 28):S167–74.
21. Peh W. Ankylosing spondylitis. Available at http://www.emedicine.com/radio/topic41.htm.
22. Gladman DD, Antoni C, Mease P, et al. Psoriatic arthritis: epidemiology, clinical features, course, and outcome. Ann Rheum Dis. 2005;64:14–7.
23. Scoggins T, Boyarsky I. Reactive arthritis. Available at http://www.emedicine.com/emerg/topic498.htm. Last updated 15 Feb 2007. Accessed 30 Jun 2007.
24. Peluso R, Di Minno MN, Iervolino S, et al. Enteropathic spondyloarthritis: from diagnosis to treatment. Clin Dev Immunol. 2013;2013:631408.
25. Wilson DJ, Casar-Pulliccino V. Spine degeneration and inflammation. In: Musculoskeletal disease (2017–2020). Cham: Springer; 2017.
26. Campbell SE, Reed CM, Liem T, et al. Radiologic-pathologic conference of Brooke Army Medical Center: vertebral and spinal cord sarcoidosis. AJR Am J Roentgenol. 2005;184:1686–7.

Infection

15

William B. Morrison and Mark J. Kransdorf

Learning Objectives
- The reader will learn the advantages of various imaging modalities for musculoskeletal infection.
- The reader will review imaging appearances of manifestations of infection on radiologic exams.
- The reader will incorporate current recommendations for terminology regarding musculoskeletal infection.
- The reader will understand mimickers of infection to help generate a differential diagnosis.

15.1 Introduction

Diagnosis of infection can be challenging clinically, based on a number of factors including location, organism, and mode of spread. Other entities can simulate infection clinically or radiologically. Radiologic examinations can improve patient care, if applied appropriately early in the disease process. However, misdiagnosis or delayed diagnosis can lead to poor outcomes. This article discusses the advantages and disadvantages of imaging modalities, the imaging appearance of various types, and manifestations of infection, as well as complicating factors and entities that can simulate infection.

W. B. Morrison (✉)
Department of Radiology, Thomas Jefferson University Hospital, Philadelphia, PA, USA
e-mail: William.morrison@jefferson.edu

M. J. Kransdorf
Department of Radiology, Mayo Clinic, Scottsdale, AZ, USA
e-mail: Kransdorf.mark@mayo.edu

15.2 General Principles

15.2.1 Routes of Infection

There are three routes for introduction of infection around the body: hematogenous, direct implantation, and contiguous spread [1, 2]. Hematogenous spread is the most common cause of osteomyelitis in most areas of the body, including the spine. Direct implantation is relatively common in the hands and feet (i.e., puncture wounds, penetrating trauma) and in various areas of the body as a result of open surgery and percutaneous procedures. Contiguous spread is related to transmission of infection through the skin or from adjacent tissues. The most common clinical scenarios involving contiguous spread of infection include diabetic pedal infection and pelvic osteomyelitis in paralyzed patients.

Key Points
- Three routes for MSK infection: hematogenous, direct implantation, and direct spread.
- Most common: hematogenous spread.
- In diabetic patients and paralyzed patients, contiguous spread is important.

15.3 Modalities

15.3.1 Radiography

For patients with clinical suspicion of infection, radiographs are typically the initial radiologic examination acquired [3, 4]. Early infection in the extremities is seen as soft tissue swelling, representing cellulitis. However, this finding is nonspecific. In more central locations such as the sacroiliac joints, soft tissue swelling is obviously not as sensitive.

Septic arthritis is characterized in the early stages by joint effusion. Depending on location (i.e., deep joints), effusion may not be detected radiographically. As the disease progresses, erosions and joint space narrowing representing chondrolysis are observed. Finally, with onset of osteomyelitis, frank bone destruction is seen. Periosteal reaction may be seen in later stages. Radiographic changes of osteomyelitis can be delayed as much as 2 weeks after onset of infection. Overall, radiographs are insensitive to osteomyelitis in early stages and cannot determine the extent of involvement of osseous or soft tissue disease. Therefore, whether negative or positive, additional imaging is necessary. Despite low utility for diagnosing osteomyelitis, the wide availability and excellent overview of anatomy make radiography excellent for follow-up examinations; evaluation of postoperative changes; identification of soft tissue calcification, gas, and foreign bodies; and characterization of the pattern and distribution of arthritis, including neuropathic osteoarthropathy.

15.3.2 Computed Tomography

CT provides similar findings on radiographs but with more anatomic definition [5]. If intravenous contrast medium is administered, soft tissue enhancement reflecting cellulitis and rim-enhancing fluid collections indicating abscess formation can be detected. In later stages of infection, as osteomyelitis sets in, periostitis and rarefaction of bone will be seen. Eventually, frank bone destruction ensues. Joint effusion, articular narrowing, and marginal erosions indicate septic arthritis. Determining the extent of involvement within the bone as well as in the soft tissues remains limited with CT. Given these limitations as well as associated expense, its use as a clinical tool for this purpose is limited. However, if anatomic information is needed and MRI cannot be obtained, or if there are metal implants, CT may be useful [6].

15.3.3 Ultrasonography

The use of a high-frequency transducer offers excellent depiction of soft tissue anatomic detail, and ultrasonography can be useful for answering specific questions, such as whether there is an infected fluid collection in the subcutaneous tissues [7]. Abscesses and effusions are seen as focal regions of hypoechogenicity often with complex internal characteristics. Joint effusions and tendon sheath fluid can be detected, but these findings are common in the absence of infection. Power Doppler can demonstrate hyperemia of the synovium and surrounding tissues, suggestive of inflammation. Although ultrasonography cannot visualize the marrow compartment, a focused examination can demonstrate cortical breakthrough and periosteal elevation. Owing to avail-

ability of other modalities that offer a more comprehensive evaluation, the use of ultrasonography for this purpose is limited.

15.3.4 Magnetic Resonance Imaging

MRI is the imaging modality of choice for evaluation infection [8, 9]. Soft tissue and bone marrow pathology can be detected with high sensitivity. High contrast between different tissue types as well as inflammatory versus non-inflammatory tissue combined with anatomic definition has made this modality useful to surgeons interested in acquiring a "road map" of pathologic tissue before surgery. Additionally, with intravenous contrast administration, it is possible to identify abscesses and extension of phlegmonous tissue and to evaluate areas of devitalization that may require debridement [10, 11].

15.3.5 Nuclear Medicine

Three-phase bone scintigraphy and labeled leukocyte imaging are the most commonly performed radionuclide tests in the evaluation of pedal infection [12, 13]. Although the three-phase bone scan is sensitive for detecting osteomyelitis, many conditions in the diabetic foot demonstrate focal hyperperfusion, hyperemia, and bony uptake, mimicking infection, and, consequently, specificity is low. When there is no increased uptake, the test is excellent for excluding the presence of osteomyelitis, except in the setting of severe vascular disease. Labeled white blood cell examination has higher specificity and is generally interpreted in conjunction with the three-phase bone scintiscan.

The uptake in three-phase bone scintigraphy using 99mTc-labeled methylene diphosphonate is related to blood flow and osteoblastic activity. Localized bone uptake on the delayed third phase is nonspecific, but if all three phases are positive with clinical suspicion of infection, the test is highly sensitive for diagnosis of osteomyelitis. Cellulitis, abscess, and other soft tissue infections show increased uptake on the initial blood flow and second blood pool phases that fail to concentrate in bone on the third phase. Occasionally, and especially, in ischemic feet, there is persistent blood pool activity which can be suspected if there is poorly defined tracer distribution. Residual bony uptake on a fourth phase, acquired after 24 h, can help distinguish osteomyelitis from overlying cellulitis in this setting. Severe ischemia results in photopenia or relative lack of uptake and chronic osteomyelitis, or partially treated infection may not show characteristic uptake on the first two phases resulting in false-negative examinations [12, 13]. Persistent radiotracer uptake may be seen with treated osteomyelitis. Bone turnover and hyperemia caused by neuropathic osteoarthropathy, trauma, recent

surgery, or inflammatory arthropathy can appear similar to infection, leading to a false-positive examination. Specificity is lower as a result of vascular insufficiency and complicating neuroarthropathy. In the setting of underlying complicating conditions, where there is nonspecific uptake on the delayed phase, corresponding uptake on a labeled white blood cell scan increases specificity.

White blood cell scanning is based on accumulation of labeled leukocytes in infected tissue with reported sensitivity and specificity ranging from 75% to 100% and 69% to 100%, respectively. Combined with three-phase bone scintigraphy, specificity increases to 90% to 100%. Focal uptake in the foot, without appreciable amounts of red marrow, is generally indicative of infection. It may be difficult to separate soft tissue from bone infection, both of which will accumulate leukocytes. Corresponding delayed uptake on a three-phase bone scintiscan can make the diagnosis of osteomyelitis. False negatives may be seen with prior antibiotic treatment and ischemia. Noninfectious inflammatory conditions such as rheumatoid arthritis and hyperemic conditions such as acute neuropathic disease can occasionally show increased uptake, a false positive.

15.3.6 Positron Emission Tomography and Cross-sectional Imaging

18-F-FDG positron emission tomography (PET) combined with CT (PET/CT) has shown promise for imaging infection, related to increased metabolism of glucose in areas of inflammation [14]. The high resolution of PET is a significant advantage over bone and labeled leukocyte imaging. However, to date, limited data exist to test its efficacy in the diabetic foot and the jury is still out. Hybridization of PET with MRI (PET/MRI) is emerging as a new tool to provide important diagnostic information, with data predominantly limited as of yet, to oncological applications. Perhaps, in the future hybridization techniques may play a useful role in the evaluation of diabetic foot infection.

Key Points
- Radiographs: inexpensive, widely available; good for initial screening, follow-up.
- Ultrasound: limited use; best for answering specific questions, evaluating for soft tissue pathology such as abscess, tendon involvement.
- CT: usually reserved for bone biopsy localization.
- MRI: generally the test of choice for diagnosis and evaluation of extent for surgical planning.
- Nuclear medicine: limited anatomic information; can be used when MRI is contraindicated.

15.4 Imaging Manifestations of Infection

15.4.1 Cellulitis

Cellulitis is seen as replacement of the normal fat signal in subcutaneous tissues on T1-weighted images, with high signal (though less than fluid) on T2-weighted or STIR images and diffuse enhancement after contrast agent administration, with swelling and loss of fat density on CT [1, 5, 9, 11]. The margins are typically poorly defined. Abscesses appear as a focal collection of signal approximating fluid on T2-weighted or STIR images, with thick rim enhancement on post-contrast T1-weighted images. Sinus tracts are characterized by a thin, discrete line of fluid signal extending through the soft tissues with enhancement of the hyperemic margins. Sinus tracts are visualized as linear tracts of fluid signal or parallel lines of enhancement in a "tram-track" configuration.

15.4.2 Septic Arthritis

Septic arthritis results from seeding of microorganisms, usually bacteria, either with direct inoculation or more commonly hematogenously [15]. The risk for joint infections is related to IV drug use, immunocompromised state, and diagnostic and therapeutic injections. The earlier the diagnosis, the lower is the risk for irreversible destruction of the articular cartilage. The clinical and serologic findings are suggestive of pyogenic septic arthritis which is established with drainage and culture. The role of imaging is secondary and is mainly related to suggest a clinically unsuspected septic arthritis. Absence of joint effusion on US shows a high negative predictive value. Radiographs cannot exclude septic arthritis. The earliest radiographic findings are soft tissue swelling and joint effusion which lack reproducibility and are nonspecific. MRI findings suggesting septic arthritis include joint effusion, synovial thickening, and surrounding soft tissue changes such as fasciitis and myositis (Fig. 15.1). Contrast administration may show diffuse synovitis and soft tissue abscess formation. Limited subchondral bone marrow edema is usually reactive, whereas diffuse marrow edema, particularly if obvious on T1-weighted images, is suggesting osteomyelitis [16]. Although sensitive, MRI lacks specificity as most of the above described findings may be seen in inflammatory joint disease as well [17].

Rapid development of effusion in infected joints can cause intense capsular and pericapsular soft tissue edema on MR imaging ("angry effusion"), which can help differentiate bacterial septic arthritis from chronic arthropathies in which capsular expansion is more gradual.

Tuberculous arthritis has a more chronic course compared to pyogenic arthritis and is common in endemic areas, but in developed countries, it is seen in immunosuppressed
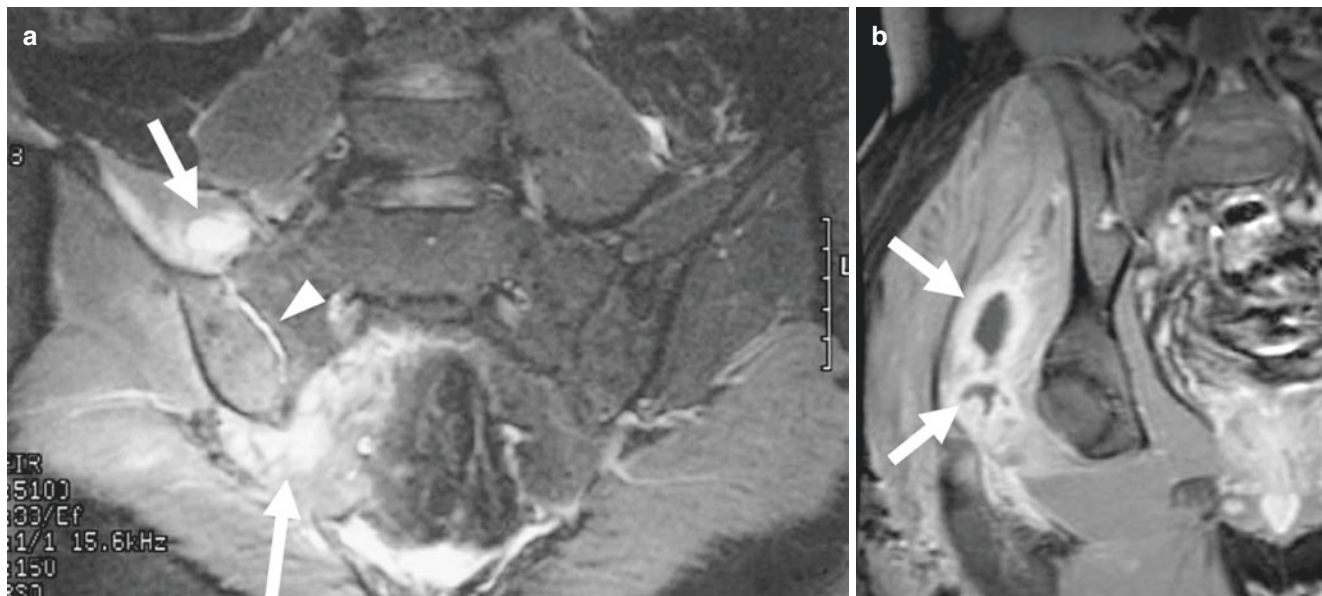
Fig. 15.1 A 35-year-old male patient with right lower back pain for 2 weeks; recent onset of right sciatic pain. Low-grade fever. Aspiration-proven *Staphylococcus aureus* septic sacroiliitis. Coronal STIR image (**a**) shows fluid signal within the joint (arrowhead) with distension of the joint recesses superiorly and inferiorly (arrows), the latter extending into the sciatic notch. Note surrounding soft tissue edema representing inflammation. Coronal T1-weighted fat-suppressed post-contrast image (**b**) shows rim-enhancing abscesses (arrows) in the gluteus musculature

patients, immigrants, and elderly patients. Tuberculous arthritis is considered to occur secondarily to hematogenously induced osteomyelitis, is mostly monoarticular with the hip being involved up to 15%, and if untreated results in joint destruction [18, 19]. Establishment of diagnosis is not possible based on imaging findings alone. The *Phemister triad* refers to the presence of *periarticular osteopenia*, *peripheral erosions*, and *gradual joint space narrowing* on radiographs. Minimal subarticular sclerosis, soft tissue swelling, osteolysis, and minimal periosteal reaction may also be seen [18, 19]. Joint space will be narrowed late in the course of the disease. Effusion and synovial hypertrophy are seen on MRI and are indistinguishable from those seen in other arthropathies. Sacroiliac joint involvement may show abscesses, often calcified, and are best appreciated with CT.

Patients with joint effusion and clinical suspicion of septic arthritis should undergo image-guided aspiration of the fluid with fluoroscopy, ultrasonography, or CT, depending upon the individual joint involvement and the body habitus of the patient.
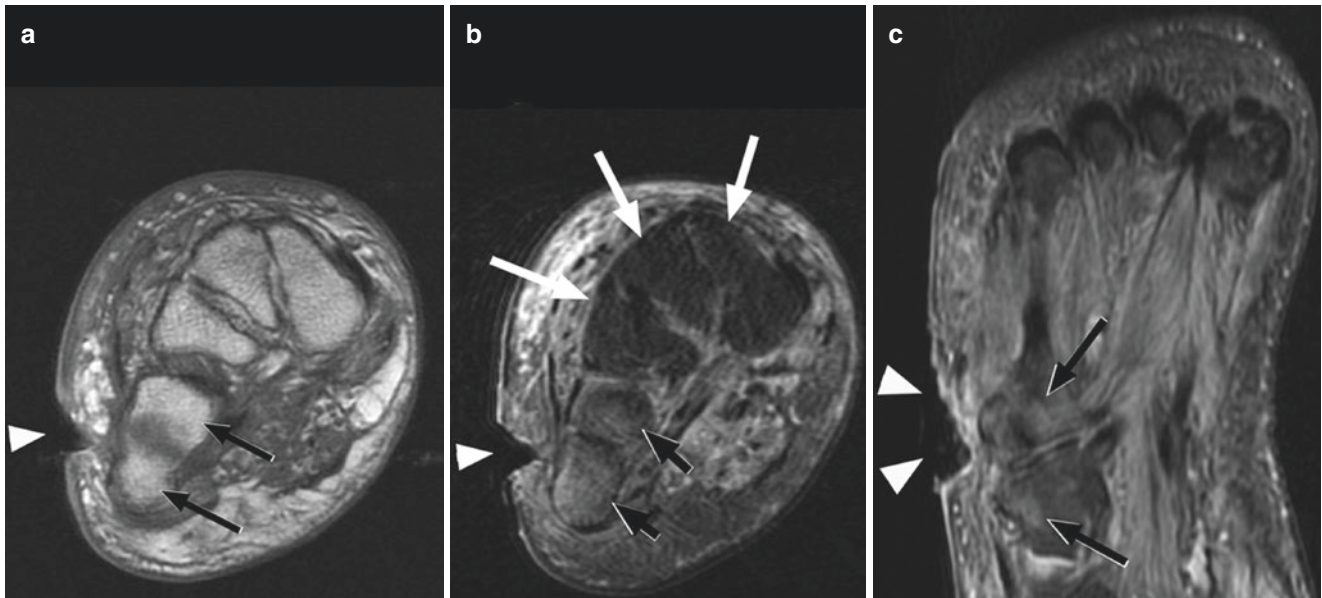
15.4.3 Osteomyelitis

Osteomyelitis is characterized by altered bone marrow signal, with low signal (loss of the normal fat signal) on T1-weighted images, edema signal on T2-weighted or STIR images, and enhancement on postgadolinium T1-weighted images (Fig. 15.2). Other MRI findings in cases of osteomyelitis include cortical disruption and periostitis. Periostitis is seen as a thin, linear pattern of edema and enhancement sur-

rounding the outer cortical margin that will appear thickened if the periostitis is chronic [2–5, 8–10].

Recognition of abnormal bone marrow signal in the appropriate clinical setting results in high sensitivity for diagnosis of osteomyelitis. Other entities can mimic this alteration in signal, including fracture, tumor, active inflammatory arthritis or neuropathic disease, infarction, or recent postoperative change. However, these other processes usually have different morphology than osteomyelitis and recognition of these patterns often enables differentiation. For example, identification of a fracture line, a discrete lesion, adjacent arthritis or neuropathic disease, or postoperative metal artifact improves specificity. Correlation with radiographs and clinical history is also important. Additionally, over 90% of the time, osteomyelitis of the foot and ankle is a result of contiguous spread through the skin with the majority of cases demonstrating skin ulceration, cellulitis, soft tissue abscess, or a sinus tract. These findings can be thought of as "secondary signs" of osteomyelitis, recognition of which improves specificity [10, 11].

In a significant proportion of cases, the MR imaging findings are not "classic"; this has been reported in cases of soft tissue ulceration and adjacent bone marrow edema but with absence of fat replacement on T1-weighted images. This appearance has been referred to as "osteitis"—a nebulous term that has been defined differently by different authors (Fig. 15.2). A recent white paper from the Society of Skeletal Radiology (in press) recommends against use of this term, instead describing likelihood or risk of underlying osteomyelitis or progression to frank bone infection. The idea is that "reactive edema" can occur in the bone marrow adjacent to a

Fig. 15.2 A 58-year-old woman with poorly controlled type 1 diabetes and early osteomyelitis. Coronal T1-weighted MR image (**a**) of the midfoot shows deep ulceration (arrowhead) adjacent to the 4th and 5th metatarsal bases. Underlying bone marrow signal appears normal (arrows) on T1-weighted images. Coronal (**b**) and axial (**c**) T2-weighted fat-suppressed images show the ulcer (arrowheads) with soft tissue edema representing cellulitis. Bone marrow edema is present (black arrows) in the metatarsal bases (compared to normal marrow signal in the cuneiform bones (white arrows)). Considering proximity to soft tissue ulceration and cellulitis, this should be reported as suspicious for early osteomyelitis (i.e., not *osteitis*)

soft tissue infection, and this does not necessarily mean that there is a bone infection. If the T1 signal is normal, there is a lower probability of osteomyelitis than if the fat signal is partially or completely replaced (high probability). In addition, if there is close proximity to a surface ulcer and the ulcer abuts the bone, any T2 marrow signal should be considered suspicious for early osteomyelitis. Expressing findings in terms of probability helps standardize therapeutic algorithms.

15.4.4 Chronic Osteomyelitis

Chronic osteomyelitis can have additional findings. Chronic manifestations of osteomyelitis include bone sclerosis, sinus tracts, abscesses (in soft tissue or bone), and devitalized areas; devitalized bone is called a sequestrum. The importance of a sequestrum (as well as devitalized soft tissue) is that intravenous antibiotics may not reach these areas, leading to persistent infection.

15.4.5 Abscess and Phlegmon

Abscess can occur in acute or chronic infections, often with sinus tracts connecting areas of infection with collections [1–5, 7]. Abscesses are seen as complex fluid collections on MRI with rim enhancement following contrast administration. A "phlegmon" is a mass-like region of infection without liquefaction. Chronic, smoldering intra-osseous abscess in a pediatric population is referred to as a Brodie abscess (Fig. 15.3). This typically occurs at the metaphysis of long bones, especially around the ankle. The classic finding of a Brodie abscess is an ovoid focus of fluid signal on MRI (corresponding to focal lucency and surrounding sclerosis on radiographs) "dripping" to the physeal plate. An appearance of multiple Brodie abscesses (or intermittent lesions in multiple locations) is seen in the condition known as chronic recurrent multifocal osteomyelitis (CRMO, also known as chronic nonbacterial osteomyelitis, CNO), which is of undetermined etiology but appears to be immune-modulated.

15.4.6 Devitalization

Changes related to ischemia should be taken into account in infection, particularly when interpreting MRI of the diabetic foot. Documentation of the presence and extent of ischemic and devitalized areas facilitates surgical planning for debridement and limited, foot-sparing amputations. Pre- and postcontrast MR images can detect ischemia and devitalization of the foot as focal or regional lack of soft tissue contrast enhancement. Devitalization, or foot "infarction," is seen as a focal area of nonenhancement with a sharp cutoff with increased enhancement in the surrounding reactive, hypervascular tissue. Only contrast-enhanced images allow reliable recognition of gangrenous tissue because T2- and T1-weighted images reveal uncharacteristic signal alterations [11].
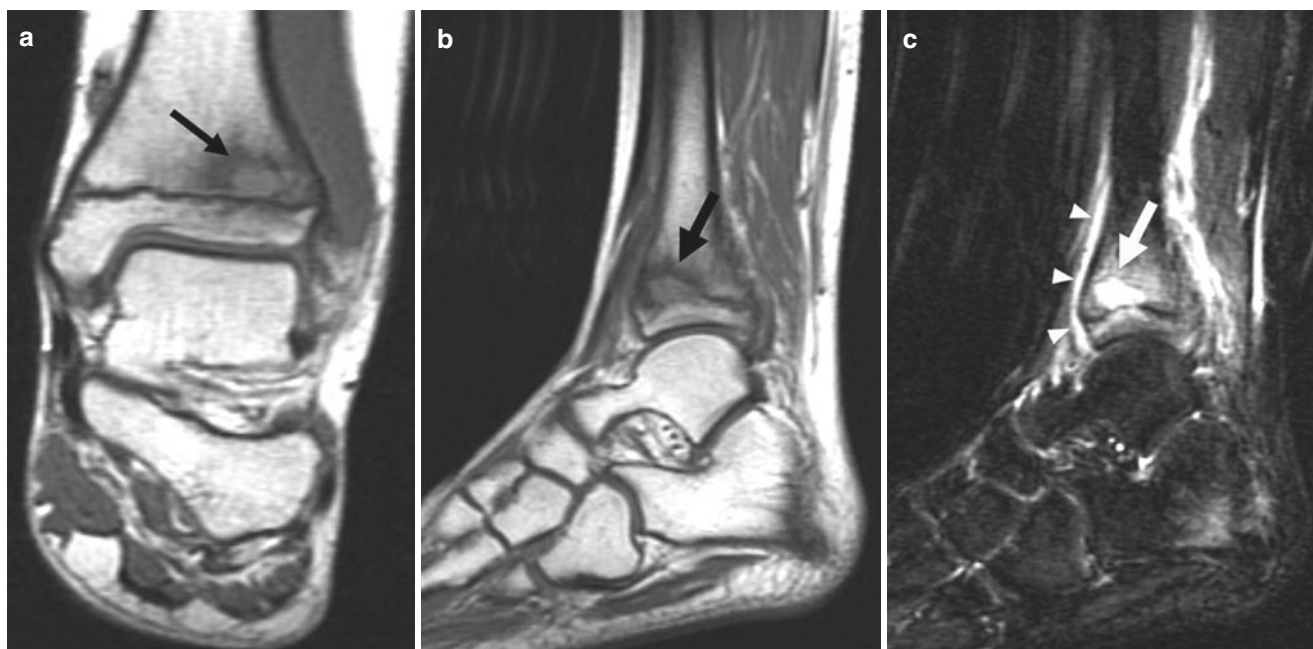
Fig. 15.3 A 10-year-old boy with chronic pain in the lower leg and intermittent fevers. Brodie abscess. Coronal (**a**) and sagittal (**b**) T1-weighted MR images of the ankle show a focal lesion (arrow) in the metaphysis of the distal tibia with slightly ill-defined margins. Sagittal STIR image (**c**) reveals fluid signal within the lesion (arrow) and surrounding bone marrow edema. Note periosteal reaction (arrowheads)

Underlying infection, including osteomyelitis, cellulitis, and abscess, would not be expected to enhance within necrotic areas (Fig. 15.4). In this setting, signal characteristics on T1- and T2-weighted images should be primarily relied on for diagnosis of soft tissue and osseous infection. If intravenous contrast is provided, the radiologist should be familiar with the appearance of devitalized tissue to reduce false-negative readings for infection.

15.4.7 Evaluation of Extent of Involvement

Extent of infection in soft tissue and bone is fairly well delineated on post-contrast MR images. However, infection does not tend to remain confined by fascial planes and spreads centripetally from the inoculation site across fascial compartments, into and across joints, and through tendons. Soft tissue involvement is often more extensive than the osseous disease, requiring careful examination of the soft tissues proximal to the source of infection. Without proper debridement the patient may eventually require more extensive amputation.

15.4.8 Spinal Involvement

Spine infection deserves special consideration; it is a relatively common clinical condition that can result in serious morbidity [20–22]. Recognition of early radiographic and MR manifestations is extremely important to avoid serious complications.

Radiologic diagnosis of spine infection is best made with MR imaging which is very sensitive for early detection of infection and accurate for delineation of extent of involvement and identification of paraspinal abscess for operative planning. However, identification of spine infection using other modalities is important because radiographs, CT, or bone scan is often ordered initially.

Radiographs are typically the first study obtained as part of the radiologic workup of suspected infection. Early manifestations of infectious spondylitis on radiographs include disc narrowing, vertebral endplate osteolysis or irregularity, and paraspinal soft tissue mass. Eventually, gross destruction of the endplates, collapse of the vertebral body, deformity, and sclerosis may occur. Generally, only one disc level is involved, although more severe or chronic cases spread to adjacent vertebral levels can occur along paravertebral ligaments or fascial planes. MRI is the primary modality for the diagnosis of infectious spondylitis. High sensitivity (ranging from 90% to 100%) and specificity (ranging from 80% to 95%), combined with anatomic detail, allow accurate diagnosis as well as delineation of extent of involvement and identification of paraspinal and epidural abscess.

The infected disc demonstrates low signal on T1-weighted images and high signal (approximating fluid) on T2-weighted images (Fig. 15.5). Fat suppression technique is recommended on the T2-weighted images to best demonstrate the associated endplate edema. On T1- and T2-weighted
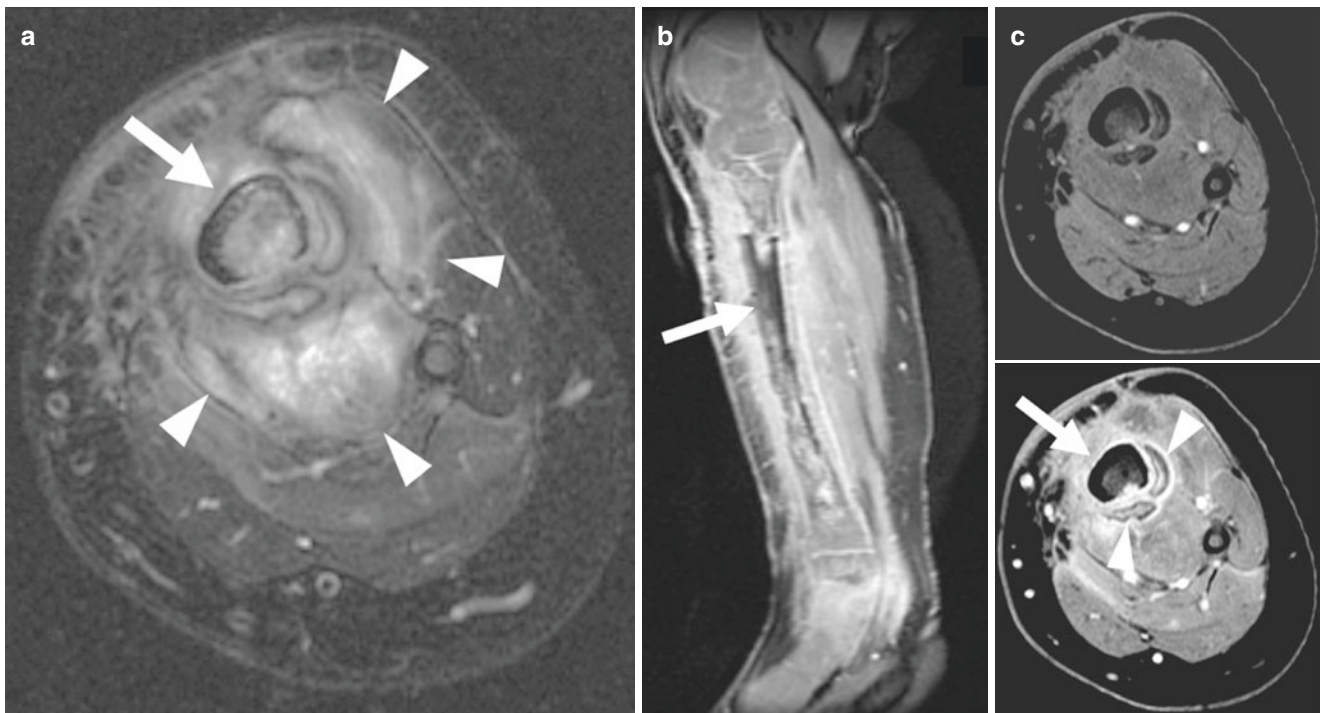
Fig. 15.4 A 6-year-old boy with chronic leg pain and fevers. Biopsy-proven osteomyelitis. Axial T2-weighted fat-suppressed MR image (**a**) of the lower leg demonstrates abnormal signal in the tibia (arrow) representing osteomyelitis. Note surrounding phlegmonous tissue (arrowheads). Sagittal T1-weighted fat-suppressed post-contrast image (**b**) and axial T1-weighted fat-suppressed pre- and post-contrast images (**c**) show nonenhancement of the mid tibial shaft (arrow) consistent with devitalization (a sequestrum). A rim of enhancing new bone formation (involucrum, arrowheads) is present

sagittal images, the endplates may be irregular, with loss of the normal low signal cortical line. Administration of intravenous gadolinium in conjunction with a fat-suppressed T1-weighted imaging sequence can aid diagnostic confidence; the infected disc demonstrates rim enhancement along the margins, with enhancement of the adjacent vertebral endplates. Occasionally, the entire vertebral body above and below the affected disc level enhances diffusely.
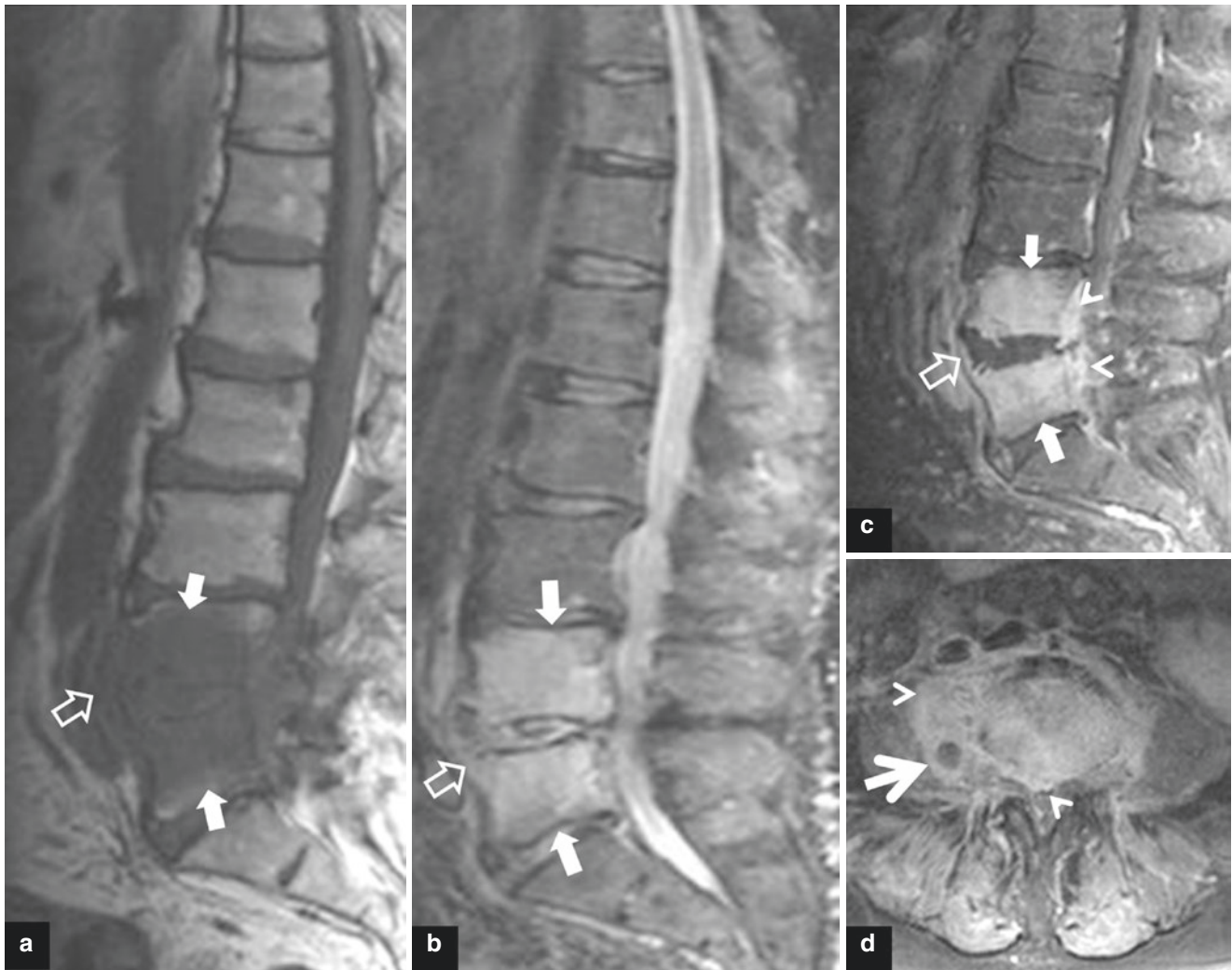
T2-weighted images and fat-suppressed T1-weighted gadolinium-enhanced images are particularly useful for identification of paraspinal or epidural abscess. These abscesses are typically longitudinally oriented, extending along paraspinal ligaments or fascial planes, often far from the original site of infection. On T2-weighted images, the abscess shows increased T2 signal intensity, approximating fluid, but often with lobulated margins and internal complexity representing septations, debris, or devitalized tissue. Gadolinium-enhanced images show rim enhancement at the margins of the abscess, which is generally thick and irregular.

Like infection, degenerative disc disease results in disc narrowing with associated endplate irregularity and sclerosis. In addition, Schmorl's nodes (intravertebral disc herniation) cause the appearance of endplate irregularity and in early stages show marrow edema on MRI. Although soft tissue mass is absent (except for disc bulge), this is not a reli-

able discriminator on radiographs or CT. However, disc degeneration is commonly associated with a vacuum phenomenon, a finding that is nearly 100% specific for absence of infection. As a result, vacuum disc should be sought in cases of suspected infection; lateral radiographs in flexion and extension can aid in identification of a vacuum phenomenon. CT is excellent for detection of small vacuum phenomena at suspected levels. On MRI, Modic type 1 endplate changes can mimic infection, with decreased T1 signal and increased T2 signal. However, the associated disc will show low signal on T1- and T2-weighted images if degenerated compared with the high T2 signal characteristic of infection. MRI can also detect paraspinal edema and mass effect, which are absent in degenerative disc disease.

15.5 Aspiration/Biopsy and Atypical Infections

Most hematogenous musculoskeletal infections are caused by bacteria, with the vast majority being *Staphylococcus aureus*. This and other bacterial infections generally have similar ("classic") imaging characteristics as described above, with diagnosis made by aspiration or biopsy. Culture of infections resulting from transcutaneous spread (i.e., diabetic ulcer) or

Fig. 15.5 A 70-year-old male patient with a history of 5 months of low back pain and a final diagnosis of tuberculous spondylodiscitis. MRI with sagittal T1-weighted (**a**), STIR (**b**), and contrast-enhanced fat-suppressed T1 on sagittal (**c**) and axial (**d**) planes show bone mar- row edema in the L4 and L5 vertebral bodies (arrows), subligamentous spread sparing the disc (open arrows), epidural and paraspinal phleg- mon (arrowheads), and paraspinal abscess formation (thick arrow)

inoculation (i.e., stepping on a nail) can exhibit more fastidi- ous organisms and multi-organism involvement. In these situ- ations, a PCR (polymerase chain reaction) assay can be useful to analyze the DNA or RNA of the organism to quickly deter- mine the causative organism rather than waiting for culture results. Additionally, in as many as 75% of cases, culture results are falsely negative [23]. Finally, PCR can be useful in differentiating chronic infection from other pathologies, espe- cially in diagnosis of prosthetic joint complications [24].

In the case of transcutaneous spread, care must be taken not to inadvertently inoculate the bone with the organism infecting the soft tissues. For example, if there is a diabetic foot ulcer with questionable abnormality in the adjacent bone on MRI, a biopsy through the infected soft tissue will virtually guarantee bone infection.

Nontraditional infections (fastidious organisms, nonbacte- rial infections) can have non-classic imaging features. This can be due to the preferred food source of the organism; where *S. aureus* feasts on standard agar culture medium (and disc material), mycobacterial infection grows poorly on bac- terial agar culture plates and in discs. As a result, discs are often involved only later in tuberculous spinal infections, with paraspinal spread predominating. It can also be due to the chronicity of the infectious process; whereas bacterial infections usually exhibit rapid onset and progression, fungal, parasitic, mycobacterial infections and others can grow slowly and insidiously leading to radiological manifestations relating to chronic inflammation. These include bone sclerosis and erosion, bone destruction and deformity, necrosis, "cold" abscesses in soft tissue and bone, and soft tissue calcification. The classic example is tuberculosis of the spine, leading to gibbus deformity and calcified paraspinal abscesses.

Many atypical infections involving the musculoskeletal system are actually manifestations of systemic infection, and

other organ involvement is the primary concern. This can occur in tuberculosis, where musculoskeletal infection is usually a consequence of lung or genitourinary disease [18, 19]. Fungal and parasitic infections are often diffusely disseminated, affecting multiple organ systems [25, 26]. Disseminated or chronic infections are often associated with an underlying immunocompromised state which can be related to HIV infection, steroid treatment, malnutrition, and diabetes as well as other chronic metabolic conditions.

15.6 Mimickers of Infection

15.6.1 Neuropathic Osteoarthropathy

Differentiation of osteomyelitis and neuropathic osteoarthropathy can be difficult, because both can demonstrate marrow abnormality, joint effusion, and surrounding soft tissue edema [27]. Some rules may be used to help differentiate these entities on MR images. First, the vast majority of cases of osteomyelitis of the foot and ankle are due to contiguous spread. Therefore, a bone marrow abnormality without adjacent skin ulceration, sinus tract, or soft tissue inflammation is less likely to represent infection. This concept is particularly useful when there are extensive bone marrow signal abnormalities and lack of subcutaneous tissue involvement. Second, neuropathic osteoarthropathy is predominantly an articular process manifesting as instability, often with multiple regional joints involved (e.g., the Lisfranc, Chopart, or multiple adjacent metatarsophalangeal joints). This and other articular manifestations of neuropathic disease (subluxation, cysts, necrotic debris) are not as common in infection. Associated neuropathic marrow changes can be extensive (especially at the midfoot) but tend to be centered equally about a joint and at the subarticular bone. Osteomyelitis shows more diffuse marrow involvement, and unless there is a primary septic arthritis, the marrow changes are generally greater on one side of the joint. Finally, location of disease is important. Neuropathic osteoarthropathy by far is most common at the Lisfranc and Chopart joints. Osteomyelitis occurs predominantly at the metatarsal heads, toes, calcaneus, and malleoli, a distribution that mirrors that of friction, callus, and ulceration. However, contiguous spread of infection can occur at atypical sites if there is a foot deformity (e.g., the cuboid in cases of rocker-bottom deformity) (Fig. 15.6).

15.6.2 Renal Failure

Chronic renal failure can lead to resorption of bone at the joints and enthesial attachments, as well as the intervertebral discs, leading to an appearance on imaging similar to that of infection [28]. This is also referred to as "dialysis-associated spondyloarthropathy" or "spondylosis of renal failure" due

to high incidence in the spine. However, other joints with high stress and bone turnover can be involved, including the sacroiliac joints. The appearance is related to bone resorption, hyperemia, and instability due to secondary hyperparathyroidism. Radiographs show bone resorption that can simulate erosion. Edema and joint effusion are observed. A background of altered bone density typical of secondary hyperparathyroidism can be sought (i.e., "rugger jersey spine"). There may also be amyloid deposition within or around the joints or discs; amyloid is low signal on T1- and T2-weighted images. If there is history of renal failure, this diagnosis can be entertained in the setting of imaging features concerning for infection. However, if the clinical picture is compatible with infection (increased WBCs, fever, positive blood culture), biopsy may be needed. The pathologist should be prompted to look for amyloid and perform a Congo red stain.

15.6.3 Crystalline Disorders

Crystalline diseases can simulate infection on various modalities [29–32].

Gout (monosodium urate crystal deposition) can present in various ways including tophaceous versus non-tophaceous and intra-articular versus extra-articular. Extra-articular involvement can include infiltration of tendons and bursae. Cases with more severe involvement can present with bone destruction and even a mutilans pattern of joint erosion. Intra-articular crystal deposition can simulate infection, with joint effusion and erosions. The inflammatory nature of arthritis also results in subchondral bone marrow edema as well as periarticular edema which can be very difficult to differentiate from osteomyelitis. Demonstration of tophi, which are mass-like foci in or around the joint, can suggest the true diagnosis; tophi demonstrate low signal on T1- and T2-weighted images, unlike infection-related abscess or phlegmon [32]. Additionally, since gout is a systemic disease, involvement of other joints should be sought in the patient's imaging file. Recently dual-energy CT has proven useful for diagnosis and determination of extent of involvement [33].

CPPD (calcium pyrophosphate deposition) and HADD (hydroxyapatite deposition disease) are calcium-based crystal disorders involving joint cartilage (CPPD) and tendons/bursae (HADD). In the case of CPPD, inflammatory involvement can lead to joint effusion and periarticular edema that can simulate gout or infection; the clinical manifestation is often referred to as "pseudogout" due to paroxysmal pain and swelling. Radiographs can be helpful in this circumstance with demonstration of chondrocalcinosis (calcium deposition in fibrocartilage and/or articular cartilage); this appearance is nonspecific and is often incidental in older patients. However, association with soft tissue swelling/joint effusion with the typical clinical presentation can reveal the
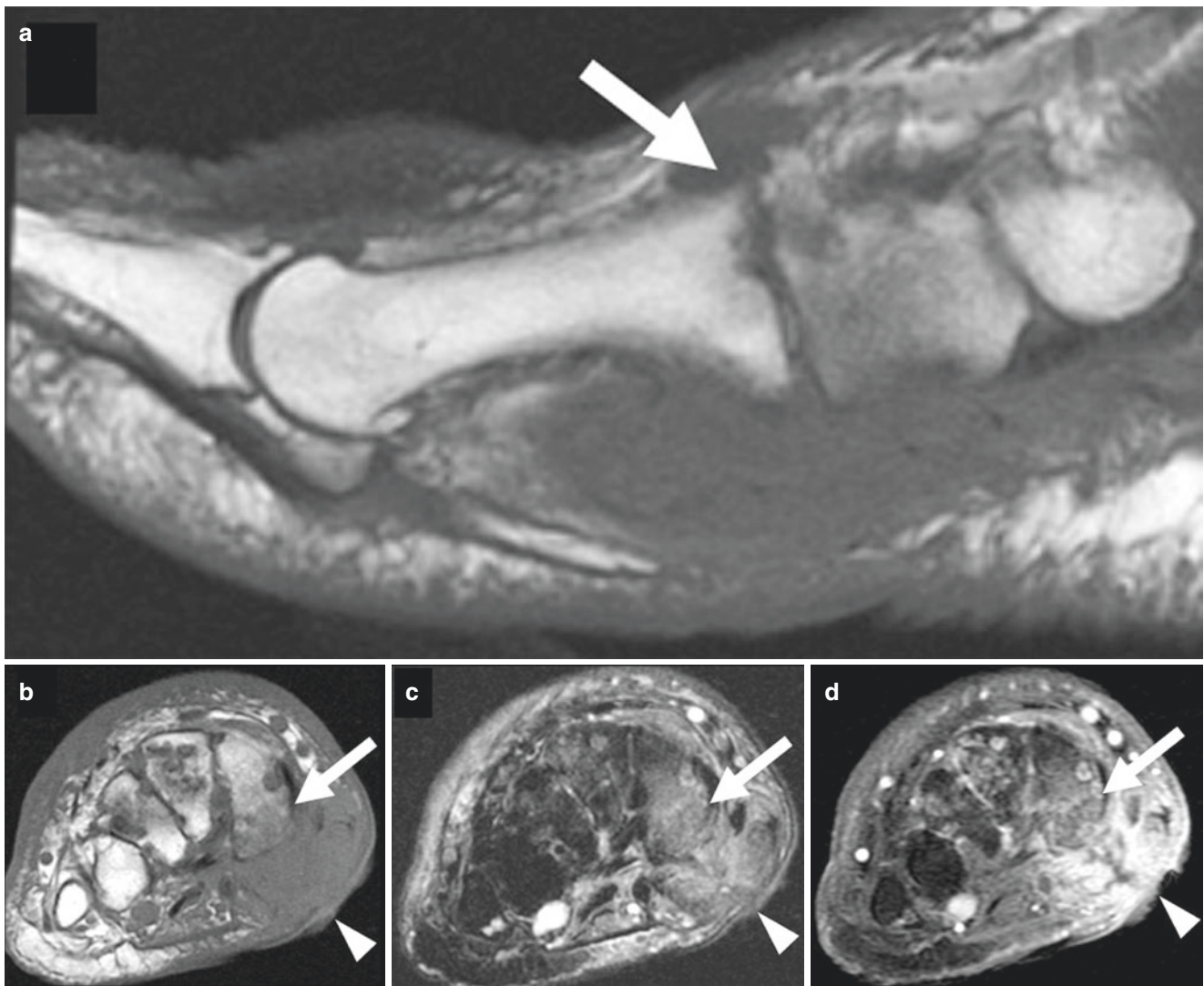
Fig. 15.6 A 56-year-old man with neuropathic osteoarthropathy of the midfoot presents with an ulceration and concern for superimposed osteomyelitis. Sagittal T1-weighted image (**a**) shows Charcot arthropathy involving the Lisfranc joint (arrow). Coronal T1-weighted (**b**), T2-weighted fat-suppressed (**c**), and T1-weighted fat-suppressed post-contrast images (**d**) of the midfoot demonstrate ulceration (arrowheads) with cellulitis and adjacent sinus tract extending to the medial cuneiform (arrows) where marrow signal alteration is consistent with superimposed osteomyelitis

diagnosis. HADD is also characteristic on radiographs, with focal calcification at a tendon attachment or bursa. This most commonly occurs at the rotator cuff; but if the location is atypical (i.e., hand tendon or gluteal attachment), the clinical presentation can mimic infection.

15.6.4 Inflammatory Arthropathies

Rheumatoid arthritis, reactive arthritis, and psoriatic arthritis (as well as less common arthropathies resulting in synovial proliferation) can simulate septic arthritis and osteomyelitis on imaging exams, with joint effusion, joint space narrowing, erosions, and subchondral bone marrow edema [34, 35]. One useful differentiating feature is periarticular edema. Inflammatory arthropathies are generally chronic processes with slow distention of the joint capsule, whereas at least bacterial infection results in marked hyperemia and rapid joint distention resulting in aggressive appearing pericapsular edema ("angry effusion"). This effect is accentuated in smaller, lower capacity joints (i.e., the sacroiliac joint). Additionally, chronic inflammatory arthropathies (especially rheumatoid arthritis) may exhibit synovial proliferation with a mass-like quality, whereas bacterial arthritis progresses rapidly without proliferative synovial hyperplasia, except in later stages or in poorly treated cases. Finally, septic arthritis, except in rare circumstances of disseminated infection, is a monoarticular process. Chronic inflammatory arthropathies listed above are associated with systemic disease and can exhibit similar findings in other joints and locations such as tendon sheaths and enthesial attachments.

15.6.5 Tumor

Certain neoplasms can have characteristics similar to infection on imaging exams. Imaging findings that can be seen in both infection and tumor include bone destruction, periosteal reaction, fluid collections and necrosis, and soft tissue mass effect [36–38]. Tumor is generally easily differentiated from septic arthritis or discitis because neoplasms rarely cross joints. Involvement of both sides of a joint therefore indicates an arthritic process, inflammatory or degenerative. However, tumors involving the shaft of a bone can result in

destruction and periosteal reaction similar to osteomyelitis. Tumors at the epiphysis can cause a joint effusion (i.e., osteoid osteoma). Small round cell tumors result in a permeative pattern similar to infection. Classic lesions simulating osteomyelitis include Ewing sarcoma, leukemia and lymphoma, and Langerhans cell histiocytosis. Conversely, atypical infections such as tuberculosis and fungal and parasitic infections can cause focal bone destruction simulating tumor. When biopsy is performed, one should always consider sending samples for both histologic and microbiologic analysis (Fig. 15.7).
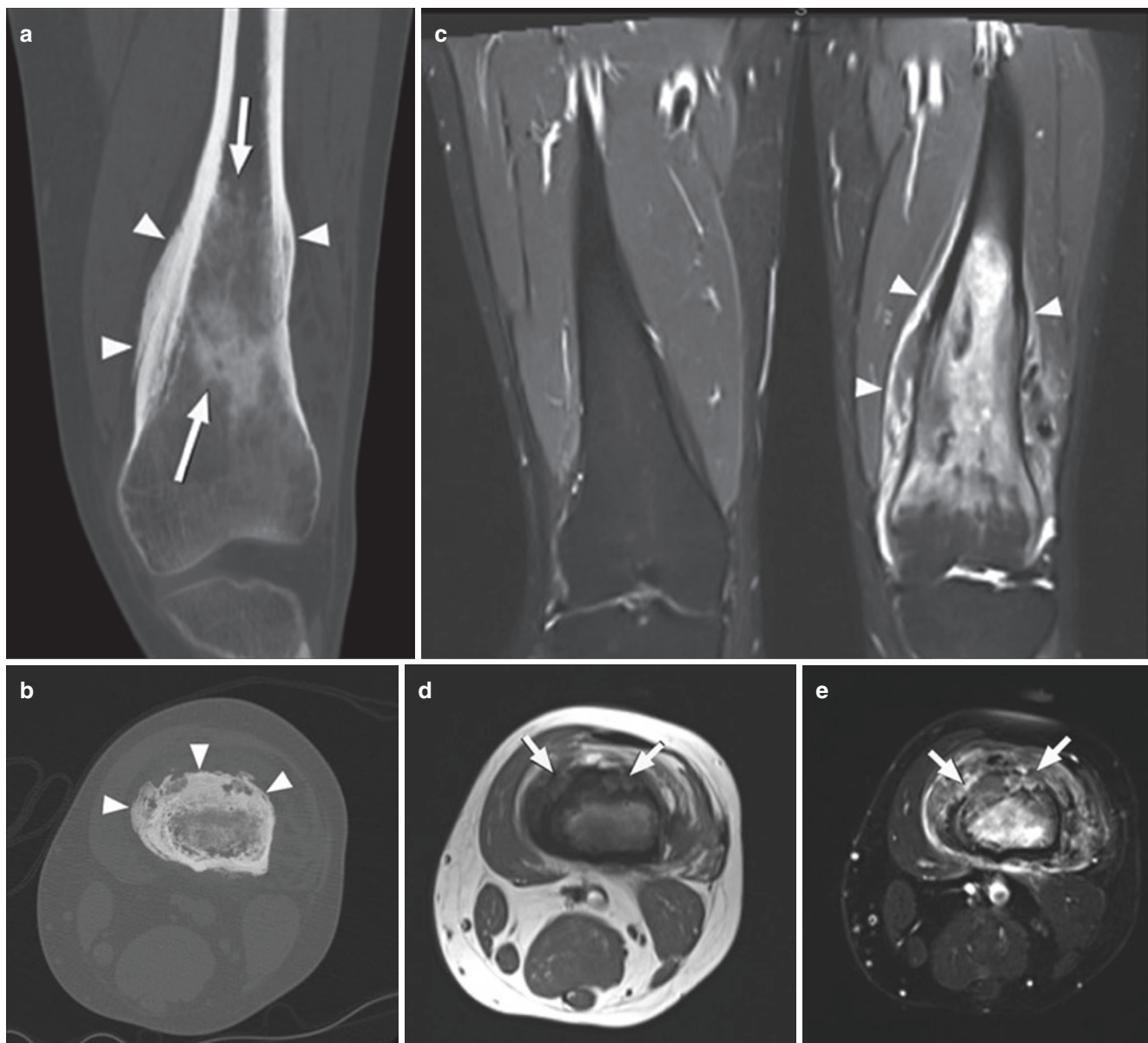
Fig. 15.7 A 38-year-old man with aching leg pain for a year. Chronic osteomyelitis simulating lymphoma. Coronal (**a**) and axial (**b**) CT images show a sclerotic lesion in the distal femoral shaft (arrows) with thick periosteal reaction (arrowheads). Corresponding coronal STIR image (**c**) shows an extensive, ill-defined intramedullary lesion with periosteal reaction and soft tissue mass effect (arrowheads). Based on course of symptoms and imaging features, biopsy was performed with differential diagnosis of chronic osteomyelitis or lymphoma. In retrospect cortical sinus tract formation (arrows) can be seen on axial T1-weighted (**d**) and T2-weighted (**e**) images

Key Points

Mimickers of infection
- Neuropathic osteoarthropathy.
- Manifestations of renal failure.
- Crystalline diseases: i.e., gout.
- Inflammatory arthritis: i.e., rheumatoid arthritis.
- Tumor: i.e., lymphoma, leukemia, Ewing sarcoma.

15.7 Concluding Remarks

Radiologic examinations play an essential role in diagnosis and management of infection. The practitioner should maintain up-to-date knowledge regarding advantages and limitations of the different imaging modalities to provide the most efficacious care.

Take Home Messages
- MRI is the test of choice for diagnosis and management of MSK infection.
- Current terminology guidelines recommend against use of the term "osteitis" for description of early/borderline cases of osteomyelitis.
- Beware of performing percutaneous biopsy in questionable cases that let you iatrogenically introduce infection.
- When performing biopsy, always consider the possibility of alternate etiology such as neoplasia.

References

1. Turecki MB, Taljanovic MS, Stubbs AY, Graham AR, Holden DA, Hunter TB, Rogers LF. Imaging of musculoskeletal soft tissue infections. Skelet Radiol. 2010;39(10):957–71.
2. Christian S, Kraas J, Conway WF. Musculoskeletal infections. Semin Roentgenol. 2007;42(2):92–101.
3. Santiago Restrepo C, Giménez CR, McCarthy K. Imaging of osteomyelitis and musculoskeletal soft tissue infections: current concepts. Rheum Dis Clin N Am. 2003;29(1):89–109.
4. Gold RH, Hawkins RA, Katz RD. Bacterial osteomyelitis: findings on plain radiography, CT, MR, and scintigraphy. AJR Am J Roentgenol. 1991;157(2):365–70.
5. Ma LD, Frassica FJ, Bluemke DA, Fishman EK. CT and MRI evaluation of musculoskeletal infection. Crit Rev Diagn Imaging. 1997;38(6):535–68.
6. Fayad LM, Carrino JA, Fishman EK. Musculoskeletal infection: role of CT in the emergency department. Radiographics. 2007;27(6):1723–36.
7. Smith SE, Salanitri J, Lisle D. Ultrasound evaluation of soft tissue masses and fluid collections. Semin Musculoskelet Radiol. 2007;11(2):174–91.

8. Erdman WA, Tamburro F, Jayson HT, Weatherall PT, Ferry KB, Peshock RM. Osteomyelitis: characteristics and pitfalls of diagnosis with MR imaging. Radiology. 1991;180(2):533–9.
9. Soldatos T, Durand DJ, Subhawong TK, Carrino JA, Chhabra A. Magnetic resonance imaging of musculoskeletal infections: systematic diagnostic assessment and key points. Acad Radiol. 2012;19(11):1434–43.
10. Morrison WB, Schweitzer ME, Bock GW, et al. Diagnosis of osteomyelitis: utility of fat-suppressed contrast-enhanced MR imaging. Radiology. 1993;189:251–7.
11. Ledermann HP, Schweitzer ME, Morrison WB. Nonenhancing tissue on MR imaging of pedal infection: characterization of necrotic tissue and associated limitations for diagnosis of osteomyelitis and abscess. AJR Am J Roentgenol. 2002;178:215–22.
12. Glaudemans AW, Israel O, Slart RH. Pitfalls and limitations of radionuclide and hybrid imaging in infection and inflammation. Semin Nucl Med. 2015;45(6):500–12.
13. Vijayanathan S, Butt S, Gnanasegaran G, Groves AM. Advantages and limitations of imaging the musculoskeletal system by conventional radiological, radionuclide, and hybrid modalities. Semin Nucl Med. 2009;39(6):357–68.
14. Andersen KF, Jensen KE, Loft A. PET/MR imaging in musculoskeletal disorders. PET Clin. 2016;11(4):453–63.
15. Graif M, Schweitzer ME, Deely D, Matteucci T. The septic versus nonseptic inflamed joint: MRI characteristics. Skelet Radiol. 1999;28:616–20.
16. Karchevsky M, Schweitzer ME, Morrison WB, et al. MRI findings of septic arthritis and associated osteomyelitis in adults. AJR Am J Roentgenol. 2004;182:119–22.
17. Kompel A, Murakami A, Guermazi A. MRI of non traumatic musculoskeletal emergencies. Magn Reson Imaging Clin N Am. 2016;24:369–89.
18. Moore SL, Rafii M. Advanced imaging of tuberculosis arthritis. Semin Musculoskelet Radiol. 2003;7:143–53.
19. De Backer AI, Mortele KJ, Vanhoenacker FM, et al. Imaging of extraspinal musculoskeletal tuberculosis. Eur J Radiol. 2006;57:119–30.
20. Torres C, Zakhari N. Imaging of spine infection. Semin Roentgenol. 2017;52:17–26.
21. Prodi E, Grassi R, Iacobellis F, et al. Imaging in spondylodiscitis. Magn Reson Imaging Clin N Am. 2016;24:581–600.
22. Diehn FE. Imaging of spine infection. Radiol Clin N Am. 2012;50:777–98.
23. Hoang D, Fisher S, Oz OK, La Fontaine J, Chhabra A. Percutaneous CT guided bone biopsy for suspected osteomyelitis: diagnostic yield and impact on patient's treatment change and recovery. Eur J Radiol. 2019;114:85–91.
24. Suren C, Feihl S, Cabric S, Banke IJ, Haller B, Trampuz A, von Eisenhart-Rothe R, Prodinger PM. Improved pre-operative diagnostic accuracy for low-grade prosthetic joint infections using second-generation multiplex polymerase chain reaction on joint fluid aspirate. Int Orthop. 2020;44(9):1629–37.
25. Arkun R. Parasitic and fungal disease of bones and joints. Semin Musculoskelet Radiol. 2004;8(3):231–42.
26. Chhem RK, Wang S, Jaovisidha S, Schmit P, Friedman L, Bureau NJ, Cardinal E. Imaging of fungal, viral, and parasitic musculoskeletal and spinal diseases. Radiol Clin N Am. 2001;39(2):357–78.
27. Ahmadi ME, Morrison WB, Schweitzer ME, et al. Neuropathic arthropathy of the foot with and without superimposed osteomyelitis: MR imaging characteristics. Radiology. 2006;238:622–31.
28. Jevtic V. Imaging of renal osteodystrophy. Eur J Radiol. 2003;46(2):85–95.

29. Teh J, McQueen F, Eshed I, Plagou A, Klauser A. Advanced imaging in the diagnosis of gout and other crystal arthropathies. Semin Musculoskelet Radiol. 2018;22(2):225–36.

30. Buckens CF, Terra MP, Maas M. Computed tomography and MR imaging in crystalline-induced arthropathies. Radiol Clin N Am. 2017;55(5):1023–34.

31. Soldatos T, Pezeshk P, Ezzati F, Karp DR, Taurog JD, Chhabra A. Cross-sectional imaging of adult crystal and inflammatory arthropathies. Skelet Radiol. 2016;45(9):1173–91.

32. Wadhwa V, Cho G, Moore D, Pezeshk P, Coyner K, Chhabra A. T2 black lesions on routine knee MRI: differential considerations. Eur Radiol. 2016;26(7):2387–99.

33. Desai MA, Peterson JJ, Garner HW, Kransdorf MJ. Clinical utility of dual-energy CT for evaluation of tophaceous gout. Radiographics. 2011;31(5):1365–75; discussion 1376–7.

34. Lambert RGW, Østergaard M, Jaremko JL. Magnetic resonance imaging in rheumatology. Magn Reson Imaging Clin N Am. 2018;26(4):599–613.

35. Reijnierse M, Helm-Mil AV, Eshed I, Schueller-Weidekamm C. Magnetic resonance imaging of rheumatoid arthritis: peripheral joints and spine. Semin Musculoskelet Radiol. 2018;22(2):127–46.

36. Peterson JJ, Bancroft LW, Kransdorf MJ. Principles of tumor imaging. Eur J Radiol. 2005;56(3):319–30.

37. Murphey MD, Senchak LT, Mambalam PK, Logie CI, Klassen-Fischer MK, Kransdorf MJ. From the radiologic pathology archives: Ewing sarcoma family of tumors: radiologic-pathologic correlation. Radiographics. 2013;33(3):803–31.

38. Murphey MD, Kransdorf MJ. Primary musculoskeletal lymphoma. Radiol Clin N Am. 2016;54(4):785–95.

Ultrasonography: Sports Injuries

16

Gina M. Allen and Jon A. Jacobson

Learning Objectives
- To understand the value of ultrasound in the examination of sports injuries.
- To be familiar with common sport-related disease of the upper extremity.
- To be familiar with common sport-related disease of the lower extremity.

16.1 Upper Extremity

16.1.1 Introduction

Ultrasound is an effective imaging method for evaluation of upper extremity sports injuries. For evaluation of the shoulder, ultrasound is ideal in assessment of the rotator cuff, the biceps brachii tendon and the subacromial-subdeltoid bursa. Evaluation of the cartilaginous structures of the shoulder is significantly limited, and therefore MRI and preferably MR arthrography are considered in this scenario. An algorithm based on patient age is often used, where patients over the age of 40 years often are evaluated with ultrasound and patients under 40 years are evaluated with MRI or MR arthrography. This algorithm is used as patients under the age of 40 years will often have articular-sided partial-thickness rotator cuff tears and concomitant labral pathology, both of which are ideally seen with MRI [1]. Beyond the shoulder, ultrasound is most accurate when the indication for imaging is targeted and the structure imaged is superficial. Last, ultrasound complements MRI given its ability to dynamically assess pathology of the upper extremity. Given the superficial location of soft tissue abnormalities, a linear transducer of greater than 12 MHz is preferred, and a small footprint probe is used for the most distal aspects of the upper extremity.

16.1.2 Shoulder

The rotator cuff is the most commonly imaged tendon group using ultrasound, where its accuracy in the diagnosis of cuff pathology is equal to MRI. Unlike the distal aspects of the upper extremity, a protocol-based evaluation with ultrasound is recommended as symptoms do not always directly correlate with pathology, and symptoms may also be multifactorial in aetiology [2]. Each individual rotator cuff tendon (supraspinatus, infraspinatus, subscapularis, teres minor) is imaged in short and long axis. Given the curvature of the humeral head and the overlying supraspinatus, care must be taken not to misinterpret artefactual hypoechogenicity from anisotropy as tendon abnormality. Pathology of the rotator cuff, similar to other tendons, include tendinosis and tendon tear. The term tendinosis is used rather than tendinitis as inflammation diminishes after the first week after a tendon injury [3]. Tendinosis refers to mucoid degeneration and chondroid metaplasia of the involved tendon [4, 5]. At ultrasound, tendinosis will appear as abnormal hypoechogenicity with possible increased in tendon thickness [6]. Tendon tear will appear as a well-defined hypoechoic or anechoic defect in the normal hyperechoic fibrillar tendon architecture. Such tendon tears may be partial-thickness and only involve the articular surface, bursal surface or may be intrasubstance (or interstitial) not contacting either the articular (Fig. 16.1) or bursal surface of the tendon, although isolated greater tuberosity extension is common. A full-thickness tear will extend from the articular to bursal surface of the tendon. Of note, most supraspinatus tendon tears extend to the greater tuberosity footprint, which creates the cortical irregularity as a

G. M. Allen
St Luke's Radiology Oxford Ltd, Oxford, Oxfordshire, UK
e-mail: gina@slro.co.uk

J. A. Jacobson (✉)
Radiology, University of Michigan, Ann Arbor, MI, USA
e-mail: jjacobsn@med.umich.edu
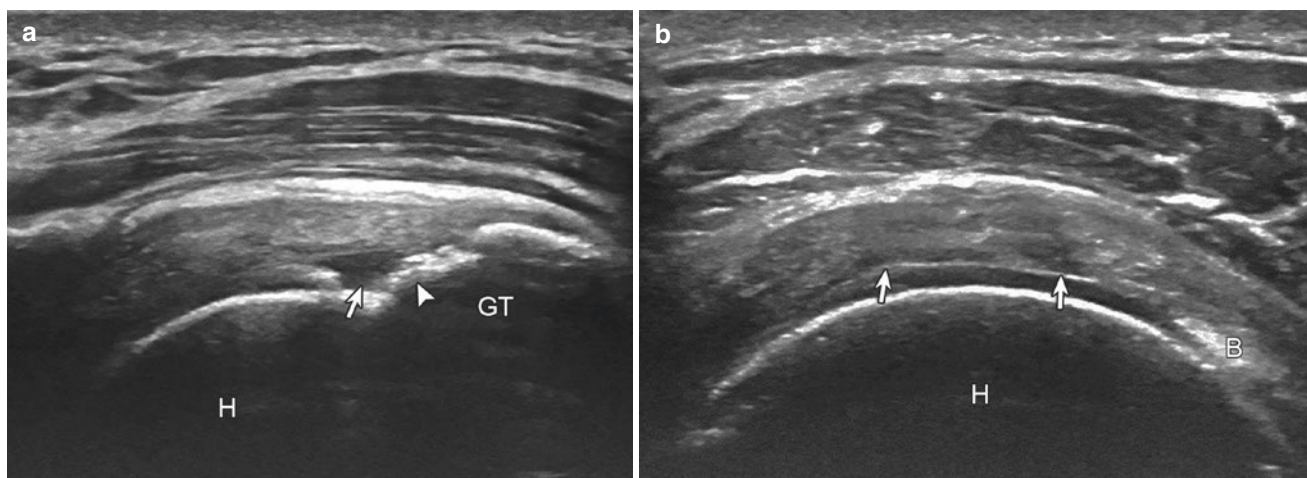
Fig. 16.1 Supraspinatus tear: articular side partial-thickness. Ultrasound images long axis (**a**) and short axis (**b**) to supraspinatus tendon show hypoechoic tendon tear (arrows) extending to the articular surface of the humeral head (H). Note cortical irregularity (arrowhead) of greater tuberosity (GT). *B* Biceps brachii long head tendon in rotator interval

very important indirect sign in such tears in patients over the age of 40 years [6, 7]. Once a tear is identified, the short- and long-axis dimensions, as well as per cent tear depth (in the case of partial-thickness tears), are measured and included in the imaging report. Chronic and large full-thickness tears, especially those involving the anterior aspect of the supraspinatus, are associated with tendon retraction and subsequent infraspinatus and supraspinatus fatty infiltration and possible muscle atrophy [8]. This information should be included in the imaging report as muscle atrophy is associated with poor outcomes after surgical repair of a rotator cuff tear [9].

Another structure commonly imaged with ultrasound is the biceps brachii long head tendon. While the most proximal aspect of the biceps brachii long head tendon at the labrum is not visible with ultrasound, the segment in the bicipital groove and more proximally into the glenohumeral joint are well seen, with the latter best seen with the shoulder in the modified Crass position. Fluid distention of the biceps brachii long head tendon sheath is most commonly from extension of a glenohumeral joint effusion. Heterogeneous or focal distention with hyperemia and focal symptoms would suggest true tenosynovitis. Tendinosis will appear as abnormal hypoechogenicity and possible increased tendon thickness, partial-thickness tears will appear as surface irregularity and hypoechoic or anechoic clefts, and a full-thickness tear will show complete tendon discontinuity [10]. The thin hyperechoic aponeurotic expansion of the supraspinatus should not be confused with a longitudinal split of the biceps brachii [11]. Unlike a longitudinal split, the aponeurotic expansion characteristically is located anterior the tendon

and blends into the supraspinatus tendon when imaging proximally. Ultrasound may also be used to dynamically assess for biceps brachii tendon subluxation and dislocation and guide percutaneous tendon sheath injection [12].

Another common structure that is abnormal with overuse injuries is the subacromial-subdeltoid bursa. This composite bursa is quite extensive located deep to the deltoid and covering portions of the supraspinatus, infraspinatus, subscapularis, biceps brachii long head and proximal humerus. Distention of the bursa may range from anechoic fluid to hypoechoic or hyperechoic synovial hypertrophy [13]. To diagnose subacromial impingement with ultrasound, the arm is abducted, and ultrasound will reveal gradual distention of the subacromial-subdeltoid bursa at the edge of the acromion; however, this finding may be found in asymptomatic individuals, and clinical correlation is required [14]. Ultrasound may also be used to guide percutaneous bursal injection.

Key Points
- Cortical irregularity of the greater tuberosity is a helpful secondary sign of a supraspinatus tear.
- Fluid surrounding the biceps brachii long head tendon is most commonly due to a communicating glenohumeral joint effusion.
- Subacromial-subdeltoid bursal distention can range from anechoic fluid to hyperechoic synovial hypertrophy.
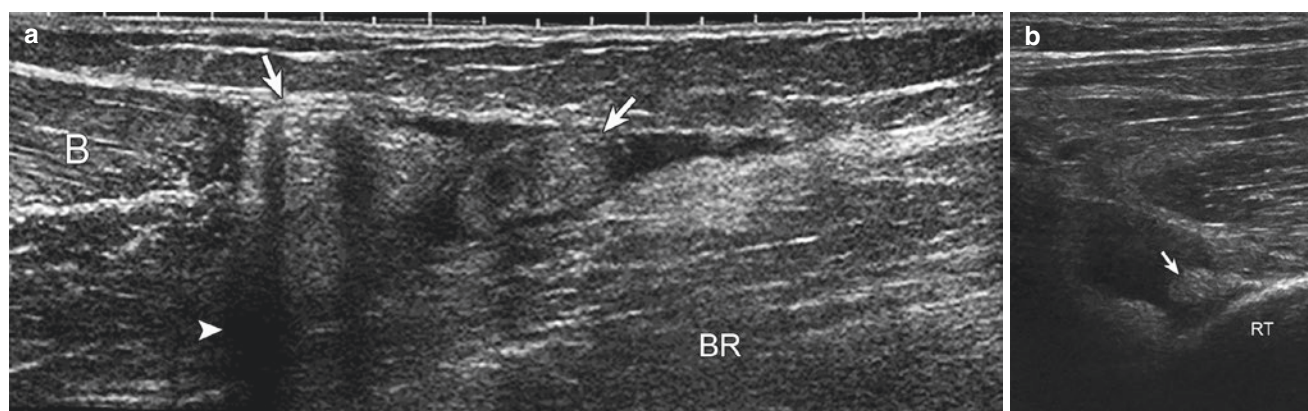
Fig. 16.2 Biceps brachii: full-thickness tear. Ultrasound images show (**a**) proximal and (**b**) distal stumps of the torn and retracted biceps brachii (arrows). Note refractions shadowing (arrowhead) deep to recoiled proximal stump in (**a**). *B* biceps brachii muscle, *BR* brachialis muscle, *RT* radial tuberosity

16.1.3 Elbow

The distal biceps brachii tendon may show findings of tendinosis (hypoechoic enlargement), partial-thickness tear (anechoic clefts) and full-thickness tear (complete tendon discontinuity) (Fig. 16.2) associated with sports injuries [15]. Ultrasound imaging of the distal biceps brachii tendon is often difficult given the oblique course of the distal tendon and resulting anisotropy. Imaging the biceps tendon from a medial or pronator window approach, with possible elbow flexion, is often helpful [16]. Partial-thickness biceps tears may involve one of the two heads, commonly the more superficial short head, which can create refraction shadowing artefact possibly obscuring the deeper long head tendon. In differentiating partial-thickness from a full-thickness tendon tear, the use of dynamic evaluation is helpful, either imaging from a medial or lateral approach [17]. With supination and pronation, lack of tendon movement to the same degree as radial tuberosity rotation is indirect evidence of a full-thickness tear. Often full-thickness distal biceps brachii tendon tears will be associated with significant tendon retraction.

Distal triceps brachii tendon tear are also effectively assessed with ultrasound. Partial-thickness tears often involve the superficial combined long and lateral heads, associated with an avulsed enthesophyte bone fragment (Fig. 16.3) [18]. The deeper medial head is often intact but may be erroneously interpreted as torn given that the medial head tendon is very short. Tendinosis may uncommonly involve the distal triceps brachii tendon, as well as distention of the overlying olecranon bursa.

Epicondylitis may also be diagnosed with ultrasound. With lateral (tennis elbow) more common than medial (golfer's elbow), the term "epicondylitis" is a misnomer in that it is not a primary epicondyle problem and is not actively inflamed [19]. The underlying pathology, similar to other tendons, represents tendinosis, interstitial tear or uncommonly full-thickness tear (Fig. 16.4). The presence of hyperemia on colour Doppler imaging correlates with symptoms and represents neovascularity rather than an indirect sign of inflammation.

The ulnar collateral ligament is evaluated dynamically with ultrasound and complements MR arthrography where the accuracy in diagnosis of tear is highest when both imaging methods are used [20]. With the elbow flexed at least 30°, valgus stress is placed across the elbow. Asymmetric widening of the medial joint space between the humerus and ulna with valgus stress can indicate ligament tear [20]. The ulnar nerve can also be imaged by dynamic ultrasound to assess for injury or subluxation.

> **Key Points**
> - Evaluating the biceps brachii tendon medially and laterally complements anterior evaluation.
> - Triceps brachii partial tears most commonly involve the superficial layer with avulsion of an enthesophyte.
> - Hyperemia of the common extensor tendon represents neovascularity and not inflammation.
> - Dynamic evaluation of the ulnar collateral ligament with valgus stress assesses joint space gapping to indicate tear.

Fig. 16.3 Triceps brachii: partial-thickness tear. Ultrasound image long axis to triceps brachii (T) shows retracted tear of superficial combined lateral and long head tendons (between arrows) with hyperechoic and shadowing enthesophyte avulsion fragment (curved arrow). Note intact deep medial head of triceps brachii (arrowheads). *O* olecranon process
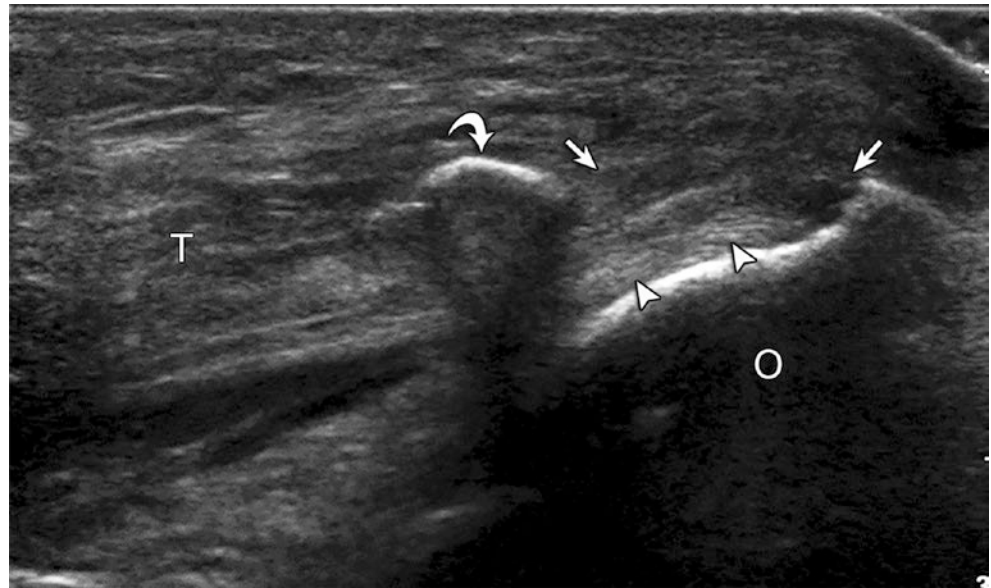
Fig. 16.4 Common extensor tendon abnormality (lateral epicondylitis). Ultrasound image long axis to common extensor tendon shows hypoechoic tendinosis (arrows). Note radial collateral ligament proper (arrowheads). *E* lateral epicondyle, *R* radial head, *a* annular ligament
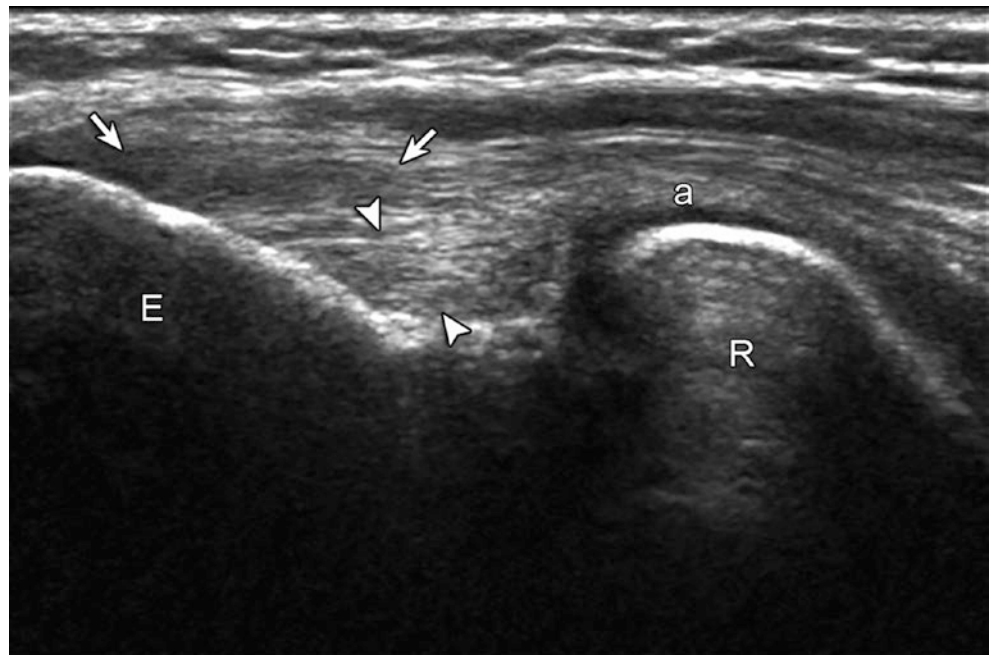

16.1.4 Wrist and Hand

Sports injuries of the hand and wrist are often ligamentous or related to the triangular fibrocartilage complex, which are best evaluated with MR or preferably MR arthrography; however, ultrasound can be used to evaluate focal tendon abnormalities. For example, intersection syndrome will appear as asymmetric hypoechoic swelling, oedema and possible hyperemia where the first extensor wrist compartment muscles (extensor pollicis longus and abductor pollicis brevis) cross over the second extensor wrist compartment (extensor carpi radialis longus and brevis) [21]. This can be very subtle and a very light pressure on the transducer is needed to see fluid in these cases. Full-thickness tendon tears are often associated with tendon retraction. Related to the extensor tendons, sagittal band injury at the level of the metacarpophalangeal joints is diagnosed when abnormal hypoechogenicity is seen with asymmetric location of the extensor tendon, best seen dynamically with flexion at the metacarpophalangeal joints, termed Boxer's knuckle [22]. Related to the flexor tendons of the fingers, ultrasound is effective in evaluation of the pulleys of the digits. Non-

visualisation of a pulley can indicate injury; however, the finding of tendon bowstringing is an important indirect sign of pulley injury, which appears as an abnormal position of the flexor tendon not approximated to the phalanx (Fig. 16.5). Bowstringing is evaluated dynamically with active finger flexion against resistance where a distance between the flexor tendon and phalanx greater than 1 mm indicates pulley injury; a distance greater than 3 mm indicates a complete A2 pulley tear; and a distance of 5 mm indicates a combined complete tears of A2 and A4 pulleys [23].

One ligament that is ideally assessed with ultrasound is the ulnar collateral ligament of the thumb [24]. Injury to this ligament, termed skier's or gamekeeper's thumb, can range from sprain (hypoechoic swelling), partial tear (partial anechoic defect) and complete tear (discontinuous ligament), with the latter either being non-displaced or displaced [25]. A displaced ulnar collateral ligament tear with an interposed adductor aponeurosis is termed a Stener lesion. Ultrasound is able to diagnose a Stener lesion with 100% accuracy [24]. Key to evaluation is correct placement of the transducer in the coronal plane relative to the thumb with visualisation of the characteristic bone contours at the expected attachments of the ulnar collateral ligament. The adductor aponeurosis is identified as a thin hypoechoic structure that normally overlies the intact ulnar collateral ligament, where flexion and extension at the interphalangeal joint cause isolated movement of the aponeurosis, which aides in its identification. The distal aspect of the displaced ulnar collateral ligament is identified as a hypoechoic round abnormality proximal to the metacarpal joint (Fig. 16.6), with a possible hyperechoic and shadowing avulsion bone fragment. The end of the torn ligament may be seen superficial to the adductor aponeurosis or may be seen along the distal metacarpal shaft with the ligament coursing proximal.
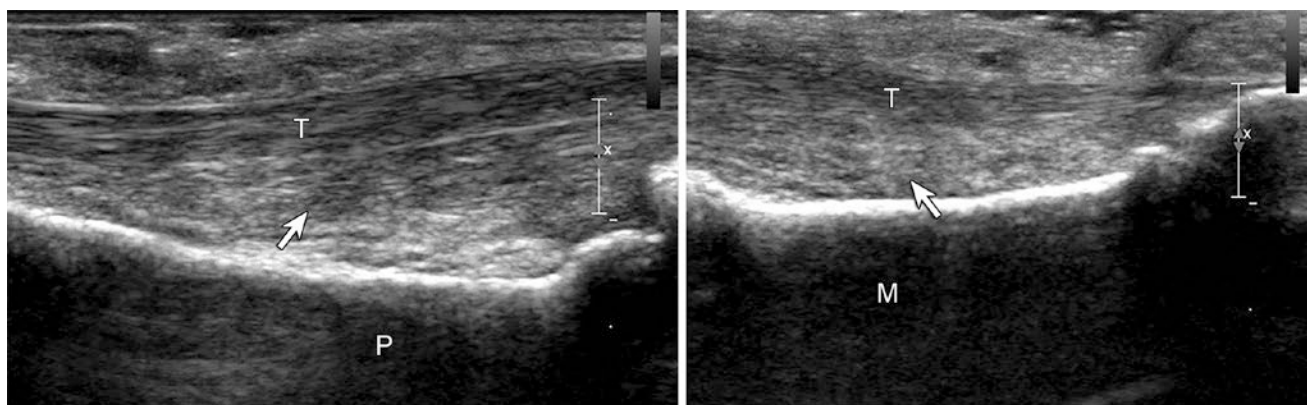
Fig. 16.5 Pulley injury. Ultrasound image long axis to the flexor tendons (T) of the finger shows abnormal volar displacement or bowstringing of the tendons (arrows) opposite the proximal (P) and middle (M) phalanges indicating A2 and A4 pulley tears, respectively

Fig. 16.6 Ulnar collateral ligament tear of the thumb (skier's thumb). Ultrasound image long axis to the ulnar collateral ligament of the thumb shows torn and proximally displaced ligament (arrow) with interposed, hypoechoic and thickened adductor aponeurosis (arrowheads). *MC* metacarpal, *P* proximal phalanx
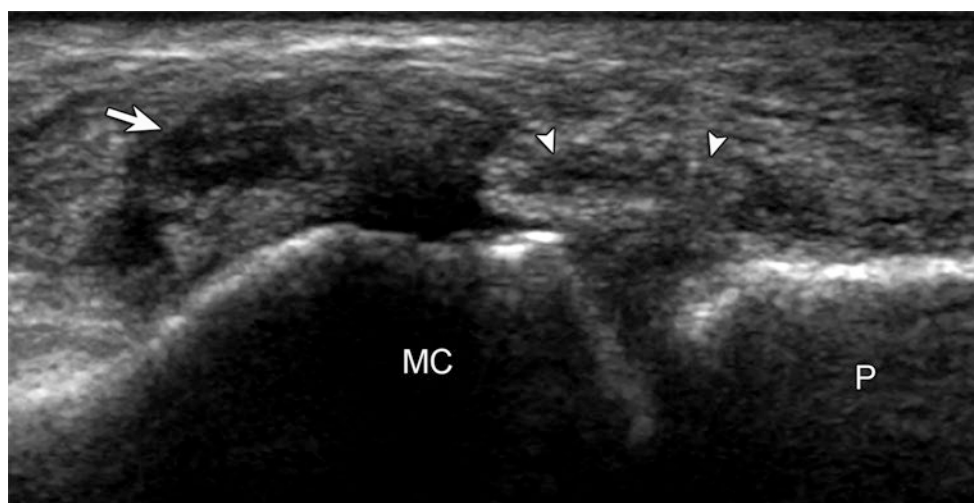
Key Points
- Tendon retraction indicates full-thickness tear.
- Flexor tendon bowstringing indicates pulley injury.
- Ultrasound can diagnose a Stener lesion with very high accuracy.

16.2 Lower Extremity

16.2.1 Introduction

For athletic injuries, diagnostic ultrasound is used daily as a "stethoscope" to confirm injury and guide treatment. It is not only performed by radiologists but also by sports physicians, physiotherapists and orthopaedic surgeons, to name a few [26].

Ultrasound examination is very important in the assessment of lower limb injuries because of its dynamic capabilities and excellent line pair resolution. Vascularity can be demonstrated within a structure without the need for intravenous contrast agent by pressing a button. Recently microvascular imaging allows us to observe subtle vascularity. Vascular supply is important in determining the nature and the time course of an injury. If increased, it indicates that an injury is in the acute or subacute phases, while its absence means that the injury is old. It is also be used to date tendinopathy. There may be some correlation with a painful tendon, but it is particularly useful in determining resolution after treatment.

In our practice diagnostic ultrasound is the first-line investigation for tendon, ligament and nerve-related disorders. It is also useful in detecting effusions and synovitis within joints. Ultrasound can reliably demonstrate small avulsion fractures at the site of ligamentous attachment which are difficult to see on conventional radiography and MRI. Dynamic stress across a ligament or tendon in the con-

text of injury can determine and emphasise the degree of separation of the injured fibres. With high-resolution ultrasound probes, normal or diseased nerves can be directly seen. When metal work is present ultrasound will demonstrate structures that would be obscured by artefact on other imaging. The presence of intermittent impingement of a tendon, ligament or nerve can be assessed dynamically and precisely. Ultrasound examination is often the only imaging that will demonstrate this important phenomenon.

16.2.2 Pelvis

16.2.2.1 Groin Pain

To examine the groin, you will need a probe that has a range of frequencies demonstrating superficial to deep structures.

Ultrasound is a very useful technique in the diagnosis of groin pain as it can cover many areas that can cause pain [27, 28]. Dynamic assessment for hernias is important (Fig. 16.7). In a study of groin pain, 89% of symptomatic athletes had inguinal hernias compared to 12% asymptomatic controls. Most of the athletes returned to normal sporting activity after surgery [29].

With diagnostic ultrasound, you can assess the exact site of the pain as demonstrated by the patient and examine the nearby joint, tendon insertions and muscles.

16.2.3 Hip

Ultrasound examination of the hip needs a probe covering the 12–8 MHz range due to the joint's depth. Imaging should start obliquely along the line of the femoral neck.

Diagnostic ultrasound can detect an effusion, synovitis within the hip joint and sometimes labral tears especially if they are associated with paralabral cysts. The technique has greater sensitivity for cysts than MRI but less sensitivity for labral tears than MRI arthrography. The presence of synovi-

Fig. 16.7 Direct inguinal hernia. Soccer player with groin pain but no clinical evidence of a hernia. The hernia is best appreciated on the dynamic assessment. You can see a loop of bowel moving forward on Valsalva. Static view is provided in this article
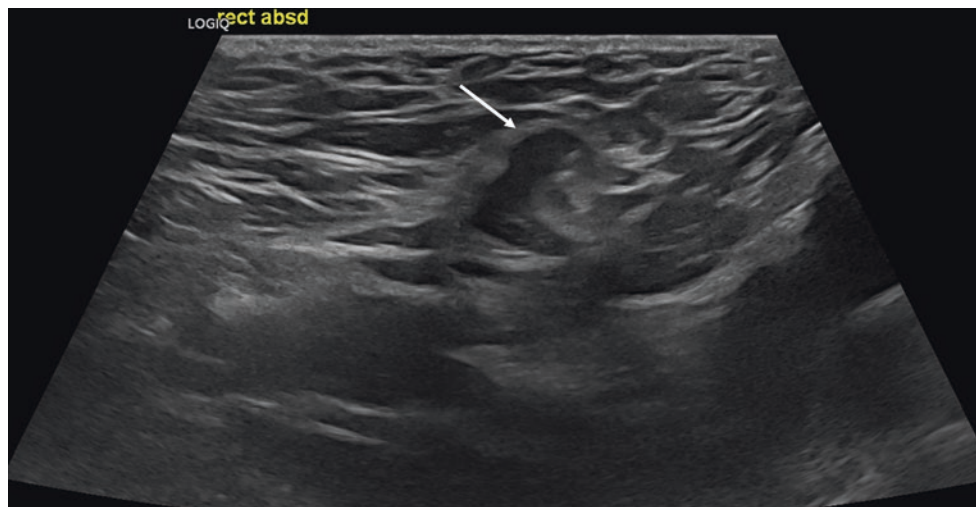
tis with its higher echogenicity, neovascularity and frondlike appearance against the anechoic fluid of an effusion is seen with standard ultrasound. MRI would require intravenous contrast agent enhancement and a longer examination to achieve similar results. A substantial benefit of diagnostic ultrasound is that it clearly differentiates cystic versus solid mass lesions. This is often difficult using MRI.

In younger athletes the most injured areas are the joint and the labrum. These are best seen with MR arthrography, but ultrasound can be used to guide the arthrography injection and guide pain-relieving injections such as steroid and sodium hyaluronic acid in the treatment of conditions that do not need surgery.

> **Key Points**
> - Groin pain can be due to hernias which can be reliably identified by dynamic ultrasound examination.
> - To detect a hip effusion, the probe is best placed obliquely along the line of the femoral neck.

16.2.4 Insertional Tendinosis (Traction Enthesopathy)

Diagnostic ultrasound is useful in the athlete in detecting tendinopathies around the hip.

Age determines the weakest area of the tendon. Before apophyseal closure, the apophyseal attachment is the weakest, and avulsion injuries usually pull off a fragment of bone. These fragments may be very difficult to identify using MRI but are obvious when using ultrasound as they cast an acoustic shadow and a sharp margin [30]. In adults with repetitive stress, the tendon insertion may be injured. The appearances on ultrasound of an abnormal tendon are identical to that described in the upper limb, with reduction in echogenicity, often neovascularisation and irregularity of the bone cortex due to enthesopathy.

In the adolescent, the pelvis is a common area for apophyseal injuries. Without the need for radiation, comparing both sides, the area of tendon insertion can be imaged by diagnostic ultrasound. The injuries occur before the age of 20. The most common apophyseal injuries occur at the insertion of the hamstrings, rectus femoris, sartorius and iliopsoas at the ischial tuberosity (54%), anterior inferior iliac spine (22%), anterior superior iliac spine (19%) and the lesser tuberosity of the femur, respectively. Less common sites are the adductor tubercle and the iliac crest [31].

In adult athletes the hamstring insertion is a common site of injury. This can be seen in runners, soccer players and cross-country skiers. Rectus femoris injuries are also seen (Fig. 16.8). Soccer players also acquire adductor insertional injuries and injuries at the insertion of the rectus abdominis muscle.
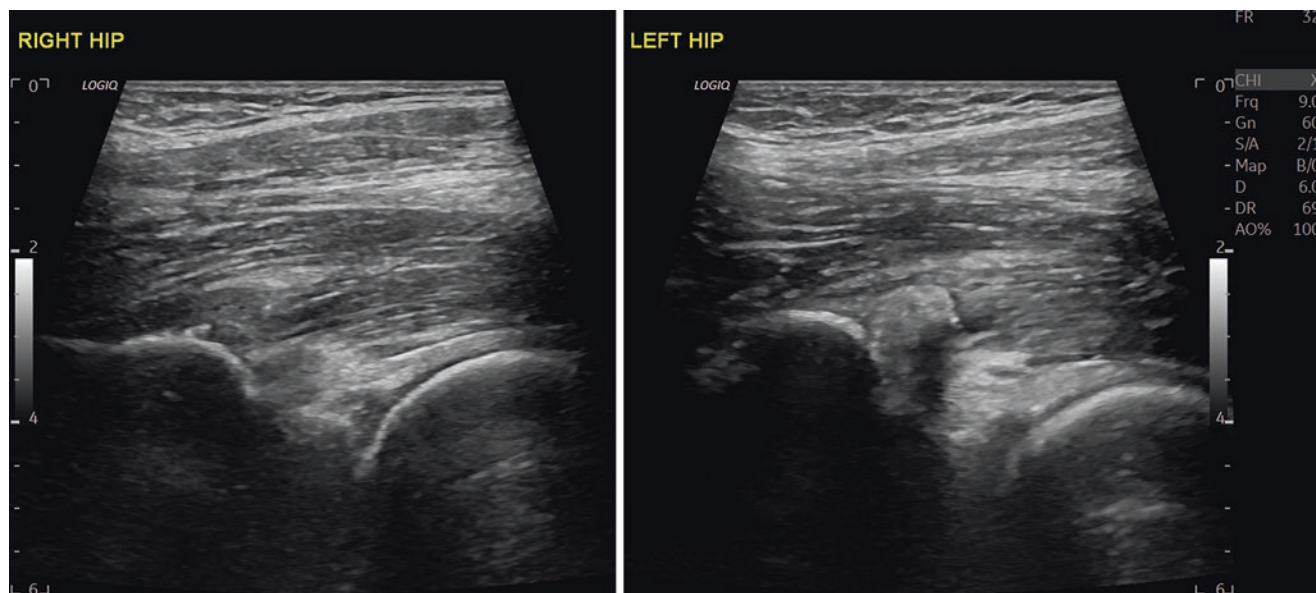
Fig. 16.8 Rectus femoris insertional injury. Horse rider. Left anterior groin pain after gym session 3 weeks before. Clinically thought to be a labral tear. Note the calcification in the insertion of the direct tendon as it joins the anterior inferior Iliac spine compared to the asymptomatic normal right side. Side-by-side comparison is very useful in these cases

Key Points

- Apophyseal injuries in the adolescent can be detected more accurately by ultrasound than by radiographs or MRI by looking for detached fragments of bone that cause acoustic shadowing.
- Insertional tendinosis or enthesopathy shows reduction of the tendon echogenicity, neovascularity and irregularity of the bone cortex at the insertion.

16.2.5 Knee

Most knee injuries are best assessed by MRI to determine both bony and ligamentous injury; however, diagnostic ultrasound is a very useful technique, if there is an area of pinpoint pain or swelling. It can detect effusions and synovitis within the joint and is useful in the assessment and treatment of patellar and quadriceps tendinosis. Collateral ligament injuries and other tendinosis can also be accurately detected and assessed dynamically by ultrasound examination.

The proximal patella tendon is most affected by traction tendinosis. At the insertion into the patella, it becomes thickened and lower in echogenicity and contains neovascularisation (Fig. 16.9). In young athletes, there is also the possibility of an apophyseal injury of both the inferior pole of the patella in Sinding-Larsen syndrome and the tibial tuberosity in Osgood-Schlatter's disease. In its early appearance, these disorders may only show fluid surrounding the tendon with-
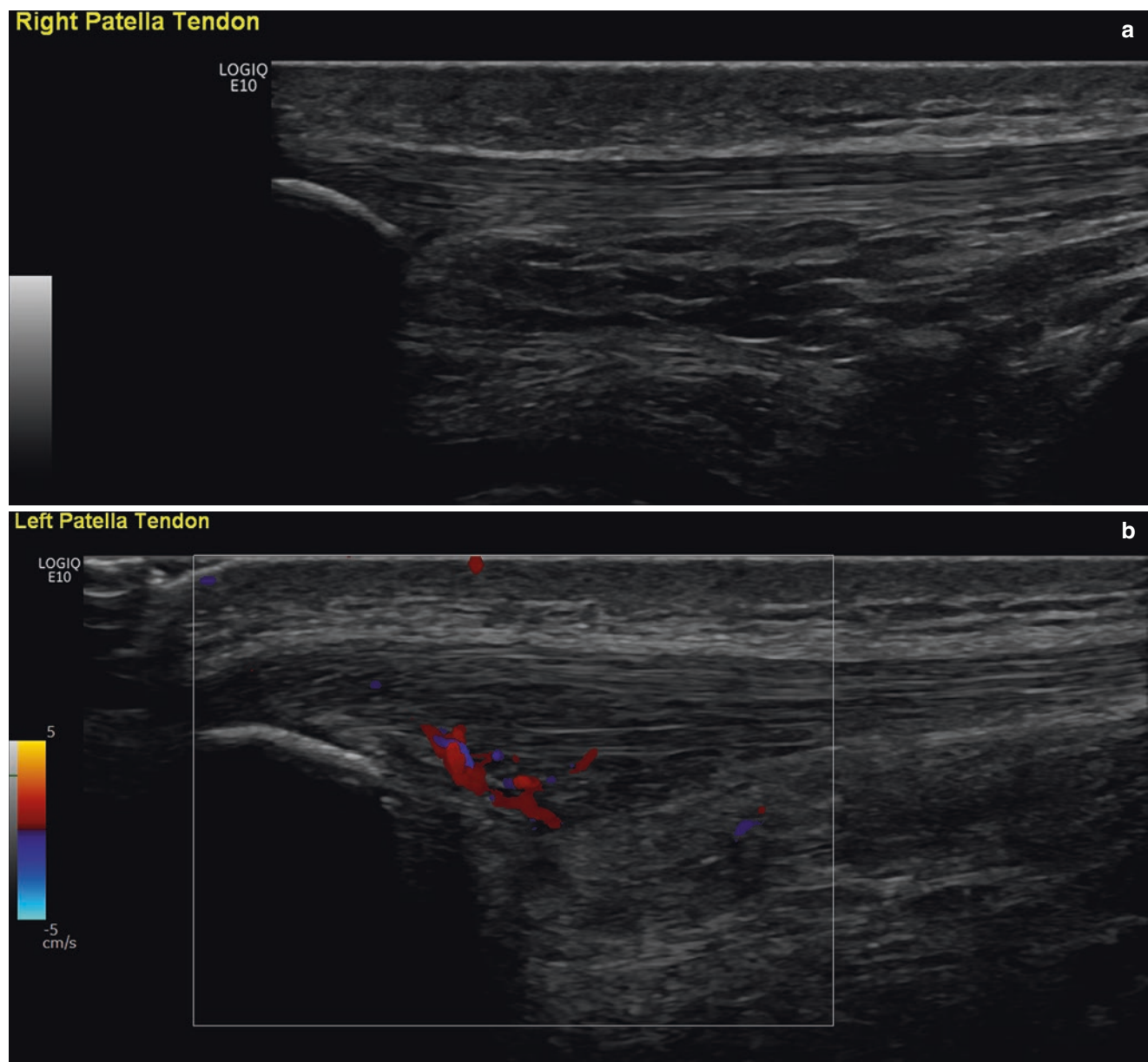
Fig. 16.9 A 22-year-old ballet dancer. (**a**) Normal right patellar tendon. (**b**) Insertional patellar tendinosis. Note the thickened proximal tendon with reduced echogenicity and neovascularisation

out the bony fragmentation as seen in more established cases. These disorders are a traction apophysitis for which offloading is the primary treatment.

Rupture of the patella tendon or quadriceps tendon may occur in the older age group of athletes and can be seen by ultrasound. Here there is a discontinuity of the tendons, and dynamic assessment allows the differentiation of partial- and full-thickness tears. In this last role, diagnostic ultrasound is a much more accurate technique than MRI whether severity and extent of the injuries are difficult to judge.

> **Key Points**
> - Knee effusions are best seen in the suprapatellar region using ultrasound.
> - Collateral ligament injuries are easily and accurately assessed by ultrasound, but the other internal knee injuries can only be fully appreciated by MRI.
> - Proximal patellar tendinosis is identified by thickening of the tendon with reduced echogenicity and neovascularisation.

16.2.6 Ankle

Perhaps the most important area in sports imaging is the ankle. It is important to use a large amount of coupling gel and light touch around this area as pressure over the bones of the ankle can be very painful and you can compress fluid around joints and tendons.

The Achilles tendon is commonly affected in athletes, especially runners. It is best seen by lying the patient prone with the foot dangling off the end of the couch so that movement of the foot can be performed. An 18 MHz probe is the most useful with a larger footplate. Midsubstance tendinosis and insertional tendinosis can be assessed in detail using diagnostic ultrasound. In midsubstance tendinosis, there is a fusiform swelling of the tendon with reduction in echogenicity and neovascularisation. In insertional tendinosis, there is thickening of the tendon, reduction in echogenicity, neovascularisation and often an enthesopathy involving the calcaneal insertion (Fig. 16.10). The presence of a plantaris tendon can also easily be identified. This can be involved in Achilles tendinosis as well or have an isolated tendinosis of its own. The plantaris tendon is important as it may be the
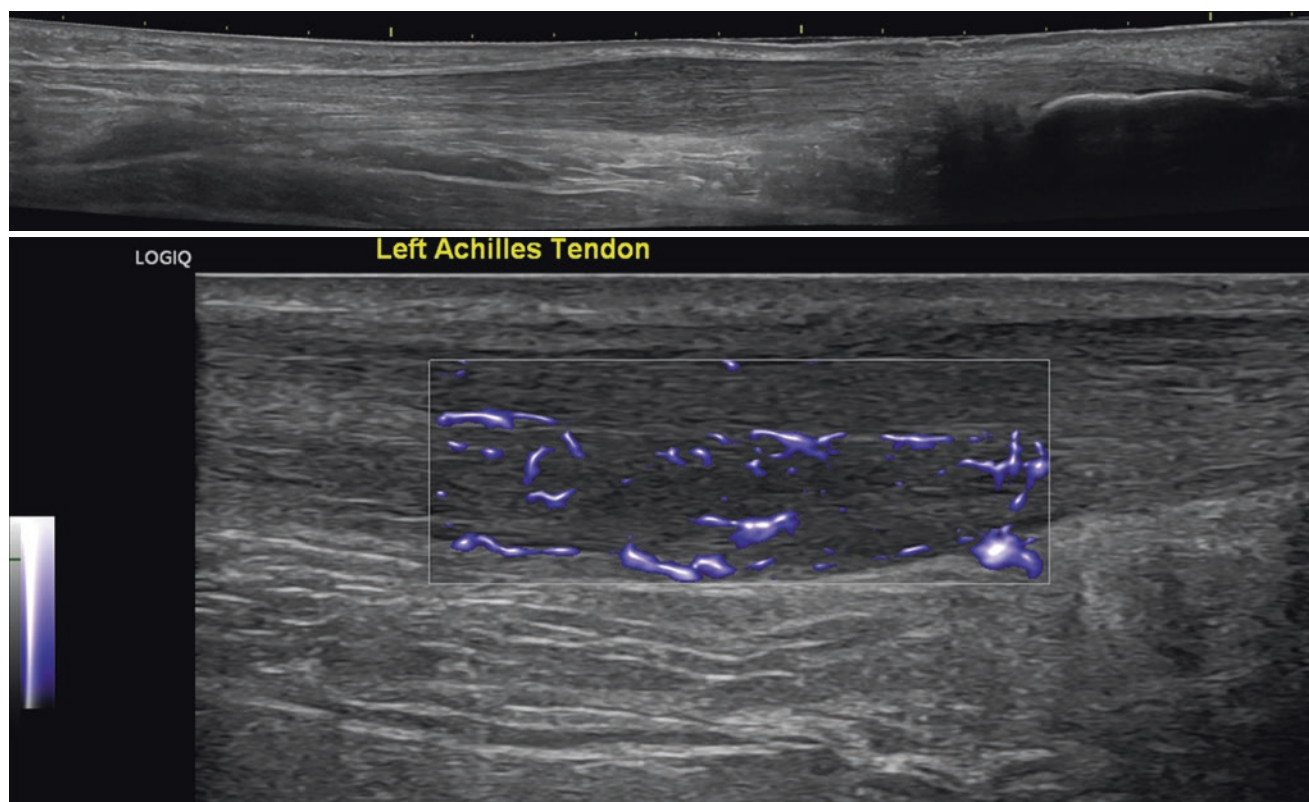
Fig. 16.10 Marathon Runner with Achilles tendinosis. Fusiform swelling of the Achilles tendon with reduction in echogenicity on this extended field of view US image and neovascularity

reason the patient with Achilles tendinosis is not responding to physiotherapy. Sometimes surgical excision can aid recovery in these cases.

Achilles rupture can occur in athletes. A complete rupture can be identified on diagnostic ultrasound by discordant movement at the site of injury when the tendon ends move in different directions producing a gap in the tendon that increases with dorsiflexion. Ultrasound can precisely locate the area of rupture which allows for measurements to be made and allows the possibility of small incisions to repair the tendon surgically. In the acute injury, it is fortunate that the only movement required is a very minor movement of the foot; if the examination is performed gently and carefully, it should not cause pain even on the day of the injury. The presence of an intact plantaris tendon spanning the Achilles tendon can falsely reassure the clinician that the Achilles tendon is intact as compression of the calf muscles will still cause movement of the foot even though the Achilles tendon itself is fully separated.

Ligamentous rupture is the most common abnormality in athletes. Ankle sprains commonly cause injury to the anterior talofibular ligament in 86%. This can either be a sprain to the ligament or a full rupture. The other lateral ligaments can also be assessed by ultrasound including the anterior tibiofibular ligament which can be injured in association with the anterior talofibular ligament or on its own. In isolation this injury often occurs when an athlete wears high boots such as ski boots or large walking boots. Injury to the calcaneofibular ligament occurs in approximately 30% of ankle sprains and is a much more significant injury with relatively poor outcome (Fig. 16.11). The posterior tibiofibular and talofibular ligament can also be injured and assessed by ultrasound. Deltoid ligament injury is also common (in 50% of lateral ligament injuries) [32]. Dynamic assessment of all the ankle ligaments is possible with ultrasound including the posterior ligaments best seen using a small footprint. High-frequency probe with dynamic assessment is especially useful in assessing a syndesmotic injury to the distal tibiofibular joint. On moving the foot in dorsiflexion and plantar flexion, the tibia and fibula should remain at an equal distance apart and in the same location. If there is any dynamic separation of the bones, then this is the diagnosis. This is often missed on any other imaging because you cannot dynamically stress this area on MRI or CT unless you have the facility to perform standing MRI or CT for comparison with supine examination!

Damage to the peroneal retinacula can also occur. The retinacula can become thickened in a chronic injury (Fig. 16.12). If the superior retinaculum is ruptured, this may lead to sublux-
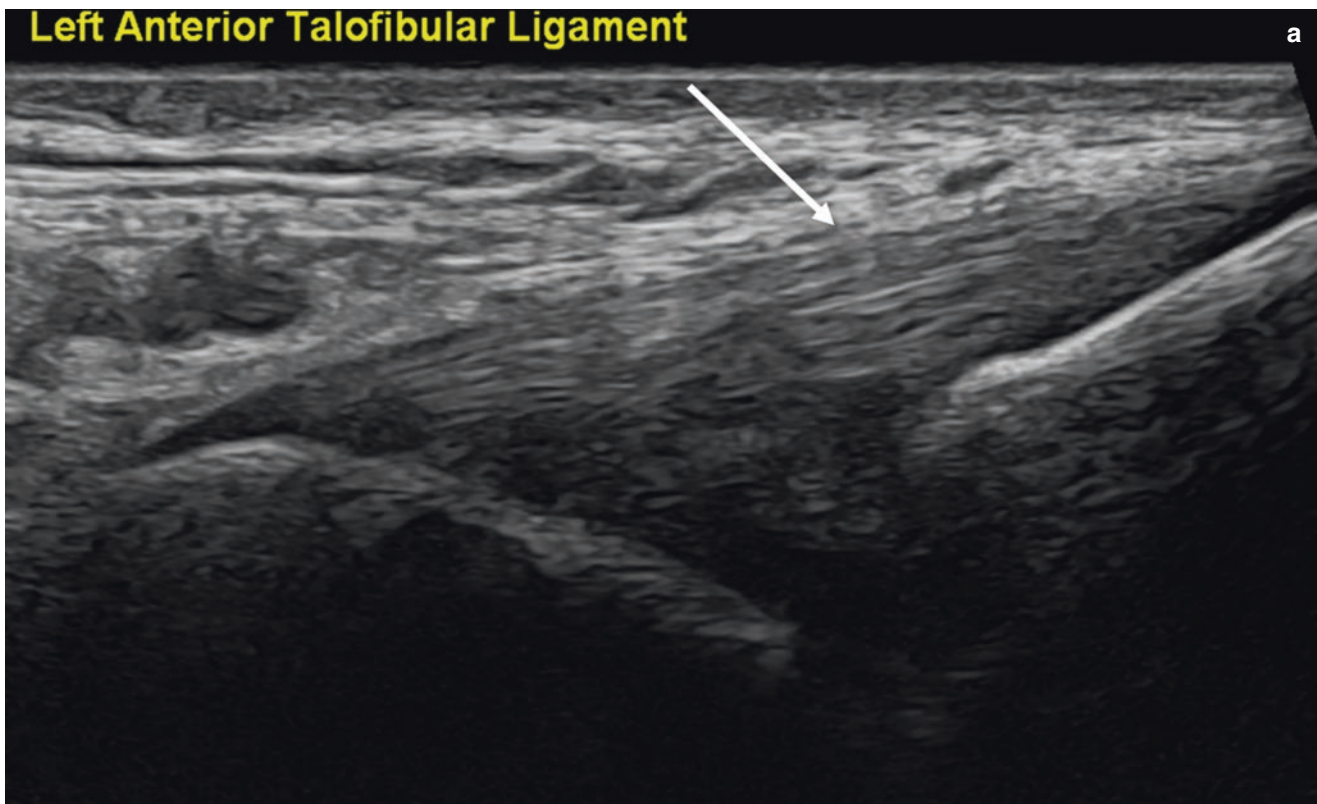
Fig. 16.11 Ruptured anterior talofibular ligament. A 19-year-old soccer player. (**a**) Normal left anterior talofibular ligament. (**b**) Torn right anterior talofibular ligament. (**c**) Injured right calcaneofibular ligament. (**d**) Right ankle effusion
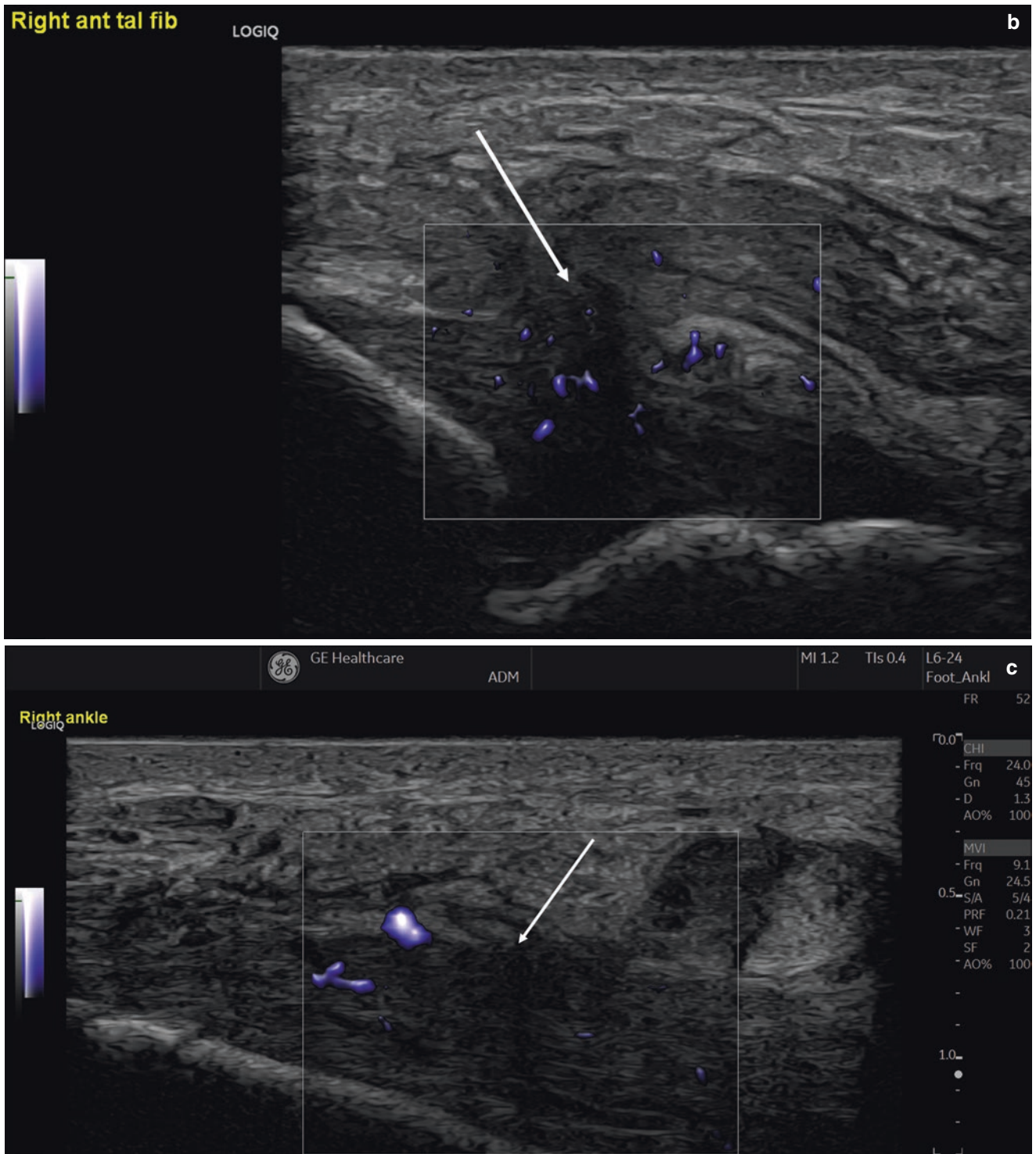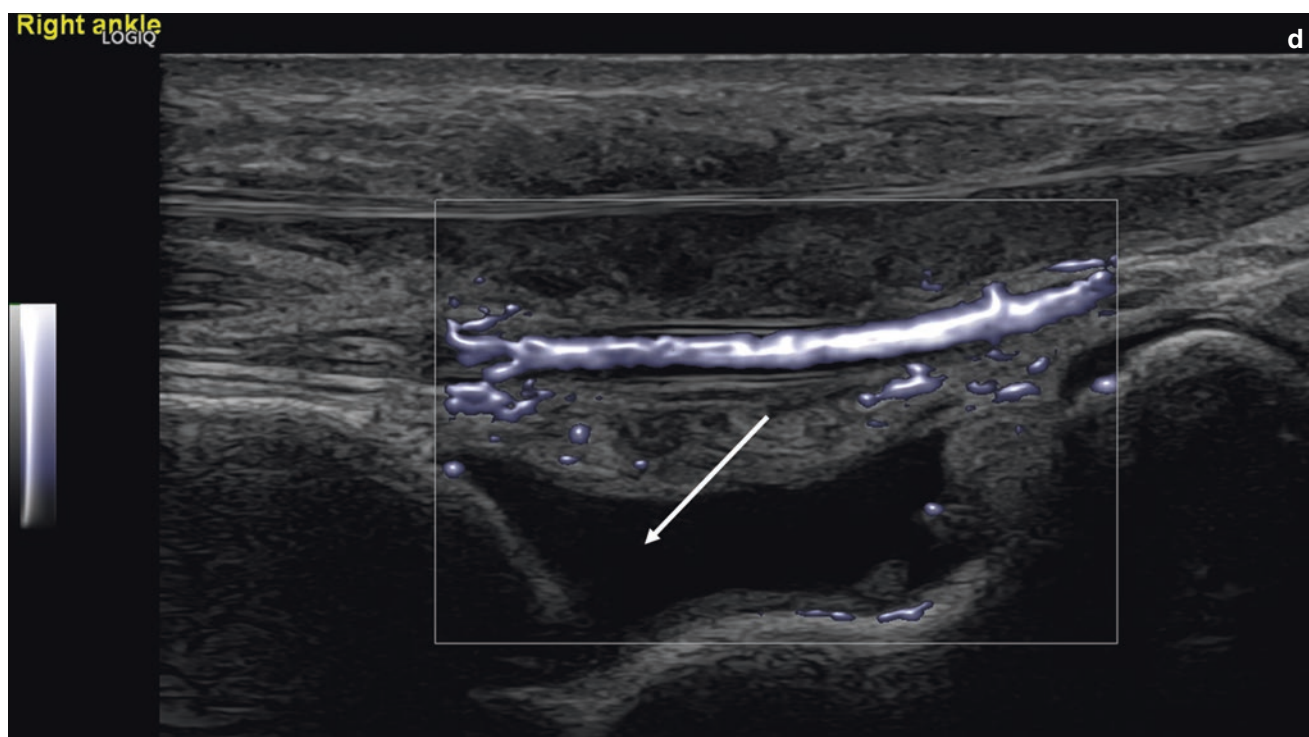
Fig. 16.11 (continued)

Fig. 16.11 (continued)

ation of the peroneal tendons. Injury in this region can also lead to pseudo-subluxation of the peroneal tendons when there is an abnormal movement of the peroneus brevis tendon against the peroneal longus. Both of these abnormalities can be a cause of clicking of the tendons in this region [33]. Dynamic assessment of tendon movement and retinaculum function is only available with diagnostic ultrasound. Intermittent or transient symptoms are often not identified using MRI or CT.

Ballet dancers suffer problems with the flexor hallucis longus tendon due to dancing on pointe over many years. This tendon is naturally larger than the other tendons in these dancers. Active tendinopathy with neovascularisation is easily demonstrated using diagnostic ultrasound.

> **Key Points**
> - Complete Achilles rupture is best assessed by ultrasound due to dynamic movement of the tendon showing the tendon ends moving in different directions. This technique has greater precision than MRI.
> - Clicking of the peroneal tendons can either be due to pseudo subluxation or true subluxation which can be dynamically demonstrated using ultrasound.
> - Ligamentous injury in the ankle is best seen by ultrasound due to the different obliquities of the ligaments; integrity of the ligament may be judged stressing the ligament while scanning.

16.2.7 Foot

The scanning technique is similar to that of the ankle using a large amount of coupling gel, and light touch around this area as pressure over the bones of the ankle can be very painful and you can compress fluid around joints and tendons.

The tibialis anterior tendon is affected in fell walkers. This is usually due to an insertional tendinosis.

The tibialis posterior tendon can rupture or develop tendinopathy. As this tendon forms part of the arch of the foot, these abnormalities can both cause a new flat foot deformity. The spring ligament can also be injured causing an acute flat-foot. These conditions are readily diagnosed using diagnostic ultrasound with high-resolution probes and good-quality Doppler imaging.

Ligamentous injury of the small ligaments of the foot can be identified using diagnostic ultrasound, especially if they are superficial. Injury to the talonavicular ligament can occur in isolation or in association with lateral ligamentous injury [34]. This destabilises the midfoot allowing movement across the talonavicular joint which is vital in the normal windlass mechanism of walking; this is the dynamic tightening of the arch of the foot by long and short stabilisers prior to pushing off from the ball of the foot. Deficiency in the strength of the arch prevents this movement and is associated with premature osteoarthritis of the midfoot.

Nerve damage can occur in athletes due to poor fitting shoes or the constant agitation of the deep peroneal nerve on
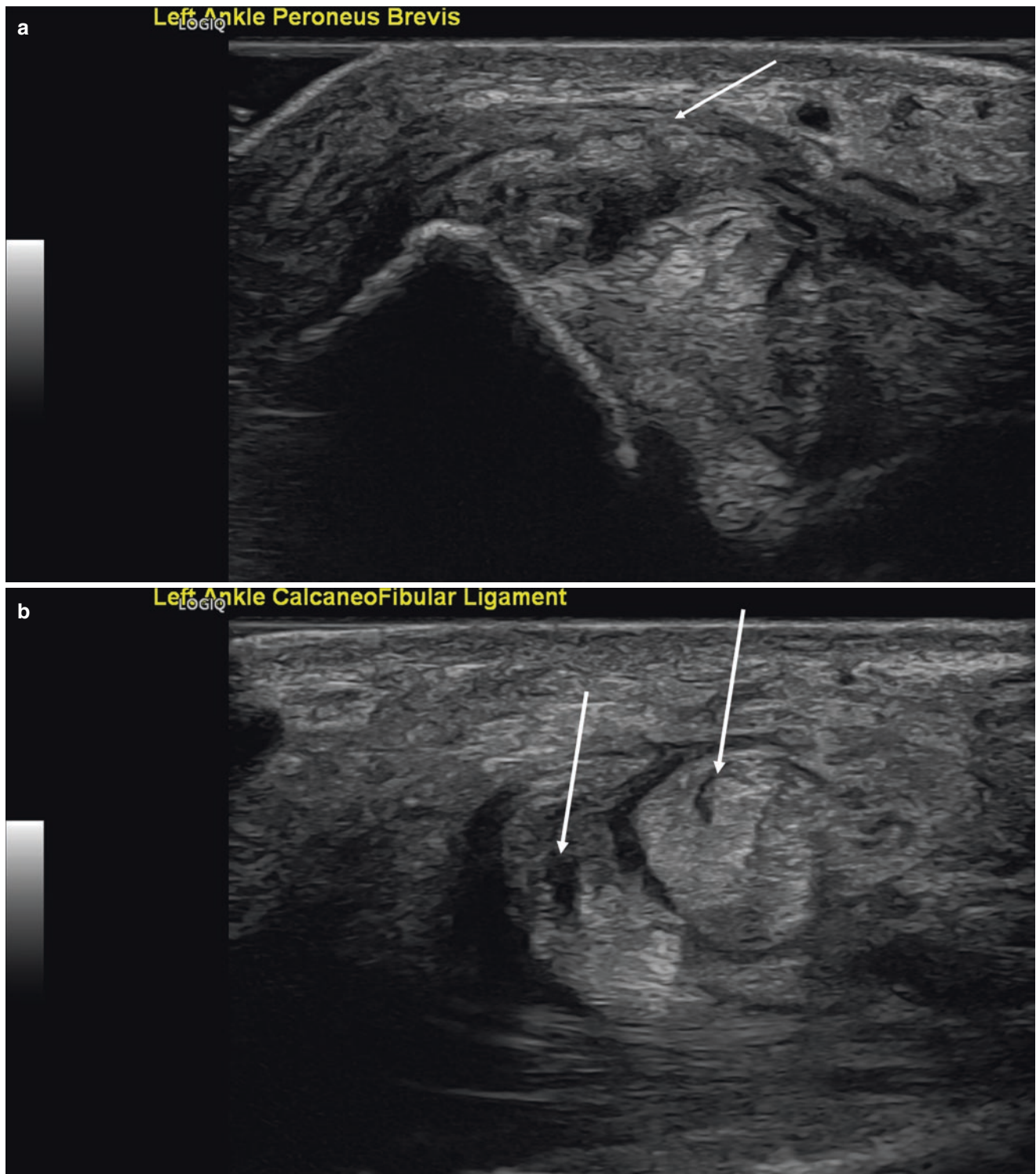
Fig. 16.12 An elite 55-year-old jockey. Peroneus longus and brevis tendinosis and superior peroneal retinacular injury. (a) Note the thickening of the superior peroneal retinaculum. (b) The peroneal tendons show central mucoid degeneration

the dorsum of the foot of the ball in soccer players kicking a ball. This can easily be seen by ultrasound examination ideally with a high-resolution small footplate probe such as 18–24 MHz. Microvascular imaging allows study of the normal blood supply to small nerves, and comparison of both sides will determine whether flow is abnormally increased.

Key Points
- The cause of a sudden flat foot deformity can be tibialis posterior tendon rupture, tendinosis or spring ligament rupture. These can all be determined by ultrasound.
- Nerves can be clearly seen on ultrasound examination with high-resolution (18–24 MHz) probes.

16.2.8 Muscle Injury

Diagnostic ultrasound may be used to assess muscle tears 6 h after injury. Before this, acute haemorrhage is echogenic and blends with the fibro-fatty interfaces of the muscle and is therefore invisible. This makes the use of pitch side ultrasound inaccurate as significant muscle damage can be overlooked. Within a few hours, liquefying haematoma forms. This is low in echogenicity and is easy to see within the muscle. It forms in the gap of the muscle injury. Ultrasound can be used to dynamically assess the size of the tear by contracting the muscle passively or actively; the movement involved is minimal and should not be enough to cause any pain. MRI can be useful in the initial phase of an injury but will overestimate the extent of injury after 24 h due to distant spread of muscle oedema in association with the injury. MRI is rarely accurate in distinguishing between partial- and full-thickness rupture. In chronic injury muscle atrophy is seen as a change in size with fatty infiltration (increased echogenicity) and best determined by comparing sides. MRI provides similar information but sometimes only one limb is examined preventing comparison. In those with chronic injury the ultrasound practitioner should always compare sides looking for chronic muscle change.

The technique of muscle ultrasound examination requires a lower frequency probe such as 8–12 MHz dependent on the depth and size of the muscle. It is best to use a fast sweeping motion over the muscle to detect the initial area of injury and then closing in on abnormal areas with slower movement to demonstrate more detail. Too much pressure can compress a liquefying haematoma making it more difficult to identify. Comparison with the opposite limb is essential to detect small areas of injury.

Diagnostic ultrasound can precisely identify scarring and myositis ossificans if the injuries are more established. Both these conditions are difficult to appreciate on MRI and are commonly overlooked. Scarring is of high echogenicity when established. Myositis ossificans is of high echogenicity and has acoustic shadowing behind it once it is established. The early calcification can be much easier to see using diagnostic ultrasound when compared to conventional radiography. Re-tearing can also be seen as low echogenicity and blurring of the normal muscle fibre pattern with vascularity in the region of a new tear [26].

Injuries may occur in any lower limb muscle group. The commonly seen injuries are of the hamstrings, quadriceps, adductors and calf muscles. Thigh muscle injury has been extensively researched in footballers. The presence of a musculotendinous injury or a large injury makes the time of returning to sport longer and the chance of a re-injury higher [35, 36].

Calf injuries commonly occur between the medial gastrocnemius and soleus muscles and are known as tennis leg. This can be mistaken for deep venous thrombosis or a ruptured popliteal cyst, but to the experienced ultrasound examiner, it is easy to distinguish between these disorders (Fig. 16.13).

Key Points
- Muscle injury may be invisible to ultrasound examination in the first 6 h after an injury as acute haemorrhage is echogenic and may mimic muscle.
- After 6 h, ultrasound accurately detects the injury as haematoma starts to liquefy. At this stage MRI may exaggerate the nature of the injury because of adjacent muscle oedema.

16.3 Guided Injections

Ultrasound is becoming essential to the safe guidance of all interventions in both the upper and lower limb. This is beyond the remit of this article but is an extension of its use once you become proficient [37, 38].
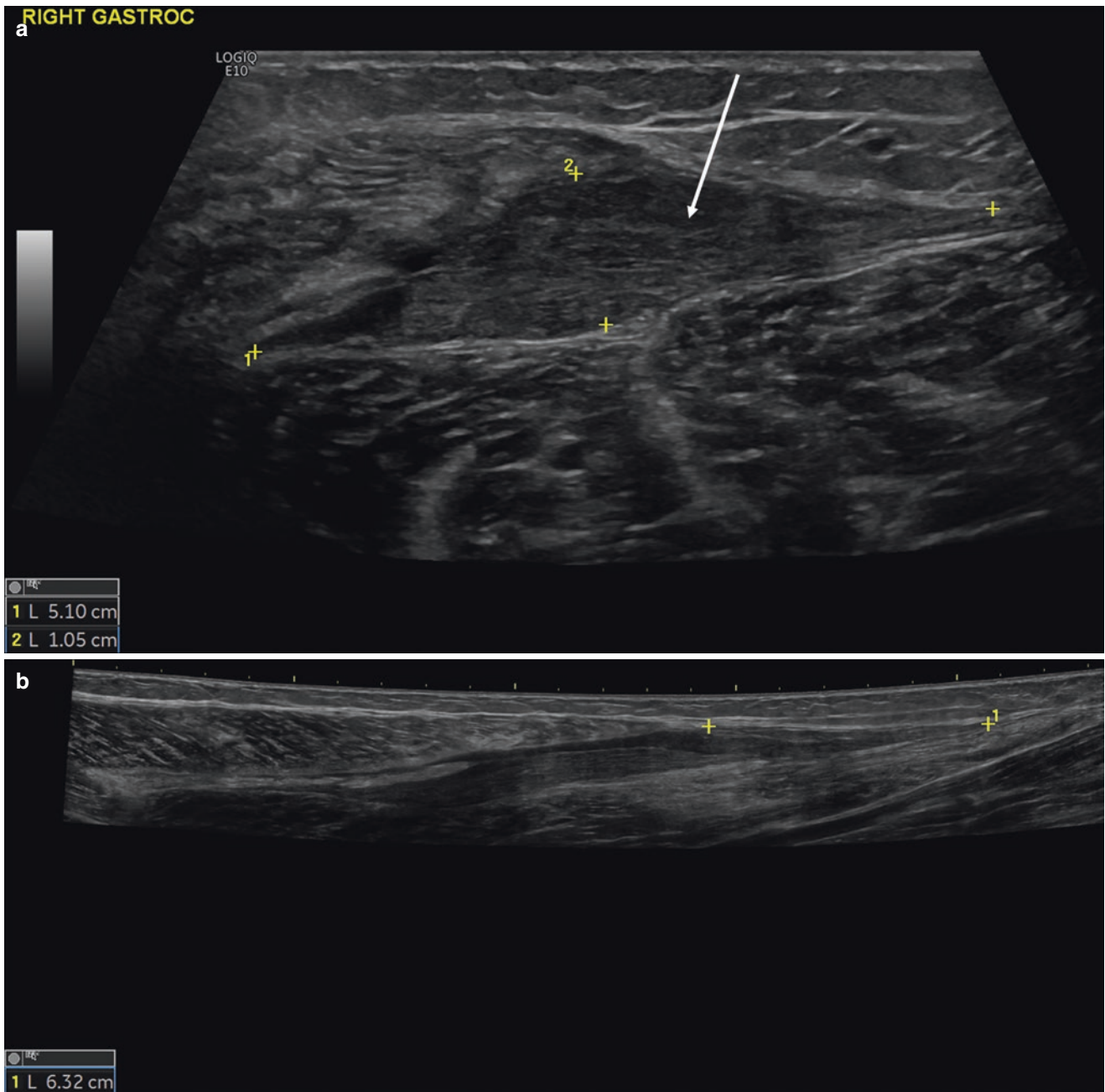
Fig. 16.13 A 50-year-old female skier. Injury in March 2020 just before lockdown for Covid 19. Stretching injury to the calf as she fell with ski moving forward. Imaged 5 months after injury as still symptomatic. (**a**) Poorly liquefied haematoma at site of injury between the gastrocnemius and soleus muscles. (**b**) Extended field of view ultrasound to show the amount of retraction of the medial gastrocnemius muscle with respect to the Achilles tendon

16.4 Concluding Remarks

Ultrasound can play a significant role in the evaluation of sports injuries. The most common application is evaluation of tendon pathology, such as tendinosis and tendon tear. While any tendon about the extremities can be evaluated, the high-resolution capabilities of ultrasound are especially ideal in evaluation of the distal extremities. The dynamic capabilities of ultrasound are also important showing tendon retraction in the setting of a full-thickness tendon tear, tendon subluxation and muscle hernias. Muscle injuries may also be evaluated for tear and haematoma although sensitivity is lower acutely after an injury. Ligaments may be assessed with ultrasound where dynamic imaging can also be used to demonstrate joint space gapping as an indicator of ligament tear. Dynamic assessment is also important in the evaluation of groin hernias. Ultrasound may be used to guide various procedures, such as injections and aspirations, as they relate to sports injuries.

> **Take Home Messages**
> - Ultrasound is effective in the evaluation of tendon and ligament injuries.
> - Ultrasound may be limited in the early evaluation of muscle injury.
> - Dynamic imaging is important in evaluation of muscle and ligament tears, tendon subluxation as well as various hernias.
> - Ultrasound may be used to guide percutaneous procedures.

References

1. Schaeffeler C, Mueller D, Kirchhoff C, Wolf P, Rummeny EJ, Woertler K. Tears at the rotator cuff footprint: prevalence and imaging characteristics in 305 MR arthrograms of the shoulder. Eur Radiol. 2011;21(7):1477–84. Epub 2011/01/27. https://doi.org/10.1007/s00330-011-2066-x.
2. Jacobson JA. Shoulder US: anatomy, technique, and scanning pitfalls. Radiology. 2011;260(1):6–16. Epub 2011/06/24. https://doi.org/10.1148/radiol.11101082.
3. Galloway MT, Lalley AL, Shearn JT. The role of mechanical loading in tendon development, maintenance, injury, and repair. J Bone Joint Surg Am. 2013;95(17):1620–8. Epub 2013/09/06. https://doi.org/10.2106/JBJS.L.01004.
4. Buck FM, Grehn H, Hilbe M, Pfirrmann CW, Manzanell S, Hodler J. Magnetic resonance histologic correlation in rotator cuff tendons. J Magn Reson Imaging. 2010;32(1):165–72. Epub 2010/06/26. https://doi.org/10.1002/jmri.22222.
5. Kjellin I, Ho CP, Cervilla V, Haghighi P, Kerr R, Vangness CT, et al. Alterations in the supraspinatus tendon at MR imaging: correlation with histopathologic findings in cadavers. Radiology. 1991;181(3):837–41.
6. Jacobson JA, Lancaster S, Prasad A, van Holsbeeck MT, Craig JG, Kolowich P. Full-thickness and partial-thickness supraspinatus tendon tears: value of US signs in diagnosis. Radiology. 2004;230(1):234–42.
7. Wohlwend JR, van Holsbeeck M, Craig J, Shirazi K, Habra G, Jacobsen G, et al. The association between irregular greater tuberosities and rotator cuff tears: a sonographic study. AJR Am J Roentgenol. 1998;171(1):229–33.
8. Araki D, Miller RM, Fujimaki Y, Hoshino Y, Musahl V, Debski RE. Effect of tear location on propagation of isolated supraspinatus tendon tears during increasing levels of cyclic loading. J Bone Joint Surg Am. 2015;97(4):273–8. Epub 2015/02/20. https://doi.org/10.2106/JBJS.N.00062.
9. Park JS, Park HJ, Kim SH, Oh JH. Prognostic factors affecting rotator cuff healing after arthroscopic repair in small to medium-sized tears. Am J Sports Med. 2015;43(10):2386–92. Epub 2015/08/20. https://doi.org/10.1177/0363546515594449.
10. Skendzel JG, Jacobson JA, Carpenter JE, Miller BS. Long head of biceps brachii tendon evaluation: accuracy of preoperative ultrasound. AJR Am J Roentgenol. 2011;197(4):942–8. Epub 2011/09/24. https://doi.org/10.2214/AJR.10.5012.
11. Moser TP, Cardinal E, Bureau NJ, Guillin R, Lanneville P, Grabs D. The aponeurotic expansion of the supraspinatus tendon: anatomy and prevalence in a series of 150 shoulder MRIs. Skelet Radiol. 2015;44(2):223–31. Epub 2014/09/03. https://doi.org/10.1007/s00256-014-1993-4.
12. Hashiuchi T, Sakurai G, Morimoto M, Komei T, Takakura Y, Tanaka Y. Accuracy of the biceps tendon sheath injection: ultrasound-guided or unguided injection? A randomized controlled trial. J Shoulder Elb Surg. 2011;20(7):1069–73. Epub 2011/07/26. https://doi.org/10.1016/j.jse.2011.04.004.
13. van Holsbeeck M, Strouse PJ. Sonography of the shoulder: evaluation of the subacromial-subdeltoid bursa. AJR Am J Roentgenol. 1993;160(3):561–4. Epub 1993/03/01. https://doi.org/10.2214/ajr.160.3.8430553.
14. Daghir AA, Sookur PA, Shah S, Watson M. Dynamic ultrasound of the subacromial-subdeltoid bursa in patients with shoulder impingement: a comparison with normal volunteers. Skelet Radiol. 2012;41(9):1047–53. Epub 2011/10/15. https://doi.org/10.1007/s00256-011-1295-z.
15. Lobo Lda G, Fessell DP, Miller BS, Kelly A, Lee JY, Brandon C, et al. The role of sonography in differentiating full versus partial distal biceps tendon tears: correlation with surgical findings. AJR Am J Roentgenol. 2013;200(1):158–62. Epub 2012/12/21. https://doi.org/10.2214/AJR.11.7302.
16. Smith J, Finnoff JT, O'Driscoll SW, Lai JK. Sonographic evaluation of the distal biceps tendon using a medial approach: the pronator window. J Ultrasound Med. 2010;29(5):861–5. Epub 2010/04/30
17. Kalume Brigido M, De Maeseneer M, Jacobson JA, Jamadar DA, Morag Y, Marcelis S. Improved visualization of the radial insertion of the biceps tendon at ultrasound with a lateral approach. Eur Radiol. 2009;19(7):1817–21. Epub 2009/02/14. https://doi.org/10.1007/s00330-009-1321-x.
18. Downey R, Jacobson JA, Fessell DP, Tran N, Morag Y, Kim SM. Sonography of partial-thickness tears of the distal triceps brachii tendon. J Ultrasound Med. 2011;30(10):1351–6. Epub 2011/10/05
19. Potter HG, Hannafin JA, Morwessel RM, DiCarlo EF, O'Brien SJ, Altchek DW. Lateral epicondylitis: correlation of MR imaging, surgical, and histopathologic findings. Radiology. 1995;196(1):43–6.
20. Roedl JB, Gonzalez FM, Zoga AC, Morrison WB, Nevalainen MT, Ciccotti MG, et al. Potential utility of a combined approach with US and MR arthrography to image medial elbow pain in baseball players. Radiology. 2016;279(3):827–37. Epub 2016/05/18. https://doi.org/10.1148/radiol.2015151256.

21. De Maeseneer M, Marcelis S, Jager T, Girard C, Gest T, Jamadar D. Spectrum of normal and pathologic findings in the region of the first extensor compartment of the wrist: sonographic findings and correlations with dissections. J Ultrasound Med. 2009;28(6):779–86. Epub 2009/05/28

22. Lopez-Ben R, Lee DH, Nicolodi DJ. Boxer knuckle (injury of the extensor hood with extensor tendon subluxation): diagnosis with dynamic US—report of three cases. Radiology. 2003;228(3):642–6.

23. Klauser A, Frauscher F, Bodner G, Halpern EJ, Schocke MF, Springer P, et al. Finger pulley injuries in extreme rock climbers: depiction with dynamic US. Radiology. 2002;222(3):755–61.

24. Melville D, Jacobson JA, Haase S, Brandon C, Brigido MK, Fessell D. Ultrasound of displaced ulnar collateral ligament tears of the thumb: the Stener lesion revisited. Skelet Radiol. 2013;42(5):667–73. Epub 2012/09/25. https://doi.org/10.1007/s00256-012-1519-x.

25. Ebrahim FS, De Maeseneer M, Jager T, Marcelis S, Jamadar DA, Jacobson JA. US diagnosis of UCL tears of the thumb and Stener lesions: technique, pattern-based approach, and differential diagnosis. Radiographics. 2006;26(4):1007–20.

26. Allen GM. The use of ultrasound in athletes. Eur J Radiol. 2018;109:136–41. https://doi.org/10.1016/j.ejrad.2018.10.028.

27. Brandon CJ, Jacobson JA, Fessell D, Dong Q, Morag Y, Girish G, et al. Groin pain beyond the hip: how anatomy predisposes to injury as visualized by musculoskeletal ultrasound and MRI. AJR Am J Roentgenol. 2011;197(5):1190. https://doi.org/10.2214/AJR.10.4890.

28. Jacobson J, Khoury V, Brandon CJ. Ultrasound of the groin: techniques, pathology, and pitfalls. Am J Roentgenol. 2015;205(3):513–23. https://doi.org/10.2214/AJR.15.14523.

29. Vasileff WK, Nekhline M, Kolowich PA, Talpos GB, Eyler WR, van Holsbeeck M. Inguinal hernia in athletes: role of dynamic ultrasound. Sports Health. 2017;9(5):414–21. Epub 2017/07/22. https://doi.org/10.1177/1941738117717009.

30. Allen GM. Tendon and ligamentous trauma. In: Vanhoenacker FM, Maas, M., Gielen, J. L., editor. Imaging of orthopaedic sports injuries: Springer, New York; 2007. p. 61–72.

31. Rossi F, Dragoni S. Acute avulsion fractures of the pelvis in adolescent competitive athletes: prevalence, location and sports distribution of 203 cases collected. Skelet Radiol. 2001;30(3):127–31. Epub 2001/05/19. https://doi.org/10.1007/s002560000319.

32. Allen GM, Wilson DJ, Bullock SA, Watson M. Extremity CT and ultrasound in the assessment of ankle injuries: occult fractures and ligament injuries. Br J Radiol. 2020;93(1105):20180989. https://doi.org/10.1259/bjr.20180989.

33. Bianchi S, Becciolini M. Ultrasound features of ankle retinacula: normal appearance and pathologic findings. J Ultrasound Med. 2019;38(12):3321–34. https://doi.org/10.1002/jum.15026.

34. De Dea M, Loizou C, Allen G, Wilson D, Athanasou N, Uchihara Y, et al. Talonavicular ligament: prevalence of injury in ankle sprains, histological analysis and hypothesis of its biomechanical function. Br J Radiol. 2017;90(1071):20160816. https://doi.org/10.1259/bjr.20160816.

35. Ekstrand J, Askling C, Magnusson H, Mithoefer K. Return to play after thigh muscle injury in elite football players: implementation and validation of the Munich muscle injury classification. Br J Sports Med. 2013;47(12):769–74. https://doi.org/10.1136/bjsports-2012-092092.

36. Pollock N, Patel A, Chakraverty J, Suokas A, James SL, Chakraverty R. Time to return to full training is delayed and recurrence rate is higher in intratendinous ('c') acute hamstring injury in elite track and field athletes: clinical application of the British Athletics Muscle Injury Classification. Br J Sports Med. 2016;50(5):305–10. Epub 2016/02/19. https://doi.org/10.1136/bjsports-2015-094657.

37. Lee JC, Ahmed N, Allen GM. Image guided injection therapies in athletes—do they work and what should we be using? Eur J Radiol. 2019;110:193–202. https://doi.org/10.1016/j.ejrad.2018.12.001.

38. Allen GM, Wilson DJ. Ultrasound guided musculoskeletal injections. Amsterdam: Elsevier; 2018.

Muscle Imaging

17

William Palmer and M. K. Jesse

Learning Objectives
- Review the role of imaging in muscle diseases.
- Detect and classify acute muscle injury by imaging.
- Review unique imaging features in idiopathic inflammatory myopathy.
- Identify the imaging features of other common infectious, traumatic, and vascular muscle pathologies.
- Discuss the differential considerations in muscle lesions.

17.1 Introduction to Muscle Imaging

Evaluation and characterization of skeletal muscle pathology is a frequently encountered indication for musculoskeletal imaging. Causes of muscle pathology are diverse and include traumatic, autoimmune, infectious, inflammatory, neurologic, and neoplastic. Each etiology while dramatically different in the pathophysiology may present with similar imaging features. An understanding of the subtle differences in imaging features between the pathologic conditions may serve to guide diagnosis and treatment in these often complex cases. In this section, we will discuss the various skeletal muscle pathologies and the imaging features associated with each.

17.2 Imaging Modalities in Skeletal Muscle Evaluation

Radiograph, while excellent for bone pathology, has limited utility in the evaluation of muscle. Although the majority of muscle pathology is occult on routine radiographic images, X-ray may be useful in a few conditions. Certain inflammatory or autoimmune myopathy, for example, is characterized by unique soft tissue calcifications of which radiographs may be the most reliable modality for detection. Magnetic resonance imaging and ultrasound offer excellent special resolution, allowing for the detailed evaluation of muscle microanatomy. Ultrasound offers an added benefit of dynamic imaging but is less sensitive than MRI for muscle edema and low-grade injury. Because of the superior sensitivity in detecting subtle injury, MR imaging evaluation is largely considered the diagnostic gold standard.

17.3 Traumatic Muscle Injuries

Muscle injury is common among athletes and poses a serious limitation to continued performance. The location and extent of a muscle injury has implications on the recovery and functional outcome.

17.3.1 Muscle Strain/Tear

Key Point
- Acute muscle strains/tears most frequently involve the gastrocnemius, biceps femoris, and rectus femoris muscles of the lower extremity.

W. Palmer (✉)
Department of Radiology, Mass General Hospital, Boston, MA, USA
e-mail: wpalmer@partners.org

M. K. Jesse
Department of Radiology, University of Colorado Hospital, Aurora, CO, USA

Acute muscle strains/tears are commonly encountered muscle injury in the athlete, most frequently involving the gastrocnemius, biceps femoris, and rectus femoris muscles of the lower extremity [1, 2]. Muscle strains are characterized into three grades with progressing severity and complexity of the injury and increasing time to recovery (Table 17.1).

Table 17.1 Grades of muscle strain [3–6]

Injury	MR findings	Extent of injury	Example
Grade 1	• T2 high signal edema with feathered appearance, usually at the myotendinous junction. No architectural distortion • Thickened or edematous tendon without tear or laxity	<10% fiber disruption	Figure 17.1
Grade 2	• T2 high signal edema with focal/partial fiber disruption • ± intramuscular hematoma	10–50% fiber disruption	Figure 17.2
Grade 3	• Complete muscle fiber/tendon disruption with laxity with/without retraction • ± intramuscular hematoma	50–100% fiber disruption	Figure 17.3

## 17.3.2 Delayed Onset Muscle Soreness

Subacute or delayed muscle injury can be seen in the setting of overuse and is referred to in radiology literature as delayed onset muscle soreness (DOMS). DOMS is thought to occur as a result of muscle fiber microtrauma followed by a delayed inflammatory phase. This injury, while painful, results in no permanent muscle damage or functional deficit. Ultrasound interrogation often yields diffuse hyperechoic foci in an enlarged muscle belly but may be insensitive in mild injury [7]. Fluid-sensitive MR imaging is the gold standard diagnostic exam, demonstrating diffuse muscle edema involving all utilized muscles of a compartment [8] (Fig. 17.4).

17.3.3 Muscle Herniation

Muscle hernias, or myofascial defects, represent focal protrusion of the muscle fibers through a focal defect in the overlying superficial muscle fascia. Muscle hernias are most commonly seen in the lower extremity with the anterior compartment of the lower leg the most common location. Ultrasound is the
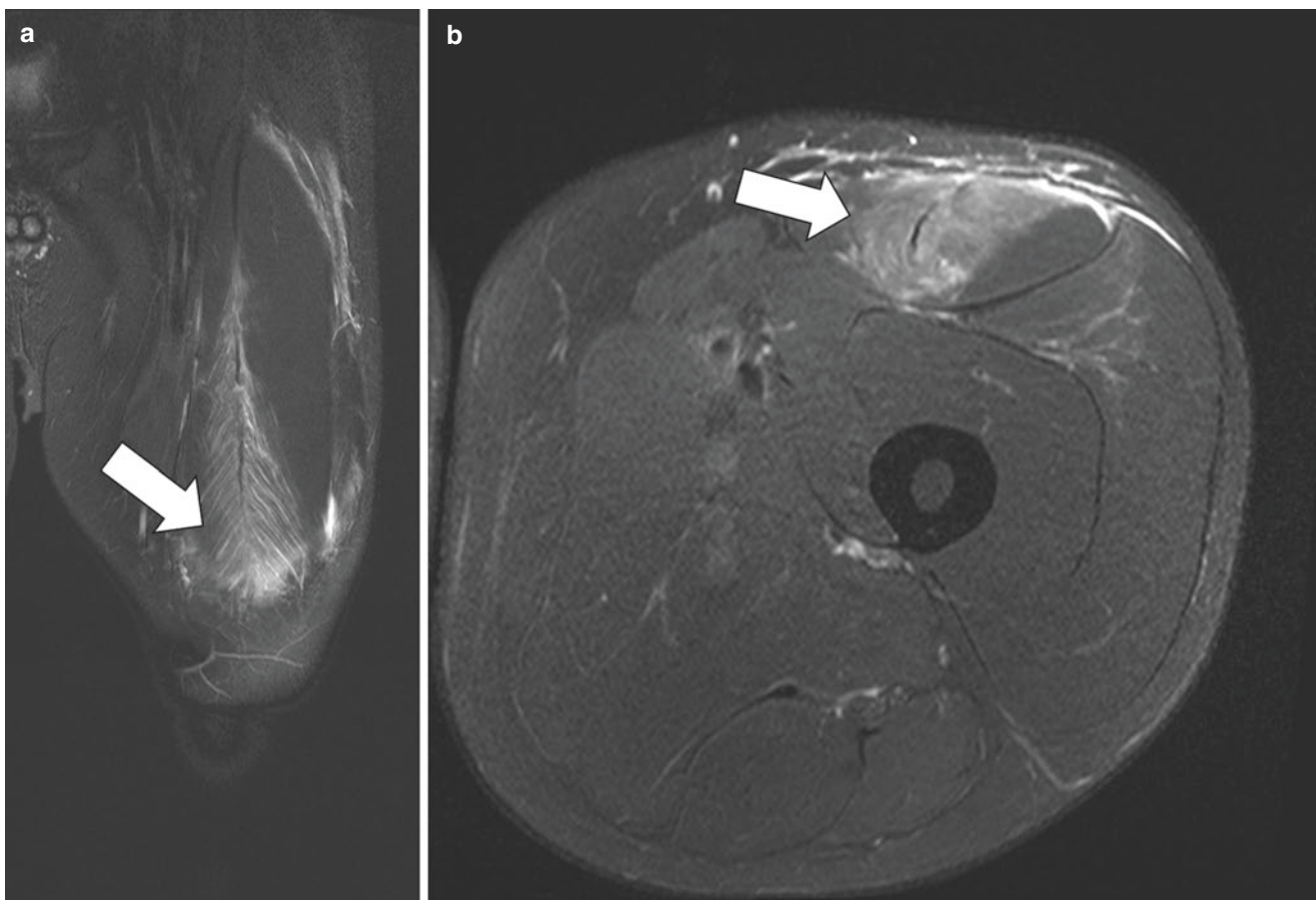
Fig. 17.1 Coronal (**a**) and axial (**b**) fat-saturated STIR MR images of the left thigh demonstrate feathered edema along the myotendinous junction of the rectus femoris muscle. No fiber disruption is identified in keeping with a grade 1 muscle injury
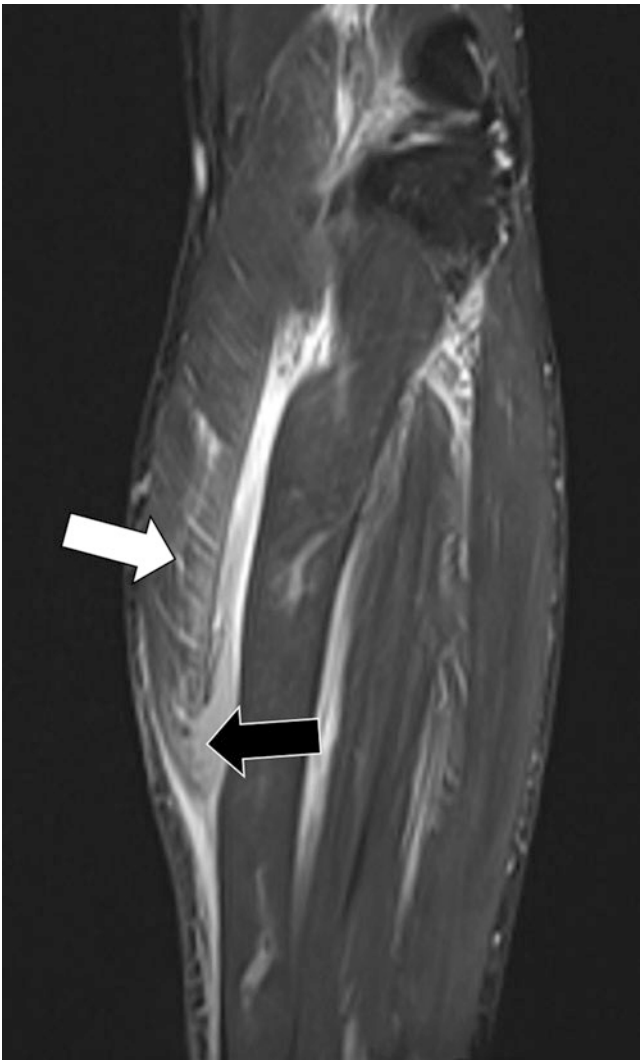
Fig. 17.2 Coronal fat-saturated STIR MR image of the lower leg demonstrates extensive intramuscular and fascial edema at the distal gastrocnemius muscle (white arrow). Partial-thickness fiber disruption at the distal myotendinous junction (black arrow) is in keeping with grade 2 muscle injury

modality of choice for the evaluation of muscle hernia as it may provide dynamic visualization of a reducible protrusion. Herniated muscle on US appears hypoechoic and mushroom-shaped with a smaller neck at the location of the fascia [9] (Fig. 17.5). MRI may be useful in the quantification of the fascial defect and herniated muscle bulk [10].

17.4 Inflammatory Myopathies

Inflammatory myopathy is classified as idiopathic or secondary. Secondary inflammatory myopathy is most frequently associated with autoimmune/connective tissue disorders such as Sjogren's disease or systemic lupus but can also be seen as a consequence of endocrine disorders or paraneoplastic syndromes. Inflammatory myopathy is a subset of heterogeneous muscle diseases that share similar pathophysiology, imaging features, and clinical presentation. Progressive and symmetric proximal to distal muscle pain and weakness in the setting of elevated muscle enzymes and abnormal EMG is suggestive of idiopathic myositis. MRI is the gold standard modality for the identification and characterization of these disorders.

17.4.1 Polymyositis/Dermatomyositis

Polymositis and dermatomyositis are related idiopathic inflammatory diseases of muscle that are characterized by muscle pain, weakness, and edema in a proximal to distal progressive distribution often involving the anterior compartment musculature of the thigh [11]. On MRI, both entities are defined by muscle edema involving one or more muscles in a symmetric distribution [12]. These entities while similar differ slightly in clinical and imaging features. Dermatomyositis, for example, is often seen in conjunction with esophageal dysfunction and may present with classic "sheet-like" cutaneous/dermal calcifications [13] (Fig. 17.6). The microanatomy of muscle involvement between these two entities also differs, with the endomysium (lining between small muscle fibers) preferentially involved in polymyositis and the perimysium and epimysium (around the larger muscle fascicles and muscle belly) preferentially involved in dermatomyositis. While both entities are characterized by feathered muscle edema in the proximal muscle groups, the differences in preferential involvement may help to differentiate these two on MR imaging. Muscle edema in polymyositis is seen centrally within the muscle belly, often sparing the peripheral muscle fascia and myotendinous junction (Fig. 17.7). Dermatomyositis by contrast presents as muscle edema predominantly peripheral with notable myotendinous and myofascial involvement [14, 15] (Fig. 17.8).

> **Key Point**
> - Muscle edema in polymyositis is seen centrally within the muscle belly, often sparing the peripheral muscle fascia and myotendinous junction.
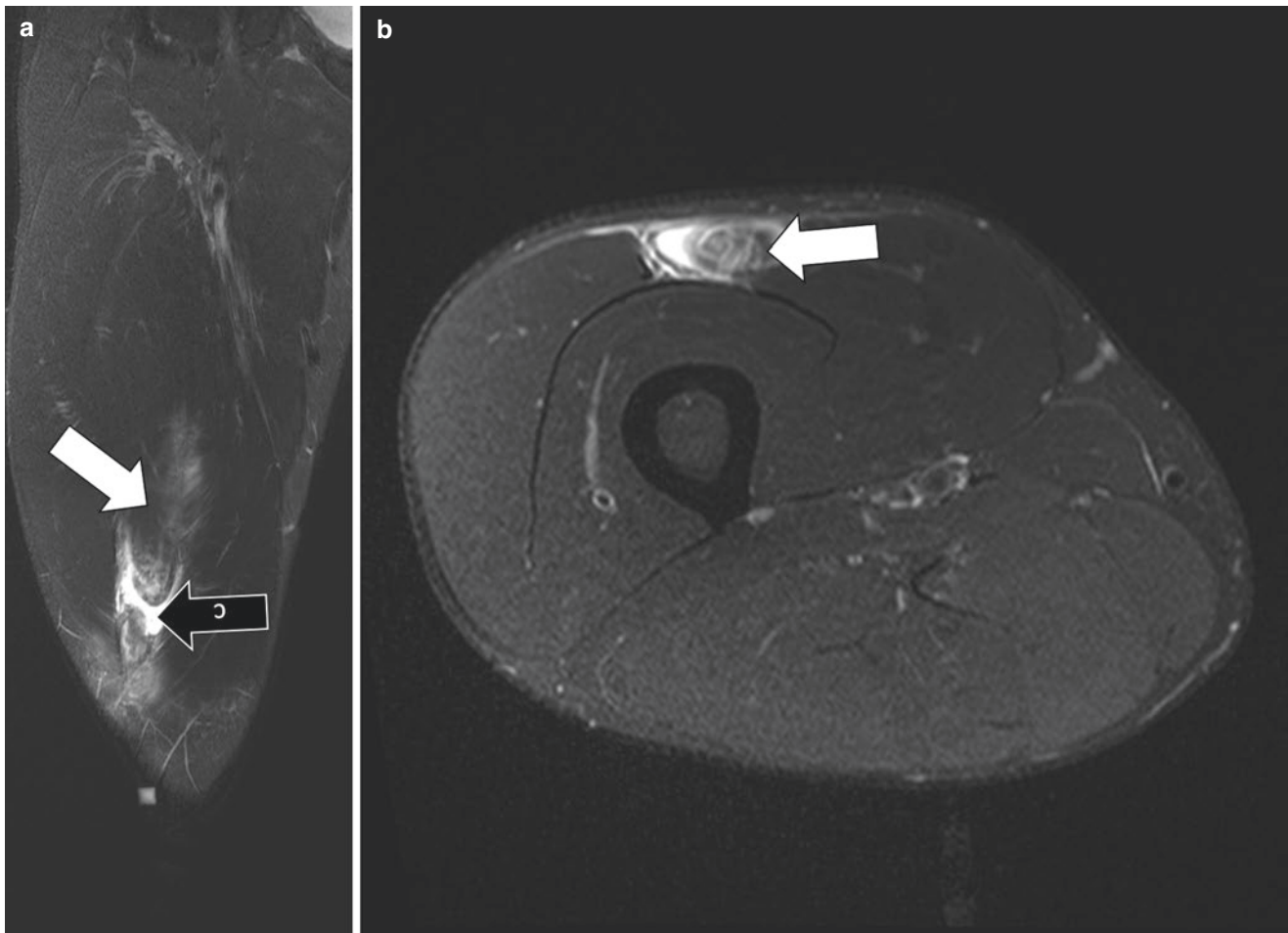
Fig. 17.3 Coronal (**a**) and axial (**b**) fat-saturated STIR MR images of the right thigh demonstrate extensive edema in the distal rectus femoris muscle belly (white arrows). This is a grade 3 injury given the complete fiber disruption and retraction apparent on the coronal image (black arrow)

17.4.2 Inclusion Body Myositis

Inclusion body myositis (IBM) is the most common idiopathic myopathy and is distinctly different in its pathophysiology compared to other idiopathic conditions. IBM is defined by inclusions of amyloid-B-protein within the skeletal muscle [16]. The onset of IBM is more common in the elderly and is often a distal to proximal distribution. MR imaging can easily differentiate IBM through the classic muscle involvement and the presence of often profound fatty infiltration [17, 18] (Fig. 17.9). The medial head of the gastrocnemius and flexor digitorum profundus muscles are commonly involved. IBM also frequently involves the anterior compartment muscles of the thigh, but unlike polymyositis and dermatomyositis, the rectus femoris muscle is notably spared in IBM [14] (Fig. 17.10 and Table 17.2).

17.5 Myonecrosis

Myonecrosis is the infarction of skeletal muscle. It has many etiologies such as trauma (e.g., crush injury), compartment syndrome, prolonged immobilization, poorly controlled diabetes, radiation treatment, and toxin (e.g., snake venom) [19]. On MRI, the infarcted muscle typically demonstrates nonspecific swelling and edema with heterogeneity that may suggest the presence of necrosis [20]. The feathery, striated pattern of muscle architecture usually remains visible. After contrast administration, infarcted muscle does not enhance (Fig. 17.11). It may not be feasible to inject contrast, however, if acute myonecrosis is complicated by rhabdomyolysis. Myonecrosis is sometimes incomplete. Enhancing linear and curvilinear foci indicate residual viable muscle tissue along vascular pedicles [21]. Once the healing process begins, contrast MRI can show
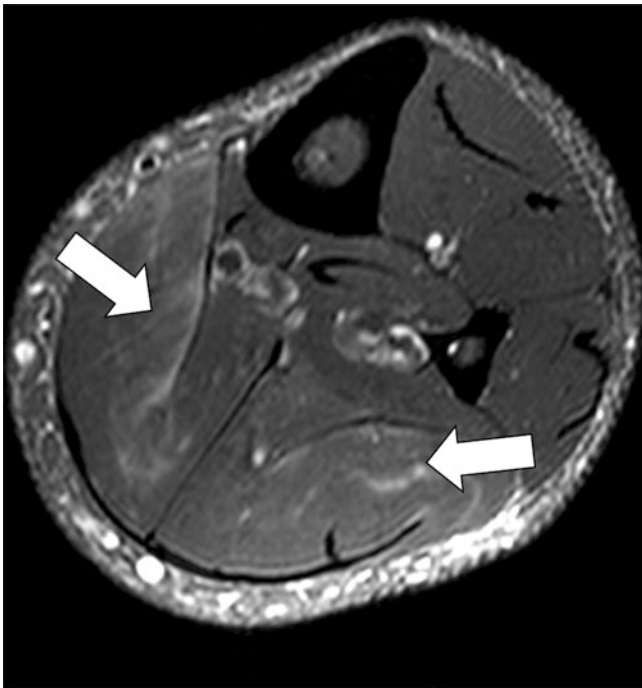
Fig. 17.4 Axial fat-saturated T2 MR image of the left calf in a 31-year-old male with severe calf pain after cross-fit workout. The feathered edema in the posterior compartment musculature (white arrows) is consistent with delayed onset muscle soreness (DOMS). This finding may persist for months following the initial insult
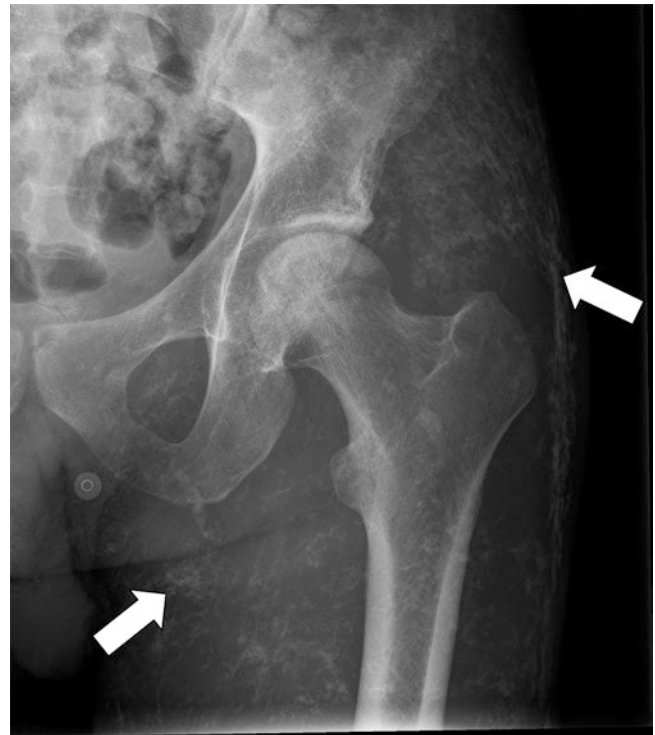
Fig. 17.6 Anteroposterior radiograph of the left hip demonstrates "sheet-like" linear calcifications (white arrows) within the soft issues in a patient with known dermatomyositis
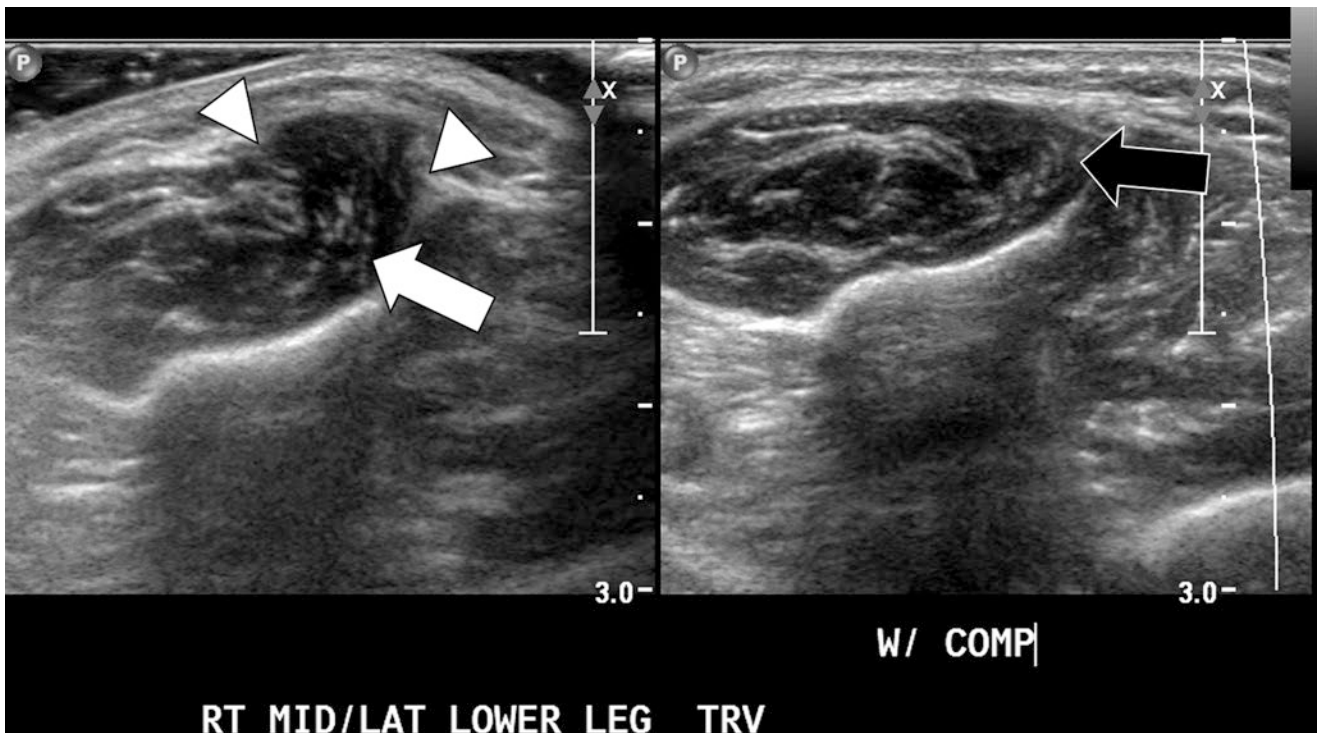
Fig. 17.5 Transverse gray-scale sonographic image of the right lower leg anterior compartment demonstrates a short segment defect in the superficial fascia (white arrowheads) with associated hypoechoic mushroom-shaped herniation of the peroneus longus muscle belly (white arrow). Comparison images of the normal left peroneus longus muscle are provided (black arrow)

rim enhancement due to granulation tissue at the interface of viable and nonviable tissue. This appearance can be confusing because it can mimic a phlegmon or abscess. In the late stages of healing, chronic sequelae of myonecrosis include cystic cavitation and dystrophic calcification.

17.6 Compartment Syndrome

In compartment syndrome, elevated pressure reduces arterial blood flow to muscles. The clinical diagnosis is confirmed by measuring intracompartmental pressure. Decreased circulation causes ischemia that can be reversed if the pressure is relieved. If intracompartmental pressure rises above perfusion pressure, blood flow is arrested causing irreversible myonecrosis. Infarcted muscle cannot be salvaged. The most common etiologies include trauma (crush injury, fracture), burn, overexertion, infection, and prolonged compression as might result from overly tight bandaging. The anterior compartment of the lower leg is particularly susceptible to compartment syndrome due to its confinement by surrounding
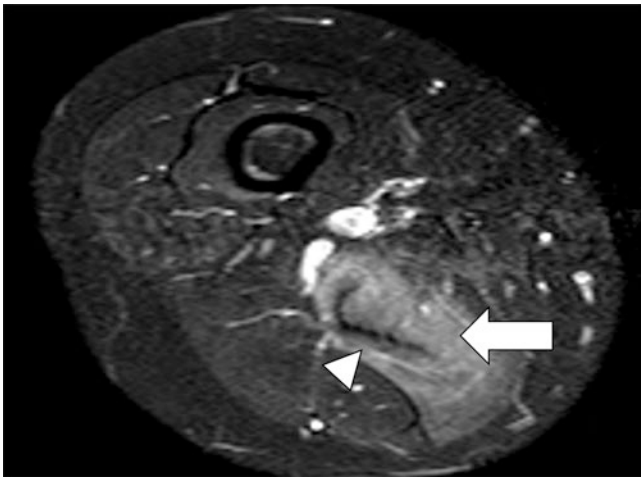
Fig. 17.7 Fat-saturated STIR MR image of the right thigh in a patient with known Sjogren's disease and polymyositis demonstrates marked diffuse edema isolated to the semimembranosus muscle (white arrow). Notice the diffuse endomysial pattern of muscle involvement with sparing of the fascia and myotendinous junction (white arrowhead)
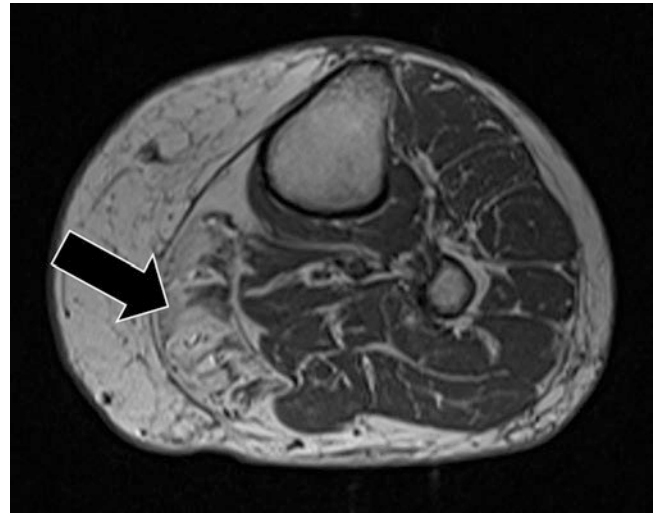
Fig. 17.9 Axial T1 MR image of the left lower leg in an 82-year-old male demonstrates profound isolated fatty infiltration of the medial head of the gastrocnemius muscle (black arrow). This pattern when symmetric is in keeping with chronic changes of inclusion body myositis
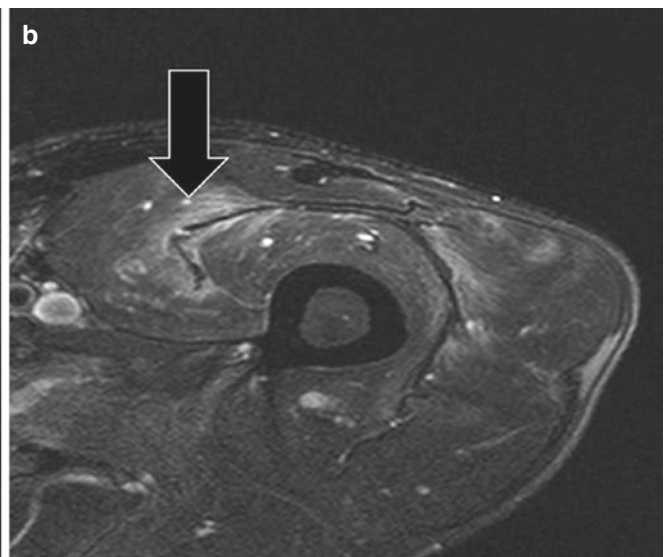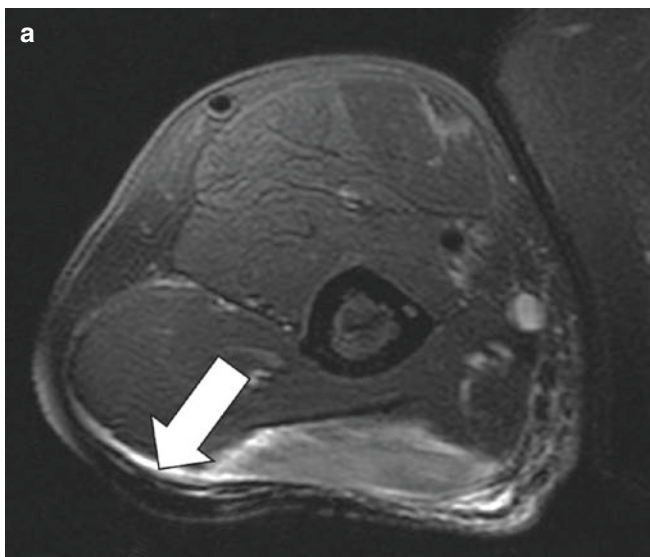
Fig. 17.8 Fat-saturated STIR MR images of the upper right arm (**a**) and right thigh (**b**) in a 27-year-old patient with dermatomyositis. Notice the perimysial pattern of edema with preferential involvement of the superficial fascia (white arrow) and myotendinous junction (black arrow)
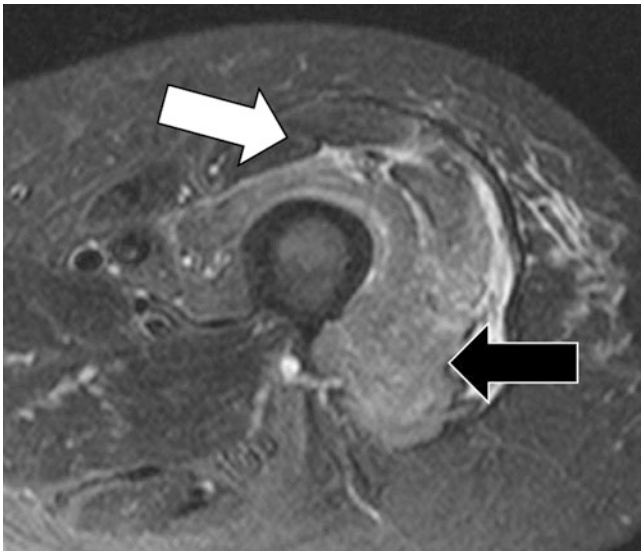
Fig. 17.10 Axial fat-saturated STIR MR image of the left thigh in a patient with inclusion body myositis and acute pain. Notice the diffuse edema in the anterior compartment musculature (black arrow) with notable sparing of the rectus femoris (white arrow)

Table 17.2 Clinical and imaging features of idiopathic myopathies [11, 12, 14, 17, 18]

Polymyositis	Dermatomyositis	Inclusion body myositis
• Symmetric • Proximal > distal • Female > male • Adults peak 30–60 • Endomysial involvement (diffuse muscle edema on MR) • Anterior thigh compartment	• Symmetric • Proximal > distal • Female > male • Juvenile and adult onset • Classic dermal calcifications • Perimysial involvement (facial or myotendinous edema on MR) • Anterior thigh compartment	• Symmetric • Proximal = distal • Male > female • Elderly predisposition • Fatty infiltration • Anterior compartment with rectus femoris sparing • Classic muscle involvement (medial head of the gastrocnemius, flexor digitorum profundus)

bone and fascia. Compartment syndrome can be acute or chronic. Acute compartment syndrome is a surgical emergency that requires fasciotomy for decompression and preservation of remaining viable tissue. Chronic and exertional compartment syndromes are aggravated by intense activity. On US and MRI, edema and swelling efface the normal muscle striations [22]. Following contrast administration, ischemic muscle enhances heterogeneously, whereas infarcted muscle lacks enhancement. Long-term complications include scarring, atrophic change, and mineralization. Calcific myonecrosis represents a severe complication of post-traumatic compartment syndrome and typically affects the anterior compartment of the lower leg.

17.7   Myositis Ossificans

Heterotopic ossification is biologically and histologically identical to normal bone but is located in soft tissues [23]. Many different insults can damage tissue and trigger a physiological reaction that leads to the formation of heterotopic bone. For example, orthopedic surgeries may be complicated by postoperative heterotopic ossification following hardware implantation, arthroplasty, and fracture fixation. Juxtaarticular heterotopic ossification may develop in immobilized patients after severe burn or brain or spinal cord injury. Surgical resection may be necessary to relieve debilitating pain and mechanical symptoms. On radiographs, mature heterotopic ossification demonstrates a pathognomonic cortical shell. On CT, low attenuation of the central cavity follows the attenuation of fat in cancellous bone. On MRI, heterotopic ossification can be misdiagnosed as lipoma because the cortical shell can have the appearance of a fibrous pseudocapsule, and the cancellous bone can demonstrate reticulations similar to adipose tissue [24].

The most frequent type of heterotopic ossification is myositis ossificans (also known as myositis ossificans circumscripta and myositis ossificans traumatica) which usually results from traumatic injury [25]. Myositis ossificans evolves in three general stages [26]. During the first 3–4 weeks, tissue injury causes organizing fibroblastic reaction, osteoblastic differentiation, and osteoid formation. During the second 3–4 weeks, the osteoid matrix becomes mineralized and produces immature lamellar bone. Finally, after 8–10 weeks, immature bone progresses to mature bone with characteristic cortex and intramedullary cavity. The imaging findings evolve with each of the three general stages. Radiographs are negative at first. If the patient presents with a painful, palpable mass, MRI is requested because of the concern for neoplasm. MRI features depend on the degree of tissue damage and surrounding inflammation [27]. MRI can show a mass-like lesion with enhancement following contrast administration simulating sarcoma. If the lesion is biopsied at this early stage, histopathological analysis can lead to the misdiagnosis of pseudo-malignancy [28]. In the middle stages of evolution, radiographs and CT show a zonal arrangement of perimeter mineralization. After full maturation, myositis ossificans exhibits a pathognomonic rind of cortex that is better characterized by radiographs and CT than MRI (Fig. 17.12).

> **Key Point**
> • In the early stage of myonecrosis, MRI can show an enhancing mass-like lesion simulating sarcoma.
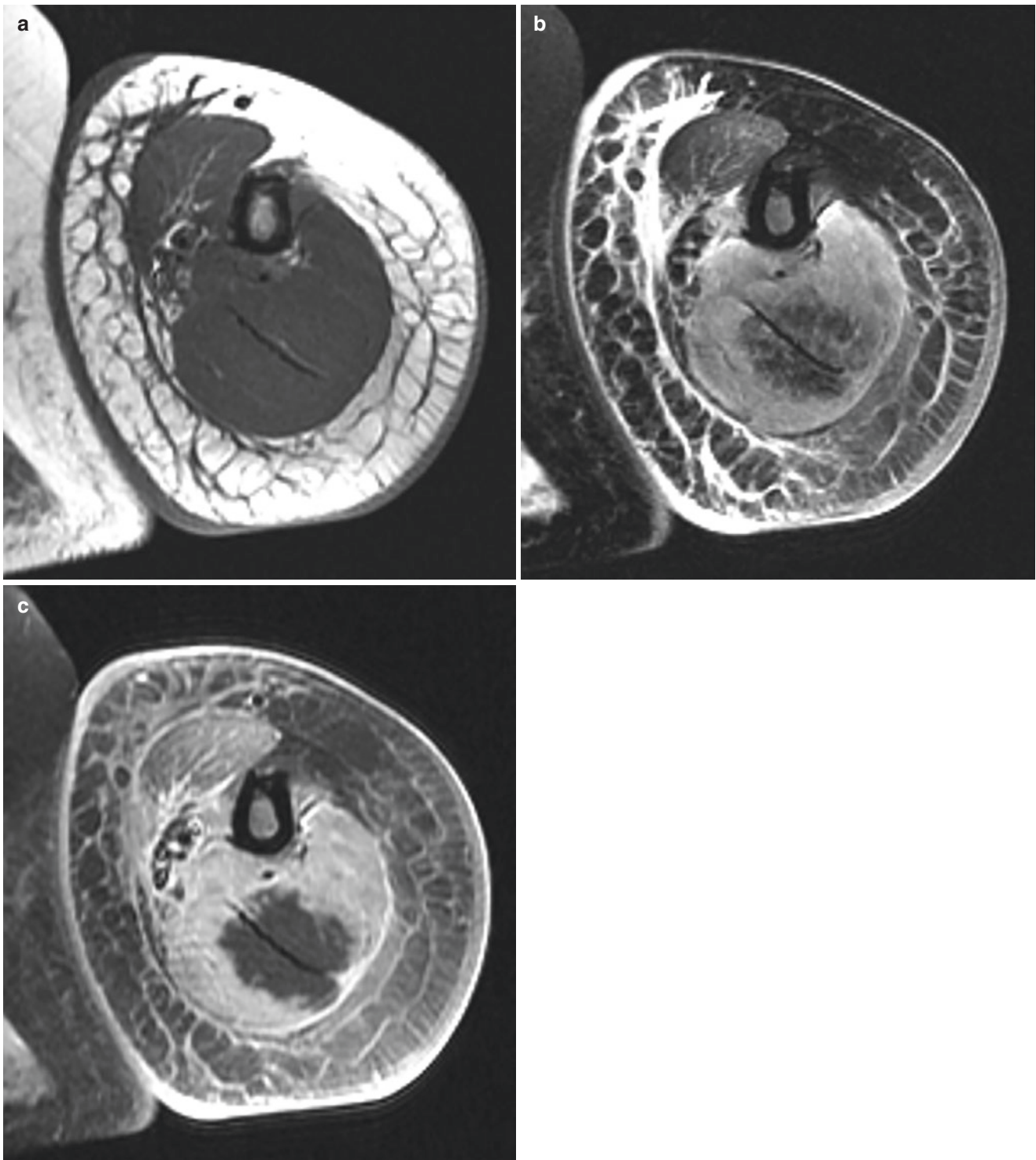
Fig. 17.11 Myonecrosis in a 73-year-old woman complaining of arm pain following drug overdose and stroke. (**a**) T1-weighted axial image shows swelling of the triceps muscle. (**b**) T2-weighted, fat-suppressed axial image shows diffuse edema of triceps muscle and low-signal region surrounding the central tendon. (**c**) Following intravenous contrast administration, T1-weighted, fat-suppressed axial image shows non-enhancing infarcted muscle corresponding to the low-signal T2-weighted region
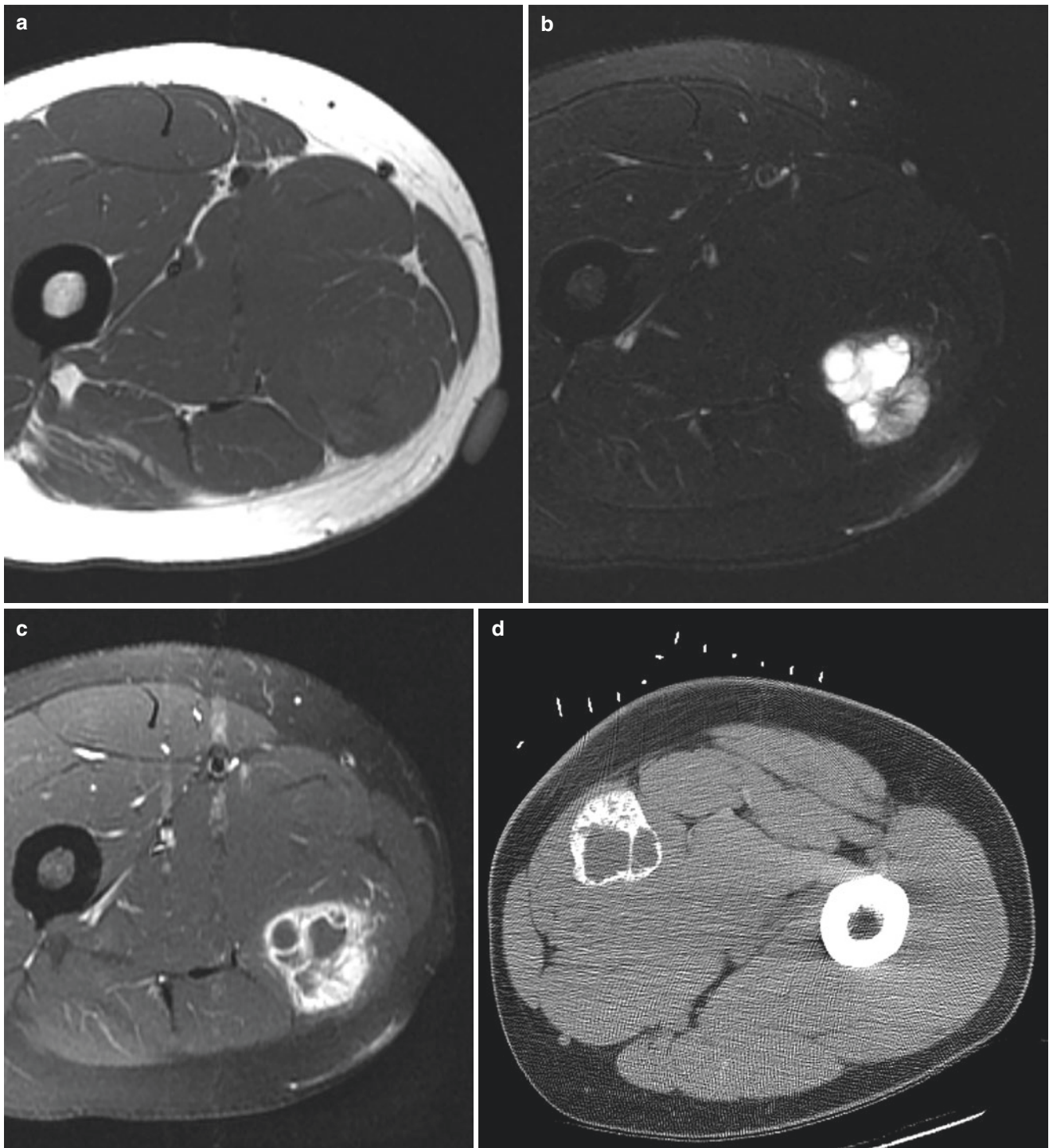
Fig. 17.12 Myositis ossificans in a 31-year-old man presenting with a painful, palpable thigh mass. (**a**) T1-weighted axial image demonstrates skin marker and swelling of underlying adductor muscle. (**b**) T2-weighted, fat-suppressed axial image demonstrates a sharply demarcated mass with cystic and solid regions. (**c**) Following intravenous contrast administration, T1-weighted, fat-suppressed axial image demonstrates dense enhancement of periphery, septations, and solid regions. (**d**) The patient was referred for CT-guided biopsy 2 weeks after the MRI study. With the patient prone, axial image obtained for procedural planning demonstrates grid placement and mineralized lesion corresponding to the MRI abnormality. The biopsy was canceled due to predominantly peripheral mineralization in pattern typical for myositis ossificans

17.8 Myopathy

Myopathy refers to the dysfunction of skeletal muscle and encompasses a spectrum of diseases. Symptoms include myalgias, muscle tenderness, and weakness. Hereditary myopathies result from enzymatic deficiencies and inborn errors of metabolism (e.g., glycogen storage disease). Endocrine myopathies are caused by adrenal, thyroid, parathyroid, and pituitary disorders. Myopathies may be induced by numerous different drugs (e.g., statin, steroid). Myositis is a subcategory of myopathy and refers to the presence of inflammation on histopathological analysis. Inflammatory myopathies are idiopathic, immune-mediated diseases such as dermatomyositis, polymyositis, and inclusion body myositis. They include conditions that affect multiple organs such as sarcoidosis. Myositis can be associated with viral infection (e.g., HIV) or bacterial infection. A complication of bacterial infection is pyomyositis. On MRI, edema-like signal, fatty muscle infiltration, and atrophic change can correlate with disease activity, intensity, and chronicity [19]. On fluid-sensitive MRI sequences, active disease locations show edema-like signal that can provide targets for biopsy [29]. Regions of active inflammation enhance after contrast administration. T1-weighted MRI images are useful for estimating the degree of muscle atrophy and fat replacement related to long-standing or burned-out myositis. Whole-body MRI provides an assessment of disease distribution and helps to gauge therapeutic response. PET can demonstrate corresponding regions of FDG uptake due to hypermetabolism.

17.9 Necrotizing Fasciitis

In necrotizing fasciitis, aggressive bacterial infection spreads rapidly between muscle compartments along deep fascial planes and subcutaneous fat. The organisms produce toxins that infarct and liquefy muscle and fat. After a short period of nonspecific symptoms, necrotizing fasciitis swiftly progresses to limb discoloration, systemic toxicity, and sepsis. Although antibiotics can be successful against non-necrotizing cellulitis and fasciitis, necrotizing infections are often fatal without surgical treatment such as debridement, fasciotomy, or amputation [30]. In patients with suspected necrotizing fasciitis, CT is obtained first because of its availability and sensitivity for gas in the soft tissues. The presence of gas is a specific but insensitive imaging sign. Therefore, the lack of gas cannot exclude necrotizing fasciitis. CT and MRI depict the size and locations of fluid collections [31]. Although intravenous contrast can better delineate muscle liquefaction and tissue infarction, intravenous contrast is contraindicated when necrotizing fasciitis is complicated by

rhabdomyolysis and renal failure. Nonspecific imaging features include subcutaneous edema, muscle edema, fascial enhancement, and small intracompartmental fluid collections [32].

> **Key Point**
> - In patients with suspected necrotizing fasciitis, the presence of gas on CT is a specific but insensitive imaging sign. The lack of gas cannot exclude necrotizing fasciitis.

17.10 Denervation Myopathy

Denervation occurs when the nerve supply to muscle is partially or completely blocked. This blockade can be symptomatic or asymptomatic and temporary or permanent. More common etiologies include penetrating trauma, surgical transection, and prolonged stretching or compression. Less common etiologies include autoimmune disease, viral infection, and carcinomatosis (nerve infiltration by malignancy). In some locations such as the spinoglenoid notch in the shoulder, slowly growing lesions (e.g., paralabral cyst, intraneural ganglion) may compress the neurovascular bundle and gradually lead to myopathic symptoms. In the acute stages of denervation, MRI shows diffuse muscle edema with uniform contrast enhancement. Muscle bulk remains normal. In the later stages of denervation, MRI findings can overlap with other disorders. Denervated muscle can become atrophic and infiltrated by fat. Edema-like signal may or may not be present. Parsonage-Turner syndrome, also known as idiopathic brachial neuritis, affects one or more muscles of the shoulder girdle. Progressive pain and weakness can mimic the clinical presentation of other shoulder disorders such as rotator cuff tear or capsulitis and, therefore, lead to a delay in diagnosis [33]. In Parsonage-Turner syndrome, supraspinatus and infraspinatus muscles are more commonly involved than deltoid, teres minor, and subscapularis muscles.

17.11 Muscle Lesions: Differential Considerations

Myotendinous strain shows pathognomonic localization to the myotendinous junction [34]. Other disorders show a random distribution in muscle. Any localization to the myotendinous junction is coincidental. For example, focal myositis may simulate acute strain if it happens to be contiguous with the myotendinous junction. However, it is usually located in the muscle

belly separate from the myotendinous junction. Intramuscular neoplasms can displace the myotendinous junction due to mass effect, but they rarely disrupt or encase it.

In myonecrosis, nonviable and adjacent viable muscle can have identical appearances on T1-weighted, T2-weighted, and STIR images because infarcted muscle maintains its normal fiber architecture, similar to necrotic cancellous bone which maintains its normal trabecular architecture. Therefore, the diagnosis of myonecrosis is made with greatest confidence when intravenous contrast is injected. The non-enhancing, avascular tissue stands out prominently against the densely enhancing viable muscle. Although infection (e.g., pyomyositis) can also cause diffuse muscle edema, non-enhancing phlegmon or abscess is distinguished from myonecrosis by the disruption of muscle architecture.

On MRI, hematoma is characterized by a bull's-eye configuration due to degradation of blood products, hemoglobin breakdown, and hemosiderin deposition. On T1-weighted images, the central region is increased in signal intensity. Neoplasms containing fat, such as hemangioma, angiolipoma, and liposarcoma, may also have a central region that is increased in T1-weighted signal intensity and, therefore, similar in appearance to intramuscular hematoma. On fat-suppressed images, however, the signal from fat is decreased, whereas the signal from hematoma is unchanged. Neoplasms complicated by hemorrhagic necrosis also can be mistaken for hematoma, but they have mass affect and displace surrounding structures, including the myotendinous junction. Hemorrhagic necrosis can be mistaken for enhancement following intravenous contrast administration.

Myositis ossificans can pose diagnostic pitfalls. It may present as a painful, palpable soft tissue mass with vague, remote, or absent history of trauma. Clinically, these symptoms and signs are suspicious for neoplasm. On MRI, myositis ossificans has a variable appearance depending on the age of injury, extent of myonecrosis, and degree of adjacent inflammation. In earlier stages, a mass-like abnormality can enhance densely after contrast administration, support the clinical suspicion of malignancy, and result in patient referral to an oncological center for biopsy and surgical resection. Imaging evidence of benign myositis ossificans may not occur until the time of CT-guided biopsy, when the pre-procedural scan demonstrates a characteristic peripheral rim of calcification (Fig. 17.12). In that case, the biopsy can be canceled.

17.12 Concluding Remarks

Although muscle is susceptible to multiple traumatic, inflammatory, neoplastic, and neuropathic disorders, imaging often enables a narrow differential diagnosis. Acute traumatic and activity-related injuries such as strain, contusion, and overuse may be complicated by myonecrosis, myositis ossificans, or compartment syndrome. Chronic sequelae are less specific, including muscle atrophy and fatty infiltration. In inflammatory myopathy, imaging is useful clinically in guiding biopsy and assessing treatment response. Imaging has a critical role in the early diagnosis and characterization of necrotizing fasciitis.

> **Take Home Messages**
> - Different imaging modalities have targeted roles in assessing muscle disorders.
> - In most muscle disorders, imaging enables a narrow differential diagnosis.
> - Clinical and imaging features of early myositis ossificans can simulate sarcoma.
> - Contrast administration may be necessary to confirm the diagnosis of myonecrosis.

References

1. Flores DV, Gómez CM, Estrada-Castrillón M, Smitaman E, Pathria MN. MR imaging of muscle trauma: anatomy, biomechanics, pathophysiology, and imaging appearance. Radiographics. 2017;38(1):124–48.
2. Mueller-Wohlfahrt HW, Haensel L, Mithoefer K, Ekstrand J, English B, McNally S, Orchard J, van Dijk CN, Kerkhoffs GM, Schamasch P, Blottner D, Swaerd L, Goedhart E, Ueblacker P. Terminology and classification of muscle injuries in sport: the Munich consensus statement. Br J Sports Med. 2013;47(6):342–50.
3. Grassi A, Quaglia A, Canata GL, Zaffagnini S. An update on the grading of muscle injuries: a narrative review from clinical to comprehensive systems. Joints. 2016;4(1):39–46. https://doi.org/10.11138/jts/2016.4.1.039.
4. Blankenbaker DG, De Smet AA. MR imaging of muscle injuries. Appl Radiol. 2004;33:14–26.
5. Gyftopoulos S, Rosenberg ZS, Schweitzer ME, et al. Normal anatomy and strains of the deep musculotendinous junction of the proximal rectus femoris: MRI features. AJR Am J Roentgenol. 2008;190:W182–6.
6. Dixon J. Gastrocnemius vs. soleus strain: how to differentiate and deal with calf muscle injuries. Curr Rev Musculoskelet Med. 2009;2:74–7.
7. Longo V, Jacobson JA, Fessell DP, Mautner K. Ultrasound findings of delayed-onset muscle soreness. J Ultrasound Med. 2016;35(11):2517–21.
8. Theodorou DJ, Theodorou SJ, Kakitsubata Y. Skeletal muscle disease: patterns of MRI appearances. Br J Radiol. 2012;85(1020):e1298–308.
9. Beggs I. Sonography of muscle hernias. Am J Roentgenol. 2003;180:395–9.
10. Mellado JM, Pérez del Palomar L. Muscle hernias of the lower leg: MRI findings. Skelet Radiol. 1999;28(8):465–9.
11. Adams MA, Chow CK, Premkumar A, Plotz PH. The idiopathic inflammatory myopathies: spectrum of MR imaging findings. RadioGraphics. 1995;15:563–74.
12. Hernandez RJ, Sullivan DB, Chenevert TL, Keim DR. MR imaging in children with dermatomyositis: musculoskeletal findings

and correlation with clinical and laboratory findings. AJR Am J Roentgenol. 1993;161(2):359–66.

13. Sanyal S, Atwal SS, Mondal D, Garga UC. Radiographic patterns of soft tissue calcinosis in juvenile dermatomyositis and its clinical implications. J Clin Diagn Res. 2014;8(12):RD08–11.

14. Phillips BA, Cala LA, Thickbroom GW, Melsom A, Zilko PJ, Mastaglia FL. Patterns of muscle involvement in inclusion body myositis: clinical and magnetic resonance imaging study. Muscle Nerve. 2001;24(11):1526–34.

15. Reimers CD, Schedel H, Fleckenstein JL, Nägele M, Witt TN, Pongratz DE, Vogl TJ. Magnetic resonance imaging of skeletal muscles in idiopathic inflammatory myopathies of adults. J Neurol. 1994;241(5):306–14.

16. Mendell JR, Sahenk Z, Gales T, Paul L. Amyloid filaments in inclusion body myositis: novel findings provide insight into nature of filaments. Arch Neurol. 1991;48(12):1229–34.

17. Cox FM, Reijnierse M, van Rijswijk CS, Wintzen AR, Verschuuren JJ, Badrising UA. Magnetic resonance imaging of skeletal muscles in sporadic inclusion body myositis. Rheumatology (Oxford). 2011;50(6):1153–61.

18. Fraser DD, Frank JA, Dalakas M, Miller FW, Hicks JE, Plotz P. Magnetic resonance imaging in the idiopathic inflammatory myopathies. J Rheumatol. 1991;18(11):1693–700.

19. Smitaman E, Flores DV, Mejía Gómez C, Pathria MN. MR imaging of atraumatic muscle disorders. Radiographics. 2018;38(2):500–22. https://doi.org/10.1148/rg.2017170112.

20. Filli L, Winklhofer S, Andreisek G, Del Grande F. Imaging of myopathies. Radiol Clin N Am. 2017;55(5):1055–70. https://doi.org/10.1016/j.rcl.2017.04.010.

21. Cunningham J, Sharma R, Kirzner A, et al. Acute myonecrosis on MRI: etiologies in an oncological cohort and assessment of interobserver variability. Skelet Radiol. 2016;45(8):1069–78. https://doi.org/10.1007/s00256-016-2389-4.

22. Rominger MB, Lukosch CJ, Bachmann GF. MR imaging of compartment syndrome of the lower leg: a case control study. Eur Radiol. 2004;14(8):1432–9.

23. McCarthy EF, Sundaram M. Heterotopic ossification: a review. Skelet Radiol. 2005;34:609–19.

24. Palmer WE, Bancroft L, Bonar F, et al. Glossary of terms for musculoskeletal radiology. Skeletal Radiol. 2020;49:1–33. https://doi.org/10.1007/s00256-020-03465-1.

25. Robinson P, Salehi F, Grainger A, et al. Cadaveric and MRI study of the musculotendinous contributions to the capsule of the symphysis pubis. AJR Am J Roentgenol. 2007;188(5):W440–5.

26. Kransdorf MJ, Meis JM, Jelinek JS. Myositis ossificans: MR appearance with radiologic-pathologic correlation. AJR Am J Roentgenol. 1991;157(6):1243–8.

27. De Smet AA, Norris MA, Fisher DR. Magnetic resonance imaging of myositis ossificans: analysis of seven cases. Skelet Radiol. 1992;21:503–7.

28. Nuovo MA, Norman A, Chumas J, Ackerman LV. Myositis ossificans with atypical clinical, radiographic, or pathologic findings: a review of 23 cases. Skelet Radiol. 1992;21:87–101.

29. Endo Y, Miller TT. Myositis and fasciitis: role of imaging. Semin Musculoskelet Radiol. 2018;22(3):286–98.

30. Edlich RF, Cross CL, Dahlstrom JJ, Long WB. Modern concepts of the diagnosis and treatment of necrotizing fasciitis. J Emerg Med. 2010;39(2):261–5. https://doi.org/10.1016/j.jemermed.2008.06.024.

31. Kim KT, Kim YJ, Won Lee J, et al. Can necrotizing infectious fasciitis be differentiated from nonnecrotizing infectious fasciitis with MR imaging? Radiology. 2011;259(3):816–24. https://doi.org/10.1148/radiol.11101164.

32. Schmid MR, Kossmann T, Duewell S. Differentiation of necrotizing fasciitis and cellulitis using MR imaging. AJR Am J Roentgenol. 1998;170(3):615–20.

33. Parsonage MJ, Turner JW. Neuralgic amyotrophy; the shoulder-girdle syndrome. Lancet. 1948;1(6513):973–8.

34. Palmer WE, Kuong SJ, Elmadbouh HM. MR imaging of myotendinous strain. AJR Am J Roentgenol. 1999;173(3):703–9.

Peripheral Nerve Imaging

18

James F. Griffith and Roman Guggenberger

Learning Objectives
- To understand the ultrasound and MRI appearances of different nerve pathologies.
- To understand the complementary roles of US and MRI in evaluating different nerve pathologies.

18.1 Introduction

The main peripheral nerve abnormalities that lead to referral for imaging are, in order of frequency: entrapment, tumours, trauma, perineural fibrosis, neuralgic amyotrophy, and inflammatory neuropathy. These conditions are best imaged with either ultrasound or magnetic resonance imaging (MRI). Both modalities allow nerves to be seen in high resolution and have their own advantages that make them complimentary in peripheral nerve imaging. Ultrasound is more readily available, allows large segments of nerves to be imaged relatively quickly, and has a dynamic component. MR neurography (MRN) provides an excellent overview of the neural anatomic environment; enables more consistent visualisation of the smaller peripheral nerves, such as those in the foot; can visualise nerves in areas where transducer access is limited, such as the intraforaminal part of the brachial plexus; is less operator dependent; enables the functional capacity of nerves to be explored in greater depth through, for example, diffusion tensor imaging; and allows the effect of motor denervation, i.e. muscle atrophy, to be seen and quantified more accurately.

J. F. Griffith (✉)
Department of Imaging and Interventional Radiology, The Chinese University of Hong Kong, Shatin, Hong Kong
e-mail: griffith@cuhk.edu.hk

R. Guggenberger
Institut für Diagnostische und Interventionelle Radiologie, Universitätsspital Zurich, Zurich, Switzerland

This chapter discusses imaging of the peripheral nerves by ultrasound and MRI.

18.2 Peripheral Nerve Basics

Peripheral nerves range in diameter from 1 to 20 mm and are formed by multiple axons, grouped into fascicles which, in turn, are grouped into nerves. The endoneurium is the connective tissue surrounding the axon-Schwann cell unit and contains collagen fibres, fibroblasts, capillaries, and a few mast cells and macrophages. The perineurium binds groups of axon-Schwann cell units into nerve fascicles. The number and size of the nerve fascicles generally diminish as the nerve gets smaller more peripherally. The epineurium is the outermost connective tissue sheath that encloses all the nerve fascicles, providing mechanical support to the nerve and reducing friction with adjacent tissues [1]. The endoneurium and perineurium form a blood-nerve barrier akin to the blood-brain barrier. As such, peripheral nerves, except for the dorsal nerve root ganglia, do not enhance with intravenous contrast unless the barrier is compromised by inflammation or malignancy [2].

18.3 Pathophysiology Basics

Pathological nerves may show neural ± fascicular oedema, altered calibre, irregular contour, discontinuity, abnormal enhancement, perineural fibrosis, or rarely intraneural fatty replacement [3, 4]. In acute nerve pathologies, fascicular pattern is usually accentuated due to intra- and perineural oedema, leading to increased nerve calibre and signal intensity. With increasing chronicity, oedema subsides and fibrotic nerve changes lead to reorganisation of nerve tissue with decreased nerve diameter and loss of T2-hyperintensity on MRI. MR imaging is more sensitive at detecting target muscle denervation oedema or atrophy than ultrasound. Diffuse

muscle oedema and contrast enhancement can be seen within 1 day of denervation. Both probably reflect increased muscle engorgement and increased muscle blood volume due to denervation. Muscle atrophy and fatty replacement are features of chronic denervation.

18.4 MR Neurography: Technical Considerations

MR neurography (MRN) aims to provide high-resolution high-contrast images of nerves. This is aided by suppression of the background fat as well as pulsation and breathing artefact suppression. While homogeneous fat suppression is challenging on 3T imaging, the increase in contrast-to-noise ratio and spatial resolution achieved by the higher field strength outweigh the issues with inadequate fat suppression. Dedicated peripheral coils ensure high-quality nerve detail and can, if necessary, be combined with surface coils when larger sections of the nerve need to be examined. For example, the brachial plexus is usually imaged with a combined head-neck coil to cover the cervical spine, foramina, and neck regions along with a torso coil to cover the parascapular and axillary regions.

Since nerves have a long (e.g. 80–100 ms) T2 signal and are usually surrounded by fat, fast or turbo spin-echo sequences with spectral saturation using the adiabatic inversion pulse and Dixon technique are preferred [5]. The Dixon technique allows larger areas to be imaged with homogenous fat suppression when, for example, imaging the brachial or lumbosacral plexuses.

Focal T2-weighted neural hyperintensity may occur if the course of the nerve changes relative to the B0-field into a plane higher than 55°. This is known as magic angle artefact which may also persist at TEs beyond 66 ms. Mild T2-hyperintensity of nerves can be seen in asymptomatic subjects [6]. If in doubt regarding the significance of any neural hyperintensity, comparison with the contralateral healthy side is helpful, as is assessing the target muscles for signs of denervation. Also, true pathologic intraneural T2-hyperintensity is usually higher than any maximal magic angle effect [7].

Recent advancements with extended echo train lengths and parallel imaging have enabled 3D T2-weighted imaging volumetric visualisation of nerves using fast or turbo spin-echo sequences in acceptable scan times [8, 9]. Suppression of adjacent vasculature can be achieved by motion-sensitised driven equilibrium or diffusion moment, improving the discrimination of small nerves in the extremities and skull base [10–12]. Contrast administration is not routinely used when imaging peripheral nerves though it can help to enhance vessel conspicuity and demonstrate inflammatory or neoplastic uptake on T1-weighted fat-suppressed images as well as

simultaneously suppressing vessel signal on T2-weighted spin-echo and STIR images to increase neural delineation.

Diffusion tensor imaging (DTI) provides additional information on nerve integrity and can be a useful adjunct to standard MRN protocols. Random multidirectional motion of water molecules is restricted when the highly organised neural membranes are intact. The amount of restriction can be quantified by apparent diffusion coefficient (ADC) which is an estimate of mean water diffusivity in all directions. Diffusion can be further directionally quantified by fractional anisotropy with 0 being full isotropy and 1 being full anisotropy. Diffusion tractography, by connecting voxels of similar diffusivity, helps visually confirm neural integrity [13].

> **Key Point**
> - The highly organised structure of peripheral nerves is similar throughout the peripheral nervous system. Nearly all nerves look the same. Similarly, the ultrasound and MRI appearances of entrapment, tumour, injury, or inflammation tend to be similar irrespective of the nerve(s) affected.

18.5 Neural Entrapment

Carpal tunnel syndrome (CTS) is the commonest nerve entrapment. The main ultrasound and MR criterion of CTS is undue swelling of the median nerve. The carpal tunnel inlet and outlet are determined on ultrasound and MRI by direct visualisation of the transverse retinaculum. On ultrasound and MRI, one should measure the cross-sectional area (CSA) of the median nerve at the distal forearm, just proximal to the tunnel, at the tunnel inlet, at the tunnel outlet, and just distal to the tunnel.

The more swollen the median nerve, the more likely the possibility of CTS. The normal median nerve CSA at any of these locations on ultrasound is <10 mm^2. A median nerve CSA of >14 mm^2 at any of these locations is diagnostic of CTS [14]. Measurements between 10 and 14 mm^2 should be taken as suggestive of, but not diagnostic of, CTS. Ultrasound CSA measurements do not include the epineurium, and, hence, MRI measurements are about 20% greater than ultrasound measurements [15]. On MRI, a median nerve CSA > 15 mm^2 either proximal to or distal to the tunnel is a useful diagnostic criterion for CTS while a CSA > 19 mm^2 proximal to the tunnel is indicative of severe CTS [16]. Intraneural hyperaemia on ultrasound is a specific but insensitive ultrasound sign of neural compression. Other ultrasound and MR signs of CTS such as increased palmar retinacular bowing or retinacular thickness, loss of neural

fasciculation, flattening ratio, and reduction in carpal tunnel CSA are not specific enough to be very discriminatory on a case-by-case basis in everyday clinical practice.

Ultrasound is as sensitive as nerve conduction studies in confirming the presence of CTS. Patients with equivocal nerve conduction study findings for CTS will also usually have equivocal findings on ultrasound so the two examinations are not necessarily complimentary. Elastography and DTI studies have shown that CTS patients slower elasticity (i.e. stiffer) and median nerves with lower fractional anisotropy values (i.e. less unidirectional diffusion) though currently elastography and DTI do not provide additional information over that provided by CSA measurements alone.

Primary CTS is more common than secondary CTS due to, for example, tenosynovitis, ganglion cysts or other carpal tunnel masses, or crystal deposition within the carpal tunnel. All of these secondary causes can be screened with ultrasound or MRI, with MRI being particularly helpful in this regard.

Following carpal tunnel release, the median nerve will usually remain unduly swollen for at least 1 year following successful surgery and may never return to normal size despite good amelioration of symptoms [17]. This persistent median nerve swelling is due to neural fibrosis and congestion secondary to chronic compressive neuropathy. Therefore, a swollen median nerve following surgery on ultrasound or MRI should not be taken as a sign of incomplete decompression. Similarly, the retinaculum will reform in most patients at 3–12 months following surgery, though in a more elongated fashion such that the overall volume of the carpal tunnel is increased [17].

The next most common entrapment is *cubital tunnel syndrome* which occurs due to compression of the ulnar nerve either within the cubital tunnel deep to Osborne's ligament or within the cubital tunnel proper deep to the arcuate ligament. Any imaging of the cubital tunnel should extend from 8 cm proximal to the elbow joint, to include the arcade of Struthers, to 5 cm distal to the joint to include the ulnar nerves between the two heads of flexor carpi ulnaris [18].

Primary cubital tunnel syndrome is less common than secondary cubital tunnel syndrome due to, for example, a prominent anconeus epitrochlearis muscle osteophytosis, synovitis, or ganglion cysts encroaching from the ulnohumeral joint into the cubital tunnel. Secondary cubital tunnel syndrome tends to be mainly seen in older patients.

The greater the ulnar nerve CSA in the cubital tunnel, the more likely the diagnosis of cubital tunnel syndrome. The normal ulnar nerve CSA is <8 mm^2. An ulnar nerve CSA > 14 mm^2 at the cubital tunnel is considered diagnostic of cubital tunnel syndrome. CSA values between 8 and 12 mm^2 are suggestive of, but not diagnostic of, cubital tunnel syndrome.

Ultrasound also allows one to examine for ulnar nerve subluxation during elbow flexion more easily than MRI. Subluxation occurs due to a redundancy of Osborne's ligament. Although ulnar nerve subluxation is usually asymptomatic and can be seen in about one-fifth of healthy subjects, one can still appreciate how repeated subluxation of the ulnar nerve over the medial humeral epicondyle could lead to friction neuritis ('ulnar neuritis') in patients who frequently flex their elbows during daily, occupational, or sporting activities.

Although not discussed much in the literature, it is likely that two pathologies, namely, neural compression and inflammation, may act in isolation or in unison to produce symptoms of cubital tunnel syndrome. Some patients may have an inflamed ulnar nerve which is not compressed. This is different to other entrapment syndromes such as carpal tunnel syndrome, where the primary aetiology is solely that of neural compression. In this respect, MR has an advantage over ultrasound in allowing one to determine neural oedema by T2-hyperintensity. Adjacent muscle acts as an internal reference to standardise ulnar nerve signal intensity [19]. Then measure the contrast-to-noise ratio (CNR) as follows:

$$CNR = \frac{\text{Ulnar nerve signal intensity} - \text{muscle signal intensity}}{\text{Standard deviation of air}}$$

A CNR of >50 has high accuracy for has high accuracy for cubital tunnel tunnel syndrome.

The third most common entrapment syndrome is *supinator syndrome* where the motor branch of the radial nerve (the posterior interosseous nerve) is entrapped at the inlet or just beyond the inlet of the supinator tunnel, known as the arcade of Frohse (Fig. 18.1). One will appreciate undue swelling of the deep branch of the radial nerve just proximal to or within the supinator tunnel. There is often also localised deep tenderness at this point.

Less frequent sites of neural entrapment include the suprascapular groove, the spinoglenoid notch (Fig. 18.2), the radial groove, the radial tunnel, Guyon's canal, the peroneal canal, and the tarsal tunnel.

> **Key Points**
> - Entrapment syndromes are common in the upper limb, uncommon in the lower limbs.
> - At the relevant sites, the greater the degree of nerve swelling, the more likely the possibility of entrapment.
> - The CSA of peripheral nerves on MRI is 20% larger than on ultrasound.
> - Both ulnar nerve entrapment and friction neuritis can produce cubital tunnel syndrome symptoms.
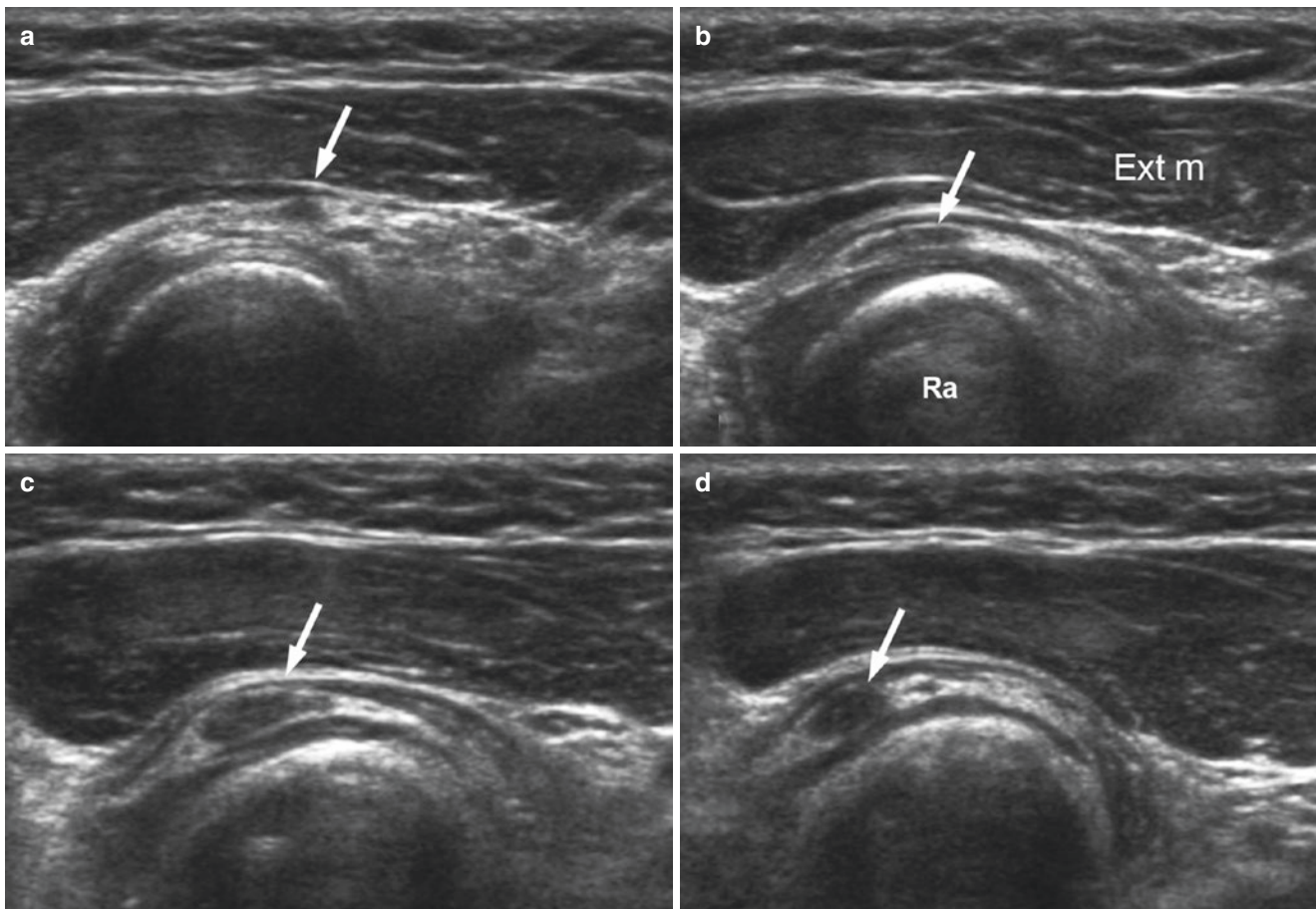
Fig. 18.1 Series of transverse ultrasound images showing posterior interosseous nerve (arrows) (**a**) proximal to and (**b–d**) within the supinator tunnel of a 9-year-old boy with quite abrupt onset of weakness of finger extension. The PIN is swollen within the supinator muscle ('supinator tunnel') located between the radial neck and the extensor forearm muscles. This swelling was due to an hourglass constriction at the arcade of Frohse confirmed surgically. PIN swelling is more commonly seen immediately proximal to the supinator tunnel inlet. Ext m Extensor carpi radialis brevis muscle

18.5.1 Tumours

More than 90% of peripheral nerve tumours are benign and more than 60% of these benign nerve sheath tumours are schwannomas. The next most common benign nerve sheath tumour is neurofibroma. Other benign nerve sheath tumours include intraneural lipoma and intraneural ganglia.

Schwannomas arise from Schwann cells, while neurofibroma comprises a mixture of neural cells. There are no known imaging features that allow one to accurately distinguish between a neurofibroma and schwannoma. As such, one should refer to the presence of a 'nerve sheath tumour' rather than a particular tumour type. Neural continuity is the most specific ultrasound or MR sign of a nerve sheath tumour (Fig. 18.3). Other less specific ultrasound or appearances are a fusiform or oblong-shaped mass, internal cystic, myxoid or haemorrhagic areas, posterior acoustic enhancement (on ultrasound), and moderate tumoural hyperaemia or enhancement. On MRI, the so-called target sign may be more sug-

gestive of a schwannoma, while more fascicular patterns are seen with neurofibromas. Only about 70% of nerve sheath tumours have visible neural continuity on ultrasound examination, and it is only in this setting that one can make a definitive diagnosis of a nerve sheath tumour based on the ultrasound appearances alone. When neural continuity is present, one should ascertain whether the tumour is located eccentric or concentric to the parent nerve as this has a bearing on the success of surgical excision. Percutaneous biopsy of nerve sheath tumour is occasionally very painful and should not be undertaken when a confident diagnosis can be made based on ultrasound appearances alone provided malignancy is not suspected.

The remaining 30% of nerve sheath tumours do not have imaging appearances specific enough to make a definitive diagnosis based on ultrasound appearances alone. In this situation one can offer a probable or possible diagnosis of a nerve sheath tumour. Potential differential diagnoses are vascular leiomyomas, vascular malformation, glomus, fibroma,
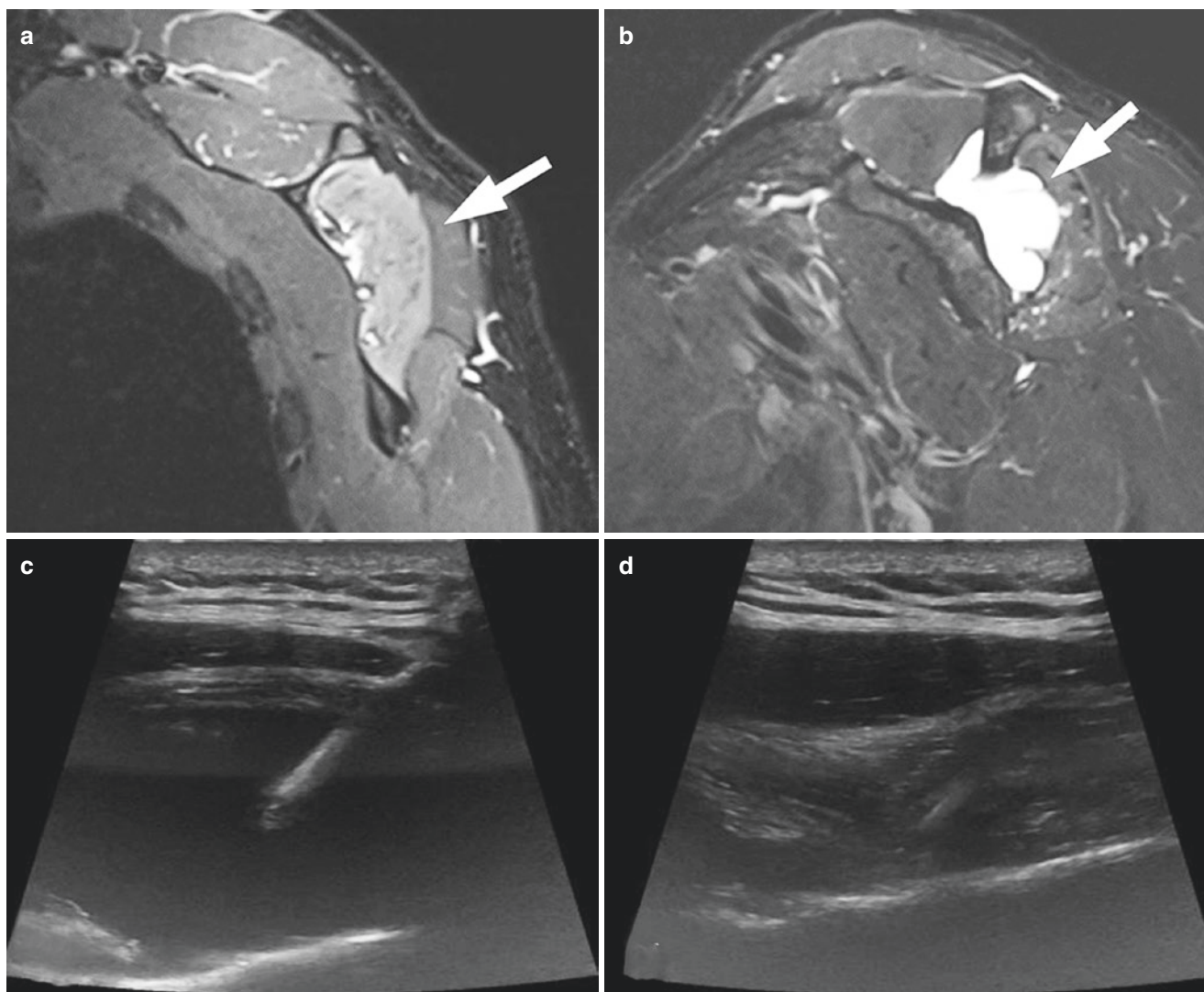
Fig. 18.2 Adult patient with increasing shoulder weakness while working overhead in vineyard. (**a**) MRN shows moderate infraspinatus denervation oedema (arrow) with (**b**) a large paralabral ganglion (arrow) causing suprascapular nerve compression in the spinoglenoid notch. This compression was relieved by US-guided cyst aspiration as seen on (**c**) pre- and (**d**) post-aspiration images

and ganglia. Appearances that would favour a nerve sheath tumour over these tumours are an oblong configuration to the mass, a regular margin, more pronounced internal speckling, and lack of vascular convergence.

Less common types of neurofibroma are diffuse and plexiform neurofibromas. Diffuse neurofibroma may be sporadic or associated with neurofibromatosis type I (NF1). They originate from the subcutaneous nerves and spread extensively along the subcutaneous connective tissue septae. One will see localised dermal and subcutaneous thickening, subcutaneous reticulation, and hyperaemia which can mimic localised cellulitis or panniculitis. Plexiform neurofibroma is only seen in NF1 and is associated with a moderate risk of malignant transformation. It has a more distinctive 'bags of worms' appearance with diffuse enlargement of nerves in a discrete lobulated mass and may occur in the subcutaneous as well as the deep tissues.

One in two malignant peripheral nerve sheath tumours (MPNST) occur in patients with NF1, while 1 in 20 patients with NFI will develop a MPNST. There are currently no imaging features that allow one to distinguish atypical nerve sheath tumours from MPNSTs [20] (Fig. 18.4). Both whole-body MRI with diffusion-weighted imaging and PET/CT imaging are currently being explored in this regard [20]. If there is clinical or imaging suspicion of MPNST, then a percutaneous biopsy should be undertaken to confirm or refute this possibility.
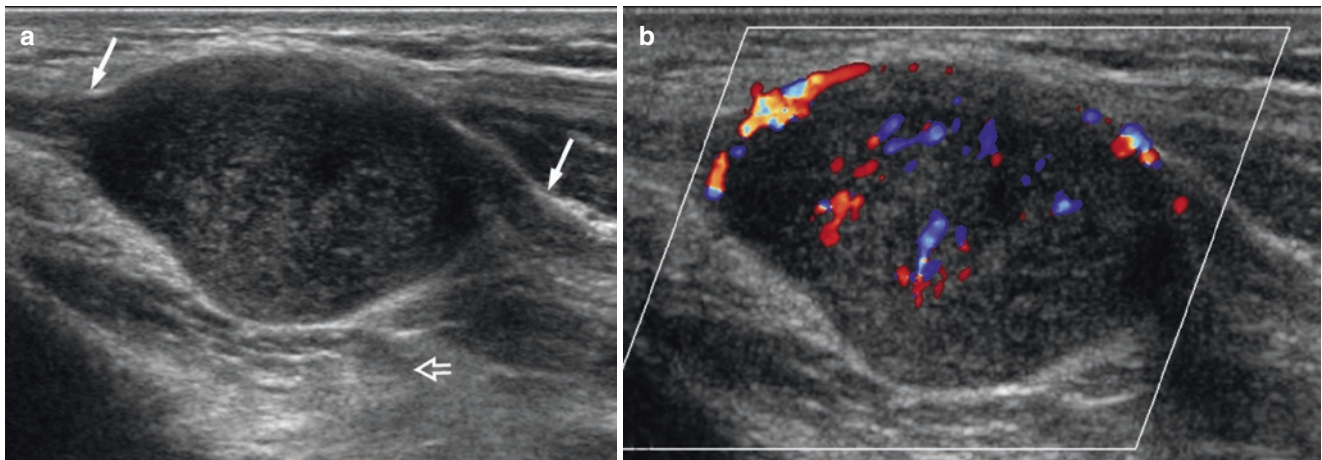
Fig. 18.3 Longitudinal ultrasound of distal forearm showing (**a**) medium-sized nerve sheath tumour arising eccentrically from the median nerve (arrows) with neural continuity and acoustic enhance-ment (open arrow). (**b**) The tumour shows moderate tumoural hyperae-mia. These are diagnostic ultrasound appearances of a nerve sheath tumour
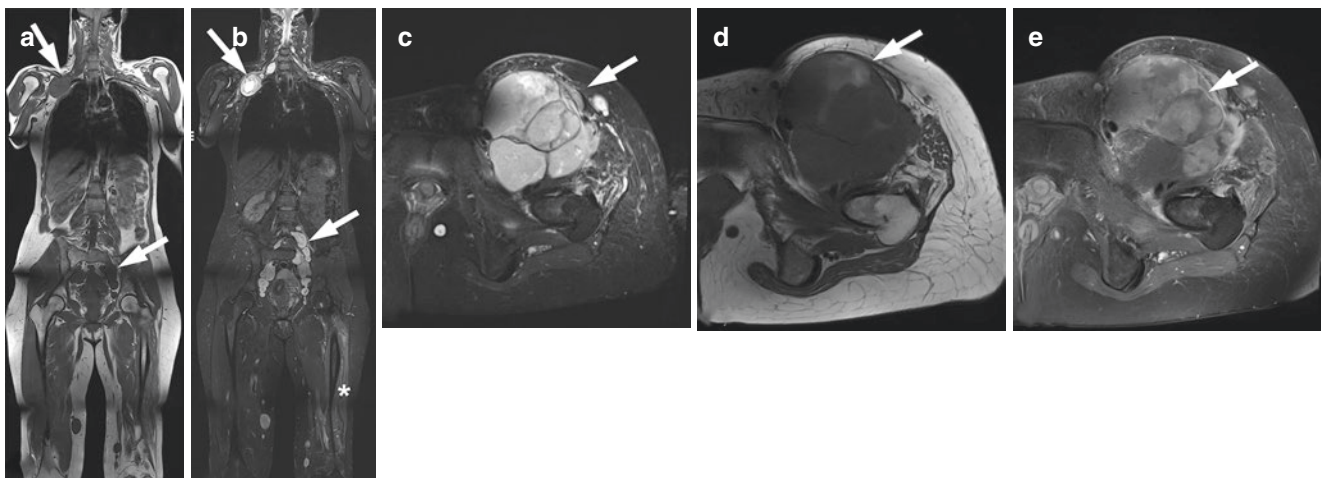
Fig. 18.4 Middle-aged women with hereditary schwannomatosis. (**a**) Multiple tumours are seen on T1-weighted and (**b**) T2-weighted STIR images (arrows). Severe denervation oedema and atrophy of the left quadriceps muscle is present (asterisk in **b**) as a consequence of a large dedifferentiated malignant schwannoma (confirmed histologically) of the femoral nerve with inhomogeneous signal on (**c**) T2-weighted STIR, (**d**) T1-weighted, and (**e**) T1-weighted fat saturated post-gad images

Key Points
- About 70% of nerve sheath tumours have neural continuity evident on imaging. Only in this setting, can one make a definite diagnosis based on imaging signs alone.
- Diagnostic accuracy of imaging for identifying nerve sheath tumours is much less when no neural continuity exists.
- Increase in size over time is the most reliable sign of the MPNST. If doubt exists, percutaneous biopsy is warranted.

18.5.2 Nerve Injury

Blunt injury to nerves usually recovers spontaneously and is not imaged. Conversely, sensory or motor denervation fol-lowing a penetrating injury usually results in early surgical exploration without the need for imaging.

Imaging is, therefore, usually undertaken to investigate either traction injury or the delayed recognition of nerve injury following penetrating trauma. In traction injury, imag-ing should focus on those nerves which have been clinically compromised, while in penetrating trauma, imaging should focus on examination of those nerves close to the path of injury. A neuroma-in-continuity (NIC) or stump neuroma

can be seen some months following partial or complete nerve transection, respectively, and should not be mistaken for a nerve sheath tumour [21].

Features of nerve injury to ascertain on imaging are:

(a) Is the nerve visibly injured, i.e. is it not swollen or mild/moderately/severely swollen? What is the length of the affected segment? Is there perineural fibrosis, haematoma, or inflammation present? Is there neural adhesion? If perineural fibrosis is present, what percentage of the neural circumference is affected?
(b) Is there neural transection present and, if so, is this complete or incomplete?
(c) If neural transection is incomplete: what is the approximate percentage of neural transection. What is the length (in mm) of the gap between the retracted fibres? Is there any fibrosis or neuroma-in-continuity (NIC) present? What is the size of this NIC?
(d) If neural transection is complete: What is the length (in mm) of the gap between the retraced nerve endings? Is there any end fibrosis or end neuroma present at the cut ends of the nerve? If present, what is the size of the neuroma? What is the distance between the visibly normal sections of nerve at either end of the transection? (Fig. 18.5).

Peripheral nerve damage is usually graded according to Seddon and Sunderland, where corresponding signal changes can be seen on MRN (Table 18.1).

However, the Sunderland classification was devised on the basis of neural crush injury. Hence it does not apply to traction injury or penetrating injury which is the most common in practice. It does not, for example, include incomplete neural transection which is a common traumatic neural injury.

> **Key Points**
> - Most neural injury does not require imaging.
> - The main points to consider are as follows: (1) is the nerve injured, i.e. swollen or with altered echotexture or signal intensity; (2) is there neural transection present and, if so, is it partial or complete; and (3) is there a neuroma present.
> - A normal looking nerve or a mildly abnormal nerve on imaging has a good clinical outcome.

Table 18.1 Sunderland grade with commonly used terminology, neural integrity, and MR appearances

Grade	Terminology	Integrity	MRN
I	Neuropraxia	Intact	Hyperintense nerve
II	Axonotmesis (mild)	Axons torn	Hyperintense, thickened with prominent fascicles
III	Axonotmesis (moderate)	+ Endoneurium torn	
IV	Axonotmesis (severe)	+ Perineurium torn	Heterogeneous nerve
V	Neurotmesis	+ Epineurium torn	Complete nerve transection
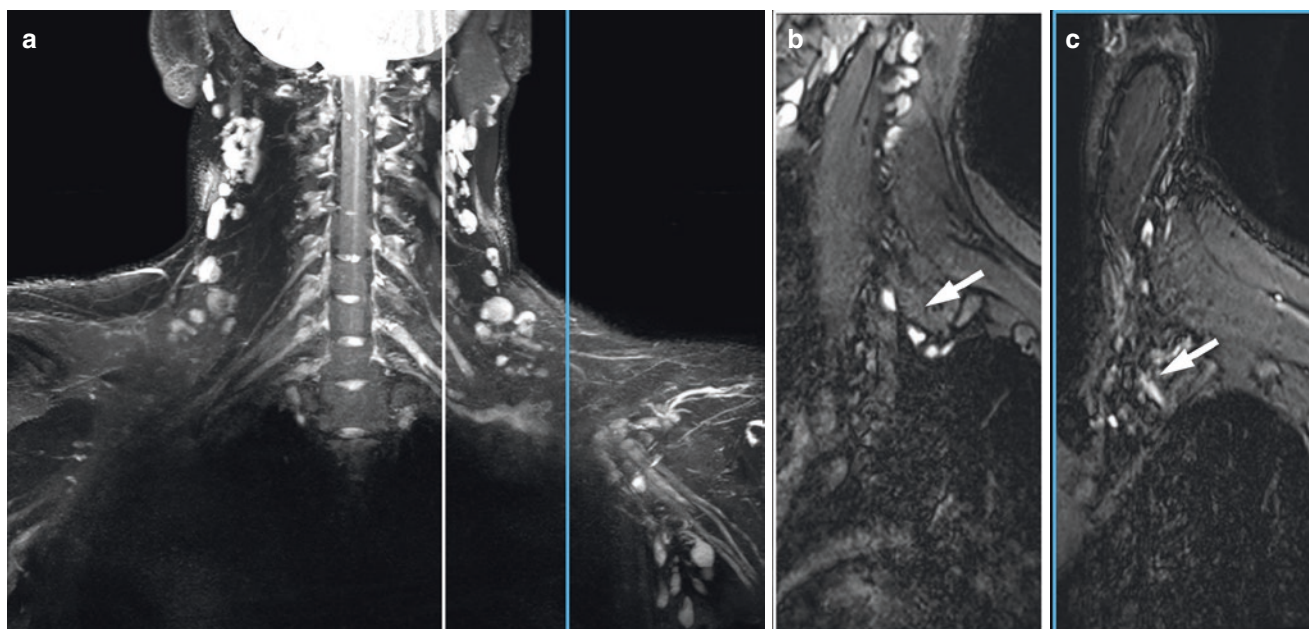
Fig. 18.5 Young man with transection of the entire left brachial plexus following an avalanche injury. (**a**) Coronal MIP of 3D SPACE STIR shows enlarged, retracted nerve stumps with (**b**) small stump neuroma formation (arrow) and (**c**) missing plexal structures more laterally (arrow)

18.5.3 Perineural Fibrosis

Perineural fibrosis is nearly always related to either prior radiation, surgery, or trauma. The most common site of post-irradiation perineural fibrosis is the brachial plexus, following irradiation for breast or nasopharyngeal carcinoma, usually with a 1–2-year latent period before symptoms emerge. The ultrasound and MR appearances of brachial plexopathy are as follows: increased size of the neural elements, poor delineation, obliterated or 'dirty' perineural fat, clumping or adhesions of the neural elements, intraneural or perineural hyperaemia/enhancement, and distortion of the neural and perineural tissues.

The main differential diagnosis, both clinically and on imaging, is metastatic infiltration of the brachial plexus. Metastatic infiltration of the brachial plexus is often, though not always, a feature of end-stage metastatic breast, head and neck, or lung carcinoma and appears, on imaging, as a discrete, often hyperaemic, mass infiltrating or adjacent to the brachial plexus. One may sometimes see metastatic infiltration of adjacent structures, such as the vertebrae or lung apices, as well as accompanying metastatic-type adenopathy. Occasionally, percutaneous biopsy may be necessary to distinguish between nodular post-irradiation fibrosis and metastatic disease. In such cases, this biopsy can be performed safely under ultrasound guidance.

> **Key Points**
> - Radiation is the most common cause of peripheral perineural fibrosis with the brachial plexus being most affected.
> - Imaging appearances of perineural fibrosis are increased size, poor delineation, 'dirty' perineural fat, adhesion, hyperaemia/enhancement, and perineural distortion.

18.5.4 Neuralgic Amyotrophy

Neuralgic amyotrophy (or Parsonage-Turner syndrome) is preferable a term to 'brachial neuritis' as the nerves beyond the brachial plexus are not infrequently affected. Neuralgic amyotrophy is an inflammatory condition of unknown aetiology which, as the name implies, leads to both severe pain and muscle weakness, particularly in the periscapular region though also more peripherally in the upper limb. There is often a preceding trigger such as infection or vaccination. Neuralgic amyotrophy may wax and wane over several months with different nerves being affected. Usually only one side is affected, and even when both upper limbs are affected, it is typically sequential rather than simultaneous. The mixed suprascapular nerve is the most frequently affected nerve. A suprascapular nerve CSA of >4.2 mm² on ultrasound has a sensitivity of 86% and a specificity of 92% for neuralgic amyotrophy.

MRI is excellent at demonstrating the atrophic and denervation changes in the parascapular and other muscles (Fig. 18.6). Ultrasound, on the other hand, is particularly advantageous in allowing ready examination of potentially affected nerves beyond the brachial plexus. Extraplexal nerves that tend to be most affected are the long thoracic, axillary, median, and radial nerves as well as the anterior and posterior interosseous nerves. Affected nerves may show localised neural swelling ± neural fascicular entwinement ± hourglass constriction. These features can be appreciated on US and MR. The hourglass constriction is thought to result from a swollen inflamed nerve becoming twisted with limb movement and being unable to return to a normal position. Hourglass constriction requires surgical intervention. If one sees neural swelling on transverse ultrasound scanning, longitudinal scanning should be performed to evaluate the presence of incomplete or complete hourglass constriction. Similarly, on MRI if the nerve changes in diameter abruptly along its course along with MRN signal

Fig. 18.6 In this patient with neuralgic amyotrophy, there is denervation oedema and moderate atrophy of the supraspinatus and infraspinatus muscles seen on both (**a**) T1-weighted (arrows) and (**b**) T2-weighted STIR images (arrows). (**c**) The suprascapular nerve is slightly thickened with a slightly irregular calibre (arrow) highly suggestive of neuralgic amyotrophy
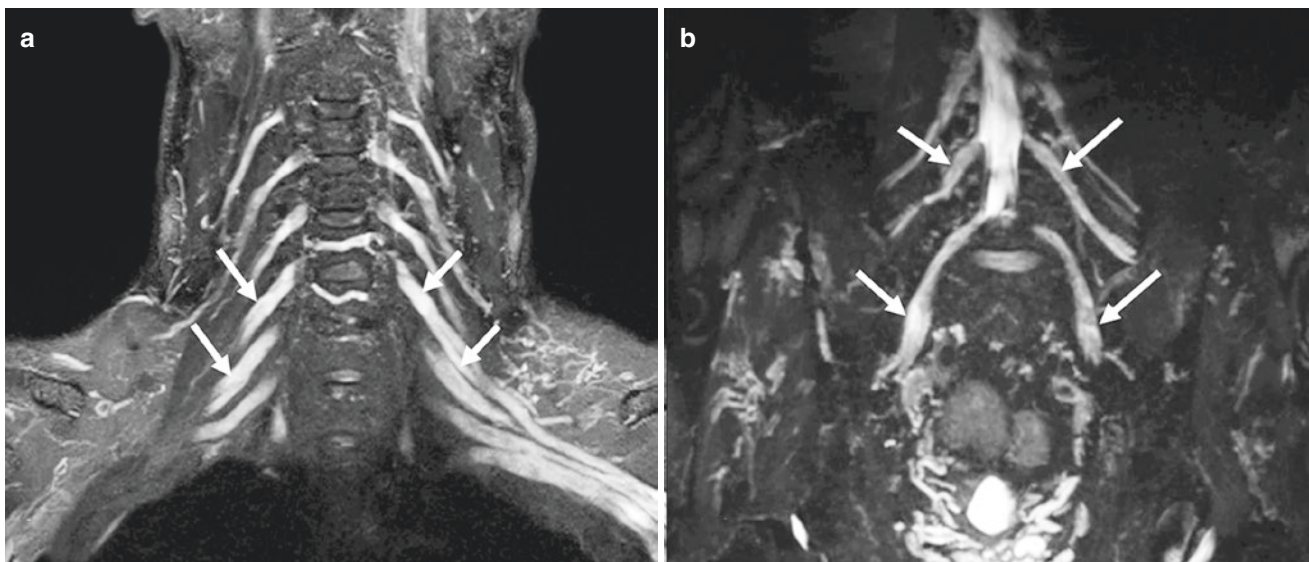
Fig. 18.7 MRN of patient with CIDP and characteristic enlargement of nerve roots and more peripheral plexal components on coronal MIP 3D SPACE STIR images, both in the (**a**) brachial (arrows) and (**b**) lumbosacral plexuses (arrows)

changes from hyper-, to hypo-, to hyperintensity, this may well represent focal hourglass constriction [22].

> **Key Points**
> - Neuralgic amyotrophy commonly affects the supra-scapular nerve though extraplexal nerves are sometimes also affected.
> - The imaging signs are neural swelling and, less frequently, fascicular entwinement ± hourglass constriction of an affected swollen nerve.
> - MR is more accurate than US at showing target muscle denervation.

18.5.5 Inflammatory Neuropathy

Inflammatory neuropathies are amenable to anti-inflammatory treatment. The two main types of inflammatory neuropathy are chronic inflammatory demyelinating polyneuropathy (CIDP) and multifocal motor neuropathy (MMN). CIDP is a mixed neuropathy while MMN is predominantly motor. Both upper and lower limbs tend to be affected. Ultrasound and MR features are increased neural size and muscle denervation ± atrophy (Fig. 18.7). Any brachial trunk size of

>8 mm^2 and swelling of the median nerve >13 mm^2 in the arm or >10 mm^2 in the forearm is 99% specific for inflammatory neuropathy [23]. Multiple sites of nerve swelling may be present.

> **Key Points**
> - Imaging is helpful in assessing inflammatory neuropathy.
> - Bilateral, diffuse, and multifocal involvement is common.

18.6 Concluding Remarks

One can appreciate that imaging of the peripheral nerves comprises a wide pathological spectrum. Imaging has greatly increased our knowledge and perception of peripheral nerve disorders enabling these disorders to be diagnosed and treated with greater clarity and precision. When imaging the peripheral nerves, one needs to be particularly mindful of the patient's history regarding previous trauma, malignancy, surgery, irradiation, as well as neurological symptoms and deficit. Ultrasound and MRI are, in many instances, complementary in this regard with considerable clinical practical benefit.

Take Home Messages
- Ultrasound and MRI are incredibly helpful in the assessment of peripheral nerve disorders.
- High-resolution, targeted imaging is required.
- Usually either imaging modality will suffice, but to fully address some problems, both may be required and are usually complementary in this regard.

References

1. Filler AG, Maravilla KR, Tsuruda JS. MR neurography and muscle MR imaging for image diagnosis of disorders affecting the peripheral nerves and musculature. Neurol Clin. 2004;22:643–82.
2. Wasa J, Nishida Y, Tsukushi S, Shido Y, Sugiura H, Nakashima H, et al. MRI features in the differentiation of malignant peripheral nerve sheath tumors and neurofibromas. AJR Am J Roentgenol. 2010;194:1568–74.
3. Baumer P, Kele H, Kretschmer T, Koenig R, Pedro M, Bendszus M, et al. Thoracic outlet syndrome in 3T MR neurography fibrous bands causing discernible lesions of the lower brachial plexus. Eur Radiol. 2014;24:756–61.
4. Menorca RM, Fussell TS, Elfar JC. Nerve physiology: mechanisms of injury and recovery. Hand Clin. 2013;29:317–30.
5. Stanisz GJ, Midha R, Munro CA, Henkelman RM. MR properties of rat sciatic nerve following trauma. Magn Reson Med. 2001;45:415–20.
6. Husarik DB, Saupe N, Pfirrmann CW, Jost B, Hodler J, Zanetti M. Elbow nerves: MR findings in 60 asymptomatic subjects – normal anatomy, variants, and pitfalls. Radiology. 2009;252:148–56.
7. Kästel T, et al. Magic angle effect: a relevant artifact in MR neurography a 3T? AJNR Am J Neuroradiol. 2016;32(5):821–7.
8. Chhabra A, Lee PP, Bizzell C, Soldatos T. 3 Tesla MR neurography – technique, interpretation, and pitfalls. Skelet Radiol. 2011;40:1249–60.
9. Vargas MI, Viallon M, Nguyen D, Beaulieu JY, Delavelle J, Becker M. New approaches in imaging of the brachial plexus. Eur J Radiol. 2010;74:403–10.
10. Madhuranthakam AJ, Lenkinski RE. Technical advancements in MR neurography. Semin Musculoskelet Radiol. 2015;19:86–93.
11. Kasper JM, Wadhwa V, Scott KM, Rozen S, Xi Y, Chhabra A. SHINKEI – a novel 3D isotropic MR neurography technique: technical advantages over 3DIRTSE-based imaging. Eur Radiol. 2015;25:1672–7.
12. Chhabra A, Soldatos T, Subhawong TK, Machado AJ, Thawait SK, Wang KC, et al. The application of three-dimensional diffusion-weighted PSIF technique in peripheral nerve imaging of the distal extremities. J Magn Reson Imaging. 2011;34:962–7.
13. Guggenberger R, et al. Assessment of median nerve with MR neurography by using diffusion-tensor imaging: normative and pathologic diffusion values. Radiology. 2012;265:194–203.
14. Ng AWH, Griffith JF, Lee RKL, Tse WL, Wong CWY, Ho PC. Ultrasound carpal tunnel syndrome: additional criteria for diagnosis. Clin Radiol. 2018;73(2):214.e11–8.
15. Lee RKL, Griffith JF, Ng AWH, Tipoe GL, Chan AWH, Wong CWY, Tse WL, Ho PC. Cross-sectional area of the median nerve at the wrist: comparison of sonographic, MRI, and cadaveric measurements. J Clin Ultrasound. 2019;47(3):122–7.
16. Ng AWH, Griffith JF, Tong CSL, Law EKC, Tse WL, Wong CWY, Ho PC. MRI criteria for diagnosis and predicting severity of carpal tunnel syndrome. Skelet Radiol. 2020;49(3):397–405.
17. Ng AWH, Griffith JF, Tsai CSC, Tse WL, Mak M, Ho PC. MRI of the Carpal Tunnel 3 and 12 Months After Endoscopic Carpal Tunnel Release. AJR Am J Roentgenol. 2021;216(2):464–70.
18. Rhodes NG, Howe BM, Frick MA, Moran SL. MR imaging of the postsurgical cubital tunnel: an imaging review of the cubital tunnel, cubital tunnel syndrome, and associated surgical techniques. Skelet Radiol. 2019;48(10):1541–54.
19. Bäumer P, Dombert T, Staub F, Kaestel T, Bartsch AJ, Heiland S, Bendszus M, Pham M. Ulnar neuropathy at the elbow: MR neurography—nerve T2 signal increase and caliber. Radiology. 2011;260(1):199–206.
20. Ahlawat S, Blakeley JO, Langmead S, Belzberg AJ, Fayad LM. Current status and recommendations for imaging in neurofibromatosis type 1, neurofibromatosis type 2, and schwannomatosis. Skelet Radiol. 2020;49(2):199–219.
21. Chhabra A, Ahlawat S, Belzberg A, Andreseik G. Peripheral nerve injury grading simplified on MR neurography: as referenced to Seddon and Sunderland classifications. Indian J Radiol Imaging. 2014;24:217–24.
22. Sneag DB, Saltzman EB, Meister DW, Feinberg JH, Lee SK, Wolfe SW. MRI Bullseye sign: an indicator of peripheral nerve constriction in parsonage-turner syndrome. Muscle Nerve. 2017;56(1):99–106.
23. Goedee HS, van der Pol WL, van Asseldonk JH, Franssen H, Notermans NC, Vrancken AJ, van Es MA, Nikolakopoulos S, Visser LH, van den Berg LH. Diagnostic value of sonography in treatment-naive chronic inflammatory neuropathies. Neurology. 2017;88(2):143–51.

Sports-Related Injuries of the Pediatric Musculoskeleton

19

Lower Extremity

Kirsten Ecklund

Learning Objectives
- To recognize unique injuries of the pediatric musculoskeleton commonly associated with athletic activity.
- To differentiate these pathologic entities from imaging features associated with normal growth and development.

19.1 Epiphyseal and Osteochondral Injuries
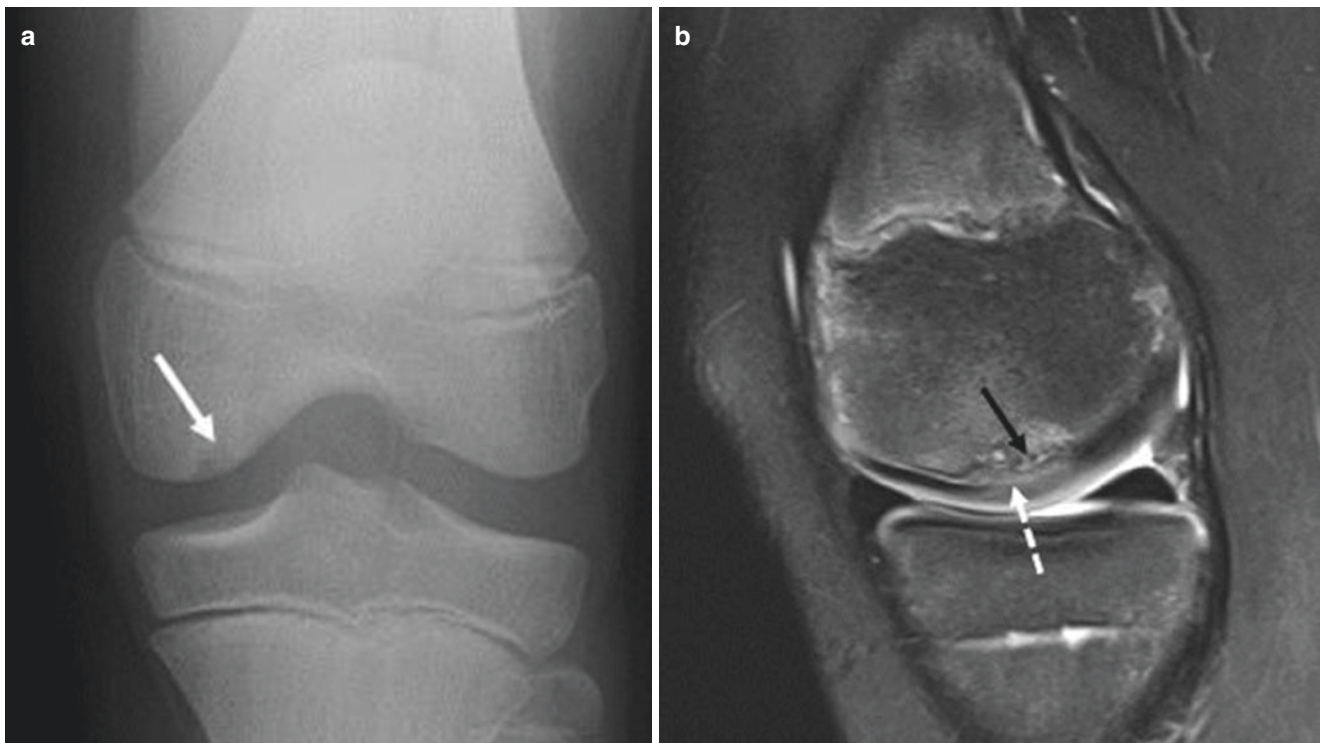
19.1.1 Osteochondritis Dissecans

Osteochondritis dissecans (OCD) was first described in 1888 by Franz Konig [1] as a cause of loose bodies within the joint. Historically, juvenile and adult-onset OCD were felt to represent the same process but with a better prognosis in skeletally immature patients. While the pathogenesis and natural history of juvenile OCD (JOCD) remain uncertain, most agree that it is acquired likely due to repetitive trauma and that it is distinct from osteochondral lesions seen in adults. The term JOCD should be reserved for patients with open physes, typically between the ages of 10 and 15 years. Surgical versus conservative management remains controversial due to the ambiguity around etiology and prognosis. Juvenile OCD of the lower extremity is most frequently encountered in the femoral condyles and the talar dome. Several reports including those from the multi-institutional Research in Osteochondritis dissecans of the Knee (ROCK) Group [2] suggest that the lesion originates within the unos-

sified epiphyseal cartilage with subsequent involvement of the subchondral bone and potentially the articular cartilage [3]. Radiographic findings may include subchondral lucency, marginal sclerosis, and osteochondral bony sequestrum partially or fully separated from the parent bone (Fig. 19.1a).

Numerous MR imaging classifications, most notably the De Smet classification [4], exist with the aim of assessing stability of the OCD. These have primarily focused on breach of the articular cartilage and fluid insinuating between the parent bone and the bony progeny as signs of instability. More recently, high-resolution MR with detailed description of the lesion is being used to assess healing and prognosis. The chondral "fragment" is better termed the progeny of the parent bone, and ossification of the progeny is a sign of healing. Fluid signal intensity sandwiched between the parent bone and unossified epiphyseal cartilage, linear vertical low signal intensity in the overlying articular cartilage, and full-thickness defects are poor prognostic signs (Fig. 19.1b).

Normal developmental ossification of the femoral condyles may be confused with OCD, though it is typically seen in children. Radiographically the femoral condylar ossification centers may appear irregular, fragmented, and spiculated. MR imaging features of developmental ossification rather than OCD include location in the posterior condyle as opposed to the intercondylar notch, accessory ossification centers, a large amount of residual epiphyseal cartilage, and lack of bone marrow edema [5] (Fig. 19.2). Additionally, disruption of the trilaminar secondary ossification center (SOC) physis overlying chondral abnormality, best seen on fat-suppressed fluid-sensitive sequences, is indicative of JOCD [6] (Figs. 19.1 and 19.2). This finding is most helpful in young children with substantial residual epiphyseal cartilage.

In children less than 6 years of age, physiologic T2 hyperintensity will be seen in the posterior epiphyseal cartilage of both medial and lateral femoral condyles, likely related to advancing ossification within the cartilaginous epiphysis.

K. Ecklund (✉)
Department of Radiology, Boston Children's Hospital, Boston, MA, USA
e-mail: kirsten.ecklund@childrens.harvard.edu

Fig. 19.1 (**a**, **b**) Osteochondritis dissecans in a 10-year-old soccer player with knee pain. The frontal radiograph (**a**) shows subchondral lucent lesion with marginal sclerosis involving the weight-bearing, intercondylar notch region of the medial femoral condyle (white arrow). The sagittal T2-weighted image with fat suppression (**b**) shows increased signal in the overlying epiphyseal cartilage, disruption of the overlying secondary physis (white dashed arrow), and subchondral marrow edema. Hyperintense T2 signal at the bone-cartilage interface (black arrow) and subchondral fibrovascular foci are further signs of JOCD and likely indicate poorer prognosis
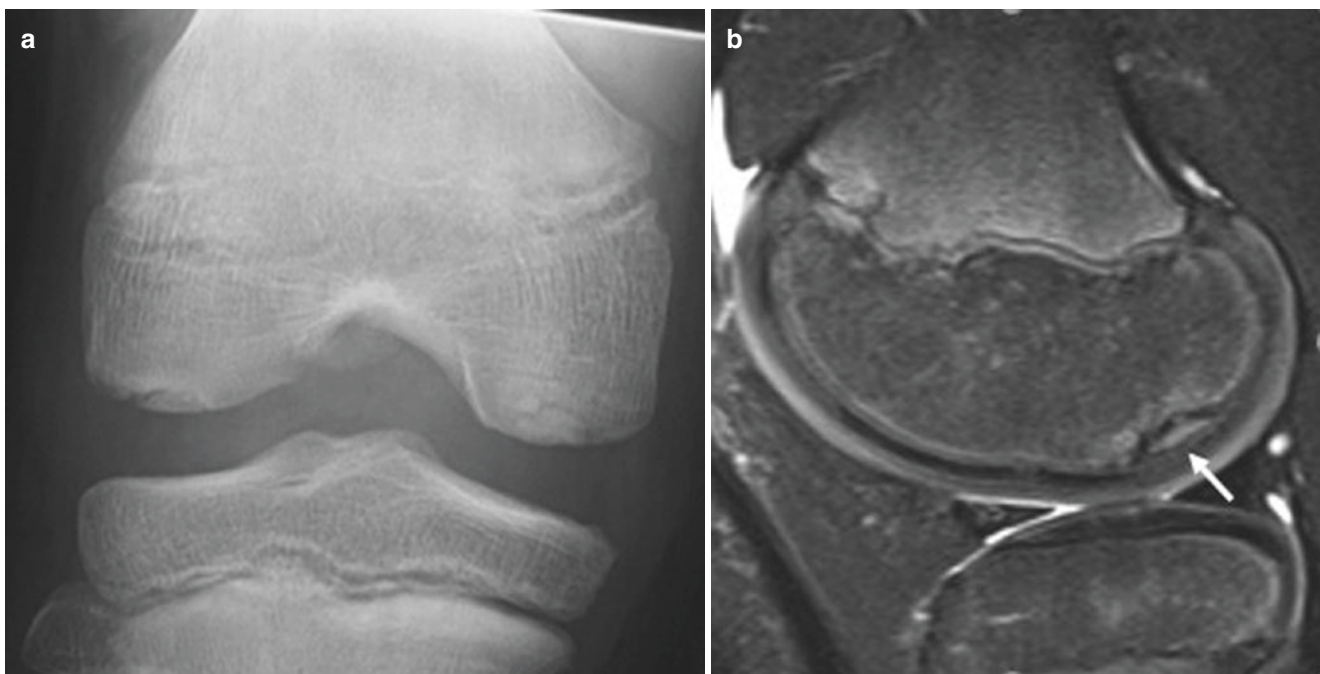
Fig. 19.2 (**a**, **b**) Normal developmental ossification in a 12-year-old baseball player with anterior knee pain after sliding into base. The frontal radiograph (**a**) and sagittal T2-weighted image with fat suppression (**b**) show osteochondral irregularity in the non-weight-bearing, posterior aspects of the medial and lateral femoral condyles. The MR features which favor developmental ossification rather than JOCD include posterior location, intact overlying secondary physis (arrow), and minimal subchondral marrow edema
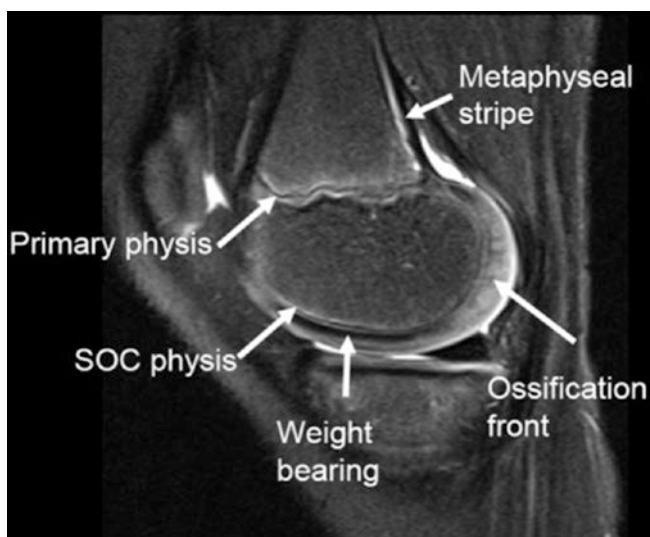
Fig. 19.3 Normal MR signal variation in a 7-year-old boy. Sagittal T2-weighted image with fat suppression shows the normal trilaminar primary and secondary (SOC) physes. Low signal intensity in the weight-bearing epiphyseal cartilage is thought to be due to desiccation of free water, while higher signal in the posterior cartilage relates to the metabolically active ossification front. The image also shows the normal hyperintense metaphyseal stripe reflecting vascular tissue between the periosteum and subchondral bone. Axially, this structure is circumferential and has the appearance of a metaphyseal ring or collar (not shown)

In these young children, low signal intensity is normally seen in the inferior aspect of the cartilaginous epiphysis, presumably due to weight-bearing [7]. This normal maturation process should not be confused with osteochondral injury (Fig. 19.3). Additionally, physiologic focal increased fluid signal intensity in the epiphyseal cartilage is common just prior to ossification and has been termed the "pre-ossification center" [8]. Misinterpretation of developmental variants as OCD may, in part, account for the higher rate of spontaneous resolution of juvenile OCD compared to the adult form.

> **Key Points**
> **MRI features suggestive of normal variant, not OCD**
> - Posterior location (not intercondylar).
> - Absent bone marrow edema.
> - Accessory ossification centers and spiculated cortical margins.
> - Intact secondary ossification center physis.
> - Young age; large amount of epiphyseal cartilage.

19.1.2 Acute Osteochondral Fractures

Acute traumatic chondral injuries are significantly more common than meniscal and anterior cruciate ligament injuries in the immature knee. In patients with open physes, femoral condylar injuries are more common than patellar and femoral trochlea [9]. Low-grade chondral injuries can be subtle with chondral thickening and abnormal signal intensity. MR has a higher sensitivity for the detection of more severe lesions with full-thickness chondral or osteochondral fracture. Subchondral bone marrow edema, best seen on fat-suppressed fluid-sensitive sequences, should alert the radiologist to scrutinize the overlying articular cartilage for associated injury (Fig. 19.4). The images should be scrutinized for free intra-articular fragments. In contrast to OCD, these acute injuries always involve the articular cartilage with or without extension to the epiphyseal cartilage and subchondral bone. As a reminder, T2 hyperintensity in the femoral condylar epiphyseal cartilage posteriorly in young children represents normal signal variation associated with the advancing ossification front [10] and should not be misinterpreted as chondral injury.

19.2 Avulsion Injuries

Avulsion injuries in children are most frequent during puberty and adolescence, when the physis is the weakest region of the musculoskeleton. In this age group, acute apophyseal avulsion fractures are more common than ligament and tendon injury. Unlike epiphyses, apophyses are growth centers which do not contribute to linear growth and are sites of tendon or ligament attachment. Acute, displaced apophyseal avulsion fractures may result from sudden, forceful muscle contraction. In contrast, myotendinous forces applied to the apophysis due to repetitive activity may lead to microavulsion at the interface between the bony apophysis and adjacent cartilaginous physis. Associated inflammation identified on MR imaging as increased fluid signal in the apophysis, physis, and soft tissues is termed traction apophysitis [11]. Acute and repetitive overuse apophyseal injuries are most common in the pelvis but are also commonly seen at the knee and ankle.

Acute patellar sleeve fractures, named for the sleeve of unossified cartilage which surrounds the osseous patella, are avulsion injuries at the inferior and rarely superior poles of the patella at the sites of patellar and quadriceps tendon attachment which occur with forceful quadriceps contraction against resistance, usually with a flexed knee. Radiographic features of the much more common inferior patellar sleeve
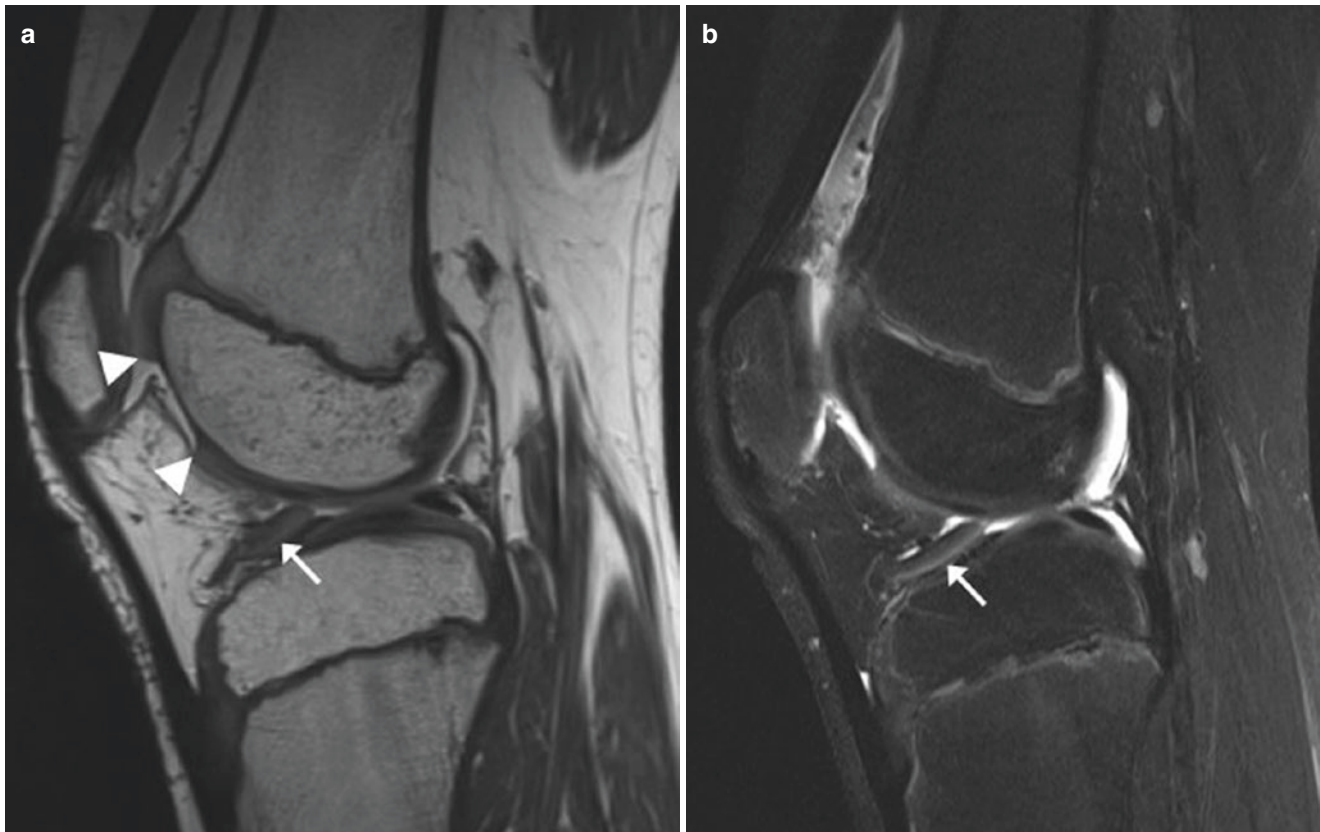
Fig. 19.4 (**a**, **b**) Acute osteochondral fracture in an 11-year-old boy who fell onto his knee playing soccer. Sagittal proton density WI (**a**) and T2-weighted image with fat suppression (**b**) reveal a large osteochondral defect (margins marked by arrowheads) in the anterior medial femoral condyle. The displaced osteochondral fracture fragment is in the anterior joint, sitting atop the tibial plateau (arrow). Note the absence of subchondral marrow edema related to normally limited epiphyseal vascularity

fracture include patella alta, a sliver-like patellar fracture fragment, joint effusion, and soft tissue swelling (Fig. 19.5a, b). MRI maybe performed to confirm the integrity of the patellar tendon and will also show the chondral component of the fracture, which if large is an indicator of operative fixation. Chronic avulsive stress at the same location results in inferior patellar traction apophysitis, called Sinding-Larsen-Johansson disease. The MR and radiographic appearances can be similar to a nondisplaced patellar sleeve fracture; however, there is no history of an acute traumatic event (Fig. 19.5c, d).

Apophyseal injury at the opposite end of the patellar tendon, the tibial tubercle insertion, can also be acute leading to a Salter-Harris type II or III fracture through the tubercle physis or chronic resulting in Osgood-Schlatter traction apophysitis (Fig. 19.5e). Radiographs show soft tissue swelling overlying the tibial tubercle, while MR images show marrow edema in the tibial tubercle and fluid signal in the distal patellar tendon and infrapatellar bursa. Fragmentation of the tubercle often reflects normal developmental ossification and should not be used to make the diagnosis of Osgood-Schlatter. The term "jumper's knee," used to describe patellar tendon pathology, should be reserved for skeletally mature patients with fused physes.

Traction apophysitis at the Achilles tendon calcaneal insertion is termed Sever's disease. Calcaneal apophyseal sclerosis is a manifestation of physiologic stress associated with weight-bearing and is not an indication of apophysitis. As with Osgood-Schlatter, MR imaging features include fluid in the distal Achilles tendon and the adjacent retrocalcaneal bursa, overlying soft tissue swelling, and marrow edema within the apophysis.

While the incidence of anterior cruciate ligament (ACL) tears in adolescent athletes, especially females, has increased dramatically in the last two decades, acute avulsion fracture of the tibial eminence ACL attachment is common in younger skeletally immature children, especially boys ages 8–14 years old, when the intercondylar eminence is incompletely ossified [12]. The Meyers and McKeever classification is most commonly used to describe the epiphyseal osteochondral displacement: type I, nondisplaced; type II, posteriorly hinged attachment with elevation of the anterior margin of the fragment; type III, completely displaced; and type IV, comminuted or rotated fragment [13]. MR images should be
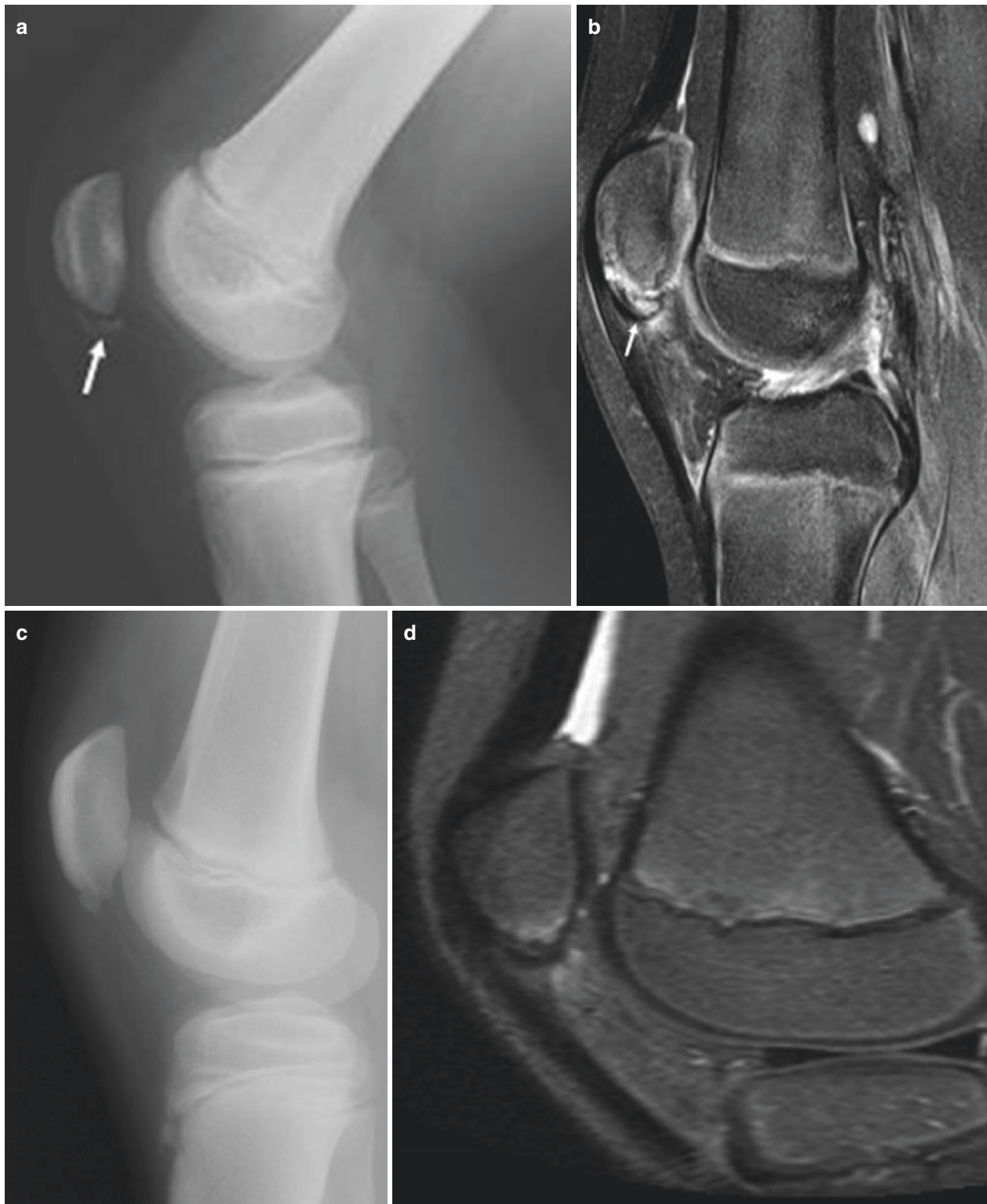
Fig. 19.5 (**a**, **b**) Acute patellar sleeve frature: Lateral radiograph (**a**) and sagittal T2-weighted image with fat suppression (**b**) in 11 y.o. boy with acute anterior knee pain after landing on his flexed knee when tackled from behind in football show a thin inferior patellar fracture fragment (arrow) and associated marrow and soft tissue. The patellar tendon is intact. (**c**, **d**) Proximal patellar tendon traction apophysitis, Sinding-Larsen-Johansson: Lateral radiograph (**c**) and sagittal T2-weighted image with fat suppression (**d**) in a 9 y.o. female ice skater with months of inferior patellar pain show fragmentation and marrow edema in the inferior patella and as well as subtle edema in the proximal patellar tendon and in the superior aspect of Hoffa fat pad. The history differentiates this from patellar sleeve fracture. (**e**) Distal patellar tendon traction apopysitis, Osgood-Schlatter: The final sagittal T2-weighted image with fat suppression (E) in 13 y.o. hockey player with 6 weeks of tibial tubercle pain, tenderness to palpation, and recent growth spurt shows intense marrow edema within a hypertrophied tibial tubercle. Associated edema is present in the distal patellar tendon and inferior Hoffa fat pad
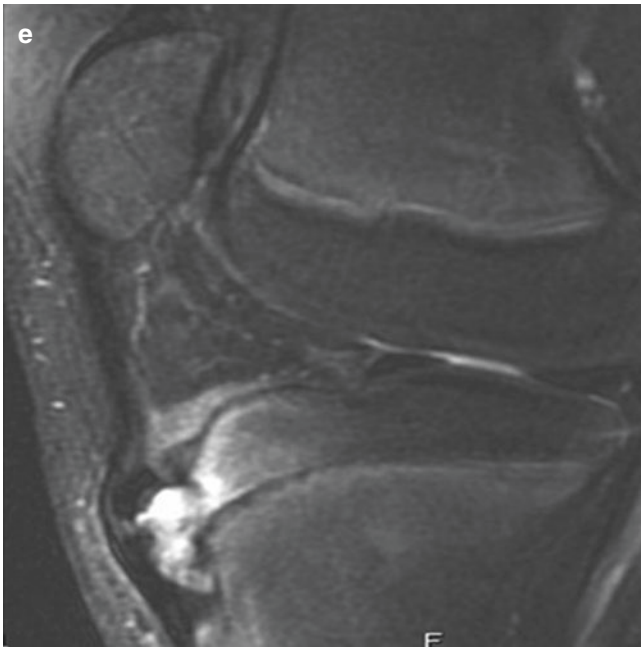
Fig. 19.5 (continued)

scrutinized for impingement of the transverse intermeniscal ligament, anterior horn of the medial meniscus, or anterior horn of the lateral meniscus between the fracture fragment and the donor site, impediments to closed reduction (Fig. 19.6).

> **Key Points**
> **Traction Apophysitis**
> - Patients must have open physes.
> - MR shows edema in the apophysis and overlying soft tissues and fluid in the tendon at the apophyseal attachment.
> - Fragmentation or irregularity of the apophysis can be normal.
> - Acute apophyseal fractures may have a similar appearance and are distinguished by history of trauma.

19.3 Physeal Fractures

The physis, or growth plate, is an exclusively cartilaginous structure throughout growth. As such, it is the weakest component of the bone-joint unit in children. Mechanical forces which result in ligamentous or tendinous injury in adults tend to cause physeal fractures in children. This is especially true in early adolescence when the physis becomes wider due to increased metabolic activity associated with the phys-

iologic growth spurt. Simultaneous increased athletic endeavors in many middle and upper school children further predisposes to growth plate fractures [8]. The Salter-Harris classification of growth plate fractures was initially described in 1963 and remains widely used. Type I is a fracture confined to the physis. Type II involves the physis and metaphysis. Type III extends from the epiphysis into the epiphysis. Type IV is an obliquely oriented fracture which extends through both the metaphysis and epiphysis, traversing the physis. Type V is a crush injury of the physis [14]. More than 30% of pediatric long bone fractures involve the physis with approximately 15% going on to develop post-traumatic growth arrest [15]. The risk of growth disturbance is less related to the Salter-Harris type than to the specific physis with lower extremity locations and those with undulating physes most at risk. When the fracture plane separates the physis from the epiphysis and disrupts the blood supply, vascular communications between the epiphysis and metaphysis may develop allowing a bony bridge to form across the physis. Large, central bridges lead to limb shortening, while smaller, peripheral bridges lead to angular deformity. In the lower extremity, physeal fractures are most common in the distal tibia with up to a third resulting in growth arrest (Fig. 19.7).

Distal femoral and proximal tibial physeal fractures are often radiographically occult, identified only when MR imaging is performed for persistent post-traumatic knee pain. These images should be scrutinized for widening and increased fluid signal within the physis and disruption of the perichondrium indicating nondisplaced fracture. Associated stripped periosteum can become entrapped within the injured physis and be an impediment to closed reduction [16] (Fig. 19.8).

19.4 Physeal Overuse Stress Injury

Growth disturbance can also occur from chronic repetitive overuse trauma in young athletes. Physeal dysfunction without premature transphyseal bone bridge formation occurs secondary to recurrent microtrauma leading to vascular compromise and disruption of enchondral ossification. Unossified bands or tongues of hypertrophic physeal cartilage extend into the metaphysis. Radiographically, this appears as physeal widening and irregularity. MR images in these patients show focal or band-like physeal widening and T2 hyperintensity related to the excess unossified cartilage as well as edema. The normal trilaminar appearance of the physis is disrupted in the area of injury. The most well-described locations of these injuries are the distal radius and olecranon in gymnasts and the proximal humerus in pitchers; however, similar physeal stress injury occurs in the knees in child athletes involved in football, basketball, soccer, gymnastics, and tennis [17]. Similarly, MR images in these children with knee pain show focal bands of physeal cartilage signal

Fig. 19.6 (**a**–**c**) Acute tibial eminence avulsion fracture. Lateral radiograph (**a**), coronal T1-weighted image (**b**), and sagittal T2-weighted image with fat suppression (**c**) in a 12-year-old girl who crashed while ski racing. The tibial spine fracture plane is clearly delineated (arrows). The anterior cruciate ligament is intact and attached to the avulsed uplifted, displaced fragment (Meyers-McKeever type III). Note the transverse meniscal ligament interposed between the fracture fragment and donor site anteriorly (dashed arrow)

Fig. 19.7 (**a–d**) Salter-Harris II fracture with premature growth arrest. This 11-year-old girl landed on her inverted ankle when doing gymnastics on a trampoline. Lateral radiograph (**a**) at the time of injury shows the fracture plane through the physis anteriorly and extending through the metaphysis posteriorly. MR sagittal proton density (**b**) and 3D gradient echo steady state with fat suppression sagittal (**c**) and coronal (**d**) reformats 11 months after the fracture reveal a bone bridge with fatty marrow signal intensity (arrow, **b**) traversing the physis anteriorly, interrupting the normally high signal intensity physeal cartilage (* **c**, **d**). The growth recovering line (dashed arrow, **b**) tethered to the bone bridge indicates absent growth anteriorly and normal growth posteriorly
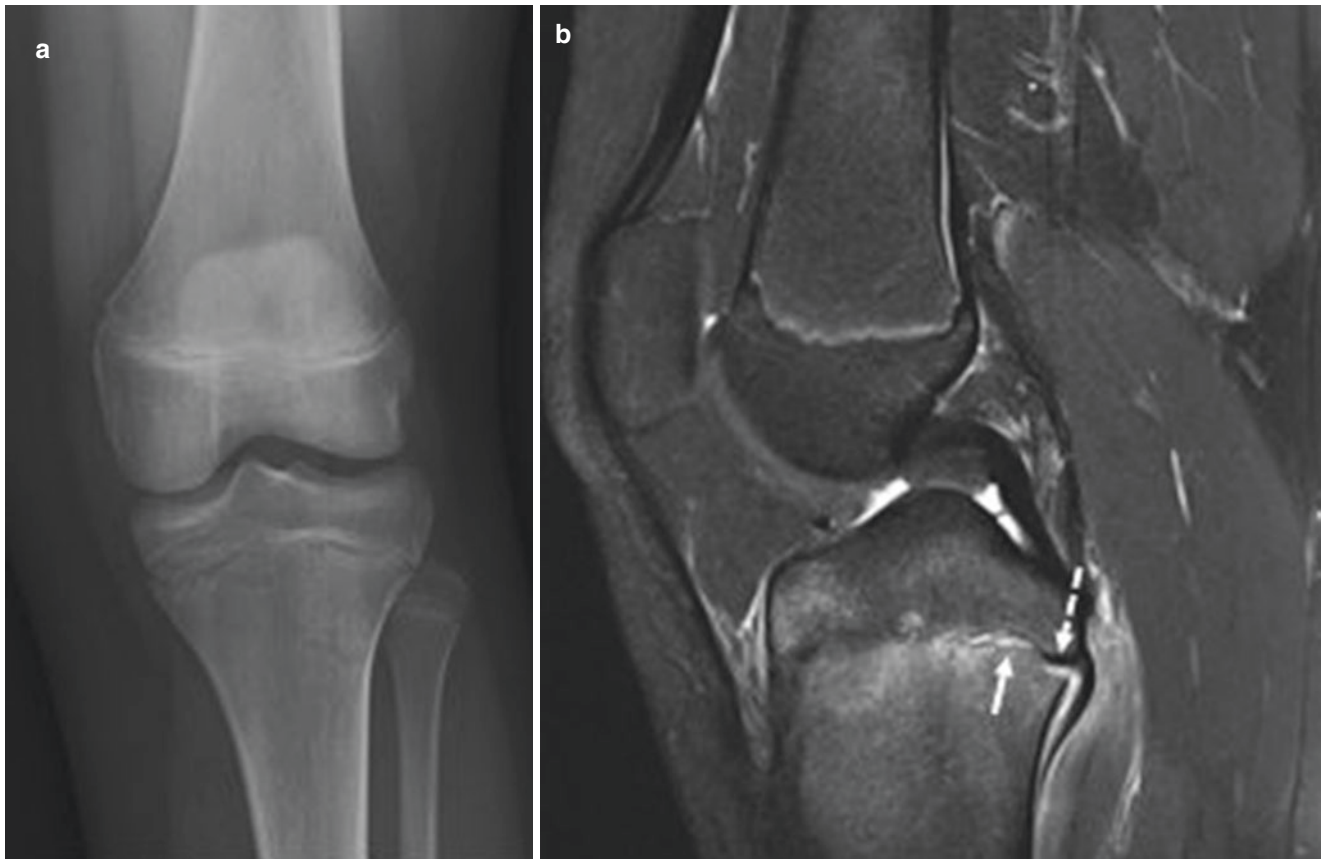
Fig. 19.8 (**a**, **b**) Radiographically occult proximal tibial fracture. AP radiograph (**a**) in a 13-year-old girl with lateral knee pain after colliding with another player in a soccer game shows no abnormality. MR sagittal T2-weighted image with fat suppression (**b**) obtained 1 week later for evaluation of persistent pain shows hyperintense fluid signal in the widened posterior physis (arrow) and marrow edema in the periphyseal epiphysis and metaphysis. Importantly, a low signal intensity linear structure within the posterior physis (dashed arrow) represents stripped periosteum which has become entrapped in the physis and may be an impediment to closed reduction

extending into the distal femoral, proximal tibial, and proximal fibular metaphyses (Fig. 19.9). The abnormalities are medial or lateral depending upon the sport. The clinical symptoms and imaging findings of these chronic physeal stress injuries tend to resolve in 1 to 2 months with strict rest and/or immobilization. Continuation of athletic activity leads to persistent pain and growth disturbance with malalignment. Importantly, these abnormalities should not be confused with focal periphyseal edema (FOPE) zones commonly seen in the proximal tibia and distal femur in adolescence thought to be a manifestation of early physiologic physeal closure [18]. FOPE zones are predictably seen just prior to the normal physeal fusion, age range 11–15 years (Fig. 19.10). While FOPE zones may be symptomatic, they do not require treatment, and they resolve as normal physeal fusion progresses.

> **Key Points**
> **Physeal Injuries**
> - Acute physeal fractures may lead to growth arrest with bony bridging across the open physis.
> - Post-traumatic growth arrest is more dependent upon the specific anatomic location (distal femur, distal tibia, proximal tibia most common) than on the Salter-Harris type.
> - Overuse or repetitive stress injury of the physis results in bands or tongues of unossified physeal cartilage extending into the metaphysis.
> - Do not confuse normal physiologic FOPE zones with physeal injury.
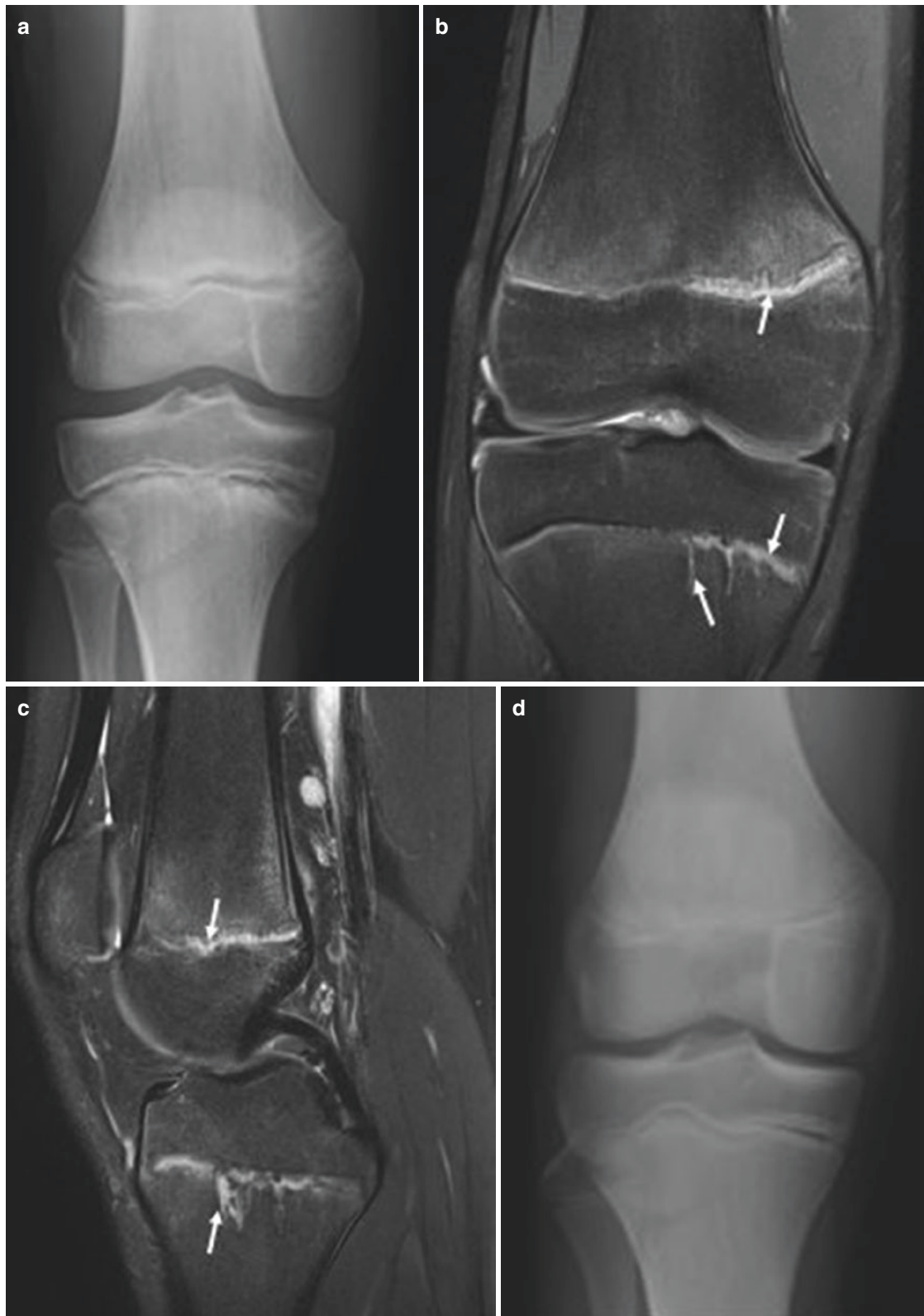
Fig. 19.9 (**a–d**) Overuse physeal stress injury. A 14-year-old ice hockey player with 3 months of knee pain. AP radiograph (**a**) shows medial physeal widening in the distal femur and proximal tibia. Coronal PD fat-suppressed (**b**) and sagittal T2-weighted fat-suppressed (**c**) images show medial physeal widening and hyperintensity (arrows). The high signal reflects unossified physeal cartilage that seems to extend into the metaphysis. The cartilage may be band-like, as in the femur, or more spiculated and tongue-like, as in the tibia. The AP radiograph (**d**) obtained 3 months later after strict rest shows normalization of the physes
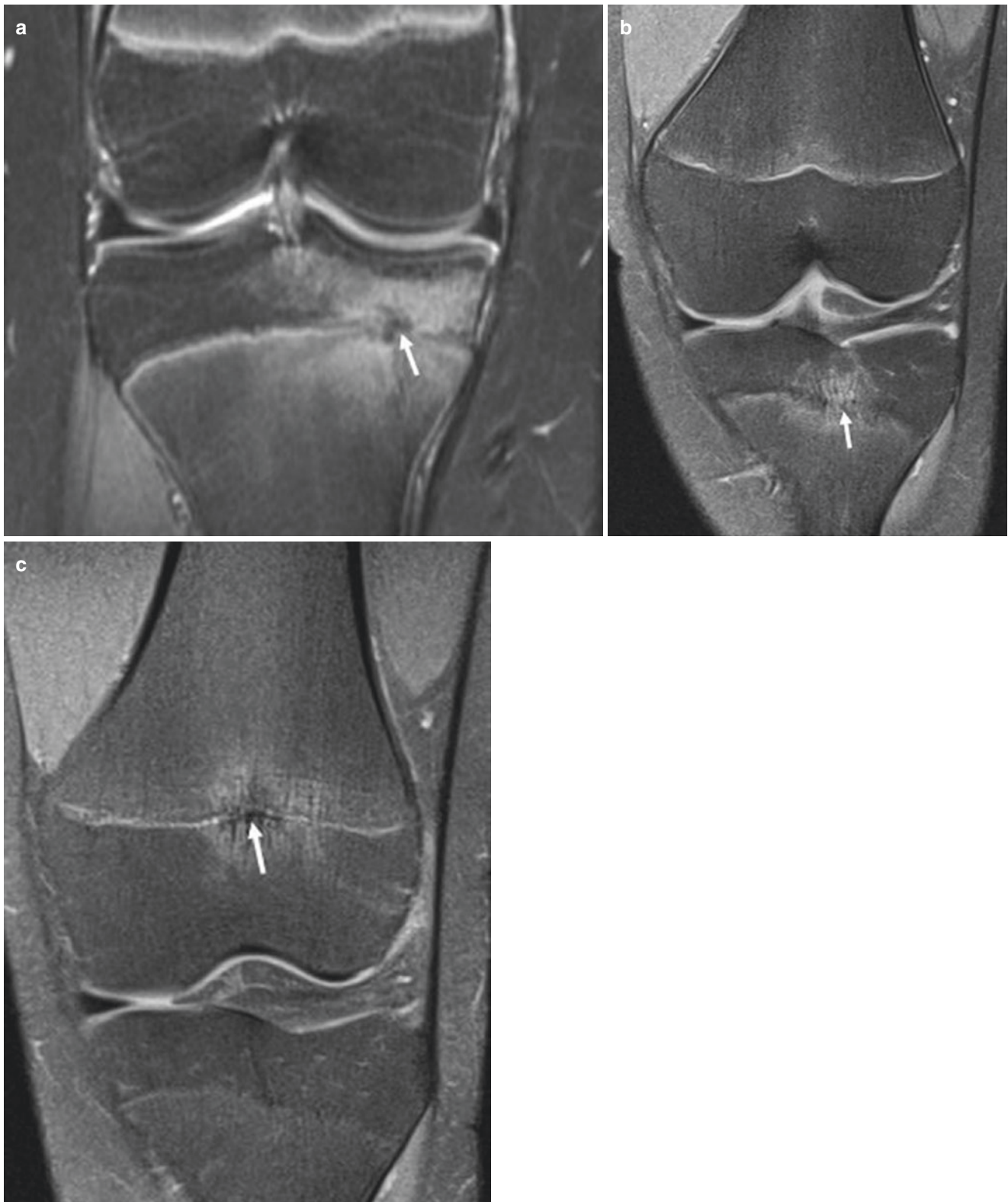
Fig. 19.10 (**a–c**) Focal periphyseal edema (FOPE) zones. Coronal PD fat-suppressed MR image (**a**) in a 13-year-old ballet dancer with medial knee pain shows marked bone marrow edema within the medial epiphysis and metaphysis centered around the fusing proximal tibial physis (arrow). Cor PD fat-suppressed MR image (**b**) in a 14-year-old female asymptomatic research volunteer shows similar but less intense edema around the fusing proximal tibial physis (arrow). One year later (**c**) the tibial physis has fused normally and the edema has resolved. A new FOPE zone is present in the distal femoral physis centrally (arrow). This is consistent with the normal growth pattern—the proximal tibial physis fuses approximately 1 year prior to distal femoral fusion. Periphyseal edema should only be ascribed to this phenomenon in adolescents with normally fusing physes
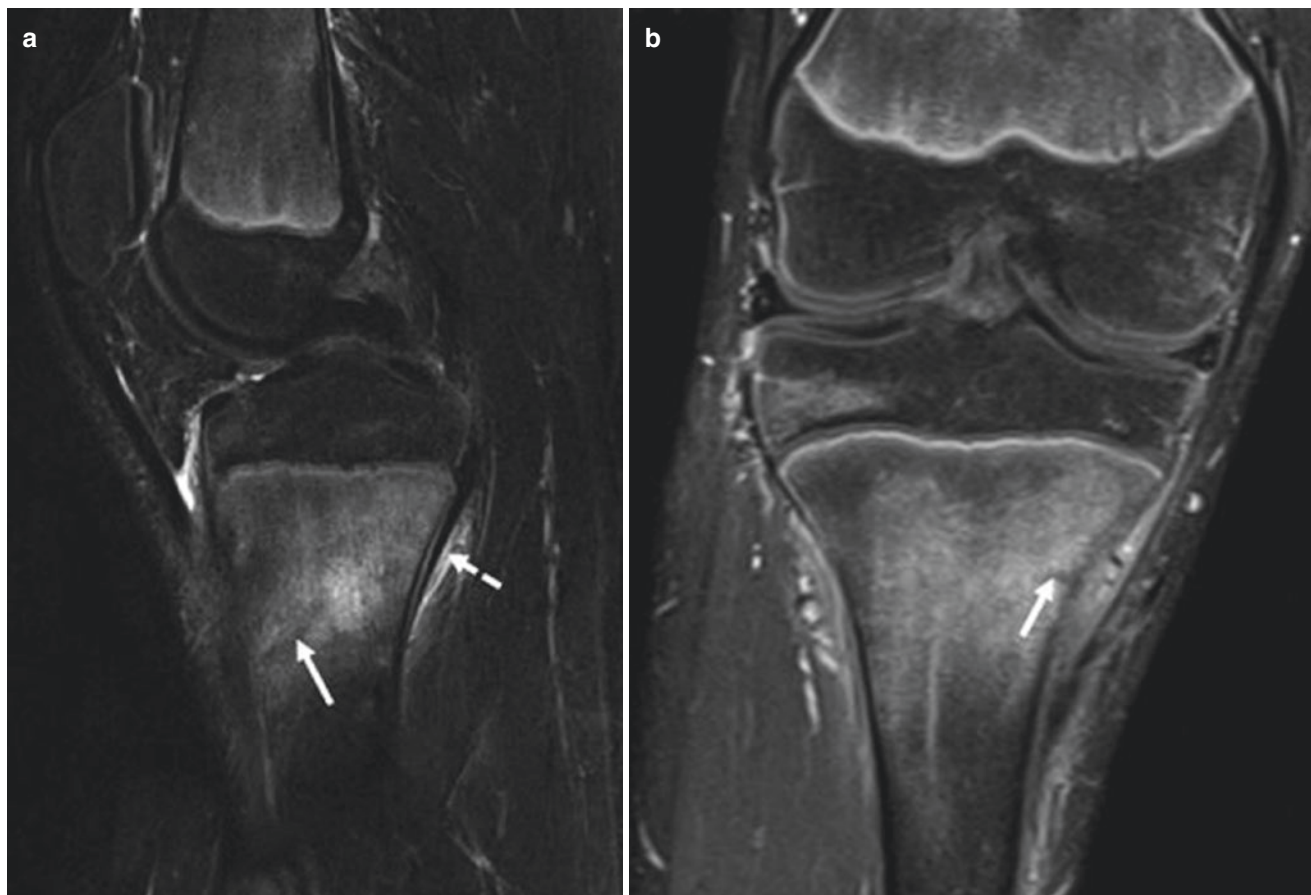
Fig. 19.11 (**a**, **b**) Tibial stress fracture. Sagittal T2 fat-suppressed MR image (**a**) in a 14-year-old boy with proximal tibial pain in the setting of increased lacrosse training shows metaphyseal marrow edema with a subtle low signal intensity oblique line centrally (arrow) and posterior periosteal fluid (dashed arrow). The coronal T1 fat-suppressed post-contrast MR image (**b**) more clearly identifies the medial cortical fracture line (arrow). Contrast is generally unnecessary for stress injury evaluation but, when administered, nicely outlines fracture lines

19.5 Long Bone Stress Injuries

Stress fractures and stress reactions in children, once considered rare, are seen with increasing frequency presumably related to increased participation in athletics. Stress is the force applied to a bone that arises from weight-bearing and from muscular contractions. Lower muscle mass, decreased bone mineral density, and thinner cortices in addition to hormonal influences predispose the immature skeleton to stress injury. A 7-year prospective study of 6831 adolescent girls found a nearly 4% incidence of stress fractures with high-impact activities (running, basketball, cheerleading, and gymnastics) as significant risk factors [19]. Almost 50% of all stress fractures in athletic children are tibial, with the remainder occurring in the fibula, femur, metatarsals, and tarsal bones. Unfortunately, the sensitivity of early radiographs is as low as 15% and delayed radiographs only reveal findings in 50% of patients. At MR imaging, STIR sequences and T2-weighted sequences with frequency selective fat saturation are exquisitely sensitive to the high signal intensity periosteal and marrow edema associated with stress reactions. A low signal intensity line within the high signal marrow edema allows the lesion to be upgraded to a stress fracture (Fig. 19.11). This line allows the lesion to be confidently identified as a stress fracture. Multidector CT with long-axis reformations can also be very helpful in delineating the occult fracture lucency.

19.6 Concluding Remarks

With the increased participation of children in athletics, radiologists are more frequently asked to assist in the diagnosis and management of acute and chronic injury to the growing skeleton. Initial radiographic assessment is often sufficient. However, we are increasingly expected to accurately evaluate soft tissue, ligamentous, tendinous, and cartilaginous injuries in competitive child athletes. MRI is often required for evaluation of injury to these radiolucent structures. Familiarity with the normal MR appearance of the growing

musculoskeleton is essential to accurate interpretation of these imaging studies in young athletes. Accurate diagnosis and management are critical to mitigate the impact upon the growth mechanism and associated lifelong disability.

> **Take Home Messages**
> - MR depiction of normal musculoskeletal development must be differentiated from physeal and osteochondral injury.
> - Overuse injuries in children are more common than previously realized.
> - Growth disturbance associated with acute and overuse injuries can lead to lifelong morbidity.

References

1. König F. Ueber freie Körper in den Gelenken. Deutsche Zeitschrift für Chirurgie. 1888;27(1):90–109. https://doi.org/10.1007/BF02792135.
2. Edmonds EW, Polousky J. A review of knowledge in osteochondritis dissecans: 123 years of minimal evolution from Konig to the ROCK study group. Clin Orthop Relat Res. 2013;471(4):1118–26. https://doi.org/10.1007/s11999-012-2290-y.
3. Ellermann J, Johnson CP, Wang L, Macalena JA, Nelson BJ, LaPrade RF. Insights into the epiphyseal cartilage origin and subsequent osseous manifestation of juvenile osteochondritis dissecans with a modified clinical MR imaging protocol: a pilot study. Radiology. 2017;282(3):798–806. https://doi.org/10.1148/radiol.2016160071.
4. De Smet AA, Ilahi OA, Graf BK. Reassessment of the MR criteria for stability of osteochondritis dissecans in the knee and ankle. Skelet Radiol. 1996;25(2):159–63. https://doi.org/10.1007/s002560050054.
5. Gebarski K, Hernandez RJ. Stage-I osteochondritis dissecans versus normal variants of ossification in the knee in children. Pediatr Radiol. 2005;35(9):880–6. https://doi.org/10.1007/s00247-005-1507-6.
6. Laor T, Zbojniewicz AM, Eismann EA, Wall EJ. Juvenile osteochondritis dissecans: is it a growth disturbance of the secondary physis of the epiphysis? AJR Am J Roentgenol. 2012;199(5):1121–8. https://doi.org/10.2214/AJR.11.8085.
7. Laor T, Jaramillo D. MR imaging insights into skeletal maturation: what is normal? Radiology. 2009;250(1):28–38. https://doi.org/10.1148/radiol.2501071322.
8. Jaimes C, Chauvin NA, Delgado J, Jaramillo D. MR imaging of normal epiphyseal development and common epiphyseal disorders. Radiographics. 2014;34(2):449–71. https://doi.org/10.1148/rg.342135070.
9. Oeppen RS, Connolly SA, Bencardino JT, Jaramillo D. Acute injury of the articular cartilage and subchondral bone: a common but unrecognized lesion in the immature knee. AJR Am J Roentgenol. 2004;182(1):111–7. https://doi.org/10.2214/ajr.182.1.1820111.
10. Varich LJ, Laor T, Jaramillo D. Normal maturation of the distal femoral epiphyseal cartilage: age-related changes at MR imaging. Radiology. 2000;214(3):705–9. https://doi.org/10.1148/radiology.214.3.r00mr20705.
11. Bedoya MA, Jaramillo D, Chauvin NA. Overuse injuries in children. Top Magn Reson Imaging. 2015;24(2):67–81. https://doi.org/10.1097/RMR.0000000000000048.
12. Merrow AC, Reiter MP, Zbojniewicz AM, Laor T. Avulsion fractures of the pediatric knee. Pediatr Radiol. 2014;44(11):1436–45; quiz 3-6. https://doi.org/10.1007/s00247-014-3126-6.
13. Meyers MH, Mc KF. Fracture of the intercondylar eminence of the tibia. J Bone Joint Surg Am. 1959;41-A(2):209–20; discussion 20–2.
14. Salter RB, Harris WR. Injuries involving the epiphyseal plate. JBJS. 1963;45(3):587–622.
15. Peterson HA. Physeal fractures: Part 3. Classification. J Pediatr Orthop. 1994;14(4):439–48. https://doi.org/10.1097/01241398-199407000-00004.
16. Chen J, Abel MF, Fox MG. Imaging appearance of entrapped periosteum within a distal femoral Salter-Harris II fracture. Skelet Radiol. 2015;44(10):1547–51. https://doi.org/10.1007/s00256-015-2201-x.
17. Laor T, Wall EJ, Vu LP. Physeal widening in the knee due to stress injury in child athletes. AJR Am J Roentgenol. 2006;186(5):1260–4. https://doi.org/10.2214/AJR.04.1606.
18. Zbojniewicz AM, Laor T. Focal Periphyseal Edema (FOPE) zone on MRI of the adolescent knee: a potentially painful manifestation of physiologic physeal fusion? AJR Am J Roentgenol. 2011;197(4):998–1004. https://doi.org/10.2214/AJR.10.6243.
19. Field AE, Gordon CM, Pierce LM, Ramappa A, Kocher MS. Prospective study of physical activity and risk of developing a stress fracture among preadolescent and adolescent girls. Arch Pediatr Adolesc Med. 2011;165(8):723–8. https://doi.org/10.1001/archpediatrics.2011.34.

Non-traumatic Musculoskeletal Diseases in Children

20

Rutger A. J. Nievelstein

Learning Objectives
- To gain knowledge about the differences between the pediatric and adult musculoskeletal system.
- To learn how these differences will result in differences in clinical and radiological presentation of musculoskeletal diseases in children.
- To discuss the optimal imaging strategies for specific disease entities in the pediatric musculoskeletal system.

20.1 Introduction

The pediatric musculoskeletal system differs from the adult musculoskeletal system in many ways, which accounts for many unique features in pediatric musculoskeletal imaging. These unique features include:

- *Anatomical differences*: such as growth plates with surrounding epiphyses and metaphyses and differences in vascular supply (the Haversian canals in pediatric bones are relatively larger and more extensive compared to adults).
- *Physiological differences*: such as increased metabolism at the metaphyses related to growth and physiological subperiosteal new bone formation in infants.
- *Psychological differences*: in case of pain, young children experience the uncomfortable sensation, but they are not worried by it and do not seek medical attention themselves. Instead they try to relief the pain by crying, limp-

ing, or disuse, and this is what is noted by the parents. Moreover, young children usually cannot give an appropriate history. Finally, "referred pain" is more often seen in children than in adults: for example, pain in the knee in a young child may be the result of referred pain from the distal tibia (e.g., a toddler fracture) or from the hip (e.g., in Perthes disease).

In addition to these differences, several pathologies in the musculoskeletal system are unique for the pediatric age and do not or seldomly occur in adults (except for some late sequelae). These include congenital and hereditary disorders, many inborn errors of metabolism and skeletal dysplasias, and some subtypes of bone and soft tissue tumors.

These differences between the pediatric and adult musculoskeletal system can result in differences in clinical and radiological presentation. Therefore, radiologists who deal with children require specific knowledge and skills, including knowledge of the (combination of) imaging modalities of first choice to answer the clinical question and optimization of the imaging techniques used (while limiting the risks of ionizing radiation, sedation, and unnecessary biopsies). In this chapter on non-traumatic pediatric musculoskeletal diseases, we will focus on (a) hip pathologies, (b) infectious and inflammatory diseases, and (c) bone and soft tissue tumors.

20.2 Hip Pathologies [1–4]

20.2.1 Developmental Dysplasia of the Hip (DDH) [3–7]

Developmental dysplasia of the hip (DDH), also known as congenital hip dysplasia (CHD), is one of the commonest musculoskeletal pathologies in the newborn. It is a developmental (and not a congenital!) disease of the hip as newborns with normal hips at birth can be affected later during infancy. Therefore, CHD is a misnomer and should be avoided.

R. A. J. Nievelstein (✉)

Department of Radiology & Nuclear Medicine, Division Imaging & Oncology, Wilhelmina Children's Hospital – University Medical Center Utrecht & Princess Maxima Center of Pediatric Oncology, Utrecht, Utrecht, The Netherlands
e-mail: r.a.j.nievelstein@umcutrecht.nl

DDH occurs in approximately 1:1000 live births with a female predominance. The left hip is more commonly involved than the right hip, and it can occur bilaterally. Risk factors include breech position during pregnancy (girls 12%, boys 2.6%) and a positive family history (girls 4.4%, boys 0.9%). Clubfoot has been thought to be a risk factor but this no longer holds true.

Ultrasound (US) is the imaging technique of first choice in infants younger than 6–9 months of age with suspicion of DDH. After this age the physiological ossification of the femoral epiphyses usually obscures an adequate overview of the entire hip joint and a pelvic X-ray is preferred. With US we are looking at the same anatomic structures as on a pelvic X-ray, with the advantage of also displaying the cartilaginous structures of the hip joint (Fig. 20.1). DDH on US is classified according to the Graf classification in types I–IV based on the morphology of the iliac bone, including the shape of the acetabulum, the bony and cartilaginous acetabular rim, labrum, and position of the femoral head (Table 20.1). It has been shown that US can also be used for guidance and follow-up of manually as well as operatively reduced dislocated dysplastic hips.

20.2.2 Transient Synovitis (Coxitis Fugax) [1, 2]

Transient synovitis of the hip is an aseptic inflammation. It is the most common cause of hip pain or limping in children under the age of 10 years and is thought to have a postviral etiology. Although limping or hip pain is usually the only complaint at presentation, affected children might be mildly ill or recently have suffered from a low-grade upper respiratory tract infection. Transient synovitis is a self-limiting disease, usually only requiring rest and analgesics as treatment. Although imaging is not strictly indicated, an US is often performed to confirm the diagnosis and/or rule out other causes. The only finding on US is a (small) joint effusion. Pelvic X-ray is only indicated when other differential diagnoses are considered. In case of a sick child, a septic arthritis should always be considered.

20.2.3 Legg-Calvé-Perthes Disease (Perthes Disease) [2–4, 8–10]

Perthes disease is an idiopathic avascular necrosis of the proximal femoral epiphysis. It typically occurs between the

Table 20.1 Graf's classification for developmental dysplasia of the hip (short version) [4, 5]

Type	α angle[a]	Additional features
Type I	>60°	
Type IIa	50–59°	Appropriate for age
Type IIb	50–59°	Inappropriate for age
Type IIc	43–49°	
Type D	43–49°	Decentering hip
Type III	<43°	Eccentric hip
Type IV	<43°	Inverted labrum

[a]The α angle is a measurement of the bony roof of the acetabulum on ultrasound
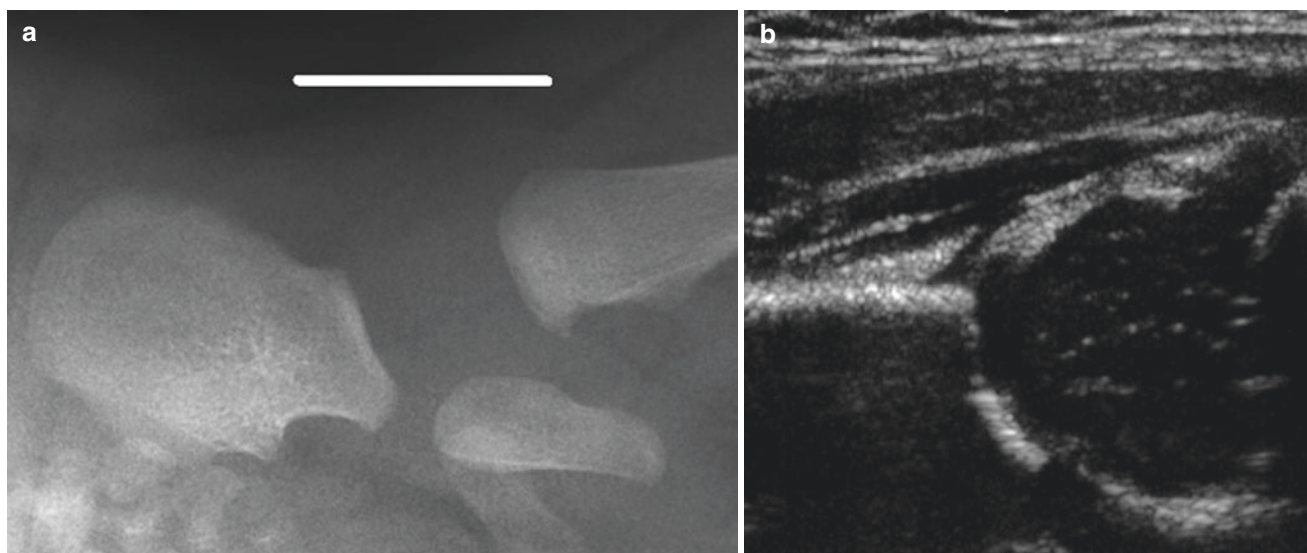
Fig. 20.1 Illustration of how the ultrasound (US) of the hip in DDH is performed (**a**) and displayed (**b**). The white horizontal line projected on the X-ray of the pelvis (**a**) represents the position of the US transducer. (Courtesy of S.G.F. Robben, MUMC, Maastricht, the Netherlands)
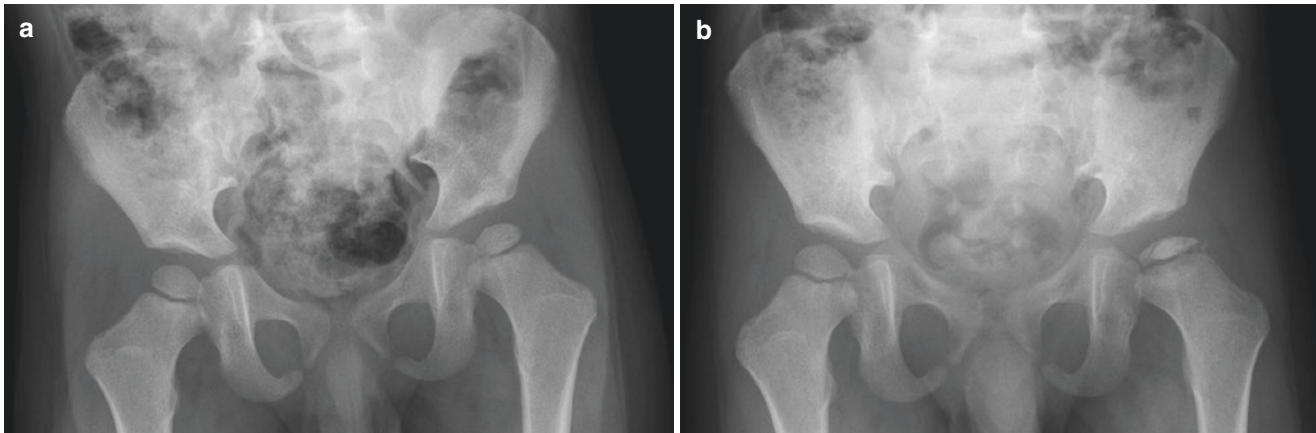
Fig. 20.2 Pelvic X-rays in Perthes disease. (**a**) In the early phase, only subtle flattening and sclerosis of the epiphysis of the left hip is seen. (**b**) A few months later progressive flattening with fragmentation and sclerosis of the epiphysis has developed

age of 5 and 8 years (range 3–12 years) with a male predominance. Although usually unilateral, Perthes disease can occur bilaterally. In bilateral cases its presentation is usually asymmetric in contrast to epiphyseal skeletal dysplasias. On US a joint effusion can be the only sign in early stages. Other US findings include collapse and fragmentation of the epiphysis and atrophy of the quadriceps muscles (due to disuse). Pelvic X-ray is, however, the most commonly used imaging modality in (suspicion of) Perthes disease but might be normal or show only subtle flattening of the epiphysis in early stages (Fig. 20.2). In later stages, progressive flattening and collapse, sclerosis, and subchondral fractures can develop, best appreciated on the frog-leg lateral view. Furthermore, metaphyseal lucencies can occur. During the healing phase, Perthes disease often results in a broad femoral head and collum (also called coxa magna) with a secondary enlarged and somewhat shallow acetabulum. Magnetic resonance imaging (MRI) can be performed but is usually only indicated in complex cases in which surgical reconstruction is considered. In the early phase, MRI will show bone marrow edema in the proximal femoral epiphysis on T2-weighted images with loss of high (fatty) bone marrow signal on T1-weighted images. A subchondral (and sometimes radiographically occult) fracture can be detected on MRI as a double rim sign on T2-weighted images with fat saturation. Furthermore, joint effusion may be present and the cartilage may become hypertrophic. Although treatment is usually conservative and symptomatic, sometimes surgical reconstruction is indicated (e.g., Salter osteotomy) to prevent development of early osteoarthritis. Besides epiphyseal skeletal dysplasias, the most important differential diagnostic consideration should include secondary avascular necrosis (due to corticosteroid therapy, sickle cell anemia, SLE or as complication of hip dysplasia treatment). In the latter, the clinical information will usually help to distinguish it from Perthes disease.

20.2.4 Slipped Capital Femoral Epiphysis (SCFE) [2–4, 9]

Slipped capital femoral epiphysis (SCFE) is an idiopathic Salter-Harris type 1 epiphysiolysis of the proximal femoral epiphysis. It more commonly affects boys and obese children with a typical age at presentation between 12 and 15 years. In approximately one-third of cases, SCFE occurs bilaterally. On imaging the epiphysis is displaced posteriorly and slightly medially, which is best appreciated on the frog-leg lateral view (Fig. 20.3). To prevent further slippage, SCFE is treated by surgical fixation. Avascular necrosis of the femoral head is a potential complication.

> **Key Point**
> • Ultrasound (US) and conventional radiography (CR) are the imaging modalities of first choice in pediatric patients with suspicion of hip pathology.

20.3 Infectious and Inflammatory Diseases

20.3.1 Osteomyelitis [11–16]

Infections of the bone and bone marrow are rare in children with a reported incidence of approximately 1:5000 children. More than half of the cases occur in children under 5 years of age, and boys are twice as often affected than girls. The lower limb is involved in over 70% of cases with the knee as most common location. It is usually mono-ostotic at presentation but can be polyostotic, particularly in neonates (22%) and infants (6.8%). Children with hemoglobinopathies (e.g., sickle cell disease) and immunodeficiencies are at increased risk of developing osteomyelitis.

Osteomyelitis usually develops via hematogenous spread, often after a minor trauma. Other routes of infection include direct inoculation and local extension from contiguous soft tissue infection. The most common organism involved is *Staphylococcus aureus*. Less frequently, β-hemolytic *Streptococcus*, *Streptococcus pneumonia*, *Escherichia coli*, *Pseudomonas aeruginosa*, and *Haemophilus influenzae* are cultured from blood or aspirates, although the incidence of *Haemophilus influenzae* osteomyelitis has decreased dramatically since the introduction of HIB vaccination. In neonates, *Enterobacteria* and *Candida albicans* can also cause osteomyelitis, and in infants *Kingella kingae* is increasingly cultured. It should be mentioned, however, that blood cultures are only positive in 30–50% of cases.

The presentation of osteomyelitis in children is age-dependent and related to the developing skeleton. In infants diaphysial vessels still penetrate the growth plate to reach the epiphysis, facilitating epiphyseal and joint infections in this age group. In contrast, in older children, the growth plate constitutes a barrier for the diaphysial vessels. These vessels terminate at the metaphysis in slow flow venous sinusoidal lakes, predisposing the metaphysis as the starting point for acute hematogenous osteomyelitis. Furthermore, because the periosteum is less firmly attached to the cortex in infants and children than in adults, elevation will be more pronounced in childhood osteomyelitis. Sequestration is infrequently seen and rare in neonates.

When osteomyelitis is suspected, conventional radiography (CR) is usually the modality of first choice (Fig. 20.4a). In the early phase, soft tissue swelling is often the only sign detected, as bone destruction and periosteal reaction become obvious only 7–10 days after the onset of disease and periosteal thickening is a late finding. With US, cortical defects and subperiosteal as well as juxtacortical soft tissue swelling and abscesses can be easily detected. The detection of these abscesses is important as these patients often require US-guided or surgical drainage instead of antibiotics only. Although computed tomography (CT) will demonstrate osseous changes earlier than CR, it is not a preferred technique because of its higher radiation dose. However, CT is superior to other imaging modalities (including MRI) in visualizing osseous destruction, gas in the bone, and bone sequestration. Because of its excellent soft tissue contrast, MRI is an invaluable imaging technique for more clearly demonstrating intra- and extraosseous extension of the osteomyelitis, particularly in complex cases (Fig. 20.4b). Imaging characteristics include ill-defined low T1 and high T2 signal intensity of the bone marrow, periosteal thickening, poorly defined soft tissue planes, lack of cortical thickening, and poor interface between normal and abnormal marrow. Another imaging sign that can be seen are the so-called "fatty globules" in the infected bone marrow best seen on T1-weighted sequences.

Fig. 20.3 Frog-leg view of the pelvis demonstrating the posterior and slightly medially displaced epiphysis of the left hip in slipped capital femoral epiphysis (SCFE)
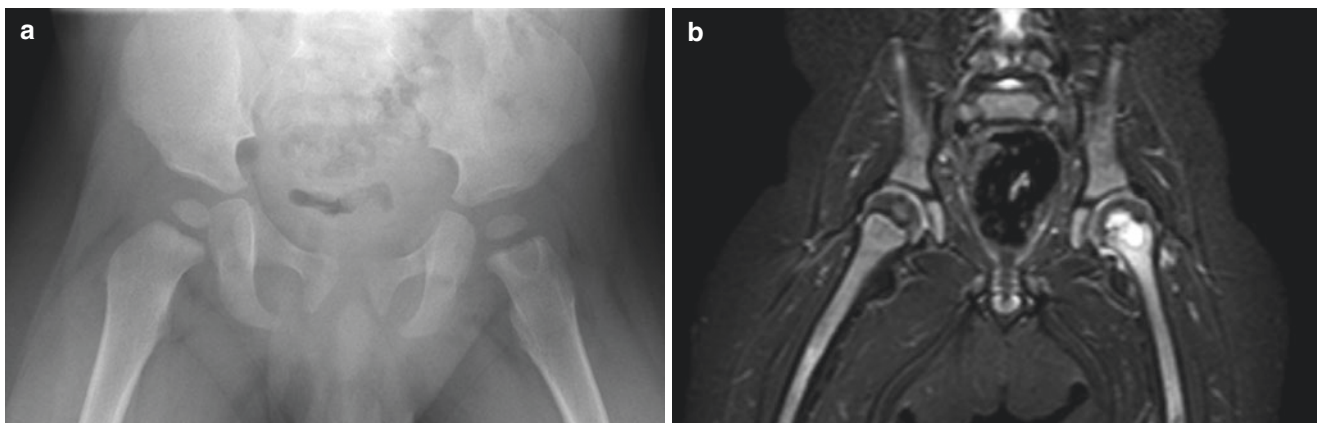
Fig. 20.4 Osteomyelitis in a 1-year-old boy with fever and left limb pain. (**a**) Pelvic X-ray demonstrating a metaphyseal located radiolucency suspicious of osteomyelitis. (**b**) Coronal T2 STIR-weighted MR image of the pelvis and hip nicely illustrating the involvement of both the metaphyses and epiphysis of the left hip with surrounding bone marrow edema, joint effusion, and only minor soft tissue changes

The use of gadolinium is mandatory and increases the diagnostic confidence as well as the detection of (small) abscesses and draining sinuses. Nuclear medicine (including 99mTc-methylene diphosphonate scintigraphy (99mTc-MDP scintigraphy) or 18F-fluorodeoxyglucose positron emission tomography/CT (18F-FDG-PET/CT)) can be used for the detection of osteomyelitis but at the expense of higher radiation doses. These techniques are usually reserved for those cases where the site of infection is unclear or if MRI is not possible or available (e.g., because of sedation/anesthesia).

20.3.2 (Spondylo)discitis [17]

Spondylitis or (spondylo)discitis in children is usually a low-grade infection of the vertebral body and/or intervertebral disc. The average age at diagnosis is 2–8 years, which is explained by the fact that the vascularization of the vertebral bodies in young children is made up of vessels across the cartilaginous vertebral plate and into the ring. After the age of 8 years, these vessels disappear, but a rich anastomotic network of vessels remains in the periphery of the disc until adolescence. (Spondylo)discitis in children mainly involves the lumbar and lumbosacral spine. Many organisms can cause spondylodiscitis, but again positive cultures are only seen in up to 50% of cases. In the early stages of the disease, CR has low sensitivity and specificity. The first radiological signs include intervertebral disc space narrowing with indistinct endplates on either side and eventually destruction of the endplates, but these signs can occur for the first time up to 2–8 weeks after the onset of symptoms. MRI is the imaging modality of choice in case of (suspected) (spondylo)discitis, demonstrating signal intensity abnormalities in the intervertebral disc and adjacent vertebral bodies. Paravertebral soft tissue extension (including abscesses) can also be easily seen.

20.3.3 Septic Arthritis [14, 16, 18]

Intra-articular infections in children are most commonly caused by hematogenous spread of microorganisms into the joints. However, in infants direct extension into the joint space from adjacent osteomyelitis can also cause septic arthritis, due to the diaphysial vessels that still penetrate the growth plate to reach the epiphysis. The hip joint is the most frequent location, followed by the knee, shoulder, and elbow. Early diagnosis is mandatory to prevent cartilage destruction, joint deformity, growth disturbance, and eventually premature arthrosis. As in osteomyelitis, the most common etiologic organism is *Staphylococcus aureus*. Other etiologic organisms include group A *Streptococcus* and *Streptococcus pneumoniae*, group B *Streptococcus* and *Escherichia coli* (in neonates), and *Neisseria gonorrhoeae* in adolescents.

As many children do not present with an obvious clinical picture, imaging is important to detect septic arthritis and give additional information of the suspected joint. CR has low sensitivity and specificity for septic arthritis, can be normal, or can demonstrate joint space widening with adjacent soft tissue swelling. US is a very sensitive technique for the detection of joint effusion, and small amounts up to 1 ml can be detected. However, the specificity toward the diagnosis is poor as neither the amount nor the echogenicity of the effusion can distinguish infectious from noninfectious effusion. On the other hand, the absence of joint effusion virtually excludes septic arthritis. Again, MRI is very sensitive for the detection of joint effusions and synovial disease. In the early stage of the infection, the joint effusion tends to have a non-specific T2 high signal intensity, whereas in later stages, it tends to have a more intermediate and heterogeneous signal intensity. Fat suppression sequences after intravenous gadolinium injection will show synovial enhancement. Moreover, MRI can demonstrate cartilage destruction and adjacent soft tissue involvement.

> **Key Point**
> - The clinical and radiological presentation of osteomyelitis, (spondylo)discitis, and septic arthritis in children is age-dependent and related to the developing skeleton.

20.3.4 Soft Tissue Infections [19, 20]

This includes cellulitis, soft tissue abscesses, pyomyositis, and necrotizing fasciitis. In children there is a predilection of these types of infections for the extremities. The most common etiologic organisms are *Staphylococcus aureus* and *Streptococcus pyogenes*. The preferred imaging techniques to investigate these infections include US (including color Doppler imaging) and MRI (including contrast-enhanced and diffusion-weighted imaging) because of their high spatial resolution and excellent soft tissue contrast. A detailed discussion falls beyond the scope of this chapter and the interested reader is referred to the literature.

20.3.5 Chronic Recurrent Multifocal Osteomyelitis (CRMO) [21–23]

Chronic recurrent multifocal osteomyelitis (CRMO) or chronic nonbacterial osteomyelitis is a rare and poorly understood disease that primarily occurs in late childhood and adolescence. It is believed to be the pediatric variant of SAPHO syndrome, which is a combination of synovitis,

acne, pustulosis, hyperostosis, and osteitis. The exact etiology is unknown although it is thought to be an autoimmune disorder. CRMO most commonly affects the lower limbs followed by the pelvis, spine, and anterior chest wall (including the claviculae). MRI is the imaging modality of choice showing nonspecific multifocal and often symmetric bone marrow signal intensity changes (T1 hypointense and T2 hyperintense), usually located in the metaphysis of the long bones, and with minimal soft tissue involvement. MRI is especially useful to demonstrate the extent of the disease, detecting asymptomatic sites in up to 20% of cases. CR has low sensitivity and specificity but may demonstrate focal lysis at the involved sites, reactive hyperostosis, and periosteal reaction.

20.3.6 Juvenile Idiopathic Arthritis (JIA)
[18, 24–27]

Juvenile idiopathic arthritis (JIA) encompasses seven subtypes of (aseptic) arthritis with onset before the age of 16 years and persistence of symptoms for more than 6 weeks (Table 20.2). Its prevalence varies between 0.07 and 4.01 per 1000 children. JIA most commonly involves the knee, followed by the ankle, wrist, hand, and others. The etiology and pathophysiology of JIA are still not completely understood. Early manifestations of JIA include synovial inflammation, causing periarticular demineralization and joint effusion. Ongoing inflammation will result in synoviocyte prolifera-

tion, increased metabolic requirements, and neovascularization which causes pannus formation. Furthermore, it is thought that autoantibody depositions and degradative enzyme activation lead to cartilage damage and bone changes, which in the end can progress to joint space narrowing and ankyloses.

Traditionally, CR is used to assess the bone (osteopenia, periostitis, erosions), joint (narrowing, effusion, synovitis), and growth (malalignment, length discrepancy) abnormalities in JIA. Recently introduced pediatric scoring systems have increased the value of CR in JIA. However, as CR can be normal or only show minor changes early in the disease and outcome and prognosis correlate with early initiation of treatment, there is an increasing emphasis on the detection of articular inflammation before radiographically detectable changes occur. This is much better evaluated with US and MRI. Several studies have shown that US outperforms clinical evaluation in the identification of synovitis and in distinguishing joint disease from tenosynovitis. US appears to be particularly useful in the evaluation of deeper joints, such as the hip, and smaller complex joints, such as the ankle, midfoot, and wrist. Imaging findings on US include synovial hypertrophy (uniform, nodular, fibrous stands, villi), joint effusion, and increased color Doppler signal. It is good to realize that isolated joint fluid is not specific for articular inflammation because joint effusion is common in healthy children; e.g., it is present in up to 60% of knees and often seen in at least one joint of the wrist. Tenosynovitis is another imaging finding that is frequently seen in JIA, characterized

Table 20.2 Subtypes of juvenile idiopathic arthritis (JIA) according to the Revised Criteria of the International League of Associations for Rheumatology [24]

Subtype	Definition	Frequency (%)	Age at onset	Sex ratio
Systemic arthritis	Presence of arthritis accompanied or preceded by daily fever of at least 2-week duration plus at least one of the following: typical evanescent erythematous rash, hepatomegaly or splenomegaly, generalized lymphadenopathy, or serositis	4–17%	Throughout childhood	F = M
Oligoarthritis	≤4 joints affected during the first 6 months of disease, subtypes: – Persistent: confined to ≤4 joints throughout the disease course – Extended: extension to >4 joints after first 6 months of the disease	27–56%	Early childhood	F >>> M
Polyarthritis, RF negative	≥5 joints affected during first 6 months of disease and absence of IgM RF	11–28%	Biphasic: 2–4 years 6–12 years	F >> M
Polyarthritis, RF positive	≥5 joints affected during first 6 months of disease and presence of IgM RF on at least two occasions more than 3 months apart	2–7%	Late childhood or adolescence	F >> M
Psoriatic arthritis	Combination of arthritis and typical psoriatic rash or (if rash is absent) presence of arthritis and any two of the following: family history of psoriasis in a first-degree relative, dactylitis, or nail pitting	2–11%	Biphasic: 2–4 years 9–11 years	F > M
Enthesitis-related arthritis	Enthesitis and/or arthritis; most common sites of enthesitis are calcaneal insertion of the Achilles tendon, plantar fascia, and tarsal area; arthritis commonly affects joints of lower extremities; sacroiliac involvement and lumbosacral spine may occur; most children are HLA-B27 positive or have family history of HLA-B27-associated disease	3–11%	Early childhood or adolescence	M >> F
Undifferentiated arthritis	Arthritis that either does not fulfill any of the subtypes or can fulfill ≥2 other subtypes	11–21%	NA	NA

RF rheuma factor, *NA* not available

by abnormal hypoechoic or anechoic thickening of the tendon sheath with or without accumulation of fluid. Color Doppler signal can be present but is not required for diagnosis. Tenosynovitis is most commonly seen around the ankle joint and in the extensor compartment of the wrist. Other US findings include increased color Doppler signal in the epiphyseal cartilage, decreased thickness of the joint cartilage, periarticular erosions, and enthesopathy. On MRI involved joints will show synovial thickening, joint effusion, and/or synovial enhancement on contrast-enhanced sequences. Furthermore, MRI can demonstrate signs of tenosynovitis and enthesitis, cartilage damage and bony erosions (epiphyseal), bone marrow edema, and increased vascularity of epiphyseal cartilage. It is good to realize that the widespread adoption of US and MRI in the diagnosis and follow-up of JIA requires a good understanding of the imaging findings and its clinical implications, as well as the development of validated pediatric joint assessment protocols. Furthermore, a substantial number of healthy children appear to have "abnormalities" in one or more joints, including bone marrow edema, joint effusion, erosion-like lesions, and even synovial thickening and signs of tenosynovitis. That is why current research is focusing on differentiating pathologic bony, cartilage, and other articular abnormalities from normal developmental variants.

> **Key Point**
> - Knowledge of the many normal variants in the pediatric musculoskeletal system that can simulate disease is essential to be able to differentiate them from pathologic bony, cartilage, and articular abnormalities.

20.4 Neoplastic Diseases

20.4.1 Bone Tumors [28, 29]

The vast majority of pediatric bone tumors are benign and include osteochondroma, nonossifying fibroma, unicameral or simple bone cyst (UBC), aneurysmal bone cyst (ABC), and osteoid osteoma. They are most frequently found between 5 and 25 years of age, often incidentally (e.g., after minor trauma). Benign bone tumors usually do not require treatment or follow-up, although some might become symptomatic and may require (surgical) intervention (e.g., pedunculated osteochondroma and osteoid osteoma). When patients are symptomatic, they most commonly present with pain that is mild, only activity-related, and nonprogressive. Nonprogressive nocturnal pain reliably relieved with aspirin or nonsteroidal anti-inflammatory drugs is typical of an oste-

oid osteoma. Sometimes the presenting symptom is a pathologic fracture (e.g., in UBC).

Malignant bone tumors constitute around 6% of all childhood cancer in patients under the age of 20 years and are the seventh most common type of tumors in children. Approximately two-thirds of these are osteosarcomas, with the remainder largely belonging to the Ewing sarcoma family of bone tumors. Malignant bone tumors occur mainly during adolescence and young adulthood. Patients with malignant bone tumors nearly always present with complaints of deep, achy, and unrelenting pain and swelling. A pathologic fracture, although uncommon, can also be a presenting feature in a minority of malignant bone tumors.

Imaging studies are essential for diagnosis, planning biopsy (if indicated), and follow-up during treatment. They can aid in differentiating a benign from malignant lesion by providing essential information regarding its nature, size, anatomic location, and effect on surrounding bone or soft tissues. Furthermore, involvement of adjacent joints and neurovascular structures can be assessed which is particularly important when surgical intervention is considered or indicated. CR should always be obtained before advanced imaging is performed as it is very helpful in establishing a first differential diagnosis. Imaging findings that can be assessed on CR include anatomic location of the lesion and position within a given bone; whether the tumor is radiolucent or radiodense or has a mixed appearance; and what the tumor's effect is on the bone and the bone's effect on the tumor. Benign bone tumors usually have sharply demarcated margins with a narrow transition zone with a geographic pattern of bone destruction with smooth and uninterrupted periosteal reaction. Malignant bone tumors, on the other hand, usually have poorly defined margins with a wide zone of transition suggesting a fast-growing lesion and a permeative or moth-eaten pattern of bone destruction with a malignant (sunburst or onion skin-like) periosteal reaction (Fig. 20.5). In most benign bone tumors, CR will suffice and no further imaging is needed. Computed tomography has a limited role to play in pediatric patients and must be used only when a real benefit is expected (e.g., for diagnosis and/or treatment of osteoid osteoma or in CT-guided biopsies). MRI is the imaging modality of choice, in particular in (suspected) malignant bone tumors, to define tumoral extension within the bone and in the soft tissues, involvement of adjacent joints and neurovascular structures, and presence/absence of skip lesions. It should be performed before a (needle) biopsy is performed as this can induce edema or hematoma, which will impact the image quality and interpretation. Furthermore, MRI is used as follow-up during chemotherapy and for preoperative planning after chemotherapy. The MRI protocol should include at least coronal T1-, axial T2-, 3D T1-weighted contrast-enhanced fat saturation sequences, as well as DWI. A T1- or STIR-weighted sequence in the sagittal or coronal

Fig. 20.5 X-ray of the right distal femur illustrating a malignant periosteal reaction (sunburst aspect with Codman's triangles) in a 9-year-old child with osteosarcoma. Furthermore, a permeative sclerotic mass is seen with osteoid formation and extension into the adjacent soft tissues

plane covering the entire bone should be added to look for skip metastases metastases. 18F-FDG PET/CT has also been used to assess metastatic disease as well as the response to neoadjuvant chemotherapy, but its use depends on the type of malignant bone tumor and/or treatment protocol.

20.4.2 Soft Tissue tumors [30–33]

As in pediatric bone tumors, the overwhelming majority of soft tissue tumors in children is benign. The most common benign soft tissue tumors are the vascular tumors and malformations, followed by lipomas, pseudotumors, fibrohistio-cytic tumors, and peripheral nerve sheath tumors. The presenting symptom is usually a bump or fullness which can be symptomatic or entirely painless. In general, benign soft tissue tumors are less than 4 cm in diameter. Malignant soft tissue tumors are rare, accounting for only 1% of all soft tissue tumors in children. Soft tissue sarcomas constitute 7% of all the childhood cancers in patients under the age of 20 years and are the sixth most common type of tumor in children. Rhabdomyosarcoma (RMS) represents 50% of all soft tissue sarcomas. The most frequent non-RMS malignant tumors are peripheral primitive neuroectodermal/Ewing sarcoma family tumors (pPNET/Ew) (19%), malignant peripheral nerve sheath tumors (6.5%), infantile fibrosarcomas (6%), and synovial sarcomas (SNVS) (5%). Age of the patient, site of the lesion, clinical history, and especially chronicity of the lesion are cornerstones in the differential diagnosis. Furthermore, predisposing diseases and/or syndromes must be taken into account (e.g., neurofibromatosis, Li-Fraumeni syndrome). Clinical criteria that are suspicious of a malignant soft tissue tumor include a size greater than 5 cm, increasing size over time, pain, and a deep location of the tumor.

US is the imaging modality of first choice, especially for small lesions. Imaging features to look for include size, regular/sharp versus irregular margins, solid versus cystic components, echogenicity, fluid-fluid levels, calcifications, and vascularity on color Doppler imaging. CR can be used to detect and characterize calcifications and involvement of the adjacent bones (scalloping and erosion versus a destructive/invasive appearance). If a definitive diagnosis cannot be made based on the US and/or CR appearance, MRI is the imaging modality of choice to further explore the lesion. As in bone tumors, this should be done prior to biopsy or surgery to accurately delineate tumor composition and extension, as well as its relation to adjacent anatomical structures such as bone, joints, and neurovascular bundle. The MRI protocol should at least include T1- and T2-weighted sequences without/with fat saturation and contrast-enhanced T1-weighted sequences. The addition of DWI is recommended but not mandatory, as its role in distinguishing benign from malignant tumors and evaluation of response to therapy has not yet been conclusively demonstrated.

> **Key Point**
> - The vast majority of bone and soft tissue tumors in children is benign.

20.5 Concluding Remarks

Imaging plays an essential role in the diagnosis and follow-up of musculoskeletal diseases in children. The radiological evaluation is challenging because of anatomical and physiological differences between the pediatric and adult musculoskeletal system, as well as the great variety of diseases and its typical presentation in children. Knowledge of these differences and the optimal choice of imaging techniques are essential to prevent any unnecessary delay in diagnosing pediatric musculoskeletal diseases.

> **Take Home Messages**
> - The clinical and radiological presentation of musculoskeletal diseases in children differs in many ways from adults, in particular related to anatomical and physiological differences of the musculoskeletal system.
> - There are many normal variants in the developing skeleton that may simulate pediatric musculoskeletal disease.
> - Knowledge of these differences and of the optimal choice of imaging techniques is essential for an adequate diagnosis of musculoskeletal diseases in children.
> - Ultrasound (US) and conventional radiography (CR) are the imaging modalities of first choice in most pediatric musculoskeletal diseases.

References

1. Perry DC, Bruce C. Evaluating the child who presents with an acute limp. BMJ. 2010;341:c4250.
2. Zucker EJ, Lee EY, Restrepo R, Eisenberg RL. Hip disorders in children. AJR. 2013;201:W776–96.
3. Silva MS, Fernandes ARC, Cardoso FN, Longo CH, Aihara AY. Radiography, CT, and MRI of hip and lower limb disorders in children and adolescents. Radiographics. 2019;39:779–94.
4. Parcels BW. Pediatric hip and pelvis. Pediatr Clin N Am. 2020;67:139–52.
5. Graf R. Hip sonography. Diagnosis and management of infant hip dysplasia. Berlin: Springer; 2006.
6. Robben SGF, Smithuis R. Developmental dysplasia of the hip – Ultrasound (2017) Radiology Assistant. 2017. https://radiologyassistant.nl/pediatrics/hip/developmental-dysplasia-of-the-hip-ultrasound.
7. Beek FJ, Nievelstein RJ, Pruijs HE, de Jong PA, Sakkers RJ. Transinguinal sonographic determination of the position of the femoral head after reposition and follow-up in a spica cast. Pediatr Radiol. 2010;40(11):1794–9.
8. Dillman JR, Hernandez RJ. MRI of Legg-Calvé-Perthes disease. AJR. 2009;193:1394–407.
9. Dwek JR. The hip: MR imaging of uniquely pediatric disorders. Magn Reson Imaging Clin N Am. 2009;17:509–20.
10. Shah H. Perthes disease: evaluation and management. Orthop Clin N Am. 2014;45:87–97.
11. Cardinal E, Bureau N, Aubin B, et al. Role of ultrasound in musculoskeletal infection. Radiol Clin N Am. 2001;39:191–201.
12. Karmazyn B. Imaging approach to acute hematogenous osteomyelitis in children: an update. Semin Ultrasound CT MRI. 2010;31:100–6.
13. Kan JH, Young RS, Yu C, et al. Clinical impact of gadolinium in the MRI diagnosis of musculoskeletal infection in children. Pediatr Radiol. 2010;40:1197–205.
14. Jaramillo D. Infection: musculoskeletal. Pediatr Radiol. 2011;41(Suppl 1):S127–34.
15. van Schuppen J, van Doorn MM, van Rijn RR. Childhood osteomyelitis: imaging characteristics. Insights Imaging. 2012;3:519–33.
16. Montgomery NI, Rosenfeld S. Pediatric osteoarticular infection update. J Pediatr Orthop. 2015;35:74–81.
17. De Moraes Barros Fucs PM, Meves R, Henzo Yamada H. Spinal infections in children: a review. Int Orthopaed (SICOT). 2012;36:387–95.
18. Nguyen JC, Lee KS, Thapa MM, Rosas HG. US evaluation of juvenile idiopathic arthritis and osteoarticular infection. Radiographics. 2017;37:1181–201.
19. Struk DW, Munk PL, Lee MJ, et al. Imaging of soft tissue infections. Radiol Clin N Am. 2001;39:277–303.
20. Trusen A, Beissert M, Schultz G, et al. Ultrasound and MRI features of pyomyositis in children. Eur Radiol. 2003;13:1050–5.
21. Khanna G, Sato TS, Ferguson P. Imaging of chronic recurrent multifocal osteomyelitis. Radiographics. 2009;29:1159–77.
22. Falip C, Alison M, Bourty N, et al. Chronic recurrent multifocal osteomyelitis (CRMO): a longitudinal case series review. Pediatr Radiol. 2013;43:355–75.
23. Zhao Y, Ferguson PJ. Chronic nonbacterial osteomyelitis and chronic recurrent multifocal osteomyelitis in children. Pediatr Clin N Am. 2018;65:783–800.
24. Damasio MB, Malattia C, Martini A, Tomà P. Synovial and inflammatory diseases in childhood: role of new imaging modalities in the assessment of patients with juvenile idiopathic arthritis. Pediatr Radiol. 2010;40:985–98.
25. Chauvin NA, Doria AS. Ultrasound imaging of synovial inflammation in juvenile idiopathic arthritis. Pediatr Radiol. 2017;47:1160–70.
26. Dimitriou C, Boitsios G, Badot V. Imaging of juvenile idiopathic arthritis. Radiol Clin N Am. 2017;55(5):1071–83.
27. Malattia C, Rinaldi M, Martini A. The role of imaging in juvenile idiopathic arthritis. Expert Rev Clin Immunol. 2018;14(8):681–94.
28. Shah JN, Cohen HL, Choudhri AF, et al. Pediatric benign bone tumors: what does the radiologist need to know? Radiographics. 2017;37:1001–2.
29. Singla A, Geller DS. Musculoskeletal tumors. Pediatr Clin N Am. 2020;67:227–45.
30. Navarro OM, Laffan EE, Ngan BY. Pediatric soft-tissue tumors and pseudotumors: MR imaging features with pathologic correlation (Part 1). Radiographics. 2009;29:887–906.
31. Laffan EE, Ngan BY, Navarro OM. Pediatric soft-tissue tumors and pseudotumors: MR imaging features with pathologic correlation (Part 2). Radiographics. 2009;29(4):e36.
32. Brisse HJ, Orbach D, Klijanienko J. Soft tissue tumours: imaging strategy. Pediatr Radiol. 2010;40:1019–28.
33. Inarejos Clemente EJ, Navallas M, Barber Martínez de la Torre I, et al. MRI of rhabdomyosarcoma and other soft-tissue sarcomas in children. Radiographics. 2020;40:791–814.